Multiscale approach in the assessment of nanocellulose-based materials as consolidants for painting canvases

Alexandra Bridarolli

Submitted for the degree of Doctor of Philosophy

University College London

Eastman Dental Institute

August 2019

Abstract

This thesis investigates mainly the use of nanocellulose-based treatment for the consolidation of degraded cotton canvases of modern paintings and includes within this some case studies on linen canvases (sized and unsized) and 19th cent. historical samples from paintings. It. uses a multi-scale analytical approach where primarily controlled relative humidity dynamic mechanical analysis (DMA-RH) was used to evaluate the effect of the novel nanocellulose based preparations. It aims at quantifying the advantages, disadvantages, and limitations of their application.

Initially, the baseline viscoelastic response to RH variations of a degraded cotton canvas was measured by DMA-RH. This technique was used further together with SEM to assess morphologically and mechanically 6 traditional consolidants including natural such as animal glue and synthetic materials.

Following the same protocol, two solutions of nanocellulose-based consolidants developed in the frame of the Nanorestart project were assessed. These materials consisted of nanocellulose dispersions in water or water/ethanol and nanocomposites of nanocellulose-reinforced cellulose derivatives in polar/apolar solvents. Overall, higher consolidation at lower weight added was measured for the nanocellulose-based treatments tested when compared to the traditional consolidants. The penetration of the consolidant in the canvas also shows to greatly differ between treatments with the nanocellulose showing low penetration. Higher mechanical response to RH was also measured after treatment in particular with the water-based treatment. The results demonstrate how the adhesion, measured here at the nanoscale, and consolidant penetration into the canvas are dominant factors for the development of consolidation treatment for painting canvases.

The assessment of the novel consolidants was finally carried out on historical canvases. Most treatments show to perform well on historical paintings in terms of handling properties, penetration and surface appearance and consolidation.

Preliminary time-resolved neutron radiography with new purpose built sample chamber and RH controller provided visual information on time-dependent moisture response of the samples.

Declaration

I confirm that the work presented in this thesis is my own original work. When information has been derived from published work, it has been cited when appropriate. Results that have been published by my colleagues and me are also indicated. Samples obtained as a results of collaborations have been noted.

Alexandra Bridarolli

Acknowledgements

Firstly, I must extend my gratitude to my two supervisors, Dr Marianne Odlyha and Dr Laurent Bozec for their continued advice and support during the PhD. Without their support, this thesis would not be where it is today. Their consideration allowed me to pursue the varied topics found in this thesis.
I must then thank my two other supervisors Dr Aurelia Chevalier and Dr Manfred Anders who I am grateful for their support, the recommendations they were able to give me throughout this PhD and the ideas that were raised during our discussions and exchanges.

This research would not have been possible without funding from the H2020 Nanorestart European project and from the Engineering and physical Research Council (EPSRC) through the Centre for Doctoral Training In Science and Engineering in Arts, Heritage and Archeology.

I should also thanks other partners from the Nanorestart project who have always been there when I needed help. For their help, support, friendship, open-minded attitude and curiosity, I would like to thanks in particular: Romain Bordes, Oleksandr Nechyporchuk, Marta Oriola, Nadine Böhme, Katharina Schumann, Katrien Keune and Giovanna Poggi.

Because this PhD has shown me that research can sometimes be very competitive, I would first like to thank first John Duncan at Lacerta Technology for his unconditional support and help with the DMA. I also thank Dale Moulding at the Institute of Child Health UCL for his help with ImageJ and collaborators in Switzerland R. Fischer and Dr Mannes who have given their time to answer my very basic questions about neutron radiography. I would also like to thank collaborators at the institute of conservation of Copenhagen Dr Krarup Andersen and Dr Dorte Sommer and Dr René Larsen. All these people have showed me that research should always be driven by curiosity.

For their time and help, I am grateful to Dr Nicky Mordan, Dr George Georgio, Dr Graham Palmer and Dr Isabel Kingston. I would not have known that much about Eastman and its devices without them.
Because this PhD would have been far less special without it, I also thank the team at SEAHA. The first year of PhD has been the most challenging and exciting thanks to the lectures of Dr. Matija Strlic and Josep Grau-Bove and my colleagues Danae, Sarah, Vladimir, Mark, Isabella, Lucie, Scott and Nathalie. Finally, because life is not all about cultural heritage and conservation, my final words will be for my peers at the Eastman Dental Institute: Adam, Lucia, Ana, Nabih, Nazanin, Sarah, Mayda. There are many more people throughout UCL and London who provided their help.

Nanorestart European project

This research project has been carried out in the frame of the European NANOrestart project which has been running from September 2014 to September 2018. As such, most of the materials and consolidants used in this project were provided by project partners. This includes the cotton canvas and the nanocellulose-based consolidants tested. The main collaborators of this research are cited below:

- Romain Bordes and his research group at the Department of Chemical and Biological Engineering, Chalmers University (Gothenburg, Sweden) who provided with the nanocellulose dispersions and the treated degraded cotton canvas samples (solution 1 in Chapter 2) and consolidant consisting of multi-layered nanoparticles (solution 3 in Chapter 2) presented in Chapter 5 and 6.
- Manfred Anders and his group at the Zentrum für Bucherhaltung (Leipzig, Germany) who provided the nanocomposite consolidants (solution 2 in Chapter 2).
- Piero Baglioni and his research group at CSGI, University of Florence (Italy) who provided a consolidant consisting of multi-layered nanoparticles (solution 3 in Chapter 2)
- Marta Oriola and her team at the Department of Fine Arts, University of Barcelona (Spain) who provided the cotton canvas and prepared the samples described in chapter 6.
- Aurelia Chevalier from the Aurelia Chevalier Atelier (Paris, France) who participated in the research carried out in Chapter 7.

Impact statement

This project has used a comprehensive nanometrology and mechanical approach to review the potential of new consolidants for the structural consolidation of canvas paintings supports. It is hoped that these treatments will offer an alternative to lining and consolidants currently in use and prevent the re-occurrence of the issues highlighted in the Greenwich conference. It is also expected that the results of this project will enable further research groups worldwide, from heritage scientists to conservators to consider the approach that we present in this manuscript to assess the performance of the materials used in conservation.

This work in this thesis has been presented in approximately a dozen conferences, seminars, workshops and internal meetings of the Nanorestart European project, and published as 3 articles with several co-authors. One of the papers was published in a high impact factor journal as first author. Three more papers are currently under preparation.

This research was also presented to larger, non-specialized audiences, at the Cheltenham Science festival as well as at the UK semi-final 3MT thesis competition which was also podcasted.

The work in Chapters 4, 5 and 6 was performed in collaboration with other European institutions in the framework of the Nanorestart European project. Chapter 4 and 6 benefited from the close collaboration with professional painting conservators. Chapter 5 consists of the assessment of a range of canvas consolidants developed by research groups based in various universities and a private conservation centre.

Part of the work presented in Chapter 5 was also carried out with two MRes students from Birkbeck University (University of London, UK). Several collaborations were also set up with other institutions. The work presented in Chapter 7 is the result of one of these collaborations. The study was successfully carried out at the neutron facility at ISIS (UK) and involved the participation of another group from the private company Lacerta Technology Ltd (UK).

New collaborations were also started with heritage institutions such as the Munch Museum in Oslo and the school of conservation in Copenhagen. Samples from an original canvas used by the Norwegian painter Edvard Munch were obtained for further testing. Complementary analysis of samples of this thesis could also be obtained in the framework of the thesis of a 1st-year conservation student from the school of conservation in Copenhagen.

Scientific publications

(1) Odlyha, M.; Lluveras-Tenorio, A.; Lucejko, J.J.; di Girolamo, F.; Hudziak, S.; Strange, A.; **Bridarolli,** A.; Bozec, L. Violin varnishes: microstructure and nanomechanical analysis. (To be submitted)

(2) **Bridarolli**, A.; et al. Evaluation of the Adhesion and Performance of Natural Consolidants for Cotton Canvas Conservation. ACS Applied Materials & Interfaces. 2018, 10 (39), 33652–33661.

(3) **Bridarolli**, A. et al. Nanocellulose-based Materials for the Reinforcement of Modern Canvas-supported Paintings. Studies in Conservation. 2018, 63(1), 332–334.

(4) Nechyporchuk, O.; Kolman, K.; **Bridarolli**, A.; Odlyha, M.; Bozec, L.; Oriola, M.; Campo-Francés, G.; Persson, M.; Holmberg, K.; Bordes, R. On the Potential of Using Nanocellulose for Consolidation of Painting Canvases. Carbohydrate Polymers. 2018, 194, 161–169.

Table of contents

List of Figures

List of Tables

Abbreviations

AFM; Atomic force microscopy

BC: Bacterial nanocellulose

CA: Contact angle

$CaCO_3$/PEI/CMC: $CaCO_3$ nanoparticles/ Polyethylenimine/Carboxymethylated cellulose

CMC: Carboxymethylated cellulose

CNC: Nanocrystalline cellulose

CNF: Nanofibrillated cellulose

CCNF: Carboxymethylated CNF

DP: Degree of polymerisation

E': Storage modulus

FTIR: Fourier transform infrared reflectance

Tyl: Tylose

DEA: Dielectric analysis

DMA: Dynamic mechanical analysis

DMA-RH: DMA under controlled RH

DVS: Dynamic vapour sorption

MC: Methylcellulose

Mp : Melting point

NC : Nanocellulose

NP: Nanoparticles

RH: Relative humidity

PAAE: Polyaminoamide epichlorohydrin

PEI: Polyethylenimine

SEM: Scanning electron micorscopy

SEM-EDX: Scanning Electron Microscope/Energy Dispersive Using X-Ray

SNP: Silica nanoparticles

SNP/PEI/CMC: Silica nanoparticles/Polyethylenimine/Carboxymethylated cellulose

T: Temperature

Tg: glass transition temperature

Tyl: Tylose MH50

Y: Young's modulus

1 Introduction

The first mention of an easel painting dates back to ancient Egypt and was made by the 1st-century AD author Pliny the Ancient in his book *Natural History* (book XXXV). Yet, the use of canvas as support for paintings only became popular in the 13th century when easel paintings gradually replaced panel and wall paintings (Stephenson, 1989). Easel paintings are multi-layered structures with 2 faces which have triggered different level of interest in conservation. Early research in the field mostly focused on the front, painted, face, of high esthetical value. The canvas itself has been often neglected and regarded by art historians and conservators as a support with historical but no specific artistic value. From the 17th to mid-20th centuries, it was thus common practice for the structural consolidation of paintings to glue a second canvas on top of the original one (Bomford, 1981; Percival-Prescot, 1974). This practice called lining was routinely applied, sometimes very early the lifetime of a painting as a durability warranty. The lining of the painting was also often associated with a preliminary step which consisted in the impregnation of the canvas (Bomford & Staniforth, 1981b; Ruhemann, 1953; Teixeira, 2016). The adhesives used for lining and impregnation were natural glues such as drying oils, animal glues, starch or wax-resins. However, at the conference of Greenwich of 1974 organised at the National Maritime Museum (UK) (Percival-Prescot, 1974; Caroline Villers, 2003), the first awareness about the damaging consequences of these practices was raised (Ackroyd, 2002; Berger, 1974) . This awareness marked the beginning of significant changes in painting conservation and with it an increased interest in researching this field. Lining and/or canvas impregnation of a painting is now done reluctantly and considered as a last resort solution by many conservators (Bomford, 2001; Joyce Hill Stoner, 1994). Simultaneously, the technique has also continued to evolve with the developments of new adhesives and lining processes (Mehra, 1981; Phenix, 2010; Ravnikar, 2014; C. Young, 2012). At the end of the 20th and beginning of the 21st centuries less invasive techniques such as strip lining, tear mending or loose lining techniques flourished (Ackroyd, 2002). With the development of new materials in art production and the growing awareness about the risks such as reversibility, unstability upon ageing associated with current adhesives in used

in conservation, the need for a simple, compatible, effective and durable alternative to the all available treatments for canvas consolidation is still present. The challenges set by complex artworks (Roudet, 2007) and inappropriate use of lining on more recent paintings (Hummelen, 2012; Richardson, 1983) marks this as a particularly relevant challenge in the field.

1.1 State of the art in canvas consolidation

1.1.1 Anatomy of easel paintings

Traditional easel paintings present a multi-layered structure made of the canvas, the sizing layer, the ground, the paint layer(s) and the varnish (Figure 1.1). While the materials used to make these different layers have changed over time, the painting structure itself has remained almost the same. These layers present different composition, role and physicochemical properties and will, therefore, be described in more detail separately.

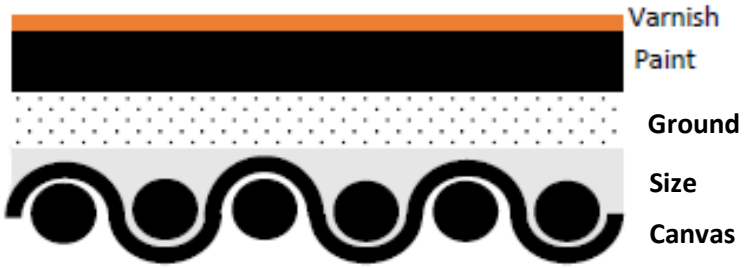

Figure 1.1: Scheme of an easel painting cross-section showing the painting's structural layers.

Painting canvases can be made out of a range of different materials. These comprise linen and cotton, for the most common, but also hemp, jute and synthetic fibres like polyester, polyamides, and carbonized fibres (Hackney, 2004a; Hedley, 1993a; Young, 2012). The natural fibres linen and cotton remain the preferred surfaces for artists and in particular linen as it is often considered to be more durable and stronger (Gerry Hedley, 1993a). Canvases are also woven structures which comprise two thread directions defined as warp and weft (Figure 1.2). The threads in warp differ from those in weft by their higher curvature as well as lower stiffness. The threads of a canvas can also be made of a various number of yarns, and the yarn of a different

number of fibres. Finally, canvas fabrics can be found in different weave patterns and weights (Figure 1.3).

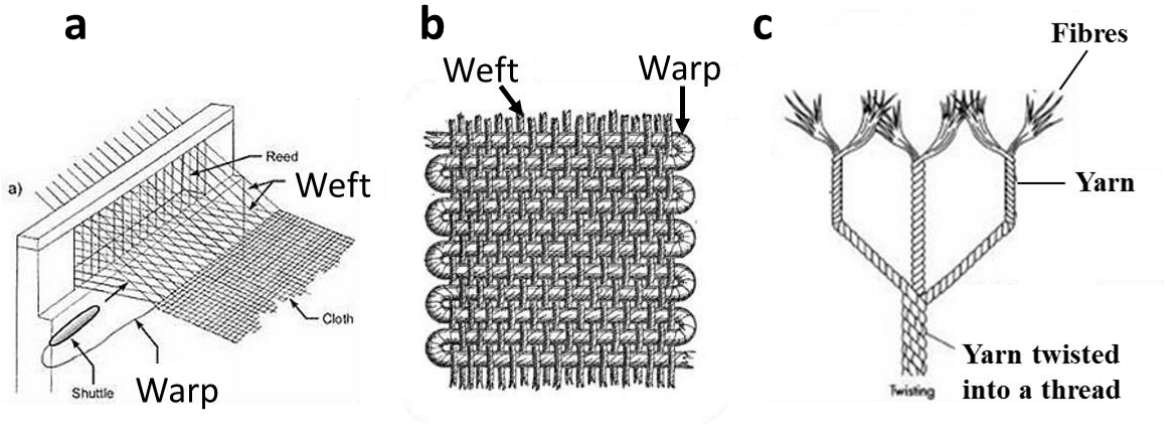

Figure 1.2: Warp and weft characteristics in a plain weave fabric from the weaving process (a) to the fabric structure (b). The structure of a thread made of twisted yarns is shown in (c) (taken from (Burnham, 1980) and in Textile Innovation Knowledge Platform website("Weaving process," n.d.) (accessed 2019) showing reproductions from (Watson, 1921)).

The woven structure of canvases and/or woven fabrics is responsible for their well known and studied anisotropic behaviour or directional-dependent properties. It has been shown that strength, initial modulus and recovery at crease, for example, vary according to the direction of measurement (Sengupta, 1972). In term of properties, textile finishing, structural parameters (yarn twist, weave, etc..) and material have an influence on the fabric's final physicochemical and mechanical properties. Finally, in a painting, the canvas plays a major role in providing a mechanical support for the other layers. It is, therefore, the main focus of work on painting structural consolidation. Lining is one option but other alternatives such as more gentle approaches to lining which include strip lining or mist lining or others such as backboarding were more recently explored (Stoner, 2012). It is now common practice to carry out tear mending works and localized consolidation such as strip lining on painting in need of structural consolidation ("Conserving canvass symposium," 2019). Backboarding has also now become a common procedure which offer a buffer to the painting thus reducing the risks associated to variations in temperature and relative humidity (Ackroyd, 2002; Hackney, 2004a).

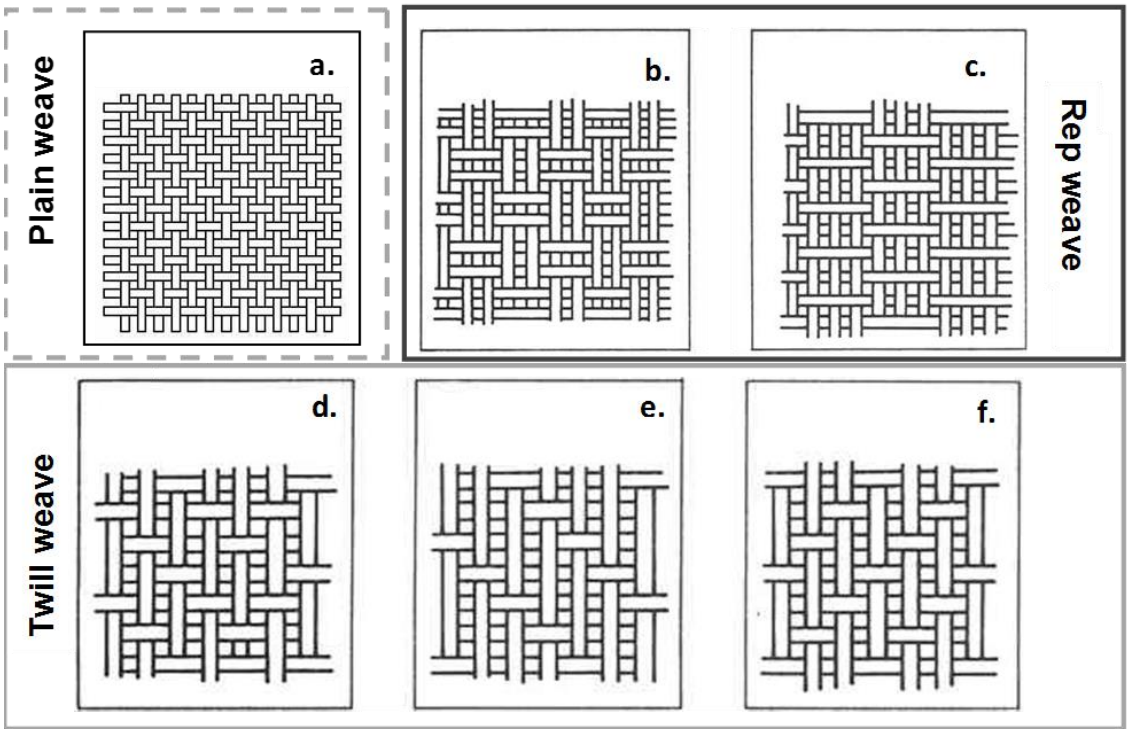

Figure 1.3: Examples of weave patterns found for canvases.

On top of the supporting canvas, the sizing and ground layers are applied to fill the voids of the canvas and also provide a physical separation between the canvas and the paint layers. Sizing materials commonly used in the past or currently in paintings are proteinaceous materials (i.e. hide glue or animal glue) or polyvinyl acetate (PVA) or acrylic resins. The ground layers are often made of a white material (gypsum, chalk, zinc or tin white) used to reflect light mixed with animal glue (aqueous-based gesso grounds) or with oil (oil grounds) (Doerner, 1984; Janson, 2006; Mayer, 1973). Acrylic emulsion based grounds have also been used since 1955 (e.g. Liquitex) (Maor, 2007; Ormsby, 2008). Sizing a canvas is not necessary for acrylic paintings but is particularly important for oil painting. The size provides a protection to the canvas against the oxidation and corrosive effects of the oils present in the ground. It also reduces, but not entirely eliminate, the absorbency of the canvas. The ground layer helps binding the paint layers onto the canvas. It traditionally offers some tooth to make the paint adhere better. It also offers a uniform surface to the support, contributes to the final texture and colour and decrease porosity at the interface with the paint layers (Dei, 2013). As such, it forms a homogeneous and continuous layer

for the application of the paint while allowing the binding between the absorbent paint layers and the support itself (Kühn, 1986).

Paint layers and varnish layers are then applied on top of the materials previously mentioned. Their role is mainly aesthetic. The varnish also acts as a protective layer for the painting and paint layers (Doerner, 1984; Hackney, 2007). The paint consists of a pigment mixed or suspended in a binder. Traditional binders are natural binders such egg tempera and oil (Mayer, 1973) whereas modern binders include synthetic resins mainly poly(vinylacetates) or PVAs, acrylic resins and alkyd resins (Cappitelli, 2000; Learner, 2007; Lodge, 1988; Sonoda, 2006). Developments in the paint industry to obtain paints with, for example, various drying times or improved surface appearance account for the large range of solvents in which paints are found: water, aliphatics, aromatics, alcohols, white spirit, etc. Finally, the varnishes currently in use can be classified between more traditional natural (shellac, dammar) and modern synthetic varnishes (ketone or acrylic resins dissolved in mineral spirits) (Gettens, 1966; Gottsegen, 1993). This variability has an impact on the choice of conservation treatment to apply. The carrier solvents of nanoparticles dispersion used to consolidate a canvas, for example, should not affect the paint and varnish layers.

1.1.2 Canvas degradation through chemical and physicomechanical processes

When the painting canvas becomes too brittle as a result of its degradation, the stretching of the painting cannot be done without the risk of breaking and damaging it, and that can occur when a lining or strip lining is performed. Several studies have investigated the degradation of paintings and its meaning in terms of mechanical properties (Hackney 1981, Carr 2003). Paintings canvases have been shown to undergo chemical as well as mechanical processes of degradation. Both these processes are strongly intertwined as described in the next chapters.

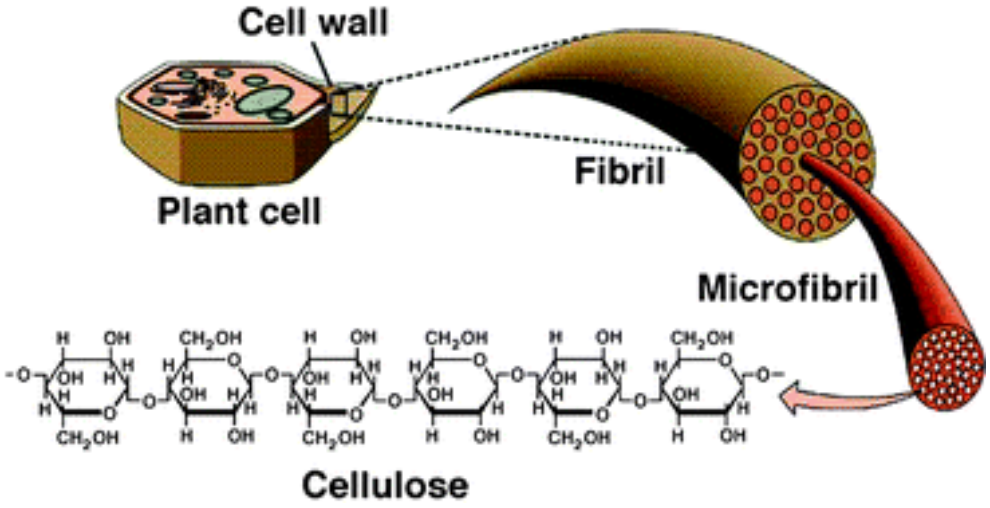

Figure 1.4: From plant cell to the individual cellulose chains (Malmstrom 2012).

1.1.2.1 Chemical degradation of canvas

Linen, hemp and more recently cotton are the materials mostly used for the support of paintings. Linen, hemp and cotton are cellulose-based materials. Cellulose is a polysaccharide made of a succession of β (1→4) linked D-glucose monomer units. Hundreds to thousands of monomer units can be found in a polysaccharide linear chain (see Figure 1.4). Many examples of studies on the cellulose degradation reactions and kinetics can be found in the literature (Area, 2011; Malešič, 2005; Stamm, 1956; Strlic, 2003; Van Der Reyden, 1992). These reactions involve the hydroxyl groups present on the glucose as well as the glycosidic groups linking the units together. The degradation is triggered mainly by light and heterogeneous acid-catalysed hydrolysis (Whitmore, 1994). It can be caused by the humidity because of the hydrophilic behaviour of cellulose. In an alkaline environment, cellulose can also undergo alkaline-catalysed hydrolysis and oxidation reactions of the hydroxyl groups with the formation of carbonyl groups (aldehydes, ketones) (Van Der Reyden, 1992). These groups can be further oxidised and trigger acid-catalysed hydrolysis (Williams, 1981). In both cases, the degradation of the cellulosic material is characterised by the cleavage of the main polymeric chain between glycosidic units. The length of the polymeric chain also called the degree of polymerization (DP), is decreased (Area, 2011; Oriola, 2011; Strlic, 2003). The degradation of the canvas is, therefore often quantified by the decrease in DP or by the acidification of the canvas. Losses in DP from 2000 to

875 have been measured for example for model paintings thermally aged for 700 hours at 105°C (Seves, 2000). The DP of original canvases from old linings were found to be around 600-700 (Oriola, 2015; Oriola, 2011).

Loss in DP has shown to translate into a loss of fibre strength and stiffness, elasticity as well as changes in material colour (Testa 1994). As a result of cellulose degradation, a loss in the macroscale mechanical properties of the cellulosic material and colour change is thus observed for aged canvases. Losses in strength and elasticity (i.e. elongation at break) of canvas fabrics (including textiles) after ageing has been quantified by Hedley (1993), Peacock (1983) and Abdel Kareem (2004). Tests conducted by Hedley and Hackney (Hackney, 1981; Hedley, 1988, 1993b) on samples naturally aged at the Tate gallery (London, UK) revealed that in only 24 years old linen canvas samples had reduced to practically one-third of their original strength. The samples, restrained under frames, had been exposed to extreme conditions following daily RH and temperature variations, protected from rain but exposed to air, on the roof of Tate Britain. Abdel Kareem (2004) reported higher losses in tensile strength (i.e. ultimate tensile strength) up to 60% and 17% for an unrestrained linen textile under artificial thermal and light ageing respectively. These tests provide a first assessment of the strong impact of ageing on fabrics mechanical properties.

Mechanical stresses can also trigger chemical degradation. The stress undergone by these fabrics will cause irreversible deformation and physical damages but also favour chemical degradation (Pertegato, 1993). This is seen, for instance, in tapestries that are hung for long periods of time. Their top edges are more degraded than the rest because they hold the weight of the whole textile.

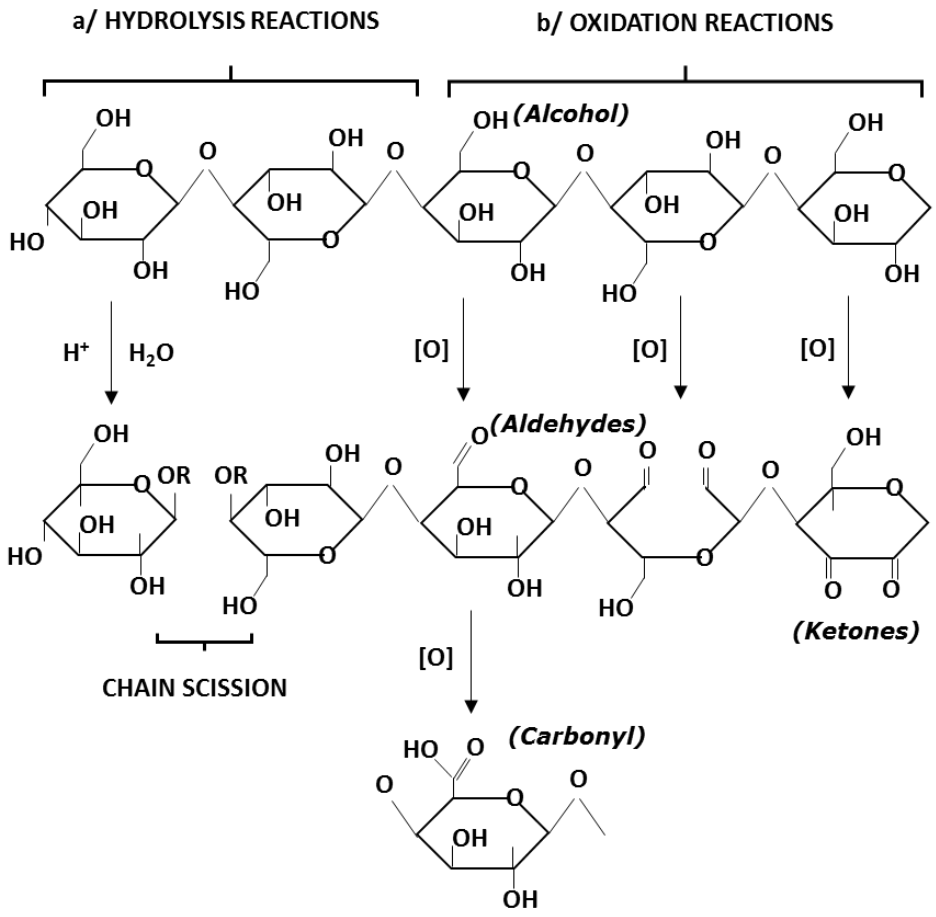

Figure 1.5: Hydrolysis and oxidation reactions leading to the degradation of the cellulosic polymeric chain (Van Der Reyden, 1992).

1.1.2.2 Mechanical degradation of easel paintings

The mechanical stresses experienced by a painting are also often caused by environmental factors: variations in relative humidity (RH) and temperature (T). Some constitutive layers of a painting are hydrophilic and highly responsive to RH while others are less so. Cotton and linen canvases, for example, are moisture sensitive supports. At 65%RH, linen and cotton can take up moisture to 12% and 8.5% in mass respectively (Hill, 2009). The individual layers also present differential mechanical responses to fluctuations in RH and T. Mecklenburg (1982) and Hedley (1988) have shown for example that the canvas and the glue layers, being responsive to moisture, will swell or contract and respond faster to the other layers to changes in RH. A more hydrophobic material such as the paint layer will be more sensitive to change in temperature. It will become more brittle or more plastic at low and high RH levels respectively. These differential behaviours

toward RH and T variations observed between constitutive layers of a painting can lead to the building up of strong shear and tensile stresses which are stresses coplanar and perpendicular, respectively, to the face of the material on which the load is acting. As a result, delamination or the rupture of the different layers resulting from the release of the accumulated tension can occur and spread onto and across the entire painting (Bergeaud, 1997; Karpowicz, 1989). In a new canvas, the glue layer and to a lower extent the stiff paint and ground layers carry much of the load. Mecklenburg (1982) showed that physical degradation of a typical painting occurs first, through embrittlement and cracking of the ground and paint layers, then through long-term relaxation of the canvas under tension (see Figure 1.6).

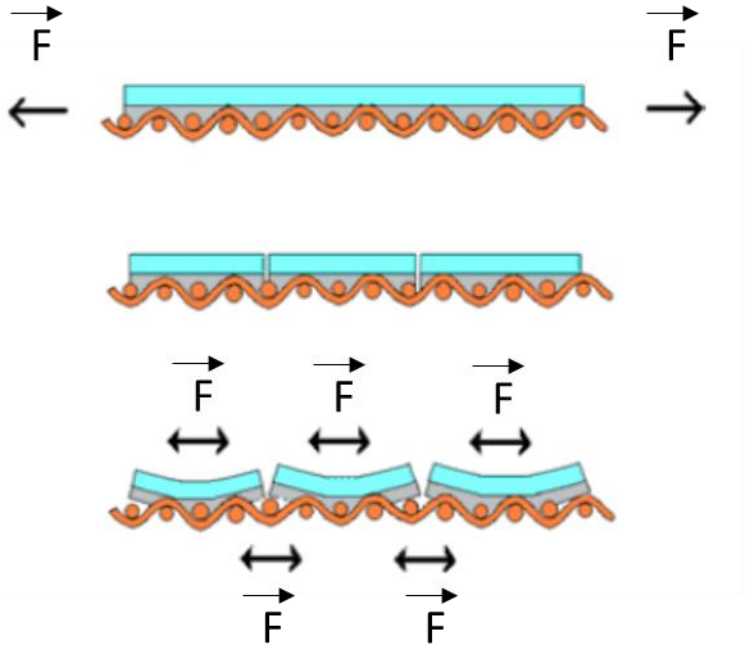

Figure 1.6: Scheme of the embrittlement of the ground and paint layer of a painting leading to paint cupping and its mechanical degradation (from Mecklenburg, 1982). The vector F refers to the tension felt by the painting and distribution of this tension before and after embrittlement of the paint and ground layers.

Much of the tension is carried in the paint and ground, and not in the canvas which is inherently much more flexible. Where the paint cracks, all the tension is then transferred to the canvas (Mecklenburg, 1982). These ruptures can, however, also start on the canvas. When it happens, threads rupture and tears appear. They are often observed along the lines marking the

interface between two materials which are areas where mechanical stresses are highly concentrated (Oriola, 2011).

1.1.3 Paintings and canvas mechanical assessment

1.1.3.1 Techniques for the assessment of paintings mechanical properties

The various structural characteristics of the canvas such as the weaving pattern, the weaving density, the amount of thread crimp, the twist of the yarn and thread have an influence on its bulk properties (Young, 2012). Similarly, the composition of the several layers of a painting, their size, their layout within the painting may lead to a range of mechanical behaviours and responses to external stresses such temperature, relative humidity (RH) (Hedley, 1988, 1993a; Mecklenburg, 1982). The development of accurate ways of assessing the mechanical properties of materials, such as textiles (Saville, 1999; Young, 1999), as well as the increased use of finite element modelling (Cook, 1995; Eischen, 1996; Wood, 2018), have enabled a better understanding of painting and canvas mechanical behaviour. It has, in particular, given access to the role of each individual painting layer of a painting in the overall response to RH (Erhardt, 1994; Hedley, 1975; Young, 2001).

Different approaches have been taken to address the evaluation of canvas and paintings properties. In the early assessments by Mecklenburg (1982) and Hedley (1988), large pieces of bare canvas were tested uniaxially with the load applied in either the warp or weft direction. During the same period, following developments in mechanical engineering for textile testing, biaxial testing, i.e. load applied simultaneously in the warp and weft directions, was also introduced in works of Berger and Russell (1982) and later in those of Young (1999). These several studies provide a more accurate assessment of a painting by replicating the tensions and mechanical stresses applied to the painting when restretching or lining it. Biaxial assessment of the canvas is particularly important due to its anisotropic behaviour. This implies that the mechanical properties of canvas, as other woven materials, will differ depending on the direction in which the fabric is tested. Hence, as shown by Penava (2016), miscalculations in canvas and

painting mechanical properties often arise from the mistaken belief that paintings mechanically behave isotropically, i.e. as opposed to anisotropic, material which has the same properties in every direction. They also show that when increasing the number of layers (sizing glue, ground layers), deviations between experimental and theoretical values decrease. The results indicate that the anisotropic behaviour of the coated canvas (such as painting) is gradually reduced and replaced by the more regular isotropic behaviour of the layers above. Although biaxial testing frames are considered as more accurate for canvas mechanical assessment, they are not commonly available for purchase and require some basic engineering skills to be made which limits their wide access for research purposes. Uniaxial testing, despite its limitations, can still provide valuable information on the mechanical properties of the canvas (i.e. elastic modulus, ultimate strength, elongation at rupture, etc.). Finally, it is important to note that most of the studies on the mechanical assessments of paintings or paintings materials focused on the measurement of the elastic response of these materials (i.e. immediate mechanical response to any stress applied). In these type of measurements, the time-dependant (or viscous) response of the materials is not taken into account. The viscoelastic response, hence the deconvolution of the purely elastic response (energy stored upon application of a stress) from the viscous, time-dependent (dissipated energy), response, is rarely explored despite its importance. It is partly due to the lack of access to devices enabling such analyses, but also because some measurements require long-term testing as will be shown later (cf. 1.1.4.1.2). The few studies looking at viscoelastic properties of painting materials include the use of dynamic mechanical analysis (DMA) by Hedley (1991) on oil paint films and Odlyha (1995) and Foster (1997) on oil primed canvases and more recently by Ormsby (2007a, 2007b) on acrylic emulsion paints and Chiriboga Arroyo (2013) on films of primer, paint and PVA glue.

More recently, several non-destructive or almost non-destructive techniques for which sampling of the artwork is not necessary have made their way into conservation for the assessment of painting mechanical properties. Nanoindentation enables the measurement of forces at the microscale (Vanlandingham, 2001). It was used in 2011 to measure bulk properties such as the

reduced elastic modulus, i.e. elastic deformation that occurs in both sample and indenter tip, and hardness of original historical paints (Salvant, 2011). Differential mechanical response between paint layers of different nature as well as loss in reduced modulus resulting from ageing were measured showing the potential of the technique. However, irreversible deformation of the surface, seen as indentations of 10 µm in diameter caused by the indenter, could be observed under the optical microscope for certain types of paints at the microscale. On small samples, this deformation will impact on the number of measurements possible. Differential image correlation (DIC) was also investigated to quantify the degree of response of the entire painting to relative humidity (RH) variations as occur in historical houses (Vilde, 2016). If implemented in museums and galleries it could enable the remote monitoring of deformation in woven canvas at various relative humidities. Computer modelling of painting behaviour has also attracted much interest in recent years (Chiriboga Arroyo, 2013; Mecklenburg, 1994). Chiriboga Arroyo (2013) used finite element (FE) modelling to investigated and predict the mechanical response of paintings subjected to loading vibrations. The goal was to evaluate the risks associated with the transport of paintings on loan, for example (Lasyk, 2014; Michalski, 1991). Despite the great potential of FE modelling (non-destructive, strong calculation power), the technique is still in its early stages of use in cultural heritage. The development of accurate models faces two limitations: the variability between mechanical behaviour of different canvases as well as the lack of extensive mechanical data gathered on paintings by previous studies. Thus, while all the techniques presented previously, i.e. mechanical (micro and macroscale, uni- or bi-axial) or computational, are valid and can bring valuable insights on the mechanical properties or response of the painting to external stress (e.g. environment, vibrations), they also present limitations. These limitations should be kept in mind when interpreting the results from the studies carried out on the mechanical properties of canvases and paintings.

1.1.3.2 Quantification of forces applied during painting restretching.

Uniaxial, biaxial and non-contact tests have provided conservators with the first quantitative mechanical assessments of practices usually based on empirical knowledge. Hence,

paintings are often restretched by conservators until they feel "tough", i.e. until they feel stretched enough to support the painting and avoid buckling of the canvas without but not high enough to endanger the paint and ground layers. The tensions applied can thus greatly varied between conservators. Several studies have looked into the quantification of the optimal tension at which a painting should be stretched (see Table 1.1). The variability in the results is, however, important. For Berger and Russell (1988), classic easel paintings should have stresses around 200N.m^{-1}. Hedley also found that a stable load for canvas test strips lies between 120-320N.m^{-1} (Gerry Hedley, 1988). However, in the same study, it is also shown that small to medium paintings could undergo much higher stresses, up to 4000N.m^{-1}. This very high value in tension seems out of proportion. Hence, Young (1999) showed later that a bare canvas tested at that level of tension felt very taut compared to a typical stretched canvas. Interestingly, the use of computer modelling also given high values of tension equivalent to 2000N.m^{-1} as suitable for the tensioning of paintings (Mecklenburg 1991). More recent work by Young (1996) and Iaccarino Idelson (2009) produced lower tension levels around 200-250 N.m^{-1} similar to those identified by Berger and Russell (1988) and Hedley (1988) found between 200 and 600 N.m-1. Using a biaxial stretcher, Young (1996) documented that tension between 200-600 N.m^{-1} produced a tautness equivalent to that of a newly stretched or lined painting (Young 1996). More recently, Iaccarino Idelson (2009) used an optical technique for measurement. He identified a threshold value beyond which there is no significant improvement in the resistance to deformation. For 5 paintings tested biaxially, the threshold lay between 200-250 N.m^{-1}. Although a consensus on the ideal tension around 200 N.m^{-1} seems to arise from these different studies, the variability in the results remains quite high Table 1.1). These scattered results highlight the influence of the analytical technique used. They also indicate the inherent singularity of each painting. Thus, if general conclusions can be drawn regarding the mechanical properties of paintings and canvas, a case-by-case study is always required.

Testing type	Tension measured	Studies	Sample type
Uniaxial testing	120-320 $N.m^{-1}$ 4000 $N.m^{-1}$ (for small painting)	Hedley 1988	Closely woven linen canvas primed with lead white and calcium carbonate. The weave counts were of the order of 14·2 x 14·6 ends/cm, 14·6 x 15 ends/cm and 14·2 x 15 ends/cm. Weight≈300g/m^2 (canvas) and 300g/m^2 (ground only)
Biaxial testing	200 $N.m^{-1}$	Berger and Russell 1988	Light linen canvas (sample (16-6 thread/cm, weight=200g/m) Heavy linen lining canvas (10 double thread/cm in the warp. 11.2 , double thread/cm in the weft direction, weight=350g/m^2
	200-600 $N.m^{-1}$	Young 1999	Superfine Plain Weave Belgian Linen (Russell & Chappell L184), weight=230gm^2)
Computer modelling	2000 $N.m^{-1}$	Mecklenburg and Tumosa 1991	Linen canvas (0.064 cm thick), 38.6 MPa average constant modulus
Optical analyse of a painting.	200-250$N.m^{-1}$	Iaccarino Idelson 2009	7 paintings mounted on original stretcher with springs

Table 1.1: Overview of the results found in the literature regarding the optimal tensions to be applied to stretch an easel painting.

1.1.4 Reinforcement of paintings

The evaluation of the desirable reinforcement is one of the main concerns for the development of new treatments for painting structural consolidation. A rigid support enables the transfer of the load away from the , canvas and uppermost layers, thus reducing the likelihood of mechanical failure (Young, 2001). Another means to achieve this goal is to reduce the response of the painting to variations in RH by rendering it less hygroscopic (Berger, 1972; Hedley, 1993a; Mecklenburg, 1982). In this part, we review existing lining canvas, consolidants, adhesives and consolidation techniques with the attempt to define their advantages and disadvantages in terms of mechanical behaviour and long-term stability.

1.1.4.1 Lining canvases, adhesives and procedures for their application.

The first lining of works on canvas which started to be carried out to a large extent in the 18th century were done using cotton and linen canvases. New synthetic materials such as polyamide or polyester canvases were tested to replace these two traditional canvases 40 years ago (Hedley 1981). However, the lack of more thorough investigation into the synthetic fabrics available as

well as their limited access in the conservation market, is responsible for their rather low success. Some of them are in use but did not reach a wide-scale acceptance expected among painting conservators (Ackroyd, 2002; Young, 2012). A more detailed investigation of all the synthetic lining canvas available was recently carried out by Young (2012). Physical, as well as aesthetic and kinaesthetic properties, were investigated. Among the materials tested, polyester was found to be the most suitable lining fabric as it exhibits, when compared to cotton, linen, polyester, polyamides, and carbonized canvases, the best combination of properties in terms stiffness, ultimate tensile strength, moisture response, crimp, drape, and lustre.

Lining using glue-paste (mixture of animal glue and flour) or wax-resin used to be the most common procedure to prevent mechanical damage in a painting (Ackroyd, 2002). Lining is still done today but the technique has greatly evolved and, in the west, is only applied in extreme cases where the painting could be entirely lost if no action is taken. When the painting is still in a good state or only needs local structural consolidation, preventive techniques of consolidation which are less intrusive are available. These are, for example, loose lining (absence of lining adhesive), strip lining (lining of the tacking edges) or backboarding (backing placed on the reverse of a painting) (Hackney, 2004). They are increasingly used by conservators (Coddington, 2018; "Conserving canvass symposium," 2019; Ridge, 2006). Their advantages and drawbacks remain relatively poorly studied and are based on a more empirical knowledge. The only research available on backboarding, for example, was performed by Stephen Hackney at the Tate (London, UK). His findings show that backboarding is beneficial to paintings by providing a protection from impacts during transport, as dust seals and barriers to moisture (Hackney, 1981; 1984; 2007). However, the practice of backboarding is still questioned as this could lead to a microclimate with enhanced volatile organic compounds (VOCs) emitted by the paint, varnish or wooden stretcher and frame (Bonaduce, 2013; Grøntoft, 2010; López-Aparicio, 2010). In the 1980's, Ackroyd reported that traditional approaches to lining continue to be used but that new adhesives and techniques are also mentioned by conservators (Ackroyd, 2002b; Stoner , 2012).

The first significant improvement of the lining technique dates from 1965 with the introduction of Beva 371 by Berger (1972). Beva 371 results from the combination of ethylene vinyl acetate (EVA) resins with waxes and ketone resins. The formulation was designed to be inert to moisture and capable of providing a non-impregnating treatment with optimal wetting properties. Its formulation was slightly modified later when the ketone resin consisting of a condensation product of cyclohexane was replaced by a condensation product of cyclohexanone. It is currently one of the most used synthetic adhesives. Other synthetic adhesives have been used from this period onwards; some of them for decades (Chevalier 2006). These adhesives are poly(vinyl acetates), acrylic or poly(vinyl alcohol) polymers. The most famous and broadly used in relining works are the vinyl acetate/paraffin/ketone mixture Beva 371 (Lascaux) formulated by Berger (1972) and the acrylic adhesive emulsion Plextol B500 (Rohm & Haas) introduced by Mehra (1975, 1972). Lascaux adhesives HV-360 and HV-498, two other acrylic emulsions are also commonly found in researches on lining adhesives (Duffy 1989; Abdel 2000). Among the poly(vinyl acetate) adhesive group, Mowilith DMC2 and Mowilith DM5 are often mentioned in conservation for painting varnishing as well as fillers of missing parts or for the repair of tears (Doménech-Carbó 2009).

The introduction of new adhesives in painting conservation follows an improvement in the handling properties and application of these adhesives. The use of heat during lining was shown to be detrimental to the painting as it will soften the paint film, and together with the applied load can irreversibly flatten impasto (Hackney, 2012; Hedley, 1991). The heat needed to apply the natural adhesives is decreased with synthetic adhesives such as Beva371. Cold-lining, lining with no use of heat, was also introduced by Mehra with the use of Plextol B500 (Mehra, 1975). New tools for lining such as low suction tables or vacuum tables also appeared from the 80's. They allow a better control over the adhesive penetration and thus a gentler approach to lining.

New options for lining are now commonly found in conservation workshops and have replaced the old techniques. Synthetic adhesives are more often used in lining but have not totally

replaced natural adhesives. The list of adhesives given above is not exhaustive. The variety of adhesives available reflects the singularities found in paintings structure and materials. Hence, depending on the type of repair (tear mending, tear repair, strip lining, consolidation by impregnation), the adhesives employed differ (Ackroyd 2002).

The range of adhesives currently available also highlights the difficulty in conservation to find treatments with optimal properties in terms of consolidation, stability, removability and handling properties. As noted by Ackroyd (2002), “these adhesives exhibit diverse properties and there appears to be little consensus (among conservators) as to those preferred: 'stiff', 'flexible', 'strong', 'not too strong', 'minimal', 'resembling the original' and 'good' were typical comments”. With the research by Ackroyd (2002), Michalski (1991), Hedley (1991) and Young (2001; 1999), a better understanding of the effects of lining was gained and with it the development of rational procedures for testing appropriate consolidation materials and techniques. The quantification of the mechanical stresses taking place in paintings benefited conservation practices. Influence of lining on mechanical properties of paintings’ canvas

Several studies have attempted to quantify the reinforcement and/or the mechanical protection provided by linings. These assessments were carried out in different ways from studying each painting component individually (Erhardt, 1994; Mecklenburg, 2007) to the quantification of the physical properties of entire objects (Young, 1999). For example, the performance of a range of PVA, such as Mowilith® DM912 and Beva® 371 (film), and acrylic adhesives, such as Paraloid® B72, Rhoplex® and Plextol®, was measured in terms of mechanical (elongation at break), physical (adhesion on flaking paint, appearance) and chemical properties (colour change upon ageing) on free-films (Horton-James 1991). The assessment of the individual materials bulk properties should however not be solely used to predict the properties of the overall multi-layered structure. First, the parameters influencing the mechanical response of layered structure will be discussed. The mechanical response of some example of linings to RH variations will be presented.

1.1.4.1.1 The impact of adhesive penetration and adhesive power on the response of linings to RH variations

The application of an adhesive onto a canvas modifies the mechanical performance of the adhesive as well as the canvas. Two main factors are behind this:

- The degree penetration of the adhesive into the canvas (Buzzegoli, 2006; Van de Vorst, 1997). This depends on the composition of adhesive, the mode of application and lining technique used, the temperature or the pressure applied during the lining process and the adhesive viscosity (D'haenens, 2013)

- The adhesion, chemical or physical, between canvas and adhesive (Cognard, 2004; Darque-Ceretti, 2003)

Penetration

First, the degree of penetration of the adhesive has an impact on the mechanical response to RH of the canvas. This is mentioned by Young (2001) for the vinyl acetate adhesive Beva371, an adhesive considered as not hygroscopic. Applied as gel lining adhesive on linen, the resulting lining (i.e. canvas with adhesive) would surprisingly showed the highest response at high RH compared to all the linings tested including other canvas materials and adhesives (wax-resin and glue-paste). However, in the same study, when Beva371 was used with polyester sailcloth, the lining obtained was almost non-responsive to RH variations. This combination provided the highest protection and stable support to changes in RH. Similar observations were made by Krarup Andersen (2013) for wax-resin used for lining works. She highlighted the discrepancy in the mechanical response measured for a film of wax-resin and for a linen canvas treated with wax-resin. Wax-resin (highly hydrophobic material) alone is not mechanically responsive to RH. However, when applied on a linen canvas, a higher shrinkage at RH level (>60%RH) was observed for the treated canvas. Shrinkage in canvas is caused by the swelling of fibres caused by moisture sorption. This leads, in tightly woven or spun threads, to the consecutive swelling of the threads, hence an increase in the diameter of the threads, causing the crimp of the threads (measure

of waviness of the threads) to increase and the fabric to shrink (Collins, 1939; Gray, 1971). This will be shown in more detail in Chapter 3.

Following these observations, Andersen (2013, p.5) suggests that the high RH shrinkage in wax-resin linings might result from the fact that the fibres of the canvases are embedded in wax-resin. The penetration of water molecules into the canvas fibres is not hindered by the surrounding wax-resin and the effect of the swelling fibres is, then, enhanced by the wax-resin as there is no free space around each swelling fibre (Figure 1.7). When there is a certain amount of free space around swelling fibres and yarns in a fabric, the swelling of fibres will occur at higher RH levels and be less pronounced (Bilson, 1996).

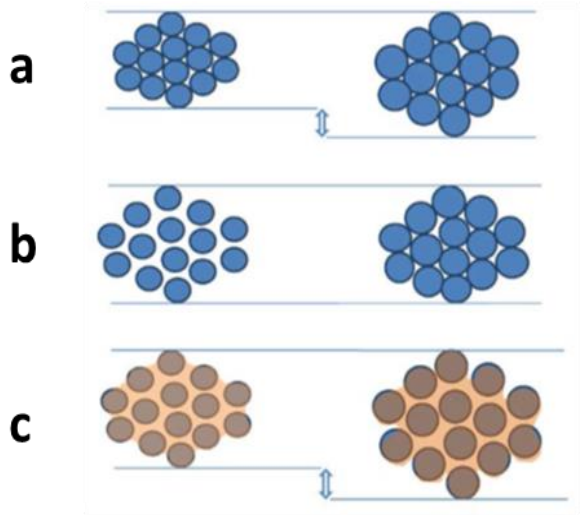

Figure 1.7: Schematic cross sections of the swelling of fibres in a non-impregnated thread and a wax-resin impregnated thread (adapted from (Krarup Andersen, 2013)). In (a), thread with no space between fibres. Swelling of the fibres caused the overall swelling of the thread. In (b), thread with space between fibres. The swelling fibres are not causing the thread to swell due to the space between fibres. In (c), wax-resin impregnated thread. The space between fibres is filled up with wax resulting in an immediate swelling of the thread.

These results highlight the strong influence of the application method (spray, from film, spatula) and lining procedure onto the overall mechanical properties of linings and the original canvas. This was expected as these parameters might lead to differences in adhesive penetration into the canvas. Second, adhesive penetration was also showed to have an impact on linings' mechanical properties such as stiffness of a lining. Young (2001) showed that a wax-resin

impregnated canvas provided the painting with a stiffer support than a canvas treated with Beva371, an adhesive with low penetration.

Adhesion

In terms of adhesion, most of the adhesives used in painting conservation, mainly for lining works, are tested for their adhesive strength (Berger, 1972; Bianco, 2015; Roche, 2003). Interestingly, adhesives often selected as consolidants are generally tested to see if they have sufficient adhesive strength (Phenix 1984; Scicolone 2011; Bianco 2015). Their cohesive strength, however, is almost never assessed possibly because of the misconception that this property is irrelevant in assessing the adhesion between two canvases. Cohesive strength, however, has an important role to play in the evaluation of the performance of the adhesives. Hence, Young and Ackroyd (2001) tested paintings for which the tacking edges had been removed. They notice that for the 4 different lining investigated (a glue-paste, a wax-resin and a Beva 371 linings with linen and a Beva 371 lining with polyester sailcloth), the movement of the glue seemed to reduce the transfer of the stress from the painting to the lining canvas. The adhesive and the adjacent weave formed a relatively flexible layer. Consequently, high shear strains must be occurring at the interfaces with the adhesive.

1.1.4.1.2 Response of lined paintings to relative humidity (RH).

Few adhesives have been assessed after being applied on canvas. Those investigated include traditional adhesives (i.e. wax-resin and glue paste) and Beva371. Mecklenburg and Hedley were among the first who noticed and quantitatively assessed the strong impact of RH on paintings lined with traditional adhesives such as beeswax and glue paste (Hedley, 1988; Mecklenburg, 1994; Mecklenburg, 2006). Beeswax is known for its hydrophobicity. It was found that the impregnation of the canvas with beeswax decreases the humidity response of a sample exposed to RH cycling (Hackney, 1981; Hedley, 1975; Young, 2001). Whereas, an old/glue paste lining is reformed by exposure to RH. Increased values of tension were measured for this sample in dry conditions (Hedley, 1988). This was later confirmed by Young (2001) who used biaxial tensile testing and RH variations from 5%RH to 85%RH. At low RH, glue-paste forms a brittle

material prone to failure. Its response to RH is also sudden and rapid. It is characterised, upon an increase in RH, by a strong decrease in tension higher than the sole creep of the linen which would have been measured at constant RH. More recently, synthetic adhesives such as the ethylene vinyl acetate-based adhesive Beva 371, the acrylics resins Paraloid B72 and B67, the cellulose ether Klucel and the polyoxazoline adhesive Aquazol were developed for conservation (Ackroyd, 2002; Barros D'Sa, 2012). Beva371, a poly(ethylene-vinyl acetate) adhesive was introduced by Berger to replace wax-resin adhesives. Mecklenburg (2012) noticed that Beva 371 alongside with two acrylic adhesives (Paraloid B72 and Paraloid B67) were those, among all the adhesives investigated, whose properties are less responsive to moisture. Their cohesive strength and stiffness were still lower than those developed by natural glues.

The canvas also plays an important role in the response of easel painting to moisture. The influence of the material chosen for the lining canvas and the glue on the overall response of the lining to RH variations was studied by Young (2012). The lower mechanical response to RH was measured for the lining using synthetic polyester sailcloth with Beva371. The protection against RH provided was, however, lower than the one obtained from a wax-resin/linen lining (Young, 2001). It was also assumed that sailcloth lining with Beva371 offers a rigid and thus protective support to a painting at ambient humidity and below but may be less effective in more humid environments at which the canvas shrinkage leads to an increase in painting tension. The response of the adhesives at different RH gives a measure of the importance of moisture levels in the evaluation of the performance of the consolidants. They also inform the limits of the reinforcement provided. However, the conclusions drawn in the short-term might not apply in the long-term. Following the results obtained by Hedley (1988) and Mecklenburg (1994, 2001), Michalski and Dale Hartin (1996) included the assessment of the long-term behaviour of lined model oil paintings (with wax-resin, Beva 371, acryloid B72 size canvas lining adhesives and size and linen canvas and polyester sailcloth) by performing stress relaxation tests over a few years. They showed that the reinforcement measured for the wax-resin lining is not maintained in the long-term. After 100 days the wax-resin lined painting had reached a lower tension than the

tension the painting would have reached if not-lined. These results seem to indicate that the painting is slipping at the adhesive bond. When drops in RH were applied from 50%RH to 12%RH, an increase in tension was noted for the model painting but a loss of tension in the wax-resin lined painting was observed. At that stage, the wax-resin lining could no longer maintain its role as support.

These studies provided initial assessments of the mechanical behaviour of lined paintings. General mechanisms of failure in the reinforcement provided by lining/adhesives arise mainly from the mechanical response of these materials to moisture. Their long-term stability should however not be neglected. Moreover, the few adhesives investigated within the lining context highlight the need for further mechanical assessment of lining adhesives in combination with the lining canvas and canvas they could be applied with and on respectively. Surprisingly, few studies have investigated the tensions induced within the fabric by the treatment process (Young, 2001) despite the stresses that may be experienced. This is due to technical limitations, such as the access in a conservation studio to a biaxial tester capable of monitoring changes in stresses or elongation experienced by the painting during the treatment process.

1.1.5 Limitations of traditional consolidants and lining practice

From the 1970s onwards, an increased number of studies were published illustrating the damaging effects of the lining (Cecil K. Andersen, Mecklenburg, Scharff, & Wadum, 2018; Bomford & Staniforth, 1981a; S. Hackney et al., 2012; Stephen Hackney, 2004a; Joyce Hill Stoner & Rushfield, 2013). The damaging effects of traditional lining procedures resulted partly from the heat and pressure used to apply the adhesives and the lining canvas which lead to flattening and the loss of important features of the painting's surface topology. These studies also highlighted the darkening of paint layers resulting from the use of wax-resin which readily impregnates into the structural openings of the painting: both lining and original canvas, ground layers and paint layers (Hackney, 2012).

From the 1970s, the rapid development of new synthetic adhesives and lining techniques in painting conservation was not supported by comprehensive analyses and understanding of these new material behaviours, including advantages as well as drawbacks. Hansen (1991) and Vinçotte (2019), for example, raised the issue of the drying time and solvent retention on the mechanical performance when testing cast films of polyvinyl acetate and Acryloid B72 (i.e. Paraloid B72). A survey carried out among practitioners by Ackroyd (2002) also highlighted a lack of assessment of these adhesives including the issue of additional weight on the stretcher.

The various protocols used for the assessment of adhesives for lining and consolidants stress the difficulty in comparing the scattered studies carried out over a few decades. Some observations and points made in those studies on the impact of ageing should, however, be recalled for their relevance, as described below.

1.1.5.1 Reversibility

Natural resin and glues used in lining works are usually removed using solvents which will dissolve them or ease their removal by mechanical action. However, these glues are never completely removed especially when the canvass has been impregnated (Bomford, 1981; Landi, 2012; Timár-Balázsy & Eastop, 1998). Several solutions have been developed and new ones are still under development in an urgent need to prevent the loss of strength of the canvas resulting from the embrittlement, the cracks the rigidity appearing in the glue paste for example. Recently the use of enzymes (Ahmed, 2012) and hydrogels (Baglioni, 2015; Pizzorusso, 2012) have been successfully employed to remove animal glue from linen and silk fabrics and the synthetic adhesive Mowilith DM5 from a linen canvas, respectively. Regarding synthetic adhesives, a loss in solubility after light ageing has been observed for Beva371 (McGlinchey, 2011). The study of acrylic/methacrylic ageing is rendered particularly difficult because of the variety of polymeric arrangements existing and additives within these materials. Generally, with ageing methacrylates are prone to depolymerization and may thus become more soluble, whereas acrylates are prone to cross-linking leading to losses in solubility (Feller, 1981; Grassie, 2008). The solubility of poly(vinyl acetate) polymer depends on the size of the chain. But generally, no changes in

solubility are observed with ageing (Reuber, 2008). Finally, Poly(vinyl alcohol) polymers are prone to cross-linking at temperatures higher than 100°C or under UV light (Horie, 2010). The thickness of the layer of adhesive as well as the material of the original and lining canvases also have an impact on the removability of the lining (Bianco, 2015) and colour change caused by ageing (Chevalier-Menu, 2010). The solvent and dilution employed in combination with the adhesives might also affect their stability (Mecklenburg, 2012).

1.1.5.2 Photo-degradation and colour change

Synthetic adhesives are also prone to photodegradation. For Beva371, the trigger of the degradation was identified as the ketone resin tackifier present in the original formulation (Ploeger, 2014). This reaction leads to loss of tensile strength and elongation (Abdel-Kareem, 2005). Photodegradation is also known to cause change in polymers. Yellowing of the adhesive has been also observed for Beva371 (McGlinchey, 2011) and the PVA adhesive Mowilith DMC2 shows discolouration (Down, 2015; McGlinchey, 2011). Moreover, a study comparing about fifty synthetic adhesives shows that PVAC adhesives yellowed approximately twice as quickly as the acrylic adhesives such as Paraloid (also called Acryloid) B72, B82 and F10 or Plextol B500 (Down, 2015).

From these studies, it is thus clear that there is still a large gap in the understanding of adhesive behaviour, stability and reversibility in relation to canvas supports (Reuber, 2008). Also, none of the available adhesives currently in use for canvas conservation seems to be stable enough to be employed routinely on paintings. Although, the criteria established for the formulation and testing of consolidants for easel painting are well-known (these will be given later in Chapter 4) and are recalled by Berger (1970), Mehra (1975) and Hedley (1993b), among others, the need for a material tailored for easel painting structural consolidation is clear. This was recently highlighted during the Conserving canvas symposium at Yale university ("Conserving canvass symposium," 2019) during which the question of whether to deline lined paintings was raised up partly because no solutions currently exist to provide a support to the delined painting without relining it. The need for more research into new materials for modern and contemporary was also

highlighted at the Conservation Issues of Modern and Contemporary Art (CIMCA) Meeting Museum of Modern Art (New York, June 2008)[1].

1.1.6 Ethics driven decision making in the choice of materials for conservation

The current trend for less invasive conservation materials and the continuous development and artistic exploration of artist in terms of technique and materials urge for the development of consolidation materials and techniques more compatible to the painting and respectful to the artist intent. This is particularly important in the context of structural conservation of painting as lining, a technique highly invasive, has been used for centuries as a routine procedure but as proven to put the painting at high risk of irreversible damages. Furthermore, replacing the support with a more rigid structure is also a major aesthetic intervention, changing the nature of the stretched canvas. As such, on top of the question around the risks associated with lining, the question of whether modern and contemporary paintings should be lined when necessary is also raised. This is because, as observed by (Pavic, (2014) in a conservation of Cakes by Vanista (1955), these recent paintings present a different making process, thus structure, than traditional oil paintings. The artists of that period experienced much more and did not waist time with proper painting preparation. Their artistic intent is also shifted from the one of traditional old painting. As such and as pointed out by Pavic (2014), it is not prudent to always use the same methodology and technology on old and modern oil paintings because their intent and making is different. If traditional consolidation can often be done on old and/or traditionally made paintings (for which the lining has often be applied earlier in their life), for modern and contemporary paintings, lining process can be perceived as an archaic and intrusive technique. Using it on a contemporary object might even be perceived as an anachronism. With modern and contemporary paintings, more than ever, new solutions for consolidation of the canvas are needed. Ethical decision-making in the treatments to be used for canvas consolidation have to encompass the preservation of the physical integrity of the painting (its shape, appearance), its meaning, function, the artist intent, its history (e.g. Auction stamps on the back of the paintings) and its materials ("Conservation Issues of

[1] https://www.getty.edu/conservation/our_projects/science/modpaints/CIMCA_meeting_jun08.pdf

Modern and Contemporary Art (CIMCA) Meeting," 2008; Gale, Lake, Sterrett, Learner, & Levin, 2009). All these criteria cannot unfortunately all be met and often compete against each other. The criteria that matter are often chosen by the conservators sometimes in collaboration with the artist and as such can strongly vary depending on the object as well as the conservator(s) in charge of the conservation.

1.2 Nanocellulose: a promising material for canvas consolidation?

New developments in nanomaterials might pave the way to promising solutions for conservation and more specifically to this project, painting conservation. Of particular interest is the development of nano-sized particles of cellulose whose promising mechanical properties have raised since 20 years an increasing interest for nanocomposites formulation (Lagerwall, 2014; Lin, 2012; Nair, 2015). Nanocellulose also offers a workable alternative to petroleum-based polymers as it is chemical similar to the canvas material (i.e. cellulose-based natural fibres). Studies for their application in conservation remain scarce despite the high potential of nanomaterials already outlined through studies on cleaning paintings (Baglioni, 2006; Pizzorusso, 2012). The decision made for this research project to develop and assess nanocellulose consolidants for painting canvas structural conservation (i.e. canvas consolidation) was partly driven by the aim of avoiding lining procedure and materials and the risks associated to their use (cf. 1.1).

1.2.1 What is nanocellulose?

Cellulose is a polysaccharide and one of the most common organic polymers on Earth. It can be found in the wall cells of plants (hemp, cotton, wood), algae (e.g. Valonia) (de Souza Lima, 2002), and it can also be produced as an exo-polysaccharide by specific species of bacteria (eg. Acetobacter xylinum) (Beltrame, 1992). The term *Nanocellulose* defines particles of cellulose generally 1-10 µm in length and 1-100 nm in diameter (Figure 1.8) (Lin, 2012). They are obtained by mechanical or bacterial breakdown of wood or plants and natural fibres (Kramer, 2006; Nakagaito, 2005; Savadekar, 2012). The process of extraction of the cellulose from vegetables is

highly energy demanding (Spence, 2011). Chemical (Boldizar, 1987) and enzymatic (Pääkkö, 2007) pretreatments of the pulps have thus been developed to ease the manufacturing of nanocellulose and create more energy efficient processes.

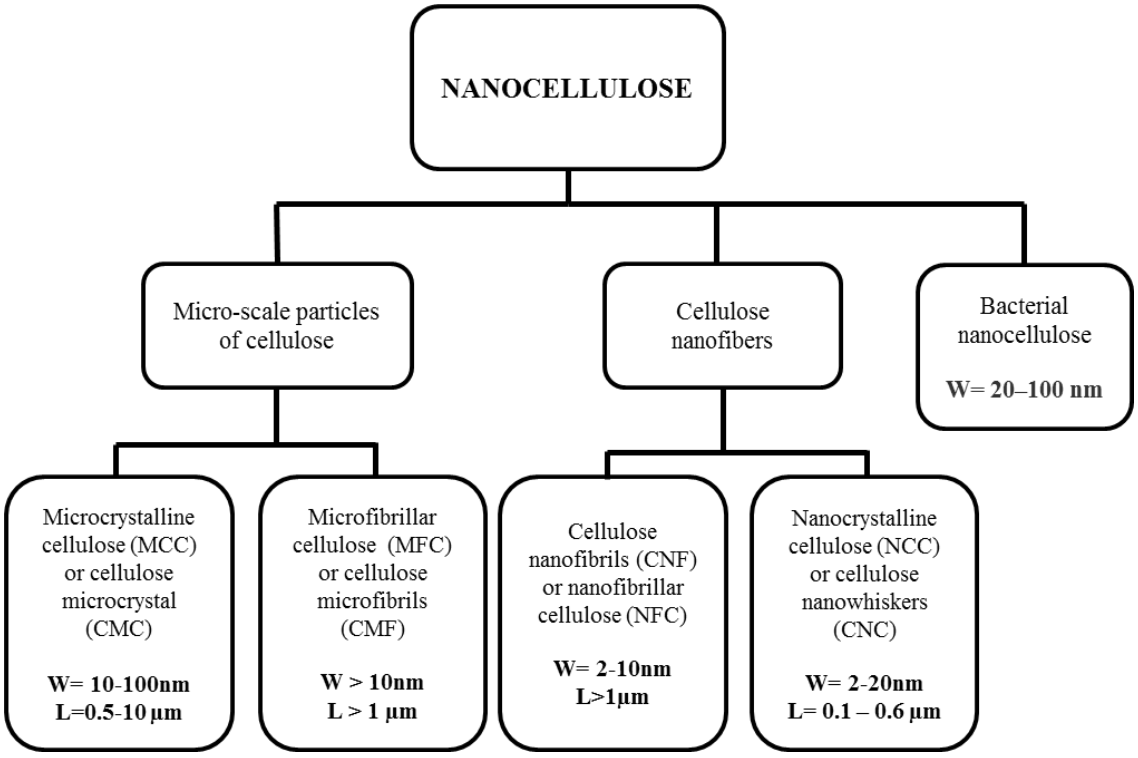

Figure 1.8: Different hierarchical levels of wood-based nanocellulose (adapted from proposed new TAPPI Standard WI 3021) adapted from Osong 2015 [W= Width, L=Length]

Depending on the cellulosic sources and applied treatments, particles of different degrees of crystallinity, crystal structure, morphology, surface chemistry and aspect ratio (see Figure 1.8) and thus with a range of mechanical, chemical and optical properties can be obtained (Habibi, 2010). The term nanocellulose defined fibril particles whose diameter or width is comprised between 1 and 100 nm. However, recently Osong et al (2016) pointed out in a review on nanocellulose that "there is still a lot of confusion regarding the terminology and nomenclature of nanocellulose". Therefore standards have been implemented (TAPPI standards established by

university labs and industries working on pulps and paper)[2]. It is however still not rare to see different terms applying to nanoparticles of cellulose of the same size. These have been reported in Figure 1.8.

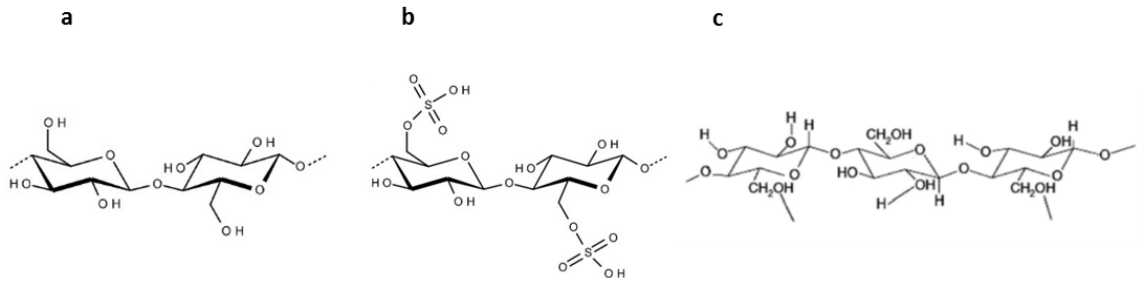

Figure 1.9: Chemical structures of cellulose nanofibrils CNF (also called microcellulose fibrils MCF) (a), cellulose nanocrystals CNC (or microcellulose crystals MCC) (b) and bacterial nanocellulose (c). CNF and CNC and bacterial nanocellulose show the polysaccharide structure of cellulose. The differences in chemical structure between the 3 nanocellulose result from the mode of extraction used to obtained them. CNF and bacterial cellulose have the same chemical structure, similar to cellulose, whereas CNC present sulfate groups (i.e. $SO4^{2-}$) which result from the sulphuric acid treatment used to remove the amorphous phase to isolate the crystalline phase of cellulose fibrils.

Microfibrillar cellulose (MCF) and Nanofibrillar cellulose (CNF) cellulose usually refer to fibres composed of crystalline and amorphous regions (see chemical structure Figure 1.9a). The microfibrils or microbundles of fibrils extracted have sizes ranging from 10 to 100nm in diameter and are µm scale in length. They are obtained using a top-down deconstruction approach based on the mechanical grinding of cellulose sources such as wood or plants. However, the cellulose fibres naturally tend to flocculate during the process. This can cause problems during homogenization treatment (Herrick, 1983) and is the step responsible for this process being highly energy-intensive. Pretreatment of cellulose by position-selective modifications on cellulose fibres such as low degrees of enzymatic hydrolysis, carboxymethylation, acetylation and oxidation is

[2] http://www.tappinano.org/resources/standards/ (Official website of the International Nanotechnology Division)

also common as it reduces the amount of mechanical energy required to liberate the microfibrils (Isogai, 2013).

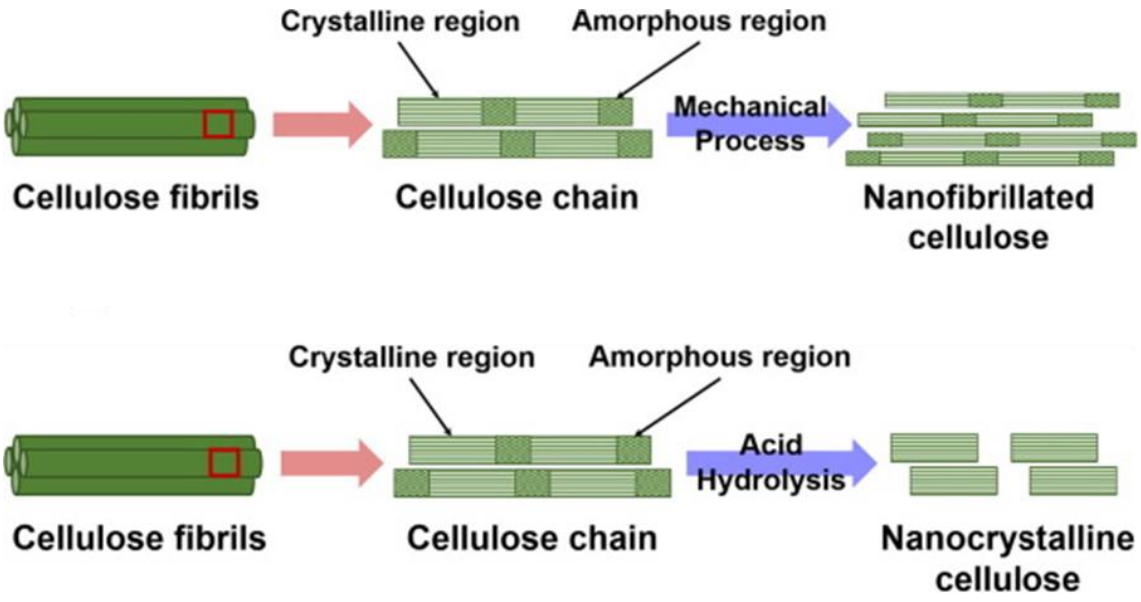

Figure 1.10: Graphic representation of the nature of the processes of extraction of nanofibrillated cellulose (CNF) and nanocrystalline cellulose (CNC) from cellulose fibrils (taken from Phanthong (2018). CNF is made of both amorphous and crystalline phases and obtained from the mechanical processing of plants. CNC is only made of the crystalline phase of the cellulose chain which is extracted by acid hydrolysis of the cellulose from plants.

Microcrystalline cellulose (CMC) and Nanocrystalline cellulose (CNC) are highly crystalline particles. They are obtained by the removal of the amorphous phase of cellulose fibrils through acid hydrolysis (Mukherjee, 1953) (Figure 1.10). This process, which often involves the use of sulphuric acid, is responsible for the sulphonate groups seen on the units of the cellulose chain (see Figure 1.9b). At the same nanocellulose concentration, CNFs led to higher strength and modulus than did CNCs due to CNFs' larger aspect ratio and fibre entanglement, but lower strain-at-failure because of their relatively large fibre agglomerates (Xu, 2013). Bacterial nanocellulose differs from CNF, CNC, CNF or CMC. It is produced by different bacteria such as *Gluconacteobacter xylinus,* which is by far the most productive and well-studied (Sheykhnazari, 2011). The cellulose produced by these organisms is pure (i.e. free of hemicellulose or lignin commonly found in wood and plants and known to weaken paper and accelerate its degradation

when not removed from the pulp ("New ways to remove lignin," 1986)) and exhibits a higher crystallinity, degree of polymerisation (DP) and mechanical strength (Klemm, 2009).

1.2.2 Nanocellulose properties: Chemical tunability, barrier and mechanical properties.

Tunable hydrophilic material

Due to their hydrophilic behaviour and the abundance of hydroxyl groups on the surface, nanocellulose particles tend to agglomerate. This phenomenon is particularly pronounced for smaller particles because of their higher specific area, which may limit the potential for mechanical reinforcement.

To overcome this phenomenon, several methods for the functionalisation of nanocellulose particles have been developed. The large number of routes of functionalization available (Lin, 2014; Missoum, 2013; Osong, 2016) account for the high tunability of these particles. Chemical modification of the surface is also a key factor to increase their compatibility and avoid agglomeration in different matrices or solvents. These procedures are, however, highly time-consuming (Dufresne, 2013).

Enhanced mechanical properties

The high tensile stiffness and strength of nanocellulose is also a key factor for choosing nanocellulose particles as consolidants which could be applied in low concentration for canvas consolidation. With high Young's modulus around 130GPa similar to Kevlar in relation with comparatively very low density around 1.5 $g.cm^{-3}$, nanocellulose is an ideal compound for the processing of reinforced polymer composite. Particles size is a key factor in particle properties. Studies have been carried out to measure the tensile modulus of microfibrils and crystalline CNCs. The modulus values registered are on average 30% higher for the CNCs than for MFCs (Lavoine, 2014a). Compared to glass fibres, another compound used to reinforce polymers, nanocellulose fibres also present higher specific Young's modulus, described as the ratio between the Young's modulus and the density of nanocellulose. For the same amount added to a material, nanocellulose

fibres bring higher reinforcement strength than glass fibres (Lee, 2014). These features suggest a promising future for these nano-sized particles.

Indeed, nanocellulose microfibrils and nanocrystals have already been used to strengthen other materials such as concrete, plastics and polymeric structures (Lee, 2014). These developments are relatively new but have given rise to a large range of nanocomposites (Kalia, 2011; Spence, 2011). For example, injectable polysaccharide hydrogels have been reinforced with aldehyde-functionalised-CNCs (Yang, 2013). The hydrogels obtained show higher elasticity, are more dimensionally stable and capable of facilitating higher nanoparticle loadings compared to unmodified CNCs. No loss in mechanical strength was measured. CNCs with specific surface modification can also act both as filler and crosslinker to reinforce hydrogel systems (Barros, 2015). CNCs have been used for example to reinforce polyacrylamide hydrogels or poly(acrylic acid) hydrogels. However, a 2014 review (Lee, 2014) points out that only 20% of the nanocomposite found in the literature show higher performance than nanocomposite made out of PLLA (poly(L-lactic acid)) another typical commercially available bulk polymer made from renewable resources. Higher performance for cellulose-reinforced polymer composites could however be obtained with nanocellulose loading greater than 30 vol%. Additionally, the thermal stability of a range of polymers has also been shown to increase by the addition of a small percentage of cellulose nanoparticles (typically around 3-5%w/w) (Barros, 2015; Kiziltas, 2011; Thummanukitcharoen, 2011).

The impressive mechanical properties of nanocellulose, its tunability and the low permeability of the nanocellulose-based film to gases might be of interest when considering application in conservation as surface treatment or as filler for existing adhesives (nanocomposite). Nanocellulose could be used as consolidant and barrier to the gases which otherwise might trigger the degradation of cellulosic materials such as paper or textiles.

Toxicity

Due to the small size of nanocellulose fibrils, questions regarding their toxicity are now often raised (Bahadar, 2016; Deloid, 2019; Harper, 2016; Sukhanova, 2018). Nanocellulose can now be found in a wide variety of products such as cosmetics, drugs, food, polymer or composite, concrete and adhesives. Studies about the toxicity of nanocellulose can be found in specific cases such as its introduction in bioscience for drugs delivery (Lin, 2014). Low inhalation and oral toxicity, as well as dermal irritation, have been measured for CNCs and CNFs (Harper, 2016; Jackson, 2011; Roman, 2015). In 2016, a review on the current state of knowledge on nanocellulose also indicates that nanocellulose, when investigated under realistic doses and exposure scenarios has limited associated toxic potential (Endes, 2016). The authors point out that at the time of writing only certain forms of nanocellulose with specific physical characteristics (length superior to 5µm, freeze-dried and re-suspended powder) can be associated with more hazardous biological behaviour . More recent studies, which evaluate the biological and predicted the environmental risks associated with the increasing use of nanocellulose materials for research and in the industry, also identified low risks of this material (Stoudmann, 2019).

1.2.3 Nanocellulose in textile finishing or cellulose substrate coating.

The use of CNF and CNC particles for textile finishing and/or the improvement of natural fibres properties has greatly evolved in the last decade due to the increasing demand for low-cost and renewable materials. Nanocellulose particles have been used for dyeing purposes (Nechyporchuk, 2017), for the fabrication of conductive materials (Li, 2017) as well as for their ability to enhance the mechanical properties of textiles (Favier, 1995; Hebeish, 2018; Silvério, 2013). Owing to their high tenability, they also offer an alternative for the surface modification of plants fibres to the common chemical treatments in use, such as mercerization, acetylation, etc.

1.2.3.1 Modification of natural fibres using nanocellulose

As reported by Kalia (2013), the modification of nanocellulose fibres can be done by surface modification of plant fibres by pretreatment or coating of the fibres with bacterial nanocellulose, by enzymatic or fungal treatment. This requires that the plant fibres are used as substrates for bacterial fermentation (Pommet 2008). As such, they need specific temperature or treatment procedure (e.g. agitator) which would not be possible for the purpose of canvas consolidation. In a study by Dai (2013), hemp fibres were modified with nanocellulose produced from hemp by dipping the fibres in the nanocellulose dispersion. The modification was however made possible by the pretreatment of the fibres by DodecylTrimethylAmmonium Bromide (DTAB) a cationic polymer possibly used to enhance the adhesion of the nanocellulose over the hemp fibres. These studies thus raised the question of the application of such modifications in conservation where soaking of the canvas is unthinkable and where the use of additional non-cellulosic substances might be discarded due to their possible instability, despite the better deposition achieved.

1.2.3.2 Use of nanocellulose in textile finishing

Several techniques both chemical and physical are currently in use for the finishing of textiles. These include plasma treatment (physical) and polymer grafting (chemical). This wide range of techniques enable the fine-tuning of the properties of textiles by modifying the fabric response to moisture, mechanical properties, colour, conductivity, inflammability. These techniques are however hardly proposed for conservation purposes due to their highly intrusive nature (e.g. low-pressure chamber for plasma treatment, immersion in chemical baths for polymer grafting).

Studies investigating the application of nanocellulose directly onto textiles and their impact on the fabric properties are scarce. Those which can be found apply to the textile industry. The tests carried out thus aim to assess the treated material in terms of wearability through the assessment of the ability of the nanocellulose to enable a better moisture management (water

transport, retention). The application to a wool fabric of a “cotton powder liquor”, consisting in a dispersion in MCC, was studied by Guan (Guan, 2008). The fabric was treated by immersion. The results indicate that the hydrophilicity of wool fibres increased after the treatment by cotton fibrils while wrinkle recovery remained unchanged after treatment. More recently, El Messiry (2015) also investigated the use of MCC which had been sprayed onto polyester and polyester/cotton blends fabrics. He also noted the increased moisture response of the treated fabrics. More recently, nanocellulose was also applied onto cotton fabrics by spraying for dying purposes. An increase in printing quality was reached after the application of a preparatory coating of CNF (Nechyporchuk, 2017).

1.2.3.3 Use of nanocellulose for the mechanical reinforcement of cellulosic substrates.

The industrial sector do not appear to have investigated the use of nanocellulose particles for the reinforcement of textiles. Such investigations were, however, found for the development of renewable paper and cardboard coating. MCF, CNF and CNC particles have been introduced in the paper industry in recent years. Used as a filler, cellulose nanoparticles have been shown to enhance the mechanical properties of filled paper. It is assumed that this enhancement is caused by a mechanism called mechanical percolation (Favier, 1995). Used as coating, the CNC, CNF or MFC coatings have not shown yet to significantly improve the bulk mechanical properties of paper or cardboard, regardless of the number of layers deposited. The techniques of coatings application commonly used (bar coating and size press processes) show to greatly weaken the paper stiffness from -36% to -30%, respectively, in comparison with a paper which would not have been through these processes (Lavoine 2011a). This is due to the large amount of water present in the nanocellulose dispersions (90%) which will modify the fibre network, and multiple drying steps. The reinforcement provided by the 5 MFC coats characterised by the increase in Young’s modulus is important in both machine direction (23%) and cross-section (41%) but is not sufficient to counterbalance the negative effect of the coating application process. The Young’s modulus values of the MFC-coated samples remain lower than the modulus of the base

paper. The same loss in mechanical performance was also observed for paper coated with CNC alone which again result from the bar coating process used (Rastogi, 2015). Slight worsening of other mechanical properties (elongation at break, breaking length, and tensile strength) was also measured in this study. This results from these successive wetting/drying cycles involving water. The surface properties of cardboard can, however, be strongly improved when coated with nanocellulose. The bending stiffness of a CNC-coated cardboard was increased by 900% for 8 CNC coatings (Gicquel, 2017). For MFC coated cardboard, an increase of 30% in bending stiffness and compressive strength was also measured (Lavoine, 2014b).

To improve the coating's flexibility and counterbalance the breakable network formed by the nanoparticles, nanocellulose is often combined a "plasticiser" or binder such PEG (polyethylene glycol) (Bardet, 2014). In another study (Lee, 2014), a composite of CNC, CMC (Sodium carboxymethyl cellulose) and cationic starch was used as a paper sizing. The authors note that the surface-sized paper with only 0.3% in CNC exhibited increases of 6, 9, 23, and 4% in the tensile index, tear index, folding endurance, and burst index, respectively, as compared to paper sized by NCC free starch-based composite suspensions.

The MFC/NFC films and coatings also offer a poor resistance against water attributed to intrinsic hydrophilic nature of cellulose (Lavoine, 2014b). They have, therefore, not been exploited at large scale for packaging applications so far. To reduce water adsorption, the nanocellulose is usually blended with water-insensitive biopolymers such as polyactic acid (PLA) and Polyhydroxyalkanoates (PHAs) (Rastogi, 2016).

The adhesion between the nanocellulose coatings and the paper substrate is little investigated in studies on paper coatings. This has gained more interest in the field of paper-making for which the cohesion of nanocellulose/cellulose fibres or additive/cellulose fibres blends is important to evaluate and quantify since it has an impact on the macro-mechanical properties of the composite papers (Gardner 2008, Wagberg 2007).

1.2.4 Nanocellulose and conservation

Despite its success in industrial applications, nanocellulose struggled to gain widespread acknowledgment in conservation because of the recent introduction of nanocellulose in the industry and . Nanocellulose might present great potential to enhance and/or modify the properties of various polymers used as glues or consolidants in conservation when mixed as a filler. Up to now, several commercial PVAs, poly(vinyl alcohol) and acrylics non specifically designed for conservation purposes, have already been successfully studied using nanocellulose as filler. Microcrystalline cellulose (MCC) was used for example to reinforce poly(vinyl alcohol) (Cheng, 2009; Li, 2011) For a specific ratio of MCC/polymeric matrix, the nanocomposite showed an improved thermal stability, and increased stiffness, tensile modulus and tensile strength up to, respectively, 69%, 60% and 28%.

However, these studies developed for industrial applications do not integrate the canvas support response to the adhesive application. Since 2014, Cataldi (2014; 2015) has thermo-mechanically characterised well-known adhesives used in conservation: Paraloid B72 and Aquazol 200 and 500, and used MCC as filler. The results published separately show an improvement in the adhesive properties attested by lower responses to environmental changes. The studies also stress the influence of the filler loading and the %RH on adhesives mechanical properties, parameters whose importance have already been pointed out in studies on nanocellulose. Indeed, these first studies despite showing the properties transferability of very specific nanocomposite onto canvas, do not bring much more answers on the stability or reversibility of these compounds. These data are however more than necessary in conservation to prove the validity of the treatment.

Moreover, in the studies cited previously, nanocellulose is used as an additive and not as a pure material. While the introduction of nanocellulose-only treatments in painting conservation has yet not been reported, it has already been reported several times for paper conservation in the literature. Notably the works of Pereira (2016), Dreyfus-Deseigne (2017). Recently, Volkel (2017) also discusses the applicability and stability of bacterial and CNF suspensions, also with

regard to their mode of application and long-term performance. A new research pathway where nanocellulose would be used alone on painting canvas or more generally on textile might be of interest, firstly, because of the suitability of nanocellulose properties with respect to the needs and requirements in canvas conservation regarding reinforcement, no visual change and compatibility. Secondly, because of the known thermochemical instability (Down, 2015) of most polymeric materials, it might be prudent to avoid their use in any restoration/conservation works. The same considerations apply to lining regarded as a heavy-treatment process by conservators. Nanocellulose was therefore introduced in this project as an alternative treatment for the consolidation of degraded and fragile painting canvases. However, the interaction of cellulose with the canvas is still too little known and should be also investigated in term of penetration, adhesion, removability and long-term stability.

Another question regarding the ethics of using this material chemically similar to the canvas substrate (cellulose on cellulose) is also raised with the use of nanocellulose for canvas consolidation. The risk that the material may not be detectable after its application is important and this risk goes against the principle of reversibility which holds in conservation (AIC Ethics and Standards Committee, 1977-1979). However, as Salvador Munos Viras observed, reversibility and minimal intervention are often impractical. This research on the developments of new materials for canvas conservation thus intends to move the discussion from reversibility which is still a major criterion of good conservation treatment to re-treatability (i.e. allowing future treatments). Because of the chemical compatibility of nanocellulose with the canvas substrate, this compound is expected to perform better than commonly-used canvas consolidants both in terms of mechanical, physical and long-term behaviour. Nanocellulose have interesting mechanical properties (cf. 1.2.3) suitable for consolidation and might as well degrade in a similar way to the canvas. A material or treatment will never be totally irreversible but it is important for conservators to be aware of the consequences of this irreversibility which led to the research presented in the successive chapters of this thesis.

1.3 Research Question, Aims & Objectives.

Whilst nanocellulose properties have been studied for several decades, the introduction of this material in conservation is currently at an early stage and its use is limited to paper conservation (Dreyfuss-Deseigne, 2017). A review of published literature has shown the potential of use of nanocellulose for the consolidation of painting canvases. This attempt is also driven by the need for alternatives to the current materials available in this field. Also, there are few references to studies were nanocellulose has been applied as a coating on fabrics made of natural fibres. This research aims to address this issue by answering the following question:

To which extent could nanocellulose materials be used for the structural reinforcement of modern painting canvases?

In order to answer the research question, the following set of objectives was established:

- Initially, study the baseline viscoelastic response of the individual layer of a painting to RH variations.
- Investigate the viscoelastic response to RH variations of traditional canvas consolidants and adhesives used in painting conservation.
- Evaluate the 3 different types of the nanocellulose-based consolidants, CNF, CCNF and CNC, on an artificially aged cotton canvas in terms of surface appearance and chemical, physical, mechanical properties.
- Verify the applicability and performance of the nanocellulose-based consolidants on naturally aged historical canvas and paintings.
- Explore further the hygroscopic response of the treated canvases by mapping the moisture distribution in real-time.

Each of the objectives will be answered in the results chapters which will address the main research question of this thesis.

This research project was carried out in the framework of the Nanorestart European project (Horizon 2020) in collaboration with 7 European institutions including universities, enterprises and private conservation studios.

2 Materials and Methods

2.1 Materials

2.1.1 Canvas

Modern unprimed and not painted cotton and linen (sized/unsized) canvases as well as a 19th century sized primed linen canvas were investigated. These canvases were selected as they are representative of the range of material that could be found in collections. The main focus was put on modern paintings and canvases as they are now considered challenging objects for conservators because of their non-conventional structure (e.g. absence of priming and paint layers directly applied onto the canvas). For that reason, lining is often non possible for this objects due to the invasive nature of the procedure. A cotton canvas was selected for most of the tests as it is a material little studied but largely found in collection of modern and contemporary paintings. Cotton fabrics also present different physical and mechanical properties than other natural fibres like linen and jute (also used for painting canvas) such as lower stiffness but higher elasticity (Reddy & Yang, 2005). The modern linen and cotton canvases were bought in art supplier shops as canvas samples from paintings of modern and contemporary paintings were not available in sufficient amount for testing at the time of the project. The cotton canvas used throughout the project is described below. Specifications of the other canvas samples used in this project are given in the Chapters/studies in which they have been used.

2.1.1.1 Cotton duck canvas

The investigated cotton canvas was a plain woven fabric of 341 ± 1 g/m2 purchased in Barna Art (Barcelona, Spain). It consists of 9 and 11 threads/cm in the warp and weft directions respectively. Each thread is made of 2 twisted yarns in both directions. This canvas was chosen for this study as it is representative of canvases used in modern and contemporary art. First, cotton is, next to linen, a material commonly used by modern and contemporary artists such as Munch (Sandbakken, 2012) or van Gogh (Van Tilborgh, 2012). However, whereas most studies on

painting structural consolidation and/or painting canvases have focused on linen canvas, cotton canvases are often neglected despite their lower chemical stability (Golden, 2013). Therefore, this study also gives the opportunity to bring more insights into the properties of canvases made of cotton. Second, the canvas was bought in an art supply shop and this suggests that this canvas is nowadays readily available to artists. Finally, this canvas was available in large quantity and presents regular weaving (as opposed to handwoven canvases) which was necessary to insure the repeatability of the measurements.

2.1.1.2 Washing and degradation protocols

Prior to the application of the consolidating treatment, the canvas was washed or degraded (Figure 2.1) following procedures which are given below. Washing the canvas prior to its use is sometimes used as a preliminary step before the preparation of the painting (Golden, 2015; Hamm, 1993); the degradation step instead was developed and used specifically for this research project in order to obtain a canvas which would mimic a highly degraded canvas.

The canvas was washed in 2 steps to eliminate additives commonly used in textile weaving processes: 1 hour at 60°C and 1 hour at 85°C. The canvas obtained following this procedure will be designated as ‘washed’ in the text.

Degradation of the canvas was also performed. Pieces of cotton canvas (10 cmx10 cm) were left under mild stirring in a 400 mL becher filled with hydrogen peroxide at 35%wt (200 mL) and sulfuric acid at 95-98% (10 mL) for 3 days at 40 °C (Nechyporchuk 2015). The resulting accelerated aged canvas had a pH of 6.5, a degree of polymerization of ca. 500, which corresponds to that of a heavily aged historical canvas (Oriola 2011). The guideline is, however, what had been measured on historical linen canvases. The cotton canvas obtained after degradation will be designated as ‘degraded cotton canvas’ in the text.

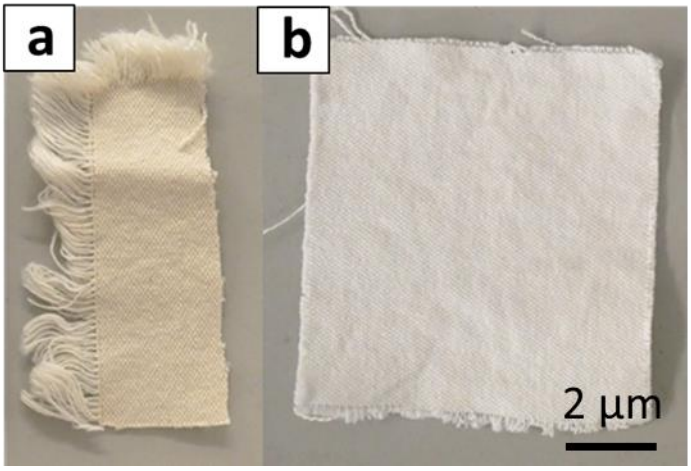

Figure 2.1: Cotton canvas before (a) and after degradation (b) showing the whitening of the canvas resulting from the use of hydrogen peroxide.

2.1.2 Newly developed consolidants

The 3 types of nanocellulose chosen in this study were selected for their potential highlighted previously (cf. 1.2.3.3) to reinforced a range of polymeric matrices including cellulose (i.e. paper). Two of these compounds, CNF and CCNF (carboymethylated CNF), were also readily available from Chalmers university (Gothenburg, Sweden), partner of the Nanorestart project. Their easy access also explains why that they were chosen for this project over other materials.

2.1.2.1 Nanocellulose-only treatments (solution 1)

Nanofibrillated cellulose (CNF) in the form of an aqueous suspension was kindly provided by Stora Enso AB (Sweden). The CNF was produced from softwood pulp (ca. 75% of pine and 25% of spruce, containing 85% of cellulose, 15% of hemicellulose, and traces of lignin, as determined by the supplier). Carboxymethylated CNF (CCNF), also in the form of an aqueous suspension, was kindly provided by RISE Bioeconomy (Sweden). The CCNF was produced from a softwood sulphite dissolving pulp (Domsjö Dissolving plus, Domsjö Fabriker AB, Sweden) by carboxymethylation, as described previously (Wågberg & Bjőrklund, 1993), followed by mechanical fibrillation. Nanocrystalline cellulose (CNC) in powder form was purchased from CelluForce (Canada). It was produced from bleached kraft pulp by sulfuric acid hydrolysis. Charge densities of −20.7 ± 0.6, −151 ± 2 and −259 ± 4 µeq/g at pH 5.2 were measured for CNF,

CCNF and CNC, respectively, using a particle charge detector PCD-02 (Mütek Analytic GmbH, Germany), titrated using poly(diallyldimethylammonium chloride). Atomic force microscopy (AFM) images and chemical structure of the three nanocellulose types are given below in Figure 2.2.

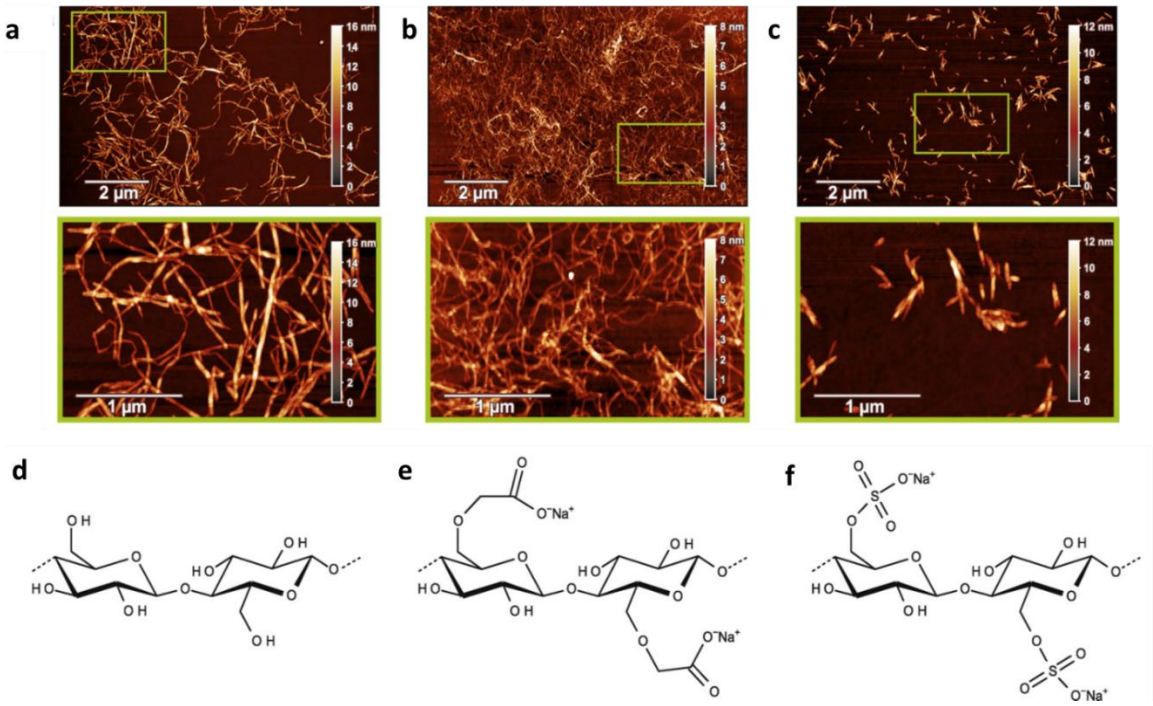

Figure 2.2: Atomic force microscopy images (a–c) and the corresponding simplified surface chemistries (d–f) of: (a,d) mechanically isolated cellulose nanofibrils (CNF); (b,e) carboxymethylated cellulose nanofibrils (CCNF) and (c,f) cellulose nanocrystals (CNC). The colour gradient bars shown in the AFM images represent the height scale, also referred to as the thickness (from Nechyporchuk, 2018).

2.1.2.2 Cellulose derivative/nanocellulose composite treatment (solution 2)

Solution 2 was proposed by ZFB, a private company for book consservation based in Leipzig (Germany) who has the experience to work with cellulose derivatives. These compounds are cellulose ethers which are commonly used in paper conservation as adhesive and consolidant. They show a good mechanical performance with paper and some, such as methyl cellulose chosen for this study, are also chemically stable on the long term (Feller, 1990). The potential of using CNC as a filler for cellulose derivatives matrices was used to explore its benefits when using the resulting composite as consolidants for painting canvases.

Tylose and methyl cellulose (MC), two cellulose derivatives.

Tylose is a water soluble hydroxyethyl cellulose. Tylose was purchased from ShinEtsu SE Tylose GmbH &Co (Wiesbaden, Germany). Tylose exist at different grades. Tylose grade MH50 (powder form) was used here because of its lower viscosity of 50 mPa•s which simplified the preparation of the aqueous solutions because of their low viscosity before film casting. The viscosity level of Tylose in solution is based on Hoeppler: 2% solution of the commercial product with 5% moisture content, 20ºC, 20ºdH (German hardness).

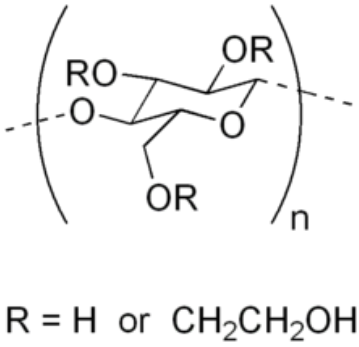

Figure 2.3: Chemical structure of Tylose, an hydroxyethyl cellulose (HEC) derivative. The degree of substitution of the product used is unknown.

Solutions of the aqueous nanocomposite MC+CNC(w) and heptane-based nanocomposite MC+CNC(h) were received, already prepared, from ZFB (Zentrum für Bucherhaltung GmbH, Leipzig, Germany). The solutions were at 1.97 % w/w in water (i.e. MC+CNC(w)) or heptane (i.e. MC+CNC(h)). The solutions are currently under development. The protocol of preparation as well as the ratio MC:CNC are covered by a non-disclosure agreement and can therefore not be disclosed.

Methyl cellulose and CNCs are water-soluble compounds and are thus insoluble in apolar solvents such as heptane. For the heptane-based nanocomposite solution, the methylcellulose compound and CNCs were chemically modified by a trimethylsilylation reaction (Mormann, 1999) in order to make them soluble in apolar solvents. A scheme of the silylation reaction and chemical structure of the silylated cellulose is given in Figure 2.5.

The water-based and heptane-based nanocomposites MC+CNC were also received mixed with $CaCO_3$ nanoparticles of deacidification present at 2% in solution. These mixtures were prepared to test the possibility of adding deacidification agent in combination with the reinforcement and to see how this addition would impact the consolidation provide on the short and long term. In paper conservation, for example, deacidification of objects has become a routine has it has proven to increase the life-time of the material (Baty, 2010). Those solutions were prepared by ZFB. The size of the particles in the dispersions was ca. 180 nm, as determined by static light scattering (Laser Scattering particle size Distribution Analyzer "Horiba LA-950")[3].

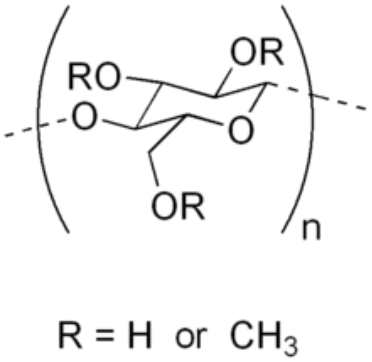

Figure 2.4: Chemical structure of methyl cellulose. The degree of substitution of the product used is unknown.

Silylated methyl cellulose

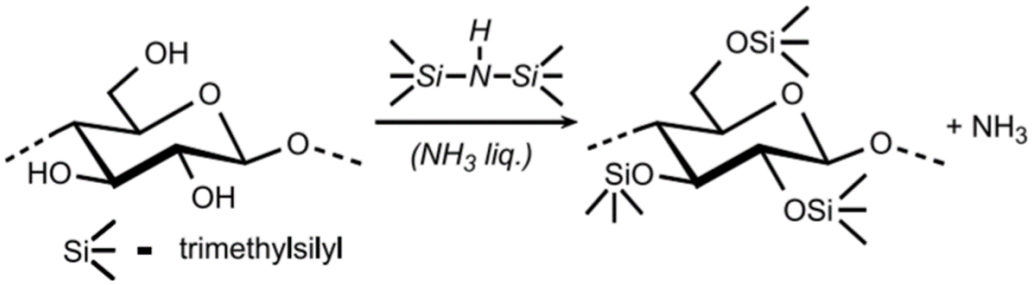

Figure 2.5: Reaction scheme of trimethylsilylation of cellulose with hexamethyldisilazane in liquid ammonia (Mormann, 2000)

[3] Nanorestart internal report (September 2018)

Cellulose, which is one of the most important natural polymers, contains one primary and two secondary hydroxy groups in its glucose units. When these hydroxy groups are partially or fully trimethylsilylated, substituted cellulose derivatives are obtained which are soluble in apolar solvents. Indeed in the paper and textile industry, cellulose from different sources was silylated to improve its solubility in organic solvents (Harmon, 1973; Mormann, 1999). This is because silylated compounds reveal reduced polarity than their original compounds (Ali, 2013; Van Look, 1995). Silylation is also well known for mitigating the effects of hydrogen bonding on physical properties (Klebe, 1964) and thus to reduce the hygroscopic behaviour of the silylated materials. The first mention of silylation of cellulose in the literature was made by Patnode (1942), who proposed it as a method of making textile materials hydrophobic.

2.1.2.3 Multilayered nanoparticles (solution 3)

The multi-layered nanoparticles consist in (1) polyelectrolyte-treated silica nanoparticles presented later in Chapter 5 and 7 and (2) the polyelectrolyte-treated calcium carbonate ($CaCO_3$) nanoparticles presented in Chapter 7.

The polyelectrolyte-treated silica nanoparticles were synthetized by Chalmers University (Gothenburg, Sweden). These nanoparticles are made of a silica nanoparticle (NP) core with polyelectrolyte multilayers (PEMs), which consisted of the cationic polymer poly(ethylenimine) (PEI) and the anionic polymer (carboxymethyl)cellulose (CMC). In the text, they are designated as Sil/PEI/CMC. The particular architecture of these NPs was achieve using a procedure that allowed the formation of multilayers without almost any aggregation and that ended with a layer of cellulosic nature (i.e. CMC). A detailed description of the preparation of Sil/PEI/CMC NPs can be found elsewhere (Kolman, 2017).

Colloidal silica, Levasil CS40-213, was kindly provided by AkzoNobel Pulp and Performance Chemicals in Sweden. The particles had a surface area of 130 $m^2.g^{-1}$ which corresponds to a spherical diameter of 21 nm (Iler, 1979). The silica particles were provided in the form of a water suspension having a pH of 9.1, a concentration of 40 % w/w and a density of

1.3 g/ml. Sodium carboxymethyl cellulose (CMC), Akucell AF0305, was provided by AkzoNobel Pulp and Performance Chemicals in a powder form. The degree of substitution was 0.77 and the viscosity of 1%w/w water solution was 12 mPa.s. The weight average molecular weight of CMC was 650000 $g.mol^{-1}$. Branched polyethylenimine (PEI) having a weight average molecular weight of 25000 $g.mol^{-1}$ was purchased from Sigma-Aldrich. Ion exchange resins Dowex Marathon A (OH^- form) and Dowex Marathon C (H^+ form), reagent grade sodium hydroxide and hydrochloric acid were used for pH adjustments. All these chemicals were purchased from Sigma-Aldrich. The Dowex Marathon C resin was washed with ethanol and dried before use, the other chemicals were used as received.

The polyelectrolyte-treated calcium carbonate ($CaCO_3$) nanoparticles were synthetized by CSGI (Florence, Italy). These nanoparticles are made of a $CaCO_3$ NP core with polyelectrolyte multilayers (PEMs), which consisted of the cationic polymer poly(ethylenimine) (PEI) and the anionic polymer (carboxymethyl)cellulose (CMC). In the text, they are designated as $CaCO_3$/PEI/CMC. The protocol of synthesis is currently under intellectual protection and should be released in the next 2 years.

2.2 Methodology

The impact of the treatments selected on the canvases properties was assessed and quantified by investigating the changes in appearance, in mechanical properties, in physical properties (i.e. hygroscopic behaviour) and in stability (chemical, physical and mechanical) over time which could be seen for the canvases after treatment. The criteria selected were inspired by those listed by Berger (1970) and Hedley (1988), among others, and are given in greater details later in Chapter 4, section 4.1.

2.2.1 Visual assessment and surface analysis

2.2.1.1 Colourimeter

For the colour measurements, an X-Rite 530 Colourimeter was used. Colour change was measured according to the CIEL*a*b* colour space. According to this colour representation, *L* is

lightness, a* is the red-green component, b* is the yellow-blue component (for the D65/10 CIE Illuminant/observer condition). Colour difference ΔE was calculated from the differences ΔL^*, Δa^* and Δb^* between the sample and a reference following the equation:

$$\Delta E = \sqrt{\Delta L^{*2} + \Delta a^{*2} + \Delta b^{*2}} \qquad (1.1)$$

2.2.1.2 Field emission -scanning electron microscopy (SEM-EDX)

The analysis was carried out using a Philips XL30 field emission SEM-EDX (FEI, Eindhoven, Netherlands) on the canvas samples. EDX detector was Oxford Instruments (UK). The system was operated at 5 kV acceleration voltage. Samples (3 x 5 mm) were mounted on aluminium stubs (Agar Scientific, Essex, UK) and sputtered with Gold/Palladium using a Palaron E5000 sputter coater for 1min30s. For the samples imaged in cross-sections, the canvas samples were glued to the aluminium stub using an epoxy resin. The samples were left to dry before imaging.

2.2.2. Quantification of chemical degradation

2.2.2.1. Infrared spectroscopy

The FTIR instrument, PERKIN ELMER – System 2000 FT-IR with SENSIR DuraScope ATR (Attenuated Total Reflectance) accessory were used to record FTIR spectra of the films and treated cotton canvas samples. Samples were stored at 20% relative humidity and room temperature prior to analysis. The analysis was performed by placing the samples onto a ZnSe crystal with applied pressure and scanning between 4000 cm^{-1} to 800 cm^{-1} by the accumulation of 12 scans with resolution of 4 cm-1. Spectra were analysed using the software, GRAMS. Spectra were then analysed and compared.

2.2.3. Static and dynamic hygroscopic response

2.2.3.1. Contact angle

The hydrophilicity of the surface was evaluated by the contact angle measurement by use of a commercial contact angle meter (CAM 200, KSV, USA). The equilibrium contact angle θ (see Figure 2.6) is determined by the Young equation:

$$\gamma^{SG} - \gamma^{SL} - \gamma^{LG} \cos\theta = 0 \qquad (1.2)$$

Where γ^{SG} is the solid–vapor interfacial energy, γ^{SL} is the solid–liquid interfacial energy and γ^{LG} is the liquid–vapour interfacial energy.

The contact angle was measured at least 5 times with the same sample in an ambient air, and the most representative curve of each set of measurements was selected for the interpretation.

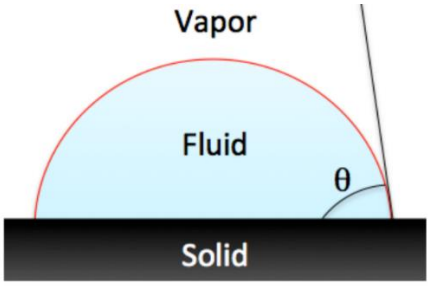

Figure 2.6: Scheme of the contact angle measurement (Santiso, 2013)

CAM 200 Optical Contact Angle Meter was employed to measure the contact angle measurements in cotton canvas specimens pre-conditioned at a fixed RH level, i.e. 30% RH, in the RH range used for the mechanical assessment (cf. 2.2.4) at room temperature. The analysis was performed by placing the samples flat on platform and letting a deionised water drop fall on it and measuring the contact angle until it was fully absorbed.

2.2.3.2. Differential vapour sorption (DVS)

The water-uptake measurements of the canvas and films samples were investigated using a Q5000 SA thermogravimetric analyzer (Q5000 SA, TA instruments, USA) having a microbalance in which the sample and reference pans were enclosed in a humidity and temperature controlled chamber. The temperature in the Q5000 SA was controlled by Peltier elements. Dried N2 gas flow (200 mL.min^{-1}) was split into two parts, of which one part was wetted by passing it through a water-saturated chamber. The desired relative humidity (RH) for

the measurements could subsequently be obtained by mixing proper proportions (regulated by mass-flow controllers) of dry and wet stream.

Samples, weighing 5–10 mg, were preconditioned using silica gel (25 °C). The amount of water absorbed was expressed as the mass percentage of water relative to the dry sample mass. The RH programs used varied according to the studies and are thus described in each chapter.

2.2.4. Mechanical assessment

2.2.4.1. Tensile testing (stress-strain curves)

In this test, the sample is subjected to uniaxial tension upon constant elongation rate. The applied force or tension necessary to induce the elongation rate is recorded as a function of elongation. In our study, the measurement was not carried out until rupture due to the limitation of the DMA used for this test. However, this was considered as sufficient since percentage of elongation around 10% and tension around 1000N/m were reached which is well beyond the 2% in elongation and 200N/m in tension to which is subjected a painting canvas (cf. Table 1.1 in Chapter 1). From the tensile tests carried out, stress-strain curves can be plotted using the dimensions of the sample. The Young's or tensile modulus is measured from the initial slope of the stress-strain curve.

For the tensile tests, rectangular samples were cut from different regions of the treated and untreated degraded canvases, parallel to the warp direction. They were cut so that 10 threads were collected in the warp direction and were typically 0.7 (thickness) x 7 (width) x 15 (length) mm in dimensions. The samples were pre-conditioned at 20%RH for at least 24 hours prior to the measurements. This is the lower bound RH level selected for mechanical assessment of the materials. It is representative of a low RH level to which paintings could be subjected in non-controlled environments (i.e. historic houses, private galleries). The DMA analyzer (Tritec 2000B, Lacerta Technology, UK) was set for measuring in tension. The tests were performed using a free length of 5mm under controlled environment (20%RH or 80%RH at 25°C). The load was applied at the rate of 0.4N/min. This method of measurement enables the evaluation of the

mechanical response of the samples at low extensions which are mechanically relevant for paintings (Mecklenburg, 1982a).

As previously mentioned, Young's moduli *Y* corresponds to the slope of the stress-strain curve measured in the elastic region of the material, i.e. where the deformation applied is reversible. It is calculated as follow:

$$Y = \frac{Tensile\ Stress}{Tensile\ strain} = \frac{F/A}{\Delta L/L} \quad (1.7)$$

where *F* is the force applied (in N), *A* the cross-sectional area of the sample (in m^2) and *L* the initial length of the sample between clamps. ΔL (in m) thus corresponds to the elongation of the sample during tensile test.

Young's moduli *Y* were measured, as seen in Figure 2.7, in the initial part of the tensile curves between 1 and 2% in elongation, range at which painting are usually stretched (M. F. Mecklenburg, 1982a).

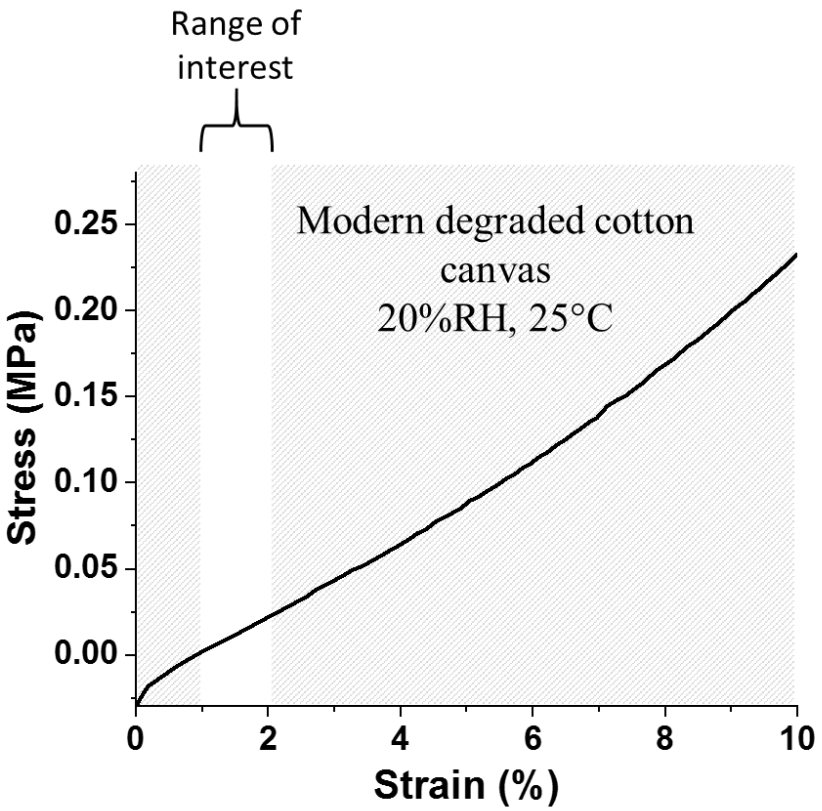

Figure 2.7: Stress-strain curve of a canvas sample showing the range of interest from which Young's modulus Y (i.e. slope of the curve) is calculated.

2.2.4.2. Dynamic mechanical analysis under controlled temperature and relative humidity (RH) (DMA-RH)

DMA is a technique commonly used for the mechanical assessment of synthetic polymers. It measures the mechanical response of a material to the application of a sinusoidal stress. When the sinusoidal stress is applied, the strain response of a visco-elastic material will lag behind the applied stress by some angle δ (Figure 2.8).

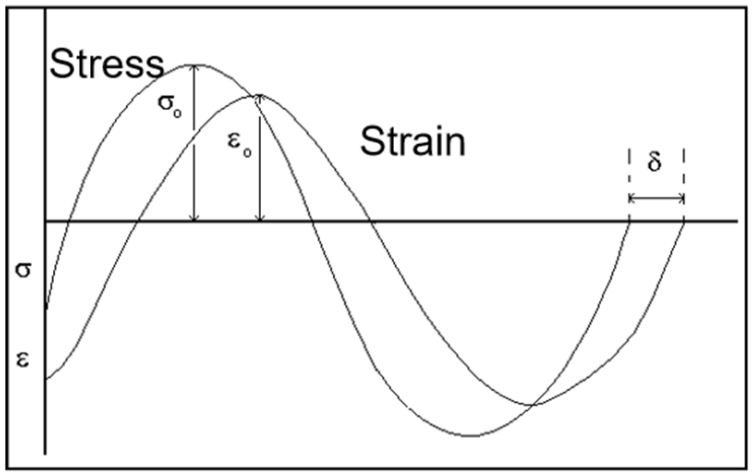

Figure 2.8: Principles of mechanical assessment using DMA. Sinusoidal stress (σ) applied during a DMA experiment and resulting strain (ε) and phase lag δ measured for viscoelastic materials.

This phase lag result from the time necessary for molecular as well as structural rearrangements. The stress σ and strain ε are expressed:

$$\sigma = \sigma_0 \sin(\omega t + \delta) \qquad (1.8)$$

$$\epsilon = \varepsilon_0 \sin(\omega t)$$

where ω is the angular frequency and δ the phase angle or phase lag. Thus, σ can also be expressed as follows:

$$\sigma = \sigma_0 \sin \omega t \ \cos \delta + \sigma_0 \cos \omega t \sin\delta \qquad (1.9)$$

After dividing this expression by the strain to obtain the modulus, two terms can be extracted which correspond to the in-phase (real) *E'* and out-of-phase (imaginary) *E''* components.

$$\sigma = \epsilon_0 E' \sin \omega t \ + \varepsilon_0 E'' \cos \omega t \qquad (1.10)$$

Then,

$$E' = \frac{\sigma_0}{\epsilon_0} \cos \delta \qquad (1.11)$$

$$E'' = \frac{\sigma_0}{\epsilon_0} \sin \delta$$

The values of these two parameters are dependent on the phase lag δ between stress applied and resulting deformation, hence strain of the sample. Tanδ is then calculated from *E'* and *E''* as follow:

$$Tan\delta = \frac{E''}{E'} = \frac{\sin\delta}{\cos\delta} \qquad (1.12)$$

If a material is perfectly elastic, the strain of the sample will occur exactly in phase with the stress applied. The phase δ, hence Tanδ, and *E''* will be equal to zero. Whereas if a material is purely viscous, the strain will be exactly 90 out of phase with the stress applied. *E'* will be equal to zero.

A Tritec 2000 B DMA connected to a humidity generator was used (Figure 2.9). Samples were pre-dried for 24 hours in a chamber whose environment was maintained at 20%RH using a glycerol/water solution (Forney, 1992)and then mounted between the tensile clamps. Due to the woven structure of the samples, a preload of 1N was added at the beginning of the data acquisition for all samples in order to maintain the sample under tension during the measurement and so that the samples did not buckle. In tension, it is indeed necessary to superimpose a static force larger than the applied dynamic force, to ensure that the sample remains under a net tensile force (Duncan, 2008).

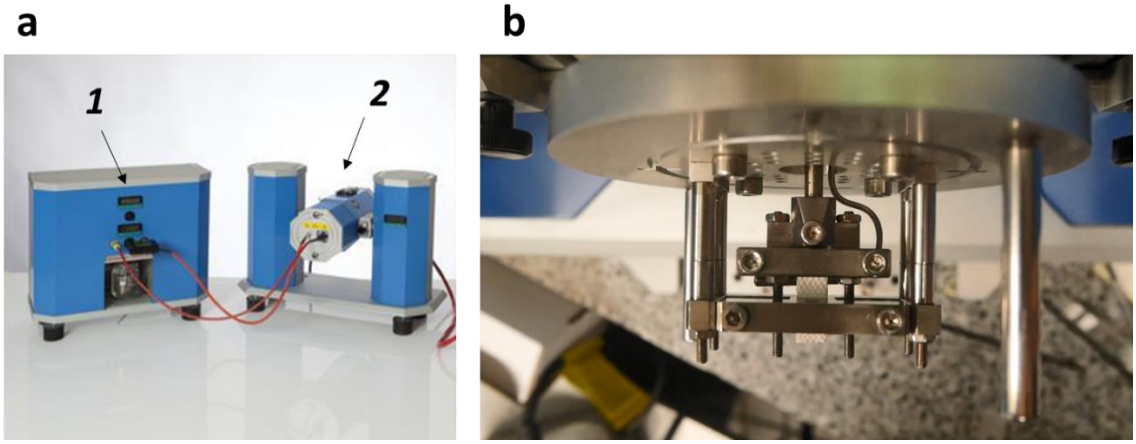

Figure 2.9: Pictures of the DMA (a2) connected to the humidity generator (a1). In (b), detail of the DMA head showing the clamps and a canvas sample clamped in tension as used for the DMA-RH and tensile test experiments.

Various RH protocols were used. They varied depending on the group of samples investigated and research questions raised. Therefore, more detailed information about the RH programs applied are given separately in each section.

Due to the anisotropic behaviour of woven fabrics (characterised by warp and weft directions as seen in Figure 1.2, chapter 1), great care was taken regarding the weave directions of the fabric when sampling and mechanically testing the samples. The weave directions and number of threads present in the direction of measurements are given for each set of measurements of this project (see in materials and methods of each chapter).

To investigate the viscoelastic properties of materials, it was also important to apply enough tension to the material in order to be avoid buckling of the canvas but also to be placed in its linear visco-elastic region or Hookean region. If the sample is not stretched enough, the mechanical response of the sample to RH variations cannot be isolated from the structural response of the canvas (slack and crimp removal). A preload of 1N was thus applied on each sample before DMA measurements to reach, prior to the DMA-RH measurements, initial stiffness in the sample between 150 and 250N.m^{-1} similar to those measured for stretched paintings (cf. Table 1.1 in Chapter 1).

2.3. Summary of materials and methods

The materials and methods given in Chapter 2 are only those which were used across several chapters of this PhD thesis. Other techniques, specific programs (e.g. RH program for DMA-RH, ageing protocol) or materials which were only use in one specific study, i.e. chapter, will be given and described in the materials and methods section of the result chapter (Chapters 3 to 8) to which they belong. The materials and methods already described in Chapter 2 will also be mentioned in each results chapter in their materials and methods section.

The chapters in which the techniques and materials described in Chapter 2 have been used are summarized in Table 2.1 (materials) and Table 2.2 (methods)

Type of material and preparation	***Material***	***Chapters***
Canvas	Cotton canvas unwashed/not-degraded	Chapter 3
	Cotton canvas washed	Chapter 3
Nanocelulose-based treatments	Solution 1: Nanocellulose-only treatments	All chapters
	Solution 2: Tylose/CNC and MC/CNC composite treatment	Chapter 5 / 7/ 8
	Solution 3: Multilayered nanoparticles	Chapter 5 (Appendix C) / 7

Table 2.1: Summary of the materials presented in Chapter 2 and chapters in which they can be found.

Type of analysis	***Instrument***	***Chapters***	***Additional information***
Visual assessment	Colourimeter	Chapter 4 / 5	
	SEM-EDX	Chapter 3 / 4 / 5	
Quantification of chemical degradation	ATR-FTIR	Chapter 4 (Appendix B) / 5	
Static and dynamic hygroscopic response	Contact angle	Chapter 3 / 5 / 8	
	DVS	Chapter 3 / 4 / 5 / 8	The RH programs used varied depending on the samples investigated. They are given separately in the materials and methods section of each chapter.
Mechanical assessment	Tensile test	Chapter 3 / 4 / 5 / 6	The RH level (20 or/and 80%RH) at which the tests were performed is given in the material and method section of each chapter.
	DMA-RH	Chapter 3 / 4 / 5 / 6 / 7	RH programs, direction of canvas measurements, number of thread in this direction and preload added varied depending on the samples investigated. They are given separately in the materials and methods section of each chapter.

Table 2.2: Summary of the techniques presented in Chapter 2 and chapters in which they can be found.

3 The role of relative humidity in the assessment of the physical-mechanical properties of painting canvases and painting constituents.

3.1 Introduction

The mechanical properties of most individual possible layers of easel paintings are well known and documented (Hedley, 1991; Hedley, 1988; Macbeth, 1993; Mecklenburg, 1982; Ormsby, 2006; Roche, 1989; Young, 2001). Variations in temperature (T) and relative humidity (RH) can affect the mechanical response of painting layers as shown, for example, for samples from 19th century paintings (Macbeth, 1993). The key findings of these investigations have been to identify the differential response of each layer to relative humidity (RH). Variations in RH as seen in Figure 3.1 are a primary cause of failures in paintings (i.e. ruptures in the paint layers) (Mecklenburg, 1982).

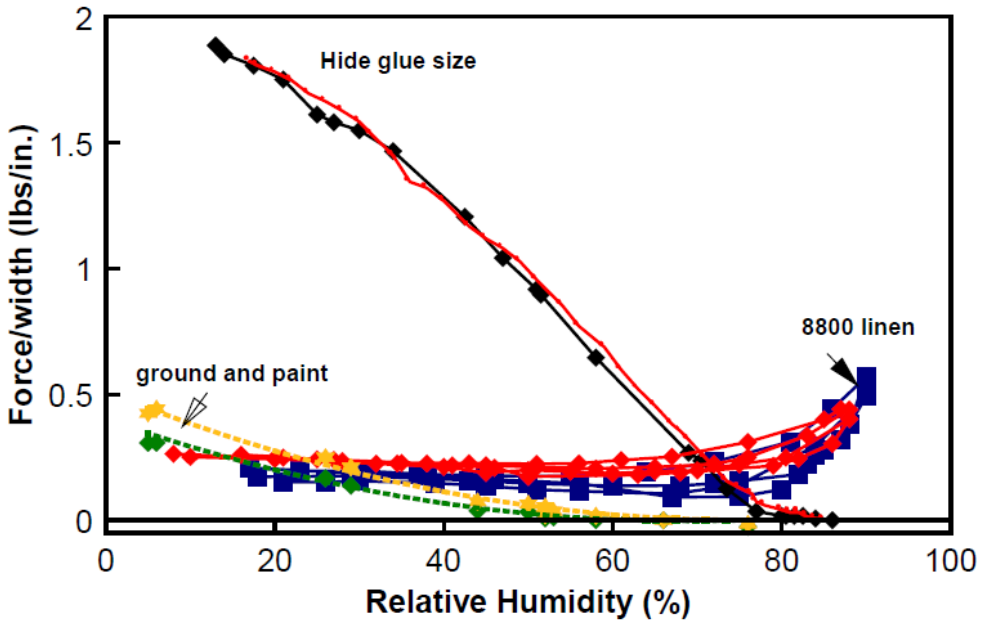

Figure 3.1: Force per width of restrained sample of linen (blue), hide glue (black), and ground and paint layers (yellow and green) made of lead white and Naples yellow, respectively. Thickness of the samples was the same and typical of a common painting. The figure shows the differential responses of the individual layers over the 10-90%RH range (figure taken from Mecklenburg, 2007).

Mecklenburg (2007) showed that the most responsive component of a painting to relative humidity (RH) is, when present, the hide glue (also called size) (Figure 3.1). When desiccated, it is the stiffest material of a painting but large decreases in elastic modulus are typically measured at high RH levels (i.e. 80%RH). The canvas also presents a high response in elongation to RH fluctuations. As seen in Figure 3.2, the force measured in either warp or weft, the two weave directions in a fabric (cf. Figure 1.2 in Chapter 1), remains quite stable between 10 and 60%RH in comparison with what was observed for the hide glue. Above 60%RH, however, the stress measured gradually increased and from 80%RH onwards each small increase in RH drastically increase the stress applied on the linen canvas (Figure 3.2).

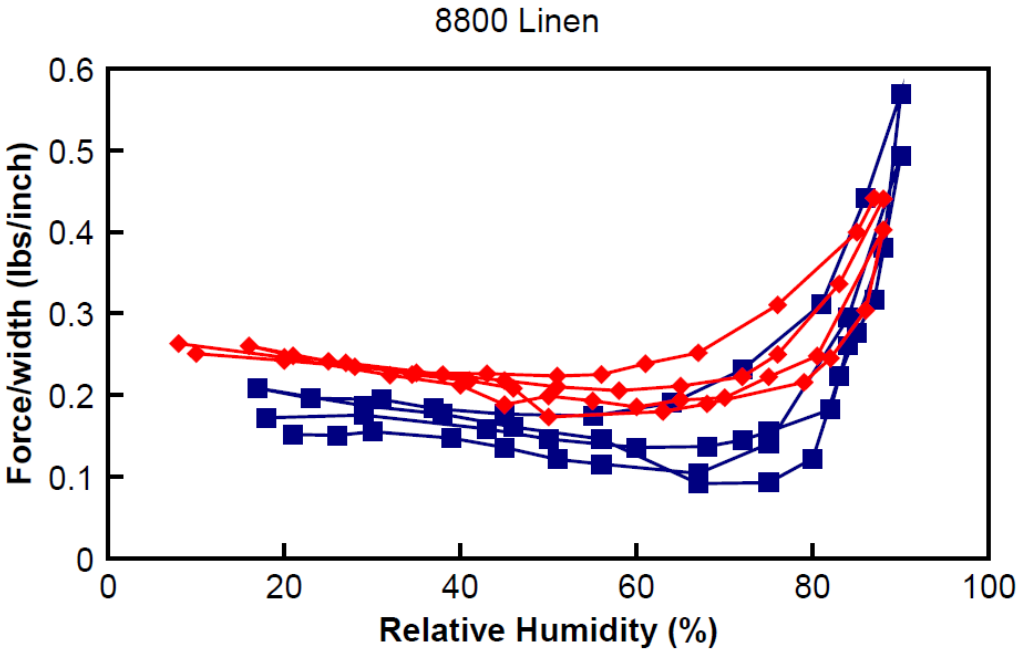

Figure 3.2: Tensile forces per width measured for restrained samples of #8800 linen measured in warp (blue) and weft (red) directions under changing relative humidity (RH) (taken from Mecklenburg, 2007).

In early works by Collins (1939) and subsequently by Gray (1971), it was shown that the stiffening of the canvas at high RH levels resulted from the swelling of the canvas fibres due to moisture sorption (Figure 3.3). This swelling leads to the consecutive swelling of the threads which subsequently increase in diameter. This causes the crimp (i.e. yarn waviness) of the threads to increase and the fabric to shrink. However, when the fabric is restrained, as in a painting where

it is fixed on stretcher, the total dimensions of the canvas, i.e. apparent dimensions and elongation, are maintained fixed. Upon moisture uptake, the shrinkage of the canvas will thus be translated into an increase in tension. The ratio of fabric shrinkage depends on the warp and weft yarns tension as well as their density (i.e. mass per unit length) (Kadi, 2015). The mechanical response to RH of paint and ground layers is so low that it is negligible in comparison to those of the hide glue and the canvas.

These different responses to RH highlighted above for the individual layer making up a painting can lead to mechanical failure in the painting. This occurs when, for a specific environment (i.e. RH, temperature), the stresses applied exceed the yield point or produce plastic or irreversible deformation of the constitutive materials of the painting (Mecklenburg, 1994).

Overall, these early studies raised awareness of the important role of RH in the risks associated with mechanical failure of materials in art and conservation. This has led to the creation of guidelines for museum environments for a wide range of materials ("Environmental Guidelines ICOM-CC and IIC Declaration", 2014; Michalski, 2016). This has also lead researchers to investigate further the impact that specific RH levels and/or variations in RH might have on the mechanical properties of objects in collections and how these could lead to an increased risk of mechanical failure.

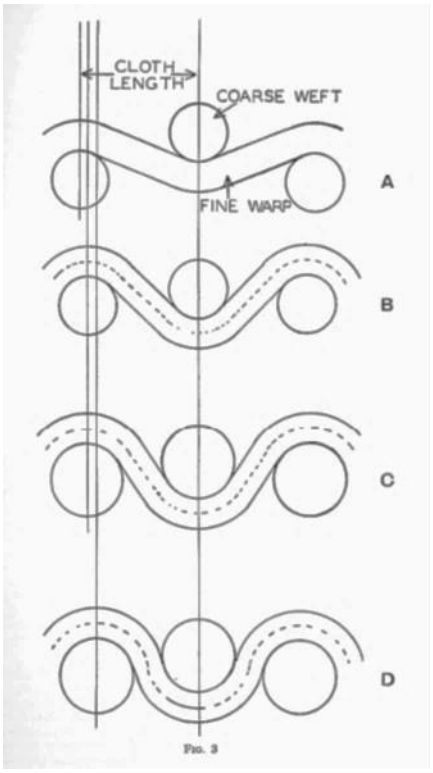

***Figure 3.3: Swelling of threads in a fabric due to wetting which causes shrinkage of fabrics in humid environments showing a cross-sectional view of the canvas before (A) and after (D) water uptake and shrinkage resulting from swelling of the threads and fibres. The caption shows the gradual swelling (B, C) of the coarse weft threads resulting in an increased crimp (i.e. weaviness) in the fine warp threads (from* Pocobene & Hodkinson (2006) *adapted from models presented by* Collins (1939) *and* Gray (1971).**

In order to investigate the mechanical properties of easel paintings and their individual layers at different RH levels, most of the studies have explored the response of samples that had been restrained with or without static load applied as well as free hanging experiments for which the sample is left to swell or contract freely. However, one notable quality of canvases or any woven fabrics is their well-known viscoelastic mechanical behaviour (Cui, 1999). This means that the material shows both elastic and viscoelastic behaviours (cf. 2.2.4.2 in Chapter 2). Dynamic mechanical analysis (DMA) is often used to quantify the viscoelastic properties of polymeric materials among which are a few woven materials (Kaka, 2015; Murugan, 2014). The elastic response corresponds to the immediate response of a material to the mechanical stress applied whereas the viscous response is associated to the time-dependent response of the material to this same stress. Creep (i.e. material deformation, elongation in uniaxial testing) or stress

relaxation (i.e. decrease in stress) of fabrics upon application of mechanical stresses or in response to a strain applied are manifestation of the viscoelastic, hence time-dependent, behaviour of fabrics.

In conservation, the time-dependent behaviour of canvas and paintings has been studied. Creep and stress relaxation tests which involve the application of a static load and static displacement, respectively, were carried out using uniaxial testing by Conti (1972), Roche (1989) and Michalski (1996). Young introduced biaxial testing (i.e. simultaneously application of stress in two perpendicular testing directions). She also used it in load-time mode to measure viscoelastic effects or the load response of the material to any external parameter (Young, 1999). In her approach, the mechanical response of a canvas submitted to cycling loads as well as the deformations of the canvas resulting from wetting were explored. All these studies provided a direct practical assessment of the painting/canvas behaviour as a response to the applied tension, the dominant force acting on a stretched primed canvas. However, their limitations lie in that few of these studies have actually intended to measure and quantify changes in viscoelastic properties resulting from changes in RH.

DMA was introduced into paintings conservation to address this problem and deconvolute the elastic (energy stored) and viscous (energy dissipated) components in the mechanical response of samples from paintings. The first mention of the technique in the field of painting conservation is made by Hedley (1990) who used it to measure paint films. DMA operates at selected frequencies (Hz) and is able to measure viscoelastic properties and relate them to internal motions of the main polymer backbone and side chains (cf. 2.2.4.2 in Chapter 2) (Menard, 2015). The technique has continued to be used on paint films on 19th cent historical canvases (Foster, 1997; Odlyha, 1998; Odlyha, 1995) as well as on other cellulosic material such as paper (Salmén, 1980) or wood (Salmén, 1984). Influence of temperature or RH on the material mechanical properties were investigated. In the particular case of canvas, DMA was shown to be a sensitive technique to changes in mechanical behaviour resulting from RH changes (Foster, 1997; Odlyha, 1998). Foster successfully followed the increase in storage modulus *E'* (i.e. elastic response) of an

unprimed linen canvas upon exposure to increased RH levels (from 50 to 75 to 100%RH). Because both viscoelastic properties as well as response to RH have been shown to be important parameters in the study of materials for conservation, it was therefore decided to evaluate the behaviour of new consolidants for conservation with this approach using DMA with controlled environment (i.e. DMA-RH). The impact of temperature on the viscoelastic response of these materials was not explored. The measurements were thus performed at a fixed temperature 25C while the RH was varied.

3.2 Aim and objectives

In this chapter, a pilot study was established to study the baseline mechanical and physical response to RH of canvas samples as well as additional painting layers (animal glue size and lead white priming). This study had two objectives:

(1) **Understanding of the viscoelastic response of the degraded cotton canvas exposed to a controlled program of RH cycles.** The understanding of its mechanical response is essential since this canvas was chosen to test the newly developed consolidants (cf. Chapter 5). It is also the first time that such as study is made on cotton canvas in comparison to linen.

(2) **Evaluation of the impact of the sizing and priming layers on the mechanical response under RH variations of linen canvases.** The effect of size was measured on a modern linen canvas that has been sized with one to four layers of animal glue. The effect of priming was measured using a historical 19th cent linen canvas sized with animal glue and primed with lead white sample which was tested before and after removal of the layer of priming.

This study provides the foundation for Chapters 4 and 5, and will allow the evaluation of the impact that the consolidants have on the model canvas samples, i.e. the degraded cotton canvas. It will also assist in interpretation of the effect of size and priming on the response of linen canvas to RH.

3.3 Materials and methods

3.3.1 Materials

The materials chosen for this study include cotton and linen canvases as well as canvas with additional layers found in painting. They were chosen to get a better understanding of canvases, i.e. the substrate to be consolidated, and the impact that preliminary treatments and preparation might have on its mechanical behaviour.

3.3.1.1 Modern cotton canvas

A modern cotton canvas was tested before and after having been washed and degraded (cf. see 2.1.1.2 in Chapter 2 for details on weave structure and washing/degradation protocols). Pictures of the canvas before and after washing/degradation are shown in Figure 3.6a. Details of the threads structure and waviness are shown in Figure 3.5 and show the higher waviness (i.e. curvature) of the warp threads over the weft. This was expected from the weaving process where the weft threads are usually hold under tension whereas the warp threads are drawn through and inserted over-and-under the weft. This was previously shown in Chapter 1 (cf. Figure 1.2).

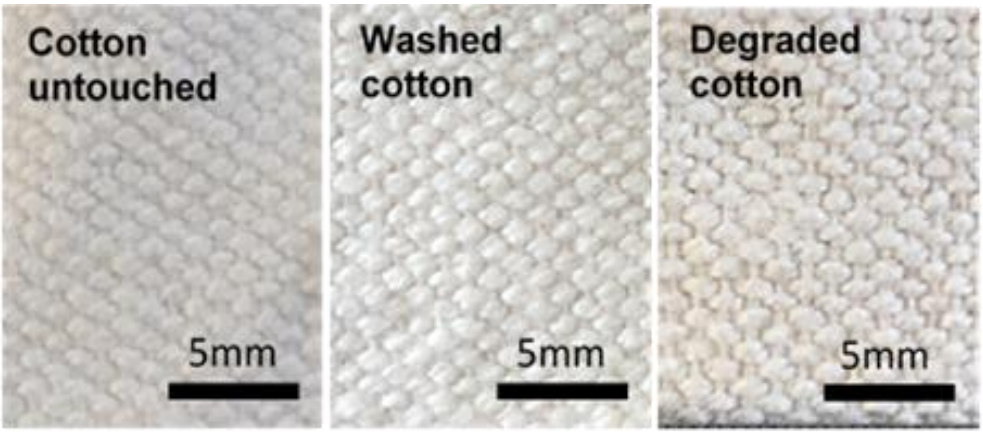

Figure 3.4: Pictures of the modern cotton canvas before and after washing and degradation

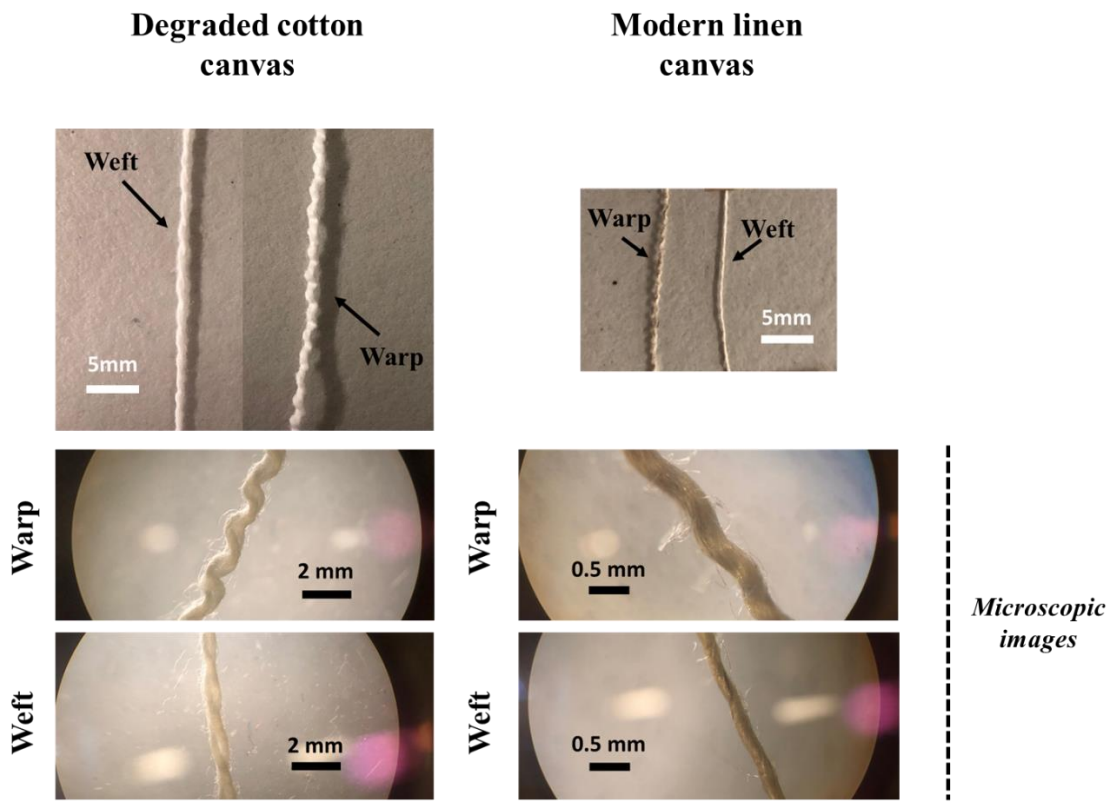

Figure 3.5: Pictures of warp and weft threads of degraded cotton and modern linen canvases showing differences in waviness of the threads as well as their structure. The microscopic images were taken at magnification of x0.66 (cotton) and x2 (linen). Note that the warp and weft threads of the cotton canvas are made of two yarns each, whereas the linen threads are only made of one twisted yarn each. The warp thread presents the wavier appearance as expected from the weaving process (cf. Figure 1.2 in Chapter 1).

The degraded cotton canvas was selected as substrate for the assessment of the newly developed nanocellulose-based consolidants. This is because cotton is, next to linen, a canvas material commonly found in paintings of contemporary art (Krueger, 2014; Oriola, 2014; Singer, 2014). Moreover, the degraded canvas used was shown to resemble naturally aged canvases in terms of its mechanical properties (Nechyporchuk, 2017). The degradation protocol resulted in a loss in tensile strength (i.e. lower breaking force or ultimate strength) and lower elongation at rupture (or elasticity). In other terms, the cotton canvas after degradation became more brittle similar to findings made by Hackney (1981), Hedley (1993), Peacock (1983) and Abdel Kareem (2004) and mentioned previously in 1.1.2.1 (p.31).

3.3.1.2 Unsized and sized linen canvases

The unsized and sized linen was provided by the Tate Conservation Dept. The linen canvas consisted of a modern superfine linen L 184, obtained from Russell and Chapple Ltd (London). It was sized using animal glue by the retired painting conservator Stephen Hackney in 2014 (see Figure 3.6b). The canvas was divided into various areas on which an increasing number of layers of size had been brushed. The number of layers applied varied from 1 to 5. The canvas presented a tight plain weaving with a density of 22 threads/cm in the warp and weft directions (Figure 3.6b). Both warp and weft threads of the canvas were made of 1 twisted yarn as seen in Figure 3.5. The threads of this canvas are thinner than the threads of the cotton canvas. Diameter of the threads was found to be mostly homogeneous across the canvas.

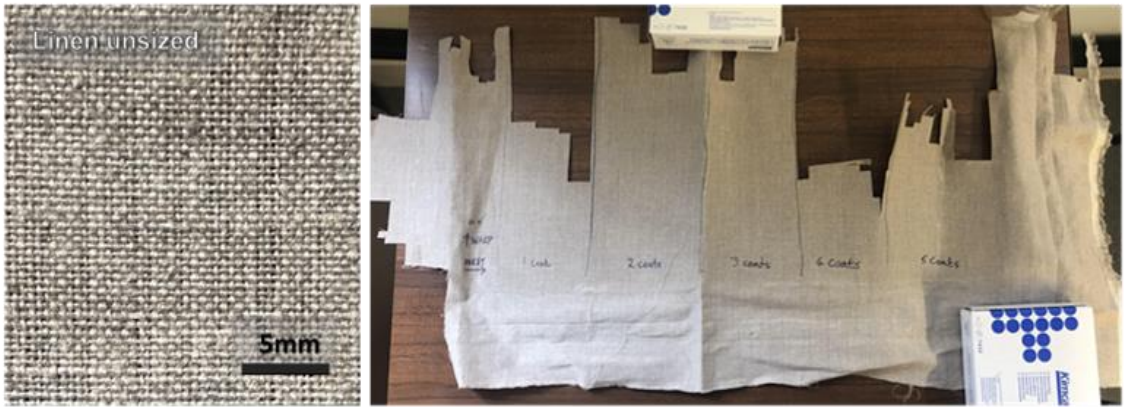

Figure 3.6: Picture of a modern unsized and sized linen canvas provided by Tate Conservation Dept.

3.3.1.3 Unprimed and primed sized linen canvas

A 19th century historical primed canvas provided by Stephen Hackney at Tate Conservation Dept. was also tested (see Figure 3.7) (Odlyha, 1998). The ground layer consisted of a layer of lead white around 100 µm thick. This ground layer was on a glue sized linen canvas.

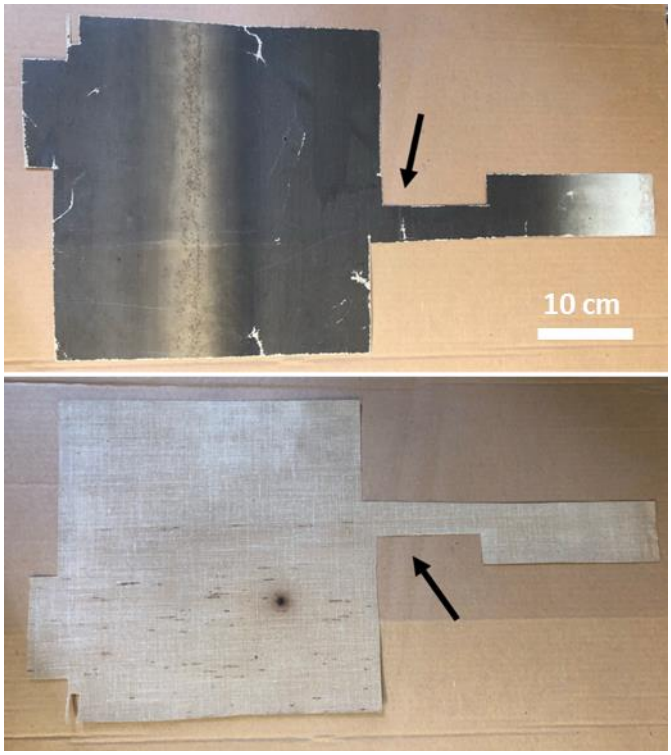

Figure 3.7: 19th century historical primed sized linen canvas provided Tate Conservation Dept. Pictures show the top primed side (top) and the canvas side (bottom). The samples were taken from the area indicated by the arrow.

3.3.2 Methods

The canvas samples unsized and sized, unprimed and prime were tested mechanically under static and dynamic variations in RH. The results were discussed and put in relation with data obtained on their surface chemistry and physical response to RH (hygroscopic behaviour).

3.3.2.1 X-ray photoelectron spectroscopy (XPS)

The XPS surface analysis was carried out for the new, washed and degraded canvases using a Quantum 2000 Scanning ESCA Microprobe (Physical Electronics, ULVAC-PHI, Chanhassen, US).

The charge shift was corrected using the binding energy of the aliphatic C-C, C-H state of C 1s at 285.0 eV as a reference signal (Pireaux, 1993). Peak fitting of the spectra was completed using the CASA XPS software.

3.3.2.2 DMA-RH

All the samples, sized/unsized, primed/unprimed were measured by DMA-RH at 1Hz and clamped in tension. A preload of 1N was used to avoid the buckling of the samples (cf. 2.2.4.2 in Chapter 2). The degraded cotton canvas and the untreated linen canvas from Tate were measured in both the warp and weft directions. For the study on sizing (i.e. unsized/sized linen from Tate), the samples were measured in the weft direction. For the study on priming (i.e. primed sized linen canvas from Tate), the samples were all measured in the same direction which could not be identified. The samples were typically 7 (width) x 15 (length) mm in dimensions.

The samples were tested by DMA-RH using 3 different programs in RH cycling inspired by a research conducted by Peresin (2010) on the viscoelastic response to RH variations of electrospun nanofibers made of nanocellulose composite. Three different RH protocols at fixed temperature (25°C) were designed to mimic variations that could be experienced by paintings in uncontrolled environments (e.g. galleries, historical houses). The RH range selected for the tests, i.e. between 20 and 80 % RH, was chosen in order to be similar to the one used in early works investigating the response of painting materials to moisture often taken between 10 and 90%RH (Krarup Andersen, 2013; Mecklenburg, 1982; Mecklenburg, 2007; Wood, 2018). The 3 RH program used are listed below:

- **RH cycles 20-80-20%RH** at 25°C (Figure 3.8). The humidity level was stabilised at 20% RH for 1 hour. RH was then increased at 4% RH/min to 60% RH and left at 60% RH for 5 min. RH was increased further to 80% RH at 1%RH/min, left for 30min at 80%RH and then decreased back to 20% RH at 4% RH/min. The 5min plateau at 60% RH was used in the program to reduce the RH overshoot that could occur at 80% RH when high rate increase in RH are used (i.e. 2-4% RH) while optimizing the time of measurement. Three consecutive RH cycles were applied.

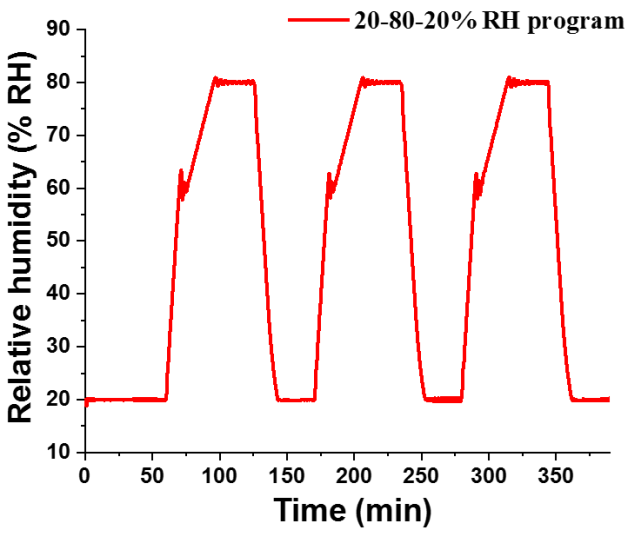

Figure 3.8: 20-80-20 %RH program (25°C) for which RH cycled between 20 and 80%RH at rates of 4%RH/min (20-60%RH), 2%RH (60-80%RH) and 4%RH/min (80-20%RH).

- **RH cycles 20-60-20 % RH** at 25°C (Figure 3.9). The rate of change from 20-60 % RH was 4%RH/min. The samples were set to equilibrate at 20 or 60 % RH for 30 min between each transition. Three (short run) to 11 consecutive RH cycles (long run) were applied. The RH cycles 20-80-20 % RH and 20-60-20% RH were designed to observe the mechanical response of different types of canvases to rapid variations in RH and to obtain a quick way to assess and quantify the stresses experienced by fabrics exposed to moisture.

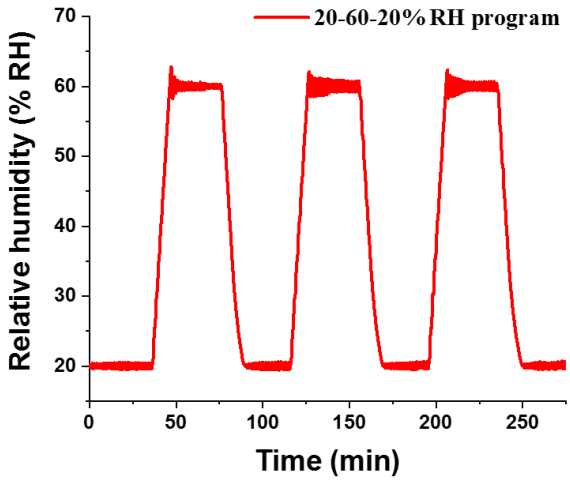

Figure 3.9: 20-60-20 %RH program (25°C) showed here for 3 successive RH cycles. RH was left to stabilized at 20 and 60%RH for 30min at each plateau. A rate of RH transition of 4%RH/min was used for both humidification (20-60%RH) and dehumidification (60-20%RH).

- **RH steps** at 25°C (Figure 3.10). The humidity was programmed to go from 20 to 80%RH and back to 20%RH at 2%RH/min with 1h equilibration every 10%RH (i.e. at 20, 30, 40, 50, 60 and 70% RH) and of 2 hours at 80% RH. RH-steps were designed to observe moisture-sorption kinetics during each step and to obtain the dynamic mechanical properties at various RH levels.

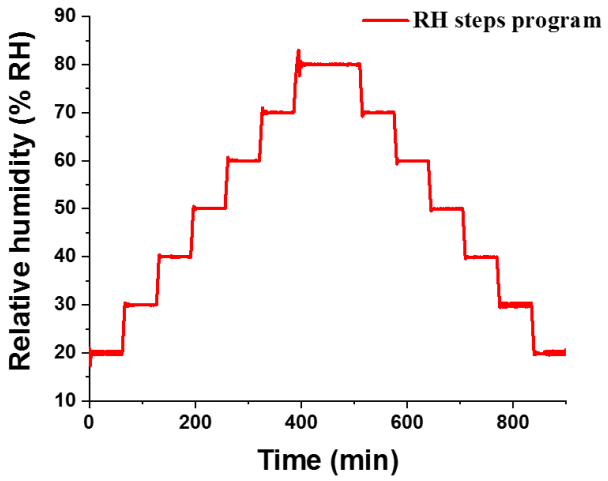

Figure 3.10: RH-steps program characterised by step increases in RH of 10% RH (4% RH/min) between 20 and 80 % RH. The RH was left to equilibrate for 1hour at each RH level, except at 80% RH at which it was left for 2 hours.

3.3.2.3 Tensile test

The degraded cotton canvas in 3.3.1.1 was measured by tensile testing at 20 and 80% RH (25°C). The samples were measured in the warp direction to investigate the impact of the treatments on the most elastic and less stiff direction of the canvas (Nechyporchuk, 2018). They were typically 0.7 (thickness) x 7 (width) x 15 (length) mm in dimensions and were cut so that 10 threads were collected in the warp direction.

3.4 Results

3.4.1 Preliminary investigations of the response of the degraded cotton canvas to moisture

As reported by Nechyporchuk (2017), after degradation of the untouched modern cotton canvas (cf. 2.1.1.2 in Chapter 2), a reduction in degree of polymerization (DP), hence reduction in length of the cellulose polymeric chains, from 1500 to 450 was measured. The DP value after degradation is similar to the DP measured for naturally aged linen canvases (Oriola, 2015). The loss in DP was associated with an important decrease in elongation, and tensile strength (Nechyporchuk, 2017). The ease of production of the pieces of degraded cotton canvas as well as their mechanical properties make them suitable mockups for the study of new treatments of consolidation for contemporary easel paintings.

3.4.1.1 Hygroscopic behaviour of the degraded cotton canvas

Cellulosic fibres such as plant fibres like cotton, linen, jute are all hygroscopic materials (Hill, 2009). Cotton fibres, for example, can absorb up to 13% their weight in water when exposed to 80% RH (Hill, 2009). As seen in Figure 3.11, with the degraded cotton canvas studied here, for example, an increase of 6% was measured between 20 and 80% RH upon 1hour exposure to 80%RH.

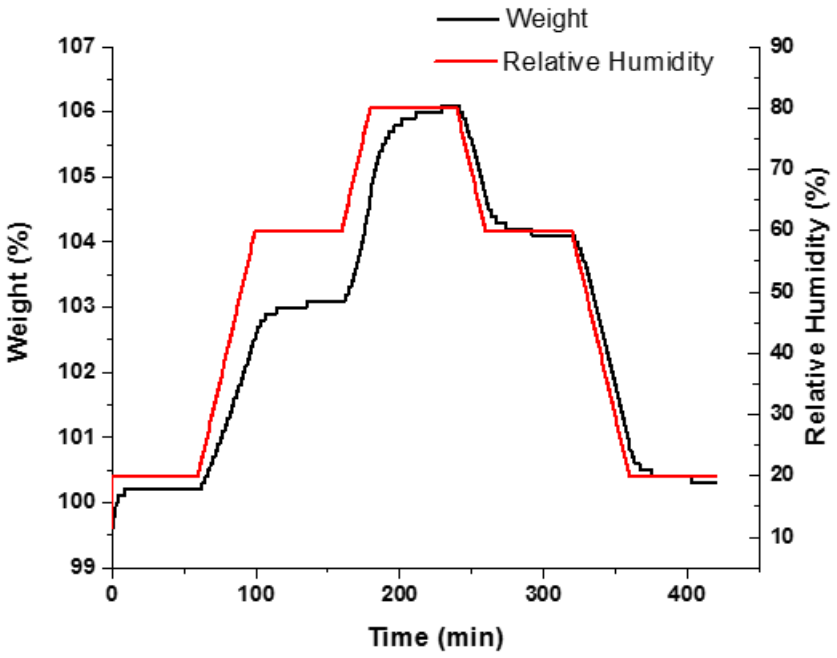

Figure 3.11: Variation in weight measured for an untreated cotton canvas (black) following changes in RH (ramp and plateaus) (red). This was measured by dynamic vapour sorption (DVS) using controlled RH cycling (20-60-80-60-20%RH). The rate of change from 20-60%RH was 1%RH/min. The samples were set to equilibrate at 20, 60 and 80% RH for 60 min between each transition.

The absorption of water by the fibres leads to the swelling of the fibres as well as modification of their mechanical behaviour. A cotton fibre, for example, tends to reach higher strength (i.e. force required to reach rupture) upon wetting (Farag, 2009). This hygroscopic behaviour will have, at the fabric level, a strong impact on the physical and mechanical properties of fabrics made of cellulose fibres subjected to moisture variations.

However, because of the woven structure of fabrics, other structural parameters such as weaving pattern, size of the fibres, yarns, threads, twist of the yarn, crimp of the warp and weft, as well as additives used during the weaving process (e.g. finishing) also come into play and can modify the physical properties of fabrics (Collins, 1939; Saiman, 2014). For example, a reduction in the crimp percentage of a fabric, hence a reduction in the waviness of the yarns/threads, was shown to increase the tensile strength at break (Saiman, 2014).

In the current study, the response of cotton and linen canvases subjected to rapid RH variations was measured. This approach was preferred here over longer times of exposure (often used to investigate the long term behaviour of materials) as it will provide more insight into the immediate mechanical response of fabric to moisture variations including the stresses undergone by fabrics and the risks of fatigue[4].

3.4.1.2 Preliminary mechanical assessment using tensile testing and static RH measurements

A preliminary assessment of the response to moisture of the degraded cotton canvas was obtained by tensile measurements as shown in Figure 3.12 using DMA in tensile mode. Tensile tests under static RH (i.e. fixed RH) have often been used to measure the mechanical properties of natural fibres at different RH (Célino, 2014). This less complex measurement will provide a baseline to deconvolute the viscoelastic response of the material which will be later monitored by DMA-RH under dynamic RH variations.

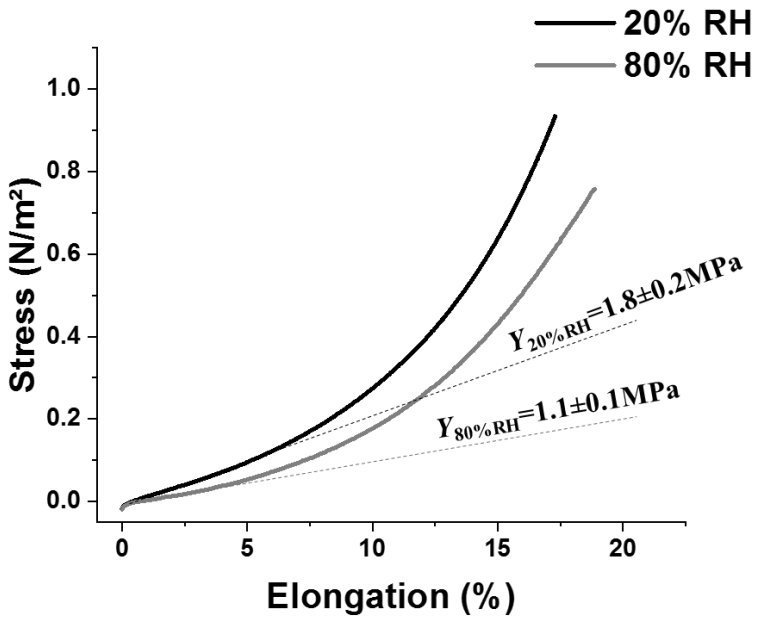

Figure 3.12: Tensile test performed at 20 (black) and 80%RH (grey) for a degraded cotton canvas measured in the warp direction. The results show the decrease in Young's modulus Y at high RH level (i.e. $Y_{80\%RH} < Y_{20\%RH}$).

[4] Mechanical degradation resulting from cycles of stress

The canvas measured was measured in the warp direction at a low and high RH level, i.e. 20 and 80% RH (Figure 3.12). Young's moduli, which give a measure of the stiffness of the sample, were calculated from the beginning of the tensile curves at elongation between 1 and 2%. It is in this range in elongation that paintings are usually restretched (Iaccarino Idelson, 2019; Mecklenburg, 1982). As seen in Figure 3.12, upon increase in RH from 20 to 80% RH, a decrease in Young's modulus from 1.8±0.2 to 1.1±0.1MPa was measured. These first results thus indicate that the mechanical response of the degraded cotton canvas exposed to high RH level, hence upon moisture uptake, is characterised by a loss in stiffness. This is in agreement with results reported in the literature on the study of the impact of moisture on natural fibres mechanical properties. In natural fibres, strength (i.e. maximal force the fibre can sustain) usually increases with moisture content and decreases with temperature, whereas the Young's modulus, i.e. stiffness, decreases as water is absorbed (Hearle, 1963). It was suggested that it is the hemicellulose, a very hydrophilic polymer (polysaccharide) present in plant fibres, which is largely responsible for the moisture sorption behaviour observed for these fibres (Davies, 1998). Water is absorbed in the pores and amorphous regions of the fibres, reducing inter-fibrillar cohesion and relieving internal fibre stress, leading to the plasticization of the fibre. The question is thus raised on how this will translate on the response of the same sample, measured by DMA-RH.

3.4.1.3 First insight into the mechanical response of the degraded cotton canvas to dynamic RH variations

The degraded cotton canvas was then measured by DMA-RH using the 20-80-20% RH RH program (cf. 3.3.2.2). The mechanical properties of the sample were measured at low elongations and in the warp as for the tensile tests previously performed. Contrary to tensile testing using the tensile tester such as Instron (static mechanical measurement), DMA in tension operates at lower strain levels which are in the region of interest for this study (Figure 3.12) and gives a measure of the viscoelastic properties of materials. With the controlled RH facility, the additional advantage is that it is possible to accurately programme the rate of increase or decrease in RH. In earlier works where programmed RH control was not available, samples were enclosed

in the sample chamber of DMA and the RH controlled environment was generated by saturated solutions and later sulphuric acid/water solutions (Foster, 1997). A unprimed linen canvas (Superfine Artists'Linen) was measured by the author of this study and the results shown below in Figure 3.13.

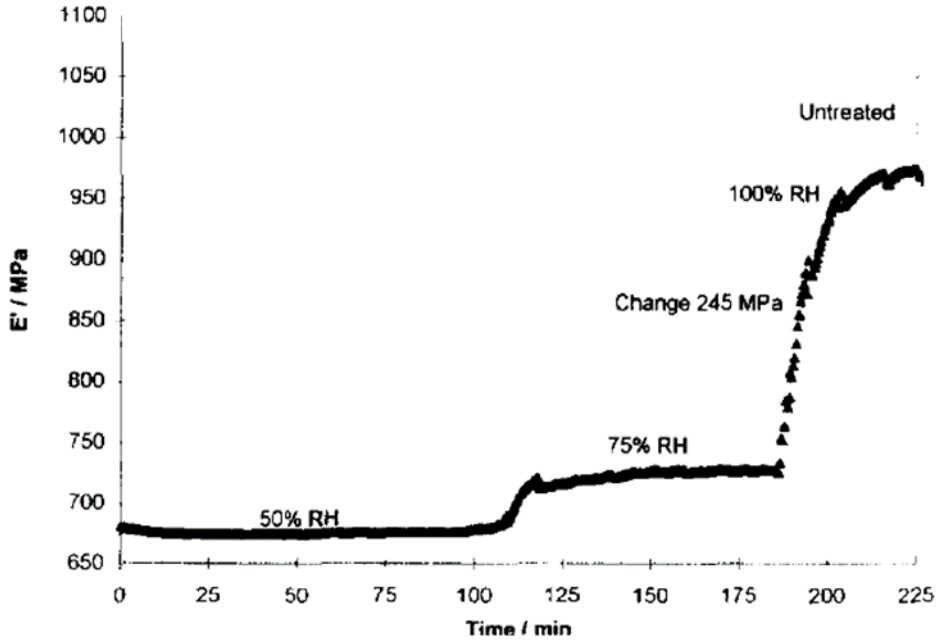

Figure 3.13: Variations in storage modulus E' with time for unprimed linen canvas samples exposed to increasing RH levels (50 to 75 to 100%RH) **(Foster, 1997).**

The typical mechanical response obtained by DMA-RH for the degraded cotton canvas subjected to the 20-80-20%RH RH cycling is given in Figure 3.14. Here, only the elastic part of the viscoelastic response, hence storage modulus *E'*, is given. *E'* gives a measured of the stiffness of a material. The results can thus be directly compared to those previously obtained by tensile tests. As seen in Figure 3.14, the cotton canvas is responsive to the change in RH as seen by the variations in *E'* measured upon RH cycling. On an increase in RH there is a sudden drop in *E'* with some recovery as it tries to reach equilibrium at 60%RH. It is likely that the sudden drop occurs due to over-plasticization of the sample. Recovery occurs as it reconfigures to include new water molecules. There is then a subsequent drop in modulus as RH goes to 80%RH and a similar effect is observed with recovery as the sample tries to reach equilibrium at 80%RH. As the RH is

decrease back to 20%RH, *E'* has not yet reach equilibrium and rapid change to higher modulus is observed.

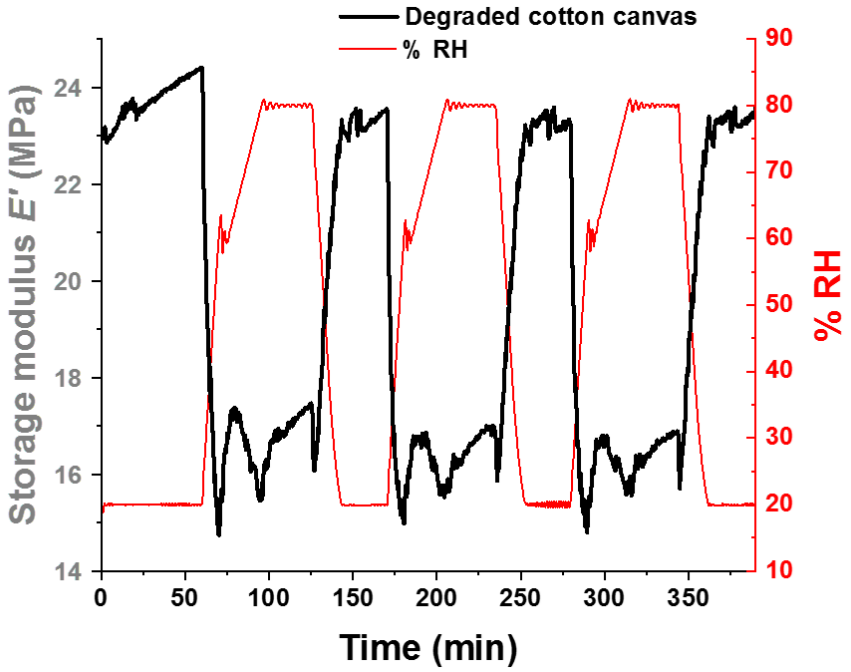

Figure 3.14: Viscoelastic response of a degraded cotton canvas (black) measured in the warp direction by DMA-RH under 20-80-20% RH cycling (red) (i.e.20-80-20%RH program). The response is shown here in terms of response in storage modulus E' (i.e. stiffness) to variation in RH. Note the decrease in stiffness measured upon increase in RH from 20 to 80% RH.

In summary, the elastic response measured by DMA-RH for the degraded cotton canvas can be characterised by the periodic decrease and increase in *E'*, hence in stiffness, upon increase and decrease in RH, respectively. The results are in agreement with the results previously obtained by tensile testing. The canvas becomes less stiff and more viscoelastic at high RH level, here at 80% RH.

3.4.1.4 Overall viscoelastic response and sample deformation measured by DMA-RH

These simple tests have thus shown the suitability of DMA-RH to monitor the mechanical of a cotton canvas to RH. The elastic and viscous responses (given indirectly by and *E'* and *Tan δ*) as well as deformation (i.e. elongation) of the sample exposed to 3 RH cycles could be

measured simultaneously. The curves obtained for these 3 parameters upon 20-80-20% RH cycling are given in Figure 3.15 for the degraded cotton canvas measured in the warp direction. The elastic response of the canvas (i.e. *E'*) is given again for comparison.

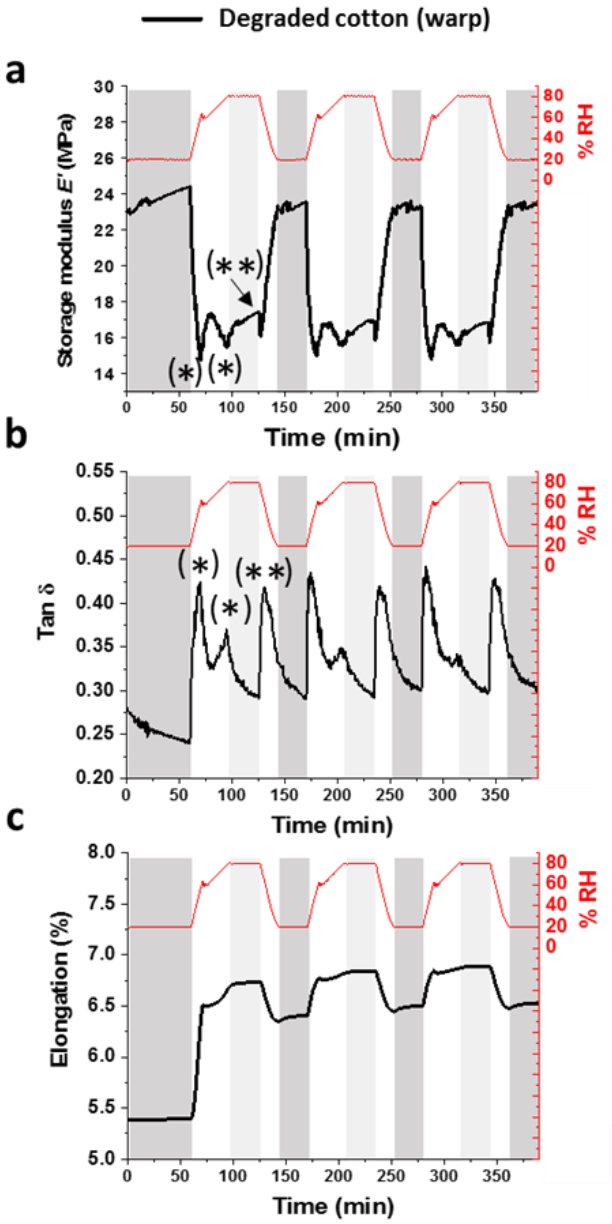

Figure 3.15: Typical mechanical response (storage modulus E' and Tan δ) and response in elongation (% elongation) of a degraded cotton canvas to RH variations. The canvas was measured in the warp direction. Note the small inflexions in the curves occurring at the beginning of each RH transition, humidification (*) and dehumidification (**).

A better understanding of the baseline physical and mechanical response of the degraded cotton to RH cycles can, therefore, only be reached by analysis of both the elastic (*E'*) and viscous (*Tan δ*) components and components of the viscoelastic response to RH as well as the response in elongation.

3.4.2 Detailed analysis of the viscoelastic and response in elongation of a degraded cotton canvas to RH cycles.

To deconvolute the main characteristics of the overall mechanical behaviour of the degraded cotton fabric uniaxially tested by DMA, four points need to be addressed:

- Elongation and creep under RH cycling
- Overall mechanical trend over the 3 RH cycles
- Differences in viscoelastic properties between RH plateaus
- Viscoelastic response during RH transitions

Due to the anisotropic behaviour of fabrics, the degraded cotton canvas was measured in both warp and weft directions. This aims at providing the representative response to RH of a fabric, taking into account discrepancies possibly arising from the weaving direction selected for uniaxial testing.

3.4.2.1 Elongation and creep under RH cycling

The percentage elongation measured in both warp and weft directions for the degraded cotton canvas exposed to 20-80-20%RH cycling is given in Figure 3.16. The curves showing the percentage elongation of the canvas have been zeroed before the application of the preload of 1N (necessary for tensioning the canvas).

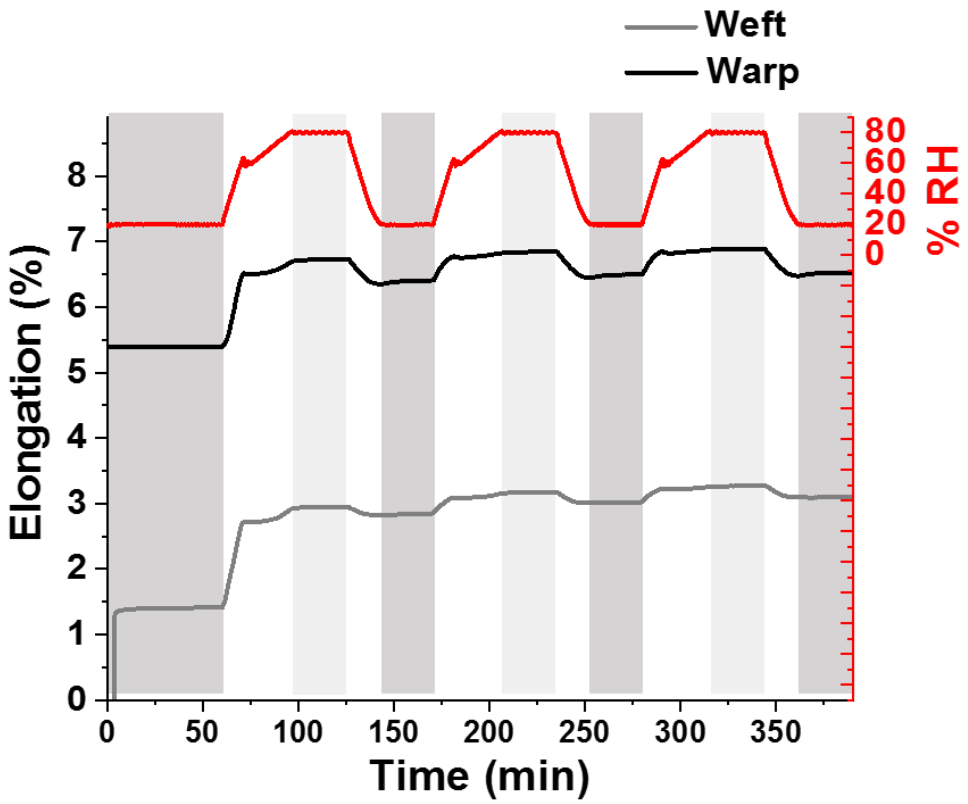

Figure 3.16: Percentage elongation of a degraded cotton canvas measured in weft (grey) and warp (black). The samples were submitted to 3 RH cycles between 20 and 80%RH (red) (i.e. 20-80-20%RH program).

The first increase in elongation is also the larger experienced by the sample and results from the application of the preload (i.e. 1N). Elongations of 5.4 and 1.4% were measured in the warp and weft directions, respectively (see Table 3.1). The higher values measured for the warp direction results from removal of the crimp known to be higher for warp threads than for weft (Collins, 1939). This was also seen previously for the degraded cotton canvas (cf. Figure 3.5).

The second important jump occurs during the first exposure to a higher moisture level, hence during the RH transitions from 20 to 60%RH and then 60 to 80%RH. As seen in Table 3.1, elongations go from 5.4% (20%RH) to 6.5% (60%RH) to 6.7% (80%RH) and from 1.4% (20%RH) to 2.7% (60%RH) to 2.9% (80%RH) in the warp and in the weft directions, respectively. Interestingly, when RH is decreased back to 20%RH, the canvas shrinks but is not restored to its previous elongation. Instead, in both directions, the elongations measured at 20%RH at the end of this first cycle are similar to those measured previously at 60%RH, first RH

cycle (Table 3.1). Increase in elongation at high RH levels (60-80%RH) and shrinkage at low RH levels (20%RH) can also be seen for the 2 following cycles and remains relatively stable. However, complete recovery of the initial elongation never occurs. Irreversible deformation of the degraded cotton canvas seems to have occurred upon application of the first RH cycle.

RH cycle	RH level	Elongation (%)	
		Weft	Warp
Initial	**20%RH**	1.4	5.4
1st cycle	**60%RH**	2.7	6.5
1st cycle	**80%RH**	2.9	6.7
1st cycle	**20%RH**	2.8	6.4
2nd cycle	**20%RH**	3.2	6.8
3rd cycle	**20%RH**	3.3	6.9

Table 3.1: Values in elongation measured for the warp and weft degraded cotton canvas at 20, 60, 80 and 20%RH of the initial part and 1st cycle of the 20-80-280%RH program as well as at 20%RH for the 2nd and 3rd RH cycles. These values correspond to the end-plateau values of each RH isotherms. The response in elongation of the warp and weft samples upon RH cycling is characterised by an important increase in elongation during the humidification step from 20-80%RH. Increase in elongation continues but at a lower rate for the following RH cycles.

This increase could be attributed to the creep of the canvas which corresponds to a time-dependent deformation of a material subjected to constant tension. This phenomenon seems to be amplified here by the use of RH cycling. This has been already described in the past for natural fibres (Chung, 2011) and cellulosic materials such as paper (Alfthan, 2004), wood (Armstrong, 1961; Ranta-Maunus, 1975) and, more recently, nanocellulose (Lindstrom, 2012). This other phenomenon is called mechanosorptive creep. It describes an increase in creep rate under cyclic humidity conditions. The creep rate measured exceeds any constant humidity creep rate within the cycling range. It was suggested that both the mechanosorptive creep undergone by the natural fibres themselves as well as the bonds between them participate to the overall

mechanosorptive creep seen in cellulosic papers made of wood fibres (Olsson, 2007). For nanocellulose papers, hence made of fibres of a smaller size, the governing mechanism of mechanosorptive creep was also found to be predominantly between molecular scales and the length-scales of the fibril diameter and to depend on interfibril bonds and possibly on the fibrils themselves (Lindstrom, 2012).

Because of the internal rearrangement occurring in the canvas samples during the first humidification from 20 to 80 % RH, the mechanical behaviour of the samples during this first phase will often be analysed independently from the rest of the measurements or discarded during future analyses. It is also important to note that the initial mechanical adaptation of the cotton canvas to the stress applied and increase in RH was also observed for the linen canvases tested in this study and might be inherent to woven materials.

In summary, this behaviour in elongation highlights the importance of using variations in RH in the evaluation of materials for conservations. This is because the dimensional, hence mechanical, responses measured for a material subjected to changes in RH can drastically varied from those measured using analyses performed at fixed RH. Mechanical preconditioning of the samples associated with the use of a first RH cycles could be suggested as a method to achieve a more stable state at which the true response of the sample could be measured. This will be later applied in chapter 4 for the study of traditional consolidants.

3.4.2.2 Overall mechanical trend

Prior to the comparison of the viscoelastic of warp and weft directions, it is important to note that the initial reorganisation identified previously by elongation (cf. Figure 3.16) can also be seen in the elastic response of the samples. In Figure 3.17, the response of the sample measured in the weft direction is characterised by a first increase in *E'* occurring during the first increase in RH. This can actually also be seen for the warp sample in Figure 3.15a. After this first increase, the 1st, 2nd and 3rd RH cycles show more repeatability in the mechanical response of the sample.

This confirms the need to assess the viscoelastic behaviour of the samples under RH cycling independently from this first phase.

The overall viscoelastic response of the weft and warp direction upon application of RH cycles is now compared. First, as seen in Figure 3.17, the degraded cotton canvas measured in the weft direction present a higher storage modulus *E'*, 4.5 to 8 times higher, than in the warp direction. This remains valid throughout the measurement and despite the application of the RH cycles and the variations in *E'* previously discussed (cf. 3.4.1.3). Since the storage modulus *E'* defines the stored energy and represents as such the elastic portion of the response of the material to a sinusoidal force (cf. 2.2.4.2 in chapter 2), this result indicates that the weft direction is proportionally stiffer than the warp direction of the canvas. This is because weft threads in plain weave fabric (such as for the canvas used) present lower crimp (Saiman, 2014). This is a result of the weaving process (cf. Figure 1.2a in Chapter 1). For the same preload applied in the experiment (i.e. 1N), the weft direction will stretch less and a higher stiffness will be measured.

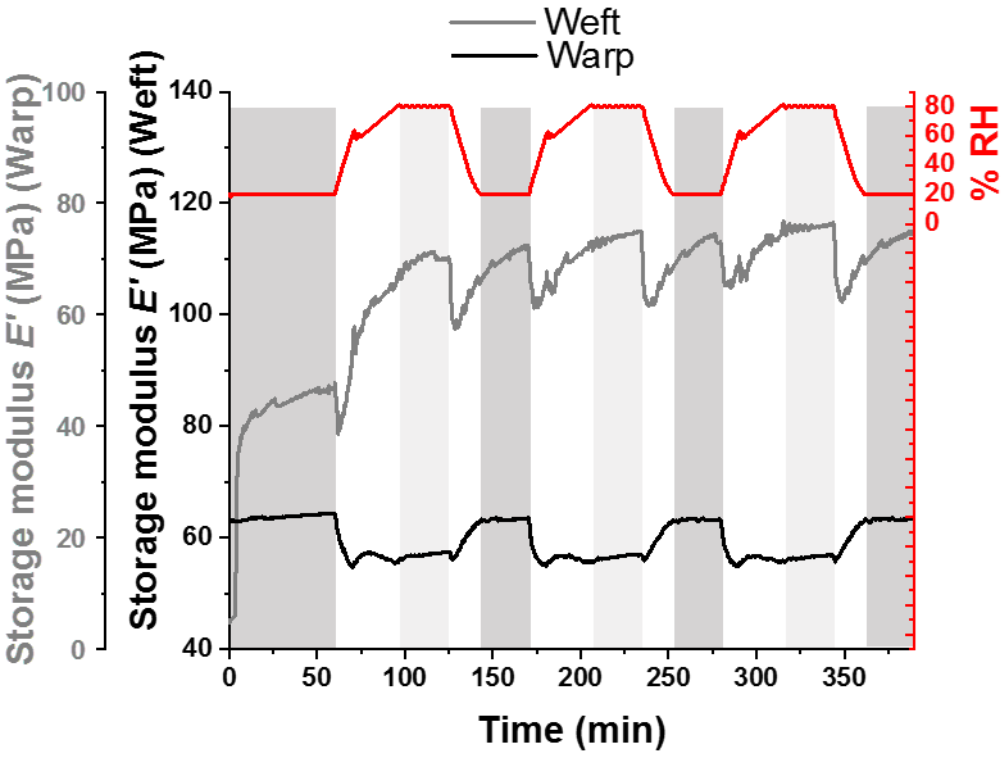

Figure 3.17: Storage moduli E' measured for a degraded cotton canvas measured in both weft (grey) and warp (black) directions upon application of the 20-80-20%RH RH program (red).

The scales of the two E' curves correspond to the same range (i.e. 100MPa) but have been vertically offset for clarity. Note the higher storage moduli measured in the weft over the warp direction.

Second, the mechanical response of the weft sample is also characterised by a period of transition during which *E'* keeps increasing after each successive RH cycles before reaching a stabilisation in trend achieved after 4-5 cycles. The stiffness of the sample, hence the energy stored by the sample while subjected to dynamic load applied by DMA, is increased. This could be seen on longer DMA runs for which 12 RH cycles were applied. Cotton samples measured in the warp and weft were tested (see Figure 3.18). Gradual increase in stiffness followed by stabilisation upon RH cycling was mainly seen for the samples measured in the weft. Interestingly, a similar phenomenon, the so-called hornification effect, has been often observed for paper and cellulose pulp (Borrega, 2010; Crawshaw, 2000; Fernandes Diniz, 2004) as well as for other hydrophilic polymers such as nanocellulose-reinforced Polyvinylacetate (PVA) films (Peresin, 2010). It relates to an increase in stiffness of the material observed upon RH cycling which results, in paper for example, from the formation between cellulosic fibres of partially reversible or irreversible H-bonds after removal of water at low humidity levels. Cellulose fibres might shrink upon drying but this has the beneficial effect of leading to a more intensely bonded structure, more dimensionally stable, and promote higher adhesion between fibres.

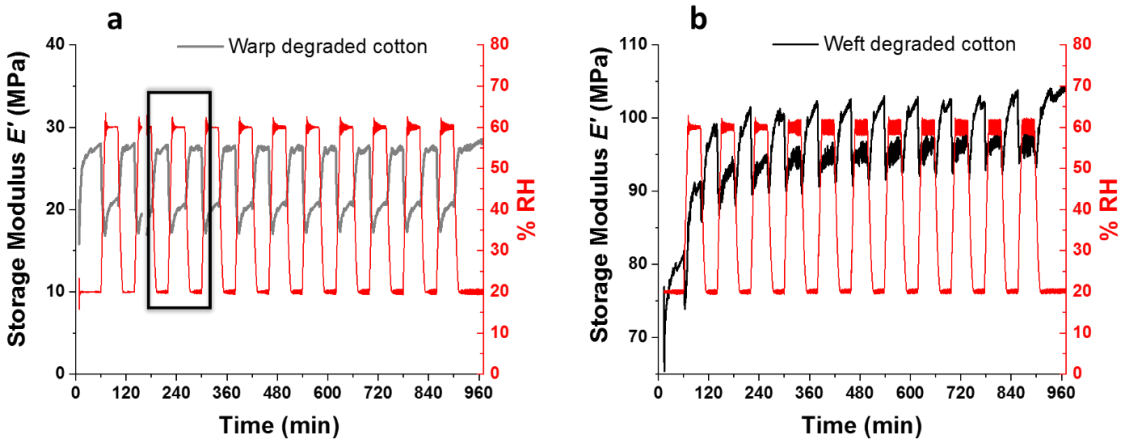

Figure 3.18: Long 20-60-20%RH runs (11 cycles) showing variations in storage modulus E' for a degraded cotton canvas measured in the warp (a) and weft (b) directions. For the weft

sample, a gradual increase in E', independent of the RH level, can be seen. Stabilisation in overall trend only occurs after 3-4 RH cycles. This was not observed for the warp sample which behave similarly throughout the test.

These first comparative results between warp and weft have provided further evidence of the impact the structure has on the mechanical behaviour of the samples. This highlights the importance of the attention to be paid to the weave direction chosen for testing when assessing mechanical properties of fabrics. Finally, it seems that the hornification effect commonly applicable to cellulose-based or hygroscopic non-woven materials, could also take place in cellulose-based woven fabrics.

In the following, further assessment of the mechanical behaviour of the warp and weft samples will be carried out, where the variations in mechanical response between RH plateaus are analysed.

3.4.2.3 Differences in viscoelastic properties between RH plateaus

As seen in Figure 3.14, the viscoelastic response of the degraded canvas in terms of variations in *E'* between high and low RH levels also differs from warp to weft. As previously mentioned in 3.4.1.3, the response of the warp canvas sample is characterised by higher *E'* values, or stiffening, of the canvas at low RH (i.e. 20%RH) and lower *E'* values, hence higher viscoelastic behaviour, at high RH levels (i.e. 80%RH). Variations in *E'* are also reversible throughout the RH cycles. As seen in Figure 3.19, variations in *E'* between 23.6±0.5MPa and 17.0±0.5MPa ($\Delta E'_{20\text{-}80\%RH}$=6.7±0.4MPa) were measured between the 20%RH and 80%RH (average of end plateau values over the 3 RH cycles). In comparison, the variations in *E'* between RH cycles are strongly reduced, almost inexistent, for the sample measured in the weft direction ($\Delta E'_{20\text{-}80\%RH}$=-0.13±2.0MPa).

a

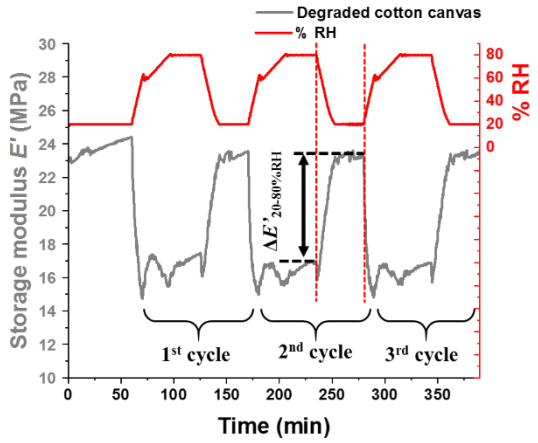

b

Direction of measurement	$E'_{20\%RH}$	$E'_{80\%RH}$	$\Delta E'_{20\text{-}80\%RH}$ (Mpa)	$\Delta E'_{20\text{-}80\%RH}$ (%)
Warp	23.6±0.5	17.0±0.2	6.7±0.4	28.4
Weft	113.5±1.6	113.7±3.2	-0.13±2.0	0.1

Figure 3.19: In (a), variations in E' measured for the degraded cotton canvas (warp direction) showing principles of calculation of the difference in E' measured between 20 and 80%RH plateaus (i.e. $\Delta E'_{20\text{-}80\%RH}$). Storage moduli at 20%RH ($E'_{20\%RH}$) and 80%RH ($E'_{80\%RH}$) as well as $\Delta E'_{20\text{-}80\%RH}$ were calculated as average over the 3 RH cycles (i.e. first 20%RH not included). They are given for the degraded cotton canvas measured in the warp and weft directions in (b).

First, the viscoelastic response of the samples measured in the warp is considered. As previously mentioned, a higher viscoelastic response of the warp sample at high RH level was observed. This is seen in Figure 3.19b by the lower values in *E'* measured at 80%RH. The higher viscoelastic response of the material at high RH was attributed to the plasticization of the material by water. This effect is widely discussed in the literature for bio-polymers (Cheng, 2006; Karbowiak, 2006; Vieira, 2011) including cellulose fibres (Apolinario, 2016; Célino, 2014; Okubayashi, 2004; Symington, 2009). Water molecules are known to bind directly on the hydroxyl groups of the external surface and the amorphous regions of the fibres (fast process) as well as on the inner voids and crystallites (slow process). It is suggested that plasticization of natural fibres occurring at high RH levels is caused by the formation of hydrogen bonds with the water molecules which, thus, replace existing bonds in hemicellulose macromolecular network (Célino, 2014). Additionally, Astley & Donald (2001) showed on a study on flax fibres that this causes the reorganisation of microfibrils inside the fibres during sorption/desorption of water molecules. At high RH levels the material, therefore, becomes more flexible and compliant.

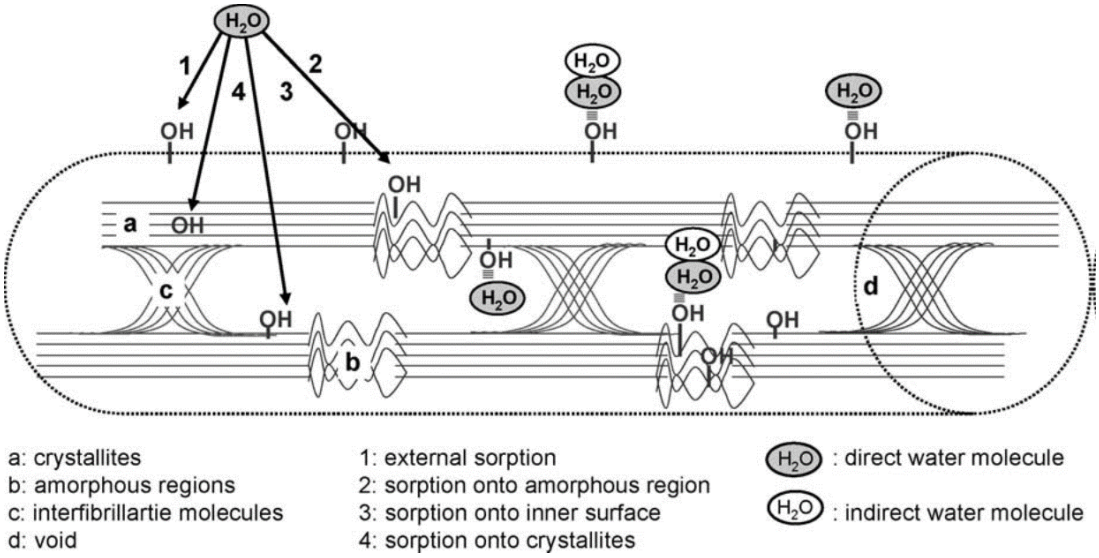

Figure 3.20: A schematic diagram of direct and indirect moisture sorption onto external surface (1), amorphous regions (2), inner surface of voids (3), and crystallites (4) (from* Okubayashi, 2004*).

Second, in view of the behaviour of the warp sample and its underlying causes, the viscoelastic behaviour of the weft sample to RH variations is reviewed. As already mentioned, the degraded cotton canvas measured in the weft direction showed instead of the warp to have a lower viscoelastic response to RH variations. This was seen as lower $\Delta E'_{20\text{-}80\%RH}$ as well as lower $\Delta Tan\delta_{20\text{-}80\%RH}$ seen for the weft sample in comparison for the warp sample Figure 3.15a and b.

This difference was initially associated with the possible lower moisture uptake of the weft threads compared to warp threads and caused by structural differences between threads. Weft thread are usually more tightly packed than the warp threads as a results of the weaving process in which weft threads are hold constantly under tension (cf. Figure 1.2 in Chapter 1). As a result, the total surface area of the weft threads which could be exposed to moisture and facilitate the diffusion of water molecule into the cellulose fibres is drastically reduced. This would have for direct consequence the lower rate of moisture sorption of the weft over the warp threads.

To confirm this assumption, further assessment of the samples using the RH steps program was carried out to resolve the viscoelastic response of the warp and weft sample at different RH levels within the 20-80%RH range.

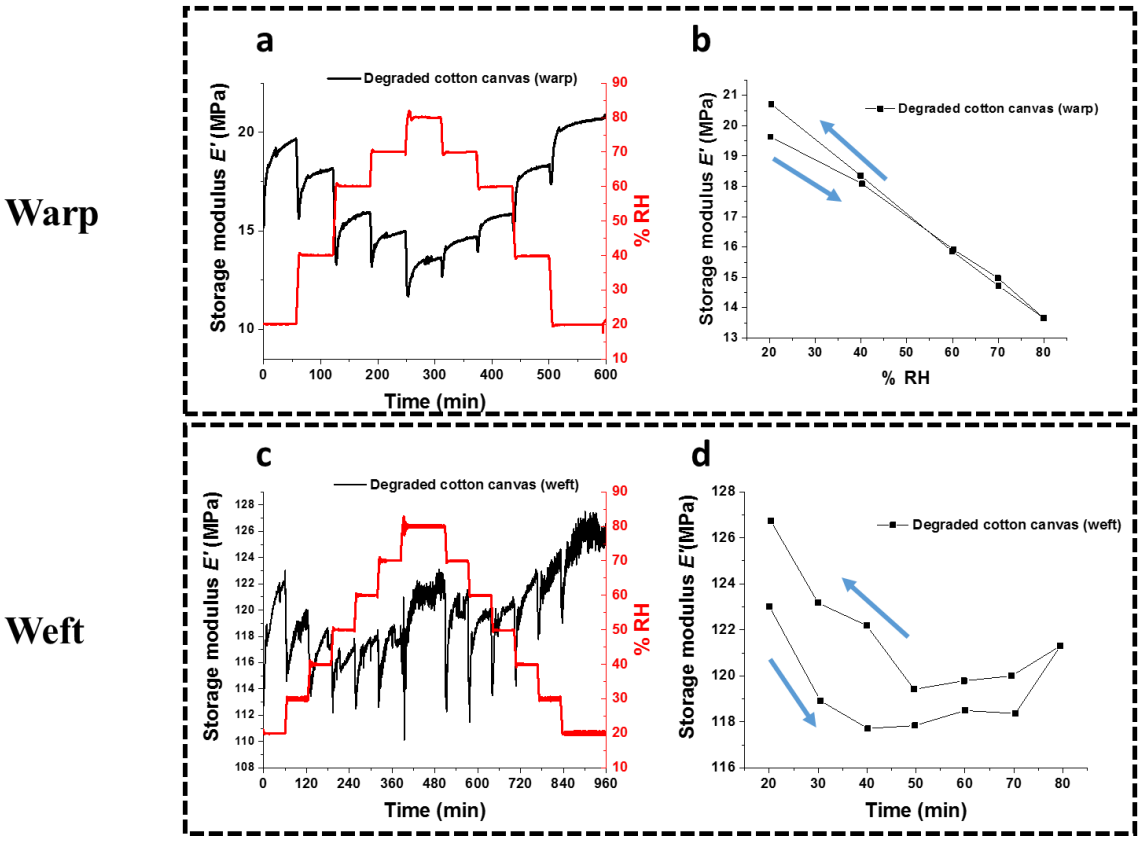

Figure 3.21: Mechanical response of a degraded sample measured in the warp (a, b) and weft (c,d) directions subjected to RH-steps (i.e. 20 to 80%RH, 2%RH/min, 1hour RH plateau every 10%RH). Note the hysteresis (the mechanical response under humidification does not follow the one measured under dehumidification) measured in the mechanical response of the weft sample (d) upon humidification (200-80%RH)and dehumidification (80-20%RH), absent from the warp sample except at 20%RH (b).

Their response, shown in Figure 3.21, however, indicates that the apparent lower mechanical response of the weft sample, in terms of *E'* (i.e. stiffness) under RH variations is the result of an inflexion seen for the mechanical response of the weft sample only. As seen in Figure 3.21, when the degraded cotton canvas is subjected to the RH-steps program with longer exposure to different RH levels, the warp sample decrease linearly following RH increases (i.e. -0.1MPa/%RH in average between humidification and dehumidification). The weft sample instead tends to follow the same trend from 20 to 40-50%RH but stiffens at higher RH, in particular above 70%RH.

The cause of the differences between the warp and weft directions highlighted in Figure 3.21 might be purely structural. It has been previously shown that shrinkage of fabrics relates to the swelling of fibres, hence of the thread. This causes the thread to increase in diameter leading to the consecutive increase in crimp of the threads (Figure 3.3). It is possible that, because of the higher initial diameter of the warp threads as well as their higher crimp, the weft threads are more affected by dimensional changes occurring in the warp threads upon moisture sorption. For an unrestrained canvas this will lead to a shrinkage of the fabric whereas when restrained, the fabric will experience an increase in tension. It is important to note that the mechanical response of the sample measured in the weft direction under RH steps seems to be governed by two independent moisture-related factors. This led to the two separate phases seen in Figure 3.21c. The initial decrease in *E'* measured between 20 and 50%RH is the result of the plasticization of the cellulose through water sorption whereas, between 50 and 80%RH, the mechanical response of the fabric is dominated by structural changes leading to an increase in tension. Where the fabric is held under tension as for the uniaxial measurement performed here, this is seen as an increase in tension.

A hysteresis in mechanical behaviour to moisture uptake/release can also be observed for the weft sample but is absent for the warp sample (Figure 3.21b and d, respectively). Again, this could be related to the hornification effect observed previously in 3.4.2.2 for the weft sample as the step RH program was only applied for one RH cycle. During that first cycle, the response of the weft sample is still mechanically evolving to a more stabilise response to RH variations (Figure 3.18b).

In summary, the results have again highlighted the structural impact of canvas or fabrics on their viscoelastic response to variations in RH. This was shown by the differential response of the warp and weft upon humidification and dehumidification.

From the results, two factors were found to possibly be responsible for the mechanical responses measured for the degraded cotton canvas to RH:

- *Water sorption factor*: cotton fibres hence cotton canvas plasticization by water molecules upon moisture uptake
- *Structural factor*: swelling of the threads caused by the swelling of the cotton fibres upon moisture uptake

The warp showed a linear mechanical response to moisture uptake and release characterised by a loss in stiffness at high RH levels. The response of the warp showed to be mainly governed by the water sorption factor. For the weft sample, instead, the two responses to moisture, physical and structural, previously described seem to compete. The weft sample behaved non-linearly with a 2-phases humidification step including a first phase of plasticization of the canvas (i.e. increase viscoelastic behaviour) followed by stiffening of the canvas. In that sense, the response measured for the degraded cotton canvas in the weft direction is very similar to the one observed for a linen canvas (direction unknown) by Mecklenburg (2007). However, it is interesting to notice that this mechanical behaviour on humidification/dehumidification could not be observed for the cotton canvas measured in the warp direction.

Overall, these results have showed that the study of the mechanical response to RH variations of fabrics could not be reduced to the simple and unique chemical, physical or structural causes but rather a combination of several factors.

It is not known how the warp and weft directions of the degraded cotton canvas measured would have mechanically behaved similarly under biaxial testing because of the limited access to the technique (cf. 1.1.3.1). It would be, however, interesting to whether an important stiffening of the canvas could have been observed for the warp sample of the degraded cotton canvas as well.

3.4.2.4 Viscoelastic response during RH transitions

Another feature of the curves in Figure 3.15 can be seen during the RH transitions. During both the humidification (20 to 80%RH) and dehumidification steps (80 to 20%RH) a rapid loss followed by a recovery in *E'* (indicated by (*) and (**) in Figure 3.15a) is seen for the degraded cotton canvas in both warp and weft. These features are shown in more details in Figure 3.22A where the warp and weft response of the degraded cotton sample exposed to reduced RH variations (20-60%RH instead of 80%RH, cf. 20-6-20%RH program in 3.3.2.2) is presented. A similar rate of RH increase and decrease (i.e. 4%RH/min) was chosen to enable the comparison of the mechanical response of the sample to moisture sorption and desorption. The viscoelastic behaviour of the samples will be discussed with regards to variations in storage modulus (stored energy) and Tan δ (dissipated energy) (cf. 2.2.4.2 in Chapter 2). The curves show the behaviour measured under the 3rd RH cycle.

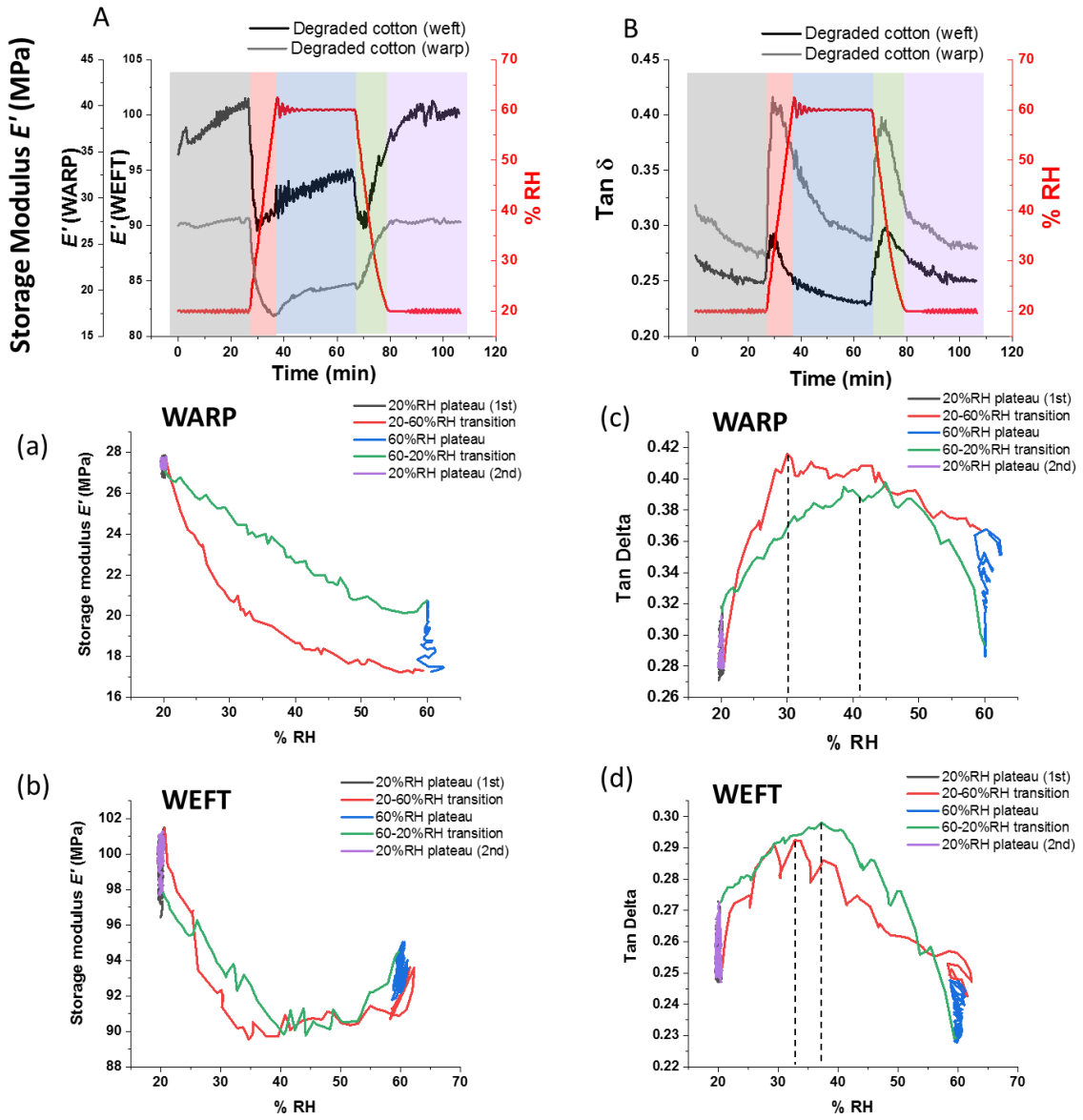

Figure 3.22: Detail of the mechanical response of a degraded cotton canvas measured in the warp and weft directions. The storage modulus E' (A) and Tan δ (B) were measured for a 20-60-20%RH cycle (3rd cycle of the measurement). In (a) and (b), the variations in E' shown in (A) have been plotted vs RH for warp (a) and weft (b). In (c) and (d), the variations in Tan δ shown in (B) have been plotted vs RH for warp (c) and weft (d).The graphs highlight the differences between warp and weft and the inversion in behaviour occuring during the RH transitions.

As seen in Figure 3.22A and B, the inflections in *E'* previously highlighted in Figure 3.15 for the warp sample are also seen in the Tan δ curve of the same sample for both humidification (20-60%RH) and dehumidification (60-20%RH). Interestingly, for the weft sample, instead, the

inflexion is absent from the *E'* curve during dehumidification. However, the inflexion is seen in *Tan δ* which supports the assumption that both warp and weft behave in a similar way to moisture transitions.

In Figure 3.22a-d, the variations in *E'* and Tan δ are plotted against RH. In Figure 3.22b (weft direction), the rapid loss in *E'* occurs at the beginning of the 20-60%RH and 60-20%RH transitions and it also associated with an increase in Tan δ, hence an increase in potential of energy dissipated. The mechanical recovery of the fabric then seems to occur between 30 and 50%RH where the inflexion in the curves is seen. For the warp sample, the same trend seems to occur as seen by the inflexion in Tan δ seen in the RH range (Figure 3.22c) and despite the absence of inflexion in the curve of *E'* (Figure 3.22a).

To understand the reasons for the mechanical behaviour of the fabric, it is important to remember the principles of moisture sorption in fabrics and in cotton and/or other natural fibres. Figure 3.23 (left side) shows the water uptake measured for a degraded cotton canvas exposed to 60%RH at 25°C. It has been shown that moisture sorption kinetics in highly hygroscopic natural fibres, such as wool or cotton, follows a two stage sorption process (Li, 2000) indicated in Figure 3.23. First, it involves a Fickian-diffusion process strongly dependent on moisture content of the fibres of the fabric (Fickian diffusion is define as a law of diffusion described by equation (1) in Figure 3.23). It is then followed by a slower process, a non-Fickian diffusion that is associated with fibre structural changes. Both of these diffusion processes lead to the overall increase, first rapid then slower, of the amount of absorbed water in the fibres.

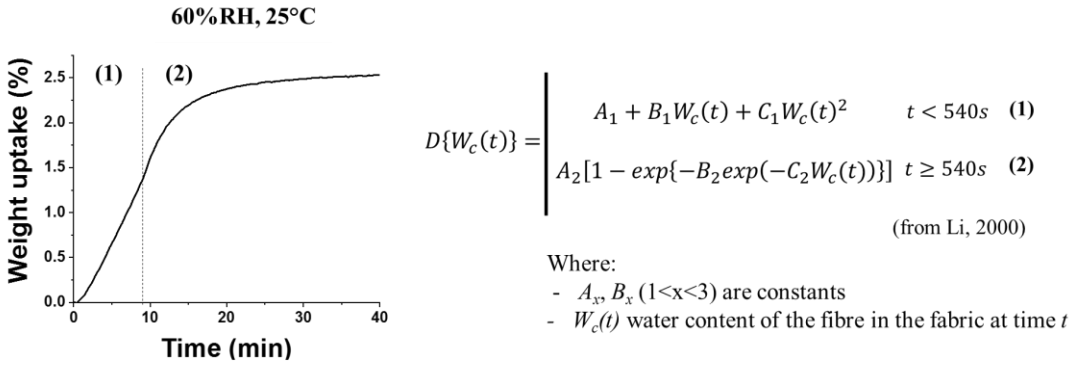

Figure 3.23: On the left, plot of the percentage moisture uptake measured for a degraded cotton canvas exposed to 60%RH (25°C). The increase in moisture uptake is characteristic of the behaviour of highly hygroscopic fibres in fabrics* (Li, 2000). *It shows a two stage sorption process described by the two equations given on the right. These equations are derived from those established by Li (2000) for wool and cotton. Li showed that fast diffusion occurs in the first stage (t<540s) and it then followed by a slower diffusion process. Diffusion is also strongly dependent on water content of the fibre, i.e. $W_c(t)$.

Interestingly, the increase in moisture content measured for the degraded cotton canvas is similar to the increase in *E'* measured during the 20 and 80%RH RH plateaus (see Figure 3.22A). This can be seen in Figure 3.24 where both weight uptake and *E'* measured for the degraded cotton canvas equilibrating at 60%RH (25°C) is shown. The canvas had been previously preconditioned at 20%RH. Both the curves of weight uptake and *E'* are characterised first by a fast increase followed by a lower increase.

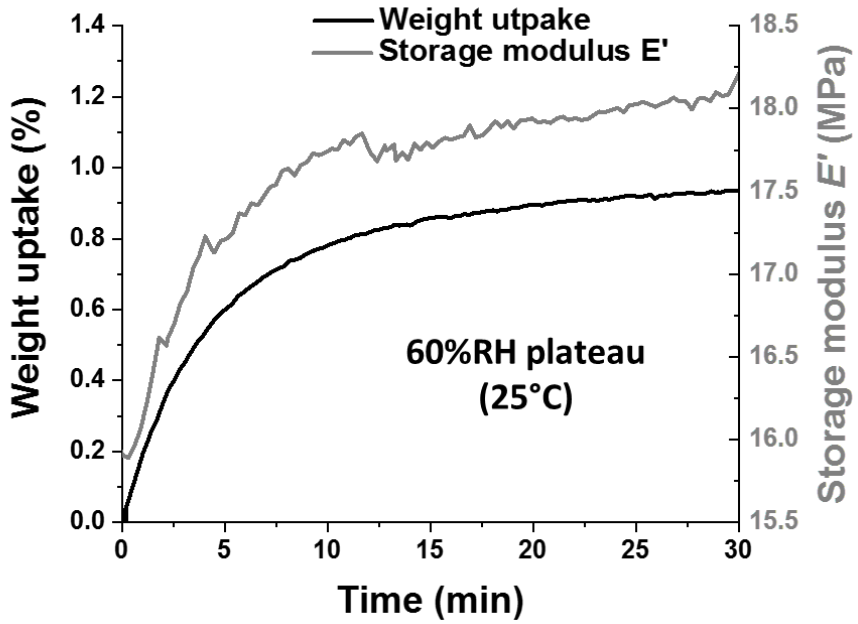

Figure 3.24: Weight uptake (DVS data) and storage modulus E' (DMA-RH data) measured for a degraded cotton canvas equilibrating at 60%RH (25C). The canvas was previously left equilibrating for 1hour at 20%RH. This is the its response for the first exposure to 60%RH. Similar increases can be seen for both curves.

This suggests that upon stabilisation of RH after the RH transitions, the mechanical response of the cotton fabric might be directly related to moisture uptake and moisture content of the fibres of the fabric. The inflexions seen in Figure 3.22a-d for the curves in *E'* and *Tan δ* of the canvas during RH transition are therefore unexpected as they do not follow the increase or decrease in RH to which they are subjected. This highlights the existence of another phenomenon competing with the kinetics of moisture sorption/desorption previously described and could be associated to the high rate of change in RH used. It is assumed that during the RH increase, given the high rate used 4%RH/min, there is more moisture than the sample can initially absorb. Non-absorbed water molecules penetrate and enter the free-spaces between canvas fibres, accumulate unbound on the surface of the fibres and act there as a lubricant for the threads and fibres of the canvas. Water facilitates internal movements and rearrangements of the threads/yarns leading to the fast apparent loss in *E'* and increase in Tan*δ* measured at the beginning of the RH transitions (i.e. inflexions in the curves in Figure 3.22). This heterogenous distribution in water content in

cotton fibres was also mentioned by Li (2000) who showed that it increases with the degree of the fibres' hygroscopicity. After the initial loss in *E'* (and increase in Tanδ), the canvas sample then recovers with a small stiffening as it tries to reach equilibrium at 80%RH or 20%RH. This leads to an apparent limitation of the DMA-RH test as designed for this study, which is that when dealing with real samples, these inflexions may not occur. The response here measured during RH transitions is characteristic of the high RH rate chosen. RH changes in museums or galleries would occur at a much lower rate.

Finally, the mechanical behaviour of the samples during RH transitions is also characterised by the hysteresis in *E'* observed for the cotton canvas measured in the warp direction (Figure 3.22a). This differential response during moisture sorption and desorption seems in agreement with the known hysteresis in moisture uptake measured upon absorption/desorption for fabric made of natural fibres (Hill, 2009) and also measured for the degraded cotton canvas (see Figure 3.11). Interestingly, this was not seen for the sample measured in the weft direction and could be an indication of differences in the chemical composition of the warp and weft threads existing prior to degradation and/or resulting from degradation. This could be, for example, traces of sizing agent often only applied on the weft threads to ease the weaving process (Farag, 2009; Hedley, 1993a; Tobler-Rohr, 2011) but not on the warp and not entirely removed upon degradation of the canvas.

In summary, the inflexions observed in both warp and weft in the viscoelastic response of the samples to RH transitions were found to most probably result from slippage of the canvas threads and fibres caused by unbound water. The mechanical response of the samples stabilises rapidly during RH transition and was maintained upon RH stabilisation at each RH plateaus. The viscoelastic response measured here during RH transitions should not, however, be considered as characteristic of cotton canvases. The inflexions observed are most probably specific to the RH program selected for the tests with fast rates in RH increase/decrease. The observations made on the untreated degraded canvas will later be used for the comparative studies presented in the

following chapters on consolidants for painting canvases and will help decoupling the mechanical response of the canvas from those of the treatments.

3.4.3 Role of canvas weave structure, pretreatments of the fabric and canvas material on the overall viscoelastic behaviour of the degraded cotton canvas.

3.4.3.1 Role of yarn and thread on fabric mechanical behaviour

The objective was here, first, to deconvolute the role of the woven structure of the canvas on its overall viscoelastic response to RH fluctuations from the impact of other parameters such as the canvas material. Individual canvas threads and yarns (cf. canvas structure in Figure 1.2c in Chapter 1) of the cotton degraded fabric were measured.

The results presented in Figure 3.25 show that the mechanical response of the yarn and thread measured in the warp direction are similar to the one of the cotton fabric. Between 20 and 60%RH, the yarn, thread and canvas measured along the warp direction stiffened at a lower humidity level (higher storage modulus *E'*) while becoming more viscoelastic at higher humidity levels (lower *E'*). Moreover, the inflection and recovery in *E'* seen during RH transitions for the cotton fabric in 3.4.2.4 (Chapter 3) could also be seen for yarn and thread. This phenomenon had been attributed to internal slippage of the yarn and thread during the humidification and dehumidification transitions and is supported by these additional findings. However, the fact that it is now seen for both the yarn and threads indicate that internal motions in the canvas could also occur on a much smaller length scale, possibly between the individual cotton fibres.

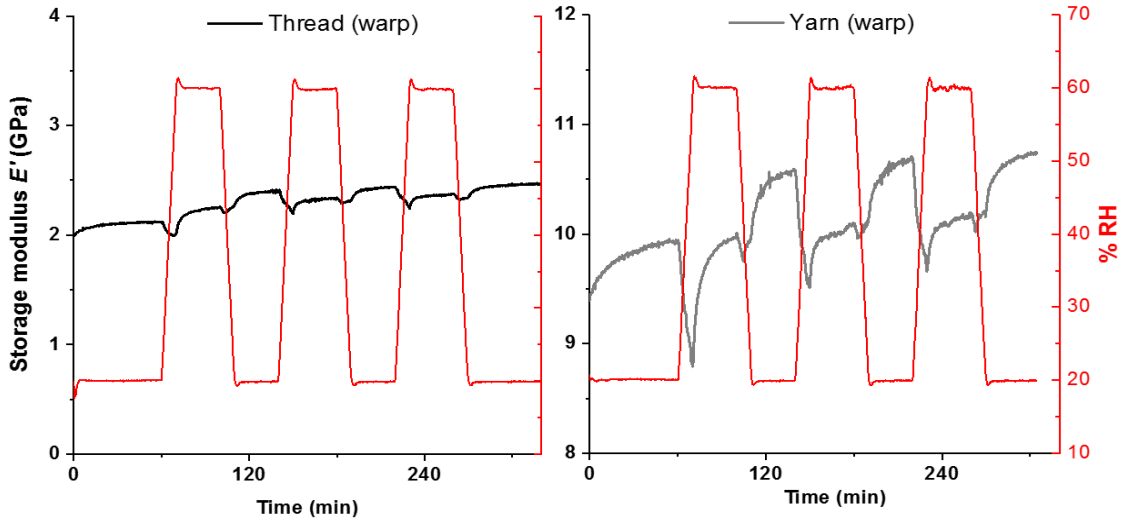

Figure 3.25: Response of a cotton thread (i.e. 2 interlaced yarns) (on the left) and a cotton yarn (on the right) from the warp direction to RH variations.

In summary, the general viscoelastic response to moisture of the cotton canvas does not seem strongly related to the yarn and thread as both of them appear to respond similarly to the canvas when subjected to variations in RH. This suggests that parameters such as number of yarns per thread and number of fibres per yarn are not responsible the overall viscoelastic response of the canvas characterised in the warp by plasticization of the canvas at high RH level. The results also indicate that the argument whereby slippage of the threads might cause the inflexions seen in the DMA-RH curves during RH transitions (cf. 3.4.2.4) should be discarded. Indeed, inflexions could also be seen for both yarn and threads during the RH transitions. Unfortunately, it was not possible to investigate whether yarn structure, such as the yarn twist, might be causing these specific features. Further analyses are thus required to understand which parameters may play a strong role in the response of the canvas to moisture variations. Single fibre work could provide meaningful information. In the following section, the impact the degradation step might have had on the viscoelastic response of the canvas to RH variations is explored.

3.4.3.2 Canvas washing and degradation: their impact on canvas properties.

3.4.3.2.1 Viscoelastic response to RH variations

DMA-RH was used to investigate the impact of canvas preparation, hence washing and degradation, on the mechanical properties of the cotton canvas. An untouched (i.e. as received from the shop), a washed and a degraded cotton canvas were tested to evaluate whether the behaviour measured for the degraded canvas was characteristic of the canvas or the result of the degradation/washing process.

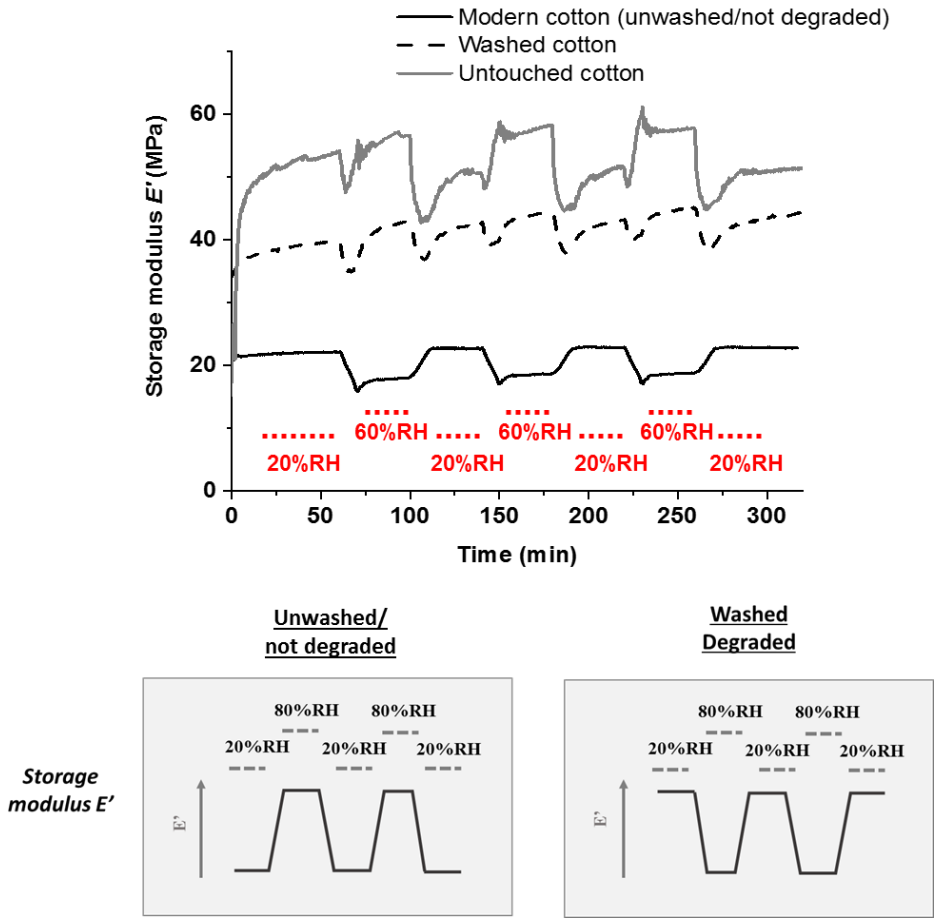

Figure 3.26: Storage modulus and elongation measured for a modern cotton canvas before washing/degradation (grey) and a washed (black dotted line) and a degraded cotton canvas (black solid line) submitted to 3 RH cycles (20-60-20%RH) (red).

The results show that the response of the cotton canvas before degradation is inverted in comparison with the response measured after degradation. As it can be seen in Figure 3.26, the response of the 3 samples to 20-60-20%RH cycle in humidity differ. While the response of the

degraded sample is characterised by the stiffening of the fabric (increase in *E'*) at 20%RH and plasticization at 60%RH, the untouched sample presents the opposite behaviour, i.e. stiffening at 60%RH and plasticization at 20%RH. The effects of this inversion can already be perceived for the washed canvas for which the storage modulus measured at 20 and 60%RH is very similar throughout the RH cycles. In Table 3.2, the average differences in *E'* ($\Delta E'_{20\text{-}60\%RH}$) measured after the first cycle between 20%RH and 60%RH (end plateau value in *E'*) are – 7.5±0.5MPa, -1.2±0.8MPa and +5.8±0.3MPa for the cotton canvas before washing/degradation, the washed and the degraded cotton canvases, respectively.

Cotton canvas	***E'$_{20\%RH}$ (MPa)***	***E'$_{60\%RH}$ (MPa)***	***ΔE'$_{20\text{-}60\%RH}$ (MPa)***	***ΔE'$_{20\text{-}60\%RH}$ (%)***
Before washing/degradation	50.4±1.1	57.6±0.7	-7.5±0.5	*-14.9%*
Washed	42.9±0.3	44.1±0.1	-1.2±0.8	*-2.8%*
Degraded	22.7±0.3	16.0±0.3	5.8±0.3	*+25.6%*

Table 3.2: Storage moduli measured at 20 and 60%RH averaged over the 3 RH cycles and calculated variations in E' (i.e. ΔE'$_{20\text{-}60\%RH}$) in MPa and % measured between the 2 RH levels for unwashed/not degraded, washed and degraded cotton canvases.

Two causes could be responsible for the changes in mechanical behaviour observed:

- Removal of compounds present on/in the cotton fibres
- Structural modification of the woven fabric, e.g. shrinkage

3.4.3.2.2 Removal of compounds present on/in the cotton fibres

The first cause of these changes could be the removal of some compounds which are commonly added to fabrics during the manufacturing processing. At that point, the threads, especially the weft, are often sized in order to ease the weaving process by improving their abrasion, reducing their hairiness and increasing their strength (Farag, 2009; Hedley, 1993; Tobler-Rohr, 2011). In more modern production methods, substances such as natural starches or synthetic waxes, polyvinyl alcohol or carboxymethyl cellulose can be used as sizing agents for

cotton in the textile industry (Schlüter, 2011). The presence of additives to the fabric was first confirmed by contact angle measurements. As seen in Figure 3.27, a droplet of water deposited onto the untouched canvas was not absorbed after 120s whereas it was totally absorbed onto the washed and degraded canvas after 53s and 7s respectively. The higher contact angle and longer time for water absorption measured for the not washed/not degraded cotton canvas is an indication of the lower surface energy between the surface of this sample and water and lower wettability of the canvas. After degradation, the initial contact angle was immediately reduced from 150° to 125° indicating the increased wettability of the degraded surface. The results thus indicate that the sizing agent present on the canvas threads renders the cotton canvas or threads more hydrophobic. Water cannot wet the canvas surface and as a result cannot reach the spaces between the fibres and spread along the fabric via capillary pressure, a phenomenon also called wicking (Das, 2007).

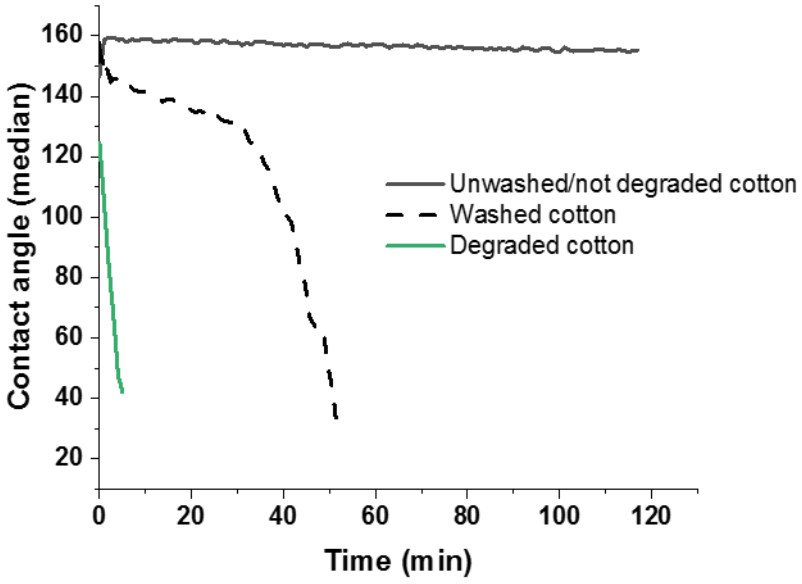

Figure 3.27: Contact angle of unwashed/not degraded, washed and degraded cotton canvases (35%RH, 25°C)

Further analysis of the surface modification of the canvas was performed using XPS. The quantitative characterisation of the surface chemical composition of the samples was obtained from the relative amount of each type of carbon-other atom interactions (C(1s)) and from the O/C

atomic ratio. The characteristic signature of cellulose consists of the C–O and O–C–O bonded carbon atoms, which correspond in XPS spectra to peaks at binding energies of 286.6 eV and 288 eV, respectively, with a relative intensity of 5:1 (Johansson, 2004; Soignet, 1976). However, non-cellulosic C–C carbon is always present due to the presence of impurities, which have been previously mentioned and detected on other cotton fabrics (Mitchell, 2005) such as fatty acids, alcohols, alkanes, esters and glycerides.

The results (Table 3.3) show an increase in the O/C ratio between the untouched and the washed sample from 0.14 to 0.21 as well as between the washed and the degraded sample from 0.21 to 0.30. This increase is likely to result from the removal of impurities present on the canvas surface as, theoretically, pure cellulose exhibits a O/C ratio of 0.83 (Ly, 2008). The surface concentration of these impurities could be reduced but even after bleaching or scouring of the fabric, non-cellulosic material residue could still be detected. This removal can be followed by the reduction in intensity of the carbon peak found at the binding energy 285.0eV and which correspond to C-C and C-H bonds. The area of the peak, assigned by deconvolution to 285.0eV, decreases from 79.17% calculated for the untouched canvas to 72.47% and 53.32% for the washed and degraded canvas, respectively (see Table 3.3, Figure 3.28).

Sample	O/C	C(1s) binding energy (eV)				
		285	286	286.6	288.1	**289.0**
		C-C or C-H	C-COO(-)	C-OH or C-O-	O-C-O or C=O	**O-C=O(-)**
Before washing/ degradation	0.14	74.9	0	17.89	5.1	**2.2**
Washed	0.21	67.5	0	23.2	6.4	**2.9**
Degraded	0.30	47.1	3.8	35.9	9.5	**3.8**

Table 3.3: XPS data of the modern cotton canvas before washing/degradation and after washing (Washed) and ageing (Degraded) steps.

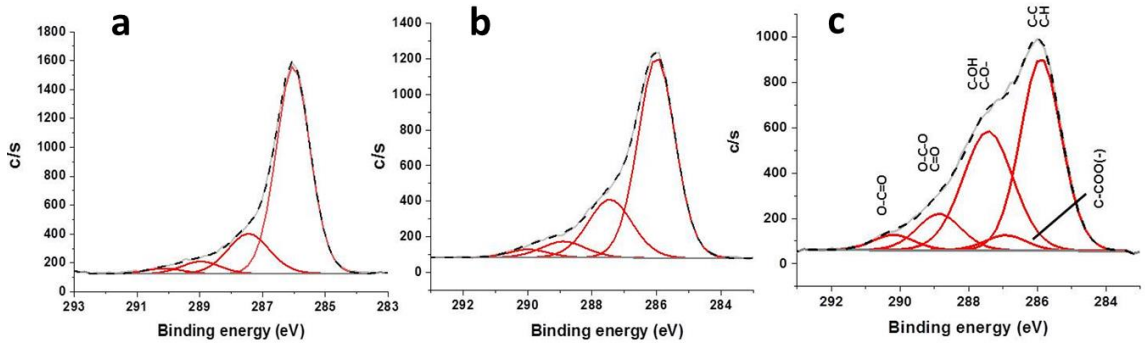

Figure 3.28: XPS spectra (in grey) of the modern cotton canvas before washing/degradation (a) and after washing (b) or degradation (c) with the deconvolution curves (in red) and the resulting fitting curve (in black).

It is not clear whether the impurities removed from the canvas are inherent to the cotton used or to the manufacturing process (e.g. cellulose wax often used in the weaving process) (Taylor, 1997). It was, for example, previously reported that upon drying from water, surface adaptation of cellulose occurs to minimize its surface free energy. This results in the adsorption of a high amount of air-borne contaminants on the surface, seen as the C–C carbon peak in XPS data (Johansson, 2011). After washing/degradation, the washed and degraded cotton canvases do seem thus to offer a purer cellulosic surface (i.e. with less non-cellulosic impurities) as indicated by the increase of the spectral intensity at 286.6eV attributed to C-O bonds but traces of residues

remain. Since XPS is a surface technique, it was not possible to determine the exact amount of impurity elimination upon washing and accelerated ageing.

Finally, the degradation procedure used appears to also modify the chemical structure of the cotton canvas cellulose. The formation of carboxylic acid species at the canvas surface, seen at a C(1s) binding energy of 289.0 eV, suggests that as oxidation and acid-catalysed chain scission increases with treatment time, carboxyl groups are formed (Seery, 2013) on the cellulose backbone. This was expected from the design of the experiment (Oriola, 2015) and was confirmed by XPS analysis.

3.4.3.2.3 Structural modification of the woven fabric

Another cause for the modification of washed and degraded canvas mechanical behaviour the shrinkage of the canvas upon wetting. During the washing and degradation steps, no mechanical restrictions such as clamping were applied on the cotton canvas. This caused upon wetting and drying a visible shrinkage of the canvas (10% and 5% in the warp and weft respectively after degradation). It could be assumed that after washing or degradation, the canvas has already reached its relaxed dimensions, meaning that the fabric will not shrink further as a result of wetting and drying (Technical bulletin Cotton Incorporated, 2004). The yarns do not change in diameter as much as before and the crimp of warp and weft threads remain unchanged. As a result, the mechanical behaviour observed for the washed and degraded canvases does not rely on the canvas morphology and weaving as much as before. It can be assumed that this behaviour might mainly translate the response of the material itself (i.e. the cotton) to moisture as well as the movement of water (causing for e.g. slippage, cf. 3.4.2.4).

Finally, while the mechanism underlying the shrinkage of textiles (see 3.1) is well accepted, another additional and less predictable type of response of canvas called relaxation shrinkage can also occur in fabrics. It is triggered by the release of internal stress in the fabric, incorporated during its manufacture (Andersen, 2009). It is sometimes associated to crimp exchange (i.e. one direction taking up the crimp of the other direction) for textiles with low crimp warp (Collins, 1939). This was not observed after neither washing nor degradation for the cotton

canvas tested. However, it is possible that this mechanism of shrinkage might have also taken place as the cotton canvas was unrestrained and internal rearrangements were free to occur during washing and degradation.

These results are particularly interesting as they tend to show that mechanical behaviour of cotton canvases, and probably any other canvas made of natural fibres, can strongly differ depending on past treatments and the use of water. For painting conservation, this implies, first, that each conservation treatments used should be carefully reported, second, that each painting should be considered as unique and its constitutive materials, among which the canvas, should be studied individually. If mechanical assessment of the canvas cannot be performed, it will be important to get technical information such as weave density, canvas/thread material and weave geometry and, if available, to know the year at which the painting was made (i.e. year the canvas might have been produced) and the techniques of support preparation that could have been used by the artist. This information can be used to define approximatively the mechanical behaviour of the canvas being conserved using the results of studies performed on canvases with known structural characteristics (Mitchell, 2005; Penava, 2016; Young, 2012b; Young, 1999)

3.4.3.3 Differences between degraded cotton and linen canvases

3.4.3.3.1 Response to RH cycling

It has been previously noted in 3.4.3.1, that the woven structure of the canvas does not seem to play an important role in the response measured in the warp upon RH cycling for the degraded cotton canvas. To investigate how the material of canvas can influence the response of the canvas, the degraded cotton canvas was here compared to a modern linen canvas. Both were again measured by DMA under RH cycling.

Linen is a material made from flax fibres. The structure of the flax fibres resembles the one of cotton fibres with primary and secondary walls made of cellulose, hemicellulose and lignin. The proportions of these 3 compounds in each wall vary between cotton and flax (Buchert, 2001; Jiang, 2019; Meinert, 1977). The main difference between flax fibres (similar to bast fibres) and

cotton fibres is that they are obtained from the stem in the form of long filaments, each of which is made up of cells, whereas cotton fibres are single plant cells (Hock, 1942). As a result, the mechanical properties flax and cotton fibres also differ. Yet, flax fibres show higher Young's modulus, tensile strength and lower elongation at break than cotton fibres (Célino, 2014).

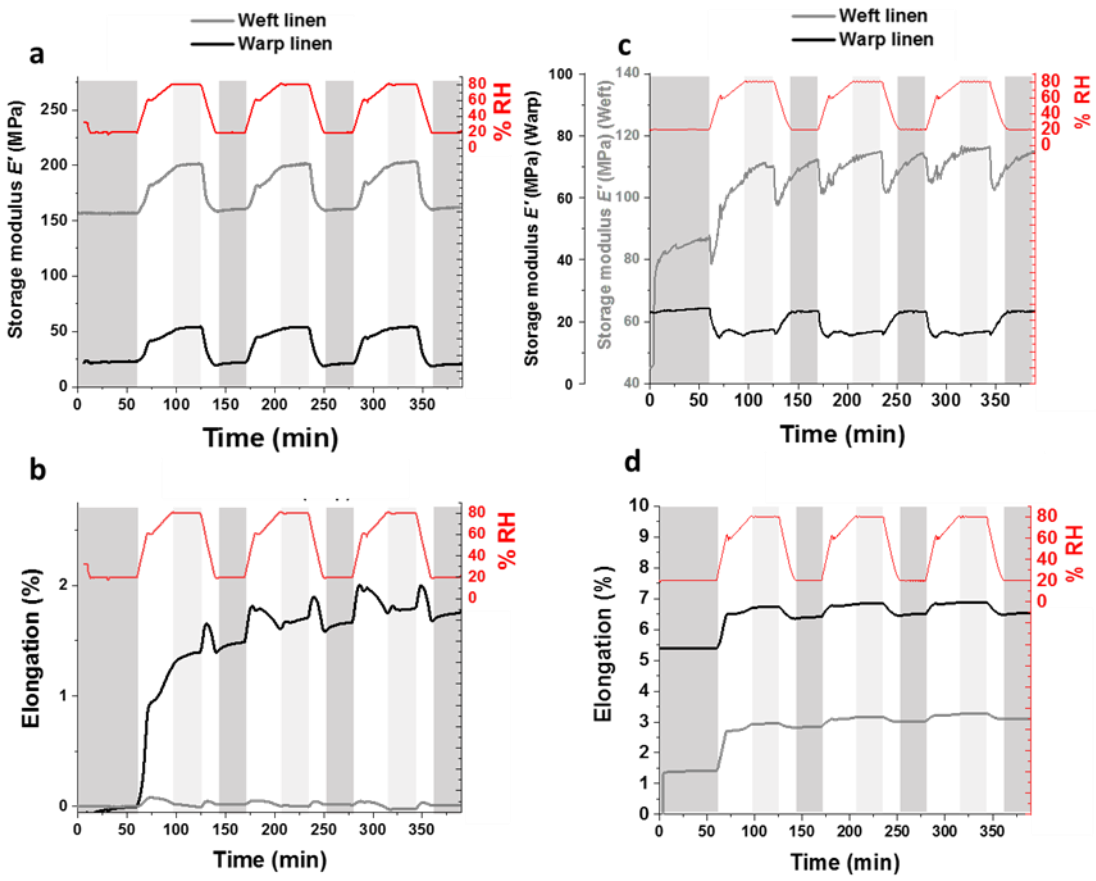

Figure 3.29: Mechanical (storage modulus E') and response in elongation in warp (black line) and weft (grey line) of a modern linen canvas (a,b) and the degraded cotton canvas (c,d) subjected to the 20-80-20%RH RH program (25°C).

Figure 3.29 shows the mechanical (a) and dimensional (b) response of a modern linen canvas to RH cycling (20-80-20%RH) in both warp and weft directions (a) compared to the response measured for the degraded cotton canvas (c and d) already shown in Figure 3.16 and Figure 3.17.

Variations in *E'* following RH cycling can be seen for both the cotton and the linen canvases. Surprisingly, contrary to the cotton canvas (cf. 3.4.1.2), the linen canvas does not show

a higher viscoelastic behaviour (i.e. loss in storage modulus *E'*) at higher RH levels. The linen fibres are not plasticised by the water diffusing in the amorphous regions of the fibres. On the contrary, the response of the modern linen canvas to RH cycling is characterised, in both warp and weft, by a loss in stiffness at low RH level (i.e. 20%RH) and increase in stiffness at high RH level (i.e. 80%RH). As such, Figure 3.29 highlights the opposite mechanical behaviours to RH cycling of the cotton and linen canvas.

Notably, this does not agree with what is reported in the literature. Symington (2009) as well as Davies (1998) noted a significant decrease in Young's modulus, hence decrease in stiffness, of flax fibres upon humidification. A decrease in Young's modulus about 23% was measured upon an increase in RH from 30 to 80%RH (Davies, 1998). Stiffening upon increase in RH was, however, observed for other natural fibres such as hemp, kenaf or jute (Symington, 2009). This increase was, however, always followed by plasticization of the fibres at high RH level, i.e. 90%RH, or upon complete immersion in water. The first stage of stiffening was attributed to fibres swelling which activate rearrangement of the microfibrils and the surrounding molecules acting as a matrix (Placet, 2012). The radial tension created lead to the increase in fibres' Young's modulus. After a certain degree of swelling the fibres become more vulnerable and hence a lowering in mechanical properties occurs seen by the loss in stiffness (Baley, 2002).

It also possible that the viscoelastic behaviour of the linen canvas measured in this study might not only be governed by the canvas material but also by the structural characteristics of the canvas. It has been shown that closely woven canvas with little separation between the yarns will by the same mechanism shrink more easily than a loosely woven canvas (Andersen, 2009). This is because there is less interfibres free space to take up for the swelling fibres in a compact yarn. Yet, the cotton canvas presents threads with a larger diameter, lower crimp of the threads, looser weaving (lower inter-threads spaces) than the linen one (see Figure 3.5). These structural differences are also shown highlighted by the values in elongation reached after application of the same preload on both canvases (i.e. 1N). As it can be seen in Figure 3.29d (cotton) and Figure 3.29b (linen), after 3 RH cycles, the cotton samples elongated by 8 and 4% for the warp and weft

respectively whereas for the linen canvas, elongation remains below 2% and 0% for the warp and weft directions, respectively. Due to the looser structure and the lower crimp of the threads of the cotton canvas, upon the application of a pre-tensioning load more movements will occur between threads, yarn or even fibres and will cause the cotton canvas to elongate more than the linen canvas.

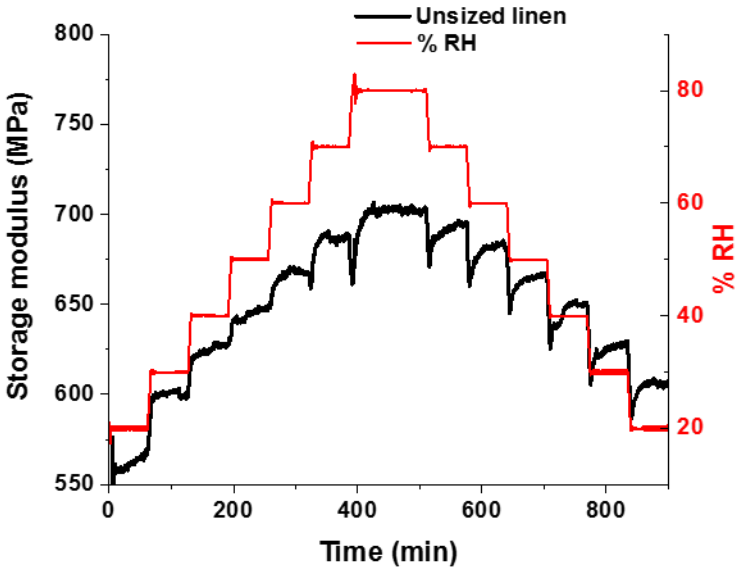

Figure 3.30: Response of an unsized linen canvas measured in the weft to the RH-steps program showing gradual stiffening and plasticization of the canvas following humidification and dehumidification, respectively.

The linen canvas of this study was also subjected to RH steps from 20 to 80%RH. From the results shown in Figure 3.30, no inflection of the curve or inversion in trend was seen. The linen canvas shows instead to respond linearly and is characterised by an increase in *E'* upon moisture sorption. The linen canvas was also tested in the warp direction as it had been shown that the direction of measurement had an influence on the mechanical behaviour of the degraded cotton canvas. The same trend in stiffening/plasticisation was again observed (see Figure A.1 in Appendix).

The mechanical behaviour of the modern linen canvas, is in accordance with previous observations made on a #8800 linen (Mecklenburg, 2007). However, the canvas stiffening seems

to start already from the first increase in RH from 20%RH. This a far lower humidity level than the one measured for a #8800 linen chosen by Mecklenburg. Mecklenburg had, indeed, noted a small decrease in tension between 10 and 75% and a sudden and important increase in tension from 75-80%RH onwards (Figure 3.2).

3.4.3.3.2 Variations in *E'* between RH plateaus

The variations in *E'* (i.e. $\Delta E'_{20\text{-}80\%RH}$) were also analysed. Variations measured for the linen canvas were particularly higher than cotton. As seen in Table 3.4, differences $\Delta E'_{20\text{-}80\%RH}$ of 40 and 38MPa were measured for linen in the weft and warp directions respectively, while $\Delta E'_{20\text{-}80\%RH}$ of 8.6±0.9MPa and -0.13±2.0MPa had been previously measured for cotton in both warp and weft directions, respectively. The lower variations in *E'* measured for the cotton canvas could indicate the lower hygroscopic behaviour of the cotton canvas compared with the linen one. This result is interesting as it could relate to the higher hygroscopic behaviour of linen over cotton fibres measured by Hill (2009). Moisture regain at 55%RH of 6.8% and 12% were measured for cotton and linen fibres, respectively (Timár-Balázsy, 1998).

Canvas material	Direction of measurement	$E'_{20\%RH}$ (Mpa)	$E'_{80\%RH}$ (Mpa)	$\Delta E'_{20\text{-}80\%RH}$ (Mpa)	$\Delta E'_{20\text{-}80\%RH}$ (%)
Linen	***Warp***	25.3±1.0	63.5±0.4	-39.2±1.4	-154.9
	Weft	167.7±0.6	214.8±1.3	-47.0±0.9	-28.0
Cotton	***Warp***	23.6±0.5	17.0±0.2	8.6±0.9	28.4
	Weft	113.5±1.6	113.7±3.2	-0.13±2.0	-0.1

Table 3.4: Comparison of the storage moduli measured at 20%RH ($E'_{20\%RH}$) and 80%RH ($E'_{80\%RH}$) (end-plateau values, average over 3 cycles) for a linen canvas (unwashed/unaged) and a degraded cotton canvas measured in both warp and weft directions. Difference $\Delta E'_{20\text{-}80\%RH}$ in E' between 20 and 80%RH is also given in MPa and % to show mechanical response of the samples to RH cycles.

In summary, mechanical assessment of a linen and cotton canvas has shown that the two canvases presented different mechanical response to RH cycling. In the warp direction, the 2 canvases had opposite behaviours (Figure 3.31). From these results, it seems thus clear that if shrinkage and resulting increase in tension at high RH levels can be observed for some canvases, this mechanism is not the same and does not always apply to all types of canvases. It relies strongly on the weave structure as well as possibly the canvas material. The testing direction when uniaxial testing is used can also have an important impact on the results.

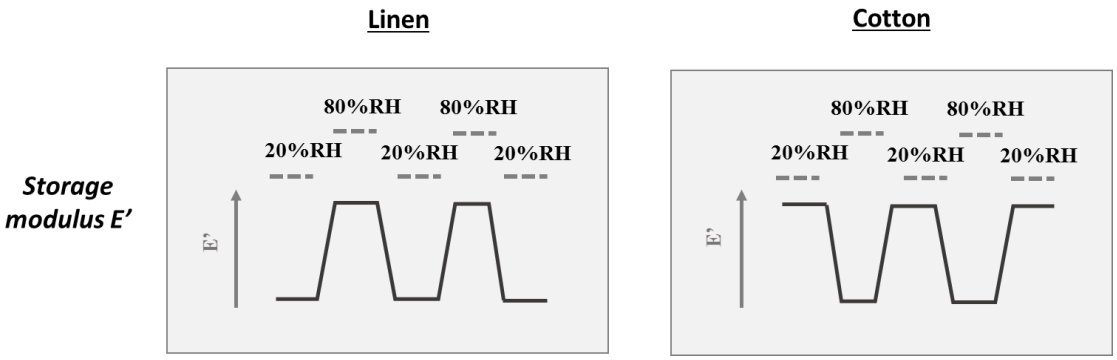

Figure 3.31: Trend in mechanical behaviour observed for a linen tightly woven canvas and a loosely woven degraded cotton canvas.

3.4.4 The mechanical impact of size and priming layers on canvas viscoelastic properties

The degradation protocol has shown to strongly modified the response of the cotton canvas to moisture. In the same way, better understanding of how size and priming modify the viscoelastic properties and response to moisture of canvases. This is of particular interest for the development of new treatments for canvas consolidation.

3.4.4.1 Sizing

It is well known that animal glue used for sizing is stiff at low RH levels and plasticises at RH levels (c.f. Figure 3.1 from Mecklenburg (2007)). Mecklenburg also showed that its mechanical response to RH variations is also known to be the stronger of all the layers making up

a painting. Unsized and sized linen canvas were investigated by DMA-RH and tested under RH variations (20-80-20%RH) in both the warp and weft directions.

The results in Figure 3.32 shown for unsized and sized (3 coats) linen canvases measured in the warp direction are in agreement with the expected behaviour previously described by Mecklenburg (2007). The sized canvas (3 coats) softens at 80%RH (decrease in storage modulus *E'*) and stiffens at 20%RH (increase in *E'*).

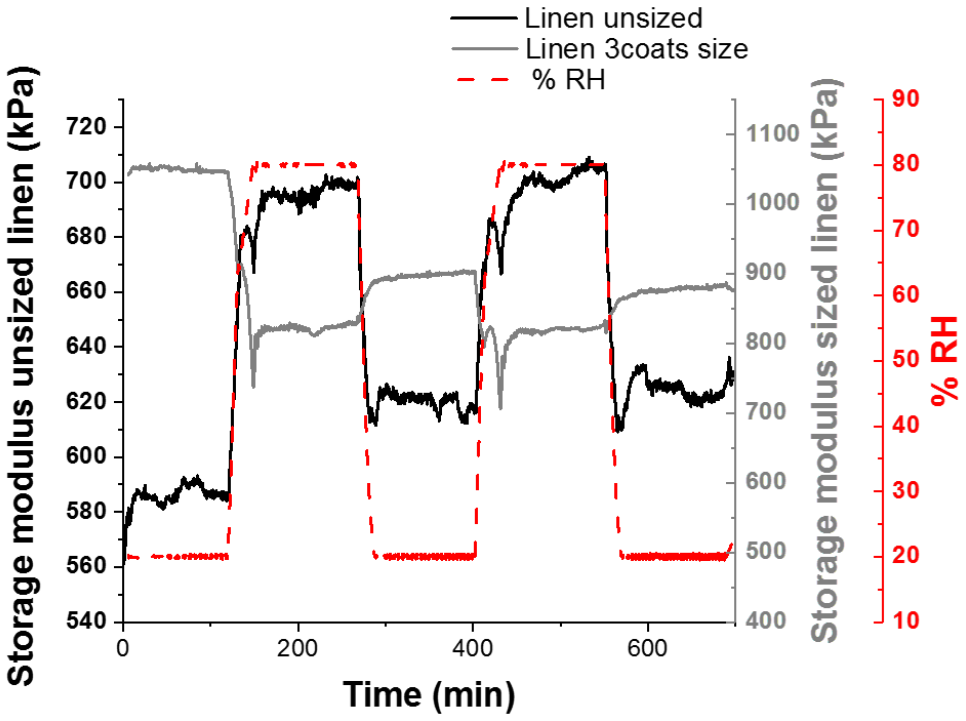

Figure 3.32: Comparison of the mechanical response of an unsized (black) and sized (3 coats) (grey) modern linen canvas (unwashed) to RH cycles (20-80-20%RH) measured in the warp.

Linen canvas	$\Delta E'_{20\text{-}60\%RH}$ (MPa)
Unsized	-40.1±0.5
3 coats size	52.0±0.8

Table 3.5: Variations in storage modulus E' measured between 20 and 60%RH plateaus (average over the 3 RH cycles) for the unsized and sized (3 coats) linen canvas measured in the warp.

The presence of sizing also shows to strongly modified the response of the canvas. An inversion in mechanical response and cycles of stiffening and plasticization can be seen between the unsized and sized canvas. The phenomenon is particularly important in the warp (see Figure 3.35) for which $\Delta E'_{20\text{-}80\%RH}$, the average difference in E' between 20 and 80%RH averaged over the 3 RH cycles, goes from -40.1±0.5 (unsized canvas) to 52.0±0.8MPa (sized canvas) (Table 3.5). As seen in Figure 3.33, a similar inversion was observed for the linen canvases measured in the weft direction.

Interestingly, this phenomenon is similar to the modification observed previously in 3.4.3.2.2 for the cotton canvas after washing and degradation. After degradation, an inversion in the mechanical response to RH variations had been measured in the warp direction and a reduction in $\Delta E'_{20\text{-}80\%RH}$ had been also observed. These results as well as the impact of washing on the mechanical properties of the cotton canvas raise the question as to whether the differences measured between unsized and sized sample might be only related to the differential response of the size applied on the canvas or if its application (i.e. wetting and possible structural reorganisation) might also be playing a role in the overall results. Further investigations are required to answer this question which fall outside the scope of this study.

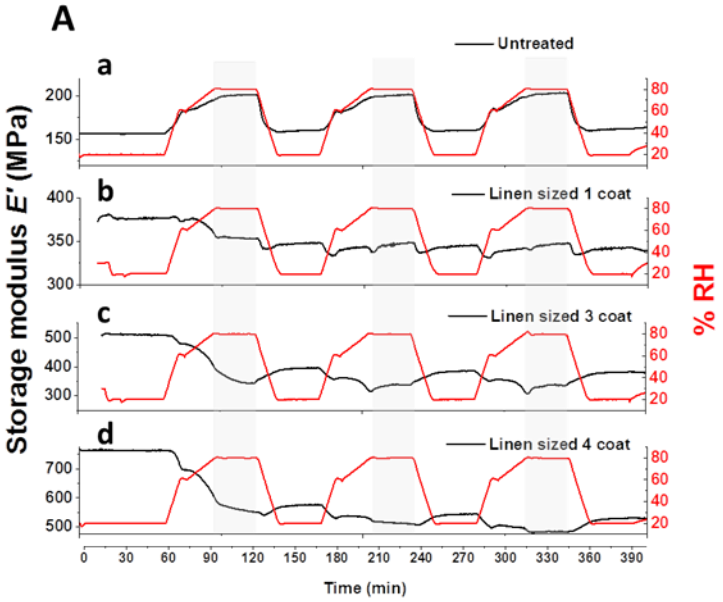

B

Samples	$\Delta E'_{20\text{-}80\%RH}$ (Mpa)
Untreated	-47.1±0.6
1 coat size	-4.7±1.2
3 coats size	48.7±1.4
4 coats size	35.5±10.9

Figure 3.33: Impact of increasing number of size coats on the response of a linen canvas to moisture cycles (20-80-20%RH). In (A), curves in storage modulus E' measured for linen canvases untreated (a) and treated with 1 (b), 3 (c) and 4 coats (d) of size. Measurements were performed in the weft. In (B), variations in E' between the 20 and 80%RH plateaus (average over the 3 cycles), i.e. $\Delta E'_{20\text{-}80\%RH}$, are shown.

The impact of sizing on the mechanical and response in elongation to RH cycling of the canvas was further investigated. Linen canvases size with 1 to 4 layers of size were analysed in the weft direction. As seen in Figure 3.33A(b), 1 coat of size already strongly modifies the response of the linen canvas to RH cycling. For this sample, an inversion of the response in *E'* of the unsized linen canvas could already be seen and caused the canvas to reduce its mechanical response to RH as seen by the lower variations in *E'* measured for the 1-coat sized linen canvas (Figure 3.33B). The absolute value of the difference $\Delta E'_{20\text{-}80\%RH}$ measured between 20 and 80%RH plateaus falls from 47.1±0.6 to 4.7±1.2MPa after 1 application of size. The layer of size thus seems to be beneficial as the sized canvas now offers a support more mechanically stable under RH variations for the painting.

However, as the number of coating of size is increased, so is the response of the sized canvases to moisture. Variations $\Delta E'_{20\text{-}80\%RH}$ in *E'* increased from -4.7±1.2MPa to 48.7±1.4 and 35.3±10.9MPa after application of 3 and 4 layers of coat, respectively (Figure 3.33B). The biggest

modification of the response seems to occur between 1 and 3 applications of size. Indeed, after the application of 3 and 4 coats of size, the mechanical response of the canvas sample does not seem to be affected anymore by additional sizing layers a seen by the stabilisation in $\Delta E'_{20\text{-}80\%RH}$.

The application of sizing also modifies the response in elongation of the canvas as seen in Figure 3.34 by the variations in percent elongation experienced by unsized and sized samples upon application of 20-80-20%RH RH cycles.

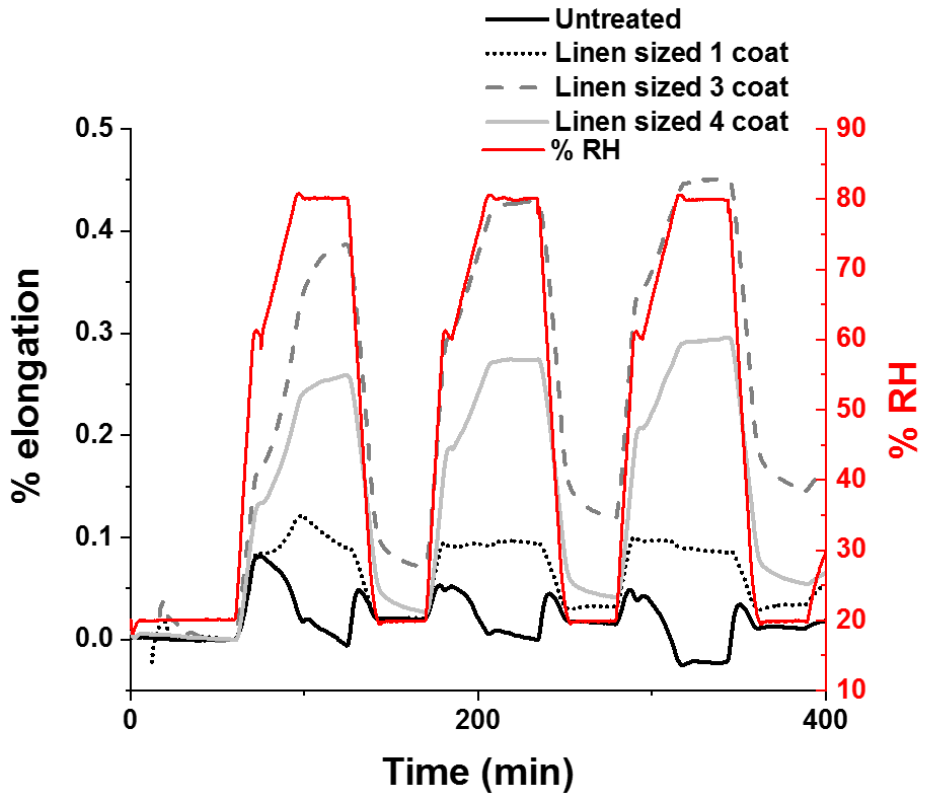

Figure 3.34: Percentage elongation linen canvases unsized (black solid line) and sized with 1 (dark grey), 3 (light grey) and 4 coats (black dotted line) of size upon application of 3 successive RH cycles (20-80-20%RH at 25°C). Measurements were performed in the weft. Application of size tends to increase the response in elongation of the linen canvas at high RH levels as seen by the increase in elongation measured at 80%RH for the samples with 3 and 4 coats of size.

Before sizing, the response in elongation of the untreated canvas is low. The response in elongation is overall stable. After a 20 to 80%RH cycle, the elongation measured for the untreated linen canvas goes back to a value similar to the initial one at 20%RH. Small shrinkage of the canvas, however, occurs upon RH cycling as seen by the reduction in elongation measured over

the 3 cycles. The canvas elongation varies the most during the episodes of RH transition were the flux of moisture pumping in our out of the chamber might induce movement, possibly slippage, of the threads of the fabric. In comparison, the size canvas samples (1, 3 and 4 coats) tend to gradually elongate throughout the cycles. As seen in Table 3.6, for the linen treated with 3 coats, the elongation measured at 20%RH goes from 0% to 0.07% (end 1st cycle), 0.12% (end 2nd cycle) and 0.14% (end 3rd cycle). The deformation is irreversible and particularly important for the linen sized with 3 and 4 coats of size.

RH cycle	**Elongation (%) at 20%RH**			
	Unsized	**1-coat size**	**3-coats size**	**4-coats size**
1st RH cycle	0.02	0.02	0.07	0.03
2nd RH cycle	0.01	0.03	0.12	0.04
3rd RH cycle	0.01	0.03	0.14	0.06

Table 3.6: Percentage elongation measured for the unsized and sized modern linen canvas with 1, 3 and 4 coats size. Note the higher elongation reached after the three 20-80-20%RH cycles for the sized samples, in particular the 3-coats sized sample.

This is likely the result of the softening of the size layer occurring during exposure to 80%RH which triggers further penetration of the glue inside of the canvas. Yet, it is known that animal glue which was used here to size the linen canvas, is sensitive to moisture and is prone to lose strength at high RH levels. This was initially suggested by Mecklenburg (2007) but will be explored in Chapter 4, during a study of traditional consolidants. At 80% RH, the size does not hold the threads, yarn and fibres together anymore which can thus move freely due to the tension applied during the test. When RH cycling goes back to 20% RH, the sizing glue re-hardens, possibly at higher RH level than 20% RH, and fixes the canvas in its new, more elongated, conformation. Since increase elongation is not observed for the untreated canvas, it is assumed

that softening of the glue could increase thread slippage. Another hypothesis is that internal stresses might have also partly built-up in the linen canvas through the application of size. This hypothesis is based on the phenomenon of crimp exchange observed upon the wetting of fabrics. The direction which presents the lowest crimp pulls out the crimp from the other direction (Collins, 1939). This is caused by the release of internal stresses in the fabric, incorporated during its manufacture such as the tension applied to hold the weft threads (cf. 3.3.1.1). In the case of the sized linen canvas samples, build-up of internal stresses could originate from the water introduced (animal glue was dissolved in water) and the tension used to stretch the canvas before sizing it. These stresses could have been released upon softening of the size layer at high RH while putting the canvas under tension. This would be partly responsible for the dimensional as well as viscoelastic responses measured and shown previously for the sized samples.

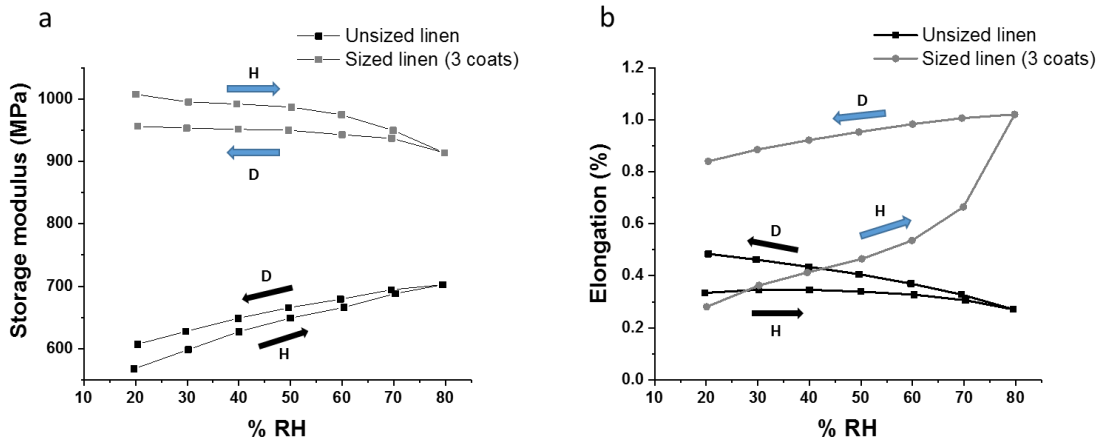

Figure 3.35: Storage modulus E' (a) and elongation (b) of an unsized (black) and 3 coats-sized linen canvas (grey) measured in the warp at each step of a 20-80-20%RH cycle. The samples were left to equilibrate 1 hour at each RH level and 2 hours at 80%RH. The humidification (H) and dehumidification (D) ramps are indicated with the arrows.

The mechanical and response in elongation of unsized and sized samples (3 coats) were also measured at different RH levels between 20 and 80%RH using the RH steps program (1hour plateau for each RH) (cf. 3.3.2.2). As seen in Figure 3.35b, the elongation of the sized linen canvas suddenly increases at 80%RH during the first 70-80%RH transition. This increase was attributed to the unlocking of canvas threads and mesh from the glue previously observed at 80%RH but

which seems to occur at slightly lower RH as seen in Figure 3.34. Under 70%RH, the more linear response of the sample to the increase in RH might result from the slow plasticization of animal glue. This is also translated into the higher loss in *E'* seen during this RH transition (Figure 3.35a).

Finally, a stronger hysteresis in elongation can be seen for the sized sample (Figure 3.35b). This highlights again the high response in elongation of the size canvas but also confirm the lubricating action of the size at high RH levels promoting canvas movement and structural reorganisation.

In summary, the size layer has shown to have a strong impact on the canvas mechanical response to RH variations. Painting canvases are commonly treated with only 1 or 2 coats of size. Figure 3.33B showed that a linen canvas with one coat of size presented the lowest variations in *E'* with RH. The lower mechanical responsiveness measured could be beneficial to the paint and ground layer, also known to be less responsive to RH. Lower stiffening /plasticizing cycles would indeed reduce the risk of mechanical fatigue of the upper layers, paint layers and varnish. In future works, a better understanding of the role of sizing on the overall viscoelastic and response in elongation of sized canvases to RH could be gained by:

- following the penetration of the size layer upon application of successive RH cycles
- studying the impact of the treatment application such as the solvent used or the level of canvas tensioning used for size application on the viscoelastic response of the unsized/sized samples.

3.4.4.2 Priming

The role of the layer of priming on the viscoelastic response of a canvas to cycling RH was also investigated. The samples investigated were taken from an historical 19th primed linen canvas. They presented a layer of cold glue size and oil priming (mixture of lead white and oil). They were measured before and after removal of the priming layer using a scalpel. In Figure 3.36, the picture of the primed sample used for the DMA-RH measurements before and after removal of the priming layer is shown. SEM-EDX images of the cross-sectional area of the primed linen

canvas before and after removal of the priming layer are also shown in Appendix (Figure A.2). Most of the 100µm thick layer of priming has been removed. Traces of the lead white priming can, however, still be observed on the surface of the canvas.

Figure 3.36: Picture of the same sample before (left) and after (right) removal of the priming layer. The sample was used as such for DMA-RH measurements.

Figure 3.37 shows the mechanical response measured for the same sample before and after the removal of the primed layer at different RH levels (i.e. RH steps between 20 and 80%RH).

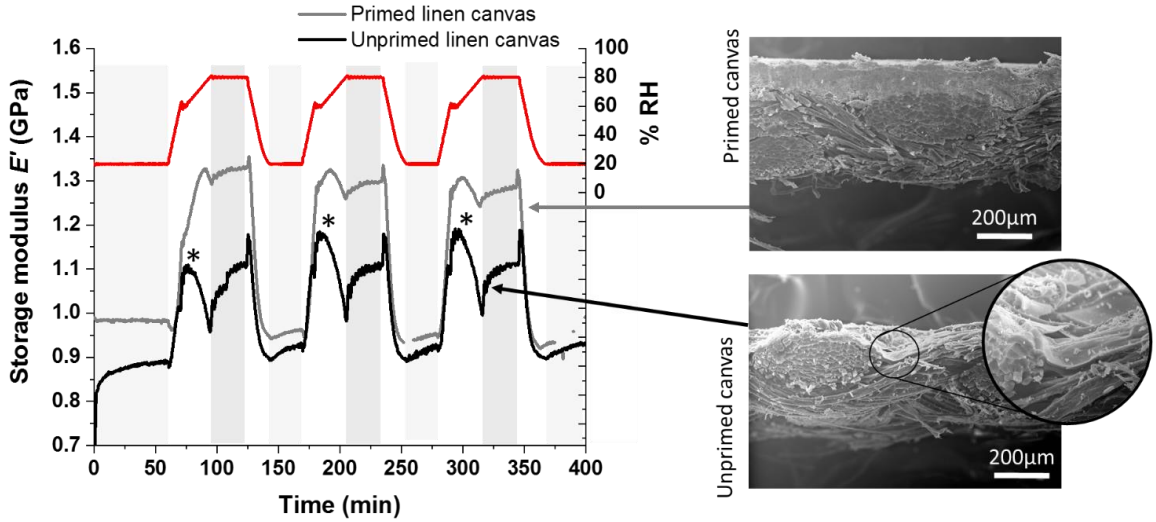

Figure 3.37: Storage modulus and elongation of a primed (grey) and unprimed (black) sample under RH variations (20-60-20%RH). Note that the unprimed sample corresponds to the primed sample after removal of the priming layer with a scalpel.

Under 20-80-20%RH cycles, the primed and unprimed samples behave in a similar way. Their mechanical responses are similar to what had been previously measured for a modern unsized linen (see Figure 3.32). The samples stiffen at high 80%RH and plasticize at 20%RH. Variations in *E'* between 80%RH and 20%RH, i.e. $\Delta E'_{20\text{-}80\%RH}$, were also lower for the unprimed sample (i.e. $\Delta E'_{20\text{-}80\%RH}$ = *-64.2±8.5MPa)* than for the primed sample (i.e. $\Delta E'_{20\text{-}80\%RH}$=*-368.5±1.2MPa)*. The removal of the priming layer seems to reduce the intensity of the mechanical stresses undergone by the canvas. This is indicated that the priming undergoes higher mechanical changes during increase or decrease RH than the canvas or size layer (also present in the canvas tested). The response of the unprimed canvas was also characterised by a strong mechanical response but this response is only at 60%RH by the high increase in *E'* (see detail (*) in Figure 3.37).

Sized 19th linen canvas	$E'_{20\%RH}$ **(MPa)**	$E'_{60\%RH}$ **(MPa)**	$\Delta E'_{20\text{-}60\%RH}$ **(MPa)**	$\Delta E'_{20\text{-}60\%RH}$ **(%)**
Primed	946.9±21.5	1305.6±23.3	-368.5±1.2	*-38.9*
Unprimed	825.1±0.6	888.3±6.2	-64.2±8.5	*-7.8*

Table 3.7: Storage moduli E' measured at 20% and 80%RH (end-plateaus value, average over 3 RH cycles) for a primed and unprimed 19th linen canvas subjected to 20-80-20%RH RH program (25°C). Variations in E' ($\Delta E'_{20\text{-}60\%RH}$) between plateaus are also given (in MPa and %). The samples were measured in the same direction.

The samples were also measured under the RH-step programme to get a better understanding of the mechanical change occurring during the 20-80%RH transitions. As seen in Figure 3.38, the two samples stiffen with increasing humidity. However, at high RH levels an inversion in trend occur and the canvas is plasticized (loss in *E'*). This inversion occurs at different RH levels for the two samples, i.e. after 60%RH for the unprimed sample and after 70%RH for the primed sample. For the unprimed sample, the loss in *E'* is particularly important. At 80%RH, after 1 hour of stabilisation, the storage modulus $E'_{80\%RH}$ reached 1057MPa, a similar value than the one achieved previously at 50%RH after 1 hour of stabilisation (i.e. 1051MPa). For the primed

sample the loss is less pronounced. At 80%RH, $E'_{80\%RH}$ has gone back to a similar value to the one previously measured at 60%RH. These results do not show the known lower mechanical response of the priming layer to moisture sorption (Hedley, 1988; Mecklenburg, 1982). More work is required to investigate this difference. It is possible that the primed 19th century historical sample tested presents a different sizing than the samples tested in the past in previous studies. This could have greatly influenced the results.

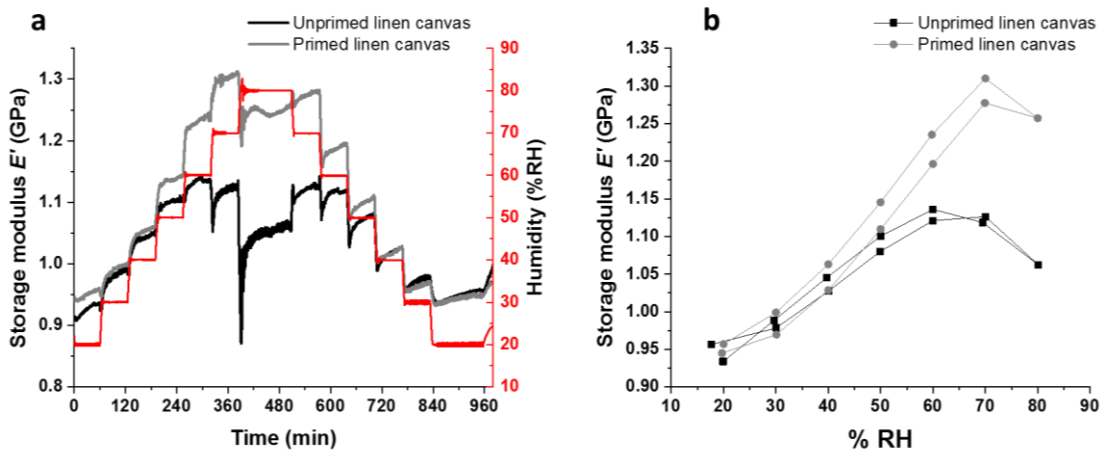

Figure 3.38: Mechanical response in E' upon time of unprimed (black) and primed (grey) samples to RH steps from 20 to 80%RH (25°C) (a). In (b), the variations in E' were also plotted upon RH taking the end-plateaus values in E' at each RH plateaus. The curves highlight the inversion in trend measured for the unprimed sized linen canvas at 60%RH upon moisture sorption/desorption. The response of the two samples to RH cycling is quite reversible as shown by the small of hysteresis seen in (b).

This work has thus shown that the priming layer is stiffer than the sized canvas at high RH levels above 40%RH and that, contrary to what was expected, governs the mechanical behaviour of the sample over the size layer between 20 and 70% RH and pushes back the inflection in E' seen for the sized and unprimed sample to 80%RH. Risks of delamination of the ground as well as paint layers are then most likely to occur at and beyond this humidity level.

3.5 Conclusions

In this chapter the viscoelastic responses of a range of canvases to RH variations was tested. This has highlighted the impact that pretreatments, weaving structure, canvas material (i.e. fibre

type) can have on the overall mechanical and physical properties of painting canvases made of natural fibres. This has also emphasised the unique characteristics of each canvas which could be found in the collections with regards to their response to RH (see Table 3.8). If overall mechanical and physical trends specific to certain kind of canvas material or weaving can be pulled-out, each canvas has its own properties.

The response of the degraded cotton canvas which was selected to be used as model for the testing of new consolidants for canvases was described in great length. This now set a basis for investigations of the impact of different newly developed consolidants for modern painting canvases. Identification of phenomenon such as mechanosorptive creep, hornification upon RH cycling has brought novel insights into the study of painting canvases.

Additionally, the assessment of the response of other constitutive layers of a painting, hence the size and the prime layers, has proven the reliability of the use of DMA-RH analysis to measure the mechanical and response in elongation of painting and painting layers to RH cycles.

	Canvases				Additional painting layer	
	Modern cotton canvas			*Modern linen canvas*	*Sizing (modern linen)*	*Priming (19th century primed sized linen)*
	Cotton canvas before washing/ degradation	*Washed canvas*	*Degraded canvas*			
Mechanical response to moisture ***(elastic response, i.e. storage modulus E')***	**Stiffening upon RH increase (warp)**	**Lower variations in *E' between RH levels* measured after washing (warp).** Threads more plasticized by RH increase than before washing.	**Plasticization upon RH increase (warp)** **Low variations in E' between RH levels (20-80%RH) (weft)**	**Stiffening upon RH increase (warp & weft)**	**Sizing induces plasticization upon RH increase (warp &weft)** -1 layer of coat on linen reduces the variations in *E'* upon RH cycling (20-80%RH) - Strong variations in *E'* measured for 3 and 4 layers of coat due to plasticization of the size glue	**Important stiffening of the primed sample (one direction measured)** Plasticization effect of the sizing observed again for the unprimed sample.

Table 3.8: Summary of the mechanical response to RH variations measured for the modern cotton and linen canvases as well as for the sized modern linen and primed 19th century linen canvases.

Further research would, however, be required to quantify the risks associated with the responses measured for the different material tested in this chapter. It is known that high variations in stiffness of the materials and layers making up a painting could be responsible for increased internal stresses, hence increased risks of mechanical failure of the painting. Yet, the acceptable range in viscolastic response of the canvas, size, priming, paint and varnish to RH cycling still need to be found. Further assessment using a combination of DMA or creep measurements under RH variations or involving computational modelling which would include the viscoelastic properties of the constitutive layers of paintings could provide some answers.

In the next chapter, the impact of traditional natural and synthetic consolidants will be investigated. Two nanocellulose consolidants (nanocellulose-only) tested in the frame of this project will also be tested for comparison. This will pave the way to a better understanding of the advantages and drawbacks of these new nanocellulose-based consolidants over traditional solutions currently available.

4 Physico-chemical and mechanical assessment of traditional consolidants

4.1 Introduction

The characteristics of a material that could be considered as adequate for canvas (and eventually painting) consolidation are well described in the literature. When the risks associated with traditional glue paste and wax resin lining were publicised in the 1970s (Ackroyd, 2002), several conservation scientist such as Berger (1970), Mehra (1075) and Hedley (1988) started to look for alternatives. To guide their research, they established lists of criteria (physical, mechanical and chemical) which would help them identify and develop suitable adhesive and consolidants for painting canvas. This led to the development of new synthetic adhesives such as Plextol and Plexisol by Mehra (Mehra, 1975) and Beva by Berger (1970). Those criteria could be classified in order of importance as follow:

- Acceptability to artists (texture, handling, appearance, etc)
- High stiffness (understood as high Young's modulus)
- Negligible hygroscopicity
- Resistance to creep and stress relaxation
- Durability
- Low extensibility
- Good elastic recovery
- Good adhesion to chosen grounds
- Low cost
- Availability
- Enable easy treatment of paintings of a large format.

In 2015, a survey was conducted to confirm these findings, in the context of the current needs of painting conservators and classify these (Oriola, 2019). The results show since the 1970s, the expectations and requirements of painting conservators for the developments of new consolidants

for painting canvases have remained broadly the same. The 67 conservators interviewed considered as essential requirements a product enabling canvas strengthening, with a good ageing and reversibility.

Consolidants or adhesives used as consolidants for fragile painting canvases can come from natural (i.e. animal glue) or synthetic compounds (i.e. Beva371). Properties well studied in terms of mechanical properties using tensile tests, adhesion between two canvases, ageing (c.f. 1.1 in Chapter 1). However, difficulties can arise when aggregating the results of these studies as the techniques of investigations may vary. Moreover, only few materials have been tested in terms of their mechanical response to RH. Animal glue and the synthetic adhesive Beva 371 are two of the most studied common adhesives but their mechanical assessment in painting conservation is often limited to their assessment as lining adhesives (Berger, 1970; Krarup Andersen, 2013; Mehra, 1975; Young, 2001; Young, 2012). Results are thus frequently given for the treated canvas or the complete canvass-adhesive-lining canvas system (Krarup Andersen, 2013, Young, 2001). Most of the studies will, therefore, only explore adhesion, bonding properties and more rarely consolidation in terms of stiffness.

This study was performed to gain a better understanding of the physical, mechanical and chemical properties of current adhesives in use and to compare those with two newly developed nanocellulose-based treatments. The six different adhesives commonly used in conservation which were chosen for this study include 1 natural, animal glue, and 5 synthetic materials: Beva 371, Paraloid B72, Klucel G, Aquazol 200 and Plexisol P550. They correspond to compounds commonly or previously used for the canvas consolidation and in lining works (Arslanoglu, 2004; Ploeger, René De La Rie, 2014; Ropret, 2007). The investigation focuses on the main criteria established previously for the evaluation of treatments for canvas consolidation. The modification in surface appearance resulting from the treatments application, quantification of the reinforcement provided as well as their response to moisture variations were assessed.

4.2 Materials and methods

4.2.1 Commonly-used paint consolidants and lining adhesives

Six different consolidants and adhesives, natural and synthetic were tested. Those are the natural adhesive animal glue and the synthetic materials Beva 371, Paraloid B72, Aquazol 200, Klucel G, Plexisol P550.

Animal glues are natural polymers obtained by partial hydrolysis of mammalian or fish collagen – the major structural protein constituent of skin, tendons, ligaments and other connective tissues (Gelse, 2003; Lodish, 2000). Collagen is a long biopolymer consisting of long polypeptide chains, wound tightly to form triple-helices of elongated fibrils. The amino (-NH-) and carbonyl (=O) groups of the amino acids (Figure 4.1) can easily form hydrogen bonds when close to another, either those present on the same chain or on different chains of the triple-helices structure. Hydrogen bonding between peptides (i.e. –NH --- O=C) can easily be broken by force or in the presence of water and reformed (Figure 4.2) (Bella, 1995; Boryskina, 2007). It is those hydrogen bonding which makes it possible for glue molecules to interact strongly with appropriate substrates such as wood and to act as powerful adhesives (Frihart, 2012; Pearson, 2003).

The animal glue used in this study was bought from Lienzos Levante (Alicante, Spain) and consists of a rabbit skin glue. The chemical, physical and mechanical properties of animal glues greatly depend on their origin (e.g. bones or skins, animal species such as fish or rabbit, etc) and mode of preparation (Schellmann, 2014).

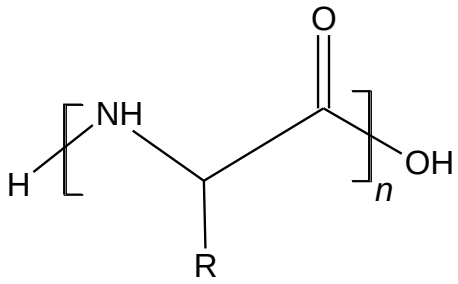

Figure 4.1: General chemical structure of an amino acid, of the constituent molecules in all proteins. "R" represents a variety of atoms or groups that can be attached to the core structure, leading 22 individual proteinogenic amino acids found in nature (see list* (Rose, 1984)*).

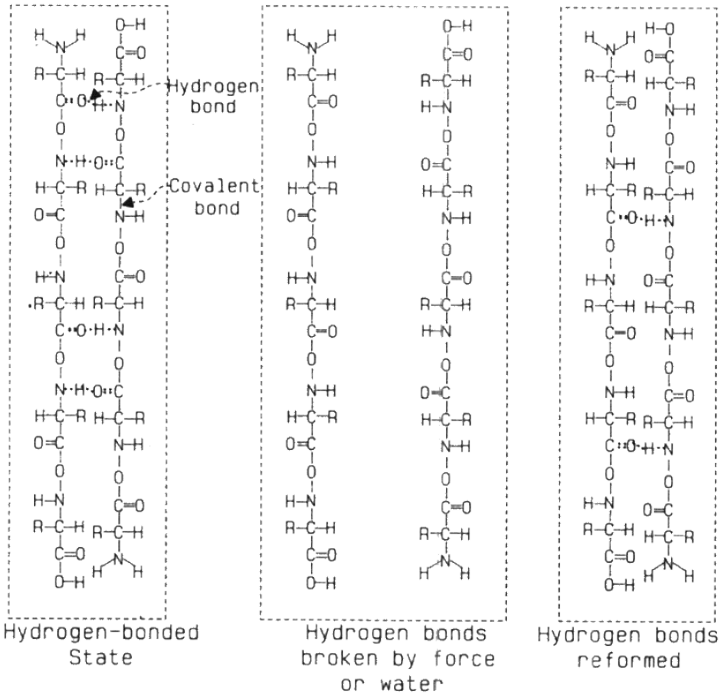

Figure 4.2: Hydrogen bonding between protein chains, which can be broken by chemical or physical stress and reformed (taken from* (von Endt, 1991)*)

Klucel G was purchased from CTS (Italy). Klulcel is an hydroxypropylcellulose existing in several grades characterised by their molecular weight (MW). Klucel G has a molecular weight of MW=370,000 g/mol. It has been used in conservation since the 1980s as a consolidating gel (e.g. for book conservation) (Martin, 2011). It is favoured in paper conservation because of its solubility in non-aqueous solvent (e.g. isopropanol). It does not have strong adhesive properties (Rodgers, 1988). Feller and Wilt (1990) showed that some cellulose ethers, including Klucel, are unsuitable to long-term applications, as they are particularly sensitive to photochemical and thermal ageing.

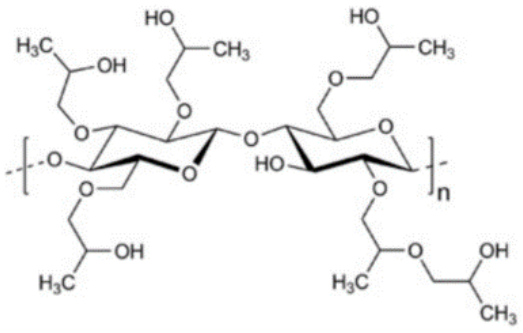

Figure 4.3: Chemical structure of Klucel hydroxypropylcellulose

Aquazol is a water-soluble synthetic resin made of Poly (2-ethyl-2-oxazoline). It was purchased from CTS (Italy). This material is known to be particularly sensitive to RH. Films of resins were found to be tacky around 60-65%RH (Muros, 2012).

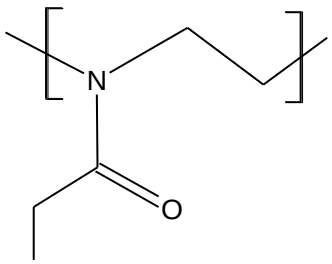

Figure 4.4: Chemical structure of Aquazol

Beva 371 was purchased from CTS (Italy). It is based on an ethylene-vinyl acetate copolymer which is one of the most widely used lining adhesive (Ploeger, 2014). Berger introduced the lining adhesive in 1970 as a substitute for wax-resin (Berger, 1970). It is made of two different Etylene vinyl acetates (EVA): Elvax® 150 (DuPont™) (45% in mass) and A-C® 400 (Honeywell) (15% in mass) as well as a resin (Laropal® K 80) (27%) and a tackifier (Cellolyn™ 21) (4%). EVA-based adhesives also contain a wax component (Paraffin), which is often added to control the melt viscosity and setting speed. The adhesive became increasingly popular, but there are some indications of drawbacks, such as its high activation temperature and deep penetration (Jaïs-Camin, 1997). Loss in solubility, or cross-linked which was also observed with in as little as five years for Beva 371 applied on cotton and silk textiles (Shore, 1994). Upon rinsing the fabric with solvent, the conservators also noticed a dark gray discoloration resulted, visible at both the front and back surfaces. Even though Beva 371 is used widely it has not been much researched in recent years. The chemical stability of Beva 371 was also questioned as new and more stable replacement formulas were tested (McGlinchey, 2011).

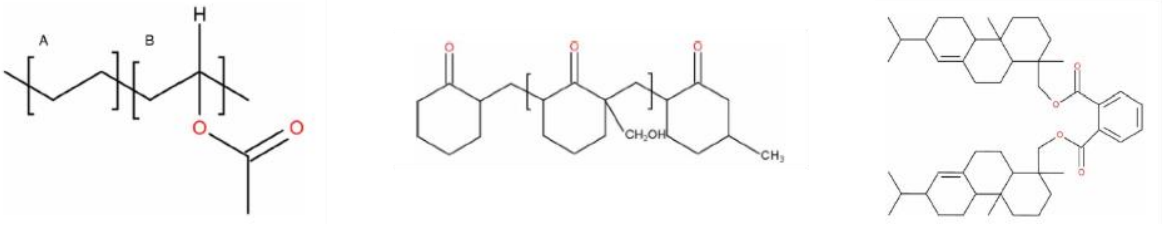

Figure 4.5:Chemical structures of the main components of Beva 371 (original product by Berger). On the left, poly(ethylene vinyl acetate) (EVA). EVA co-polymers with different properties are obtained by varying the ratio of PE (A) to VA(B) in the co-polymer. In the centre, idealized chemical structure of a keton resin like Laropal® K80 (structure can vary). On the right, Cellolyn^{TM} 21 one the right (technical grade material as some abietyl alcohol groups may be present).

Paraloid B72 was purchased from CTS (Italy). It consists of a methyl acrylate/ethyl methacrylate (MA/EMA, 30/70 %w/w) copolymer (Horie, 2010) with its composition slightly varying over time (de Witte, 1978). It has been used for more than 50 years in painting conservation as a consolidant and varnish as well as on a wide range of archaeological materials and art objects. In the US the former name of the product is Acryloid B72 (Lazzari, 2000). Paraloid B-72 has a high viscosity which makes it a good choice to readhere materials, but less well-suited for penetrating paint films or consolidating underbound paint (Farmakalidi, 2016).

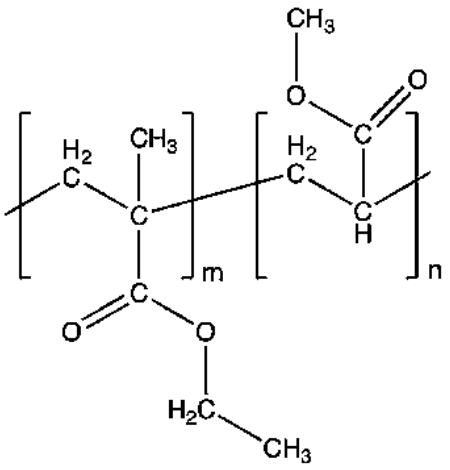

Figure 4.6: Chemical formula of Paraloid B72 acrylic resin

Invented by Mehra, Plexisol® P550 is an acrylic resin often used in painting conservation for the consolidation of the paint layer and stabilisation of the canvas (Lardet, 2014). It was recommended from the ’70s for the preparation of the canvas prior to lining by Mehra who used to provide a moisture barrier prior to lining (Mehra, 1975). This thermoplastic polymer is made of butylmethacrylate monomers. It is colourless and transparent. It is known to be photo-stable but to crosslink and become insoluble upon ageing (Delcroix, 1988). It does not offer high adhesion and increase the stiffness of the treated canvas. Plexisol P550 was purchased from Lascaux (Switzerland).

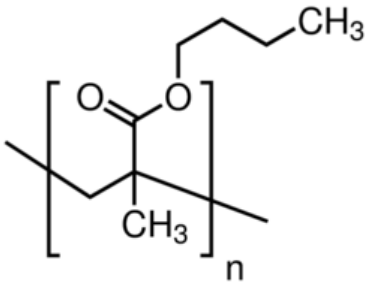

Figure 4.7: Chemical structure of Poly(n-butylmethacrylate), main constituent of Plexisol P550.

4.2.2 Sample preparation

Square samples (10 cmx10 cm) of a modern cotton canvas were artificially degraded using a protocol described in Chapter 2 (cf. 2.1.1). The degraded cotton canvases were then treated by painting conservators at the University of Barcelona (Spain) whose skills and experience ensure the optimal application of the treatments. The treatments applied consist of 6 traditional consolidants, 1 natural, animal glue, and 4 synthetic ones, Beva371, Paraloid B72, Aquazol200, Plexisol P550, KlucelG, and 2 nanocellulose-based treatments, CNF and CCNF. The treatments were applied by brush in order to reach a 5% increase in canvas weight after complete drying of the treatment. Calculations of the amount of consolidant needed were done for each product prior to the application. The canvas weight before treatment was measured at 374 g/m^2.

The dilutions used for each treatment and the solvent used were chosen by the conservators who carried out the treatment. Their choices were guided by their experience. Therefore, the viscosity of each treatment varies. Depending on the viscosity of the consolidant, one single layer to multiple ones were applied. The higher the viscosity, the lower was the number of applications needed. This is because a higher amount of product could be applied in one application until the canvas felt wet or saturated with the treatment. Between applications, the adhesive was left to dry. Description of the samples and number of applications used are given in Table 4.1.

Treatments	% w/v	Solvent	Number of layers applied	Tg (°C)	mp (°C)
CNF	1%	Water	4	-	
CCNF	1%	Water	4		
Beva 371	3%	Cyclohexane	4	40	68
Paraloid® B72	2.5%	Acetone	1	40[5]	
Aquazol 200	2.5%	Ethanol	1	69-71	
Animal Glue	1.7%	Water	2		
Plexisol P-550	5.3%	White spirit	1	29	
Klucel® G	1%	Ethanol	4	0 and 120[6]	

Table 4.1: List of treatments applied on the degraded cotton samples including the concentration used, the solvent and the number of applications which needed to be applied to

[5] Tg given on the product datasheet. However, a Tg of 25°C was measured by Farmakalis (2016) by DSC on paraloid B72 films.

[6] Klucel is a special polymer that presents a dual Tg because it has a beta transition. (See Ashland products brochure (web page: https://www.ashland.com/file_source/Ashland/Product/Documents/Pharmaceutical/PC_11229_Klucel_HPC.pdf)

reach a 5% increase in canvas weight. Physical properties of the materials, such as glass transition temperature (Tg) and melting point (mp) are given when applicable and available.

The area where the adhesive has been applied was marked with a pencil (7.5cm x 7.5 cm). The area along the borders of the sample was left untreated and used to clamp the sample onto a stretcher (Figure 4.8).

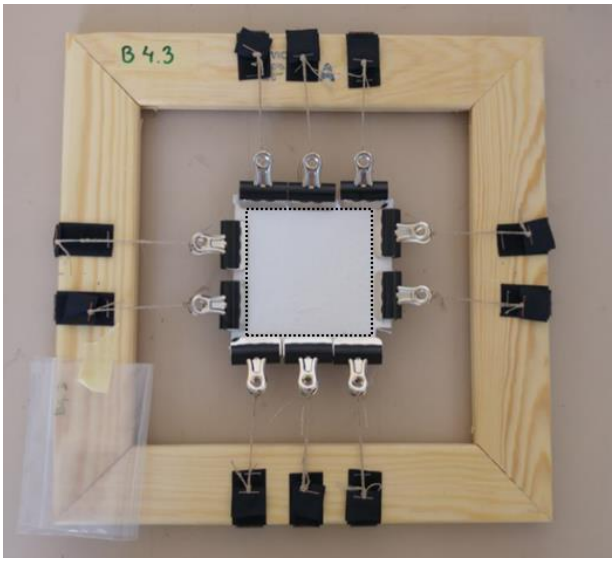

Figure 4.8: Degraded cotton canvas stretched into a wooden frame before the application of the treatment in the area delimited by the dotted line.

4.2.3 Tensile testing

The tensile testing was carried out using the DMA is tensile mode as described in Chapter 2 (cf. 2.2.4.1) at both 20% and 80%RH to investigate the influence of moisture on the mechanical performance (stiffness) of the samples and consolidants. The samples were cut so that 10 threads were collected in the warp direction and were typically 0.7 (thickness) x 7 (width) x 15 (length) mm in dimensions. Prior to the measurements, the samples were preconditioned in chambers at 11% or 75%RH (i.e. similar RH for the tensile test) for more than 48h using saturated salts solutions of lithium chloride and sodium chloride, respectively. The results obtained are given as average of 3 to 5 repeat measurements performed for each category.

4.2.4 Dynamical mechanical analysis under controlled RH program (DMA-RH)

Rectangular samples pieces were cut in order to get 10 threads in the warp direction and were typically 0.7 (thickness) x 7 (width) x 15 (length) mm in dimensions. The samples were preconditioned before the measurement for at least 24h at 20%RH at room temperature. The samples were then measured by DMA under RH control. Two RH programs were used for the DMA-RH measurements (Figure 4.9).

The first RH program to be used consists of RH cycles going from 20 to 80%RH at 25°C (*RH cycling program*). The humidity level was stabilised at 20%RH for 30min. RH was then increased at 4%RH/min to 60%RH, left at 60%RH for 1 min and increased further at 2%RH/min to 80%RH. After 30min isotherm at 80%RH, the RH level was decreased back to 20%RH at 4%RH/min and left at that RH level for 30 min. This cycle was repeated 3 times.

A longer RH program (*RH steps program*) was used as well to unravel the mechanical response of the samples during RH transition and enable more time for moisture content equilibration at the set RH. This RH program consists in 1 RH cycle from 20 to 80%RH. The samples were left to equilibrate for 1hour at 20, 40, 60, 70 and 80%RH during both humidification (20-80%RH) and dehumidification (80-20%RH). The rate of RH transition between plateaus was fixed at 4%RH/min.

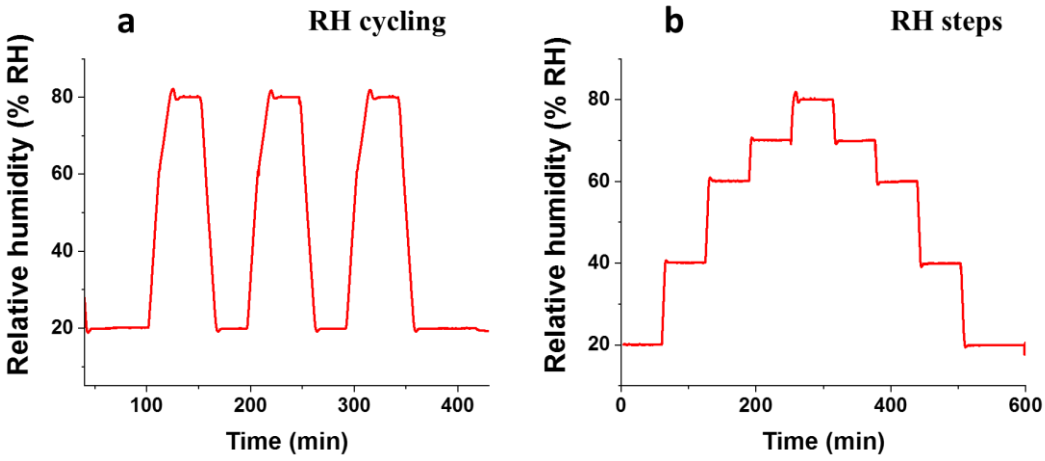

Figure 4.9: The two RH programs use for the DMA-RH measurements: the RH cycling program (a) and the RH steps program (b).

4.2.5 DVS

The principles of DVS measurements are given in Chapter 2 (cf. 2.2.3.2). Two different RH programs were used:

- RH program DVS1: 20-60-80%RH RH cycle which consists in isotherm at 20%RH for 1hour, then the RH was increase at 4%RH/min up to 60%RH and followed by an isotherm at 60%RH for 1hour. RH was increased again at 80%RH at 4%RH/min and was followed by an isotherm at 80%RH for 1 hour. RH was decreased back to 60%RH and 20%RH in a similar way (i.e. 4%RH/min during RH transitions, isotherm of 1 hour at 60%RH and 20%RH) (used on CNF and Animal glue films)
- RH program DVS2: RH stabilised at 20%RH for 30min, then increased at 4%RH/min to 80%RH and left between 30 and 1hour at 80%RH (used on 4 canvas samples treated with traditional consolidants).

4.2.6 Ageing protocol

The accelerated ageing of the samples was performed using an ageing chamber at the research laboratory of the RIJKS museum (Amsterdam, NL) which enable precise control and programming of RH and T fluctuations. The ageing program used was adapted from one previously used by Chevalier-Menu (2010). It uses fluctuations in RH and T in the dark and was developed to mimic natural degradation of painting adhesives and canvases. It has been successfully applied on canvas and canvas adhesives and consolidants such as glue paste (mixture of animal glue and flour), Beva 371 and Plexisol P550 among others. These two later materials are also included in our study. The use of cycles of RH and T for the ageing was motivated by the higher accuracy of this kind of test to simulate stresses undergone by materials in real case scenario. A painting exhibited by a collector, in a historical house or a museum without sufficient environment controls, can be subjected to widespread variations in RH and T caused by the outdoor environment.

The ageing program can be described as follow (see also Figure 4.10).

1) 80°C, 40%RH, for 54h
2) 80°C, 80%RH, for 54h
3) 20°C, 70%RH, for 54h
4) 20°C, 40%RH, for 54h
5) 80°C, 40%RH, for 54h
6) 80°C, 80%RH, for 54h
7) 20°C, 70%RH, for 54h
8) 20°C, 40%RH, for 54h
9) 80°C, 80%RH, for 168h

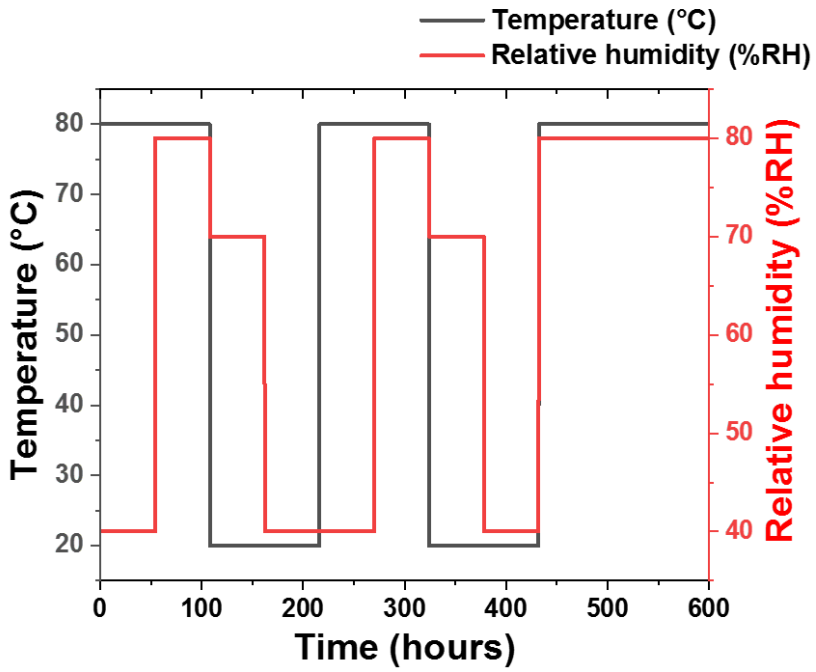

Figure 4.10: Accelerated ageing program used (from Chevalier-Menu, 2010) which consists of cycles of RH and T in the dark.

The samples were suspended as shown in Figure 4.11.

Figure 4.11: Samples hanging in the ageing chamber.

4.3 Results

Natural and synthetic traditional adhesives and newly developed nanocellulose-based consolidants were assessed to compared their respective performance in terms of effect on visual appearance, consolidation, response to fluctuations in RH and effect of ageing.

4.3.1 Appearance/penetration

First assessment of the treated samples was carried out by colourimetry used to quantify the colour of the sample. The treatment deposition was then assessed at the microscale by SEM. Crucially, the degraded cotton canvas tested has a strong white colour as opposed to its original, beige, colour (before degradation). This change in colour is a result of the degradation procedure applied which involves using H_2O_2 thus leading to canvas bleaching (cf. 2.1.1.2 in Chapter 2).

After application by brushing of the nanocellulose-based treatments, the change in appearance between treated and the untreated canvas remains minimal (see Figure 4.32 later in

the text). As seen in Figure 4.12, for all the samples, the colour variation ΔE* measured between treated and untreated cotton canvas remains below 3. Below this value, the colour change is considered as minimal and only perceptible for expert eyes or when the two colours compared are placed next to another (Wojciech, 2011).

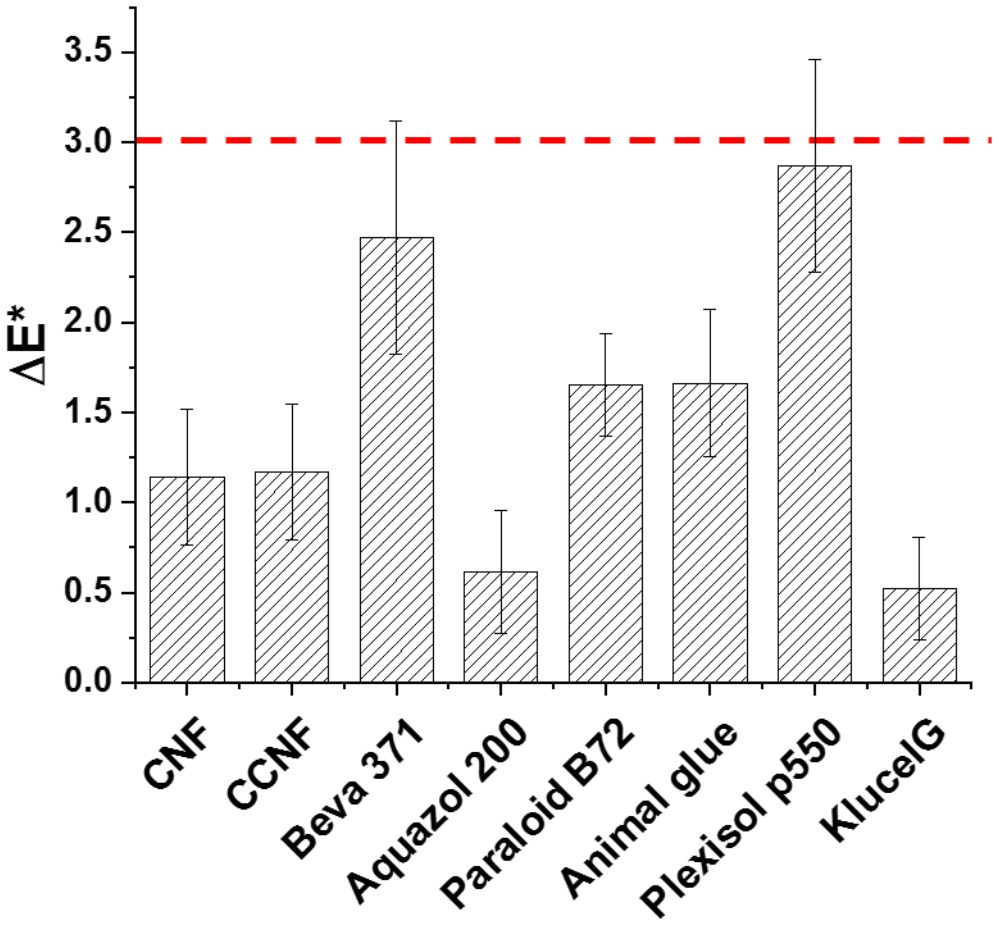

Figure 4.12: Colour change ΔE* measured after the application of traditional and nanocellulosic treatments on a degraded cotton canvas.

The surface of the canvas samples was also imaged using SEM to inform on the behaviour of the treatments when applied on the woven fabric. Figure 4.13 shows that all the traditional consolidant are not clearly visible on the canvas surface when this latter is imaged at low magnification (i.e. between x35 and x40). The nanocellulosic treatments, however, form a continuous and dense surface coating visible in the high magnification SEM image for CNF in

Figure 4.13. Similar surface deposition was observed for CCNF which is therefore not shown in the figure. The threads and fibrils of the underlying canvas are still visible after the application of the treatment. However, the weaving of the threads and cotton fibres of which they are made and which can be seen for the untreated canvas are mostly covered with a layer of treatment. If the threads are distinguished by their shape and regular size, the woven structure is no more clearly identifiable. The nanocellulose layer covers the interstices and voids seen between the threads of the untreated sample. The coated surface appears flat. Fibrils of the canvas trapped in the coating are seen across the surface of the sample.

At higher magnification, the presence of adhesive and consolidant on and in-between cotton fibres can be observed for all the traditional consolidants. The consolidants are forming bridges linking and connecting the cotton fibres together and holding them together. Those bridges are narrow as seen for animal glue, Beva 371, Aquazol 200 or Plexisol P550, or continuous and filling all the inter-fibres spaces as seen for Klucel. The Paraloid B72 treated sample is particular as the treatment does not seem to attach to the cotton fibres. Moreover, the treatment film presents a series of holes which probably result from the presence of air bubbles in the consolidant when prepared and applied on the canvas. Holes, but much smaller, can also be seen in the Klucel adhesive.

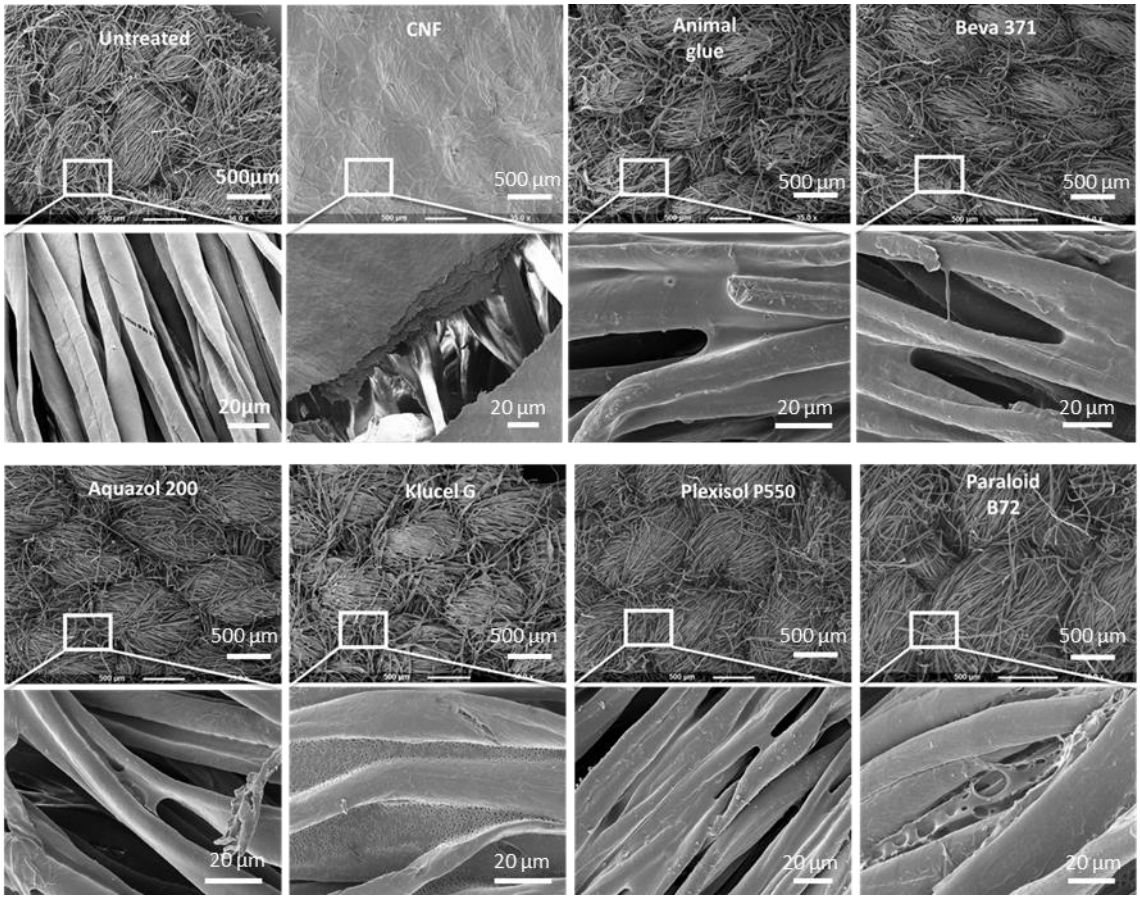

Figure 4.13: SEM images of a degraded cotton canvas before and after treatment using and the nanocellulose treatment CNF and adhesive and consolidants commonly in used in conservation: animal glue, Beva 371, Aquazol 200, KlucelG, Plexisol P550 and Paraloid B72. The images were taken at 2 different magnifications (x35-x40 in row 1 and 3, x1200-x2000 in row 2 and 4) to highlight differences in surface deposition of the treatments. The scale bars in row 1 and 3 correspond to 500 µm and those in row 2 and 4 to 20µm as shown for the untreated sample.

4.3.2 Consolidation

Following the visual assessment of the samples, consolidation provided by the traditional consolidants in comparison with the nanocellulose-based consolidants was measured by tensile testing. The tensile tests were performed at both 20 and 80%RH since it is well-known that moisture, hence RH, can greatly influence the mechanical response of materials encountered in paintings. This was previously shown for canvas (Hedley, 1988; Mecklenburg, 2007; Young, 2001) (see also Chapter 3 in 3.4.3.3 for linen canvas) which was shown to stiffen above 75%RH due to the swelling of the threads or lining adhesives such as animal glue or cellulose ether which

lose its strength with increasing RH (Mecklenburg, 2007). Therefore, tensile tests performed at 20 and 80%RH allow investigating the reinforcement achieved after treatment as well as to gain insights into the performance of the treatments at different RH.

a

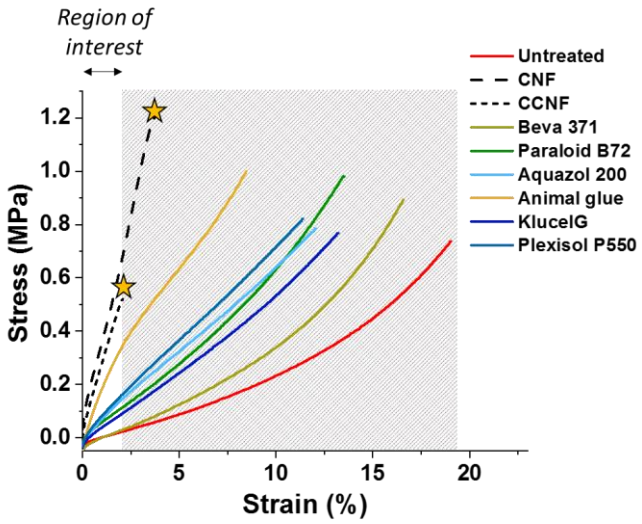

b

Sample	Young's modulus (MPa) *At 20%RH*
Untreated	1.8±0.2
CNF	23.1±1.8
CCNF	23.8±5.4
Beva 371	3.8±0.8
Paraloid B72	6.0±1.1
Aquazol 200	6.8±0.8
Animal glue	14.3±2.1
Klucel G	5.9±1.1
Plexisol P550	7.2±0.9

Figure 4.14: In (a), stress-strain curves measured at 20%RH (25°C) for untreated and treated degraded cotton canvases using traditional adhesives (Beva 371, Paraloid B72, Aquazol200, Animal glue, KluceG and Plexisol P550) and newly developed nanocellulosic consolidants (CNF and CCNF). In (b), Young's moduli measured at 20%RH from the slopes of the stress-strain curves shown in (a) in the region of interest for paintings (i.e. 0-2%) **(Mecklenburg, 1982).** ***The yellow stars seen in (a) on the tensile curves of the CNF and CCNF-treated samples are here to indicate the first loss in tension experienced by the samples and was attributed to the rupture of the CNF and CCNF coating layers. This loss was followed by an important increase in elongation and recovery of the tension starting from lower tensions. This is not shown in here but can be seen in Figure 4.15 in Appendix for the tensile tests performed at 80%RH.***

As a first step, the consolidation provided by the treatments was examined. Figure 4.14 shows the results of the tensile testing performed at 20%RH. As shown in Figure 4.14, the application of traditional as well as nanocellulose-based treatments led to an increase in stiffness of the treated degraded cotton canvases. This is seen as an increase in the slope of the stress-strain curves measured in the region of interest, i.e. between 1-2% in elongation, at which canvas are commonly stretched (Mecklenburg, 1982). Among all the treatments tested, the largest increase

in Young's modulus *Y*, resulting from the treatment application and measured in the region of interest, was obtained for the nanocellulose-based treatments, CNF and CCNF. Increases in *Y* from 1.8±0.2MPa (untreated canvas) to 23.1±1.8 and 23.8±5.4MPa for the CNF and CCNF-treated cotton canvas were measured, respectively (Figure 4.14). The increase in stiffness measured for the traditional consolidants remains, in comparison, below 5MPa. Among traditional consolidants, animal glue offers the highest reinforcement. Young's moduli of 14.3±2.1MPa was measured for the animal glue treated canvas whereas Young's moduli remain below 7.2MPa for the other traditional consolidants, hence ParaloidB72, Beva 371, Aquazol 200, KlucelG and Plexisol P550. For the same weight added, the nanocellulosic treatments seem thus to offer a more effective consolidation (for the same weight added) than traditional consolidants.

Similar observations and results were obtained from the comparison of the results of the tensile tests performed at 80%RH. The results for the 80%RH tests can be found in Figure 4.15. Overall, the consolidation provided by the traditional and nanocellulose consolidants is maintained upon exposure to 80%RH. Higher consolidation is again provided by the nanocellulose treatments in comparison to the traditional consolidants.

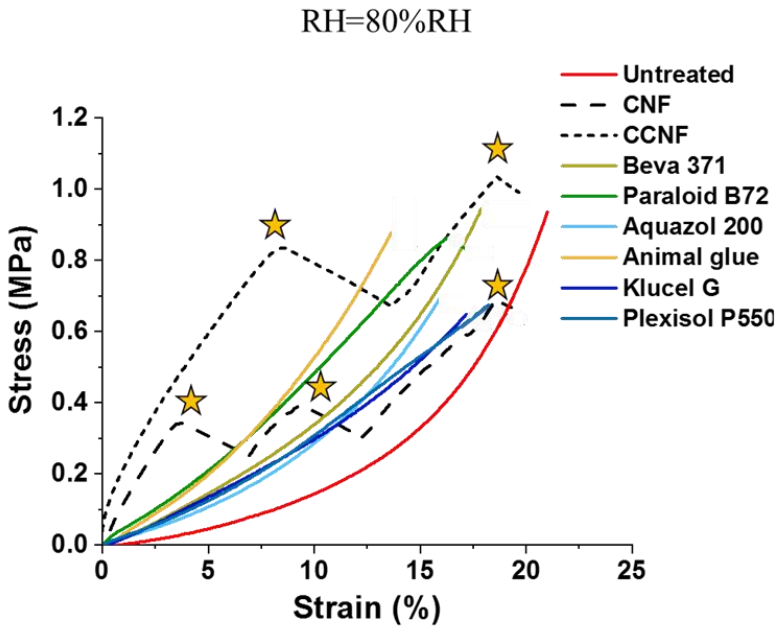

Figure 4.15: Stress-strain curves measured at 80%RH (25°C) for untreated and treated degraded cotton canvases using traditional adhesives and newly developed nanocellulosic

consolidants. Localised rupture of the CNF- and CCNF-treated cotton canvases are indicated by the stars on the stress-strain curves.

Another difference between mechanical behaviour of traditional and nanocellulose-based treatments tested here was also observed. As opposed to the tensile curves obtained for the traditional consolidants, in Figure 4.14, non-linear behaviour of the stress-strain curves for the CNF- and CCNF treated samples was seen above 2% of extension. From 2.3% and 4.1% elongation, for the CNF and CCNF-treated sample respectively, drops in tension can be observed. This behaviour has been already observed before for samples treated with CNF (Nechyporchuk, 2018). Moreover, when measured at 80%RH, the same drops could be observed for the two nanocellulose-based treatments (Figure 4.15). As shown previously in the high magnification SEM image of the CNF-treated canvas in Figure 4.13, the CNF and CCNF consolidants form a film which sits on top of the canvas (see CCNF-treated canvas in Figure B.1 in Appendix). It can be thus assumed that those drops in tension are the result of localised ruptures of the consolidant film. This will be discussed in more depth in the following chapter. Despite the higher mechanical performance of the nanocellulosic treatments, the risks associated with its brittleness combined with its tendency to form a film when applied on a canvas could be one of their limitations.

4.3.3 Response to moisture

As already mentioned (cf. 4.3.2), the consolidation provided by the treatments is maintained at low and high RH levels. It is however also important to understand how the tension of the samples varies with moisture and the magnitude of the mechanical changes resulting from variations in RH. The question is not here about the consolidation provided by the treatments over a range of RH. The focus is put, instead, on the risks associated with the built up of mechanical stresses resulting from the time-dependent response of the materials tested to variations in RH. The higher the mechanical response is (i.e. the higher variations in tensions between RH levels) the larger the risk would be that fatigue or rupture of the canvas and the other painting layers it supports occurs.

The mechanical response of the untreated and treated canvases was measured at different fixed RH levels as well as under continuous variations in RH. The first case, i.e. fixed RH, corresponds to the tensile tests partially presented in 4.3.2 which were performed at 20 and 80%RH (25°C). The second one, refers to the assessment of the canvas samples by DMA-RH for which 20-80-20%RH (4%RH/min, 25°C) RH cycles were applied. The results of both of the tests are discussed.

4.3.3.1 Loss in Young's modulus at high RH

First, variations in Young's moduli between 20 and 80%RH were analysed. An example of tensile curves measured at 20 and 80%RH can be seen for the animal glue-treated sample in Figure 4.16. The Young's moduli (*Y*) calculated at 20 and 80%RH from the tensile, or stress-strain, curves for untreated and treated cotton canvases are reported in Figure 4.17. As seen in the diagram, the increase in RH is responsible for a loss in Young's modulus *Y* (or stiffness) measured for all the canvas samples, untreated or treated.

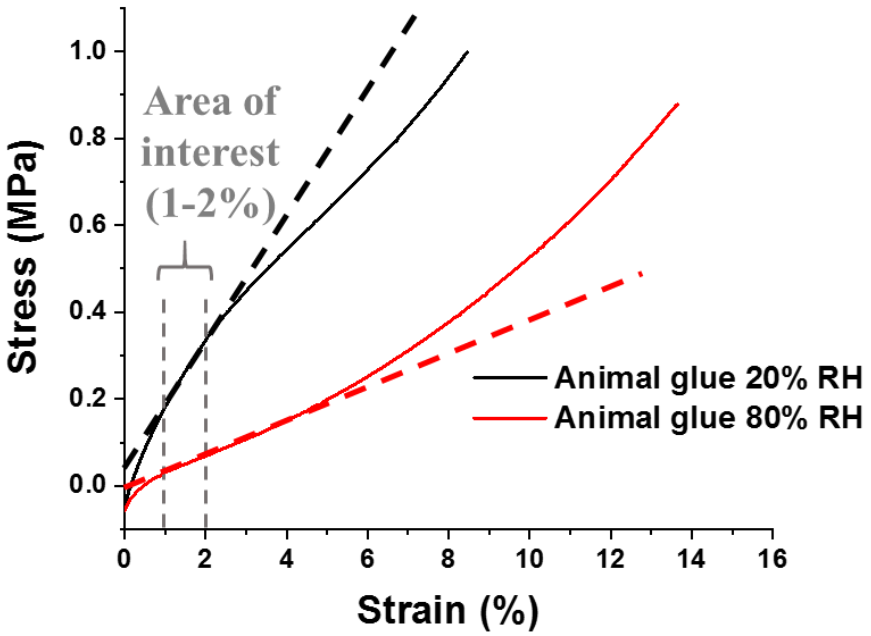

Figure 4.16: Stress-strain curves of a degraded cotton canvas treated with animal glue measured at 20 (black) and 80%RH (red). The tensile curves were fitted by linear regression in

the region of interest (1-2% in elongation) (dotted lines black (20%RH) and reed(80%RH)). The slopes of the fitted curves correspond to the Young's modulus of the tensile curves.

It has been previously argued that the plasticization of the degraded cotton canvas at increase RH level results from water diffusion in the canvas (c.f. 3.4.2.3 in Chapter 3). As water molecules quickly diffuse in the amorphous regions of the cellulose fibres, hydrogen bonding between cellulose chains are replaced by water-cellulose hydrogen bonding. The structure formed by the cellulose chains and their packing is disrupted and this would cause the loss observed in mechanical properties. It is assumed that the same occurs with the different adhesives and consolidants tested in this study. In the latter case, losses in the stiffness of the materials might be associated with a reduction in the interfacial adhesion between adhesive and cellulose fibres. This effect was observed by Bowditch (1996) in a study on the performance of epoxy-based adhesive joint for wood exposed to water.

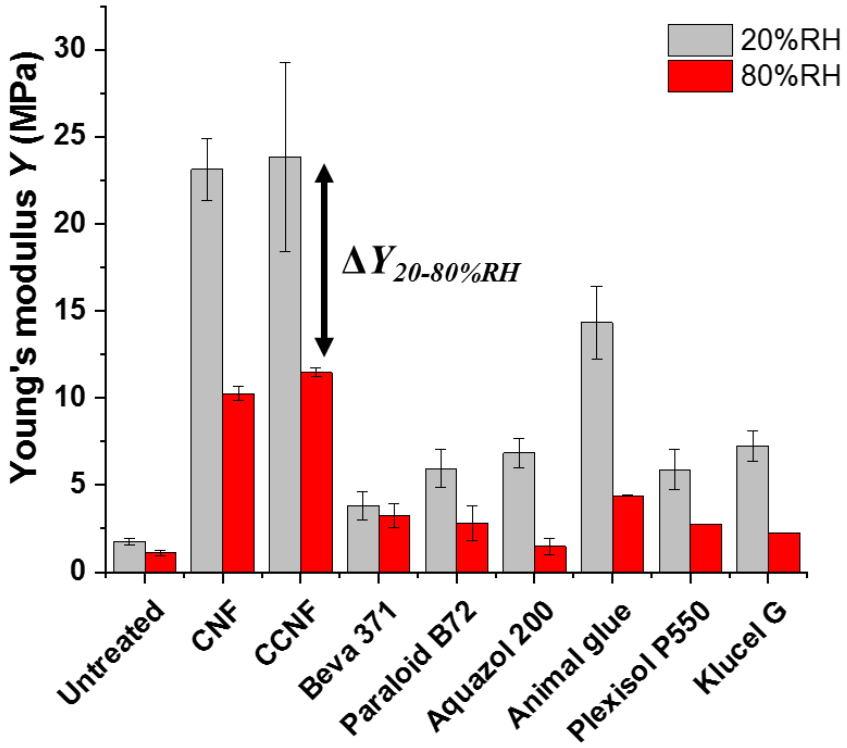

Figure 4.17: Young's moduli measured at 20%RH (grey) and 80%RH (red) for untreated and treated cotton canvases using traditional and nanocellulosic consolidants. The Young's moduli Y were calculated from the slope of the stress-strain curves in the region of interest (1-2% in elongation) as shown in Figure 4.14. $\Delta Y_{20\text{-}80\%RH}$ corresponds to the difference between Young

moduli measured at 20%RH and 80%RH which values are given for each sample in Table 4.2 below.

The decrease in *Y*, however, varies among samples. Among traditional consolidants, losses in *Y* range from 0.6±1.5 to 9.9±2.1MPa measured for Beva371 and Animal glue, respectively (Table 4.2). As expected, the water-and ethanol-based treatments Animal glue and, Aquazol200 and Klucel G (see Table 4.1) are more sensitive to water moisture, more hygroscopic. This is because these materials contain a higher number of hydroxyl groups on the surface of their polymeric chains (see 4.2.1 for chemical structure of these adhesives) which makes them more responsive to moisture and more prone to interact with the water molecules through hydrogen bonding (Burchard, 2003; von Endt, 1991). This leads to important losses in *Y* between 69 and 78% (Table 4.2) measured for these samples as opposed to Beva371 (cyclohexane-based), ParaloidB72 (acetone-based) and PlexisolP550 (white-spirit-based), for which losses in *Y* remain below 55%. The percentage in loss is particularly low (i.e. 15%) for the canvas treated with the cyclohexane-based Beva371 treatment.

Sample	**$\Delta Y_{20\text{-}80\%RH}$ (MPa)**	**% Y loss (%)**
	$\Delta Y_{20\text{-}80\%RH} = Y_{20\%RH} - Y_{80\%RH}$	$\%\ Y\ loss = \Delta Y_{20\text{-}80\%RH} / Y_{20\%RH}$
Untreated	0.7±0.2	38
CNF	12.9±1.8	52
CCNF	12.3±5.4	56
Beva 371	0.6±1.5	15
Paraloid B72	3.1±1.5	53
Aquazol 200	5.4±1.0	78
Animal glue	9.9±2.1	69
Plexisol P550	2.7±N/A	54
Klucel G	2.3±N/A	69

Table 4.2: Difference $\Delta Y_{20\text{-}80\%RH}$ calculated between Young's moduli measured at 20%RH (i.e. $Y_{20\%RH}$) and 80%RH (i.e. $Y_{80\%RH}$) for untreated and treated degraded cotton canvases. V

However, despite the loss in stiffness measured at 80%RH for all the traditional consolidants, the consolidation provided by the treatments remain effective. As seen in Figure 4.17, Young's moduli measured at 80%RH for the samples treated with traditional consolidants remain higher (>2.2MPa) than for the untreated canvas. The only exception is Aquazol 200 for which a *Y* of 1.5±0.5MPa similar to 1.1±0.1MPa measured for the untreated sample is reached at 80%RH. This indicates that at high RH, Aquazol200 fails in providing consolidation to the cotton canvas.

In comparison, the nanocellulose-treated canvases, which are also the stiffest canvas samples, register the highest losses in Y (Table 4.2). Losses from 23.1±1.8 and 23.8±5.4MPa (*Y* at 20%RH) to 10.3±0.4 and 11.5±0.3MPa (*Y* at 80%RH) were observed for the CNF and CCNF-treated cotton canvas, respectively. These losses are equivalent to a decrease of approximately 55% in stiffness for both samples. This is likely due to the higher hygroscopic behaviour of nanocellulose than natural fibres such as cotton. It has been previously shown that depending on the preparation method, the specific surface area of CNF nanofibrils can approach 500 m^2/g (Sehaqui, 2014; Sehaqui, 2011), while the specific surface area of soft cellulose pulp typically ranges between 1 and 4 m^2/g (Banavath, 2011). This increase in surface area is related to an increase in the availability of the hydroxyl groups on the surface of nanocellulose leading to a higher hygroscopicity.

Nevertheless, *Y* measured at 80%RH for these 2 samples remains higher than all the other samples, untreated or treated with traditional consolidants. This shows that the nanocellulose treatments the consolidation provided by the nanocellulose treatments CNF and CCNF to the degraded cotton canvas is maintained at 80%RH. The higher performance in terms of reinforcement of these 2 treatments compared to those of the traditional consolidants remains also unchanged at high RH level.

4.3.3.2 Viscoelastic response to moisture under dynamic RH variations: overall variations and real-time response

4.3.3.2.1 Variations in storage modulus

The mechanical response of the samples to moisture was also measured dynamically using RH variations and DMA. Here the RH was programmed to vary between 20 and 80%RH, the RH levels used for the tensile tests. The advantage of the DMA-RH measurement over tensile testing is that it enables measuring the real-time response of the same sample at different RH and during RH transitions, non-destructively (as opposed to tensile testing). An example of the mechanical response of a Beva371-treated canvas measured by DMA-RH upon use of a 20-80%RH RH program is shown in Figure 4.18. It is expected that the results of the DMA-RH experiment should be in good agreement with those of the tensile tests. This is because the same the same RH levels were tested (i.e. 20 and 80%RH) and the storage modulus *E'* obtained from the DMA-RH measurement can give a measure of the stiffness of a material (cf. 2.2.4.2 in Chapter 2).

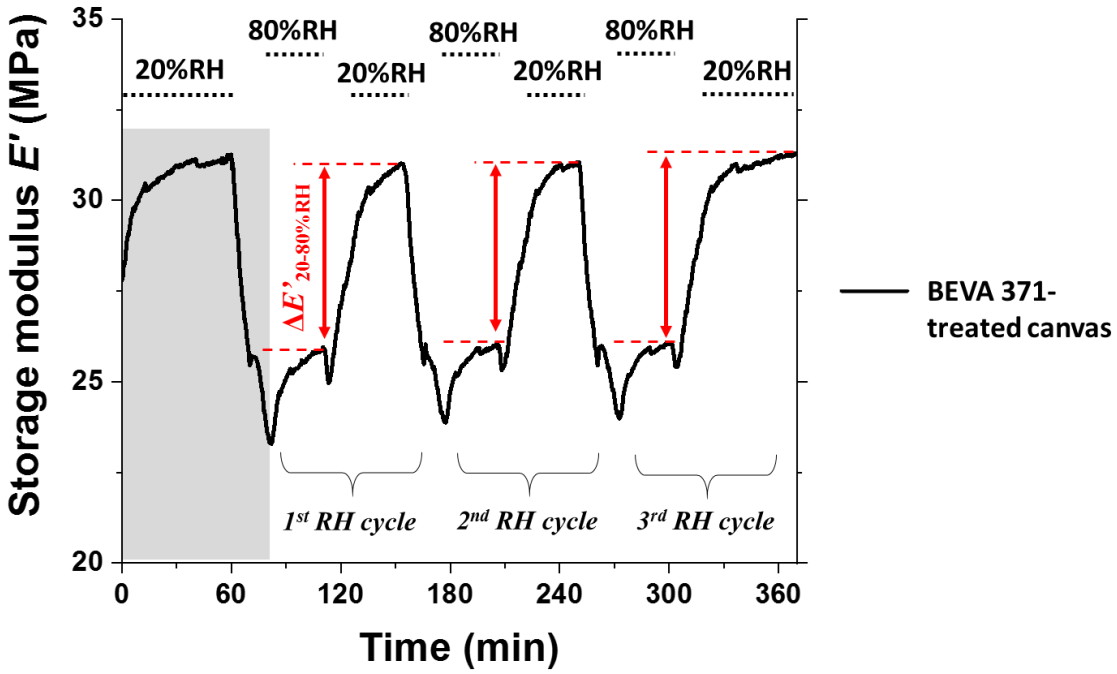

Figure 4.18: DMA-RH curve obtained for a Beva 371-treated canvas submitted to 3 RH cycles (20-80-20%RH, 4%RH/min for 20-60%RH, 2%RH.min for 60-80%RH and 4%RH.min for 80-20%RH, at 25°C). The first 20%RH will always be discarded in the analysis of the DMA-RH curves as the first 20-80%RH transition is associated to important mechanical rearrangements of the canvas (i.e. mechanical conditioning) and this variability can be a source of errors as shown in Chapter 3 (cf. 3.4.2.1). $\Delta E'_{20\text{-}80\%RH}$ is calculated from the end-plateaux values of E' at 20 and 80%RH at each RH cycle.

As seen in Figure 4.18, the response of the Beva371-treated sample is characterised by an increase in *E'* at low RH level (20%RH) and decrease in *E'* at high RH level (80%RH). This indicates that the treated canvas responds to RH variations by showing a lower viscoelastic behaviour (hence becoming stiffer) at low RH and a higher viscoelastic behaviour at high RH. This mechanical response is similar than the one measured for a degraded cotton canvas as shown previously in Chapter 3 for the same RH-program (i.e. 20-80-20%RH) (cf. 3.4.1.3). The canvas samples treated with the other traditional adhesives of this study as well as the nanocellulose-treated canvases also responded in a similar way. Representative DMA-RH curves for the canvases treated with the traditional treatments and nanocellulose consolidants are given in Figure 4.19 and Figure 4.20, respectively.

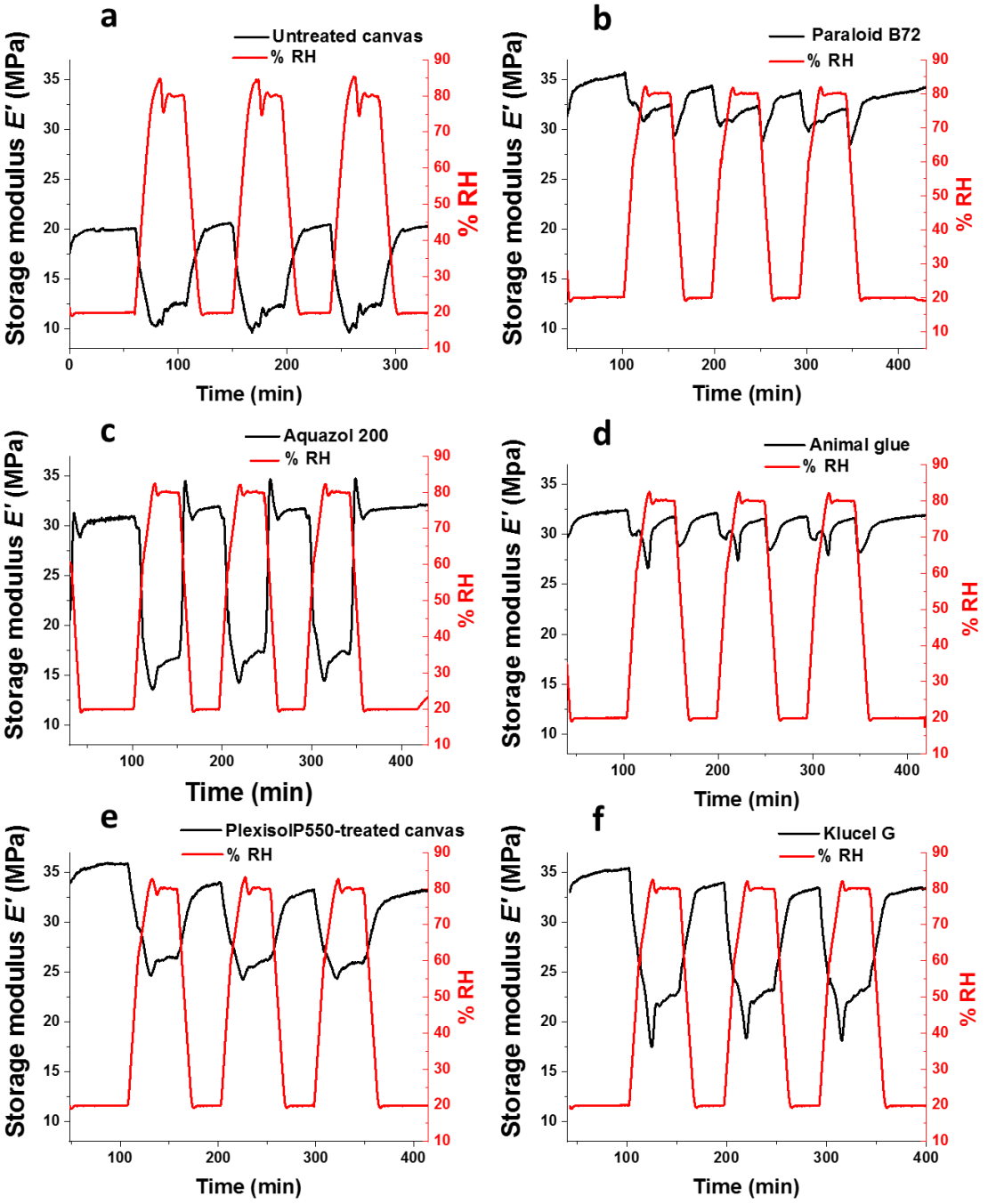

Figure 4.19: DMA-RH curves of degraded cotton canvases untreated (a) and treated by brushing with traditional consolidants such as Paraloid B72(b), Aquazol 200 (c), Animal glue (d), Plexisol P550 (e) and Klucel G (f) (5% total added weight) under 20-80-20%RH RH program.

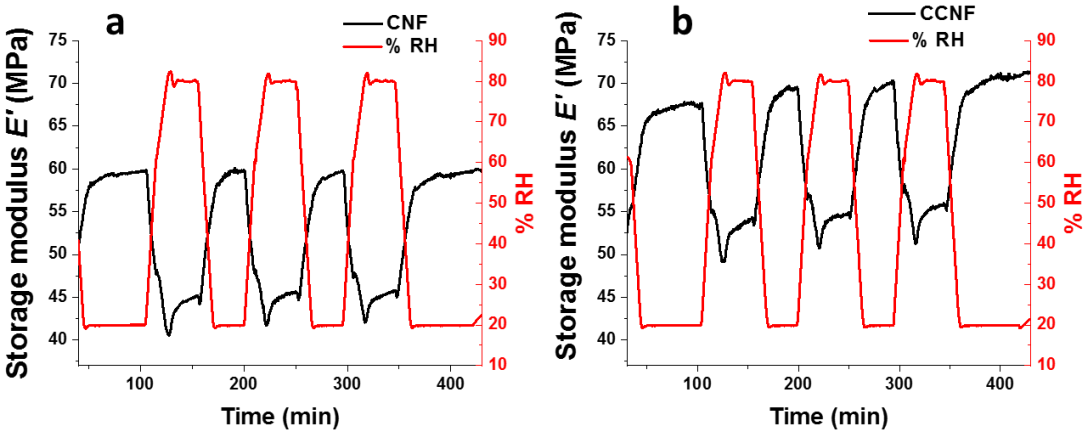

Figure 4.20: DMA-RH curves of degraded cotton canvases treated by brushing with the nanocellulose consolidants CNF (a) and CCNF (b) (5% total added weight) under 20-80-20%RH RH program.

As seen in Figure 4.19 and Figure 4.20, the untreated and treated degraded cotton canvases absorb moisture at different rates depending on whether they are in RH ramping or under steady state conditions. The RH overshoots occurring at 80%RH during the humidification transitions are responsible for example for the apparition of rapid jump and decrease in *E'* seen in the mechanical response of the Aquazol 200-treated canvas (Figure 4.19).

The focus here is the sorption that occurs in the steady state (i.e. RH equilibration). The difference in *E'* measured between RH plateaux at 20 and 80%RH (end-plateaux values) are shown in Figure 4.21. The results are given for the 2nd RH cycle. As seen in Figure 4.21, the results are partly in agreement with the variations in Young's modulus measured by tensile tests and shown in Table 4.2. High variations in *E'*, between the 20 and 80%RH plateaux were measured for the nanocellulose consolidants (i.e. $\Delta E'_{2nd\ cycle}$=13.8±0.7MPa for the CNF- and $\Delta E'_{2nd\ cycle}$ =14.9±1.9MPa for the CCNF-treated canvas). The hygroscopic treatments Aquazol 200 and Klucel G also show a higher mechanical response to moisture variations than the less hygroscopic consolidants, such as Paraloid B72 or Beva 371and Plexisol 200 and this fits with the expectations.

The Aquazol 200 treatment induces particularly strong variations in *E'* between dry (20%RH) and humid (80%RH) state as highlighted in Figure 4.21 by variations in *E'* at $\Delta E'_{2nd}$

$_{cycle}$=13.8±0.7MPa similar to those measured for CNF and CCNF. These high variations in *E'* measured for Aquazol 200 are probably due to the swelling and melting of the consolidant upon the use of high RH levels.

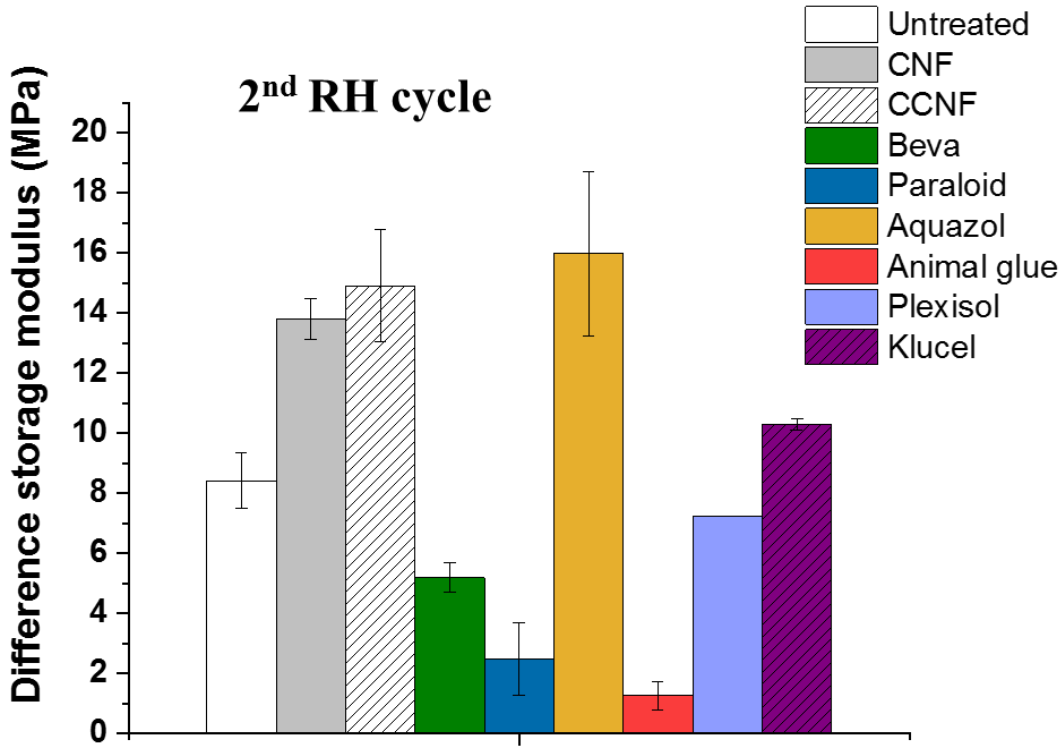

Figure 4.21: Difference ΔE'$_{20\text{-}80\%RH}$ in storage modulus E' between the 20 and following 80%RH plateaux (end-plateau values for 2nd RH cycle).

This was confirmed by performing a similar DMA-RH test on a film of Aquazol 200, using the same RH program as for the treated canvas. In Figure 4.22, the DMA-RH curves obtained for the Aquazol200-treated canvas (Figure 4.22a) and the Aquazol200 film (Figure 4.22b) are shown. From the first RH transition from 20 to 80%RH, it can be seen that the film loses all its tension which led to the measurement to be stopped. This was expected as it is known that the glass transition (T_g) temperatures is strongly dependent on the RH level and is known to decrease upon increase in RH (Kohan, 1996; Odlyha, 1998; Lawrence, 2001). Aquazol 200 has a Tg at 20%RH, 25°C of 69-71C (Table 4.1). Upon increase in RH and because of its high hygroscopic behaviour, its Tg decreases and might go below 25°C, temperature at which the

DMA-RH measurements were performed. As a result, it loses its stiffness and is enter its viscous or rubbery state.

Additionally, it has also been previously reported that Aquazol200 can become tacky at around 60-65% RH (Muros, 2012) or even undergo cold flow when stored in environments of 50-70% RH and 21-24°C (Arslanoglu, 2004). In such cases, the adhesive was seen to swell and, in a few instances, lose some of its adhesive strength. Interestingly, when the treatment is present on the canvas support, the fibrous structure seems to hold the treatment in place, which could lead to to higher penetration). Therefore, as seen in Figure 4.22, when RH cycle goes back to lower RH values after 30 min exposure to 80% RH, the consolidant is reformed and *E'* increases back to its previous value. This is highlighted by the stable variations in *E'* measured by DMA-RH. Similar observations were made for KlucelG another water-sensitive adhesive also prone to flow at high RH levels (see DMA-RH curves of the treated canvas and film in Appendix Figure B.2).

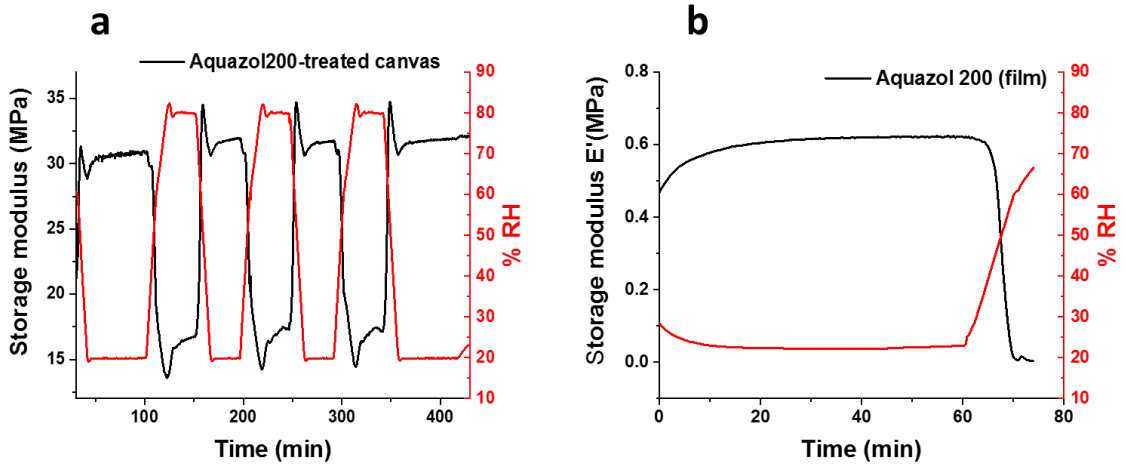

Figure 4.22: Variations in E' measured for a cotton canvas treated with Aquazol 200 (black, left) and a film of Aquazol 200 (black, right) upon application of the 20-80-20 RH program (red).

Discrepancies between the results of the DMA and tensile tests also arise from the results presented in Figure 4.21 and Table 4.2. This is particularly the case of the animal glue-treated canvas for which the lowest difference in *E'* between 20 and 80%RH plateaux (i.e. $\Delta E'_{2nd\ cycle}$=1.67±1.25 MPa) was measured. Yet, tensile tests in section 4.3.3.1. had shown that the

mechanical response of this sample was, behind those of the nanocellulose-treatments, the largest among traditional consolidants. The high mechanical response of animal glue to moisture was also shown by DMA-RH. Large losses in *E'* from 1.0GPa to 0.4GPa were measured between end-plateau values (1st RH cycle) of *E'* at 20 and 80%RH, respectively (Figure B.3 in Appendix) which is particularly high in comparison with the losses measured for a Paraloid B72 (Figure B.4 in Appendix). However, contrary to the films of Aquazol 200 and Klucel G, the animal glue film could be subjected to 20-80-20%RH cycles and did not lose all the tension at high RH.

Similarly, but to a lower extent, discrepancies can also be seen between the samples treated with less hydrophilic treatments, i.e. Beva371, Paraloid B72 and Plexisol P550. Their mechanical responses to moisture, relatively to each other, differ. Tensile tests had shown that Beva371 presented the lowest response to RH variations (i.e. $\Delta Y_{20\text{-}80\%RH}$=0.6±1.5MPa) among the canvas samples (see 4.3.3.1). The results of the DMA-RH measurements instead indicate that Paraloid B72 is the less responsive material. A difference in storage modulus of $\Delta E'_{20\text{-}80\%RH}$ =2.49±1.21MPa was measured for Paraloid B72 whereas $\Delta E'_{20\text{-}80\%RH}$ of 5.19±0.51 and 7.22±N/A MPa were obtained for Beva371 and Plexisol P550, respectively. Those differences could probably result from the time-dependant response of the treatments to moisture as further investigated in the following section.

4.3.3.2.2 Real-time response of treated canvas and treatments

Figure 4.23 shows the percentage change in weight measured for films of CNF and animal glue of the same thickness which were exposed to a single RH cycle with steps at 20, 60 and 80%RH. As shown in the figure, an animal glue film will take longer to equilibrate upon increase in RH than a CNF film. For the first 60%RH plateau in Figure 4.23, the animal glue film has not yet reached equilibrium at the end of the plateau as opposed to the CNF film which seems to have reached equilibrium almost instantly. Canvas samples treated with the hygroscopic materials Animal glue and Aquazol200 and the less hygroscopic Beva371 and Paraloid B72 were also measured by DVS using a single 20 to 80%RH RH step (4%RH/min, 20%RH (30min) to 80%RH (30min-1hour)). The results shown in Figure 4.24 highlight for the hygroscopic materials, the

lower rate (lower initial slope) of moisture sorption of the Animal glue sample in comparison with Aquazol 200. During the first 10 min of measurement, the slope of weight uptake for the animal glue sample is similar to those of the two less hygroscopic materials, Beva 371 and Paraloid B72.

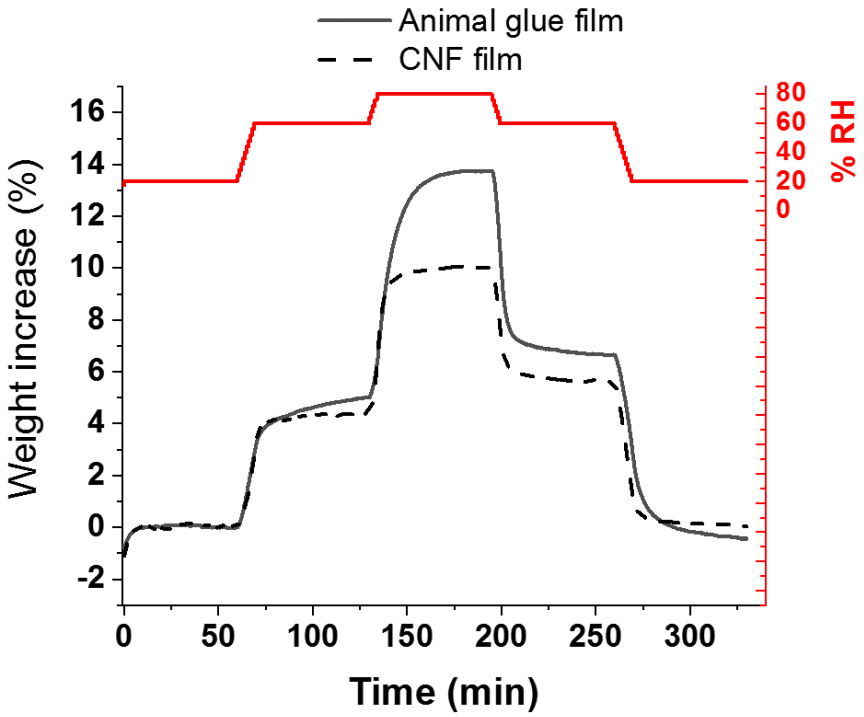

Figure 4.23: Weight uptake measured by DVS for films of CNF and animal glue exposed to a 20-60-80%RH cycle as described in 4.2.5 (DVS 1) (i.e. 4%RH/min, 1hour at the RH plateau 20, 60 and 80%RH).

Stabilisation in moisture content also seems to occur faster for the Aquazol 200 material than for Animal glue as seen by the higher slope of the curve seen for this sample than for Aquazol 200 after 30 min exposure to 80%RH. This suggest that moisture content at equilibrium of the animal glue sample could be higher than the Aquazol 200 sample upon longer exposure. These results tend to agree with the assumption previously made on the impact on distinct time-dependent responses of the samples to moisture could cause discrepancies in mechanical results. Moisture diffusion in animal glue exposed to 80%RH seems to be a slower hence longer process than for Aquazol 200.

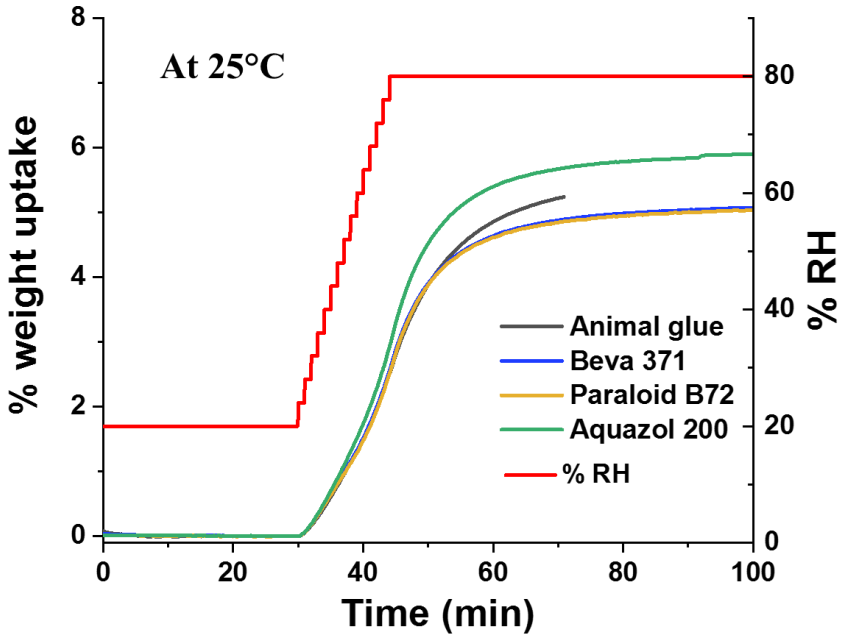

Figure 4.24: Weight uptake measured by DVS for treated degraded cotton canvases with Animal glue, Aquazol200, Beva 371 and Paraloid B72 exposed to a 20-80%RH steep cycle as described in 4.2.5 (DVS 2) (i.e. 4%RH/min, 30min at 20%RH and 30min to 1 hour at 80%RH).

From those observations, it is then possible to assume that DMA-RH may highlight differences in the real-time response of the samples to moisture. This is because the DMA measurements were carried out using fast RH cycles and short equilibration at each RH plateau (30min at 20 and 80%RH) which do not enable enough time for the samples to equilibrate in terms of moisture content. This could not be shown by the tensile tests which were performed on samples that had been left to equilibrate at a specific RH for at least 24h.

This assumption was further explored through the use of longer RH runs enabling longer time for equilibration in samples' moisture content. In Figure 4.25, the results of the longer DMA-RH run are shown for the animal glue-treated canvas. The RH was varied from 20 to 80%RH with RH equilibration at 20, 40, 60,70 and 80%RH and was stabilised at each plateau for 1h. As seen in Figure 4.25, the differences $\Delta E'$ between 20 and 80%RH remain below 5MPa which is similar to the value already measured by DMA-RH during fast RH cycling. However, the increasing slopes observed for E' at each RH plateau could also indicate that the sample has not yet reached equilibrium.

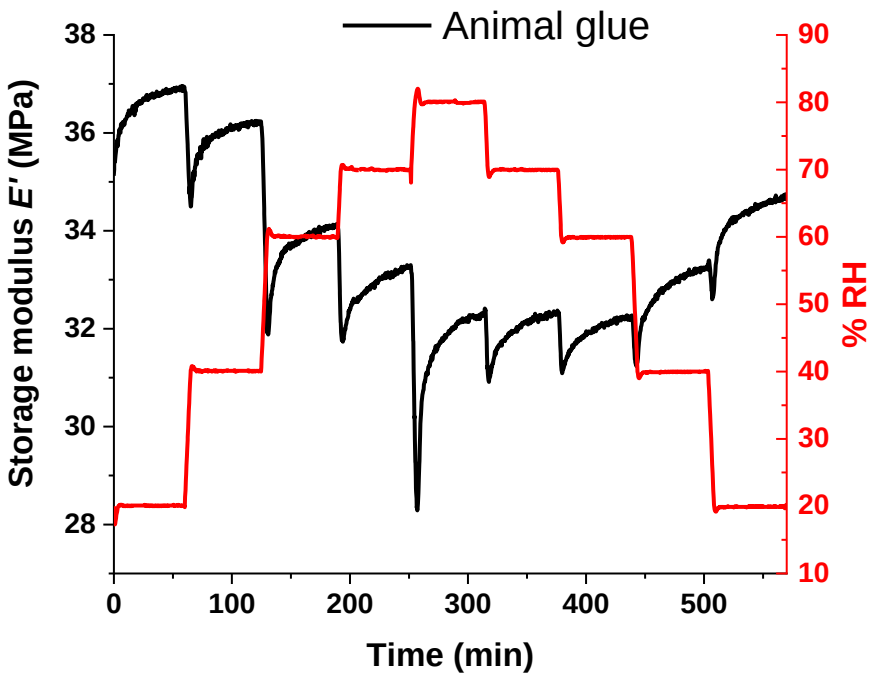

Figure 4.25: DMA-RH measurement of an animal glue treated canvas using RH steps of 10%RH from 20 to 80%RH (4%RH/min, 1hour equilibration at each RH plateau). Loss in E' was observed from low to high RH level. Variations in E' between the 20 and 80%RH levels remain below 5MPa.

The mechanical response of the samples during RH plateaux (i.e. equilibration at fixed RH) was thus analysed in more depth. The increase in *E'* observed during these RH plateaux for the samples was analysed for the untreated canvas and the Animal glue and Aquazol 200-treated samples (two hygroscopic treatments) and their response compared. These treatments were chosen since their response to moisture varied between the results of the tensile tests (cf. 4.3.3.1) and DMA-RH measurements (cf. 4.3.3.2.1). In Figure 4.26, the logarithmic increase in *E'* of the untreated and treated samples is compared for the 70%RH and 80%RH isotherms taken upon humidification (i.e. 20-80%RH transition of the RH cycle). The overall DMA-RH responses of the treated and the Aquazol 200-treated degraded cotton canvas to RH steps program can be found in Figure 3.21 (Chapter 3) and in Appendix (see Figure B.8), respectively.

At 70%RH, Figure 4.26a first highlights the faster mechanical response of the untreated and Aquazol200-treated sample over the Animal glue-treated sample occurring during the first 10 min

of the RH equilibration. The Aquazol200-treated sample then seems to mechanically stabilised as seen from 25min onwards by the low increase in *E'*, whereas the trend of the curves of the untreated and animal glue sample is similar. It is characterised by a constant increase in *E'* however lower compare to the one seen in the first minutes of exposure. These distinct trends observed between the Animal glue and Aquazol 200 samples seem to agree with the assumption that Animal glue has a lower immediate mechanical response to moisture and that this response is highly time-dependent. Aquazol200 instead has a faster mechanical response to moisture uptake which is in correlation with the faster rate of moisture sorption observed for the sample by DVS (see Figure 4.24).

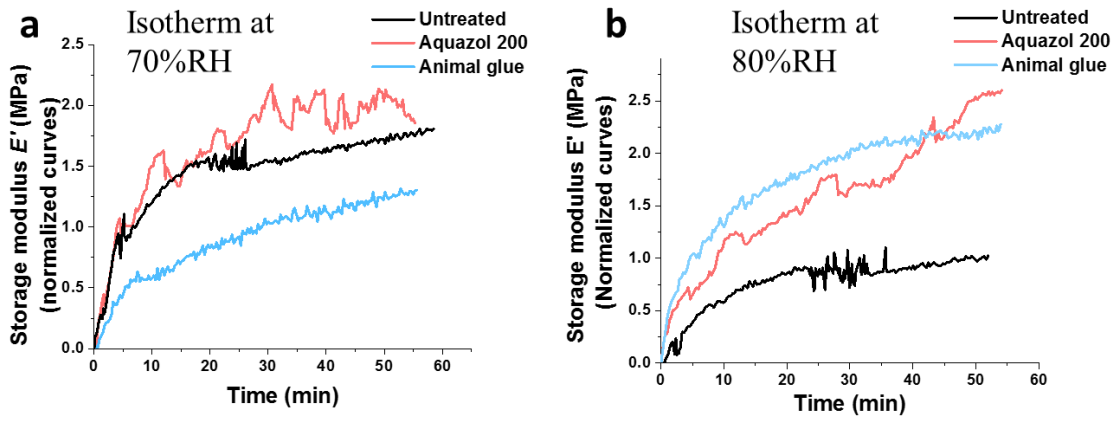

Figure 4.26: Increase in E' observed during RH plateaux (i.e. RH isotherms) at 70%RH (a) and 80%RH (b). These plots correspond to segments taken from the DMA-RH measurements using the RH step program (cf. 4.2.4 and Figure 4.25, Figure B.7 in Appendix) carried out on untreated, Aquazol 200- and Animal glue-treated degraded cotton canvas. The results shown for the 70%RH isotherm (a) are taken from the humidification ramp of the DMA-RH steps measurement.

At 80%RH, however, the animal glue sample seems to be the most responsive to RH of all the samples as seen by the rapid increase during the first 10min of exposure to 80%RH and the higher slope of the curve compared to those of the untreated and Aquazol200 samples (Figure 4.26b). Aquazol200 shows a constant increase which do not show any signs of stabilisation even after 60min of exposure. The assumptions raised during the 70%RH plateaux thus seem to be contradictory with what is shown at 80%RH. Further testing is required to understand the causes of the discrepencies observed.

In summary, the higher time-dependent response to moisture of the animal glue sample over the other samples could be seen by DVS when increasing the RH from 20 to 80% RH (Figure 4.24) This could not, however, be clearly identified by DMA-RH by analysis of the increase in *E'* during the RH isotherms (Figure 4.26) during which it would have been expected to observe a lower slope of increase in *E'* at 20% and 70, 80% RH. The results raised the question whether fitting of the *E'* curves measured during RH stabilisation could help pulling-out the long-term mechanical behaviour of the samples at a specific RH and anticipating on the final stabilised state (and final $\Delta E'$) of the canvas. Internal rearrangement and random events occurring during the arrangement could be the main difficulty faced in the analysis of the data.

There is potential for further investigation this area. The behaviour of coated or treated samples could result from a combination of factors such as mechanical response of the canvas and treatment, swelling, structural changes (slippage, stiffening) depending on the weaving. Additionally, as aspects such as modification of the treatment penetration and surface deposition during testing should be considered.

4.3.3.2.3 Mechanical damping effect of the treatments

In the studies of polymer composite structure, the incorporation of a reinforcement to the matrix is often studied in terms of visco-elastic properties. The addition of CNF as a reinforcement in a neat polymer resin of polyester was studied by Lavoratti et al. (2015). They show that the addition of CNF leads to the restriction of the free movement of the polymer molecules, thus yielding a lower Tanδ peak height, hence lower loss energy (cf. 2.2.4.2 in Chapter 2), for composites when compared to the neat polymer undoped. As a consequence, at high filler concentration (CNF=1-2%), a higher restriction of the polymer matrix molecules (lower Tan δ) were observed, compared to lower concentrations (CNF< 0.5%) (higher Tanδ).

In a dense polymer matrix, internal frictions refer to the movement between polymer molecules and any other additives added to the matrix. However, for canvas, a woven material, changes in Tan δ can result from changes in the physical and chemical properties of the cotton cellulose chains (microscale) but can also originated from purely structural properties such as

frictions between warp and weft threads, twist of the yarn which can modify the water diffusion in the yarn. In Chapter 3 (cf. 3.4.2.4), for example, the inflexions observed in the curves of *E'* and Tan delta for a degraded cotton canvas during RH transitions (humidification and dehumidification) were attributed to the slippage of cotton fibres, yarns or threads caused by unbound water. Therefore, due to the difficulty to unravel the response to moisture of fibres' type (cotton, linen) from the one of the canvas structure, interpretations of the results will be taken with care.

Figure 4.27 shows the representative mechanical responses in Tan δ of a canvas untreated and treated with the hydrophilic consolidant KlucelG. These curves highlight differences in viscoelastic behaviour between samples which will be discussed below for all the samples (untreated and treated), namely the inflexions in Tan δ seen during RH transitions (indicated by (*) in Figure 4.27) and the variations in Tan δ between the 20%RH and 80%RH isotherms (as already investigated for the DMA-RH curves in *E'* in 4.3.3.2.1).

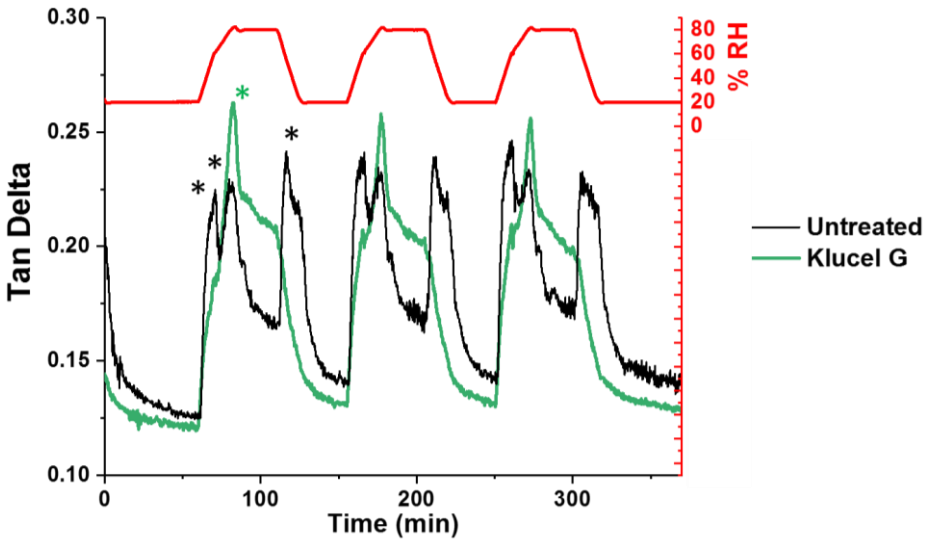

Figure 4.27: Variations in Tan δ measured over time for a degraded cotton canvas untreated (black) and treated with Klucel G (green) upon application of 20-80-20%RH cycles (RH cycling program, 25°C). Note the difference between the curves highlighted by the higher number of inflexions in the Tan δ curves seen for the untreated sample (black (*)) than for the Klucel G sample (green (*)).

The applied hydrophilic and less hydrophilic treatments are first considered separately and compared to an untreated canvas. As seen in Figure 4.28, the tan δ measured at 20%RH for all the canvas samples treated with hydrophilic consolidants are higher than the one of the untreated canvas. At 80%RH, the values in Tan δ of the treated canvases are either higher (i.e. Aquazol200 and KlucelG), either similar to the Tan δ of the untreated canvas (i.e. Animal glue). As already mentioned, Tan δ gives a measure of the part of viscous over elastic response of a material, hence the internal friction of the material. These first results could thus indicate that at 20%RH, all the consolidants provide a more stable material by reducing the free movement of the polymeric molecules of the cotton canvas. At higher RH levels, however, this stabilisation is lost and the response of the canvas seems overcome by the viscous response of the treatments. This is also translated in higher variations in Tan δ ($\Delta Tan\delta_{20\text{-}80\%RH}$ or $\Delta Tan\delta$) measured between the 20 and 80%RH plateaux (end-plateau values of Tan δ at 20 and 80%RH). Calculations and values in $\Delta Tan\delta_{20\text{-}80\%RH}$ are shown for all the untreated and treated samples in Figure 4.29.

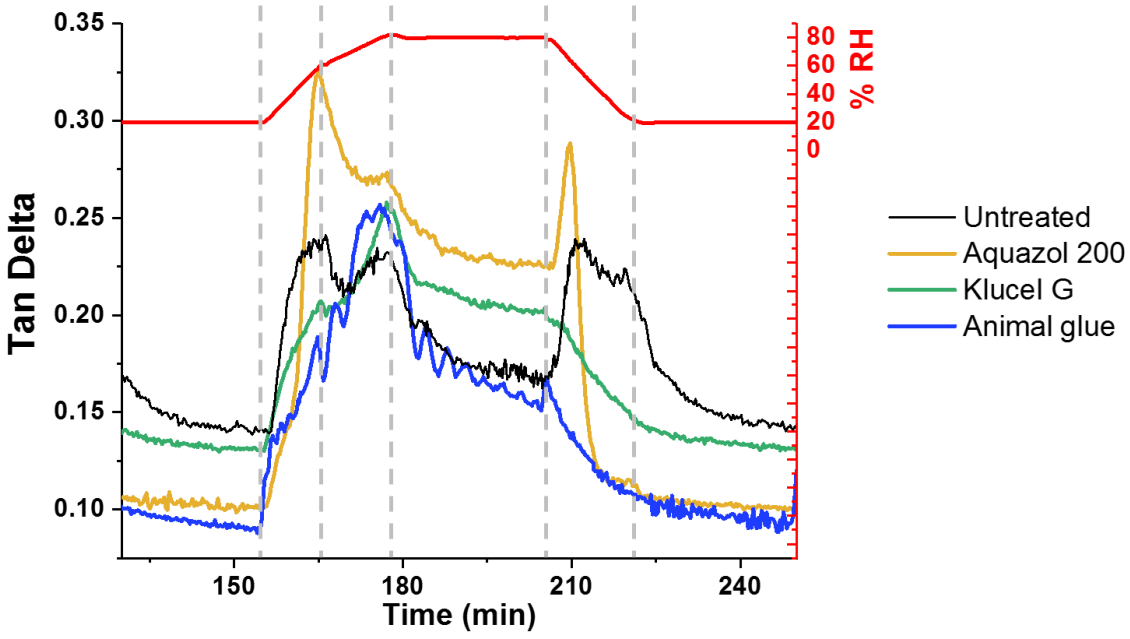

Figure 4.28: Detail of the DMA-RH results showing variations in Tan δ of untreated and treated samples upon application of one single RH 20-80-20%RH cycle (i.e. 2nd RH cycle). The results are here presented for the degraded cotton canvas untreated and treated with the hydrophilic traditional consolidants, Aquazol 200, KlucelG and Animal glue.

ΔTanδ measured for the samples treated with the hydrophilic consolidants are higher (i.e. ΔTanδ>0.07) than those measured for untreated material (i.e. ΔTanδ=0.04±0.01) (Figure 4.29a). They are probably caused by swelling of the treatments as it was previously shown that Aquazol200 and Klucel G flow at 80%RH (Figure 4.22 for Aquazol 200 and Figure B.2 for Klucel G). For the Aquazol 200-treated sample, an earlier mechanical response is observed by a jump in the Tan delta during the first 20-60%RH ramp (Figure 4.28). The jump is absent from the tan δ curves of animal glue and KlucelG. This highlights the earlier response of the treatment to RH at 60%RH. This was also seen using DMA-RH with the RH steps program where the higher loss in *E'* occurs between 40 and 60%RH for the Aquazol 200-treated sample (see Figure B.7 in Appendix). This was again not observed for the canvases treated with Klucel G or animal glue.

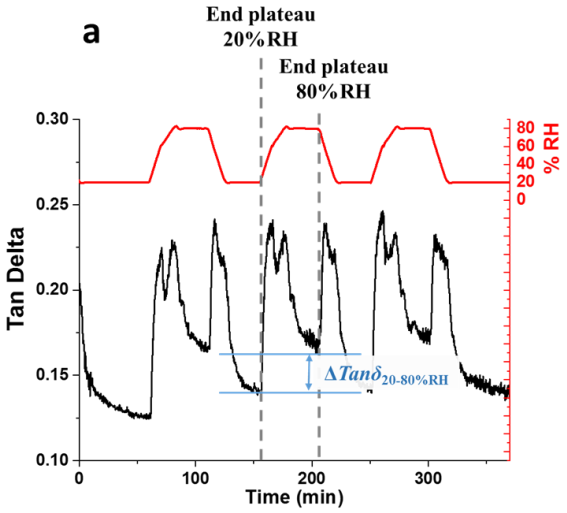

b

Sample	$\Delta Tan\delta_{20\text{-}80\%RH}$
Untreated	-0.04±0.01
CNF	-0.06±0.04
Aquazol 200	-0.19±0.02
Animal glue	-0.10±0.06
Klucel G	-0.07±0.00
Beva 371	-0.02±0.00
Paraloid B72	-0.03±0.01
Plexisol P550	-0.03±0.01

Figure 4.29: In (a), variations in Tan δ measured for an untreated degraded cotton canvas subjected to 20-80%RH RH program (cf. Figure 4.9). The variations in Tan δ (i.e. ΔTan $\delta_{20\text{-}80\text{-}20\%RH}$) calculated for the untreated and treated canvases are given in (b). These values were calculated using the end plateau values of Tan δ at 20%RH and 80%RH of the 2nd RH cycle as indicated in (b). Note in (a) that Tan δ at the end of each RH equilibration (30min plateau) had never stabilized. The values given in (b) were calculated from the difference in Tan δ between the averaged values measured in the last 1 min (i.e. 5 points on the curve) of the 20 an 80%RH plateaus of the the 2nd RH cycle. Three to five measurements were performed for each sample.

In comparison, the animal glue-treated canvas response is characterised by a lower Tan δ at 80%RH after stabilization (end plateau value). As seen previously (4.3.3.2.1), the animal glue-treated sample has a higher time of response to change in RH than Aquazol 200, Klucel G and CNF. It also seems to be more sensitive to higher RH levels than the others used in this study. As seen in Figure 4.28 and in the Appendix in Figure B.9, when the RH control went above 70%RH and then above 80%RH during the RH overshoot occurring at each 20-80%RH transition, the mechanical response of the sample is increased.

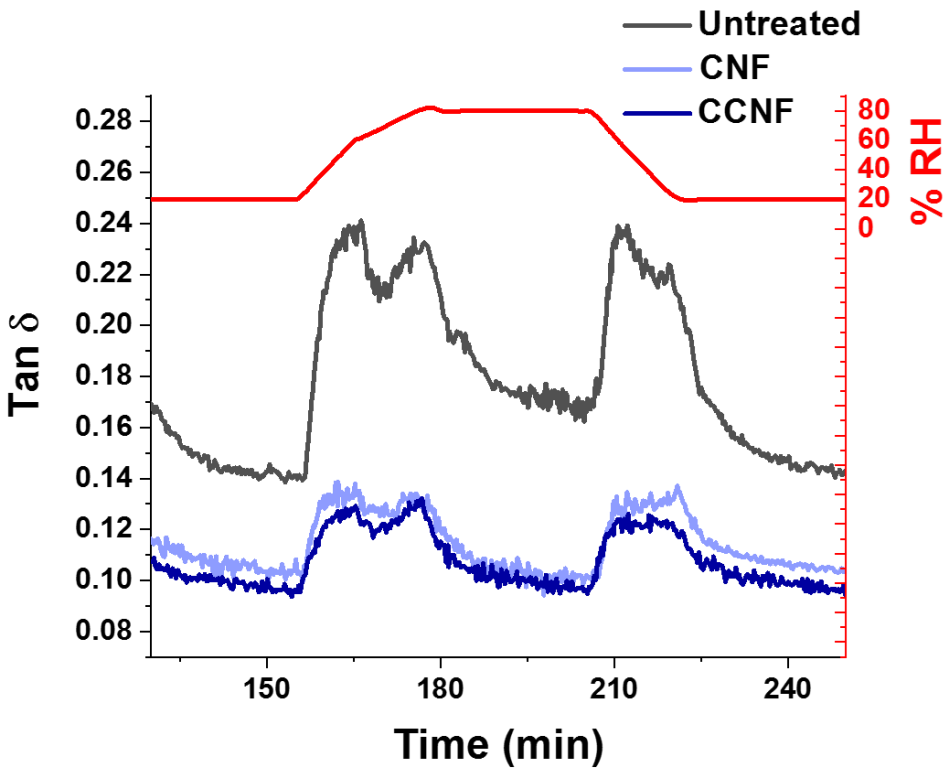

Figure 4.30: Detail of the DMA-RH results showing variations in Tan δ of untreated and treated samples upon application of one single RH 20-80-20%RH cycle (i.e. 2nd RH cycle). The results are here presented for the degraded cotton canvas untreated and treated with the hydrophilic nanocellulose consolidants CNF and CCNF.

Interestingly, as seen in Figure 4.30, the viscoelastic behaviour of the CNF and CCNF-treated canvases is similar to the untreated canvas in terms of the response to RH transitions. As for the untreated canvas, three inflexions occurring during the 20-60%RH, the 60-80%RH and the 80-20%RH transitions are seen. The fact that the CNF and CCNF treatments do not penetrate the canvas but rather remain on top of the canvas may not prevent internal motion in the canvas,

hence the response of the canvas can still be seen through the variations in Tan δ upon RH cycling similar in trend for the untreated and CNF- and CCNF-treated samples. CNF and CCNF, however, seem to reduce these motions as seen by the overall reduction in Tan δ measured between 0.10 and 0.14 for the CNF and CCNF-treated samples whereas for the untreated canvas Tan δ varies between 0.14 and 0.24. The CNF and CCNF coatings also appears to reduce the delay in response of the degraded canvas to dehumidification. This is maybe because faster diffusion of moisture occurs for these samples due to the high hydrophilic behaviour of CNF and CCNF. Comparison of the hygroscopic response of an untreated canvas with CNF and CCNF-treated canvas are shown in more detail in the next chapter (Chapter 5) which confirms this assumption.

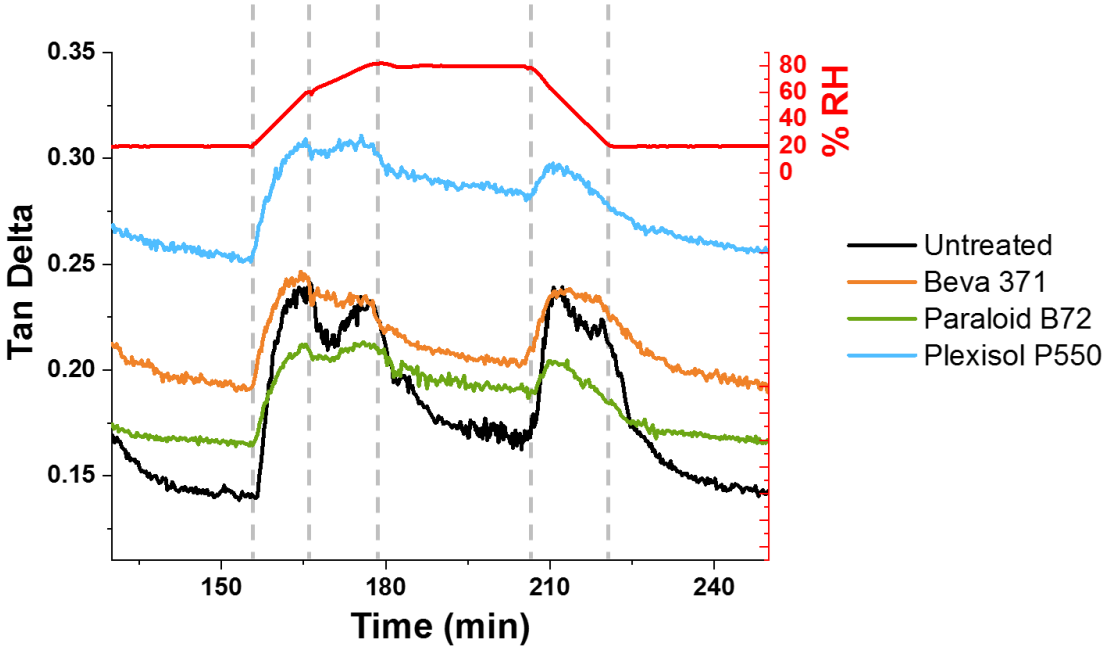

Figure 4.31: Detail of the DMA-RH results showing variations in Tan δ of degraded cotton canvas untreated and treated with less hygroscopic traditional consolidants upon application of one single RH 20-80-20%RH cycle (i.e. 2nd RH cycle). The response of Beva371, ParaloidB72 and Plexisol P550 (treatments in the less polar solvents) is compared to the untreated canvas.

In comparison, the less hydrophilic treatments, Beva 371 and Plexisol P550 do not reduce the Tan δ, i.e. internal friction in the sample, of the degraded cotton canvas either at 20%RH nor at 80%RH (Figure 4.31). The Tan δ measured for the Plexisol P550 sample is particularly high

(i.e. $Tan\delta_{20\%RH}$=0.256 compared to $Tan\delta_{20\%RH}$=0.193 for Beva 371) indicating that this sample might have the higher visco-elastic response of all the samples between 20-80%RH. This was expected since Plexisol P550 is also the material of all the consolidants tested whose Tg is the nearest to the 25°C used for testing (i.e. 29°C as seen in Table 4.1). The same applies to a lower extent to Beva 371 which was shown to exhibit a lower temperature than the 40°C indicated by the supplier. On the contrary, at 80%RH, Paraloid B72 offers a lower viscoelastic behaviour, lower internal frictions, than the untreated canvas as it was only previously observed for the animal glue and, to a lower extent, for the CNF treatments.

Overall, the results highlight the lower variations in Tan δ measured for all the less hygroscopic treatments in comparison with the untreated canvas. The untreated canvas presents a high visco-elastic response to fast change in RH as seen by the jumps in tan δ seen for all the RH transitions (20 to 60%RH, 60 to 80%RH and 80 to 20%RH). However, after stabilisation of the RH at 20 or 80%RH, Tan δ measured recover quickly to lower values as seen by the ΔTan δ measured between 20 and 80%RH in Figure 4.29a which is similar to the values calculated for the samples treated with less hygroscopic traditional consolidants.

To conclude, the hygroscopic commonly-used adhesives and consolidants, i.e. Animal glue, Aquazol 200 and Klucel G, show the highest viscoelastic response to RH fluctuations of all the samples. As seen in Figure 4.29b, the variations in Tan δ (ΔTan δ) between the 20 and 80%RH plateaux are the highest for those samples and range from 0.07±0.00 for KlucelG to 0.19±0.02 for Aquazol 200. This is higher than what could be measured for the untreated canvas ($\Delta Tan\delta$=0.04±0.01). The less hygroscopic treatments in comparison, i.e. Beva 371, Paraloid B72 and Plexisol P550, show variations in Tan δ between 0.02±0.00 (Paraloid B72) and 0.3±0.01 (Beva 371 and Plexisol P550) lower than the untreated sample. Interestingly, the CNF-treated sample has lower variations in Tan δ (i.e. $\Delta Tan\delta$=0.06±0.04) than the other hydrophilic treatments and the less hydrophilic treatments and similar to untreated canvas.

4.3.3.3 Intermediate conclusions

In summary, the results of the tensile tests performed at 20 and 80%RH and those of the DMA-RH measurements both highlight the higher mechanical response of the Animal glue, Aquazol 200 and Klucel G treatments, the most hygroscopic materials, in comparison with the Beva 371, Paraloid B72 and Plexisol P550 consolidants, less hygroscopic materials. For the most hygroscopic materials, measurements of the treated samples and films of treatments showed the impact of moisture on the mechanical properties of the samples characterised by swelling and melting of the adhesives and consolidants when exposed to high RH levels used in the tests (here max 80%RH). This results from the lowering of their T_g temperatures.

When compared to the CNF and CCNF treatments, it was shown that the first two nanocellulose-based treatments to be tested in this project behave differently from the traditional consolidants in terms of physical (penetration) and mechanical properties. First, they performed better in terms of consolidation than the traditional consolidants. At 20%RH, they offer a reinforcement up to twice higher than animal glue, identified as the stiffer traditional consolidant tested. However, CNF and CCNF are also associated with high risks of physical ruptures resulting from high brittleness and low penetration into the canvas. This was not observed for the 6 traditional consolidants tested which seem to penetrate better the canvas by filling the inter-fibres spaces and thus linking and interlocking cotton fibres together. Finally, the viscoelastic response in *E'* of the CNF and CCNF treatments to RH variations is also much stronger than those of traditional consolidants. Whether these variations could be detrimental to the ground and paint layer and lead to fatigue. This needs to be further explored using, for example, finite elements analysis integrating the viscoelastic properties measured by DMA for each layer of a painting.

Discrepancies in the results obtained with tensile testing at fixed RH (20 and 80%RH) and DMA-RH using fluctuations in RH (RH cycles) indicate that other factors than moisture level might influence the mechanical response of the canvas samples. In particular, the time-dependent response of the treatments could be responsible for the differences observed. Another important parameter influencing the mechanical response of the samples could also be the tension to which

the canvas sample are subjected when measured by DMA during the RH variations and the continuous creep undergone by the sample during each measurement. Further investigations would be required to unravel the impact it has on the results obtained by DMA-RH.

The main findings of this first part of the study are summarised below in Table 4.3.

	Surface appearance	**Consolidation** (i.e. canvas stiffening or increase in Young's modulus in 1-2% elongation range)	**Hygroscopic behaviour and mechanical response to RH variations** (DMA-RH in 20-80% RH range)
Beva 371	- Interfibrillar bridges resembling secondary arms are formed between cotton fibres. Formation of a web structure between cotton fibres and treatment. - At low magnification, treatment compliant to the surface topology. - Treatment seems to penetrate into the canvas mesh.	Low	Low - Lower response of all the less hygroscopic treatments
Paraloid B72	- A low magnification, treatment compliant to the surface topology. - Interfibrillar bridges formed but present holes - The adhesive located between fibres does not seem to attach fully to the surrounding cotton fibres	Medium	Low - Higher than Beva371 -Time-dependant response to RH transition observed
Aquazol 200	As for Beva 371	Medium	Very high Complete loss of strength at 80%RH for film
Animal glue	As for Beva 371	High Lower than nanocellulose	High - Particularly at high RH (>70%RH) - Time-dependant response to RH transition observed - Higher moisture uptake than CNF at 80%RH
Klucel G	As for Beva 371 - Apparent small porosity of adhesive films formed between fibres (Possibly trapped air bubbles)	Medium	High Complete loss of strength at 80%RH for film
Plexisol P550	As for Beva 371	Medium	Low Higher than Beva371
Nanocellulose (CNF & CCNF)	- Formation of a coating layer on the surface of the canvas (treated side). - Morphologically compliant to the surface.	High (increase Young's modulus at low elongations (i.e. 1-2%)) Ruptures of the coating observed at higher elongations	High Higher mechanical response to RH

Table 4.3: Intermediate summary of the tests performed on the traditional and nanocellulose consolidants. The treatments differ in terms of surface appearance, consolidation and hygroscopic behaviour.

4.3.4 Physico-chemical stability upon ageing

The stability of the treatments was also evaluated in terms of colour change and mechanical properties (consolidation and response to RH).

4.3.4.1 Change in visual appearance after ageing

4.3.4.1.1 Colour change

Figure 4.32 shows the untreated and treated cotton canvas before and after ageing (cf. 4.2.6). Visual assessment of the samples shows darkening and yellowing of the canvas samples after ageing. This is confirmed by quantitative colour measurements.

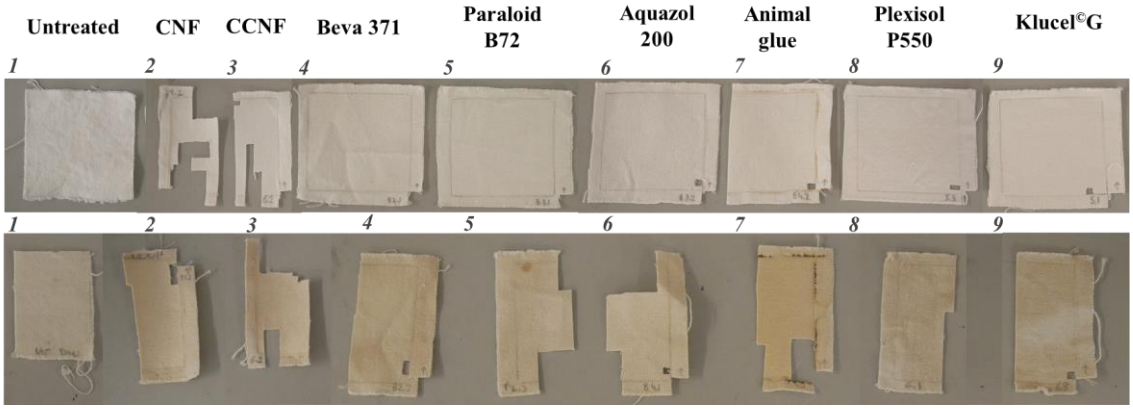

Figure 4.32: Untreated and treated cotton canvases before and after ageing

As seen in Figure 4.33, the overall ΔE^* colour change measured for all the aged samples is above 3 which is the value at which colour change is noticeable by a non-expert human eye. Interestingly, ΔE^* measured for the treated samples, all superior to 10, are statistically above the one measured for the untreated sample, hence 7.5. This shows that the treatments tend to increase the colour change resulting from degradation. The animal glue-treated sample is more prone to colour change as seen by a $\Delta E^*=17$. As seen in Figure 4.33 (right side), when analysing the colour changes in the L*a*b* or CIELAB colour space, the visual changes observed are the results of a loss in luminance (i.e. $\Delta L^*<0$) and yellowing (i.e. $\Delta b^*>0$) of the treated samples. Loss in lightness is particularly high for the nanocellulose-based treatments, as well as for animal glue, with ΔL^* measured at 9. Colour changes, in particular, the yellowing of the samples, are an issue as they

result in the strong modification of the visual appearance of the canvas. Moreover, yellowing can indicate instability or degradation of the adhesive (Down, 2015).

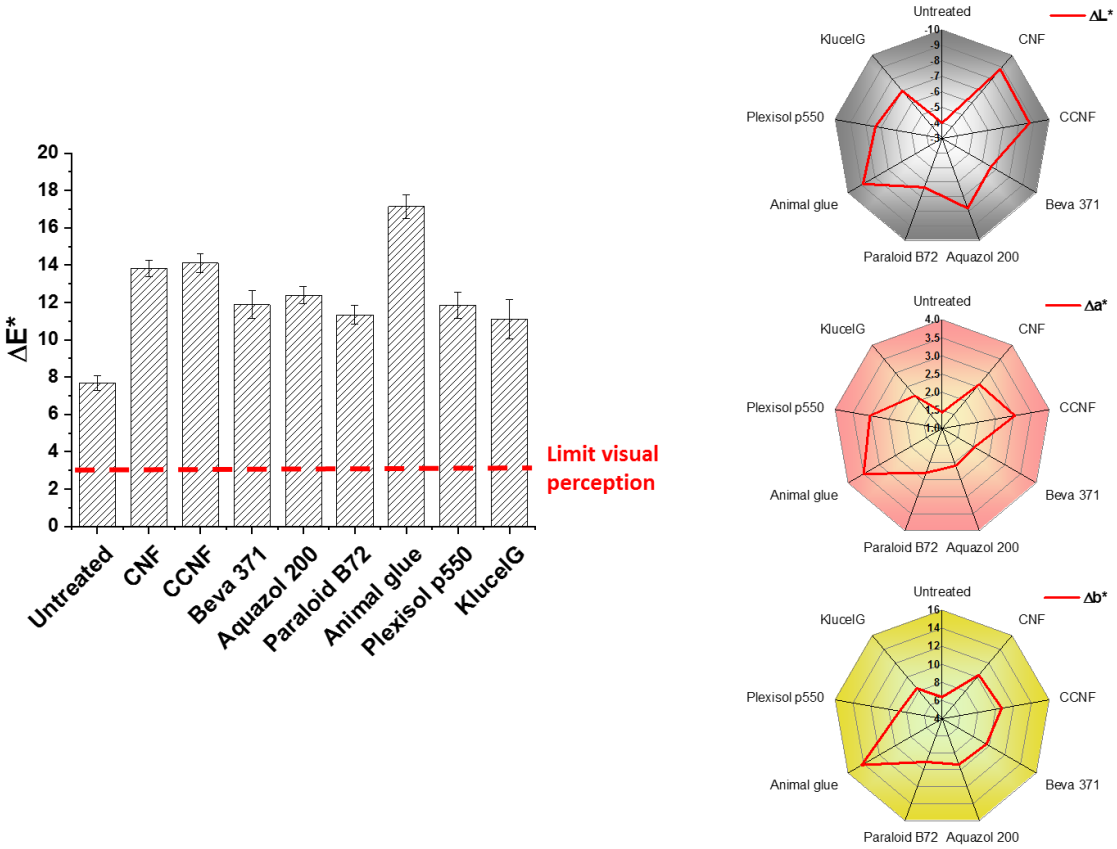

Figure 4.33: Colour change measured after ageing for untreated and treated cotton canvas using traditional and nanocellulose-based consolidants. The overall colour change (i.e. ΔE*) (left) as well as more detailed information of the changes occurring in terms of luminance (ΔL*), change along the green-red axis (Δa*) or the yellow-green (Δb*) (right) are given.

4.3.4.1.2 Modification of treatment deposition resulting from accelerated ageing

The surface appearance of the samples was imaged after ageing. The SEM images of the aged untreated and treated canvases are shown in Figure 4.34, next to the images of the untreated samples (right-hand corner of each image) already shown previously (i.e. Figure 4.13). The resulting appearance of the samples surface is particularly interesting as it highlights the numerous morphological changes which have occurred and result from ageing, in particular for the samples treated with traditional consolidants. As seen in Figure 4.34, for the Aquazol200, PlexisolP550,

KlucelG and ParaloidB72 samples, and to a lower extent for the Beva 371-treated sample, the deposition behaviour of the treatments has been greatly changed. Interfibres bridges formed between cotton single fibres by the consolidants Plexisol P550, Aquazol 200 and Beva 371 and previously observed in Figure 4.13, are hardly seen on the canvas surfaces after ageing. They still formed bridges linking cotton fibres and probably holding them together but those bridges are in a much lower amount. For Paraloid B72 and Klucel G, it has been observed prior to ageing that the treatment was filling the interfibres spaces. Holes in the treatment bulk had also been seen probably resulting from trapped air bubbles during the treatment application (smaller for Klucel G than Paraloid B72). As seen in Figure 4.34, the two adhesives seem to have been reformed by heat and the high RH level applied during ageing. The surface holes are not more visible after ageing and treatment behave like the other traditional treatments tested by forming interfibres linkers.

For the 4 treatments mentioned, Plexisol P550, Paraloid B72, Aquazol 200 and KlucelG, the high temperature and high RH level used during ageing might have caused the swelling and re-shaping seen by the change in surface texture of the consolidants. This is because at temperatures above their glass transition temperature (Tg), thermoplastic materials behave as flowing liquids (Horie, 2010). Yet, as reported in Table 4.1, the Tg of all the traditional consolidants tested range from 40 to 71°C, except for KlucelG for which two Tg (0 and 120°C) seem to have been identified (Table 4.1). Despite this, the material seems to have also been affected by the harsh ageing conditions. Moreover, for many hygroscopic materials, water acts as a plasticizer thus reducing the Tg of the material. This has been shown for example with rabbit skin glue whose Tg can decrease down to around or below room temperature at high RH levels (65-95%RH) (Timár-Balázsy, 1998). This is because the water increases the mobility of the collagen molecules.

Regarding the other commonly-used consolidants, the Beva371 adhesive seems to behave in a similar way as before ageing, interfibres bridges are seen in Figure 4.34. It is assumed that this is because Beva 371 is non-hygroscopic and has one of the higher Tg among the materials

with low hygroscopic behaviour (i.e. 40°C similar to Paraloid B72). For animal glue, on the contrary, it seems that the consolidant has become desiccated which could have been caused by the high temperature reached during ageing (i.e. 80°C). Cracks on the treatment films formed between cotton fibres are seen and seem to trigger the ruptures of the fibres to which they are attached as seen in the SEM image in Figure 4.34. Animal glue is known to desicate at low RH (Schellmann, 2014). The glue becomes more crystalline and thus more rigid and brittle. 50%RH is known to be the optimal RH level at which optimum proportions in crystalline and amorphous regions are kept in the material. The lowest RH reached during ageing was 40%RH which should not be sufficient to cause desiccation of the animal glue. However, observation of a film which had been also aged simultaneously to the treated canvas also presented visible cracks on its surface (see Figure B.10 in Appendix). In comparison to the traditional treatments, the CNF and CCNF consolidant seem very stable upon ageing in term of surface deposition. The film of CNF (also seen for CCNF) is maintained on the canvas surface. Contrary to what could have been expected, the film does not present any cracks after ageing and remains in appearance unchanged although it is not known whether the thickness of the film might have been modified.

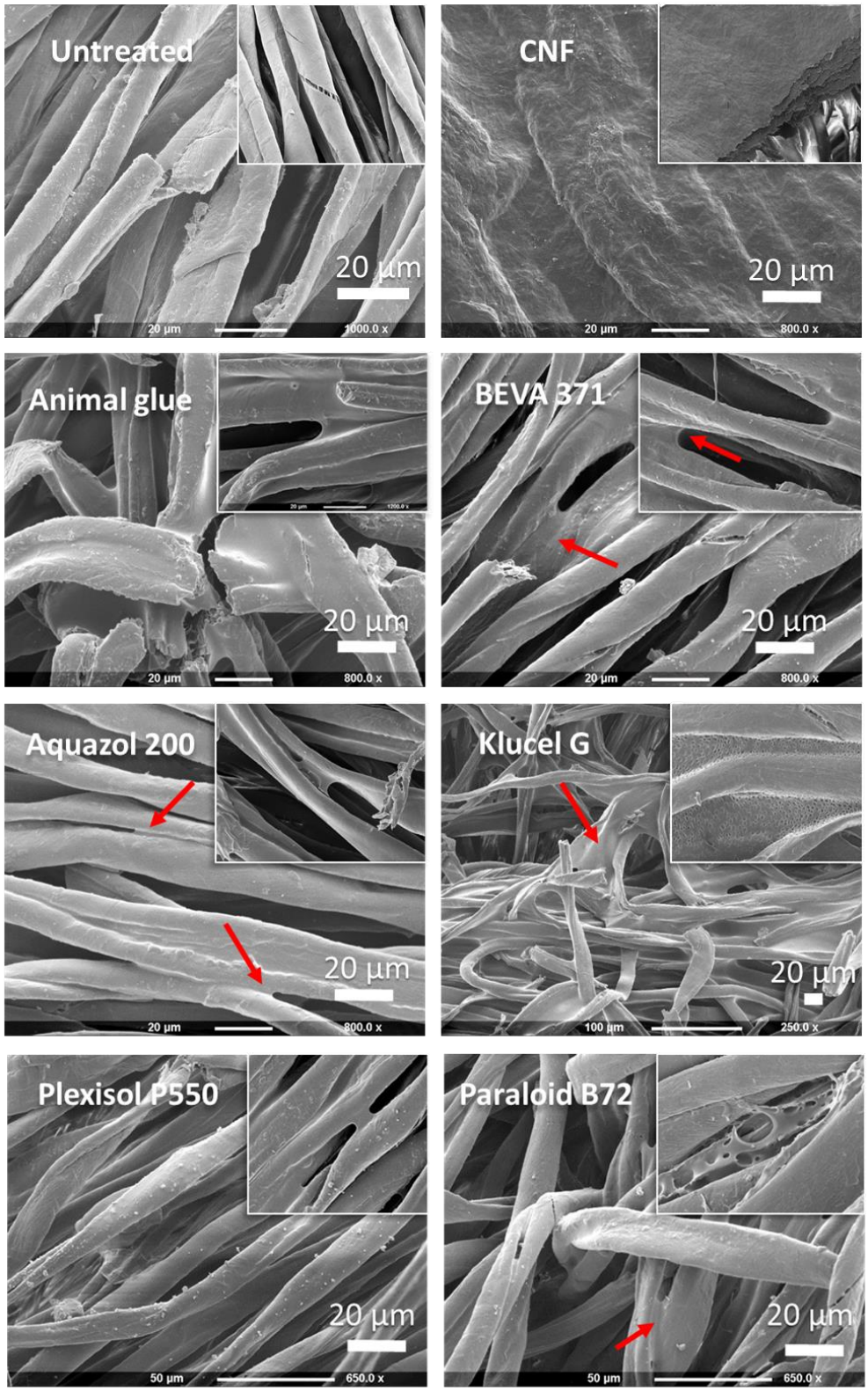

Figure 4.34: High magnification (x250-1000) SEM images of the treated degraded cotton canvases (traditional and CNF consolidants) after ageing. The surface appearance of the unaged samples, shown previously in Figure 4.13, is given in the right-hand corner of each image for comparison.

4.3.4.2 Consolidation

In terms of consolidation, tensile tests were performed on the aged sample were performed at 20%RH. In Figure 4.35, the results are compared with those obtained at 20%RH on the unaged samples. As seen in the diagram, the ageing led to different and opposite trends among the samples. For the nanocellulose-based treatments CNF and CCNF, as well as the animal glue, accelerated ageing induces a loss in Young's modulus *Y*. For the Animal glue, a loss in *Y* of ΔY =-9.8MPa was measured after ageing. This drop probably results from the cracks previously observed for animal glue interfibrillar bridges which seemed to have caused cotton fibres embedded in the consolidant to break as well. This trend aligned with properties recently reported by Tsetsekou (2018) who showed that following RH and T ageing cycles, rabbit-skin glue which was tested as adhesive for wood, appeared totally weakened and more brittle. For the CNF and CCNF-treated samples, the loss calculated is also important (i.e. -9.5±7.3 and -2.9±6 for CNF and CCNF-treated canvas, respectively). A high standard deviation was, however, calculated for the CNF-treated sample. This could account for variabilities across the sample which might have been increased by the degradation through ageing.

In terms of brittleness and decreases previously mentioned for CNF and CCNF, the ageing does not seem to increase or decrease the resistance of the treatment films to ruptures. The first ruptures observed on the tensile curves occur on average at the same elongation for the unaged and aged CNF and CCNF-treated canvas (see Figure B.11 in Appendix). Overall, even after ageing the CNF and CCNF-treated samples maintain their position and rank among the consolidants providing the higher consolidation, seen by higher Young's modulus or stiffness measured, to the degraded cotton canvas.

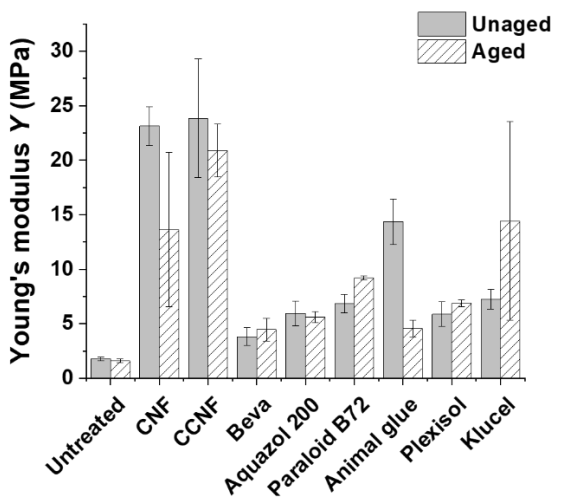

	Comparison before/after ageing	
Samples	Difference in Young's modulus (MPa) $[\Delta Y = Y_{aged} - Y_{unaged}]$	Percentage variations in Y (%) $[\Delta\%Y = \frac{Y_{aged} - Y_{unaged}}{Y_{unaged}}]$
Untreated	-0.2±0.3	-10.7±14.3
CNF	**-9.5±7.3**	-41.1±31.6
CCNF	**-2.9±6**	-12.3±25.0
Beva 371	0.7±1.3	17.2±34.7
Aquazol 200	-1.2 ±1.0	-18.2±14.5
Paraloid B72	3.2±1.1	54.5±18.8
Animal glue	**-9.8±2.2**	-68.0±15.5
Plexisol P550	1.0±1.2	17.1±20.2
Klucel G	7.2±9.2	99.4±126.8

Figure 4.35: On the left-hand side, Young's moduli measured at 20%RH for untreated and treated cotton canvas before and after ageing. On the right-hand side, table with the differences in Y measured at 20%RH between aged and unaged samples. Note that the difference in Y is given as ΔY= Y(aged)-Y(unaged).

As opposed to the samples just mentioned, after ageing some other samples reached higher stiffness than those measure before ageing. This is the case of Klucel G (ΔY=7.2, high standard deviation however measured for the aged sample) and Paraloid B72 (ΔY=3.2). Regarding the Klucel G-treated sample, the results are in accordance with the literature. Geiger & Michel (2005) showed that a film of Klucel E (another grade of Klucel with lower MW, MW=80000g/mol) loses in flexibility, and become stiffer and more brittle under moderate ageing conditions (i.e. 42°C, 32-68%RH under UV light). However, another hypothesis could also be raised stating that the high RH level (i.e. up to 80%RH) and temperature (i.e. up to 80°C) used during ageing might have led to the swelling of the treatment. This was already suggested from the SEM images of the samples after ageing (Figure 4.34) and could also be shown by DMA-RH. Under the application of 20-80%RH variations in RH, a film of KlucelG showed to flow at high RH levels (Figure B.2 in Appendix). Because the samples were hung in the ageing chamber (Figure 4.11), the flow of KlucelG at high RH levels as well as at high temperature levels might have caused the treatment to fall to the bottom of the canvas piece. This would explain the high standard deviation measured as well as the high stiffness measured. Interestingly, this was however not observed for the Aquazol 200 and animal glue treated canvases despite these

treatments having also shown to flow around 80%RH (see Figure 4.22 (Aquazol200) and Figure B.3 in Appendix (Animal glue)). Since only 3 samples were measured for the KlucelG-treated canvas, further sampling and measurement of this sample could be performed.

Compared to other consolidants, the Aquazol 200, Beva371 and Plexisol P550 performed well with almost no change in stiffness (I.e. Young's modulus) after ageing. It is however not known whether the apparent stability translates to the chemical stability of the material. Plexisol P550, for example, is known, as other poly(butyl methacrylate) substances, to be prone to crosslinking upon thermal ageing (Drinberg, 1953; Thomson, 1956; Delcroix, 1988). It is probable that physical changes (e.g. flow of Aquazol200 at 80%RH) could mask the impact of chemical ageing upon the treated-canvas mechanical properties. FTIR spectra of the samples and films of consolidants were measured but did not show any changes in the chemical structure of the samples after ageing (see Figure B.12 in Appendix). Further assessment such as py-GCMS should be required to isolate the role of the chemical ageing on the final mechanical properties of the materials.

4.3.4.3 Response to moisture

Upon ageing, the response to moisture of the samples was also re-examined. In Figure 4.36, the difference $\Delta E'$ in storage modulus (i.e. stiffness) between the 20 and 80%RH plateaus is given for each sample before and after ageing. The impact of ageing on the mechanical response of the samples to moisture (i.e. RH) variations is particularly important for the untreated canvas as well as the Aquazol 200 and animal glue samples and the nanocellulose treatments. These samples register the highest difference between $\Delta E'$ measured before and after ageing (i.e. from 2.1MPa for the untreated canvas, 3.9MPa for Aquazol 200, to 5.8MPa for the CNF-treated canvas).

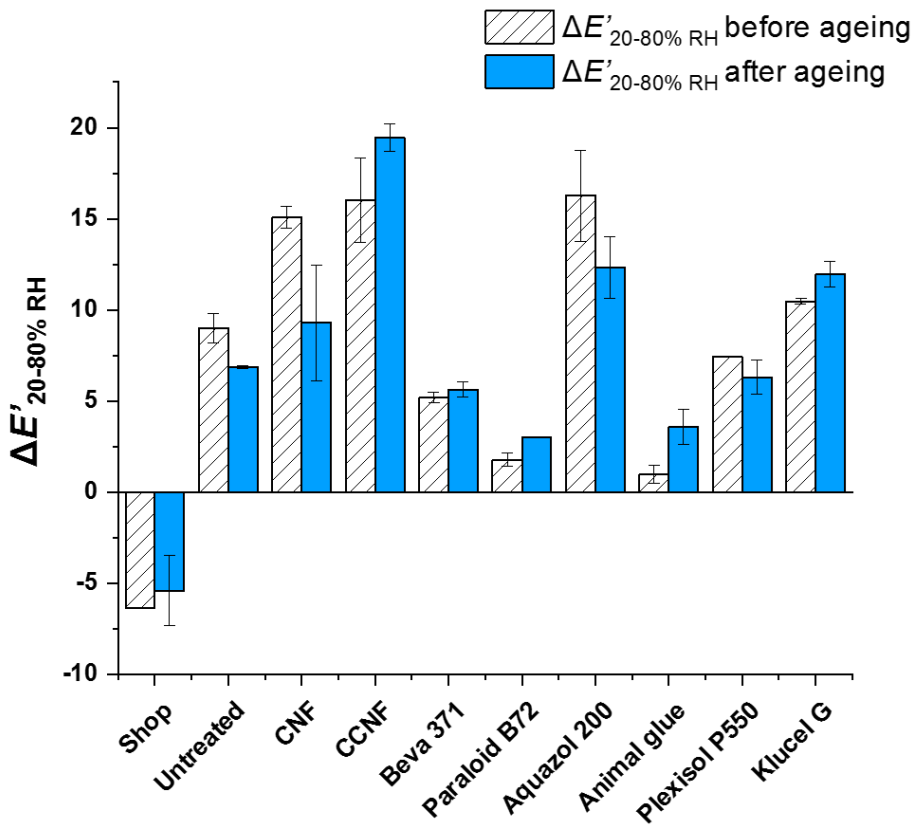

Figure 4.36:Comparison of the difference in storage moduli E' measured between 20 and 80%RH plateaux (i.e. $\Delta E'_{20\text{-}80\%RH}$) for unaged (hatched) and aged (blue) samples.

The results also show that, as for the impact of ageing on Young's moduli (i.e. 4.3.4.2), different changes in behaviour occur among the samples, hence treatments, upon ageing. For some canvas samples, the mechanical response of the canvas is decreased upon ageing (Figure 4.35, Table 4.4). This is the case of the untreated canvas as well as, among traditional consolidants, the Aquazol 200- and to a lower extent, the Plexisol P550-treated canvas. On the contrary, Animal glue, Paraloid B72, Klucel G and to a lower extent, Beva 371-treated canvases tend upon ageing to be more mechanical responsive to moisture variations as seen by the increase in $\Delta E'$ between RH plateaux after ageing. Interestingly, the trend upon ageing of the CNF and CCNF-treated canvases are opposed. The accelerated ageing seems to have lower the mechanical response of CNF-treated canvas to moisture variations, whereas it has increased the one of the CCNF-treated canvas.

Sample	$\Delta E'_{unaged}$ (before ageing) MPa)	$\Delta E'_{aged}$ (after ageing) (MPa)	$\Delta(\Delta E')_{aged-unaged}$ (i.e. $\Delta E'_{aged} - \Delta E'_{unaged}$) (MPa)
Unwashed/not degraded	-	-5.4±1.9	-
Untreated degraded	9.0±0.8	6.9±0.1	-2.1±0.8
CNF	15.1±0.6	9.3±3.2	-5.8±3.2
CCNF	16.0±2.3	19.5±0.8	3.5±2.4
Beva 371	5.2±0.3	5.6±0.4	0.4±0.5
Paraloid B72	1.8±0.4	3.0±N/A	1.2±N/A
Aquazol 200	16.3±2.5	12.3±1.7	-3.9±3.0
Animal glue	1.0±0.5	3.6±1.0	2.6±1.1
Plexisol P550	7.4±N/A	6.3±1.0	-1.1±N/A
KlucelG	10.5±0.14	11.9±0.7	1.5±0.7

Table 4.4: Comparison of the difference ΔE' measured between the 80%RH and 20%RH plateaux before (2nd column) and after ageing (3rd column). The 4th column of the table gives the difference between ΔE'(aged) and ΔE'(unaged).

To explain the changes observed, the samples and treatments will be considered individually and the results put in perspective with the literature. First, for the untreated cotton canvas, the lower variations $\Delta E'$ measured probably result from the degradation of the amorphous regions of the cellulose chains of cotton leading to an increase in crystallinity of the cotton. It was indeed shown that increased hydrolytic damage is accompanied by an increased percent fraction of the crystalline phase in cotton fibres (Bílková, 2012). This is due to the fact that the material of the amorphous region is more readily accessible by degradation factors and the cellulose molecule is preferentially distributed at these sites. Due to the higher percentage in crystalline phase, the cotton fibres become less hygroscopic. This was also shown by DVS (see Figure B.6 in Appendix). The same degradation processes leading to higher crystallinity are probably undergone by the CNF treatment which contains amorphous and crystalline regions (Dufresne, 2013). The reason why this does not seem to apply to CCNF is unclear. However, a study on the

degradation of carboxymethyl cellulose in salt form by de Britto & Assis (2009) suggests that upon thermal (150°C, 20min) and hydrothermal ageing (1 week at 100%RH), an intermediary acid or ester compound involving the carboxylate group is formed during the early step of degradation. Increase response of the CCNF-treated sample to moisture could probably result from the degradation of the carboxyl groups present on the CCNF polymeric unit (cf. Figure 2.2e in Chapter 2) and formation of more hydrophilic groups (acid and ester) than the groups formed after cellulose or CNF degradation (i.e. aldehyde and ketone as shown in 1.1.2.1 in Chapter 1 where reactions of cellulose degradation are given).

For Paraloid B72 and Animal glue, after artificial ageing, the response in terms of variations in E' between 20 and 80%RH (i.e. $\Delta E'_{20\text{-}80\%RH}$) had increased by 1.2 and 2.6MPa, respectively (see $\Delta(\Delta E')_{aged\text{-}unaged}$ in Table 4.4). The results tend to indicate that upon accelerated ageing, the Paraloid B72 and Animal glue show a higher mechanical response to RH variations possibly associated to a higher hygroscopic behaviour. An increased response to moisture of Paraloid B72 after thermal ageing (100 ± 2 °C, for 432 hours) had been already identified by Farmakalidis (2016) who uses contact angle to investigate aged films of the adhesive. This increase could result from the chemical degradation of Paraloid B72 known to be prone to cross-linking upon ageing. This was shown by several studies investigating the stability of Paraloid B72 mainly under heat and light ageing (Butler, 1988, 1989; Ropret, 2007; Sawicki, 2017). FTIR spectra remained unchanged but the material becomes more brittle and micro-cracks developed in the polymer (Ropret, 2007).

Those micro-cracks could be another cause of the increased mechanical response to moisture variations observed for both samples. Those were not observed by SEM for Paraloid B72 but it is probable that ageing might have also led to a more brittle material. For the animal glue aged sample instead, localised ruptures observed on the treatment by SEM (Figure 4.32) could indicate that the treatment does not prevent the movement of the canvas support as much as before ageing. For samples treated with animal glue or Paraloid B72, the role played by the canvas in the total mechanical response of the sample under RH variations could thus be increased. Therefore,

variations in E' upon application of RH cycles is increased toward values closer to the one measured for the aged degraded untreated canvas (i.e. $\Delta E'$=6.9MPa), hence from $\Delta E'$=1.0 to 3.6MPa and from $\Delta E'$=1.8 to 3.0MPa for animal glue and ParlaoidB72 treated canvas Table 4.4.

Aquazol 200 was not found to be thermally stable (Wolbers, 1994). It does not reticulate or crosslink during artificial light ageing but oxidation of the material could take place under light ageing as shown by pyrolysis-gas chromatography/mass spectrometry (La Nasa, 2017).

Plexisol P550, Beva371 and KlucelG, finally, did not show to have their mechanical response to moisture particularly affected upon ageing despite the fact that they are known to be prone to chain scission reactions upon ageing (see 4.2.1.) (Delcroix & Havel, 1988). As seen in Table 4.4, the difference in $\Delta E'(20\text{-}80\%RH)$ between the aged and unaged sample, remains below1.5 MPa in absolute value.

The lower response to moisture measured for the Plexisol P550 after ageing might result from the cross-linking reactions known to occur in the polymer chains upon ageing (see 4.2.1.) (Delcroix, 1988). The chains polymers are connected to each other permanently (cross-linking) which reduces the number of exposed hydrophilic groups available to interact with water through hydrogen bonding and to facilitate water diffusion. This was first pointed out by Drinberg and Yakovlev in 1953 who measured the thermal degradation of poly(butyl methacrylate) and later then by Thomson (1956). They noted a decrease in solubility of the polymer.

The chemical stability of Beva 371 was not studied in depth. As observed by Ploeger (2014), Berger often referred back to work done by Feller & Curran (Feller, 1970) in which they studied the stability of EVA co-polymers and the influence wax–resin has on the ratio of polymer main chain scission to cross-linking. EVA co-polymers are relatively stable materials; however, it is suggested that they can undergo a complex set of oxidation reactions involving interactions with moisture, oxygen, and UV radiation, which could result in the formation of acids, ketones, lactones, hydroperoxides, and conjugated dienes (Allen, 2000; Jin, 2010). There is also the competition between cross-linking and chain scission; EVA co-polymers with higher VA contents

are more susceptible to degradation involving chain-scission, since VA groups are points of weakness throughout the co-polymer (Feller, 1970; Jin, 2010).

Chain-scission is also thought to be the main aspect of degradation of Klucel. This was shown by Feller & Wiltt (1990) for Klucel G under film form which had been to thermal ageing at 90C. The viscosity of the material was shown to decrease with time of exposure and gave a measure of the chain scission occur in the polymer backbone. The behaviour of KlucelG under photochemical ageing was compare to Whatman #42 filter paper and the results showed that the rate of photochemically induced chain breaking in the Klucel G and cellulose itself were similar.

4.3.4.4 Intermediate conclusions on stability upon accelerated ageing

The main results obtained on this study on the stability of the traditional adhesives/consolidants and comparison with nanocellulose treatments is given below in Table 4.5.

	Stability upon ageing		
	Surface appearance ***(Note that colour change was stronger for all treatments than for the untreated canvas)***	***Consolidation***	***Hygroscopic behaviour and response to RH variations***
Beva 371	- Darkening -Lower amount of interfibres bridges	- Stiffness relatively unchanged	- Response to RH variations unchanged
Paraloid B72	- Darkening - Holes in interfibrillar films have disapeared	- Strong increase in stiffness (+55% in *Young's modulus*)	- Higher response to RH variations
Aquazol 200	Strong darkening -Lower amount of interfibres bridges	- Stiffness relatively unchanged	- Lower mechanical response to RH variations but remain higher than the unaged/aged degraded cotton canvas
Animal glue	- Strong yellowing and darkening - Cracks visible on film of consolidant by SEM at high magnification	- Strong loss in stiffness (-68% in *Young's modulus*) resulting in low consolidation provided	- Higher response to RH variations
Klucel G	- Loss luminance - Pores seen before ageing have disappeared. Treatment seem to have penetrated further into the canvas	- Strong increase in stiffness after ageing (+99% in *Young's modulus*)	- Small increase in response to RH variations
Plexisol P550	- Loss luminance - Lower amount of interfibres bridges	- Stiffness relatively unchanged	- Small decrease in response to RH variations
Nanocellulose (CNF & CCNF)	- High colour change, darkening and yellowing - Surface appearance under SEM unchanged (i.e. superficial coating maintained)	- Strong loss in stiffness but high consolidation is maintained (CNF/CCNF)	- Lower and higher response to RH after ageing for CNF and CCNF, respectively

Table 4.5: Summary of the results obtained for the traditional and nanocellulose treatments in terms of stability upon accelerated ageing. The results are given for changes in surface appearance, consolidation and hygroscopic behaviour.

4.3.5 Conclusions

This study was carried out to gain better understanding of the mechanical properties and response to moisture of several traditional consolidants and adhesives used in conservation. Most of these consolidants were or are still commonly used in conservation. However, not all have been thoroughly investigated in terms of mechanical response to moisture as well as stability upon ageing involving RH and T cycles. Their properties were compared to those of two nanocellulose-based treatments, proposed as new consolidants for painting canvas.

First, differences in surface deposition, probably associated with treatment penetration, between traditional consolidants (natural or synthetic) and CNF and CCNF treatments were observed. Whereas the traditional consolidants seem to cover individual cotton fibres and threads forming interfibrillar bridges, the CNF and CCNF treatments remain as a layer on top of the canvas. The results of this study also highlighted the higher stiffness reached with the nanocellulose-based consolidants than with the traditional consolidants. Higher reinforcement seems thus to be provided by the CNF and CCNF treatments. However, those treatments also show high brittleness, probably resulting from the mode of deposition. This feature is an important disadvantage for the treatments in comparison to the other adhesives tested which have shown to be indeed more flexible. Finally, the mechanical response of the samples to RH variations show to be higher for the nanocellulose-treated canvases. The results also indicate that among traditional consolidants, the more hygroscopic treatments are in general more mechanically responsive to RH variations than the other, less hygroscopic, traditional consolidants. Interestingly, the time-dependent response seems to prevail for some treatments such as animal glue or Paraloid B72 leading to lower apparent mechanical response under fast RH cycling (DMA-RH tests).

The last assessment of the treatments' stability was performed using artificial ageing combining thermal and RH ageing. FTIR spectra did not show any changes, however, colour change and modification of the mechanical response of the sample in terms stiffness and response to RH variations were measured. Beva371, ParaloidB72 and Plexisol show the lower change in

terms of mechanical properties. The CNF and CCNF-treated canvas underwent high modifications such as loss in stiffness. However, they remain stiffer than all the other consolidants tested and lower response to RH variations, hence lower mechanical stress, was also measured for the CNF-treated canvas upon ageing.

This study has highlighted the main differences between several commonly used treatments and shown the advantages and disadvantages of the CNF and CCNF treatments over traditional consolidants. It has also shown that further investigations are required to deepen the understanding of the hygroscopic behaviour of common adhesives used in conservation and the consequences it can have on their mechanical behaviour. The accelerated ageing program was successfully used in this study to draw novel conclusions. However, it should be further enhanced to account the appropriate ageing conditions for all the treatments tested. This has so far proved to be difficult because of the low Tg of most of the adhesives.

5 Study of 3 types of nanocellulose-based consolidants for cotton canvas

5.1 Introduction

The evaluation of the main chemical, physical and mechanical properties of traditional consolidants carried out in Chapter 4 has helped to give a better picture of the materials traditionally and/or currently in used for painting structural conservation. Following the same protocol of assessment, newly developed nanocellulose-based consolidants based will be studied in this chapter. They can be classified into three main categories which correspond to three different consolidation strategies: pure nanocellulose, nanocomposite and multi-layered nanoparticles consolidants (Figure 5.1).

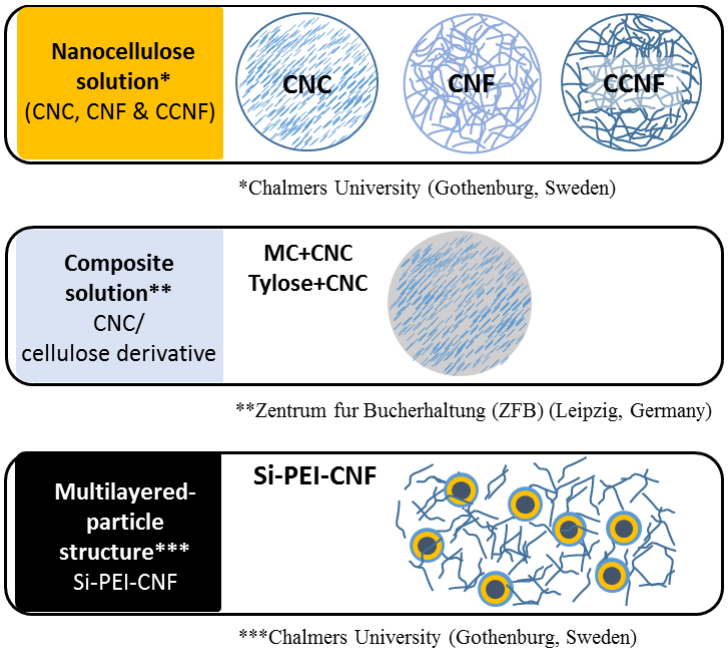

Figure 5.1: Scheme of the 3 solutions proposed in the project to consolidate degraded and fragile painting canvases made of natural fibres (e.g. cotton, hemp, jute,…): the pure nanocellulose dispersions (1), the CNC-nanocomposites (2)and the multi-layered solution (3)

Each of the strategies were proposed by a different institution of the Nanorestart project, i.e. Chalmers university (solution 1 and 3), ZFB (solution 2). The main solutions which will be presented are the two first types of consolidants (i.e. nanocellulose and nanocomposites). The

results obtained for the last solution, i.e. multi-layered nanoparticles (i.e. Si-PEI-CMC:CNF), will only be given in the appendix (cf. Appendix C, p.406).

As seen in the previous chapter (i.e. Chapter 4), the development of new lining adhesives for painting canvases can be successfully carried out if they follow specific criteria. Those criteria have been well-established for several decades by both the scientific and conservation community (Berger, 1970; Hedley, 1988). In view of the results obtained previously for traditional consolidants, five criteria were selected to assess the newly developed nanocellulose-based consolidants. They are given below next to more detailed information on their implications in conservation as this provides valuable keys of understanding for the discussion of the results.

The assessment of the three categories of nanocellulose-based materials for consolidation was carried out in terms of:

- Visual assessment and modification of the surface appearance at the macro and micro-scale

  The consolidant should have a limited impact on the visual appearance of the canvas. It should not mask any signs present on the canvas with important historical value (e.g. signatures). The aesthetical appearance of the canvas should also be preserved as it can greatly depreciate the financial value of the painting[7].

- Evaluation of the degree of penetration and surface behaviour of the treatment

  Depending on its degree of penetration, a treatment aiming at the consolidation of a material might give different results in terms of consolidation and present different pitfalls. On one hand, high penetration is favourable and often recommended for efficient mechanical consolidation of a material (e.g. wood (Cipriani, 2010; Unger, 2001)). However, it also further complicates the later removal of the treatment from the bulk of the treated material (D'haenens, 2013). This goes against the principle of reversibility which still prevails in

[7] From discussion with private painting conservator Aurelia Chevalier.

conservation (Bianco, 2015; Sease, 1998) or retreatability which is now considered in conservation (Appelbaum, 1987; Viñas, 2011). This is the case of PEG (polyethylene glycol) treatments which have shown to be efficient for the consolidation waterlogged wood but are known for their irreversibility (Graves, 2004; Hocker, 2012) or the colour change observed for wax-resin impregnations used in linings (Bomford, 1981). On the other hand, lower penetration of the consolidant would lead to the formation of a layered system with its mechanical limitations such as concentration of mechanical stresses at the interface between layers and increase risk of mechanical failure resulting from delamination or rupture of one of the layer (He, 1993; Hutchinson, 1996). This will be discussed in greater details later. The fact that the treatment does not penetrate into the canvas would, however, facilitate its removal through, for example, peeling or scratching using a scalpel.

- Quantification of the consolidation provided to establish if sufficient consolidation is provided.

The consolidation is measured in terms of stiffening of the canvas at low elongations (i.e. 1-2% elongation) at which easel paintings is usually stretched (Iaccarino Idelson, 2019; Mecklenburg, 1982).

- Hygroscopic behaviour of the samples and impact on overall mechanical response to RH.

The mechanical and dimension responses of a material to fluctuations in RH could, when these go beyond the elastic region or beyond what the material can mechanically sustain, cause fatigue of the material and lead to its consecutive mechanical failure. Assessment of the mechanical response of the consolidants to RH also informs the RH levels at which the treatment might fail in its role of consolidant, i.e. support, for the degraded and fragile canvas. Finally, the differential mechanical response of the different layers of paintings is often the main cause of damages in paintings. It is therefore important to assess the mechanical response of each individual layers and of the entire multi-layered system build.

- Long-term optical, chemical and mechanical stability upon handling and ageing

The higher stability of the treatment also ensures a reduction in the number of repeated treatments over time that are needed, leading to lower risks associated to the application of the consolidation treatment (i.e. painting handling, frame removal, application of solvents, etc.).

In addition, the study of the impact of treatment application (and therefore penetration) on the surface appearance, mechanical properties and hygroscopic response of the treated cotton canvas is included in the analysis reported here.

This chapter consists of a series of tests assessing the main advantages and limitations of different types of nanocellulose-based treatments for painting canvas consolidation. The assessment will be based on tests performed on a model artificially degraded cotton canvas also used in Chapter 4.

5.2 Materials and methods

Two main solutions for the consolidation of painting canvases made of natural fibres were developed in the frame of the Nanorestart European project. These include:

- First solution: pure nanocellulose treatments: nanofibrillated cellulose (CNF), nanocrystalline cellulose (CNC) and a chemically modified CNF, a carboxymethylated CNF (CCNF).
- Second solution: A polymer composite made of cellulose derivative reinforced with CNC. The cellulose derivatives tested include a hydroxyethyl cellulose (HEC) compound available commercially under the trade name Tylose® (grade MH50) and methylcellulose (MC). The use of nanoparticles of deacidification, calcium carbonate ($CaCO_3$) combined with the CNC-reinforced MC composite (i.e. MC+CNC) was also explored.

5.2.1 Materials

For all the nanocellulose-based consolidants, the model canvas used for the test consists of a degraded cotton canvas (cf. 2.1.1).

Solution1: Nanocellulose treatments

Details information on the chemical structure and provenance of the CNF, CCNF and CNC nanocellulose used are given in Chapter 2 (cf. 2.1.2.1).

Solution 2: Nanocellulose composites treatments

Two cellulose derivatives were studied: Tylose MH50 and methylcellulose (MC). TyloseMH50 was received in powder form whereas solutions of MC mixed with CNC (i.e. MC+CNC) at 1.97%w/w in water and heptane were received from ZFB (Leipzig, Germany). Calcium carbonate ($CaCO_3$) nanoparticles prepared by ZFB were also received in solution at 2% in water and at 2% mixed in a solution at 1.97% in water of MC+CNC. More detailed information about the products is given in Chapter 2 (cf. 2.1.2.2).

The decision to use deacidification agents on canvases came about from results reported in past works by Hackney (1994) as well as, more recently, by the outcomes of a previous European project, NanoforArt. These studies have shown that the use of basic or alkaline materials as deadification agents are efficient in neutralizing acidity within paper or canvas. They also provide an alkaline reserve which will act a buffer against the further development of acidity within the cellulosic material. $CaCO_3$ was used prior to the application of the MC+CNC consolidant in water or mixed together with it. The possible benefits provided by the deacidification agent on the long-term mechanical stability of the consolidation were explored.

5.2.2 Methods

5.2.2.1 Treatment application

Solution1: Nanocellulose treatments

The CNF, CCNF and CNC treatments were all received already applied on degraded cotton canvases. The samples had been prepared at Chalmers University. The method and protocol of application of the treatments can be found elsewhere (Bridarolli, 2018; Nechyporchuk, 2018) but are, for clarity, also given below.

In the first part of the study of the nanocellulose consolidant, a degraded cotton canvases was treated with CNF, CCNF and CNC.

The nanocellulose aqueous suspensions, CNF, CCNF and CNC, were prepared with deionized water at concentrations of 1.00, 0.25 and 3.00 wt.%, respectively, in order to achieve a similar viscosity. The suspensions were then homogenized using a Heidolph DIAX 900 (Heidolph Instruments, Germany) equipped with a 10F shaft at power 2 (around 11,600 rpm). These suspensions were homogeneously spread on the surface of the degraded cotton canvas samples (70×80 mm) using a plastic serigraphy squeegee. The coatings were deposited in 3 passes with an interval of 20 min to allow some water to evaporate. Table 5.1 shows the increase of the canvas basis weight after coating, measured by gravimetry.

Nanocellulosic treatment	Description	Basis weight uptake (%) of the canvas for 3 coatings of treatment
CNF	Canvas coated with a nanofibrillated cellulose suspension at 1%w/w	7.8
CCNF	Canvas coated with a carboxymethylated nanofibrillated cellulose suspension at 0.25%w/w	1.2
CNC	Canvas coated with a nanocrystalline cellulose suspension at 1%w/w	22.2

Table 5.1: Increase in canvas basis weight measured after coating (data taken from (Nechyporchuk, 2018))

Solution 2: Nanocellulose composites treatments

Film preparation

First, solutions of Tyl at 1.5%w/w in water were prepared. It was observed that the Tylose powder easily agglomerated when mixed to water at room temperature. It was then difficult to disperse the agglomerates of undissolved powder and this require to stir the solution overnight. To avoid this, distilled water was first heated up to 60°C and the Tylose MH50 powder (mass calculated from the volume of water used) was then slowly added to the water under continuous stirring using a magnetic stirrer (*step 1*). At that temperature, Tylose does not react immediately in contact of the water and can be homogeneously dispersed in solution. The water was then left to cool down at room temperature under continuous stirring. The Tylose solution was left under stirring for 20min until a clear and homogeneous solution had been obtained (*step 2*). The solution was then mixed thoroughly with Ultra-Turax for 5min (*step 3*) and kept in the sonicator for 15min for further dispersion (*step 4*) and then on a vacuum (*step 5*) to get rid of air bubbles created from mixing with Ultra-Turax. Finally, the Tylose solution was poured into a petri dish (Ø87mm), air dried for more than 3 days to remove any air bubbles and oven dried at 40°C overnight with half open lids (*step 5*).

For the preparation of the nanocomposite films of Tylose with CNC (i.e. Tyl+CNC), a solution of CNC at 1%w/w in water was first prepared. Contrary to Tylose, the CNC powder was easily dispersed in distilled water under mild stirring. Specific masses in Tylose (1.5%w/w) and CNC (1%w/w) were mixed together under stirring (see calculated masses in Tylose and CNC in Table 5.2). The dry casting of the Tyl+CNC film then processed as previously described or Tylose in *step 5*.

%CNC in film dry weight	0%	5%	10%	15%	20%
Tyl (1.5%w/w) (g)	15.8	15.1	14.3	13.5	12.7
CNC (1.0%w/w) (g)	0.0	1.2	2.4	3.6	4.8

Table 5.2: Composition of Tylose MH50 (1.5%) and CNC solutions to create films with a surface density of 40g.m^{-2} with different percentages of CNC

Treatments application on degraded cotton canvas

The aqueous consolidants MC+CNC(w), MC+CNC+$CaCO_3$(w) treatments and the $CaCO_3$ dispersion were applied by brushing to pieces (9x8cm) of degraded cotton canvas. Brushing was carried out in both warp and weft directions to improve the homogeneous distribution of the treatments across the canvas. Three coating were applied for each treatment in order to reach a total surface coverage of 15g.m^{-2}. The treatments were left to dry between each application.

Another degraded cotton canvas was treated with CNF for comparison. The treatments were applied by brushing in three applications to reach the same surface coverage of 15g.m^{-2} than the samples treated with the nanocomposite consolidants.

Samples for case study on penetration

An aqueous solution of Tylose at 1.5%w/w was applied on small pieces (2x2cm) of degraded cotton canvas by brushing and by spraying using an airbrush at a pressure of 3 bars. By brushing, two samples at 15g.m^{-2} and 30g.m^{-2} in surface coverage which correspond to two and four applications of the treatment, respectively, were made. By spraying, only one sample with a surface coverage in Tylose of 15g.m^{-2}.

5.2.2.2 Tensile testing

The untreated/treated canvas samples were preconditioned before the tensile tests at least 24h at 20%RH at room temperature and tested in the warp direction. They were cut so that 10 threads were collected in the warp direction and were typically 0.7 (thickness) x 7 (width) x 15

(length) mm in dimensions. The samples were measured by DMA used in tensile mode (cf. *2.2.4.1* in Chapter 2).

5.2.2.3 DMA-RH

The untreated/treated canvas samples were preconditioned before the DMA-RH measurement for at least 24h at 20%RH at room temperature. They were cut so that 10 threads were collected in the warp direction and were typically 0.7 (thickness) x 7 (width) x 15 (length) mm in dimensions. All the samples, were measured by DMA-RH at 1Hz and clamped in tension. A preload of 1N was used to avoid the buckling of the samples (cf. 2.2.4.2 in Chapter 2). The samples were tested in the warp direction.

The RH program used in the studies evaluating the performance of the solution 1 and solution 2 of the nanocellulose-based consolidants consists in three successive RH cycles 20-60-20 % RH at 25°C as shown in Figure 5.2. The rate of change from 20-60%RH was 4%RH/min. The samples were set to equilibrate at 20 or 60 % RH for 30 min between each transition.

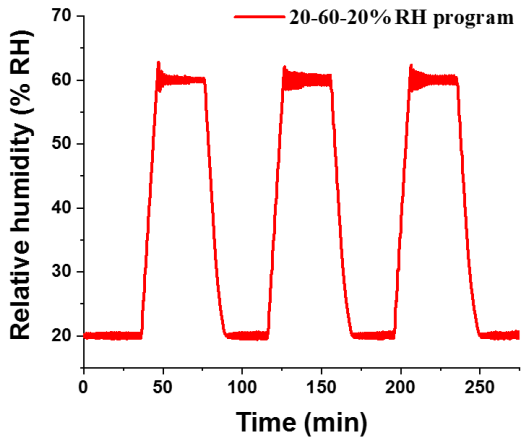

Figure 5.2: RH cycles 20-60-20 %RH program showed here for 3 successive RH cycles. RH was left to stabilized at 20 and 60%RH (isotherm at 25°C) for 30min at each plateau. A rate of RH transition of 4%RH/min was used for both humidification (20-60%RH) and dehumidification (60-20%RH).

Another RH program was used for the samples tested in the case study, i.e. the Tyl-treated cotton canvas treated by brushing and spraying. The 20-80%RH RH program used consists of RH

cycles going from 20 to 80%RH at 25°C. The humidity level was stabilised at 20%RH for 30min. RH was then increased at 4%RH/min to 60%RH, left at 60%RH for 1 min and increased further at 2%RH/min to 80%RH. After 30min isotherm at 80%RH, the RH level was decreased back to 20%RH at 4%RH/min and left at that RH level for 30 min. This cycle was repeated three times Figure 5.3.

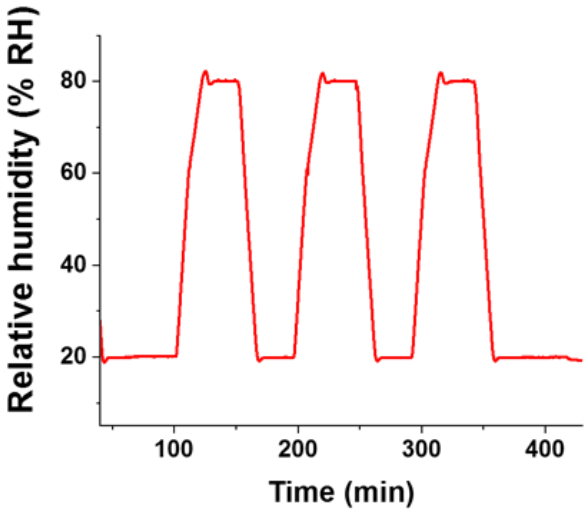

Figure 5.3: 20-80-20 %RH program (25°C) showing 3 RH cycles between 20 and 80%RH. RH plateaus of 30min were used at 20 and 80%RH. Rate of RH transitions of 4%RH/min (20-60%RH), 2%RH/min (60-80%RH) and 4%RH/min (80-20%RH) were chosen.

5.2.2.4 Ageing program

The accelerated ageing used in this chapter on the nanocomposites consolidants (i.e. solution 2) differs from the one used previously on the traditional consolidants as well as the CNF and CCNF treatments in Chapter 4 (cf. 4.2.6 in Chapter 4). This is because the ageing chamber was not available at the time of the experiment. The untreated and CNF- and CCNF-treated degraded cotton canvas were the only samples aged using both programs. The samples were here aged for 6 weeks in a ventilated oven at fixed RH and T conditions, i.e. 65%RH and 80°C. A similar program had been used in the past to follow the ageing of linen canvases (Oriola, 2011). The CNF-treated cotton canvas treated by brushing was also aged and its properties after ageing were evaluated for comparison.

5.2.2.5 Fluorescent microscopy

In the case study of this chapter, Tylose MH50 solution (1%w/w in water) was mixed with the fluorescent dye Rhodamine B. The samples cross-sections were analysed using an Olympus BX-51 upright microscope (Olympus corporation, Japan) equipped with a Bio-Rad Radiance 2100 confocal laser scanning head (BioRad, USA). The laser emissions used were argon (457 nm) and HeNe (543 nm) to excite the Rhodamine B stain. The HQ 515/30 emission filter was used and images were analysed using the LaserSharp 200 software. Prior to the measurement, the canvas samples were embedded in an acrylic resin (hard grade, Agar scientific, UK) and left overnight to dry. The embedded samples were polished using a semi-automated polishing machine.

5.3 Results Part 1: nanocellulose-only consolidants (*Solution 1*)

5.3.1 Penetration

The 3 different pure nanocellulose treatments were first investigated in terms of surface deposition and penetration by SEM. As seen in Figure 5.4, the treatments form a continuous layer sitting on top of the canvas mesh. This had been previously seen in Chapter 4 for the CNF-treated sample (cf. Figure 4.13). The homogenous coating reduces the overall roughness of the untreated canvas through the formation of a thin film over and between the canvas fibres filling the inter-fibre and inter-thread spaces, as previously observed (Nechyporchuk, 2017; Nechyporchuk, 2018). Morphologically, the treatment is highly compliant morphologically to the shape of the threads as the CNFs, CCNFs and CNCs tightly wrap tightly around the cotton fibres.

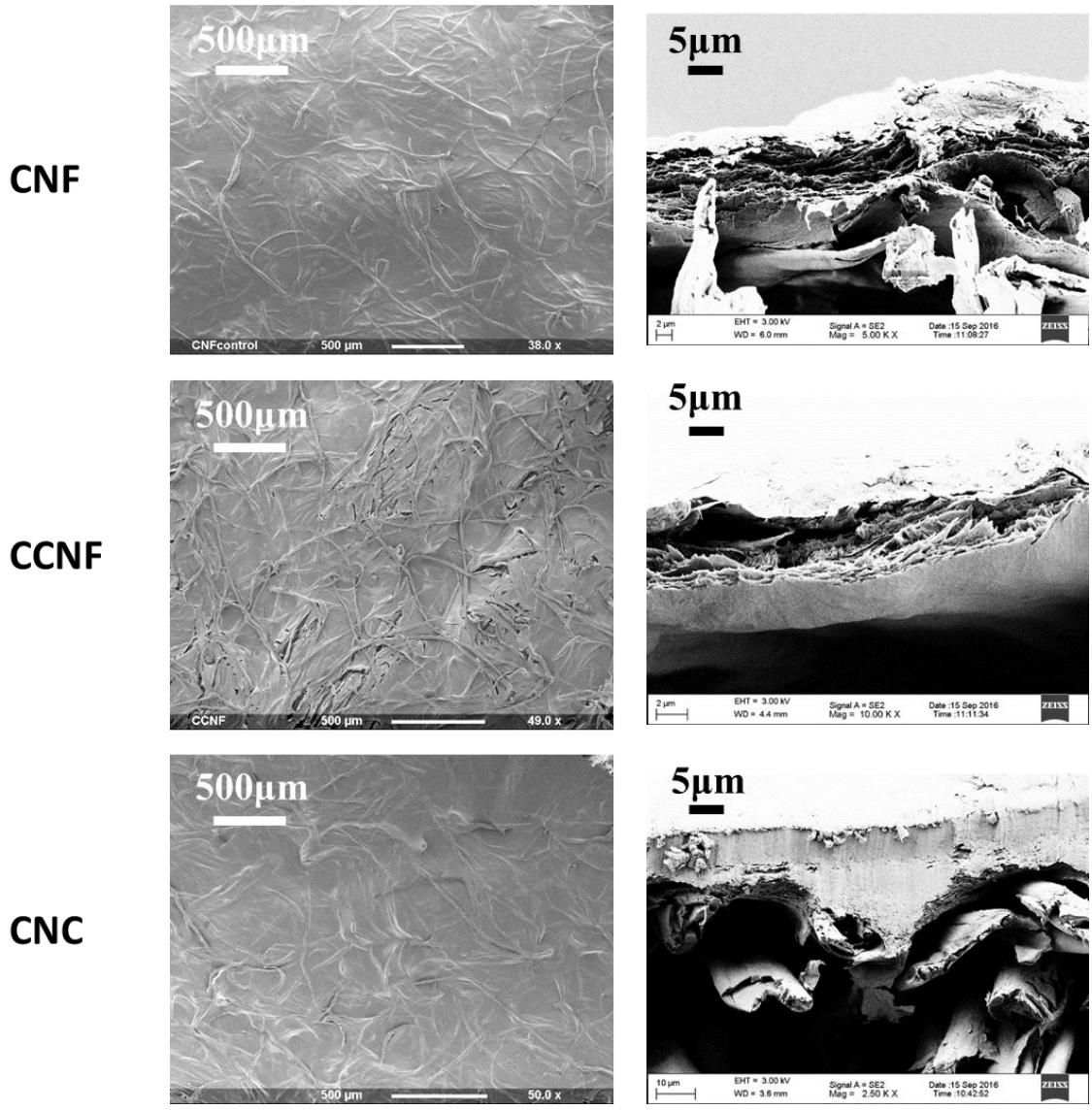

Figure 5.4: SEM images of the surface of a CNF-, a CCNF- and a CNC-treated degraded cotton canvas as well as a cross-section image (taken from (Nechyporchuk., 2018)). Note that for all the nanocellulosic treatments, a thin layer (≈5um) is formed on top of the canvas. The treatments do not seem to penetrate the canvas mesh.

The thickness of the treatment layer can be found around 5µm as seen in the cross-sectional images of the treated samples in Figure 5.4. Due to the different shape and length of CNCs and CNFs or CCNFs, they exhibited different behaviour in surface deposition. The CNF and CCNF treatments formed a layer with a fibrous aspect whereas the CNC formed a more compact and denser one. The longer nanofibrils of the CNF and CCNF treatment, their entanglement and the aggregates that are usually formed on casted CNF films (Sun, 2018; Xu, 2013) lead to a more porous layer of treatment upon drying (Figure 5.4). Because of their much

smaller size, CNC nanoparticles can form a more ordered and compact layer. The phenomenon was attributed to the self-assembly of CNCs during the drying process (Han, 2013). These differences in morphology and structure could strongly influence the mechanical behaviour of the treated canvas such as its stiffness or response to moisture.

5.3.2 Consolidation

The consolidation provided by the nanocellulosic treatments had been previously measured by tensile tests by Nechyporchuk (2018). Samples from the same batch were also tested by DMA-RH under controlled environmental conditions (20%RH, 25°C) to account for possible variations coming from the response of the samples to humidity and at lower values of applied force. The results of the measurements led to similar conclusions.

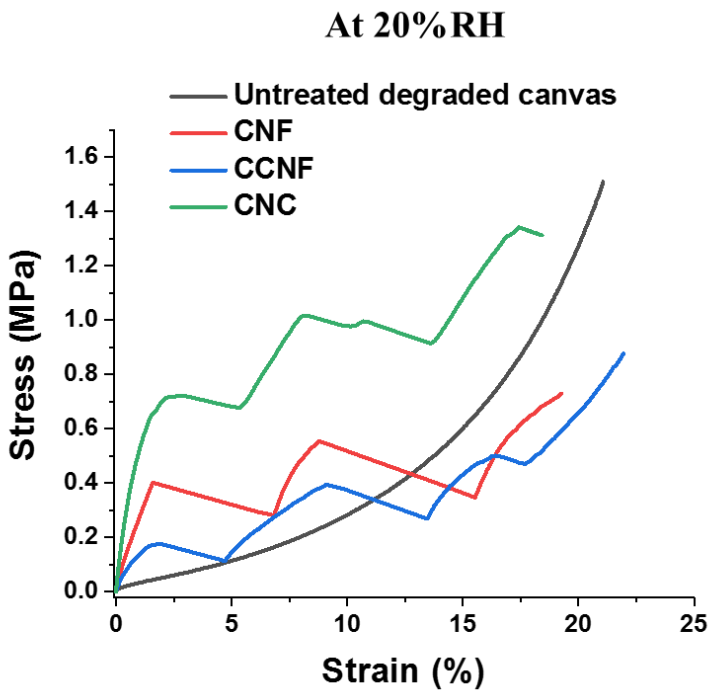

Figure 5.5: Stress-strain curves of untreated and CNF, CCNF and CNC-treated degraded cotton canvas measured by DMA in tensile mode at 20%RH and 25°C.

In Figure 5.5, the stress-strain curves obtained for the CNF-, CCNF- and CCN-treated canvas are shown. The results of those tests showed that the three treatments provided sufficient consolidation to the canvas by increase its stiffness in the range of interest, i.e. 1-2% elongation,

at which paintings are usually restretched. As seen in Figure 5.5, at low elongation, between 0 and 2%, the slope of the tensile curve of the treated canvases is significantly increased. The Young's moduli were calculated in the region of the curves corresponding to 1-2% in elongation since this is the region at which painting canvases are usually stretched (M. F. Mecklenburg, 1982a). As seen in Table 5.3, the use of CCNF resulted in a smaller increase of the stiffness ($Y_{20\%RH}$ =8.3MPa), as compared to CNF ($Y_{20\%RH}$=23.7MPa). This is because a lower amount in dry weight of CCNF was deposited. Due to the higher aspect ratio of the CCNF fibrils, at same concentration, the CCNF dispersion presents indeed a higher viscosity (Nechyporchuk, 2016). CNC coatings provided the higher level of reinforcement ($Y_{20\%RH}$=36.0MPa) but the treatment was also applied at a higher concentration of 3%w/w. Therefore, in terms of deposited weight, the CNC offered the lowest level of reinforcement normalized by the deposited weight. This can be explained by the fact that they possess the lowest aspect ratio.

Sample	**Young's modulus (MPa)** ***At 20%RH***
Untreated	1.9
CNF	23.7
CCNF	8.3
CNC	36.0

Table 5.3: Young's modulus (20%RH, 25°C) calculated for the untreated degraded canvas and the CNF-, CCNF- and CNC-treated degraded cotton canvases.

As seen in Figure 5.5, the stress-strain curves obtained for the CNF, CCNF and CNC-treated canvases are also characterised by successive losses in tension (or stress). It is important to note here that Young's moduli discussed previously had been measured from the initial part of the curves before these losses begin. The discontinuities in the stress strain data were attributed to localized ruptures of the CNF, CCNF or CNC coating sitting on the top canvas fibrils. SEM images, which were taken of the canvas after tensile testing, support this assumption (see Figure

C.1 in Appendix). Those ruptures in the layers of treatments were also observed by tensile testing on an Instron tensile tester by Nechyporchuk (2018) even at higher RH of measurement (60%RH) and despite the application of an additional number of layers (i.e. shown for 3 applications). It is the result of both the well-known brittleness of nanocellulose films (Mäkelä, 2016) as well as the low penetration and surface deposition of the treatment leading to the formation of a multi-layered system. Researches on crack propagation in multi-layered systems suggest that in the two-layers system obtained for the nanocellulose treatments, the application of a load parallel to the plane of the layers is the primary cause of delamination and rupture of the coating layer (Hutchinson, 1996). It has been seen on SEM images (Figure C.1) that rupture of the CNF layers (same of CNC and CCNF) is more likely to occur than delamination. This is because of the high differences in mechanical properties between the more elastic substrate (the canvas) and the stiffer and brittle coating layer (nanocellulose film). The competition between cracks advance within the interface and kinking out of the interface depends on the relative toughness of the interface to that of the adjoining material (Hutchinson, 1991). Since the toughness of the interface also plays an important role in the failure mechanisms, it will be investigated in more depth later in Chapter 6.

On the long-term, however, the increase number of cracks formed on the nanocellulose coating could be detrimental to the consolidation provided by the treatment. This was shown for a CNF-treated sample for a test of endurance to tensioning was carried out and consists of 3 consecutive repeats of tensile tests on the same sample (see Figure C.2 in Appendix).

Comparison of the stiffness of the untreated and nanocellulose-treated cotton canvases could also be compared by DMA-RH. The technique gives also a measure of the stiffness of the sample but allows for the deconvolution of the pure elastic (stored energy) from the viscous (loss energy) of the materials tested (cf. 2.2.4.2 in Chapter 2). The samples were subjected to three 20-60-20%RH cycles. In Figure 5.6, their mechanical response to changes in RH is seen as variations in storage modulus *E'* (i.e. stiffness).

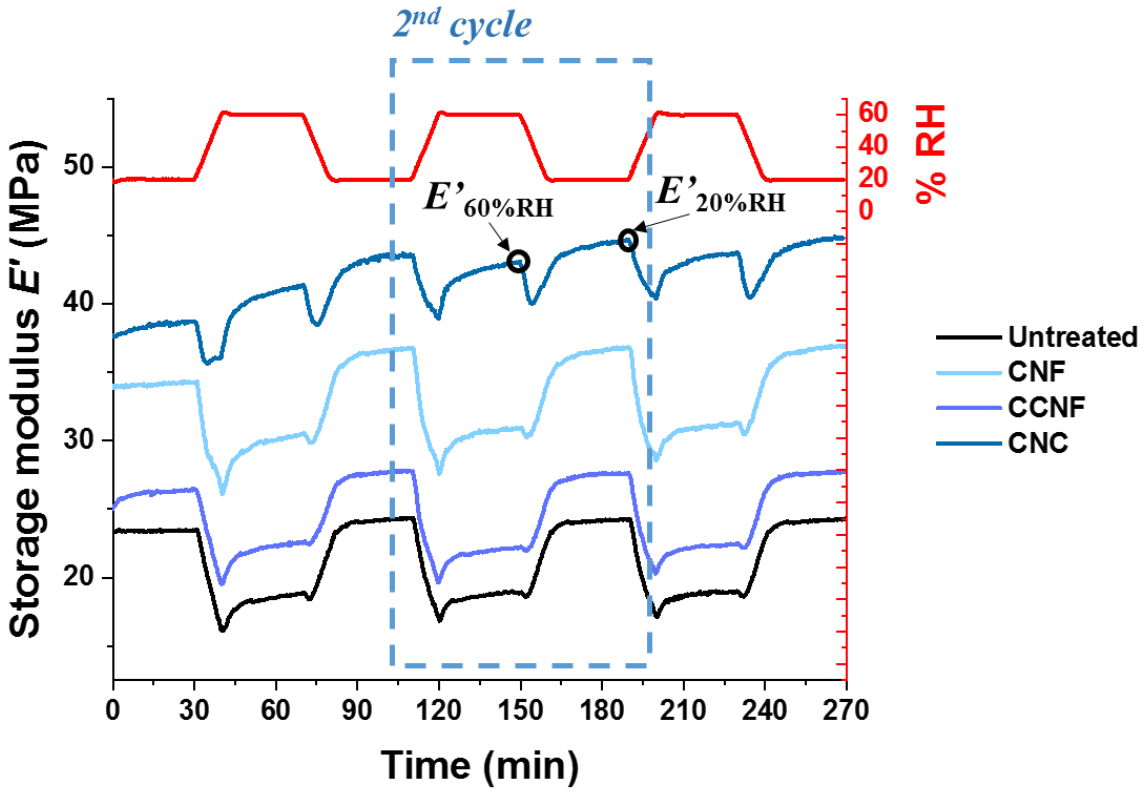

Figure 5.6: Variation in storage moduli measured for an untreated and CNF-, CCNF- and CNC-treated degraded cotton canvases tested in the warp direction.

As seen in Figure 5.6, all the treatments provide a noticeable reinforcement to the degraded cotton canvas. This is shown by the increase in *E'* measured after treatment of the degraded cotton canvas for the CNF, CCNF and CNC treated canvases. This increase is also independent of the RH level (between 20 and 60%RH) at which the sample was measured.

The results also indicated that the CNC-treated samples were the stiffest material tested followed by CNF and CCNF. The end-plateau values in *E'* measured at 20%RH and 60%RH for the untreated and treated canvas are reported in Figure 5.7. As it can be seen, a storage modulus at 20%RH, i.e. *E'*(20%RH), of 43.4MPa was measured for the CNC-treated sample. This is significantly higher to 43.0 and 29.8 MPa measured for the CNF and CCNF samples, respectively. Variability between measurements could also be observed as for example for the CNC-treated sample in Figure 5.6. Those might result from the variability in treatment deposition over the surface. The manual application of the treatment and the use of spraying instead of brushing have

shown during the preparation of the samples to be particularly difficult to control accurately. Despite the rigorous application of the treatment (same amount and same operator) for each test performed, differences between the samples are inevitable. With a sufficient number of repeat measurements (~5), the overall trends in mechanical behaviour could, however, be exposed.

5.3.3 Response to moisture

The response of the samples to moisture was also investigated. This is important since high mechanical response of the treatments to moisture could be the cause of higher risks of mechanical failure of the canvas and other painting layers (cf. 1.1.2.2 in Chapter1).

In Figure 5.7 are shown the end-plateau values in *E'* measured at 20%RH and 60%RH for the untreated and the CNF-, CCNF- and CNC-treated canvases canvas. First, it can be seen that the viscoelastic responses to RH variations for both untreated and treated samples are similar: all the samples exhibited higher stiffness (i.e. higher *E'* hence lower viscoelastic behaviour) at low RH (20%RH) and plasticization or lower stiffness (i.e. lower *E'* hence higher viscoelastic behaviour) at high RH (60%RH). The mechanical response of the samples to RH variations and in particular the lower *E'* values measured at high RH levels results from the plasticizing action of the water molecules on the cellulosic chains of the canvas and of the nanocellulose coatings. This effect has been widely reported in the literature for bio-polymers (Cheng, 2006; Karbowiak, 2006; Vieira, 2011) of which cellulose fibres (Apolinario, 2016; Célino, 2014; Okubayashi, 2004; Symington, 2009) and nanocellulose, CNF (Belbekhouche, 2011) and CNC (Belbekhouche, 2011; Dufresne, 1998; Khan, 1988; Sahputra, 2019) . The phenomenon was well explained by Khan (1988) for compressed disks of CNF and CNC. He observed that when water interacts with the cellulose in fibres or microfibrils in CNF and CNC, it disrupts the cellulose-cellulose bonds or hydrogen bonds linking the hydroxyl groups of neighbouring cellulose chains. Molecular rearrangements with moisture and changes in hydrogen bonding associated with reconfiguration of the cellulose-cellulose–water network will lead to a change in free volume of the cellulose chains. This leads to modification of the plasticity and elasticity of the cellulose material which was shown to occur preciously in Chapter 3 (cf. 3.4.1.3) for the degraded cotton canvas and apply

as well to nanocellulose coatings. This was later confirmed by Sahputra (2019) through the use of mechanics–molecular dynamics who showed in the particular case of MCC (i.e. CNC) that the plasticization by water results from the contribution from both hydrogen bound scission and free-volume mechanisms.

It is assumed that the higher the variations in storage modulus *E'* measured between high and low RH levels for the treated canvases, the higher the risk of mechanical fatigue and rupture of the priming and paint layers which are supported by the canvas.

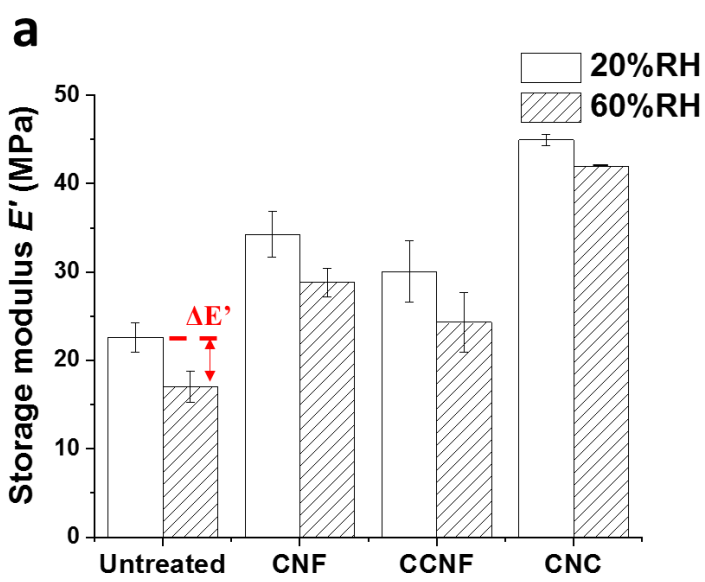

b

Sample	ΔE'(20-60%RH) (MPa)
Untreated	5.6±0.2
CNF	5.4±0.9
CCNF	5.9±0.1
CNC	3.1±0.4

Figure 5.7: Storage moduli E' measured at 20%RH and 60%RH (end plateau values, 2nd RH cycle) for untreated and CNF-, CCNF- and CNC-treated canvases (a). Difference in E' calculated between the 20%RH and 60%RH plateaus for the second RH cycle (b) (cf. Figure 3.19 in Chapter 3).

Therefore, the second stage of this study was to quantify the variations in *E'* measured between 20 %RH (i.e. *E'*(20%RH)) and 60%RH (*E'*(60%RH)). The differences Δ*E'*(20-60%RH) calculated are reported in Figure 5.7. The calculation was done for at least 3 repeat measurements per sample using the end-plateau values of the 2nd cycle since it was shown in Chapter 3 that the first cycle often undergoes mechanical conditioning (cf. 3.4.2.1). Figure 5.7 shows that the 2 types of nanofibrillated cellulose, CNF and CCNF, do not significantly modify the response of the

canvas to moisture. Variations in *E'* calculated at 5.6±0.2MPa for the untreated canvas, remain at 5.4±0.9MPa and 5.9±0.1MPa for the CNF and CCNF-treated canvas respectively. The mechanical response of the CNC-treated, on the contrary, greatly differs and is characterised by lower variations in *E'* upon application of the 20-60%RH RH cycles. A difference Δ*E'*(20-60%RH) of 3.1±0.90.4 MPa was calculated for the CNC-treated sample.

The lower mechanical response of the CNC-treatment to moisture variations could indicate the lower hygroscopic response of the CNC coating to moisture compared to CNF and CCNF. This is in agreement with a study carried out by Guo (2017) on CNF and CNC samples who showed by differential vapour sorption (DVS) that CNF was more hygroscopic (higher equilibrium moisture content, higher sorption ability) than CNC. The response of the CNC-treated canvas is also seen to be lower than the one measured for the untreated canvas. This was not entirely expected, given that both CNC and CNF are both highly hygroscopic materials due to their high surface area which is associated to higher availability in hydroxyl groups (i.e. reactive with water) (Voisin, 2017). Moreover, CNC nanoparticles also bear highly hydrophilic sulphate groups resulting from the acid hydrolysis used during their synthesis (see 2.1.2.1 in Chapter 2). It has been pointed out by Belbekhouche (2011) that not only the surface chemistry of nanocellulose particles but also the porosity of the nanocellulose films can greatly influence the overall hydrophilic response of the material. The surface chemistry of the CNC nanoparticles does not seem, indeed, to explain the low mechanical response to moisture variations observed. Instead, the reasons could be found in the more compact structure of the layer of CNC, as previously observed by SEM (see cross-section SEM image in Figure 5.4). The high density of the CNC coating might limit the diffusion of moisture in the material which could be the source of changes in the mechanical behaviour of the CNC layer. The specific arrangement of the CNCs into a dense coating layer might also explain the characteristic behaviour in elongation measured for the CNC-treated sample shown in Figure C.3 in Appendix. The CNC-treated canvas present a steady increase in elongation upon humidification (20 to 60%RH) and dehumidification (60 to 20%RH) contrary to the CNF- and CCNF-treated samples for which shrinkage is seen to occur during the dehumidification step. This could suggest that the dimensional response of CNF and CCNF

samples upon RH cycling is the result from the swelling of the nanofibrils and water desorption during humidification and humidification respectively, whereas the dimensional response of the CNC is mainly governed by reorganisation of the nanocrystals within the layer. This is supported by the fact that amorphous content of CNF is higher than that of CNC. As such, the extent of structural swelling of CNF would be greater than with CNC (Guo, 2017).

In order to explore this assumption, DVS (differential vapour sorption) measurements were performed on the treated canvases. They show the weight uptake/release with increase/decrease in RH of the untreated and treated cotton canvases. As seen in Figure 5.8, the lowest weight uptake at 60%RH measured among the 3 nanocellulosic-treated canvases was measured for the CNC-treated canvas. It is also lower than for the untreated canvas. After 30min isotherm at 60%RH, 14.7%, 15.8 and 23.2% weight increase were measured for the CNC, CCNF and CNF-treated canvas, respectively. The lower hygroscopic behaviour of the CNC-treated canvas seems, therefore, supported again by the DVS measurements and explains the lower mechanical response of the CNC-treated sample to RH variations.

In Figure 5.8, the DVS measurements also show the apparent higher hydrophilic behaviour of the CNF coating over the CCNF coating. This could be due to impurities present on the CCNF particles which have been introduced or not eliminated during processing of the nanocellulose particles (Belbekhouche, 2011). This could be, for example, the presence of traces of lignin, a polysaccharide naturally presents in wood, from which CCNFs were extracted, which is a more hydrophobic compound than cellulose. Indeed, Rojo (2015) recently reported that 13.5wt% of residual lignin in CNF nanopapers resulted in a reduction of their hydrophilicity and water vapour permeability.

This could also be the cause of the higher hygroscopic response of the untreated cotton canvas in comparison with the CCNF-treated cotton canvas. The CNF treatment instead seems to increase the hygroscopic behaviour of the canvas. Interestingly, this does not seem to have had an impact on its mechanical response to RH variations as shown by the variations in E', i.e. $\Delta E'$(20-60%RH), which are, as previously reported, similar for the untreated and CNF-treated canvases (cf. Figure 5.7b).

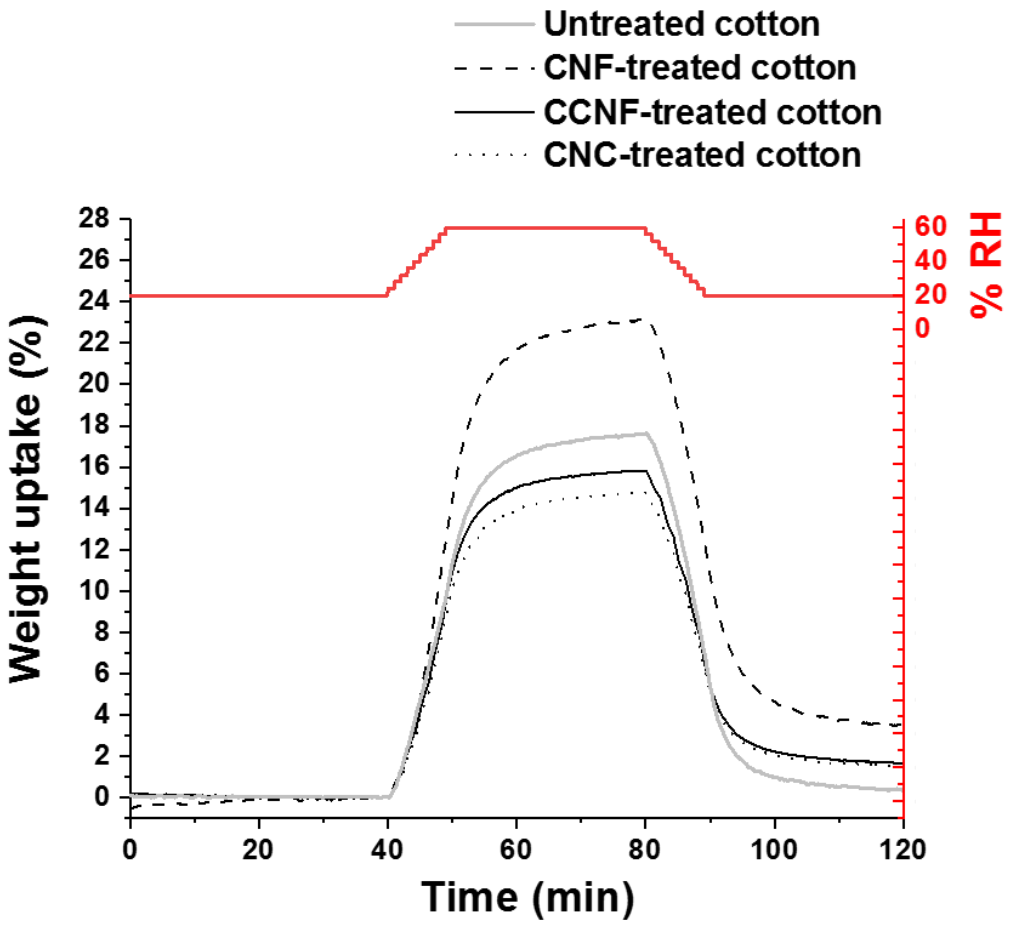

Figure 5.8: Comparison of the hydrophilic behaviour of the three nanocellulosic treatments CNF, CCNF and CNC applied on a degraded cotton canvas using vapour sorption measurement (DVS). The response of the untreated cotton canvas is shown for comparison. Note the higher response of the CNF treatment over the CCNF and CNC treatments. The lower weight uptake, hence hydrophilic response, was measured for the CNC-treated canvas.

5.3.4 Intermediate conclusions on the use of nanocellulosic treatments (solution 1) for canvas consolidation

Overall, the nanocellulose treatments investigated have shown to give an important reinforcement to the treated degraded cotton canvases. A noticeable increase in stiffness was reached for all the treated samples at low elongation in the region at which painting is usually restretched (1-2%elongation) (Mecklenburg, 1982). When comparing different types of nanocellulose, CCNF showed better performance per gained weight. However, because of the high viscosity of CCNF, the lower concentration of the CCNF dispersion compared to CNF

(1%w/w) and CNC (3%w/w) also induce that the canvas to be treated will be exposed to a higher amount of water. CNC showed the lower reinforcement for gained weight but is also the treatment which offered the lower mechanical response to variations in RH (20-60-20%RH).

Moreover, the three nanocellulose treatments tested behave in a similar way when applied on the canvas. The treatments are seen as a thin layer (≈5µm) which sits on top of the treated side of the canvas and does not seem to penetrate the canvas. Due to their low penetration and the high reinforcement provided, these treatments could be seen as nano-linings. The coating is very compliant morphologically to the shape of the threads. The method of application, spraying (shown in this chapter) and brushing (see Figure 4.13 in Chapter 4) does not modify the surface deposition and penetration of the CNF and CCNF, and probably CNC, treatments. The superficial deposition of the treatment might offer the advantage of easing the removal of the treatment in the future and thus comply with the principle of reversibility of interventions important to conservation (Sease, 1998).

A drawback of these three treatments remains, however, their high brittleness. The fact that the treatment does not either penetrate the canvas increase the risks of failure of the coating. To overcome this problem, the use of an intermediate coating to promote the adhesion between nanocellulose treatment and the canvas fibres was explored. The results of this study are given later in Chapter 6. This treatment aims to improve the binding between nanocellulose and the cotton fibres. The results of the study are presented in the section 5.4, Results Part 2.

5.4 Results Part 2: Cellulose derivative and CNC filler (*Solution 2*)

Nanocellulose, CNF or CNC, have been introduced and tested as reinforcing agents for polymer matrices for decades (Dufresne, 2013; Favier, 1995). For canvas consolidation, CNC was here selected as reinforcing agent for cellulose derivatives, Tylose and methylcellulose, commonly used in conservation and which have proven to be relatively stable with time (Feller, 1990). This choice was motivated by CNC's greater crystallinity and expected less tendency for entanglement into aggregates than CNF. This would allow for higher concentrations in the dispersions and should promote the processing properties of CNC composites compared to those containing CNF (Forsgren, 2019).

The study of the Tylose/CNC nano-composite was carried out over two years in collaboration with two students, Sobnom Mustari and Deeshani Wijesekara, enrolled in a MRes Chemical Research program at Birkbeck University (University of London, UK). Part of the results of this research can, therefore, be found in their Master's thesis (Akushla Wijesekara, 2018; Mustary, 2017). First, the reinforcement provided by CNC to the Tylose matrix was studied through the preparation of films. Second, from the results of the study on films, the formulation in Tylose (Tyl)/CNC with the higher stiffness was selected for further testing on a degraded cotton canvas.

5.4.1 Reinforcing cellulose derivative films using nanocrystalline cellulose

The use of CNC as filler for mechanical reinforcement of Tylose films was first investigated. Films of Tylose without or with different concentrations in CNC were prepared and analysed for their chemical, mechanical and hygroscopic behaviour. The aim of this study was to define the optimal ratio Tylose/CNC for which the stiffest films is obtained. The formulation selected was then tested on the model of degraded cotton canvas. Using this approach, a better understanding of the viscoelastic properties of the treatments is gained. This allows for anticipating on the response which will be measured on the treated canvases as well as highlighting the impact the surface deposition of the treatment might have on this response.

5.4.1.1 Appearance

The films of TyloseMH50 (Tyl) and Tyl+20%CNC (Tyl+20CNC) are shown in Figure 5.9. The films obtained by dry casting are transparent and mechanically resistant to handling. The addition of CNC at 20% in total dry weight of the film does not modify the appearance of the films. Both films, however, presented undissolved fibrils coming from the Tyl solution which are clearly visible to the naked eye (see zoomed image of Figure 5.9a). As seen on the microscopic images shown in Figure 5.10, these fibrils are around 1mm in length and 50µm in width. The manufacturer confirmed their presence and the impossibility to dissolve them in water. When casting the films, their heterogeneous distribution in solution and the long-time needed to dry cast the films led to the inhomogeneous distribution of those fibrils across the films. Bundles of fibres also formed as seen in Figure 5.9. Their presence and inhomogeneous distribution could lead to earlier mechanical failure of the films. This requires an increased number of repeat measurements in particular for the DMA-RH measurements due to the small size of the samples needed for measurement.

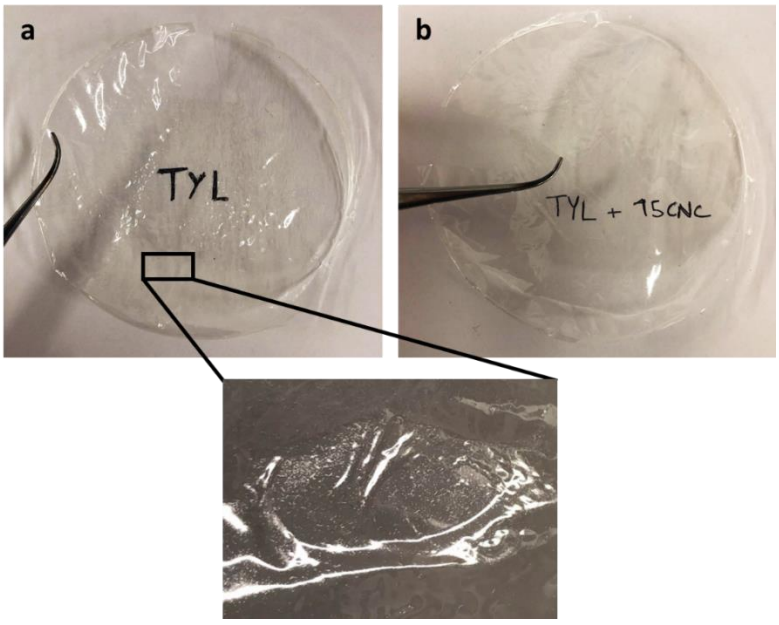

Figure 5.9: Films of TyloseMH50 (Tyl) (a) and Tyl+20%CNC (b). The films obtained are transparent. Non-dissolved fibrils coming from Tylose can be seen on both films. They could not be homogeneously distributed in solution during the dilution of TyloseMH50. They often formed bundles upon dry casting of the films which can be seen on the images.

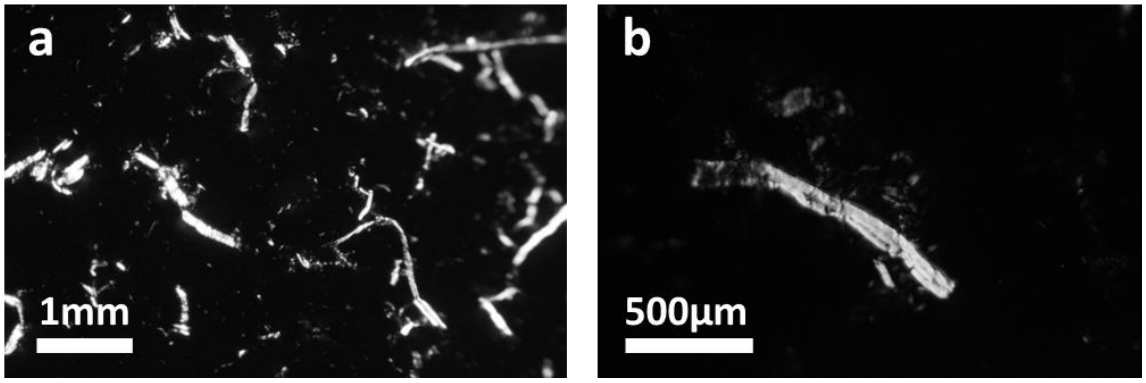

Figure 5.10: Details of the films observed under polarized light microscope (x10 (a) and x20 (b) in magnification) showing the undissolved fibres present in the films and coming from TyloseMH50.

5.4.1.2 FTIR analysis of the films

The FTIR bands in the spectra of a Tylose and Tylose+20CNC films are shown in Figure 5.12. The absorption peaks of the Tylose film spectrum (a) are mainly assignable to the stretching OH stretching vibrations at 3422 cm^{-1}. the asymmetric and symmetric stretching of C-H bonds at 2917 cm^{-1} and 2841 cm^{-1}, respectively and the bending vibration of OH in absorbed water at 1644cm^{-1} (Khan, 2010; Poletto, 2014). CH_3 deformation in cellulose is indicated by the peak at 1457 cm^{-1} and C-H bending in plane is shown at 1378 cm-1 and 1313 cm-1 respectively. The CO stretching results the strong peak at 1052 cm-1 (Poletto, 2012). The peak at 941 cm-1 is corresponding to C-H bending out of plane according to Mani and Suresh (2009).

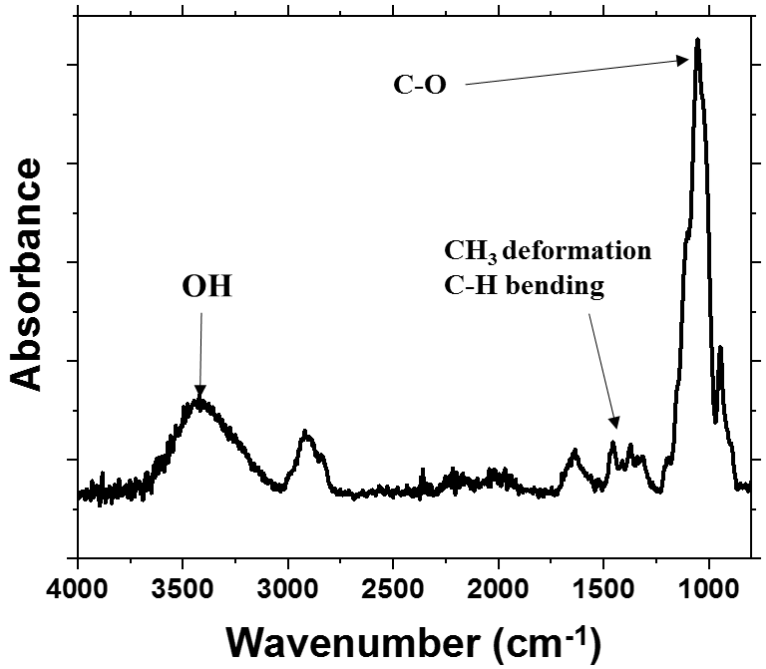

Figure 5.11: FTIR spectra of a TyloseMH50 film with indication of some peaks associated to OH stretching, CN3 deformation and C-H bending

Wavenumber/ cm^{-1}	Assignment
3422	OH stretching
2917	C-H stretching (asymmetric)
2841	C-H stretching (symmetric)
1644	O-H bending
1457	CH_3 deformation
1378	C-H bending in plane
1313	C-H bending in plane
1052	C-O stretching
941	C-H bending out of plane

Table 5.4: List of peaks of the FTIR spectra and their attribution to chemical functions of the hydroxyethyl polymer making up TyloseMH50.

As seen in Figure 5.12, the addition of CNC to the Tylose matrix led to a shift of the peak corresponding to OH bonding from 3429 to 3346cm^{-1}. This shift could be attributed to the increase in hydrogen bonding created between the hydroxyl groups of Tylose with those present on the CNC surface. A similar observation was also made by Khan (2010) who observed a shift from

3410 cm^{-1} to 3330 cm^{-1} for films of methylcellulose (MC) upon the addition of CNC between 0.25 and 1% in dry weight.

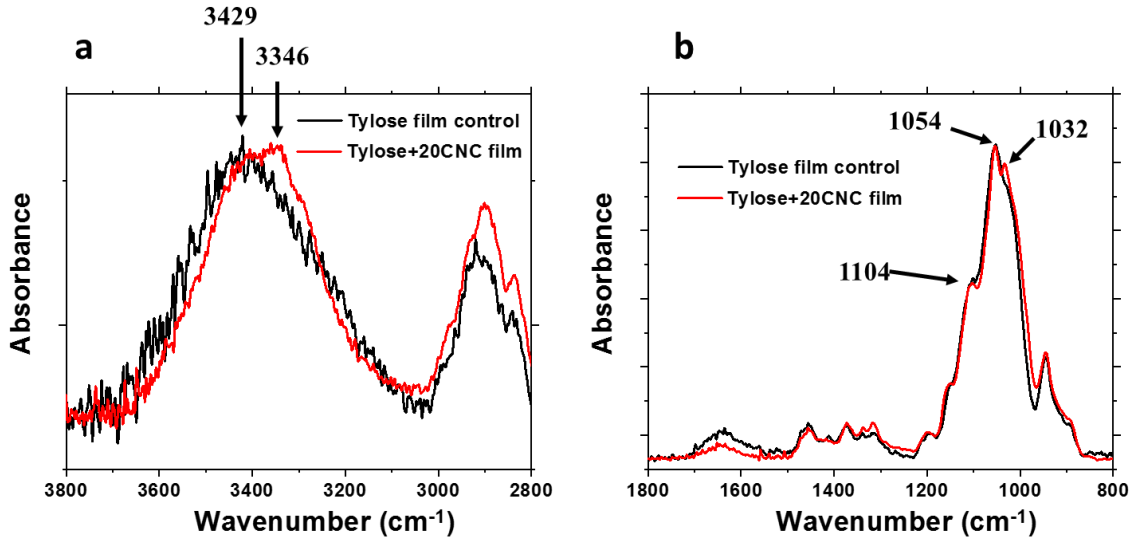

Figure 5.12: Details of the FTIR spectra of films of TyloseMH50 (black) and TyloseMH50+20CNC (red) in the wavenumber range 3800 to 2800 cm^{-1} (a) and 1800 to 800cm^{-1} (b).

An increase in absorbance at 1032 cm^{-1} of the shoulder peak of the 1054 cm^{-1} peak associated to stretching of C-O, can be seen for the Tylose+20CNC film in Figure 5.12. This may be due to the different chemical environments of carbonyl groups created after bonding with CNC with higher density of hydroxyl groups which can make polar bonds with oxygen in carbonyl group leading to different energies of carbonyl stretching vibrations

Overall, the results tend to confirm the molecular interactions of nanocellulose (CNC) and Tylose polymeric chains (i.e. Hydroxyethyl cellulose) through hydrogen bonding with carbonyl groups and hydroxyl groups of the cellulose nanocrystals and hydroxyethyl cellulose chains.

5.4.1.3 Films consolidation upon addition of CNC

The use of CNC in combination with the cellulose derivative matrices Tylose and methylcellulose was mainly driven by the knowledge that the nanocomposite formed may present improved mechanical properties compared to those of the cellulose derivative alone. Improved mechanical properties in CNC-reinforced nanocomposites has been shown in numerous studies including various polymeric matrices (Cataldi, 2015; Kalia, 2011; Lee, 2014; Peresin, 2010; Spence, 2011). It has been shown that above a certain critical volume fraction (referred to as percolation threshold), rod-shaped fillers, such as carbon nanotubes (CNT) or CNCs, interconnect to create a network inside the matrix, which usually leads to a step-wise increase in some physical properties (Dhar, 2017).

The Young's moduli measured for the Tylose films without CNC or with an increasing amount of CNC (from 5 to 20% in dry weight) are shown in Figure 5.13. Upon addition of CNC, an incremental increase in Young's modulus is observed from 1.11GPa measured for the control film of Tylose (i.e. Tyl control) to 1.41, 1.24, 1.62 and 1.99GPa for Tyl+5CNC, Tyl+10CNC, Tyl+15CNC and Tyl+20CNC films, respectively. The highest reinforcement of the Tylose film seems thus to be reached for the highest amount in CNC added (i.e. 20% of the total film weight).

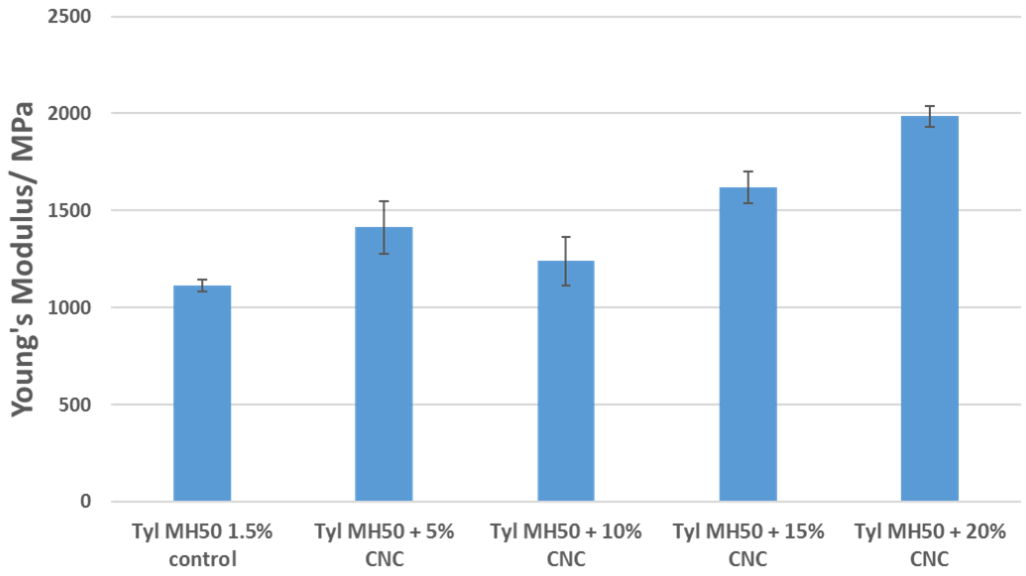

Figure 5.13: Young's moduli calculated for a TyloseMH50 film (Tyl control) and Tyl-based films containing 5%, 10%, 15% and 20% CNC (in dry weight). The results correspond to 5 repeats per sample. The results show the increase in Young's moduli upon addition of CNC to the Tylose matrix.(taken from (Akushla Wijesekara, 2018)).

The control Tylose and reinforced Tyl+20CNC films were also tested further by tensile testing using the Instron tester. In this measurement, the films were brought to rupture in order to evaluate the films ultimate strength and elongation to rupture. The results are presented in Figure C.5 in Appendix. As it can be seen, the addition of CNC particles to the film increase the stiffness of the material (increase in Young modulus shown in Figure 5.13) but simultaneously increase the brittleness of the film. This is shown by the reduction in the elongation at break of the films from 16% for the control Tyl film to 5% measured for the Tyl+20CNC film. Similar behaviour had been observed by Youssef (2015) for MC films reinforced with CNC (3 to 10% CNC in weight of the dry film).

It is, however, important to notice that the inhomogeneous distribution of the CNC particles in the polymer matrix can have an important effect on the mechanical properties of the final casted films. The method of preparation of the films and its direct impact on the films mechanical properties was, for example, highlighted by comparing the results of this investigation with those obtained previously with another batch (Mustary, 2017). The differences observed in

the results (see Figure C.4 in Appendix) probably result from the difficulty to homogeneously disperse the CNC particles in solution.

5.4.1.4 Hygroscopic behaviour upon CNC addition

The percentage increase in weight which followed the change in %RH was measured for casted films of Tylose 1.5% and Tylose 1.5% + 20% CNC (see Figure 5.14). At 60%RH, weight increases of 6.5%±0.6% and 5.7±0.4% were obtained for the Tylose and Tylose +20% CNC films respectively. These results indicate the lower moisture uptake reached by the Tyl+20%CNC film in comparison with the Tylose film without CNC. This behaviour further confirms the results obtained in previous studies (Azeredo, 2009; Cao, 2008; Kaboorani, 2016; Paralikar, 2008; Svagan, 2009) which have shown that addition of NC to different types of polymeric matrices has improved their barrier properties to water. This is because it is thought that the presence of crystalline fibres increases the tortuosity in the materials leading to slower diffusion processes and, hence, to lower permeability (Sanchez-Garcia, 2008). The barrier properties are enhanced if the filler is less permeable, and have good dispersion in the matrix and a high aspect ratio (Lagarón, 2005).

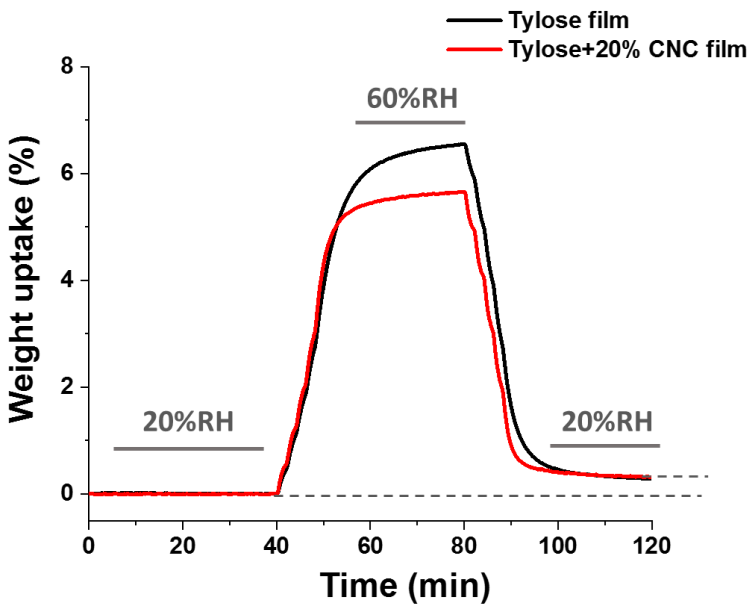

Figure 5.14: Percentage weight increase measured for a TyloseMH50 and a TyloseMH50 + 20% CNC film upon application of a 20-60-20%RH cycle. The curves were normalized at the end of the first equilibration isotherm at 20%RH (i.e. Weight uptake (t=40min)=0%).

In terms of mechanical properties, the hygroscopic behaviour of Tylose also has an impact on the response of the films to moisture variations. The typical response of a Tylose film is shown in Figure 5.15. As it can be seen, the film responds, as expected, in a similar way than Klucel (i.e. hydroxypropyl cellulose), another cellulose ether, previously investigated along other traditional consolidants (cf. Chapter 4), as well as the degraded cotton canvas. Mechanical response is characterised by a sudden drop of storage modulus during 20 to 60%RH transition. This is because moisture plasticized the film by increasing the unbound water molecules inside the film reducing the strength of the film. As RH is sitting at 60%, there is a stiffening of the film until the end of 60% RH state.

Storage modulus has increased when RH varied from 60% to 20%, in the same pattern in all 3 cycles at 20% which could result from the removal of unbound water which has plasticized the films. As RH is sitting at 20%, there is a stiffening of the film until the end of 20% RH state. The sudden drop occurs when RH changes from 20% to 60% was much bigger in 1st cycle compared to 2nd and 3rd cycles. That may be due to initial reorganisation of H-bonds in first

cycle associated with higher water absorption and molecules of bound water than for the 2nd and 3rd cycles. After this first reorganisation, the material has reached equilibrium in terms of internal molecular organisation. The material, therefore, becomes mechanically more stable under further and similar RH variations. This is seen by the stable variations in E measured between RH plateaus for each cycle after the first humidification. This time-dependent change, defined as "physical aging", was observed in the past by Padanyl (1993) when studying the absorption and desorption of water in cellulosic fibres in paper. He showed that by alternating water absorption and desorption cycles, gradual change in macromolecular packing occur until the material reaches an equilibrium state, i.e. the equilibrium free volume state.

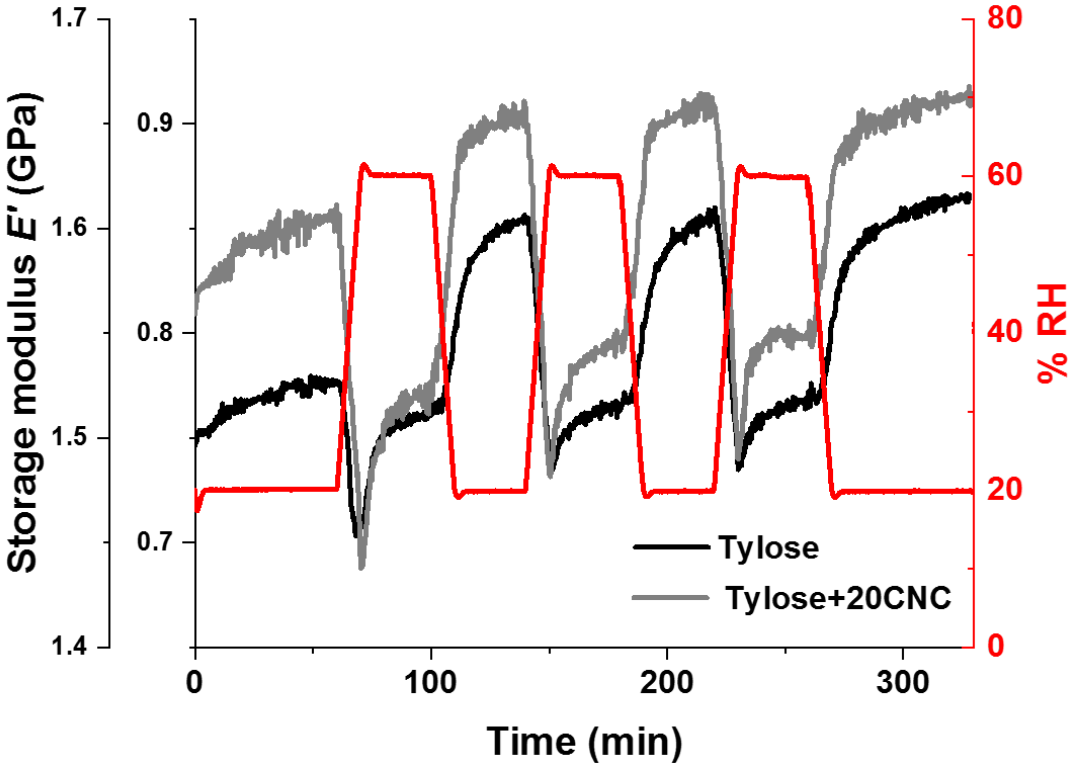

Figure 5.15: Variations in storage modulus measured upon 20-60-20%RH cycling for a Tylose (black) and CNC-loaded Tylose films at 20% in dry weight (i.e. Tylose+20CNC) (grey). The curves were normalized at the end of the first 20%RH plateau. Cycling decrease and increase in E' upon humidification and dehumidification, respectively, are seen for the two films. It is particularly pronounced for the Tyl+20CNC film. The CNC-reinforced Tyl film sample upon humidification becomes stiffer than the film without CNC.

When comparing the mechanical response to RH of the Tyl film upon addition of CNC, it was observed that the nanofiller led to a small increase in the mechanical response of the Tyl+20CNC film upon RH cycling. This occurs despite the lower hygroscopic behaviour, highlighted by DVS measurement, of the Tyl+20CNC film. This is showed by higher differences in *E'* between 20 and 60%RH (i.e. $\Delta E'_{20\text{-}60\%RH}$) plateaus obtained for the Tyl+20CNC film as seen in Table 5.5. $\Delta E'_{20\text{-}60\%RH}$ measured for the films showed an increase from 197.2 to 219.2Mpa (data from 3rd cycle RH) upon addition of CNC at 20% in dry weight of the film. This distinctive behaviour of the CNC loaded Tyl film is believed to be the result of the interaction, through hydrogen bonding, between CNC and the hydroxyethyl cellulose (HEC) polymeric chains of Tylose. It has been previously shown for PVA/CNC nanocomposite fibres that humidification cycle increased the water concentration in the CN-PVA matrix interface, and that after the removal of water molecules, the flexible hydrogen bonds between PVA chains and/or between PVA and water molecules were replaced mainly by stiffer CN-PVA bonds. (Peresin et al., 2010) It is possible that the same phenomenon applies to Tylose/CNC nanocomposite. The stiffer CNC-Tyl bonding, stiffer than Tyl-Tyl bonding, might increase differences in *E'* seen for the Tyl+20CNC film between humid state (i.e. 60%RH) at which more flexible bonds between water and Tylose are formed and dry state (i.e. 20%RH) at which Tyl-CNC bonding are formed.

		1st cycle	2nd cycle	3rd cycle
Tyl film	$E'_{20\%RH}$ (MPa)	937.9	966.5	992.2
	$E'_{60\%RH}$ (MPa)	744.6	774.5	795.0
	$\Delta E'_{20\text{-}60\%RH}$ (MPa)	***193.3***	***192.0***	***197.2***
Tyl+20CNC film	$E'_{20\%RH}$ (MPa)	1715.2	1739.5	1765.2
	$E'_{60\%RH}$ (MPa)	1471.4	1545.9	1546.0
	$\Delta E'_{20\text{-}60\%RH}$ (MPa)	***243.8***	***193.6***	***219.2***

Table 5.5: Storage moduli at 20 and 60%RH measured for Tyl and Tyl+20CNC films and calculated difference in E' between plateaus of each cycle from curves in Figure 5.15.

This increased mechanical response to RH upon addition of CNC was also accompanied with a reduction in variations in elongation of the films upon RH cycles (see Figure 5.16). The results suggest that the structure formed in the presence of CNC is more resistant to elongation. It is possible that CNCs might hinder movements of the hydroxylethyl cellulose (HEC) polymeric chains of Tylose and increase their entanglement. This would explain the lower percentage of elongation measured upon exposure to 60%RH for the Tyl+20CNC film in comparison to the Tyl film. Moreover, Figure 5.16 also indicates that the Tyl and Tyl+20CNC films are irreversibly deformed after the first RH humidification transition from 20 to 60%RH. After the first RH cycle, the elongation measured at 20%RH for both films has increased by 0.12%. For the Tyl+20CNC film, irreversible plastic deformation continues to occur through application of the RH cycles to reach after 2 and 3 RH cycles the elongations measured at 20%RH of 0.21% and 0.25%. It is due to the increased mobility of the network caused by the absorption of strongly bonded water molecules located at the interface between the reinforcing CNCs and the HEC chains of the Tylose matrix or between HEC chains. This was also observed in the past for PVA/CNC nanocomposite fibres (Peresin., 2010) as well as casein films not reinforced with CNC (Bonnaillie, 2015) measured by DMA under RH cycling.

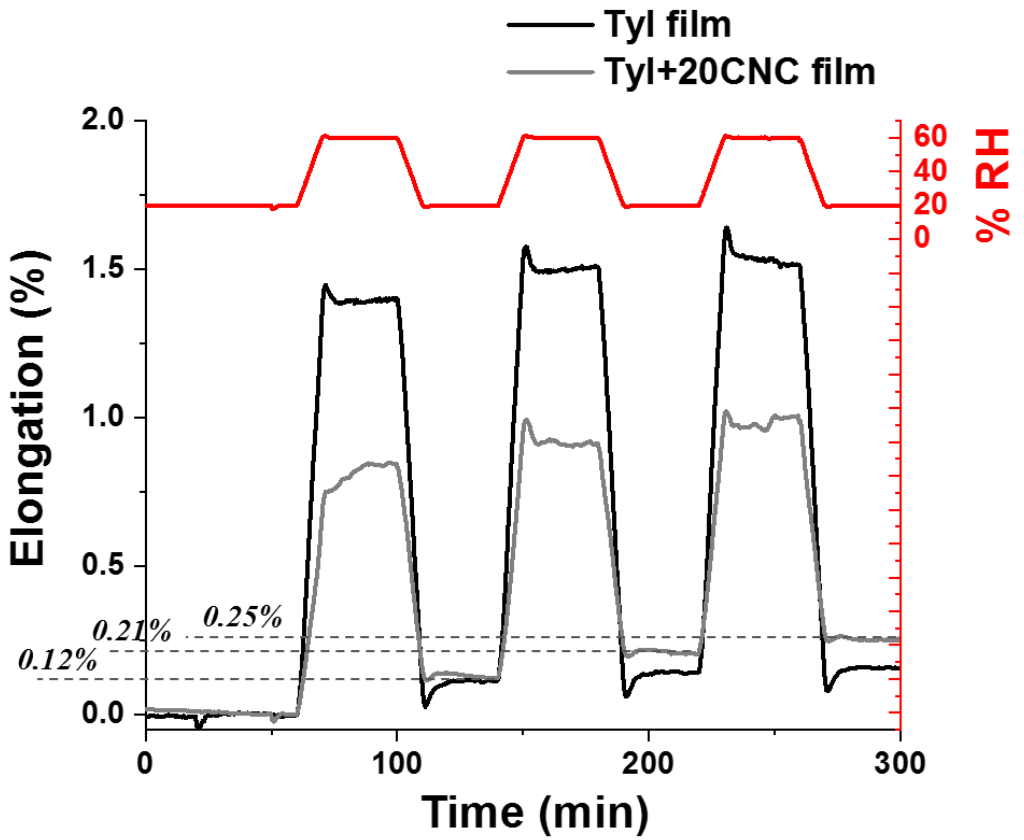

Figure 5.16: Percentage elongation of pre-dried Tylose MH 50 (black) and Tylose MH 50+20%CNC(w/w) (grey) films with respect to time (min). Note the higher elongation measured for the Tylose film at 60%RH than for the Tyl+20CNC film.

Finally, *E'* of the control Tylose film measured at 60%RH increased from about 1471.4 to 1545.9MPa after the first humidity cycles and dropped after the last, third cycle (Table 5.5). This is in contrast to the continuous increase in storage modulus observed in the case of CNC-loaded Tylose film upon humidity cycles. These results indicate that, upon water absorption-desorption, new hydrogen bonds are created between chains in Tylose film, inducing an increase in contact area that enhance the adhesion between the fibres.

5.4.1.5 Intermediate conclusions in the impact of CNC filler on the chemical, mechanical and hygroscopic properties of Tylose films.

In summary, this study has shown that CNCs used as filler for cellulose derivative matrices can improve the mechanical properties of the material as well as it hygroscopic behaviour. Reinforcement of Tylose films upon addition of CNCs was shown to result from an

increase in molecular interactions in hydroxyl groups seen by FTIR. Reinforcement of the Tyl films upon addition of CNC was confirmed by increased Young's modulus values and storage modulus values measured by tensile tests and DMA-RH, respectively. Finally, the CNC-reinforced films show a lower hygroscopic behaviour and dimensional response (i.e. percentage elongation) to RH variations than the control Tyl film. However, the stiffer bonding between CNC and HEC chains also led to an increase in mechanical response to RH seen by the increase in $\Delta E'$ upon exposure to RH variations. The question whether this should be or not detrimental to the painting on which the nanocomposite Tyl+CNC would be applied remain mainly dependent on whether or not the treated canvas retains its role of support at high RH. The results also suggest that humidity cycles have the potential to improve Tyl-Tyl and/or Tyl-CNC adhesion and consequently to enhance the physical properties of the composite films. Further studies are required to unveil the molecular basis for the observed behaviours.

5.4.2 Canvas consolidation using the nanocomposite solution (case of MC+CNC) and effect of the addition of a deacidification nanoparticles ($CaCO_3$)

5.4.2.1 Surface appearance after treatment

SEM images showing the surface (3 different magnifications) of cotton canvases before and after treatment using the nano-composite Methylcellulose (MC)/CNC with or without deacidification agent $CaCO_3$ are shown in Figure 5.17. A cotton canvas treated with $CaCO_3$ only is also given for comparison.

As seen for MC+CNC (without deacidification nanoparticles) and MC+CNC+$CaCO_3$ (with deacidification nanoparticles), the two treatments behave in a similar way indicating that the deacidification nanoparticles might not modify the deposition of the treatment over the canvas. The MC+CNC nano-composites seem to penetrate inter-threads and inter-fibres. The treatments are seen to fill those spaces and voids in the form of inter-fibres bridges. When considering these properties, the behaviour of MC+CNC (as well as MC+CNC+$CaCO_3$) resembles the one observed previously in Chapter 4 (cf. 4.3.1) for most of the traditional consolidant (e.g. Animal glue, Beva

371) including KlucelG, another type of cellulose derivative. The MC+CNC-based treatments are seen to tightly wrap the individual cotton fibres. However, the absence of clear features of the MC+CNC films makes it partially difficult to distinguish untreated from treated fibres. The presence of a treatment layer on those fibres is generally seen through the presence of the inter-fibres bridges or cracks in the films (as seen for MC+CNC in Figure 5.17, details shown by arrows).

Regarding the additional use of deacidification agent, when applied separately, the $CaCO_3$ nanoparticles were shown to be distributed homogeneously on the individual cotton fibres. When mixed with the MC+CNC, they can be seen embedded in the layer of treatments.

The Tylose/CNC composites was also investigated in terms of surface deposition. Similar observations in surface appearance and mode of deposition were made for the canvas treated with Tylose only and with the Tylose/CNC nanocomposite (see Figure C.6 in Appendix). These results indicate that the addition of CNC does not influence the surface deposition of the treatment.

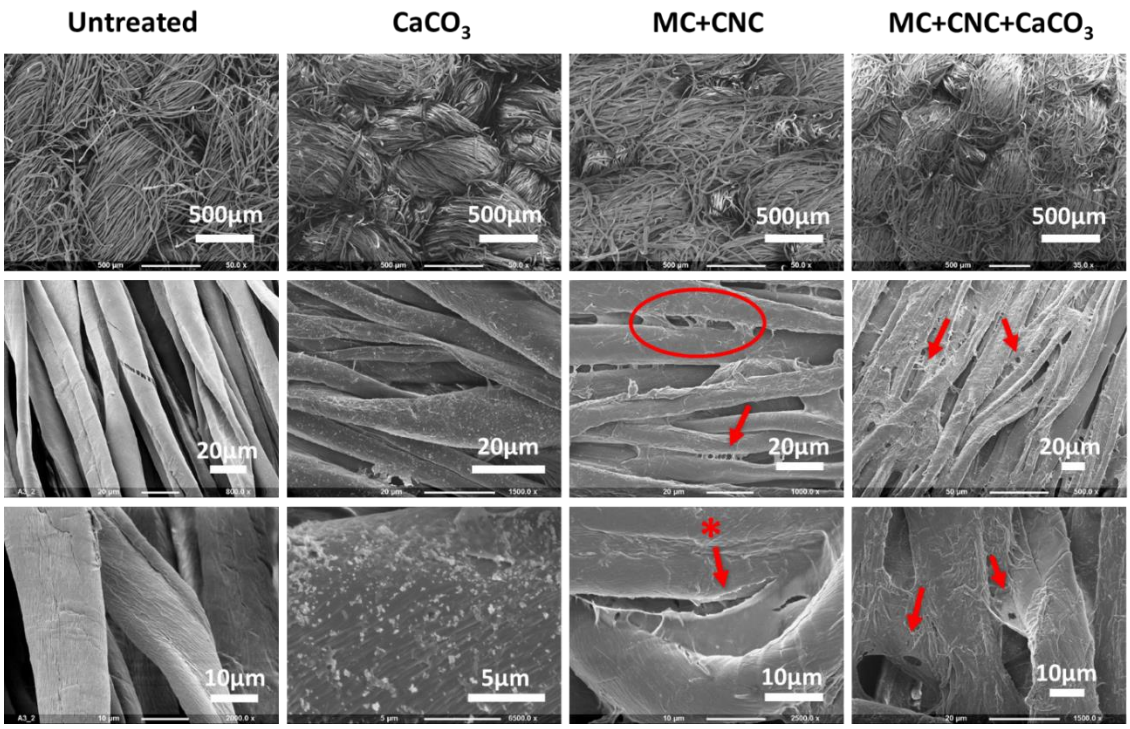

Figure 5.17: Comparison at 3 different magnifications (from top to bottom: low, medium, high) of the surface appearance under SEM of an untreated canvas and 3 canvases treated with a deacidification solution ($CaCO_3$), the methylcellulose+CNC consolidant (MC+CNC) and the mixture of deacidification and consolidant (MC+CNC+$CaCO_3$). MC+CNC and MC+CNC+CaCO3 form bridges of treatment between canvas fibres which could promote the consolidation of the cotton canvas. For these 2 samples, few ruptures in the interfibrillar films formed could also be seen (indicated by (*) for the MC+CNC-treated sample).

5.4.2.2 Consolidation

As seen in Figure 5.18, both MC+CNC and MC+ $CaCO_3$ provide high consolidation to the canvas. This is seen by the increase in slope in the stress-strain curve (Figure 5.18a), hence increase in Young's modulus *Y* (i.e. stiffness) (Figure 5.18b). The result obtained for a CNF-treated canvas with the same surface coverage (i.e. 15g.m^{-2}) is shown in Figure 5.18b for comparison. The results seem to indicate that the MC+CNC treatment might provide a higher consolidation (i.e. *Y*=15.5±0.3MPa) to the canvas than the CNF treatment at same surface coverage (i.e. *Y*=11.5±1.1MPa).

The $CaCO_3$ nanoparticles (NPs) of deacidification seem to interfere with the MC+CNC nanocomposite by lowering the consolidation provided. The Young's modulus (at 20%RH) of

15.5±0.3MPa measured for the MC+CNC-treated canvas is decreased to 11.8±1.7MPa for the MC+CNC+$CaCO_3$-teated canvas (Figure 5.18b). However, the use of the deacidification agent $CaCO_3$ and consolidant independently in a two-step application (i.e. $CaCO_3$/MC+CNC) seem, as expected, to limit the loss in stiffness. Surprisingly, the application of $CaCO_3$ prior to the MC+CNC consolidant still seems to lead to a decrease in Young's modulus measured for the $CaCO_3$/MC+CNC sample (Y=12.9±0.6MPa).

Finally, contrary to what had been previously observed for the nanocellulosic treatment, no ruptures of the treatment seem to take place during testing. As seen in Figure 5.18a, the tensile curves of the MC+CNC, MC+CNC+ $CaCO_3$ and $CaCO_3$/MC+CNC present an almost linear appearance at elongations between 0 and 10%.

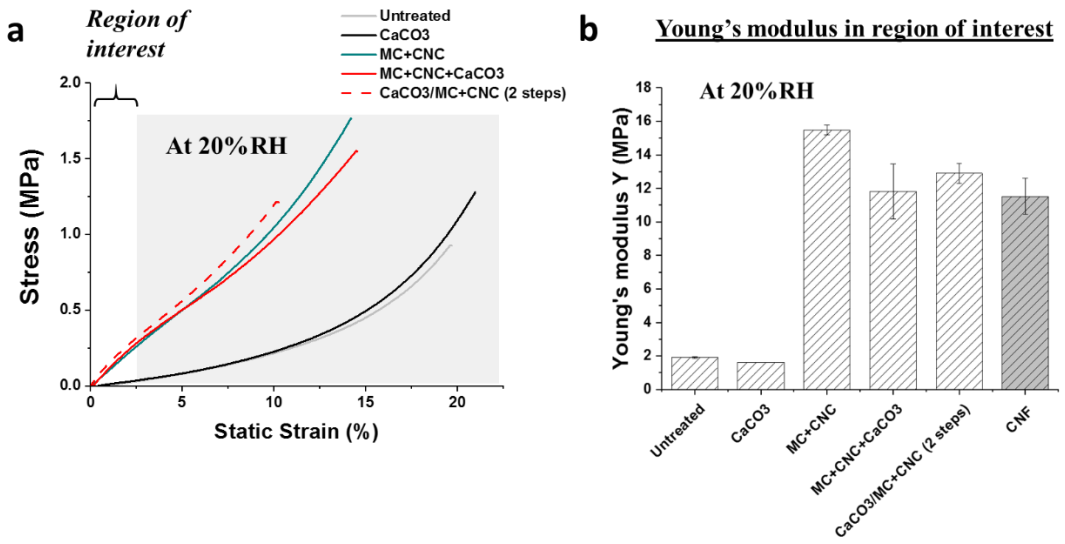

Figure 5.18: Strain-strain curves (at 20%RH, 25C) of an untreated and several treated degraded cotton canvases measured in the warp direction. The treatments tested consist in the deacidification $CaCO_3$ NPs (black), the nanocomposite consolidant MC+CNC (green) and the combined deacidification/consolidation solutions MC+CNC+$CaCO_3$ (1 step application) (red, solid) and $CaCO_3$/MC+CNC (2 steps application) (red, dotted). All the treatments were applied at the same surface coverage of 15g.m^{-2} by brushing.

5.4.2.3 Response to moisture variations

As seen in Figure 5.19, the MC+CNC and MC+CNC+$CaCO_3$ tend to lower the response of the degraded cotton canvas to moisture variations. This is seen as a reduction in the difference in storage moduli $\Delta E'_{20\text{-}60\%RH}$ measured between the 20%RH and 60%RH plateaus. The treatments reduce the response of the canvas from $\Delta E'_{20\text{-}60\%RH}$ =4.9±N/A MPa (untreated sample) to 3.8±0.0 and 1.8±0.7MPa for the MC+CNC and MC+CNC+ $CaCO_3$ treatments, respectively. The reduction in mechanical response to RH is particularly noticeable for the consolidant with the $CaCO_3$ deacidification NPs. The reduced response to moisture could come from the lower hygroscopic behaviour of the $CaCO_3$ compared to the MC+CNC matrix. It could also be associated, as previously suggested for the Tylose films upon addition of CNC, to an increase tortuosity offered to water diffusion in the material. This leads to slower water diffusion processes, hence higher permeability to moisture (Sanchez-Garcia, 2008).

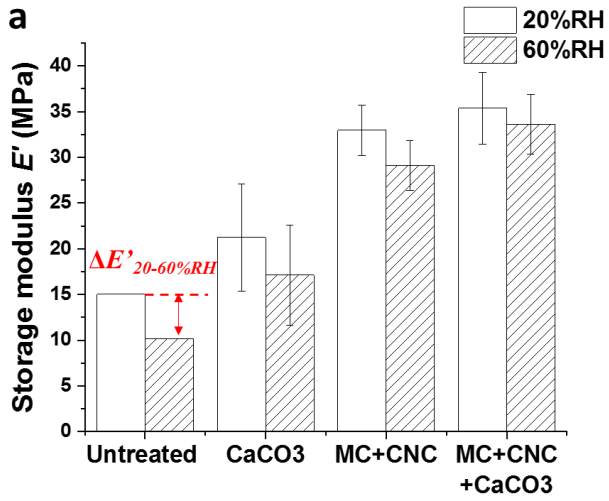

b

Sample	ΔE'(20-60%RH) (MPa)
Untreated	4.9±N/A
$CaCO_3$	4.1±0.4
MC+CNC	3.8±0.0
MC+CNC+$CaCO_3$ (1 step app)	1.8±0.7

Figure 5.19: Storage moduli E' measured at 20%RH and 60%RH (end plateau values, 2nd RH cycle) for untreated and $CaCO_3$, MC+CNC-and MC+CNC+$CaCO_3$-treated canvases as well as a CNF-treated canvas given for comparison (a). Difference in E' calculated between the 20%RH and 60%RH plateaus for the second RH cycle (b).

5.4.2.4 Stability upon ageing

Appearance

Upon ageing, an important visual change in colour was observed for all the samples (Figure 5.20). As seen in Table 5.6, this was caused by a loss in luminance ($\Delta L^*<0$), hence darkening of the canvas, and yellowing ($\Delta b^*>0$). For most of the samples treated with $CaCO_3$, however, a lower change in colour than for the untreated canvas was measured. This is the case of the $CaCO_3$- and MC+CNC+ $CaCO_3$-treated canvases for which ΔL^* *of -7.0 and -5.6 and* Δb^* of 8.9 and 9.1 were measured, respectively (Table 5.6). This is lower that what was measured for the untreated sample (i.e. ΔL^*=-11.7 *and* Δb^*=10.4*)* or any other samples. The deacidification NPs seem thus to have a beneficial impact in slowing down the degradation of the canvas upon thermal/RH ageing.

Surprisingly, when the $CaCO_3$ NPs are applied prior to the MC+CNC consolidant (i.e. $CaCO_3$/MC+CNC), the colour change measured were almost similar to those obtained for the MC+CNC-treated sample. This is probably because contrary to the mixed formulation MC+CNC+$CaCO_3$, the deacidification $CaCO_3$ NPs cannot slow down the degradation of the MC+CNC consolidant since they are not in direct contact with it but rather in the canvas.

Overall, the change in colour upon ageing is lower for the nanocomposite treatment (solution 2) than for the CNF treatment for which a particularly high loss in luminance (i.e. ΔL^*=-18.6) and yellowing (ΔL^*=15.1) has been measured. This does not, however, applied to the CNC and CCNF treatments for which similar (CNC-treated canvas) or even lower (CCNF-treated canvas) values in ΔL^* and Δb^* were measured (Table 5.6).

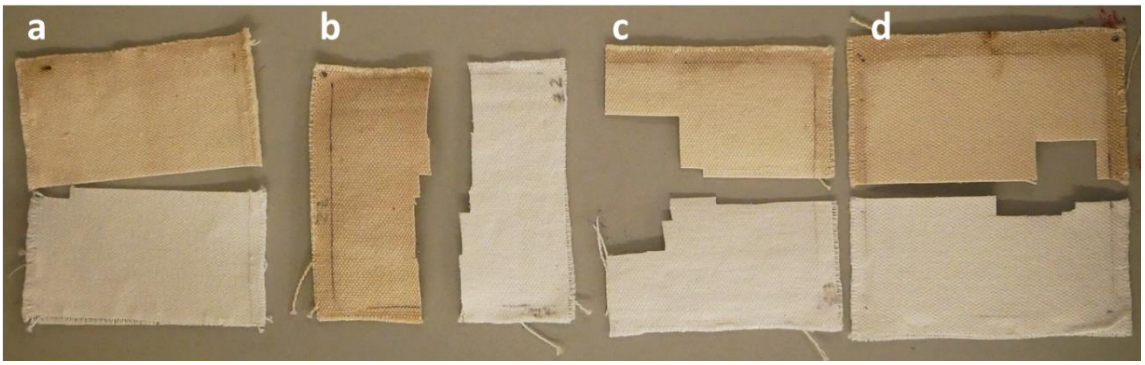

Figure 5.20: Treated degraded cotton canvas, CaCO3 (a), MC+CNC (b), MC+CNC+CaCO3 (c) and CaCO3/MC+CNC(d) before and after ageing. The darker samples in each group are the aged samples.

	Untreated	CaCO3	MC+CNC	MC+CNC+CaCO3 (1 step)	CaCO3/ MC+CNC (2 steps)	CNF	CCNF	CNC
*ΔL**	-11.7	-7.0	-12.8	-5.6	-12.0	-18.6	-9.2	-10.9
*Δa**	2.7	3.0	4.8	3.1	5.0	4.4	2.9	3.1
*Δb**	10.4	8.9	11.5	9.1	12.2	15.1	10.8	11.3
ΔE*	**15.8**	**11.7**	**17.9**	**11.1**	**17.8**	**24.4**	**14.4**	**16.0**

Table 5.6: Colour change in CIELAB colour space (ΔE*, ΔL*, Δa*, Δb*) measured for the samples and resulting from ageing. The results are shown for untreated and treated degraded cotton canvases treated with CaCO3, MC+CNC, MC+CNC+CaCO3 and CaCO3/MC+CNC (treatments from solution 2) as well as a CNF, CCNF and CNC-treated canvases (treatments from solution 1) for comparison.

Consolidation

The impact of ageing on the mechanical properties of the samples is here only discussed for the MC+CNC-treated and MC+CNC+$CaCO_3$-treated samples. Again, the results are compared with those obtained for a CNF-treated sample having the same surface coverage in treatment.

As seen in Figure 5.21, after ageing, the samples tend to have lost in stiffness and, as a consequence, to provide a lower consolidation to the degraded cotton canvas. This is true for the MC+CNC treatment and is also seen for the CNF-treated canvas for which losses in Young's

modulus from 15.5±0.3 to 11.4±0.6MPa and from 11.5±1.1 to 8.1±2.5MPa were measured, respectively. On the contrary, for the mixed consolidant with deacidification agent treatment, i.e. MC+CNC+$CaCO_3$, the ageing program does not seem to have affected the mechanical properties of the material. The Young's modulus measured after ageing remains almost unchanged and is maintained between 11.8 (*Y* before ageing) and 11.6MPa (*Y* after ageing).

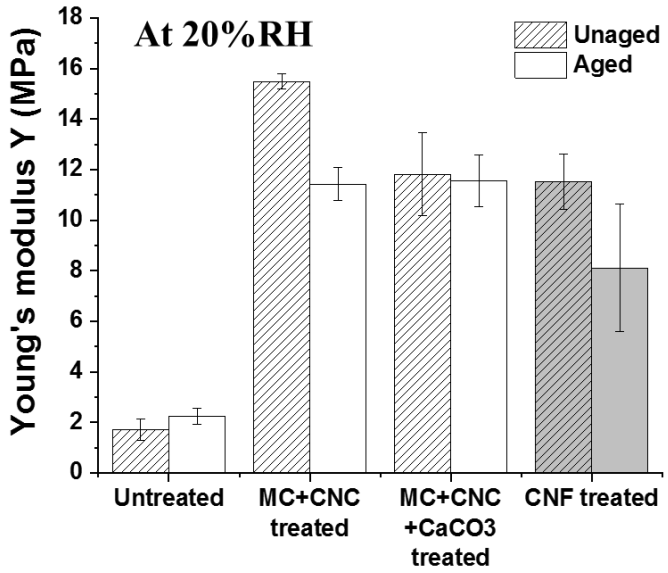

Figure 5.21: Young's modulus (at 20%RH, 25°C) measured in the warp direction before and after ageing for the untreated and MC+CNC, MC+CNC+$CaCO_3$ (1 step app), $CaCO_3$/MC+CNC (2 steps app)-treated degraded cotton canvases (at 15g/m^2). Young's moduli of a canvas treated with CNF, at the same surface coverage (i.e. 15g/m^2) is shown for comparison. Note the increase in Y, hence the stiffening, observed for all the samples after ageing.

The advantage of using deacidification NPs in combination with the consolidant seems supported by those findings. The results have shown that the lower visual changes observed after ageing for the MC+CNC+$CaCO_3$-treated sample are also associated with a good mechanical stability. Combining deacidification NPs with the consolidant seems to protect the consolidant from degradation and, as such, would ensure the long-term stability of the consolidation reducing the need for future retreatments.

Hygroscopic response (mechanical point of view)

In terms of response to moisture, the response of the samples after ageing differ (Table 5.7). The mechanical response of the untreated remains unchanged. However, whereas the response of the MC+CNC-treated sample is decreased by half from $\Delta E'_{20\text{-}60\%RH}$ =3.8±0.0MPa to 1.9±0.4MPa, the response of the MC+CNC+$CaCO_3$ sample is slightly increased from $\Delta E'_{20\text{-}60\%RH}$ =1.8±0.7MPa to 2.5±0.3MPa. The reasons for the changes observed are not clear. However, since the changes $\Delta E'_{20\text{-}60\%RH}$ after ageing are not significantly different, it is possible that they only result from differences in treatments distribution within the canvas and between sample pieces measured. Overall, the results show that the lower response to moisture previously highlighted in remain unchanged. Both MC+CNC and MC+CNC+$CaCO_3$ consolidants reduce the mechanical response of the canvas to moisture.

Sample (treatment)	**ΔE'(20-60%RH) (Mpa)**	
	Before ageing	**After ageing**
Untreated	4.9±N/A	4.7±0.6
MC+CNC	3.8±0.0	1.9±0.4
MC+CNC+ $CaCO_3$ (1 step app)	1.8±0.7	2.5±0.3

Table 5.7: Comparison of the mechanical response 20-60%RH cycles of untreated and MC+CNC- and MC+CNC+$CaCO_3$-treated degraded cotton canvases before and after ageing. The variations in storage modulus E' (i.e. $\Delta E'_{20\text{-}60\%RH}$) were measured between 20 and 60%RH RH plateau (end plateau values, 2nd RH cycle) and the test repeated 3 times per sample.

5.4.3 Intermediate conclusions for the nanocomposites consolidants (i.e. solution 2)

The addition of CNC nanocellulose particles to cellulose derivative matrices has shown to improve the stiffness (i.e. Young's modulus). Improved mechanical properties could be seen from Tylose films with 5%CNC in dry weight. It was also shown that addition of CNC reduces the hygroscopic behaviour of the cellulose derivative films.

When applied on canvas, the nanocomposite films achieve a good coating of the canvas at the thread and canvas single fibre level. Higher penetration of the treatment seems to be achieved than for CNF, CCNF and CNC treatments. The nanocomposites treatments also enable suitable consolidation of the canvas, similar at same surface coverage, to the one reached using CNF. The addition of deacidification particles to the nanocomposite MC+CNC as shown to possibly reduce slightly the consolidation achieved by the MC+CNC treatment (only seen by DMA-RH but not by tensile test). However, it also seems to be accompanied by a favourable reduction in the mechanical response of the sample to RH variations. Overall, the CNC-nanocomposite treatments, with or without deacidification agent, also decreases the canvas response to RH variations. These variations remain, however, higher than those measured for the CNC-treated canvas (cf. 5.3.3).

In the following section, the impact of the chosen application method is investigated for any potential influence on the results of the nanocomposite treatments. This case study is based on the assumption that different methods of application might lead to different degree of penetration of the treatment into the canvas, hence different results in terms of consolidation. This will be discussed in more detail below.

5.5 Case study: Note on the influence of the application method on the deposition and consolidation

During the experiments, the influence of the mode of application was also considered. It has already been noted in section 5.3.1 that for CNF, the penetration and deposition of the treatment, associated with the formation of a superficial layer or nano-lining, does not seem to be influenced by the mode of application chosen (i.e. spraying or brushing). However, it was not known if the same would be true for the nanocomposite treatments (Tyl+CNC and MC+CNC). How does the mode of application of the treatments modify their penetration and how does this influence the final mechanical and hygroscopic properties of the material? The tests were carried out using the Tyl and Tyl+20CNC consolidants.

5.5.1 Penetration

A degraded cotton canvas was treated by a solution of Tylose at 1.5%w/w in water by spraying and by brushing. To follow the penetration of the treatment into the canvas, a fluorescent dye was mixed to the Tylose solution. The cross-sections of the treated canvas samples are shown in Figure 5.22. The presence of Tylose is indicated by the white area on the images. The Tylose sprayed sample and the Tylose brushed (1 application) sample correspond to the same amount of applied treatment. As seen in Figure 5.22a and b, the application by brushing induces a higher penetration of the treatment into the canvas than when the treatment is sprayed. The presence of treatment on the sprayed sample is seen to have penetrated only the superficial cotton fibres of the canvas on the treated side (Figure 5.22a). On the contrary, at the same weight added, for the brushed sample, the treatment as penetrated the canvas up to the other side (i.e. untreated) of the canvas (Figure 5.22b). The mechanical action of the brush and small pressure applied when treating the canvas might have facilitated the passage of the Tylose solution into the canvas mesh, between threads and cotton fibres. Interestingly, it can also be seen that a higher concentration of treatment is found at the interface between threads (see arrows in Figure 5.22b). This is probably because the treatment penetration is slowed down when cotton fibres are found in perpendicular

alignment and, as a consequence, inter-fibre spaces are less accessible. When a higher amount of Tylose is applied by brushing (Figure 5.22c), the treatment can be seen filling the canvas in its entire depth and to be homogeneously distributed.

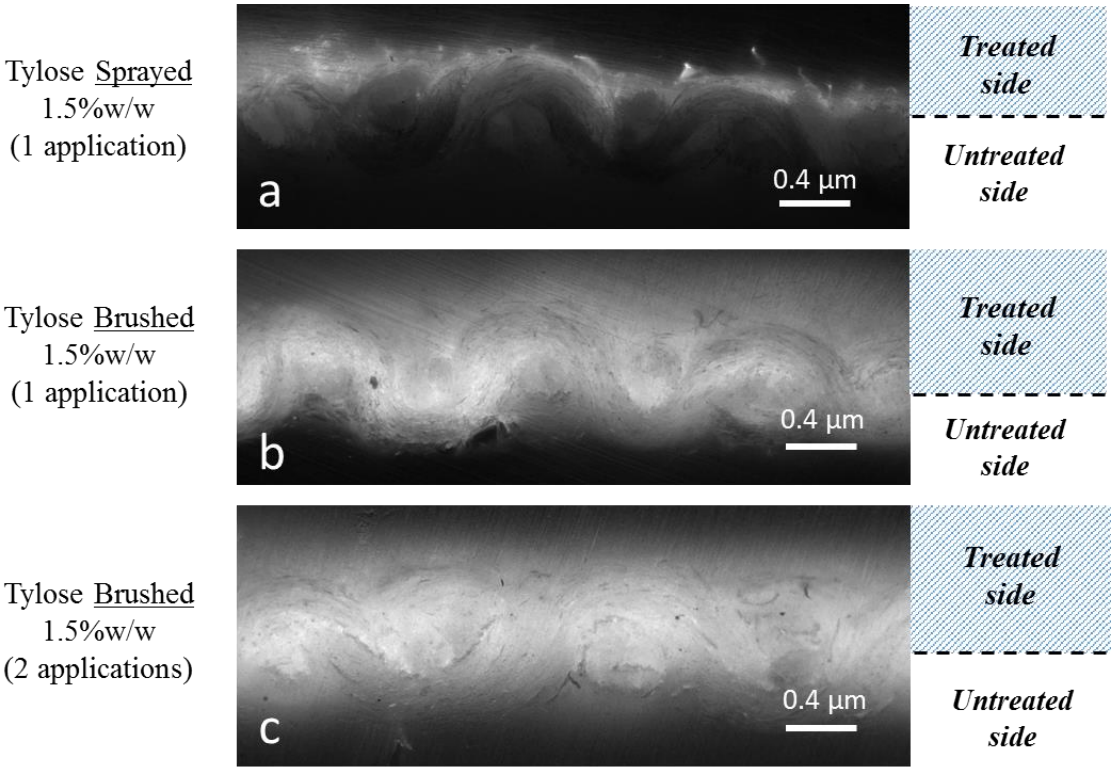

Figure 5.22: Cross-section images of cotton canvases treated with Tylose (Methyl hydroxyethyl cellulose) at 1.5%w/w in water taken by confocal microscopy. The canvas samples were measured embedded in an acrylic resin. Tylose was mixed with a fluorescent dye (Rhodamine B) to follow the penetration of the treatment within the canvas. The treatment has here been applied in 2 different ways: by spraying (a) and by brushing (b,c). A similar amount of treatment was applied in a and b whereas double the amount in Tylose was applied in c. Comparison of the images highlights the difference in treatment distribution and penetration in the canvas.

SEM images of the surface of the sprayed and brushed (single application) samples were also taken and comparison with the cross-sections images could be made. As seen in Figure 5.23, when Tylose is applied by spray, the inter-fibres spaces present on the emergent part of the threads (see arrows in Figure 5.23a) are entirely covered with the treatment. The treatment forms a dense

layer, morphologically compliant to the superficial fibres which can still be seen but which covered almost entirely the canvas surface (Figure 5.23b). The space between threads is, however, still accessible probably due to the low amount of treatment applied. For the brushed canvas, on the contrary, the treatment is much more compliant to the single cotton fibres morphology. The visible part of the threads can still be seen, as for the sprayed sample, the higher retention of the treatment (Figure 5.23c). However, details of these areas presented in Figure 5.23d shows that inter-fibres spaces remain free of treatment. Tylose forms a thin film linking partially the cotton fibres between each other. The bulk of the canvas is still visible. In conclusion, the higher penetration achieved using brushing instead of spraying seems to be supported by both fluorescent microscopy and SEM images of the surface of the sample.

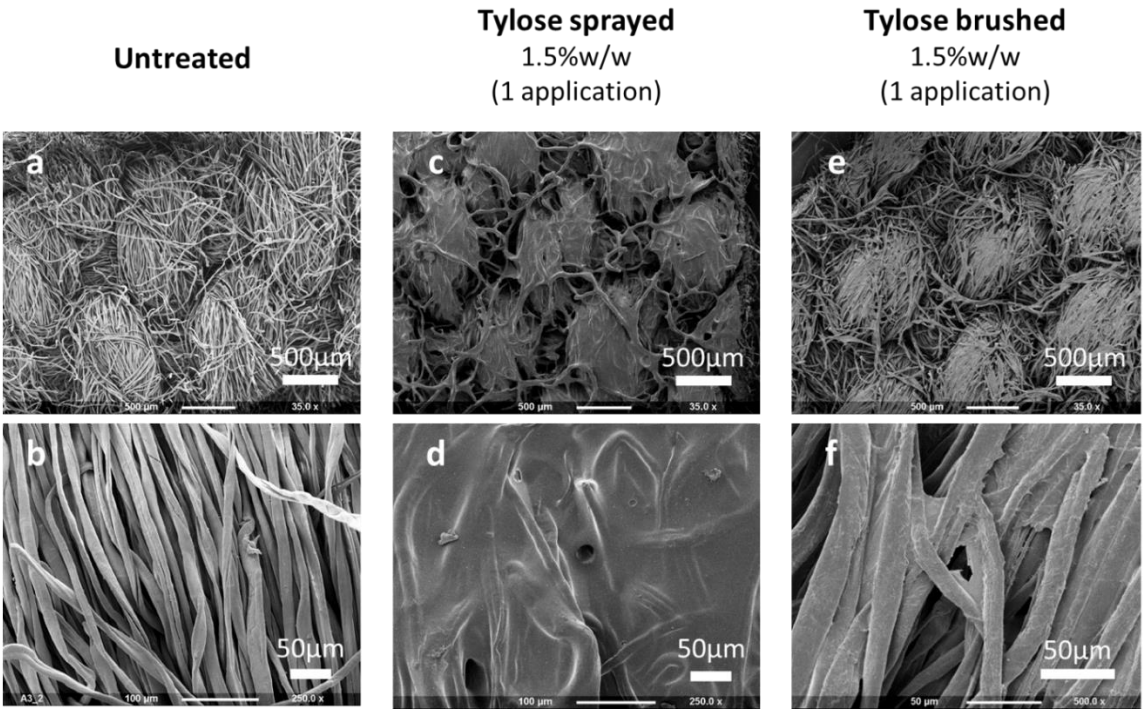

Figure 5.23: SEM images at two different magnification of the surface of degraded cotton canvases untreated (a,b) and treated with Tylose by spraying (1.5w/w, 1 application) (c,d) and brushing (1.5w/w, 1 application) (e,f). Images at low (a and c) and high (b and d) magnification are shown.

5.5.2 Consolidation

The degree of penetration of the treatment could have a direct impact on the consolidation achieved for the treated canvas. With this assumption, the sprayed sample (1 application) and the 2 brushed samples (1 and 2 applications) were tested by tensile testing and their Young's moduli measured in the region of interest for easel paintings (1-2% elongation) (see 1.1.3.2 in Chapter 1).

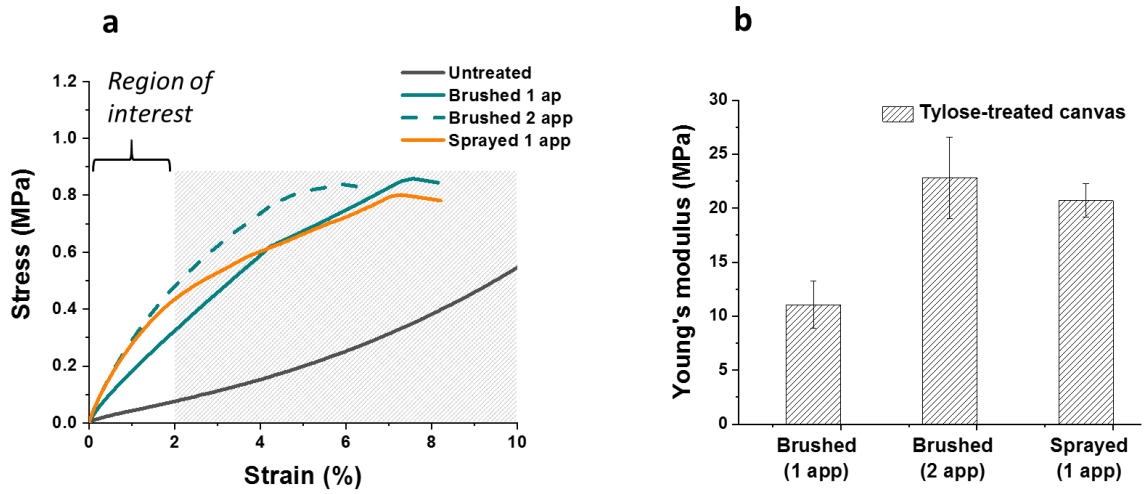

Figure 5.24: On the left, tensile curve performed at 20%RH (25°C) of untreated and treated cotton canvas with Tylose50. This graph shows the impact of the method of application (brushed or spray) and number of application (1 or 2 applications) on the mechanical properties of the treated canvas. On the right, Young's moduli at 20%RH (25°C) calculated from the slope of the tensile curves in the region of interest.

Figure 5.24a shows the representative stress-strain curves obtained for the untreated and treated cotton canvas. In the region of interest, it can be seen that the higher slopes of the stress-strain curves, hence higher Young's modulus (i.e. stiffness), are seen for the sprayed sample and the brushed sample (two applications). Young's moduli of 20.7±3.8 and 22.8±1.6MPa were measured for the sprayed and brushed (two applications) samples, respectively, whereas a lower Young's modulus of 11.1±2.2MPa was measured for the brushed sample (single application). The results indicate that at the same weight added, spraying the treatment provides a higher reinforcement at low elongation than brushing. To reach the same level of consolidation than the

one reached for the sprayed sample, twice the amount in Tylose had to be applied by brushing. The higher consolidation reached by spraying probably result from the lower penetration of the treatment observed previously for this sample. The treatment is concentrated on the treated surface of the canvas. The surface of the threads is embedded in the cellulose derivative matrix which, thus, prevent the threads to move upon application of tension. This is seen by tensile testing as a strong increase in Young's modulus (Figure 5.24b). On the contrary, due to the higher penetration of Tylose when brushing is used, the overall density of the treatment is reduced. As seen previously by SEM in Figure 5.23d, the cellulose derivative-based treatment forms thin films between cotton fibres which might mechanically fail before the thick layer observed for the sprayed sample. When a higher amount in treatment is applied by brushing, the density of treatment in the canvas volume is increased, hence Young's modulus is also increased.

Spraying the consolidant instead of brushing could be seen as more effective. However, the superficial deposition achieved by spraying also present the drawbacks already highlighted with the nanocellulose treatments (see 5.3.2), hence concentration of the mechanical stresses on the layer of treatment leading to its early mechanical failure. This can already be seen in Figure 5.24a with the inflexion at higher elongations (i.e. >2%) of the tensile curve obtained for the sprayed sample. The curve rejoins the one of the brushed (1 application) sample above 4% elongation. In that sense, the use of brushing for the application of the treatment seems more suitable for canvas consolidation. It, however, also forces to apply higher amounts of treatments to which conservators are often reluctant for reasons of reversibility and because it implies higher risks associated to the application of high amount of solvents (varnish swelling, canvas reactivity, losses of vulnerable paint layers) (Burnstock, 2014; Krarup Andersen, 2013; Phenix, 2014; Works, 2018).

5.5.3 Response to moisture

The impact of the mode of treatment application on the hygroscopic behaviour of the treated canvases was also investigated. First, the hydrophilic behaviour of the treated side of the samples was evaluated using contact angle measurements. In Figure 5.25, the time taken for a

droplet of water deposited on the treated side to be absorbed by this surface was measured. As expected, differences between the time of absorption of the water droplet were observed between the canvases treated by spraying and those by brushing. However, it is important to note that for the canvases treated by spray, the time of absorption measured is higher, 20 and 31s Tylose-treated and Tylose+20CNC-treated canvases, respectively, than those measured for those treated by brushing (<11.5s). The application by brushing thus seems to increase water absorption from the treated side.

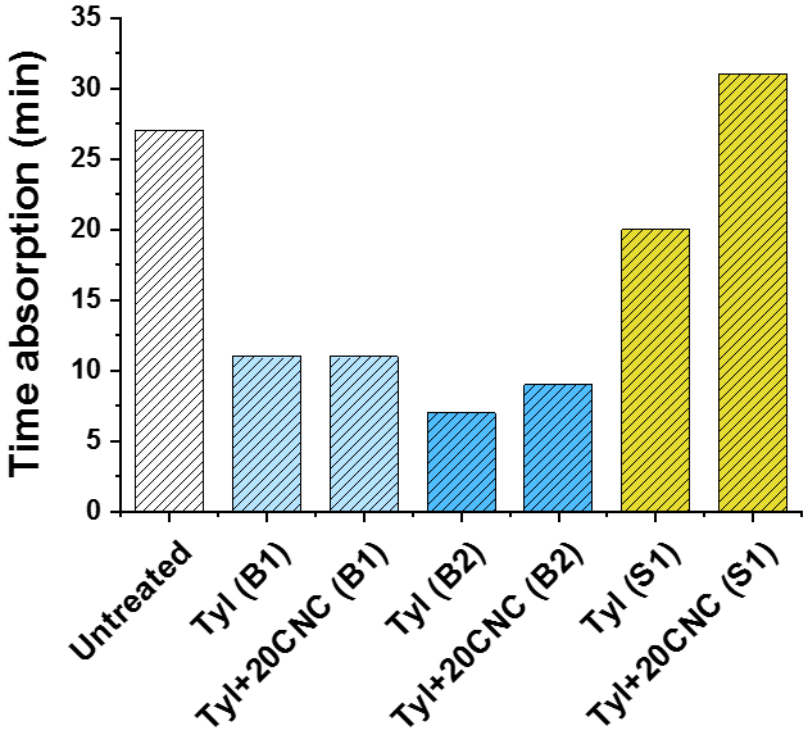

Figure 5.25: Time (in seconds) taken for untreated and treated degraded cotton canvases to absorb a water droplet measured by contact angle. A degraded untreated cotton canvas was measured before and after treatment with Tylose (Tyl) and Tylose+20%CNC (Tyl+20CNC) by brushing (1 (B1) and 2 (B2) applications corresponding to 15 and 30g.m^{-2} surface coverage, respectively) and by spraying (1 application (S1), 15g.m^{-2} surface coverage).

Two factors influence water absorption of a surface: the surface energy of the surface, water absorption in increased when surface energy is increased or the roughness of the sample (Cassie, 1944; Wenzel, 1936). For both samples, the same treatment was applied, i.e. Tylose and Tylose+20CNC, so that the same change in surface energy would be expected for both samples.

When comparing the surface appearance of the brushed and sprayed samples, at same surface coverage in treatment, the SEM images in Figure 5.23 had shown that spraying led to an overall reduction in surface roughness compared to brushing. However, it is known that for a hydrophilic surface, a large surface area or a higher roughness leads to increase polar interactions with water droplet and thus decreases the water contact angle (Kubiak, 2011; Wolansky, 1999). Cellulose derivatives are hydrophilic materials. As such, after treatment application, the canvas surface becomes more hydrophilic. Therefore, the principles which were just described should have applied for the Tyl-treated samples. The results are thus particularly surprising as they show opposite relative behaviours to what would have been expected. Moreover, for the untreated canvas, time absorption of 27s was measured. This is even lower than the time of absorption measured for the sprayed Tylose+CNC-treated canvas. These results thus suggest that for the sprayed samples, a lower surface coverage than the 15g.m-2 expected might have been applied. This was probably caused by the lower control over the weight added (losses due to evaporation during spraying, losses on the canvas edges) and homogeneous deposition of the treatment prone to occur during spraying.

The results obtained for the brushed samples, however, highlight the increase hydrophilic behaviour reached after application of the Tyl and Tylose+CNC treatments. The samples are rendered even more hydrophilic after the second application of the treatment (i.e. Tyl and Tyl+CNC brushed (2 applications)) (Figure 5.25).

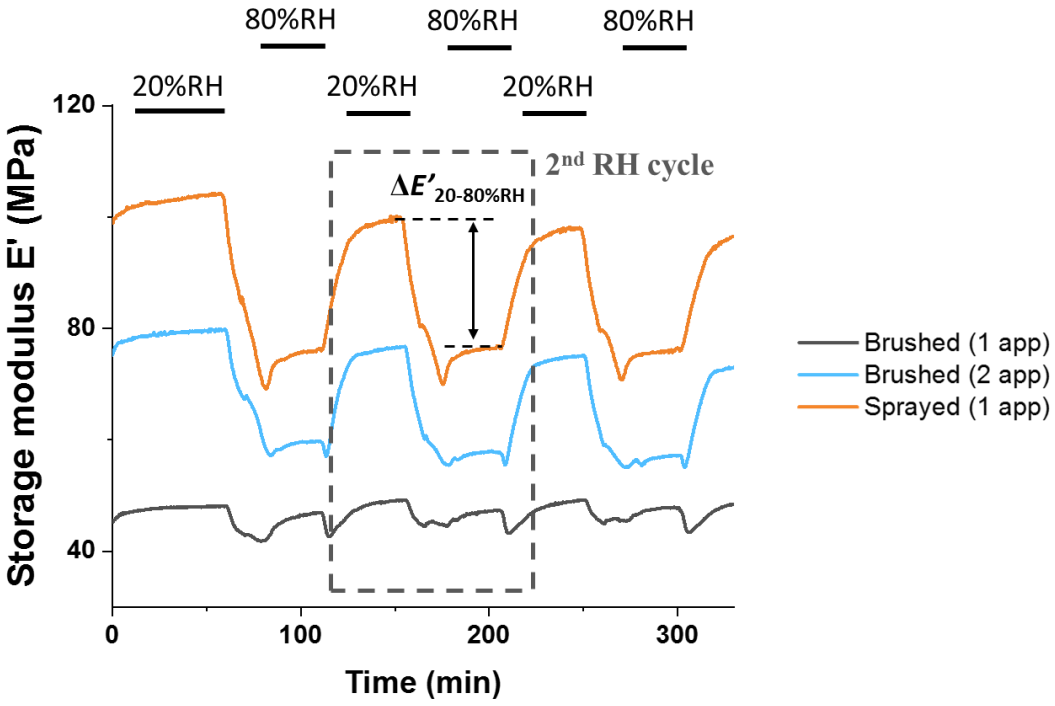

Figure 5.26: DMA-RH curves showing variations in storage modulus E' measured for Tyl+20CNC treated samples undergoing 20-80-20%RH RH cycles. Note the lower mechanical response of the brushed sample with 1 application (15g/m2) (black) than the sprayed sample (15g/m2). When a higher amount of treatment is applied by brushing (brushed (2 app, 30g/m2)) (blue), this triggers a higher response to moisture.

Further assessment of the hygroscopic response of the samples was carried out by DMA-RH using 20-80-20%RH cycles. Measurements of the variations in storage modulus *E'* (see DMA-RH curves in Figure 5.26) between low and high RH levels aim at informing on the mechanical response of the samples to moisture. The differences between *E'* measured at 20 and 60%RH (end-plateau value) were measured for the 2nd RH cycle as seen in Figure 5.26. As seen in Figure 5.27a, the values in *E'* measured at 20 and 80%RH for the 2nd RH cycle show again the higher stiffness reached by spraying over brushing for the same surface coverage. However, the increase in *E'* hence higher consolidation seems associated with an increase in mechanical response of the samples. In Figure 5.27b, the differences $\Delta E'_{20\text{-}80\%RH}$ calculated for the sprayed (1 application) and the brushed (2 applications) samples are greatly higher (i.e. 23.8±0.4 and 16.3±7.1MPa, respectively) than those measured for the brushed (1 application) and untreated samples (i.e. 3.3±2.0 and 4.9±1.4MPa, respectively.

a

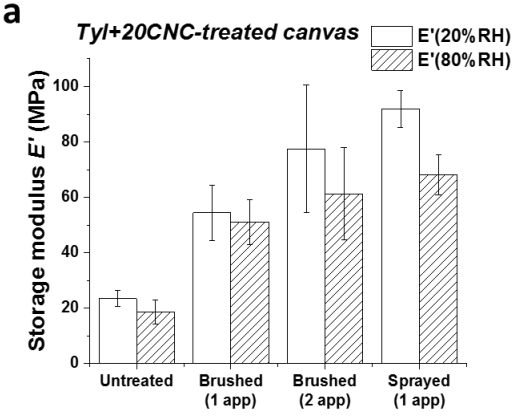

b

Tyl+20CNC treated canvas	**$\Delta E'$ (20-80%RH) (MPa)**
Untreated	4.9±1.4
Brushed (1 app)	3.3±2.0
Brushed (2 app)	16.3±7.1
Sprayed (1 app)	23.8±0.4

Figure 5.27: Storage moduli E' measured at 20% and 80%RH (end-plateau value) for untreated and Tyl+20CNC-treated degraded cotton canvases (a) and difference in E' measured between the 20%RH and 80%RH plateaus as shown in Figure 5.26 (i.e. $\Delta E'_{20\text{-}80\%RH}$) (b). The results enable to compare the impact of the mode of application used (sprayed (1app, 15g.m^{-2}), brushed (1app, 15g.m^{-2}) and brushed (2app, 30g.m^{-2})) on the mechanical properties and mechanical response to moisture variations of the treated samples.

These results are interesting as they further suggest that the mode of application of the treatments can strongly affect the mechanical response to moisture of the treated canvases. First, as seen before by tensile testing (Figure 5.24) and then by DMA-RH (Figure 5.27a), the use of one application of the nanocomposite treatment applied by brushing already provides consolidation to the canvas. As seen in Figure 5.27b, the treatment does not affect the mechanical response of the canvas to RH variations as variations in *E'* remain quite low, similar to the untreated canvas. However, when a higher amount is applied (i.e. brushed two applications), higher reinforcement is achieved but the higher density of treatment in the canvas volume or possibly the higher penetration of the treatment into the canvas seem to lead to higher mechanical response to moisture. The mechanical stresses absorbed by the canvas (and potentially the higher risk of mechanical failure of the canvas or the painting) are increased in this latter case.

Second, spraying also seems to increase the mechanical response of the treated canvas to moisture variations. At same surface coverage, spraying the treatment led to an increase in

mechanical response to RH from $\Delta E'_{20\text{-}80\%RH}$=4.9±1.4MPa (untreated) to 23.8±0.4 MPa (sprayed sample) (Figure 5.27b) whereas the response of the brushed sample (i.e. 3.3±2.0MPa) remain similar to the untreated canvas, as seen previously. However, this latter observation should be taken with care as DMA-RH results obtained for the Tyl-treated samples (see Figure C**.7** in Appendix) do not entirely match those obtained with the Tyl+20CNC-treated canvases. For the Tyl-treated samples, $\Delta E'_{20\text{-}80\%RH}$ measured for the sprayed sample remains quite low (i.e. $\Delta E'_{20\text{-}80\%RH}$ =5.3±4.6MPa) at similar values than those calculated at 4.9±1.4 and 3.3±2.6MPa for the untreated and brushed (1 app) samples, respectively. For the brushed (2 applications) sample, a higher response (i.e. higher $\Delta E'_{20\text{-}80\%RH}$) to moisture variations reached after treatment is again observed.

The role that a particular application method (e.g. brushing, spraying, blade coating) can have on the final properties of a treated canvas has been shown in the past, in particular for wax resin (Krarup Andersen, 2013) and the vinyl acetate adhesive Beva 371 (Krarup Andersen, 2013; C. Young & Ackroyd, 2001). Several authors have shown that depending on the way the treatment is applied, hence the degree of penetration of the adhesive into the canvas, the final mechanical properties of the treated canvas can greatly differ. As previously shown in Chapter 1 (cf. 1.1.4.1.1), the high penetration of wax-resin adhesive in linen canvases was shown to be responsible for the strong shrinkage observed for these linings at high RH. Krarup Andersen (2013) suggested that wax-resin might enhanced the swelling of the threads as the fibres of the canvas are embedded in the resin and because there is not free space around each swelling fibre (cf. Figure 3.3 in Chapter 3).

However, contrary to wax-resin or Beva 371, cellulose derivatives are hygroscopic materials. It thus possible that the phenomenon described above might not apply in this particular case. The results might, on the contrary, indicate that Tylose might trigger and increase the rate of diffusion of the water molecule in the canvas. This would explain the higher variations and higher viscoelastic behaviour measured for the brushed (2 applications) samples. The canvas is embedded in the Tylose (or Tylose+CNC) matrix which facilitates the absorbance of the water

molecule (as seen also by contact angle, cf. Figure 5.25). Tylose itself, as well as Tylose+20CNC, have also shown to be highly responsive to moisture and to show a higher visco-elastic behaviour above 60%RH (cf. 5.4.1.4). This could also suggest that the treatment might act as a lubricant for the canvas threads leading to an increase in mechanical response of the treated canvas to moisture.

The reasons behind the high $\Delta E'_{20\text{-}80\%RH}$ measured for the sprayed sample are not clear. The discrepancy in the results obtained for Tyl-treated and Tyl+20CNC-treated sample, however, suggests the need for further measurements and the need for improved controls of the homogeneous application of the treatment and surface coverage after the treatment has dried.

5.6 Conclusions

The two different solutions for painting canvas consolidation present advantages and disadvantages which were listed at the end of each individual study. All the treatments were assessed for their optical, hygroscopic and mechanical properties. The main observations and conclusions made for each treatment are summarised in Table 5.8 below.

As seen in Table 5.8, the properties of each solution can greatly differ from others. All, have shown to be, up to a certain point, beneficial in terms of consolidation to the canvas by providing a support through the formation of a superficial coating as in the case of the nanocellulose-only treatments (CNF, CCNF and CNC) or by impregnating the canvas as for the CNC nanocomposites treatments. The superficial coating formed by the nanocellulose-only treatments has shown, however, to increase the risk of failure of the support offered by the treatment to the canvas at low elongation (i.e. 2%). The colour change observed for the nanocellulose-treated canvases after ageing was also higher than for the CNC nanocomposite-treated canvases. Overall, however, the nanocellulose-only treatments also offer some advantage in terms of removability as the coating can be easily removed if retreatment is needed or failure of the coating occurs. The two types of consolidants presented here can thus offer a range of solutions for painting canvas consolidation. The evaluation conducted in this project enabled to

highlight the main characteristics of the treatment in terms of penetration, consolidation, colour change and response to RH variations leading thus the path for further improvements.

	Solution 1 Nanocellulosic treatments	**Solution 2** CNC nanocomposites
Visual appearance	- Formation of a coating layer on the surface of the canvas (treated side). - Morphologically compliant to the surface.	- High penetration of the treatment into the canvas (increased by brushing). - Treatment tightly wraps around cotton single fibres. - Formation of interfibrillars bridges between canvas fibres.
Consolidation	High (increase Young's modulus at low elongations (i.e. 1-2%)) Ruptures of the coating observed at higher elongations	High (increase Young's modulus)
Hygroscopic behaviour / mechanical response to RH variations	High for CNF and CCNF Low for CNC	High Lowered by addition of $CaCO_3$ (i.e. MC+CNC+$CaCO_3$ mixed solution)
Stability upon accelerated ageing	- High colour change (CNF) - Loss in stiffness but high consolidation is maintained (CNF) - Lower response to RH after ageing (CNF)	- High colour change (lower than CNF) - Loss in stiffness but high consolidation is maintained - Lower response to RH after ageing
Main advantages	- High stiffness - -Superficial coating (increased reversibility)	- High consolidation associated to high penetration reducing risks of rupture
Main disadvantages	-Superficial coating with high brittleness	-High penetration (lower reversibility)

Table 5.8: Summarize of the results of the assessment of two nanocellulose-based solutions proposed for canvas consolidation, i.e. nanocellulose and nanocellulose composites. The nanocellulose-only treatments (Solution 1) were applied by spray whereas the CNC nanocomposites (Solution 2) were applied by brushing.

6 Improvement of the adhesion and performance of a nanocellulose consolidant using polyamidoamine epichlorohydrin (PAAE) (published work (Bridarolli., 2018))

6.1 Introduction

As previously shown, the nanocellulosic treatments do not penetrate the canvas treated (cf. 5.3.1). They rather sit on top of the fabric and form what could be seen as a nano-sheet of cellulose nanofibrils or nano-lining. The surface deposition of these treatments has the advantage of facilitating their removal but it also increases the risks of mechanical failure of the treatment due to the brittleness of those nanocellulosic materials. This was highlighted by the ruptures measured for the samples and seen on the treatments coatings at low elongations.

To overcome these drawbacks, a study was conducted in which a cationic polymer polyamidoamine epichlorohydrin (PAAE) was applied prior to the application of the CNF dispersion. As for the tests conducted previously, the CNF treatment and PAAE were applied at a low weight added on canvas. This strategy is adapted by wet-end paper chemistry in which reactive water-soluble polymers are now used routinely to improve the mechanical properties of paper under wet conditions (Crisp, 2009). The cationic polymer PAAE is one of these commonly used polymers. It bears a protonated amine group that enables strong absorption on cellulose and an azetidinium group which covalently binds to the carboxyl groups present on the pulp fibres forming ester linkages (Espy, 1995; Obokata, 2007; Obokata, 2005). The resulting tensile strength of PAAE-treated paper re-wetted in water was considerably increased (Obokata, 2007; Obokata, 2005). This increase was attributed to intra and inter-fibre crosslinking as well as to an increased cellulose interfibres adhesion (Wang, 2012). These mechanisms have been thoroughly described for paper fibres, and here we hypothesize that they would apply also to woven cotton canvases.

The purpose of this case study is, therefore, to investigate if cationic polymer PAAE can be used together with CNF to enhanced the nanocellulose treatment adhesion, hence the

consolidation it has shown to provide (Chapter 3), whilst ensuring that the canvas is still able to adapt to changes in its environment (especially relative humidity RH).

6.2 Materials and methods

6.2.1 Materials

The same CNF dispersion as used in Chapters 4 and 5 was used (cf. 2.1.2.1). PAAE (polyamidoamine epichlorohydrin) was synthesized from the reaction of epichlorohydrin with polyamidoamine resin, which was formed by the reaction of diethylenetriamine and adipic acid (Figure 6.1). For this study, we used the commercially available PAAE Eka WS 505 (pH=4) from Akzo Nobel Pulp and Performance Chemicals AB (Gothenburg, Sweden) at 6%w/w in water. A more in depth study of this product is reported elsewhere (Siqueira, 2012).

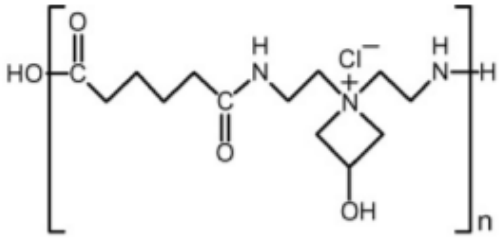

Figure 6.1: Chemical structure of polyamidoamine epichlorohydrin (PAAE)

6.2.2 Methods

6.2.2.1 Sample preparation

The use of a pre-coating of PAAE (polyamidoamine epichlorohydrin) before the application of the CNF consolidation was also tested. This is because PAAE is known to promote intra and interfibre crosslinking and adhesion between paper fibres (Wang, 2012). It was hypothesized that this would apply also to the woven degraded cotton canvas and the cellulose nanofibrils of CNF.

Both PAAE and CNF were applied by spraying on a degraded cotton canvas. For the application of the consolidants, both CNF and PAAE were applied to the surface of the degraded

canvas pieces (8 cm x 8 cm) by spraying. A Cotech Airbrush Compressor AS18B (Clas Ohlson AB, Sweden) at a pressure of 3 bar was used. PAAE (6%w/w) was initially sprayed on the degraded cotton canvas (1.3 g/m^2) which was then set to dry for 2 hours at ambient temperature. Following this step, a dispersion of CNF at 1%w/w in water was deposited via 2 spraying passes with 20 min interval, corresponding to 5.8 g.m^{-2} of deposited material. Scheme of the multi-layered canvas/PAAE/CNF system created is shown in Figure 6.2.

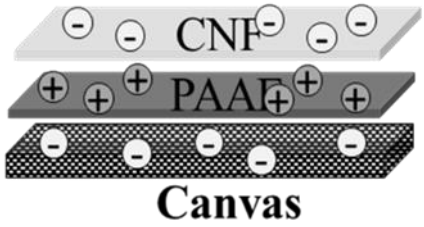

Figure 6.2: Scheme of the multi-layered structure of a treated sample with PAAE and CNF (1 application of PAAE, 2 applications of CNF). The treatments were applied by spraying and left to dry before application of the next layer.

6.2.2.2 Tensile testing

The tests were performed as described in 5.2.2.2. The samples were measured in the weft direction. Rectangular samples pieces were cut in order to get 4 threads in the weft direction and were typically 0.7 (thickness) x 4 (width) x 15 (length) mm in dimensions.

6.2.2.3 DMA-RH

The CNF, PAAE+CNF and PAAE-treated canvases of the second study (see 1.2.1.2.1) were measured in the weft direction. Rectangular samples pieces were cut in order to get 4 threads in the weft direction and were typically 0.7 (thickness) x 4 (width) x 15 (length) mm in dimensions.

The 20-60%RH RH program used for the CNF-, CCNF- and CNC-treated cotton canvases was also used for the PAAE and CNF-treated samples (cf. 5.2.2.3 in Chapter 5).

6.2.2.4 Atomic force microscopy (AFM) (adhesion measurements)

AFM is a tool which enables the measurement the topology of solid surfaces but can also be used to measure the local material properties such as elasticity, adhesion and surface charge densities (Binnig, 1987; Butt, 2005). The adhesion forces between the CNF particles and the PAAE were measured using a NanoWizard I AFM system (JPK Instruments, Berlin, Germany) mounted on an Olympus IX71 (Olympus, Tokyo, Japan) inverted microscope. Tipless NPO10 AFM cantilevers with a nominal spring constant of 0.24N/m were used. The probes were functionalized with a silica sphere (probe) of 10μm in diameter before being coated with PAAE (6%w/w) or CNF (1%w/w).

For the probe functionalization with PAAE, the probe was coated by dipping the silica sphere attached to the cantilever in a solution at 1%w/w in PAAE for a few seconds and then set it to dry in air at room conditions for 1h. For the CNF functionalization, the probe was dipped 3 times in an aqueous dispersion at 1%w/w in CNF for 1min. The freshly coated probe was set to dry for 1 min in air in between each dipping steps in order to increase the CNF adherence onto the silica sphere. The freshly coated beads were set to dry for 30 min prior to the measurement.

The functionalized probes were calibrated prior to AFM force measurements using a protocol described elsewhere (Strange, 2019). The deflection sensitivity (unit V/nm) of the functionalized probes was obtained by indenting a hard surface, in this case glass slide. The spring constant of the cantilever was obtained by non-contact thermal actuation.

The cotton fibre was fixed on a glass slide at both ends using parafilm in order to avoid contamination expected with the use of glues or solvents. The measurements were performed in contact mode in ultra-high quality (UHQ) water at room temperature. A loading force of 0.7N and a constant speed rate of 5μm/s were used. A scheme of the cantilever movement during a measurement is shown in Figure 6.3a. Force-distance curves were recorded on a minimum of 5 cotton fibres with no less than 7 locations measured for each fibre from which 300 force-curves were obtained.

The energy of adhesion was obtained by integrating the retraction curve using the JPK data processing software (JPK Instruments, Berlin, Germany) as shown in Figure 6.3b and Figure 6.3c.

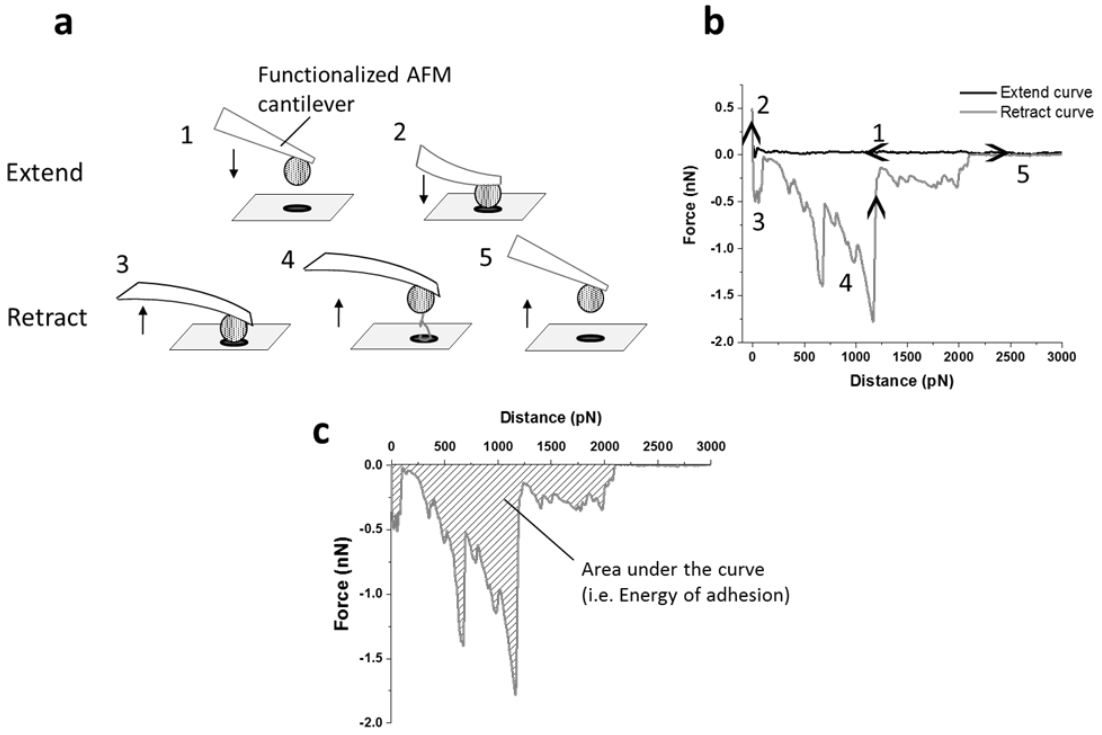

Figure 6.3: Principles behind the AFM adhesion measurements and data processing* (from Bridarolli, 2018)*: (a) scheme of the tip movement during a single approach-retract cycle of the AFM tip, (b) diagram of the resulting force-distance curve measured and (c) retract curve showing the area under the curve (shaded area) which was used to calculate the energy of adhesion.

6.3 Results

6.3.1 Penetration

The SEM images (Figure 6.4) show that for the CNF-treated sample, the treatment is visible as a thin coating deposited over the canvas surface threads. Some ruptures of the deposited CNF-film can also be seen between the threads for the CNF sample (arrows on Figure 6.4). At low magnification, it is possible to observe how the CNF layer used in conjunction with PAAE presents a similar distribution and surface deposition onto the canvas to that of the CNF-only

treated sample. However, the surface coverage of the CNF coating of these two samples slightly differs when observed at higher magnification. Several ruptures of the CNF film or its delamination from the cotton fibres can be observed in smaller number for the PAAE+CNF the anchor the CNF fibrils onto the canvas fibres. From the SEM images of the PAAE-only treated sample, the resin is not clearly seen on the surface of the fibres. As shown previously (Andreasson, 2005), this could result from the absorption of the resin by the canvas fibres. Finally, few interfibres bridges could be observed at high magnification for the PAAE-only treated sample. It is believed that these would possibly promote the formation of interfibres/threads CNF bridges observed in both cases and preserve them from ruptures.

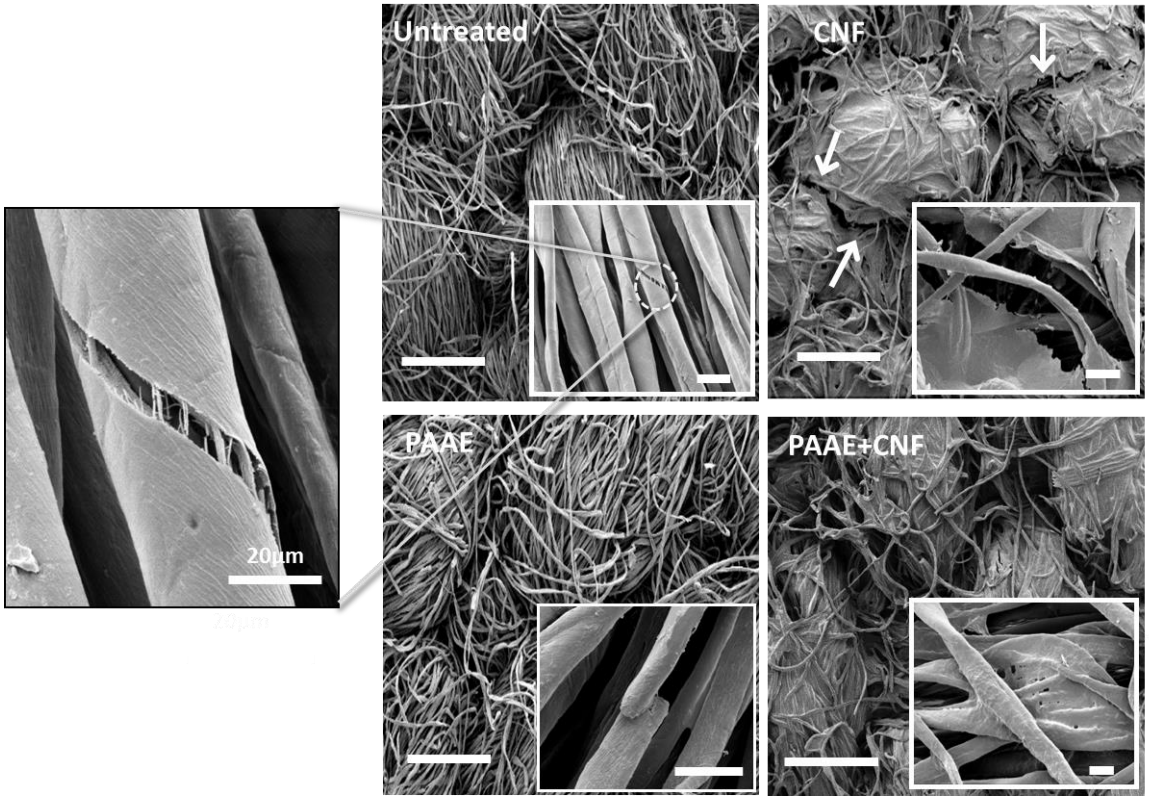

Figure 6.4: SEM images showing the deposition of the treatment onto the surface (scale bar of 500 µm) and the fibres (scale of 20 µm) of the canvas. On the left, detail of an untreated fibre shows rupture of the fibre resulting from ageing.

By applying a larger amount of CNF over the PAAE layer (i.e. 8 applications of CNF corresponding to 26 g/m^2), the treatment behaves like a surface coating (see Appendix, Figure D.1). The improvement provided by the PAAE layer seems to be lost by an excessive accumulation of CNF layers and presents a similar surface appearance to that of the 8CNF-only treated sample (see Appendix, Figure D.2).

6.3.2 Adhesion of CNF on cotton fibres improved by polyamidoamine-epichlorohydrin (PAAE)

The improved deposition of nanocellulose onto the canvas promoted by PAAE was further characterised by measuring the adhesion forces developed between the treatments (PAAE and CNF) and the canvas fibres. In painting conservation, macro-peeling tests are most commonly used to assess the adhesive performance of the lining adhesive. For our system, this test presents some limitations such as the small thickness of the PAAE-nanocellulose layer (~4 µm), which makes peeling from the surface difficult. The use of AFM with a functionalized probe (coated with CNF or PAAE) (Figure 6.5) is a way to overcome this problem while at the same time enabling quantification of the forces applied at the nanoscale.

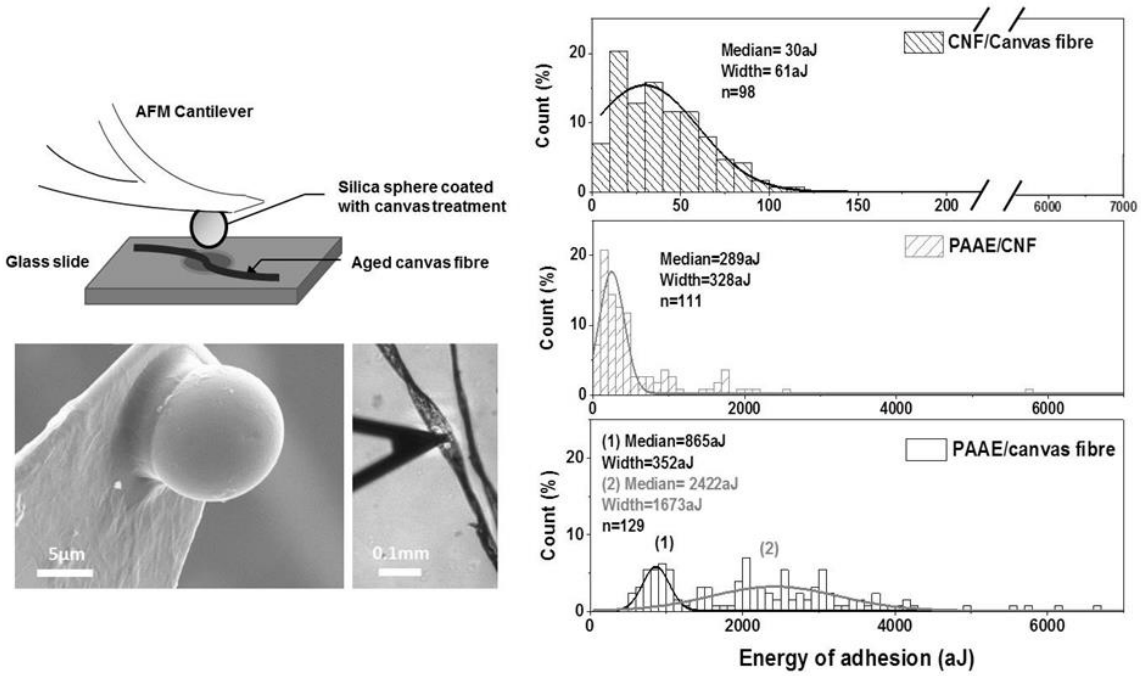

Figure 6.5: On the left, the setup designed for the quantification of the forces developed between the tested treatments and the canvas fibre using AFM (a) with the SEM image of the bead-functionalised cantilever (b) and a microscopic image showing the cantilever on a cotton fibre during a measurement.

Interface tested	*CNF/Canvas fibre*	*PAAE/CNF*	*PAAE/canvas fibre*
Distribution type	Unimodal	Unimodal	Bimodal
Energy of adhesion (mean ± width) (aJ)	30±61	289 ± 328	(1) 865 ± 352 (2) 2422 ± 1673

Table 6.1: Type and characteristic (mean and width) of the distribution of the energies of adhesion measured between the CNF/Canvas fibre, PAAE/CNF and PAAE/canvas fibre interfaces.

On the right, distribution of the energy of adhesion calculated between (from top to bottom): CNF and a degraded canvas fibre as well as between PAAE and CNF and PAAE and a degraded canvas fibre. The numbers in between parentheses correspond to the fitting curves used to determine the energy of adhesion of the corresponding regimes.

The adhesion energy was measured for the different systems in UHQ water in order to replicate the conditions of application of the treatments (all water-based). The results (Figure 6.5) firstly show that the adhesion energies measured between PAAE and CNF and between PAAE and canvas fibre are both higher than that measured between CNF and canvas fibre. As such, for the PAAE/CNF and the PAAE/canvas fibre systems, the medians of the distributions (unimodal and bimodal respectively) were calculated to be E_{adh}(PAAE/CNF)=289±328 aJ, and E^1_{adh}(PAAE/canvas)=865±352 aJ and E^2_{adh}(PAAE/canvas)=2422±1673 aJ, respectively (Table 6.1). Between CNF and canvas fibre, the adhesion energies remain below 150 aJ with a median at E_{adh}(CNF/canvas)=30±61 aJ. The adhesion energies measured when PAAE is introduced as a coupling agent are increased by one order of magnitude or more. These results suggest that the cationic sites of PAAE interact with the carboxylate groups present on the aged and degraded cellulose chains and the nanocellulose fibrils (Wågberg, 1993). This considerable increase in adhesion confirms that the use of PAAE promotes an enhanced adhesion of CNF onto the canvas, supporting the PAAE/CNF application approach for canvas consolidation.

This increase in adhesion probably result from the presence of carboxylic groups on the surface of the degraded cotton fibres. Indeed, as previously seen in Chapter 3 (cf. 3.4.3.2.2), XPS measurements previously performed on a cotton canvas before and after degradation have shown that after degradation, the cotton canvas presented an increase number of carboxylic groups on its surface 3.4.3.2.2 in Chapter 3). PAAE bears a protonated amine group that enables strong absorption on cellulose and an azetidinium group which covalently binds to carboxyl groups present on the pulp fibres and can form ester linkages (Espy, 1995; Obokata, 2007; Obokata, 2005). High adhesion between PAAE and the degraded cotton canvas was thus expected. Moreover, the degradation of the cotton canvas also leads to the removal of surface impurities which enable the obtention of a purer cellulosic surface but also present in an altered state resulting from degradation with the presence of carboxyl groups which promote interaction with PAAE.

From these measurements, one can also conclude that CNF does not attach strongly to the canvas fibre as seen by the low values in adhesion in Table 6.1. It has been previously stated that the high number of hydroxyl groups on the surface of the nanocellulose particles favours the formation of hydrogen bonding with other polymeric materials (Gardner, 2008). However, since the adhesion measurements need to be performed in a buffer environment (i.e. UHQ water), there is a competition taking place between the hydroxyl groups on the CNF surface and water for hydrogen bonding with the hydroxyl groups on the cellulose fibre. Hydrogen bonding between fibre surface hydroxyl groups and water will take over which explains the low adhesion energies measured between CNF and the canvas fibres.

Taking into consideration the shape of the energy distributions (Figure 6.5), one can observe both unimodal and bimodal behaviour for the PAAE/CNF and the PAAE/canvas systems, respectively. For the PAAE/CNF system, more than half the measurements give energies of adhesion below 500 aJ (Table 6.1). The bimodal distribution for the PAAE/canvas fibre system is also much wider. For this system, the values of adhesion energy span the range 610 to 3600 aJ. The question arises whether this wider distribution could result from differences in the state of the degradation across fibres, and/or from the chemical inhomogeneity of the fibres surface and inherent twisted morphology of cotton fibres. Up to now, no correlation could be made between the area morphology of the fibre or its state of degradation and the energy of adhesion.

6.3.3 Consolidation

In terms of mechanical reinforcement, the consolidation provided by the treatment with CNF was also improved by the use of PAAE. Paintings are usually restretched in the extension range up to 1-2 % (M. F. Mecklenburg, 1982b). In this range, the stiffening of the multi-layered PAAE+CNF sample was shown by an increase in Young's modulus, from 1.9±0.7 MPa to 9.2±3.3 MPa measured before and after application (see Figure 6.6, Table 6.2). An increase in stiffness was also measured for the CNF- and PAAE- treated samples for which Young's moduli of 2.8±0.1 and 6.8±0.5 MPa were measured, respectively. For the PAAE-only treated sample, the strong reinforcement measured could result from the inter cross-linking of cellulose by the formation of

resin-fibre chemical bonds, and the intra or self-crosslinking occurring in PAAE when drying (Espy, 1995; Siqueira, 2012). The fact that the reinforcement is weaker for the CNF-only treatment is due to the weaker hydrogen bonds that have formed upon drying of the CNF treatment. The Young's moduli values measured for these samples are, however, lower than the 9.2±3.3 MPa obtained when the treatments were combined. The greater reinforcement reached with the introduction of PAAE is probably related to its function as coupling agent between CNF and the cellulosic fibre.

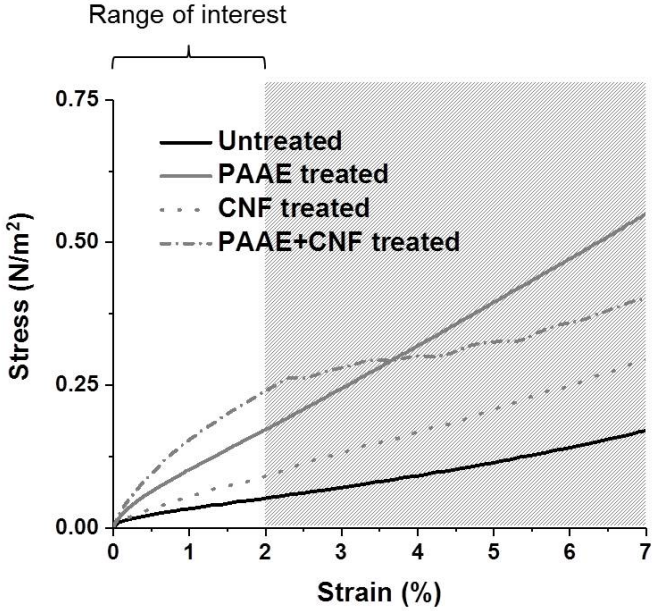

Figure 6.6: Tensile curves at 20%RH for untreated and treated samples showing the higher stiffness of the PAAE+CNF sample in the range of interest (i.e. strain at which paintings are usually re-stretched).

Sample	Young's modulus (MPa)
Untreated canvas	1.9 ± 0.7
PAAE treated canvas	6.8 ± 0.5
CNF treated canvas	2.8 ± 0.1
PAAE+CNF treated canvas	9.2 ± 3.3

Table 6.2: Young's moduli at 20%RH (calculated from the stress-strain tensile curves) for untreated and treated samples

A non-linear behaviour of the stress-strain curve for the PAAE-CNF treated sample is, however, seen in Figure 6.6 above 2% of extension. After 2.5% in elongation, the tension measured for this sample is stabilized around 0.29 N/m2 and becomes lower than the one measured for the PAAE-treated sample after 3.8% elongation. This behaviour has been already observed before in 5.3.2 (see Figure 5.5) for samples treated with a higher amount of CNF only (Nechyporchuk, 2018). The irregular slope can be attributed to localized ruptures of the CNF layer sitting on the top canvas fibrils. SEM images, which were taken of the canvas after tensile testing, support this assumption (Figure 6.7). The absence of similar drops in tension for the CNF-only treated sample could result from the low amount of CNF applied in this study. As seen in Figure 6.4, the CNF coating on the CNF-treated canvas already presents before testing some ruptures and delamination seen on its surface. The low amount of CNF deposited for 2 applications does not enable the formation of a continuous and strong enough layer which would partly hold the tension applied to the canvas during handling. Thus, reinforcement seems only provided to the canvas when the adhesion between the nanocellulose and the canvas is improved (case of PAAE+CNF) or when a higher amount of CNF is applied (as seen in 1.3.1.1.2). It should, however, be noted that the reinforcement in the case of the PAAE+CNF sample is limited to the low elongation values. These values remain in the range identified by conservators as appropriate for canvas re-tensioning. However, if the tension applied during re-tensioning should exceed 2%

extension, the brittleness of the CNF coating should always be considered as a possible limitation of this treatment.

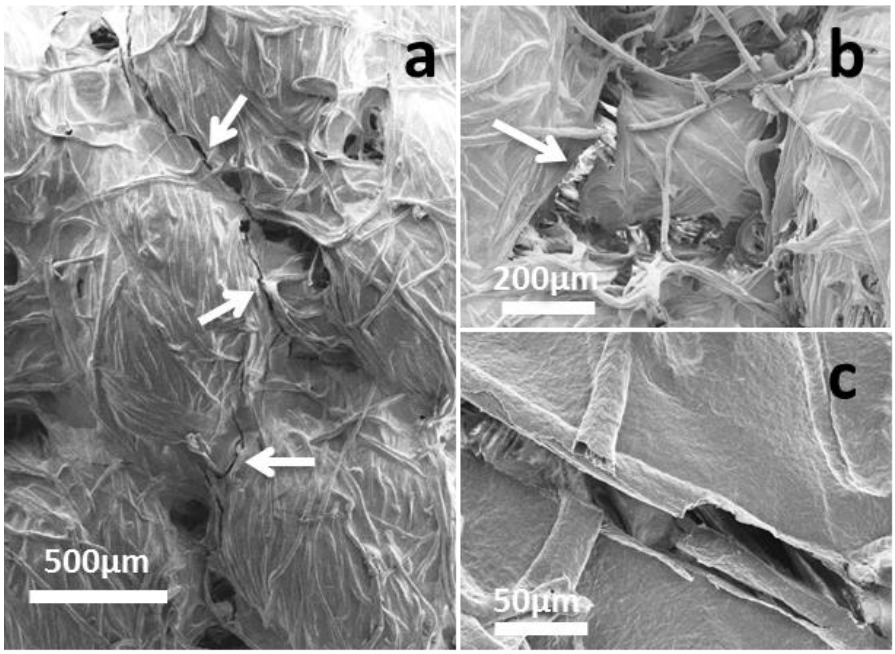

Figure 6.7: SEM images of a PAAE+CNF treated canvas after tensile test measurement showing zones of rupture of the superficial CNF film (a) in particular ruptures in the inter-threads spaces (b) and along the canvas fibres (c).

6.3.4 Response to moisture

When considering novel treatments, it is essential to ensure that the introduction of new materials does not modify the natural response of the canvas under variable environmental conditions. Figure 6.8 shows the mechanical response fingerprint of untreated cotton canvas subjected to relative humidity fluctuations. The DMA-RH response curve indicates that the canvas tends to stiffen at a lower humidity level (higher storage modulus *E'*) while becoming more viscoelastic at higher humidity levels (lower *E'*). This behaviour is directly related to the canvas material (i.e. cotton) as well as to the weave. To explore this in more detail, quantification of the mechanical stress experienced by the samples was firstly done by calculating the difference between storage moduli (*E'*) at 60 % RH and at 20 % RH (end plateau values as described in Figure 6.9).

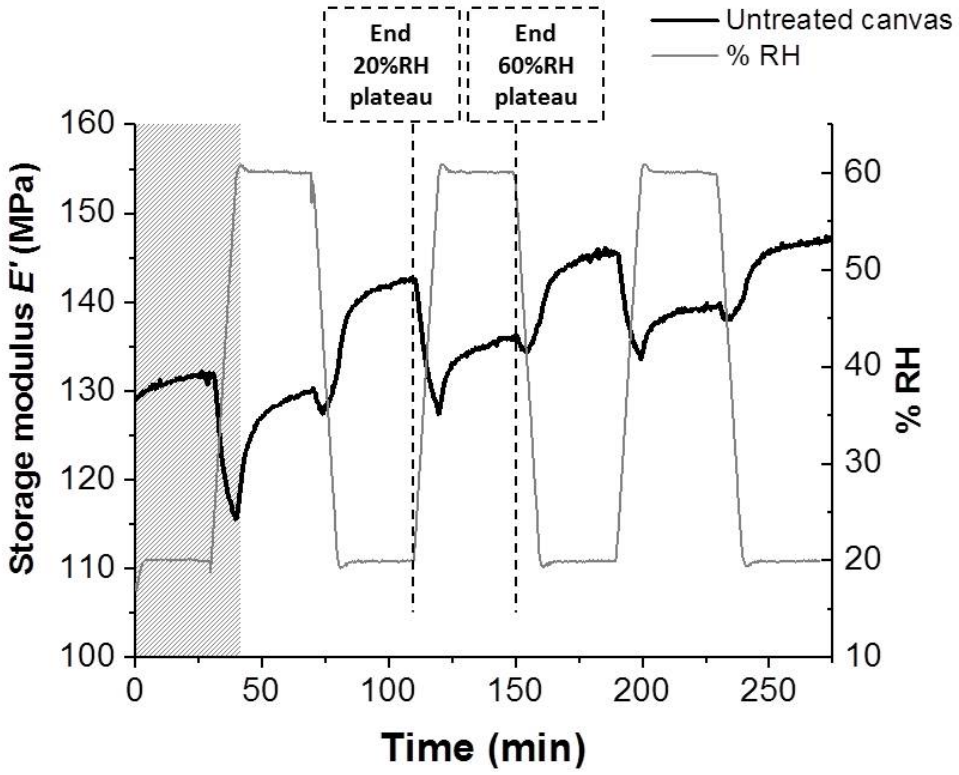

Figure 6.8: Mechanical response (E') of the untreated degraded cotton canvas (cf. 2.1.1.2) to RH-cycling (20-60-20%RH) over time. Correlation between %RH variations and E' measured are seen and highlighted by the dotted lines placed at the end of the 20 and 60%RH plateaus (2nd RH cycle).

The results are given for the 3 cycles. Using this approach, one obtains the response by the samples and the treatments to moisture and the impact on their resulting mechanical behaviour. As seen in Figure 6.9, for all the samples the difference between *E'*(60 % RH) and *E'*(20 % RH) decreases with time. For sample PAAE+CNF, the difference in *E'* goes from 16.5 to 13.1 MPa from the 1st to the 3rd cycle. This decrease might relate to the structural stabilisation of the fabric upon moisture sorption and desorption which could arise from the hysteresis in moisture sorption/desorption previously shown for the degraded cotton canvas (cf. Figure 3.11 in Chapter 3). Diffusion of moisture in fabrics is known to follow a few different paths inducing changes in the size of the cellulose fibres. Fibres swell during moisture sorption but because they are not completely elastic there is incomplete recovery after desorption. A hysteresis between sorption and desorption thus arises (Siroka, 2008). Because the response measured for the degraded cotton canvas (also similar for all natural fibres (Hill, 2009) is characterised by a faster

response to moisture sorption and lower response to desorption this could explain the observation that upon the application of various RH cycles, the canvas will slowly reach a more humidified state. The fast dehumidification steps and short times of equilibration at low RH level (20%RH) does not give enough time to the fabric to release the water absorbed at high RH. Differences in percentage water uptake between the low and high RH levels thus decrease as the sample reach its equilibrium moisture content at each RH levels.

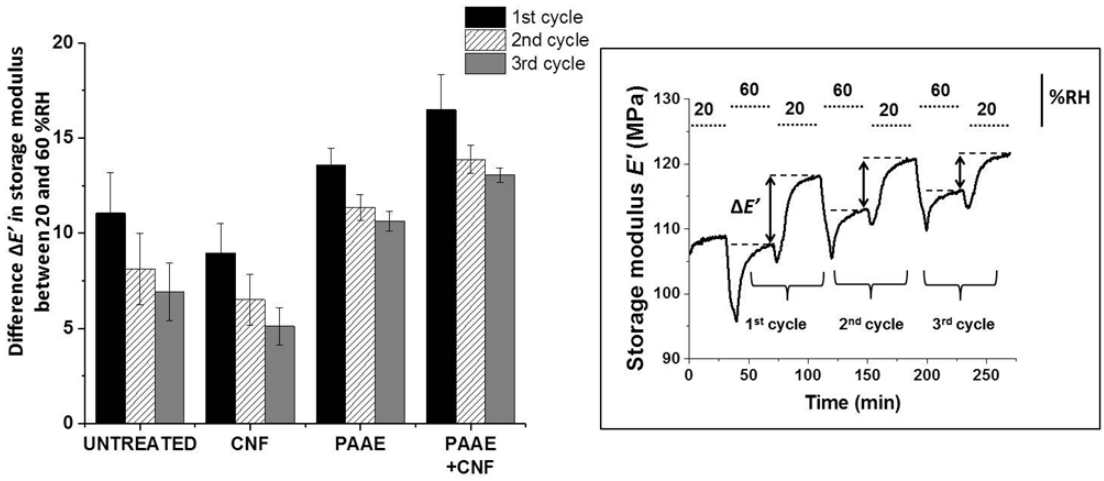

Figure 6.9: On the left, difference ΔE' calculated between storage moduli (E') measured at the end of the 60%RH and 20%RH plateaus for each of the 3 RH cycles. The results are shown for a degraded cotton canvas untreated and treated with CNF, PAAE and PAAE+CNF. On the right, details of a DMA-RH curve showing where the ΔE' were measured.

As seen in Figure 6.9, the use of PAAE tends to increase the canvas response to moisture. For the 3rd cycle, the difference in *E'* calculated for the PAAE- and PAAE+CNF-treated samples reached 10.6±0.5 and 13.1±0.4 MPa, respectively. That is almost twice as much as the values obtained (again for the 3rd cycle) for the untreated and the CNF-treated samples, which gave values of 6.9±1.5 and 5.1±1.0 MPa, respectively. Upon adding PAAE as an intermediate layer, the mechanical response of the fabric to moisture is amplified leading to the higher variations in *E'* observed across the RH cycles. However, it has been shown that the mechanism behind the wet-strength properties of PAAE in paper results from cross-linking of the resin upon drying which then offers a protective network of cross-linked molecules for the fibre-fibre contacts

(Lindström, 2005). PAAE has also shown to efficiently limit the loss in strength of paper under wet conditions by increasing the ratio wet/dry strength from 10% without PAAE to 33% for 10mg/g PAAE per gram of paper pulp (Su, 2012). Even if these mechanisms apply well to paper, they do not seem to apply here for fabrics. This different behaviour could presumably result from the method of application used (i.e. spraying) or by the limited amount used. The limited penetration of the PAAE into the fibres is also plausible as it is known that penetration can be limited by the composition, structure (pores) of the fibres (Andreasson, 2005). Higher mechanical stability was instead observed for the CNF-only treated sample. The difference in storage modulus (E') measured for this sample is similar to that for the untreated sample and confirms already published work where the CNF treatment had been applied at a higher amount (i.e. 7.2% weight uptake after coating instead of 5.8% here) by blade-coating (Nechyporchuk, 2018).

6.4 Conclusions

With these results, we show that the application of PAAE as an intermediate layer promotes adhesion of the CNF particles onto the canvas fibres by improving their morphological, chemical and mechanical coupling with the canvas fibres. The improvement can be attributed by nanomechanical analysis to the stronger adhesion taking place both between CNF and PAAE and between canvas fibres and PAAE. The combination of the good mechanical properties of CNF and the strong adhesion promoting the effect of PAAE makes this multi-layered treatment an efficient reinforcement procedure despite the low weight of CNF added. These results confirm the potential of PAAE as an anchor on the canvas for the nanocellulose fibrils. In this work, we have also demonstrated that a severe shortcoming of the use of PAAE for painting conservation is the high mechanical response to moisture that such treatments give rise to. It is, however, yet to be investigated in future work whether the stresses measured will lead to damage to the painting or reduce the stresses already present in the painting materials (Young, 2001).

This study also demonstrates the important role of adhesion in the development of new nanocellulose treatments for painting conservation. These results suggest that the mechanical performance of nanocellulose as reinforcement material can be greatly improved by combining them with additives that will promote their adhesion onto fabrics. Chemical functionalization of nanocellulose might offer an alternative route to the introduction of non-cellulosic additives (Cheng, 2016; Hubbe, 2015)(D. Cheng et al., 2016; Hubbe M., Rojas O.J., 2015) which could also be explored in future work. In the frame of the application of nanocellulose-based treatments in conservation, it is expected that compromises between good coupling and reversibility will have to be made.

7 Assessment of the newly nanocellulose-based consolidants on historical lining canvas and real paintings: from a conservator's to a scientist's perspective

7.1 Introduction

In the previous chapter, the performance of different consolidants was evaluated on a cotton canvas mock-up made to mimic a degraded canvas which would need consolidation. A better understanding of the impact of the nanocellulose-based treatment in terms of mechanical, physical, in particular response to moisture, and chemical stability could be derived from the tests. The assessment of the newly developed treatments, however, lacked in-situ evaluation, and applicability on real objects using criteria established alongside painting conservators.

The study of the treatments was thus translated across from a lab well-equipped for material studies to the workshop of a painting conservator, from a material scientist approach (more quantitative) to a conservator's practical approach (more qualitative); from degraded canvas mock-ups to more complex historical linen an cotton canvases and paintings. This application of the assessment of the consolidants to the context of conservation allow for reconsideration of the evaluations previously carried out. It also makes it possible to consider the work and skills of professional painting conservators and to explore the benefits of a more application-centric approach.

Overall, this study aims at providing with a more accurate evaluation of the real impact of the treatments, highlighting the pitfalls and advantages of the different solutions, in the frame of real paintings and current conservation practices. For this, 2 objectives were set:

- Evaluation of the 3 categories of nanocellulose-based consolidants using techniques commonly used, available or suited to a conservation studio environment as well as the empirical knowledge of trained and experienced painting conservators.

- Quantification of the improvements achieved on historical canvases in terms of visual, physical and mechanical properties.

The criteria selected for the assessment resemble those listed previously in Chapter 4 and 5. The treatments were assessed upon their handling properties, the visual appearance after treatment, the penetration through canvas and/or paint layer and the mechanical reinforcement achieved. Following this study, additional quantitative mechanical tests using DMA were performed on a selection of nanocellulose-based treatments using a historical linen canvas. This last experiment aims to confirm the effective consolidation provided by the treatments on real, more complex, objects (i.e. historical canvases and paintings).

The results of this study will help to list the main advantages and disadvantages of each consolidant when used by conservators on real objects. This list will supplement the outcomes of the quantitative measurements performed on mock-ups of a degraded cotton canvas presented in Chapter 5. The final outcome will then be the validation of the most suitable consolidant for paintings canvas consolidation.

7.2 Materials and methods

Different consolidants developed in the frame of the Nanorestart project were tested on historical linen canvases and paintings dating from the 19th to the 20th century. The results obtained for some selected treatments tested in previous chapters are reported here, as well as new solutions, not yet tested on the degraded cotton canvas. An empirical qualitative approach was first used to compare the treatments from a conservator point of view. The assessment was performed in collaboration with Dr. Aurelia Chevalier, a private painting conservation (Atelier Aurelia Chevalier, Paris, France). Additionally, the opinion of Anna Lucchini, another painting conservator from Italy present at the Nanorestart meeting in Paris, are included in this report.

7.2.1 Materials

The materials, historical paintings and canvases, mock-ups of paintings belong to the painting conservator Aurelia Chevalier. They were carefully selected with her for being

representative of the variety of paintings that could be received in as conservation studio for structural conservation (i.e. acrylics or oil paintings, cotton and linen canvases, 19th and 20th century). Because these canvases were historically used on paintings (as lining or as support for a painting), the presence of size, priming as well as traces of oil or dust on the canvases add another layer of complexity to the study of the consolidants. These samples are also more representative of the types of substrates on which the consolidants could be used.

7.2.1.1 Canvas

Canvases which used to be lining canvases (i.e. canvas glued to the original canvas of a painting) were tested. They had been removed in the past by the painting conservator Aurelia Chevalier from the back of different easel paintings which were undergoing conservation work. The 3 canvases tested are made of linen and present traces of the lining glue (not identified, probably animal glue) originally used for the lining work. The canvases differ by their weaving density. They are listed in Table 7.1.

Name of the historical lining canvas	*Weaving density*	*DP*	*Age*	*Density warp (threads/cm)*	*Density weft (threads/cm)*
Canvas high-density weaving n°1	High	1300	19th century	20	23
Canvas high-density weaving n°2	High	N/A	19th century	18	14
Canvas low-density weaving	Low	N/A	19th century	11*	14*

* For the canvas low-density weaving, the weft and warp direction could not be identified. The values given here cannot be associated with certainty to either warp nor weft.

Table 7.1: List of historical linen canvases (originally lining canvases) used for the comparative assessment of the nanocellulose-based treatments. Description of their weaving density, DP and age is given. All the canvases presented a plain weave pattern.

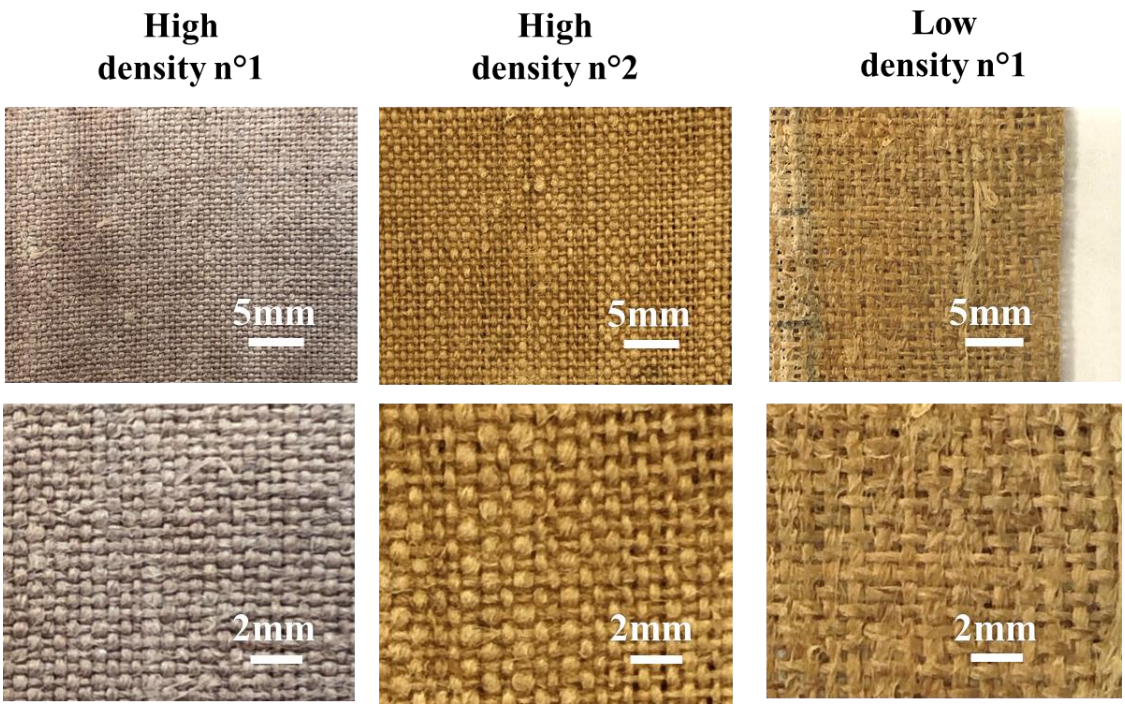

Figure 7.1: Pictures and details of threads dimensions of the 3 linen lining canvases showing high (a,b) and low weaving densities (c).

7.2.1.2 Paintings

Four paintings among which 2 acrylic- and 2 oil-based paintings were tested (Figure 7.2). They had been bought on the internet by Dr. Aurelia Chevalier. They are not of high artistic or historical value which make of them suitable items to be used for research purposes. They are also representative of a range of canvas types, nature of the paint, type periods. Information about the 4 paintings which were available from Aurelia Chevalier who gave them are listed in Table 7.2.

Figure 7.2: Pictures of the 4 paintings (linen or cotton canvas, acrylic or oil paint) tested including "The musician"(A), "Angels"(B), "Portrait of a woman"(C), "African women" (D).

Name	*Canvas material*	*Paint/preparation type*	*Date*	*Painter*	*Image*
The musician	linen	oil painting	19th century	Unknown	A
Angels	cotton	acrylic	20th century	Unknown	B
Portrait of a woman	linen	oil painting	19th century	Denise Mazet	C
African women	cotton	acrylic	20th century	Unknown	D

Table 7.2: Information available for the 4 historical paintings

The name of the painters of these artworks remain unknown, except for *Portrait of a woman* which bears the name of the painter and the titles were given in order to simplify their identification in this study.

7.2.1.3 Other painting samples and mock-ups for analysis on treatment penetration

The assessment of the treatment penetration was carried out using a historical lining canvas covered with lead white (Figure 7.3) and mock-ups of a painting (Figure 7.4). The historical lining canvas in Figure 7.3 consists in a linen canvas which has been removed from a 19th easel painting by the painting conservator Aurélia Chevalier. One side of the canvas has a thin red earth paint layer covered with a thick layer (>1mm) of white lead in oil. This stratigraphy is representative of the one encountered in 19th-century easel paintings (Chevalier, 2008) .

Figure 7.3: Lead-white treated original canvas (lead-white side(C top), canvas side(C, bottom)) for the assessment of treatment/solvent penetration.

The mock-ups consist of painted and varnished square canvas samples (10cmx10cm) prepared and provided by A. Chevalier (Figure 7.4). These samples are reproductions of the simplified stratigraphy of an oil painting characterised by a sized linen canvas with a ground layer and a red paint layer. The red paint was made at 80%w/w of red earth pigments (cadmium red)

bought at CTS France mixed with rabbit skin glue in water. Part of the painted surface was then varnished using a dammar varnish at 10% in ligroin (i.e. petroleum ether).

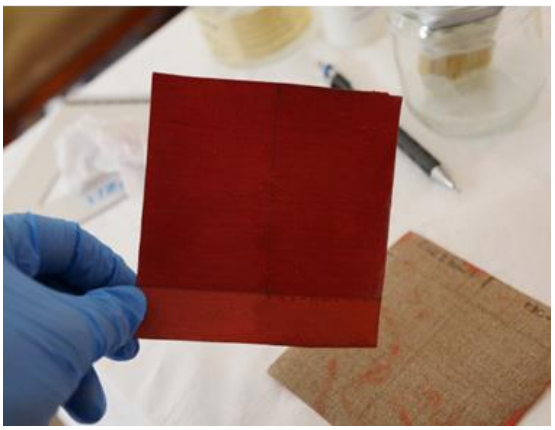

Figure 7.4: Mock-ups of a water-sensitive painting. These samples consist in a linen canvas painted with red earth pigments sensitive to water (swelling).

7.2.1.4 Treatments

Treatments belonging to the three categories of products previously mentioned in Chapter 5 were tested in this part of the study (cf. 5.2.1 in Chapter 5):

- Pure nanocellulose treatments
- Nanocellulose composites
- Nanocellulose/silica hybrid materials

The pure nanocellulose treatments consist of the CNF, CCNF and CNC dispersions already used in chapter 4 and 5. Non-surface-modified cellulose nanofibrils (CNF) in the form of aqueous suspension were provided by Stora Enso AB (Sweden). Cellulose nanocrystals (CNC) in powder form were purchased from CelluForce (Canada).

The nanocellulose composites treatments tested consisted of mixtures of methylcellulose (MC) and nanocrystalline cellulose (CNC) in water or heptane. The combination of these mixtures with deacidification such as $CaCO_3$ and MgO in water and heptane respectively was also tested. The deacidification solution of MgO (in heptane) was also tested alone.

Two types of nanocellulose/silica hybrid materials were used in this study (cf. 2.1.2.3 in Chapter 2). The first one was synthesised by Chalmers University and was already previously tested on cotton canvases (see Chapter 4). It consists of polyelectrolyte-treated silica nanoparticles (referred to here as Sil/PEI/CMC). A detailed description of the preparation of Sil/PEI/CMC can be found elsewhere (Kolman, 2019; Kolman, 2018). The second type was synthesized and provided by CSGI in Florence, Italy. It is similar in its architecture to the SIL/PEI/CMC particles but replaces the silica core with a $CaCO_3$. The dispersion is made of $CaCO_3$ nanoparticles coated with polyelectrolyte multilayers (PEMs), which consisted of the cationic polymer poly(ethylenimine) (PEI) and the anionic polymer (carboxymethyl)cellulose (CMC). They will be called $CaCO_3$/PEI/CMC. Dispersions at 1%wt in water and 1%wt in water:ethanol (50:50) of Sil/PEI/CMC and $CaCO_3$/PEI/CMC, respectively, were tested separately ($CaCO_3$/PEI, $CaCO_3$/PEI/CMC and $CaCO_3$ only) or mixed together (Sil/PEI/CMC +$CaCO_3$/PEI/CMC).

Pure nanocellulose treatments	**Nanocellulose composites**	**Nanocellulose/silica hybrid materials**
CNF at 0.75%wt (in water)	**MC+CNC** at 1.98%wt (in water)	**$CaCO_3$/PEI (+)** (in water:ethanol(50:50))
CCNF at 1%wt (in water)	**MC+CNC+$CaCO_3$** at 1.98%wt (in water)	**$CaCO_3$/PEI/CMC (-)** (in water:ethanol (50:50))
CNC at 3%w/w (in water:ethanol, 50:50)	**MC+CNC** at 1.98%wt (in heptane)	**$CaCO_3$** (in water:ethanol (50:50))
	MC+CNC+MgO at 1.98%wt (in heptane)	**Sil/PEI/CMC** at 1%wt + **$CaCO_3$/PEI/CMC** (in water:ethanol(50:50))
	MgO (in heptane)	

Table 7.3: List of the 3 different types of treatments tested. The (+) and (-) signes refer to the charge borne by the particles.

Treatments	On lining canvases and painting <u>for conservator's assessment</u>	On lining canvas <u>for mechanical testing</u>
CNF	**Y**	**Y**
CCNF	**Y**	**Y**
CNC	N/A	**Y**
MC+CNC (w)	**Y**	N/A
MC+CNC+$CaCO_3$ (w)	**Y**	**Y**
MC+CNC (h)	**Y**	N/A
MC+CNC+MgO (h)	**Y**	**Y**
MgO (h)	**Y**	N/A
Sil/PEI/CMC	N/A	**Y** (in combination with $CaCO_3$/PEI/CMC) At 1%w/w of $CaCO_3$/PEI/CMC:Sil/PEI/CMC (1:1)
$CaCO_3$/PEI	**Y** (2%wt)	N/A
$CaCO_3$/PEI/CMC	**Y** (2%wt)	**Y** (in combination with $CaCO_3$/PEI/CMC) At 1%w/w of $CaCO_3$/PEI/CMC:Sil/PEI/CMC (1:1)
$CaCO_3$ nanoparticles	**Y** (2%wt)	N/A

Table 7.4: Tests performed for each treatment ('Y'=Yes, 'N/A'=no test). Some treatments could not be tested during the workshop during which historical paintings were treated. From the treatments tested during the workshop, the most relevant ones and those which seem the most suitable in terms of final visual appearance of the treated canvas and handling properties were selected for further mechanical assessment.

7.2.2 Methods

7.2.2.1 Treatment application on historical canvases and paintings

Samples for qualitative assessment (conservator's point of view)

For the qualitative assessment of the treatments, the approach taken was conducted and designed in collaboration with painting conservators whose expertise and experience were beneficial for this project.

Prior to the treatment application, the canvases were washed following a procedure commonly used by conservators only after first being stretched on a wooden frame to avoid any shrinkage upon washing and drying. This washing step aimed to remove the layer of aged lining glue remaining on the canvas (inner side which used to be in contact with the painting canvas from which it was removed). The exposed face of the canvas (the external or visible side when

on the painting) was washed to remove traces of dirt. The canvas was brushed gently in order not to damage the canvas threads and fibres. The glue present on the other side was removed carefully using a scalpel. This removal was essential to avoid the inhomogeneous dispersion of the treatment, variabilities between areas of the same canvas which could have led to inaccuracies in the assessments. The washed canvas was then left to dry at room temperature.

The face without glue (or exposed face) was always selected for the application of the consolidation treatments as it was considered as more representative of the type of surface encountered in future real cases.

The treatments were applied on the dry canvas by brushing. The amount of treatment applied was controlled in order to reached for each treated area and each treatment, the same coverage (same amount of dry treatment per unit area) around 9g/m^2 (i.e. 2% to 4% added weight). The brushing was carried out along both the warp and weft directions, alternatively, to allow good penetration and homogeneous repartition of the treatments. The treatment application was done in several steps in order to avoid saturating the canvas with solvent (i.e. before complete wetting of the canvas). The number of steps varies according to the treatment viscosity, concentration and solvent (see Table E.1 in Appendix 5.1).

Samples for additional quantitative mechanical testing

The linen canvas dense weaving n°1 was also used for further mechanical assessment. The canvas was cut in pieces of 15 mm x 7 mm. They were clamped before the treatment application on a weighing boat cut into a frame. This was done in order to avoid shrinkage of the sample which could have led to change in the mechanical properties measured or rupture of the dried treatment layer when putting the sample back to horizontal for measurement. The same amount of treatment, resulting in a coverage of 9 g/m^2 (i.e. 2% to 4% added weight), was applied on each clamped canvas sample and spread using a spatula. Further details on the preparation of the samples will be given later in 7.2.2.3.

7.2.2.2 Qualitative assessment

The assessment of the treatments was carried out following qualitative approach that could be used in a painting conservator workshop. The criteria used for the assessment were selected and the tests elaborated in collaboration with the painting conservator, Dr. Aurélia Chevalier.

7.2.2.2.1 Handling properties

Observations made on the applicability and handling properties of the treatments are based on the experience gathered by the painting conservators Aurelia Chevalier and Anna Lucchini during the application of the treatments on historical paintings.

7.2.2.2.2 Surface appearance

Visual and physical assessments (texture to the touch) of the treated surface were performed. The assessment particularly focused on colour changes that could result from the application of the treatments (undesirable effect) and modification of the canvas visual appearance. The back of a painting often has important information (such as old stamps, signatures or writing) which can be considered as valuable as the front painted surface. Masking this information could be detrimental to the painting by lowering its cultural value, by masking important historical informations and "could also led to an important drop in the financial value of the object"[8].

7.2.2.2.3 Water sensitivity, solvent penetration

Canvas mock-ups painted using a red paint made or earth pigments and rabbit skin glue highly sensitive to water as well as lining canvas presenting a white-lead layer were tested.

For the red painted samples, one droplet of treatment was deposited on the surface of the canvas side (i.e. unpainted side). The samples were also treated by brushing. For the lead-white treated samples, the treatment was applied by brushing as in a real case scenario on the canvas

[8] Private discussion with Dr. Aurélia Chevalier who has experience working with museums as well as private collections.

side (i.e. until saturation, good penetration and homogeneous distribution of the treatment are achieved). In both cases, the assessment was carried out by observing the migration of the solvent from treated canvas side to the paint layer of the painting sample (cf. red paint or lead white paint in 7.2.1.3). Buckling of the sample or wetting of the paint layer resulting from the treatment application were reported. High penetration of the treatment could be detrimental to the paint layers and be, therefore, undesirable.

7.2.2.3 Quantitative assessment: mechanical reinforcement

This measurement aimed to give a direct assessment of the consolidation provided by the treatments on real, historical and naturally degraded canvases The quantitative assessment of the reinforcement provided by the nanocellulose-based consolidants on historical canvases was carried out using the 19th century lining canvas (linen canvas, dense weaving n°1) (cf. 7.2.1.1). The assessment was carried out using DMA-RH at constant RH and temperature (30%RH, 25°C, chosen as typical room conditions). The storage modulus of the linen canvas samples was measured before and after the application of the treatment. A scheme of the protocol followed is shown in Figure 7.5.

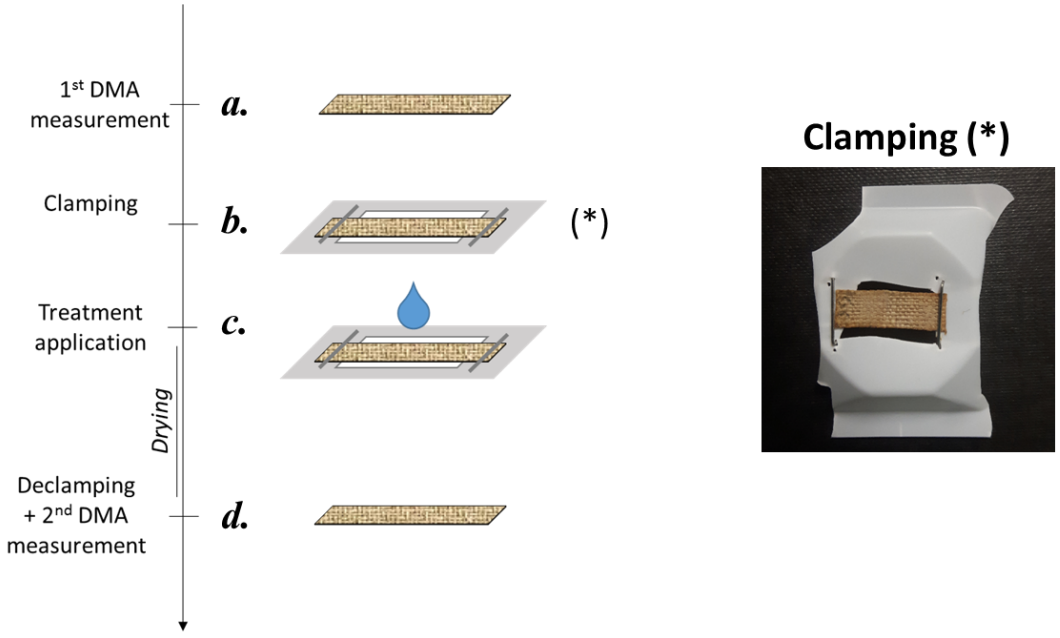

Figure 7.5: Scheme of the different steps followed to quantify the reinforcement provided by the nanocellulose-based treatments to a 19th century lining canvas (linen, dense weaving n°1).

Canvas samples of the same size were cut parallel to the same direction (typically 0.7 (width) x 15 (length) mm) which could not be identified here as weft, neither warp. After preconditioning at 30%RH (25°C) for at least 24 hours, the samples were then measured before the application of the treatment by DMA-RH (30%RH, 25°C) (a). They were pre-tensioned between the clamps of the DMA with a tension of 0.6N to remove any slack. Storage modulus *E'* was measured after 30min equilibration at 30%RH (25°C). The samples were then remeasured twice under the same conditions but *E'* was only measured after 15min equilibration. This was done to verify that the DMA measurement and handling of the canvas would not introduce error in the measurements of the mechanical properties of the samples. After clamping each sample on a small frame made using laboratory weighing bowls (b) (see image on the right in Figure 7.5), the samples were treated with the same amount (i.e. same total dry amount) of treatment (c). At least 3 canvases samples per treatment were prepared. The samples were then left to dry. After declamping the samples from their frame, they were preconditioned at 30%RH (25°C) for at least 24 hours and measured again by DMA (30%RH, 25C) (d). The DMA measurement was carried out on the treatment sample in the same way as before treatment application (i.e. 0.6N preload, 3 repeat measurements, one with 30min and the 2 others with 15 min equilibration at 30%RH).

The test was designed as such to avoid variabilities resulting from the inhomogeneities observed on the historical canvas chosen for this test, i.e. threads and fibres of different thickness and shape, traces of size glue within threads which could not be removed after washing.

7.3 Results & discussion

Following an approach designed in collaboration and for painting conservators, the different treatments were evaluated for their visual impact, their cohesion with the canvas and the risks associated to their penetration through the canvas and paint layers. The canvas and paintings chosen were as representative as possible, with considerations made for the range of objects that could be encountered in a painting conservator's workshop. Additional mechanical assessment of a selection of treatments on an historical linen canvas aimed to demonstrate the consolidation impact of the treatments on a real canvases and to support this consolidation by quantifying it.

7.3.1 Visual appearance and penetration

Both lining canvases and historical paintings with cotton or linen canvases were visually assessed (qualitative assessment) after application of the treatments. The nanocellulose-only treatments, the nanocellulose composite treatment and the hybrid treatments led to different surface appearance and will, therefore, be mentioned separately.

7.3.1.1 Nanocellulose composite treatments (MC+CNC)

Visual appearance

A first visual assessment of the treatments could be made on the lining canvases (dense and loose weaving). As seen in Figure 7.6-7, for the water-based compounds MC+CNC(w) and MC+CNC+$CaCO_3$(w), no change in colours to low darkening of the surface were observed, respectively, for the treated areas. Moreover, attenuation of the surface imperfections and colour contrast could be observed. This could be better described as a general smoothening of the features, such as darker spots, traces of glue or weaving pattern, present at the surface of the canvas (Figure 7.6). This was particularly noticeable for the canvas with the high-density weaving n°1. The surface smoothening is associated with a faint surface whitening.

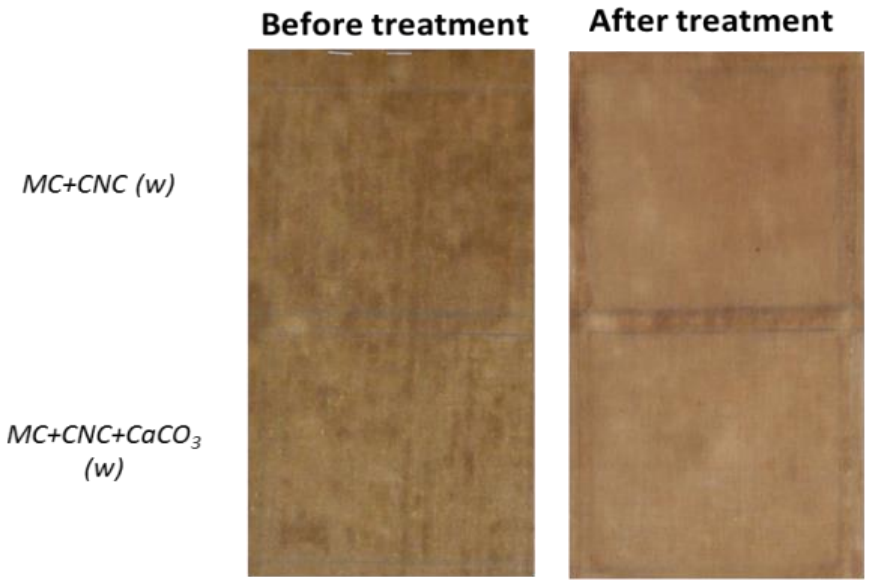

Figure 7.6: Lining canvas (high-density n°1) before and after treatment with MC+CNC (w) and MC+CNC+$CaCO_3$ (w).

As seen in Figure 7.7, the application of the heptane-based MC+CNC treatments led to similar change in appearance than the water-based solutions. Whitening of the canvas surface were however observed for the MC+CNC(h) and MC+CNC+CaMgO(h) treatments, particularly strong for this later, in comparison with their water-based counterparts.

Figure 7.7: Lining canvas (high density n°1) before (0) and after treatment with MC+CNC (w) (1), MC+CNC+$CaCO_3$ (w) (2), MC+CNC (h) (3) and MC+CNC+MgO (h) (4).

For all 4 MC+CNC treatments, the surface visual reduction of contrast and homogenisation in colour was accompanied by a reduction in canvas surface roughness, which was immediately evident after touching the surface which was smoother and flatter.

These purely qualitative observations made by painting conservators were later confirmed by microscopic investigation of the surface topography using SEM. As seen on the SEM images in Figure 7.8, the inter-fibres and inter-threads spaces have been filled or covered with the treatments.

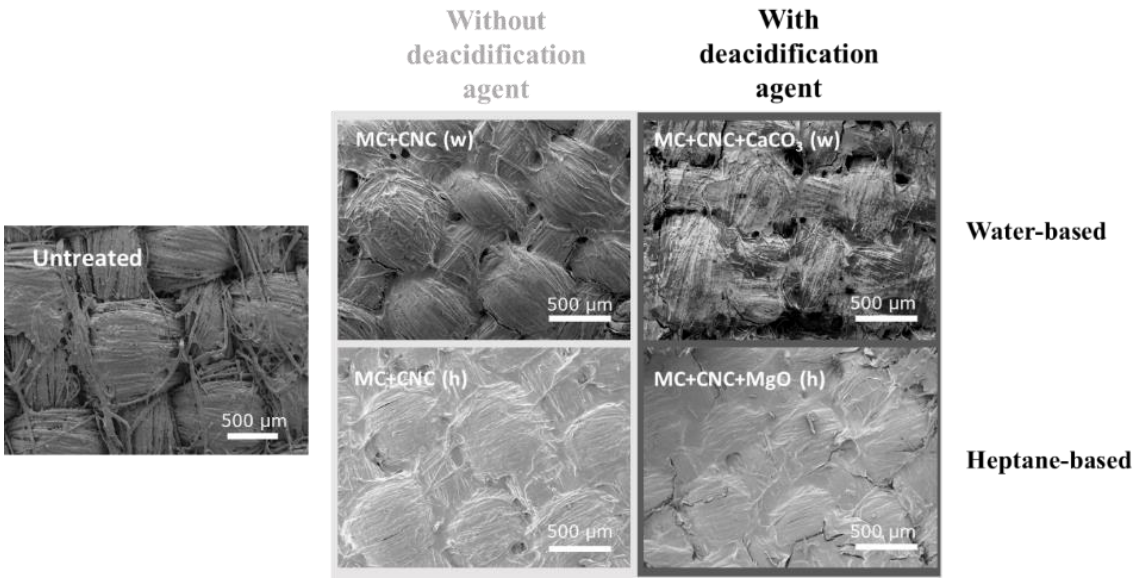

Figure 7.8: SEM images of water-based treatments MC+CNC (w) and MC+CNC+CaCO3 (w) and heptane-based treatments MC+CNC (h) and MC+CNC+MgO (h).

On both *the Angels* and *the Musician* paintings, the application of the water-based treatments resulted in a noticeable darkening and loss of lustre of the canvas (particularly visible under raking light). The cause of this darkening is unclear. It could be due to differences between the refractive index of the canvas and the treatment which is however difficult to measure. The covering effect of the canvas which fills the canvas holes and surface topological irregularities also play a role in the loss of lustre observed.

The heptane-based treatments were also tested on the historical paintings, but at a lower amount applied. For both treatments and despite the low amount applied, whitening of the canvas was observed on the treated areas of *the Musician* painting. The whitening remains low (light deposition observed) for the MC+CNC(h) treatment. For the MC+CNC+MgO(h), canvas whitening reached the same level as for CNF and CCNF for which a higher amount of treatment had been applied. For *the Angels* paintings, no change in appearance could be observed for any

of the 2 products. However, this could be due to the low amount applied and the white appearance of the cotton painting used for this painting. As opposed to *the Angels* painting, *the Musician* painting presents a dark oxidized linen canvas. As a result, this latter canvas offers more contrast with the white particles of $CaCO_3$ treatment. In both cases, the treated area offered again a smooth surface to the touch.

Figure 7.9: The musician painting before (a) and after treatment (b,c) with aqueous composite treatments MC+CNC (w) (C.1) and MC+CNC+$CaCO_3$ (C.2), the heptane-based composite treatments MC+CNC (h) (C.3), MC+CNC+MgO (h) (C.4) and the deacidification MgO solution in heptane (C.5), the nanocellulose dispersions CNF (NC.1) and CCNF (NC.2) and the hybrid treatments Sil/PEI (H.1), Sil/PEI/CMC (H.2) and the solution of $CaCO_3$ nanoparticles (NP). The modification of the reflective index of the canvas after the application of the treatments is revealed by illumination of the canvas under raking light (c).

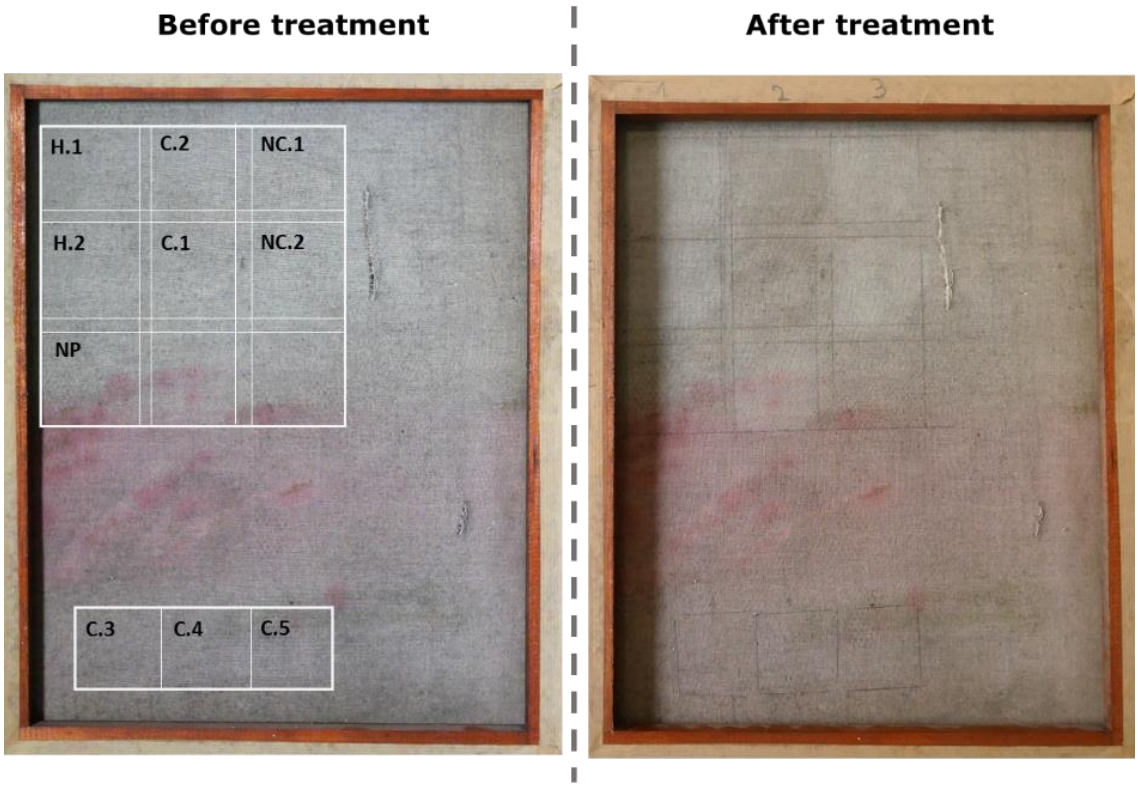

Figure 7.10: The Angels painting before and after treatment with the aqueous composite treatments MC+CNC (w) (C.1) and MC+CNC+CaCO3 (C.2), MC+CNC(h) (C.3) and MC+CNC+MgO (C.4), the nanocellulose dispersions CNF (NC.1) and CCNF (NC.2) and the hybrid treatments Sil/PEI (H.1) and Sil/PEI/CMC (H.2). The deacidification solutions MgO (C.5) and CaCO3 nanoparticles (NP) were also applied for comparison.

Treatment penetration

Cross-sections of the sample also revealed the differential behaviour between heptane-based and water-based treatment (see Figure 7.11). The degree of penetration of the treatments in the canvas was measured using SEM-EDX by plotting the distribution of calcium (Ca) and of magnesium (Mg) and silica (Si) for the MC+CNC+$CaCO_3$(w) and the MC+CNC+MgO(h) treatment, respectively. As seen in Figure 7.11, while the water-based treatment MC+CNC+$CaCO_3$(w) appears to have penetrated the fabric up to the reverse side (see detail (**)), the heptane-based treatment MC+CNC+MgO(h) remains as a coating on the surface. This was also seen on SEM images of an MC+CNC+MgO(h)-treated lining canvas (see Figure E.1 in

Appendix). As observed for the cotton canvas, the absence of full treatment penetration could result from the high viscosity of the heptane-based treatments. It could also arise from the repulsion between hydrophilic fabric and hydrophobic heptane-based treatment thus preventing the wetting of the fibres and treatment penetration (Wang, 2018). It is also known that silylation of the methylcellulose in the heptane-based MC+ CNC consolidant mitigates the effects of hydrogen bonding on physical properties (Klebe, 1964).

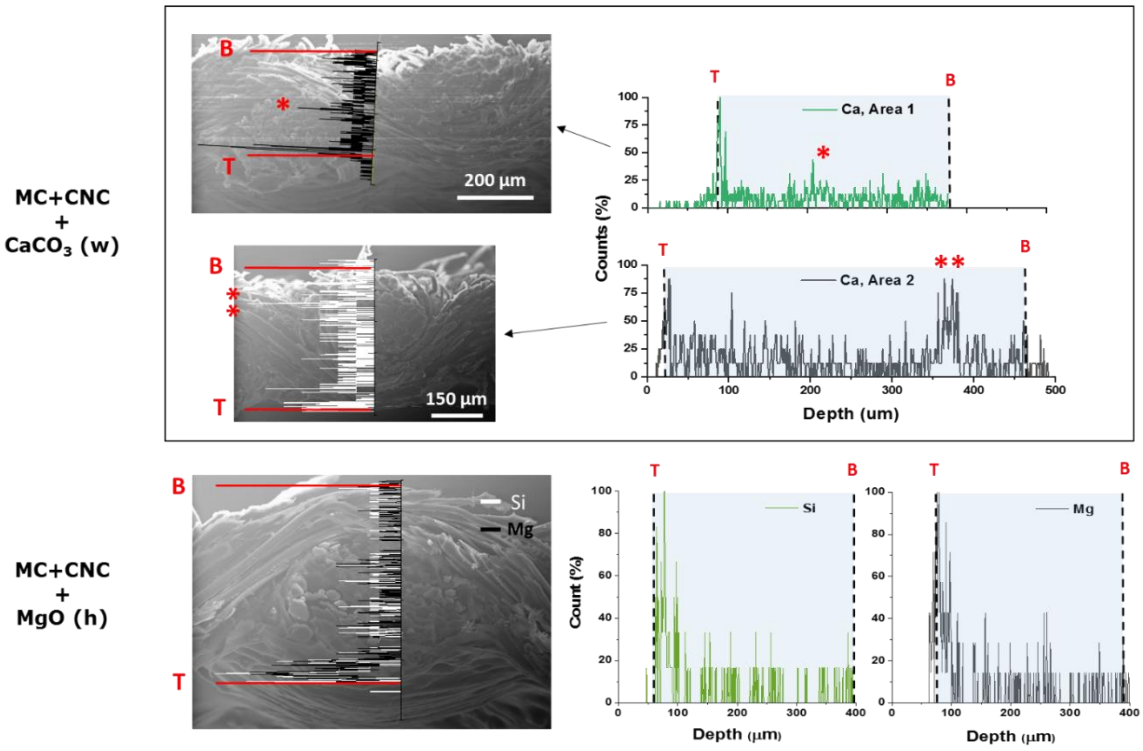

Figure 7.11: SEM-EDX images of cross-sections of treated lining canvas treated with MC+CNC+$CaCO_3$(h) and MC+CNC+MgO (h). The distribution of the elements present in the treatments (i.e. Ca Kα, Mg Kα, Si Kα) is given across a line drawn from the treated side (T) to the bottom of the canvas (B). Note the higher signal measured in (*) and (**) for Ca, indicating the penetration of the treatment.

From the distribution profile of Ca for the MC+CNC+$CaCO_3$-treated canvas, it is also worth noting that the treatment is not homogeneously distributed within the canvas. A higher amount of Ca can be measured at the interstitial spaces between threads indicated by (*) in Figure 7.11. This pattern suggests that the diffusion of the treatment within the canvas mesh could be stopped at these intersections due to the change in the alignment of the yarns and fibres from one

direction to its perpendicular. It could also indicate that the treatment diffusion is mainly trigged along and not across threads. Either hypothesis supports the current knowledge on textile wicking[9] which states that water can diffuse in fabrics by capillarity along the interstitial canals formed between yarns (in-plane wicking) (Das, 2011; Mhetre, 2010; Rossi, 2011; Wang, 2018). This in-planar wicking strongly depends on various parameters such as pores size, twist of the yarn, number of fibres and fibres density.

7.3.1.2 Pure Nanocellulose treatments

Visual appearance

The CNF and CCNF differ from the composites MC+CNC treatment in that they offer less viscous treatments terms of viscosity. Due to their low viscosity, the control over the solvent and/or treatment penetration is reduced. On the lining canvases (loose weaving in Figure 7.12 and high density weaving in Figure 7.14), this could be seen by the presence around the treated area of large water rings resulting from the water dispersion after treatment application, as seen in Figure 7.12. These rings, also called tide lines, are clearly visible and offer an inhomogeneous and non-desired surface appearance.

[9] Wicking describes the action of absorbing or drawing off a liquid by capillary forces.

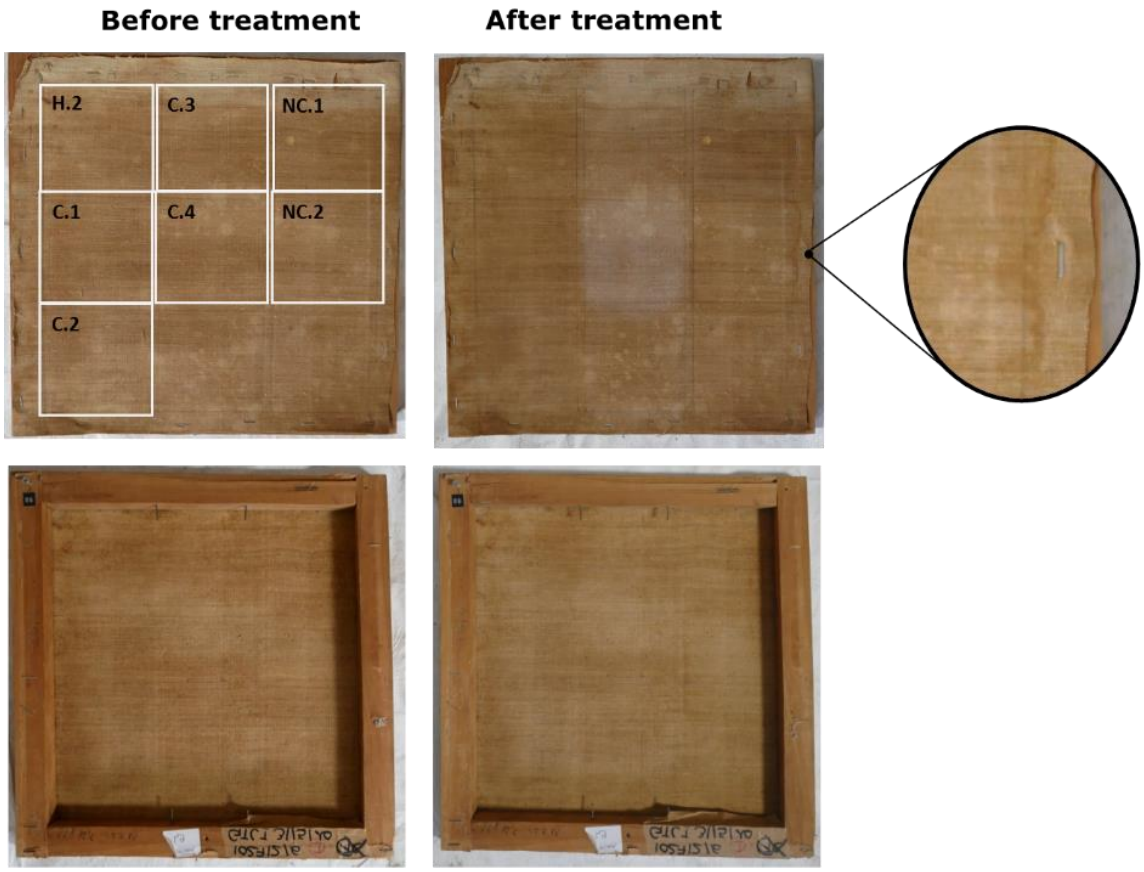

Figure 7.12: Lining canvas with a low-density weave before and after treatment application using the hybrid treatments Sil/PEI (H.1) and Sil/PEI/CMC (H.2), the aqueous composite treatments MC+CNC (w) (C.1) and MC+CNC+$CaCO_3$ (C.2) and the nanocellulose dispersions CNF (NC.1) and CCNF (NC.2).

Attenuation of the surface imperfections was observed but was not accompanied by a smoother feel to the touch as for the MC+CNC composite treatments. Further assessment using SEM (Figure 7.13) showed that the treatments behave similarly on the historical paintings and lining canvas as on the cotton mockups tested in previous chapters (see Chapter 4, 5). The CNF and CCNF treatments behave as coatings sitting on top of the canvas mesh, covering interstitial threads and fibres spaces. The smoother appearance observed at the macroscale probably results from this deposition behaviour.

On both historical paintings, the nanocellulose CNF and CCNF treatments induced a whitening of the canvas. The stronger colour change was observed for the CCNF treatment.

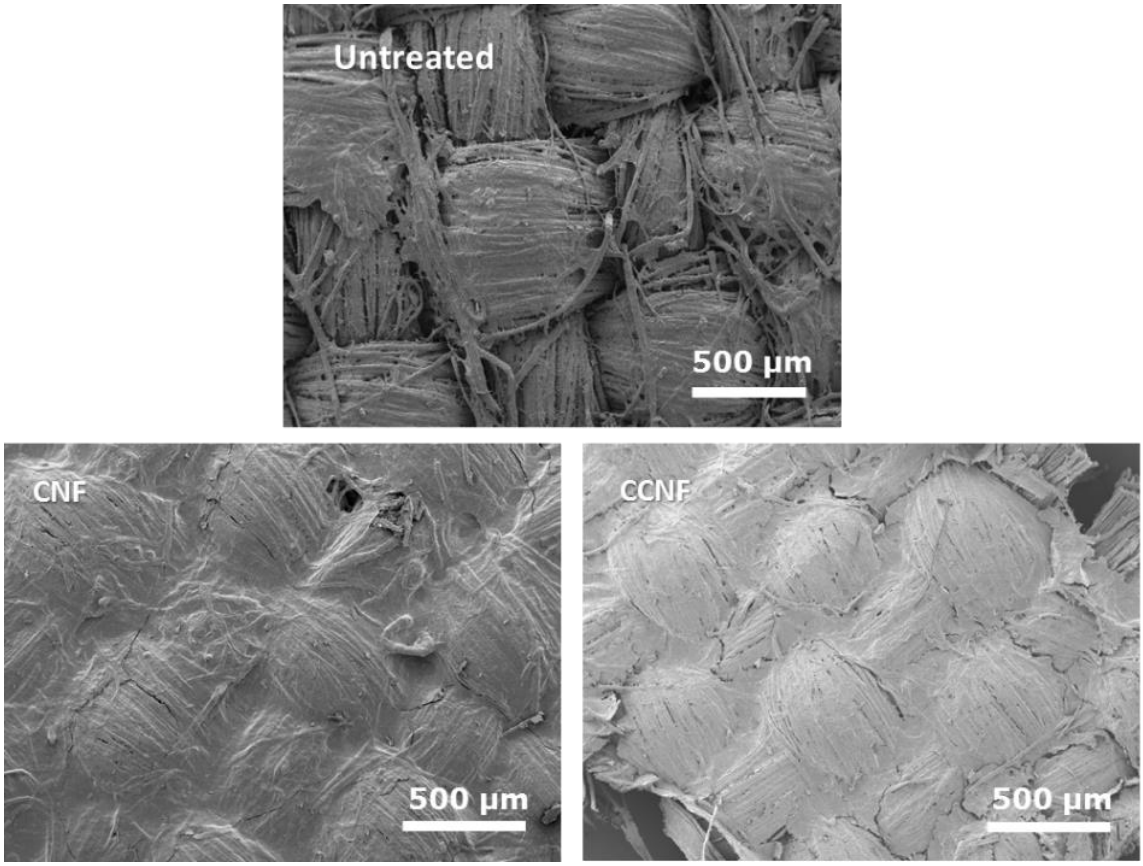

Figure 7.13: SEM images of the untreated and CNF- and CCNF-treated lining canvas (high-density weaving n°1)

Treatment penetration

As expected, the CNF and CCNF treatments behave in a similar as when applied on the degraded cotton canvas (see 5.3.1 in Chapter 5). The nanocellulosic treatments remain on top of the treated canvas and form a continuous layer of treatment, or nano-lining, suggesting that the treatment do not penetrate the canvas (see Figure E.2 and Figure E.3 in Appendix).

7.3.1.3 Nanocellulose/silica hybrid materials

Visual appearance

The last group of treatments, the hybrid treatments, is also the one that leads, among all the treatments tested, to the stronger whitening. The $CaCO_3$/PEI dispersion, in particular, made of positively charged nanoparticles, induced the stronger change in appearance.

Figure 7.14: Linen lining canvas treated with the hybrid treatments $CaCO_3$/PEI (H.1) and $CaCO_3$/PEI/CMC (H.2), the aqueous composite treatments MC+CNC (w) (C.1) and MC+CNC+$CaCO_3$ (C.2) and the nanocellulose dispersions CNF (NC.1) and CCNF (NC.2). Note the impact of water on the colour of the canvas. The darkening of the back of the canvas particularly pronounced for the area treated with CNF and CCNF treatments. Strong whitening of the canvas surface also visible for the $CaCO_3$/PEI treated area.

As seen in Figure 7.14, the canvas surface is covered with a white and inhomogeneous layer of treatment. For the dispersion of $CaCO_3$/PEI/CMC (i.e. $CaCO_3$/PEI with an added layer of CMC) the whitening of the surface was also seen but in a much lower extent. Interestingly, a dispersion of $CaCO_3$ nanoparticles was also applied for control and did not induce any colour change. On the contrary, as previously seen in Figure 7.9, the dark oxidized canvas of *the Musician* painting tends to darken after the application of $CaCO_3$.

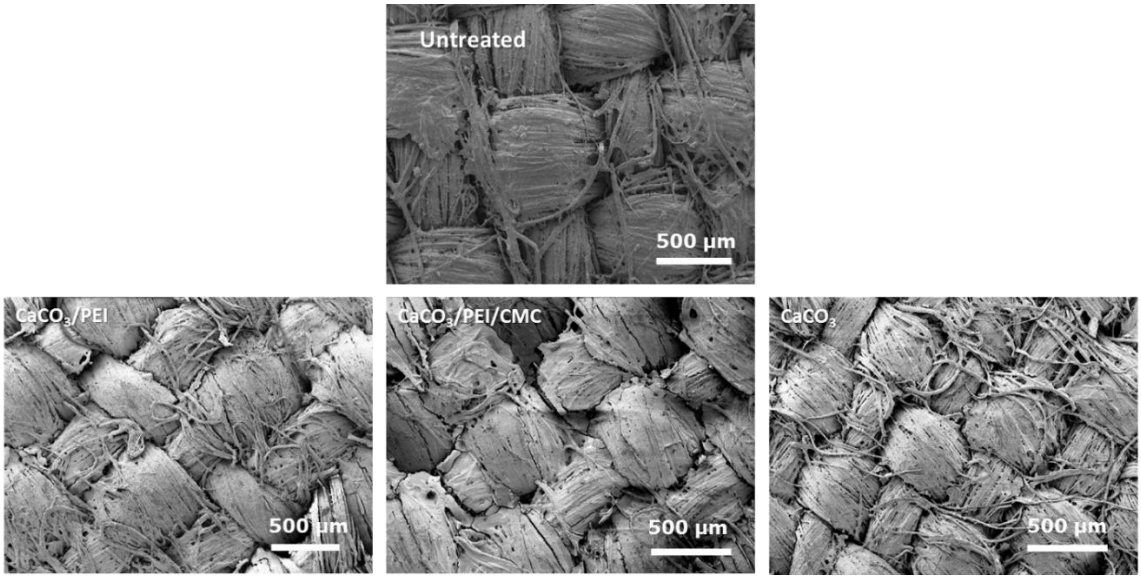

Figure 7.15: SEM images of high-density lining canvas n° 1 untreated and treated with $CaCO_3$/PEI, $CaCO_3$/PEI/CMC and $CaCO_3$ nanoparticles (NP).

Treatment penetration

Darkening observed for the canvases treated with the solutions of nanoparticles of $CaCO_3$ could be the result of the higher penetration of the $CaCO_3$ nanoparticles in comparison with the multi-layered $CaCO_3$/PEI/CMC ones. In a similar study (Kolman, 2018), silica nanoparticles (SNP) were used instead of $CaCO_3$ particles to create multi-layered nanoparticles (i.e. Sil/PEI/CMC described in 7.2.1.4). The penetration of the coated or uncoated silica particles was followed by energy-dispersive X-ray (EDX). The application of formulations solely based on SNP led to a relatively low EDX silica signal measured on the surface. It was assumed that the nanoparticles penetrated into the canvas, probably promoted by the capillary action of the fibrous network. When the silica or $CaCO_3$ nanoparticles are coated with PEI or PEI/CMC, the outer layer modifies the interaction between the single particles and the canvas fibres. The PEI-only coated $CaCO_3$ particles are expected to attach better to the fibres by electrostatic interaction between the positive charge they bear and the negative charge, resulting from acidic hydrolysis, present on degraded canvas fibres.

When looking at the SEM images of the canvas surface (Figure 7.15) as well as the EDX-SEM images taken of the cross-sections of the samples (see Figure 7.16), a higher penetration is reached with the $CaCO_3$ dispersion and the $CaCO_3$/PEI treatment than with the $CaCO_3$/PEI/CMC treatment. After the high Ca signal measured on the surface for all the samples, other concentration of Ca can also be seen in the sample bulk. As indicated in Figure 7.16 for the $CaCO_3$ and $CaCO_3$/PEI samples, traces of Ca indicated by (*) and (**) were also located at the interstitial space between the threads for $CaCO_3$ and in the canvas thread for $CaCO_3$/PEI. For the $CaCO_3$/PEI/CMC –treated sample, presence of Ca was also measured in the interstitial space between the threads (indicated by (***) in Figure 7.16). However, contrary to the $CaCO_3$ and $CaCO_3$/PEI treatments, $CaCO_3$/PEI/CMC shows higher agglomeration on the canvas surface. This treatment diffuses less into the canvas mesh than $CaCO_3$ and $CaCO_3$/PEI. This could result from the presence on the surface of the fibre of traces of lining glue (probably an animal glue or gelatine) which might modify the surface charge of the canvas fibres. It is has been established that the surface of gelatine is negatively charged at higher pH (pH 9) and positively charged at lower pH (pH 5) (Alihosseini, 2016). For acidic degraded canvases (low pH), the positively charged fibres might, therefore, cause $CaCO_3$/PEI/CMC particles agglomeration on the superficial area of the fabric. Another reason for the behaviour observed could be the bigger size of the 2-layers $CaCO_3$/PEI/CMC particles in comparison with the 1-layer $CaCO_3$/PEI nanoparticles.

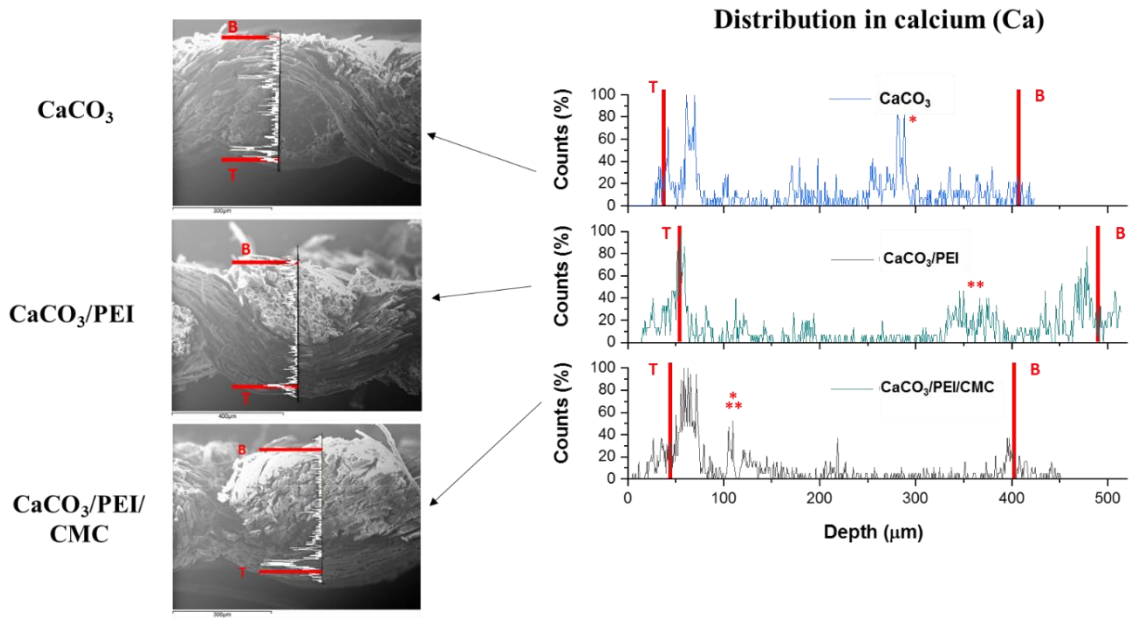

Figure 7.16: SEM-EDX images of cross-sections of treated lining canvas treated with $CaCO_3$, $CaCO_3$/PEI and $CaCO_3$/PEI/CMC. The distribution of the elements (Ca) present in the treatments is given across a line drawn from the treated side (T) to the bottom of the canvas (B). The scale bars on the SEM images correspond to 100µm.

7.3.2 Water sensitivity, solvent penetration (Red painted samples and canvas with white-lead layer)

Another, essential criterion for painting conservators is the assessment of the nanocellulose-based is their compatibility with water-sensitive objects. With this objective in mind, several mock-ups of a water-sensitive painting (cf. red painted linen canvas in Figure 7.4) which had been prepared in the past (>5 years) were used to test the consolidants. The red paint used on these mock-ups is known to respond quickly to water through darkening of the wetted area associated with swelling.

As seen in Figure 7.17, when applied in droplets, the water-based MC+CNC treatments led to the swelling of the painted layer. The paint layer swelled as a result of the water added. The same observation was made for the CNF and CCNF treatments. Surprisingly, when the treatment is not applied in droplets but homogeneously brushed onto the canvas surface, no swelling could be seen. This absence of response shows the importance of the application technique and the quantity used. Water-based treatments could be used on water sensitive painting if they are

applied properly, by a skilled conservator and in several applications. To reduce the amount of water used, the concentration in nanocellulose could be increased. However, this can be only done up to a certain amount in order to preserve the stable dispersion of the particles in solution. In fact, it is has been shown that owing to their long aspect ratio, large surface area, and high interface energy, CNF fibrils tend to intertwine together and form agglomerates. At very low concentrations (between 0.5% and 2%wt in water depending on the particle size and processing used) CNFs already present a gel-like rheological behaviour (Dufresne, 2013; Gong, 2014; Herrick, 1983). CNCs are smaller in length than the long fibrils of CNFs and CCNFs. For dispersions of the same viscosity, a higher concentration could be reached for the CNCs one than for those containing CNFs or CCNFs. This is due to the bigger size of nanofibrils in comparison with the nanocrystals (cf. Figure 1.8 in Chapter 1). Swelling could also be observed for the hybrid $CaCO_3$/PEI treatments using a water/ethanol solvent. However, the impact is much lower than for the nanocellulose treatments. Contrary to all other water-based treatments, for $CaCO_3$/PEI and $CaCO_3$/PEI/CMC, no trace of the solvent could be seen on the unvarnished area. The heptane-based treatments were the only which, as expected, did not show to modify the appearance of the water-sensitive mockups and did not induce swelling of the painted surface.

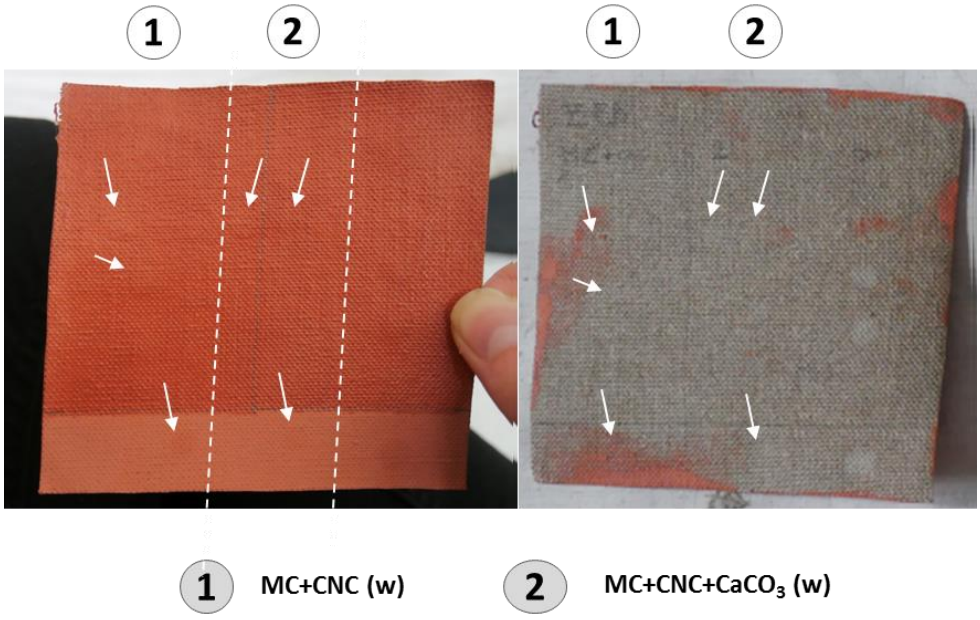

Figure 7.17: Mock-ups of a water-sensitive painting after application of droplets of the water-based MC+CNC(w) and MC+CNC+$CaCO_3$ (w) treatments.

Further mechanical assessment of a selection of treatments applied on historical lning canvas was carried out based on the results of the previous assessments (conservator's assessment) which are summarized in Table 7.5. The treatments performing the best (green square in Table 7.5) on the different tests were chosen. The MgO and $CaCO_3$ solutions which do not aim at the consolidation of the canvas but were introduced in this study as deacidification agents were not included either in the additional mechanical assessment of the treatments. Among the composite treatments, the solutions which combine both consolidation and deacidification agents were selected, i.e. MC+CNC+$CaCO_3$ (w) and MC+CNC+MgO (h). The $CaCO_3$/PEI treatment was discarded because of the strong colour change induced by the treatment and observed on the several substrates tested.

		$CaCO_3$/PEI (e) 1.3%wt	$CaCO_3$/PEI/ CMC (e) 1.3%wt	CNF (w) 1.4%wt	CCNF (w) 0.8%wt	MC+CNC (w) 1.98%wt	MC+CNC+ $CaCO_3$ (w) 1.98%wt	MC+CNC (h) 1.98%wt	MC+CNC+ MgO (h) 1.98%wt	MgO (h)
Penetration/water sensitivity	*Red paint*	Varnished ++ Unvarnished +++	Varnished + Unvarnished +++	n/a	Varnished + Unvarnished +	Varnished ++ Unvarnished +	Varnished ++ Unvarnished +	Varnished +++ Unvarnished +++	Varnished +++ Unvarnished +++	N/A
	White lead treated canvas	+	+	++	++	++	++	++	++	++
Lining canvas	*Lining canvas (tight weave)*	- (whitening, solvent traces)	++	+ (solvent traces)	++	+++	+++	(++)	(++)	(++)
Historical paintings	*Robust painting ("the musician")*	- - (whitening)	- (low whitening)	- (whitening)	- (whitening)	+++	+++	+ (low whitening)	- (whitening)	+++
	Sensitive painting ("Angels")	+/++ (whitening)	+/++ (whitening)	+ (whitening/ warping)	+ (whitening/ warping)	++ (swelling of the painting but treatment/solvent does not go through)	++ (swelling of the painting but treatment/solvent does not go through)	+++	+++	+++

Table 7.5: Overview of the results obtained for the different tests performed on lining canvas and historical paintings (Conservator's point of view assessment). The green and red squares in the table highlight the good and unacceptable results obtained with the treatments, respectively.

7.3.3 Mechanical quantitative assessment of the consolidation

The reinforcement achieved for the different treatments was measured using a historical lining linen canvas. Unfortunately, historical canvas made of cotton could not be found in order to repeat the assessment on this type of canvas. Like other historical canvases used for this project, the lining linen canvas used for these tests contained strong structural inhomogeneities. These inhomogeneities resulted from the variable diameter of the threads and inhomogeneous distribution across the fabric of the size glue which could not be totally removed by washing. Due to these structural inhomogeneities, tensile measurements of the canvas would have led to an unacceptably high variation of values within the same group of samples. To overcome this issue, dynamic mechanical analysis (DMA) was used. This technique enabled the non-destructive testing of the samples by restricting the measurement to the elastic region of the sample while a tensile test is irreversible. The storage modulus *E'* of each sample could thus be measured before and after application of the treatments (cf. 7.2.2.3). All the samples were measured at fixed environment conditions, 30%RH (between the 20-60%RH chosen for the experiments carried out in previous chapters, e.g. 3.3.2.2) and 25°C. This is because, the assessment only focuses on quantifying the consolidation achieved after treatment and because the mechanical response of hygroscopic canvases is known to be dependent on RH (Célino, 2014).

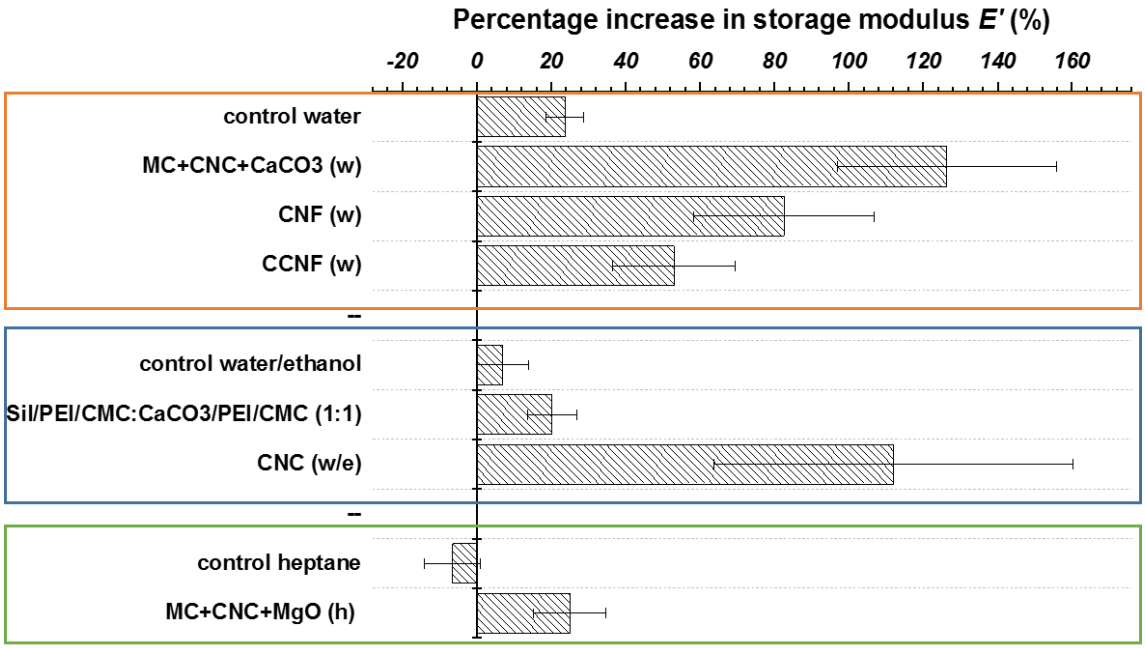

Figure 7.18: Percentage increase in storage modulus resulting from the application of 9g/m² of treatment on the high-density weaving linen canvas n°1. The impact of the different solvents used to applied the treatments (i.e. water, water:ethanol(50:50) and heptane) were also tested separately. The results are grouped by solvent, i.e. water (orange), water:ethanol (50:50) (blue) and heptane (green). For each category, five samples were measured.

Figure 7.18 shows the calculated percentage increase in storage modulus *E'* (30%RH, 25°C, 30min equilibration) measured for the linen canvas samples and resulting from the application of the treatments. The results indicate that all the treatments tested led to the consolidation of the historical canvas. As seen in Figure 7.18, an increase in stiffness (or storage modulus *E'*) was measured for all the samples treated using one of the nanocellulose-based materials. An increase ranging from $\Delta\%E'$=20±7% (Sil/PEI/CMC+$CaCO_3$/PEI/CMC) up to 126.3±29.5 % (MC+CNC+$CaCO_3$(w)) was measured (Table 7.6). The treatments for which the highest consolidation was obtained were the water-based composite treatment MC+CNC+$CaCO_3$ ($\Delta E'$=185.0±3.4 MPa, Δ%E'=126.3±29.5 %) as well as the pure nanocellulose dispersions CCNF ($\Delta\%E'$=53.0±16.6%), CNF ($\Delta\%E'$=82.6±24.3%) and CNC ($\Delta\%E'$=112.1±48.3%). The reinforcement obtained for all the treatments and the strong stiffening measured for pure nanocellulose treatments (CNF, CNC and CCNF) is in agreement with what had been previously measured on treated modern cotton canvas artificially degraded.

Category	Treatment	Increase in *E'* after treatment application ($\Delta E'_{\text{before-after treatment}}$)	Percentage increase in *E'* after treatment application ($\Delta\%E'_{\text{before-after treatment}}$)
Water-based treatments	**Water (*control*)**	28.1±9.2	23.7±5.0
	MC+CNC+ $CaCO_3$(w)	185.0±3.4	126.3±29.5
	CNF(w)	79.5±10.8	82.6±24.3
	CCNF(w)	58.5±20.2	53.0±16.6
Water:Ethanol (1:1) -based treatments	**Water:EtOH (1:1) (*control*)**	7.0±8.3	7.0±7.0
	SNP/PEI/CMC : $CaCO_3$/PEI/CMC (1:1)	22.3±12.0	20.2±6.6
	CNC (w:e)	125.6±54.2	112.1±48.3
Heptane-based treatments	**Heptane *(control)***	-7.3±9.2	-6.5±7.5
	MC+CNC+MgO (h)	27.6±10.6	25.0±9.7

Table 7.6: Increase in storage moduli E' (i.e. $\Delta E'_{\text{before-after treatment}}$) and percentage increase in E' (i.e. $\Delta\%E'_{\text{before-after treatment}}$) measured at 30%RH for an historical lining canvas (linen canvas, dense weaving n°1) before and after application of different nanocellulose-based consolidants. The linen canvas was also treated with the solvents in which the different consolidants were found. These samples were used as control to show the impact of the solvent-only on the mechanical properties of the historical canvas.

Interestingly, the strong stiffening reached using the water-based composite treatment MC+CNC+$CaCO_3$(w) was not observed for its counterpart heptane-based treatment MC+CNC+MgO(h). Moreover, the increase in storage modulus *E'* measured for MC+CNC+$CaCO_3$(w) was not expected as previous tests performed on cotton canvas had indicated a rather low increase in Young's modulus for MC+CNC (in water) in comparison with the CNF, CCNF and CNC treatments (see Chapter 5). Two explanations could be given for the discrepancy observed.

Firstly, the mechanical properties of the sample are strongly affected by the solvents used (water, ethanol or heptane). In parallel to the application of the treatments, the 3 solvents used in

this study were also applied on the linen canvas. As seen in Table 7.6, the application of water-only led to an increase in storage modulus of 23.7±5.0% ($\Delta E'$=28.1±9.2MPa). This is equivalent to the consolidation obtained using the ethanol/water-based Sil/PEI/CMC+$CaCO_3$/PEI/CMC (20.2±6.6%) and the heptane-based MC+CNC+MgO(h) (25.0±9.7%) treatments. This unexpected consolidation using water probably results from the redissolution of the glue remaining on the canvas. The water-soluble animal glue which remains on the linen canvas will swell in presence of water, dissolve and a new layer of glue is thus formed between threads and fibres and result in an apparent consolidation of the fabric. An increase in stiffness was also reached for the historical canvas treated with the ethanol/water (50/50) mixture. This increase remains however low (i.e. 7.0±8.3%) due to the lower amount of water in solution and the possible low impact of ethanol on the glue. Contrary to the results of the water and the water/ethanol solutions, the application of heptane led to a decrease of in canvas stiffness, i.e. decrease in storage modulus *E'*. This could result from the washing out of other species present in the canvas such as oil-based material with which non-polar solvents can dissolve. It could also be caused by the softening of the paint layer by the solvent and the longer time needed for the complete evaporation of heptane in comparison to water. Indeed, while it is known that water leads to swelling of the preparation layer in paintings (i.e. -7.3±9.2%) mixture of organic (Baglioni, 2013).

If the solvent used with the treatment can impact the mechanical properties of the bare lining canvas, so does the time of contact between solvent and canvas. This is the second explanation which may be provided to explain the higher stiffening measured for the water-based, MC+CNC+$CaCO_3$(w), than the heptane-based MC+CNC+MgO(h) composite treatment. Indeed, MC+CNC+$CaCO_3$(w) at 2%w/w presents a higher viscosity than the other water-based treatments CNF and CCNF. The composite treatment homogeneous application on the surface of the sample was, therefore, more difficult to achieve than for the pure nanocellulose dispersions. This might have led, in the case of the MC+CNC+$CaCO_3$(w), to exposure of specific area of the canvas to a higher amount of water thus leading to the dissolution of a higher amount of glue than for CNF

and CCNF. The time of drying was not measured but could also have an impact on the stiffening reached.

Overall, the application of the treatments on a historical painting is positive, showing that consolidation could be conferred by each selected treatments and this, independently from the impact of the solvent used. These study also shows that the inherent presence of traces of glue or oil-based substances on historical canvases may inevitability lead to modifications of their mechanical properties through the application of solvent only. These changes are somewhat independent of the nature of the treatment. The amount of change depends on the soils present on the canvas, the nature of the paint layers (e.g. oil or acrylic) and the solvent used as well as the time of contact between those and the solvent.

7.4 Conclusion

The initial study by painting conservators of the nanocellulose-based treatments that could be potentially used for canvas consolidation has been an essential step in this research. First, in-situ assessment of the newly developed treatments was performed using techniques and the empirical knowledge of trained and experienced painting conservators. Second, the tests were carried out in collaboration with professional conservators whose approach and understanding of the problem help to deepen our understanding of the advantage and disadvantages of some treatments over others. The results of these tests, highlighted the potential of some of the developed treatments for canvas consolidation. Physical and mechanical properties of the treatments already quantified on mock-ups of degraded cotton canvas were validated by testing them on historical canvases and paintings despite them being on different fibre types (i.e. linen and cotton).

Overall, the different consolidants tested offer a wide range of products in both polar and apolar solvents which is suitable for painting conservation. Their suitability varies between substrates (see Table 7.5). The water-based MC+CNC composite products are suitable canvas consolidants in terms of penetration, surface deposition, canvas visual appearance and

consolidation. They have acceptable viscosity. Slight darkening of some of the canvases could, however, be observed in some cases where a large amount of consolidant was applied.

The heptane-based MC+CNC composite products offer acceptable handling properties such as the ease of application by brushing and consolidation (despite the loss in stiffness caused by application of the solvent). They appear as the most suitable nanocellulose-based consolidants for water-sensitive paintings. However, a disadvantage of these treatments is the strong whitening observed when these treatments are used on dark canvases. This is particularly the case of the MC+CNC+MgO(h) consolidant. These products have also a fast drying time. This has the advantage to reduce the duration of the application but has, as well, the disadvantage to give less room for control during the application of the product. All the treatments of this group of products can mainly be applied by brushing or blade coating (coating spread onto the surface using a blade) only due to their high viscosity.

Nanocellulose-only treatments provide strong consolidation. Even at low amount applied, the consolidation expected should be sufficient thus reducing the risk of change in visual appearance observed for some canvases (i.e. *the Musician* in Figure 7.9). They should also be used at the highest possible concentration or dispersed in ethanol/water solvent. For consolidation of highly water-sensitive objects, the 3 solutions tested in this study should be discarded. In terms of handling properties, CNF, CCNF, CNC can be easily sprayed or brushed and in that sense have the advantage to be quite versatile.

The hybrid treatments have good handling properties and can be brushed or sprayed. The use of water/ethanol blend solvent is an advantage. However, due to the strong colour change observed after application of $CaCO_3$/PEI, this treatment should be discarded. When combined with Sil/PEI/CMC, designed to be mix with $CaCO_3$/PEI, the treatment does not seem to offer either a good reinforcement as no increase in stiffness was measured. Nevertheless, it is possible that the treatment might increase the elongation at break of the canvas (as seen in the study carried out on the Sil/PEI/CMC particles (Kolman, 2018). This would be beneficial for very brittle textiles which

would break below the typical forces and elongation applied when restretching the painting on its stretcher.

The work contained in this chapter has proven to be invaluable and necessary in the process of selection and evaluation of the treatments. The acceptation of the products and validation could not have been possible without the input of conservators. However, this project has also highlighted the importance of supporting the findings with quantitative assessment of the physical, mechanical and chemical properties of the consolidants. Empirical knowledge based on individual experience and practices was shown to vary from conservator to conservator and to highly depend on the school of conservation and country. The addition of quantitative analysis on real objects in order to replace subjective analysis may speed up the acceptance of these new treatment methods. Despite the robustness of this empirical knowledge, these differences in approaches between conservators identified during the project highlights yet again the need for quantitative and scientific assessment of the treatment properties.

Future work could focus on measuring the minimum amount of consolidant required to reach consolidation without altering the aesthetics of the canvas. The reversibility of the treatments and retreatability of the canvas should also be investigated. These points need to be to addressed as they are essential for further acceptance of the consolidants among the painting conservation community.

8 On the potential of neutron radiography for mapping and dynamic measurement of moisture sorption/desorption into cellulose-based textiles.

8.1 Introduction

The impact of RH on the nanocellulose-based treatments introduced in this project has been, so far, studied in terms of mechanical properties. In Chapter 5, this was successfully examined using tensile tests and DMA-RH measurements. Physical assessment through quantification of the rate of moisture uptake by DVS was also carried out. However, the limitation faced with this type of assessment is that it does not give access to the spatial distribution of water across the samples and does not allow either for the visualisation of the dynamics of moisture sorption/desorption.

This knowledge is critical to painting conservators as changes in RH are often encountered by paintings either on display in uncontrolled environments (e.g. historical houses) or during conservation treatments such as localised treatments of paintings and humidification applied with vacuum hot tables (Reeve, 1988). Moreover, it has been shown that the ingress of moisture either in the vapour or liquid state in easel paintings can trigger immediate or long-term non-reversible alterations of its constitutive materials (Andersen, 2018; Flor, 1989; Hedley, 1988; Macbeth, 1993; Odlyha, 1995; Van Loon, 2012). The work performed so far in this thesis raises the following questions: How do the newly developed nanocellulose-based treatments affect the canvas physical response to moisture and how is the moisture distributed in the treated canvas? This study will aim at visualising and quantifying the spatial and temporal distribution of water for different types of treated canvases samples.

Given the high sensitivity for hydrogen, neutron imaging can be used to follow water movements (diffusion, absorption or desorption) in a wide range of items and materials. After calibration, this technique can also be used to measure the absolute moisture content water content

in a given material. High precision and spatial resolution can be achieved with this method. Neutron radiography was successfully used to follow the time-dependent distribution of water for various materials (building materials, plants, narrow channels, synthetic fibres, etc.) (Alam, 2006; Carlisle, 1994; Cheng, 2012; Zhang, 2011) including cellulose-based materials such as wood (Islam, 2003; Sonderegger, 2010; Mannes, 2014). It has shown to enable the measurement of time dependent water profiles in the materials studied or the calculation of diffusion coefficients as shown by Sonderegger (2010), for example, in a study on multi-layered boards made of wood boards glued together with different wood adhesives (polyvinyl acetate, epoxy resins). Neutron radiography was therefore chosen to help understanding how moisture is distributed, before and after treatment, within the canvases.

The application of neutron radiography in this way has already been successfully demonstrated in a previous publication allowing real-time visualisation of the diffusion of water vapour with model samples of paintings (Hendrickx, 2016). The samples tested in this study consisted of mock-ups of paintings with a support (canvas), a size (proteinaceous), a priming ground, and one or more paint layers followed by a varnish layer (see following paragraph 8.2.1.1 for more detailed description of the samples). The results showed that cellulose fibres and glue sizing have a much stronger water uptake than the chalk–glue ground and the data showed that the uptake rate was not uniform throughout the thickness of the sized canvas. Neutron radiography was therefore proposed as a crucial technique to further the understanding of moisture diffusion and distribution in paintings as well as the impact of the newly developed nanocellulose-based treatments on a mesoscopic level.

For this study, a sample chamber connected to a temperature and RH controller was purpose-built (see Figure 1 later in 8.2.1.3). This chamber was inspired by a set-up developed elsewhere (Hendrickx, 2017). The RH controller enables to programme RH to increase and decrease at a selected rate. Mock-ups of a degraded cotton canvas and samples from an historical painting were then tested with 2 objectives:

- firstly, the study the impact of part of the new treatments on the different canvas samples available
- secondly, the comparison of the rate and distribution of moisture uptake of the modern cotton canvas with an historical canvas having a layer of size and a ground layer.

The results put in perspective with the outcomes previously obtained by DMA-RH (see Chapter 5) will help providing a global picture of the physical and mechanical impact of moisture on the samples.

8.2 Materials and methods

8.2.1 Materials

8.2.1.1 Canvas samples and treatments

Samples that were investigated included the following: a control untreated sample which was the modern cotton canvas that had been degraded to simulate an aged cotton canvas in need of consolidation (cf. 2.1.1.2 in Chapter 2). In addition to the cotton canvas, a historical primed canvas sample was provided by Tate Conservation Dept, UK. Such samples are of extreme value for scientific investigation since they provide a source of original samples and materials, naturally aged, for study. This sample consists of a 19th century linen canvas (plain weave) taken from the original auxiliary canvas (loose lining) of Sir Edwin Henry Landseer's painting (Study of Lion, c.1862, Tate Gallery N01350). The linen canvas is sized with animal glue and presents a preparation priming layer (lead white $(PbCO_3)_2 \cdot Pb(OH)_2$ in oil).

Figure 8.1: Picture of the primed linen canvas taken from a loose lining of a E. H. Landseer painting (c. 1862). The samples used for the experiment were taken from the area indicated with the arrow.

The cotton canvas and the primed linen canvas (Landseer) were both treated by brushing using 3 different nanocellulose treatments: CNF (in water), CNC (in water) and MC+CNC (in heptane). In addition, three other nanocellulose-based treatments were also tested on the cotton canvas: MC+CNC(w), Tylose50 (Tyl) and Tylose50+CNC (Tyl+CNC), all aqueous-based.

8.2.1.2 Sample preparation

During the experiment, both sides of the canvas samples were exposed to the humid environment generated in the sample cell (see more details in 8.2.1.3). The cotton samples were treated from both sides of the canvas, eliminating any errors that could result from the diffusion of moisture coming from the untreated side. For the Landseer primed linen sample, the treatments were applied on the canvas side only as the ground layer present on the opposite side acts as an appropriate barrier to moisture. The treatments were applied in order to reach a surface density of 30g/m^2. For the cotton canvas, this was only applied to one face. The other face presented a surface density in treatment of 15g/m^2. The samples studied by neutron radiography are listed in Table 8.1.

Canvas material	Canvas samples	Thickness (mm)	Solvent	RH-protocol
Cotton	CNC-treated cotton	0.895	water	1 cycle using 20-75%RH RH program
	Cotton degraded untreated	0.848	-	2 cycles using 20-75%RH RH program (i.e. 20-75-20%RH (60min-90min-60min), 4%RH/min)
	CNF-treated cotton	0.880	water	
	MC+CNC (h)-treated cotton	0.906	heptane	
Linen	Primed linen untreated	0.473	-	1 cycle at 20-75-20%RH (60min-90min-60min), 4%RH/min
	Primed linen CNF-treated	0.537	water	
	Primed linen (MC+CNC(h))-treated	0.492	water	

Table 8.1: List of the samples tested using the 20-75%RH program by neutron radiography. The samples were subjected from 1 to 2 RH cycles for neutron radiography. The justification for choosing 75 %RH as maximum RH level instead of 80%RH as used in Chapter 4 will be given later in this chapter (cf. 8.2.2.3).

8.2.1.3 Chamber design for experiment

This is the first time that a controlled RH experiment was performed at ISIS Neutron and Muon Beam, Harwell (UK) at the IMAT (Imaging and Materials Science & Engineering) beam-line. Studies on diffusion behaviour of water often favoured the use of liquid water since water vapour has a density 1000 times lower, hence 1000 times lower neutron attenuation coefficient, than the liquid phase. The standard set-up to study diffusion behaviour of water vapour in a material consists in dry cup/wet cup experiments. Diffusion of moisture in the longitudinal axis of the wood samples was, for example, studied that way by sealing one side of the sample to a recipient containing silica gel ("dry cup") or saturated salts ("wet cup") while the rest of the sample was exposed to the environment of a closed chamber (Mannes, 2009). The climate in the chamber was regulated with two basins filled with demineralised water or saturated salt solutions (depending on the desired humidity). A similar set-up using dry and wet cup and a chamber at 23°C and 50 ± 2%RH was later used by Hendrickx (2016) to study mock-ups of an easel oil painting.

The environment conditions in this type of experiment are therefore fixed and cannot be changed without having to stop the neutron beam, prematurely ending the experiment. This has the disadvantage of not enabling the measurement of important phases in the diffusion process such as the beginning in the starting phase of the diffusion. The use of RH-controlled chambers developed to address this problem and that can be controlled at distance is very recent, and a crucial development. Hendrickx (2017) and Mannes (2017) recently presented works in which climatic chamber connected to a remote RH controller had been used. The climatic chamber designed by Mannes (2017), in particular, allows the programming and remote control of the RH conditions inside the chamber in both static (fixed relative humidity RH) and dynamic mode (cycles in RH). It also included temperature control. This latter point is particularly important in diffusion studies as water diffusion and moisture content is greatly influenced by temperature. This was shown for example for plant fibres whose moisture content increases with temperature (Das, 2007). The same RH level will correspond to a low or high amount of water vapour at low temperature or high temperature, respectively.

To account for the small size of the samples tested, a custom made climatic chamber sample cell was built and connected to a Lacerta Technology RH controller (Figure 8.2) and a water bath. The sample cell designed in collaboration with and built at Lacerta Technology is shown in Figure 8.2a. It consists of a cylindrical chamber (1) in which a frame holding the sample in place can be inserted (2) (Figure 8.2b). The upper tube containing the sample as well as the frame that were exposed to the neutron beam were made from Grade 6082T2 of aluminium. It is important that a pure material is used in order to have minimal absorbance or scattering of the beam. The frame was welded to the cylinder lid so that the chamber can be hermetically closed for the accurate control of the RH in the chamber during the experiment. The chamber was connected via one cable to an RH sensor placed on top of the sample and chamber (3) and to the RH controller via one flexible cable placed at the bottom of the sample (4) which features on part of its length an insulation and a heating system to prevent condensation within the tube. There was always a constant flow of 0.6L/min through the cell. The RH sensor was calibrated using a

Mitchell Optical Humidity & Temperature Calibrator, based upon the chilled mirror principle. The RH controller was tuned to the specific requirements of the cell constructed for this experiment, in order to give optimal control, with minimal sag and overshoot. The temperature was controlled and maintain constant via water circulating inside a rectangular base (5) supporting the chamber cell which was connected via two cables (water inlet and outlet) (6) to a recirculating water bath.

The design was made as such that the water from the cooling system would not obstruct the path between the beam and the sample. Moreover, because of the sensitivity of electronics components to the neutron beam, the sensor which needed to be placed next to the sample in order to get a higher accuracy in the RH measurement, was protected using a cadmium cap ((1') in Figure 8.2b) and a second shield ((1'') in Figure 8.2c). Figure 8.2c and shows the complete set-up used during the neutron experiments.

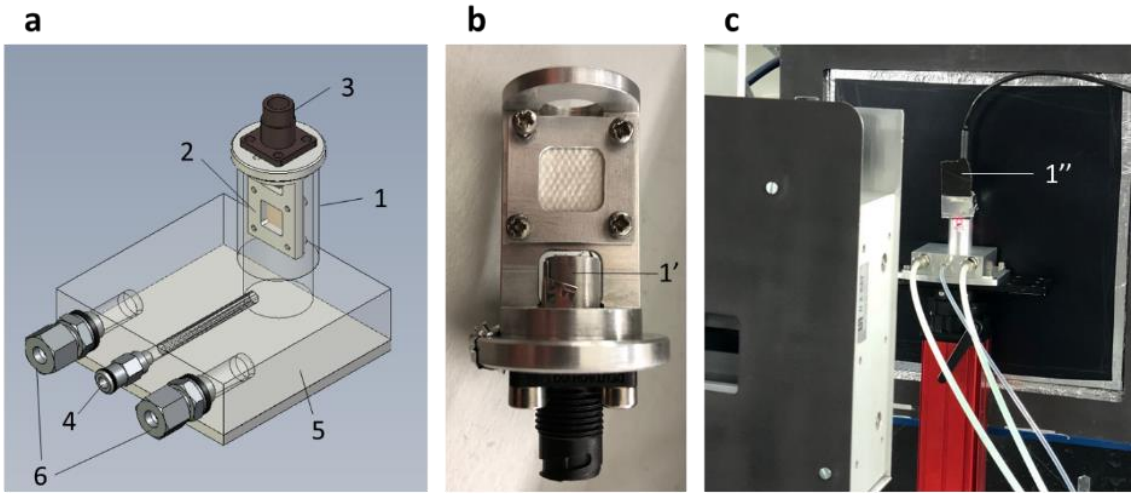

Figure 8.2: In (a), design of the sample cell (1) in which the sample holder (frame seen in (2)) is inserted. The sample is positioned so that the plane of its faces are orthogonal to the neutron beam axis. The sample cell is connected to an RH sensor (3), the RH controller (4) and a temperature control system (6) which enable the circulation of water in the base supporting the sample cell (5). In(b), sample holder showing the frame holding a cotton canvas and the RH sensor wrapped in a cadmium foil (1') in order to avoid the exposure of the electronics to the neutron beam. In (c), complete set-up during an experiment showing the second shield for the RH sensor (1").

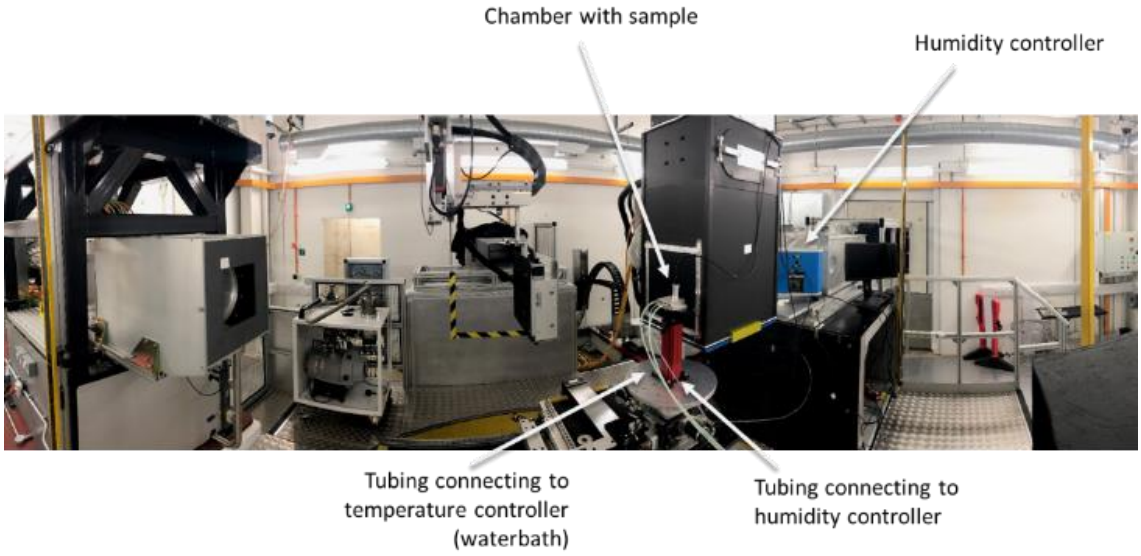

Figure 8.3: Overall view of experimental set-up with sample holder in front of the detector, RH controller, and tubing connecting the chamber to the RH-controller and to the water-bath (temperature control).

8.2.2 Methods

8.2.2.1 Neutron beam principles: basic principles

Principles

Neutron imaging, as well as X-ray imaging, is based on transmission interference. The degree at which an object within the beam path attenuates the incoming radiation (Figure 8.4) is observed and measured. The result is a shadow image of the object, which yields information on its inner structure and composition, due to the interactions between incoming beam and object. These interactions depend on the object or material elemental composition and density, and comprise of absorbance and scattering.

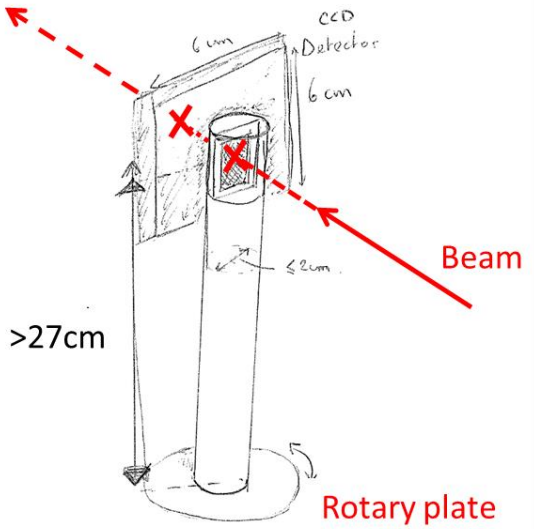

Figure 8.4: Simplified visualisation of the transmission measurement: the incident neutron beam with the intensity I0 is led on a sample with the thickness z. The transmitted beam with the intensity I is registered with a 2D-detector. The sample can be moved closer to the detector to increase the resolution. The detector is at a fixed position.

The atoms of different elements interact with the beam depends on the type of incident radiation. X-ray photons, for example, interact with the electrons of atomic shells, resulting in a strong correlation between the atomic number and the interaction probability. The larger the atomic number, the higher is the interaction probability given by the microscopic cross-section. Conversely, neutrons possess a completely different interaction pattern with matter. Being neutrally charged particles, they are unlikely to interact with electron shells of an atom. The interaction occurs with the atomic core itself and thus is not correlated with the atomic number. Instead, it shows a high interaction probability for some light elements, such as hydrogen while heavier elements, such as lead are practically transparent for neutrons.

The attenuation coefficient or macroscopic cross-section is a parameter that describes the degree to which a certain material attenuates a beam. The attenuation results from all interactions of the beam with an object, which includes scattering as well as absorbance. In a simplified first

order approach, a differentiation between both interaction types can be neglected. The transmitted mono-energetic beam with energy E can be described by the linear attenuation law:

$$I(E) = I_0 . e^{\Sigma z}$$

where I is the intensity of the transmitted beam, I_0 is the intensity of the incident beam, Σ is the neutron attenuation coefficient of the material and z is the specimen thickness. The linear attenuation law is valid under the assumptions that the beam is mono-energetic and that the thickness, z, tends towards 0.

The attenuation coefficient Σ comprises of the microscopic cross-section of an element σ, i.e. the interaction probability of an element with the radiation, and the atomic density, N, of this element. For pure specimens of only one element Σ is calculated as follows:

$$\Sigma = \sigma . N$$

For compound materials containing more than one element, the attenuation coefficients of the individual components can be summed up to give the total attenuation coefficient of the sample:

$$\Sigma = \sum_{i=1}^{n} \sigma_i . N_i$$

The measurement of neutron transmission through the sample allows in principle an absolute determination of the sum of cross–sections and densities of the sample:

$$T = \frac{I(E)}{I_0} = e^{\Sigma z}$$

This investigation was mainly concerned with the water content. The transmission coefficient was thus calculated by dividing the intensity of the intensity of each individual image of a series with the intensity from the empty chamber:

$$T = \frac{I_{wet}(E)}{I_{flat}(E)}$$

Experimental setup

The experiments were carried out at the ISIS Neutron and Muon Beam, Harwell (UK) with Genoveva Burca, principal scientist at the neutron imaging beam-line IMAT (Imaging and Materials Science & Engineering). The characteristics of the beam-line have been described by Burca (2013) and Kockelmann (Kockelmann, 2015). The chamber was positioned as close as possible from the neutron detector, which consisted of a scintillator-
CCD-camera-system with a field of view of 300x300 mm^2. The scintillator (zinc sulfide doped with lithium-6 as neutron absorbing agent thickness 100µm) converts the neutron signal into visible light, which is led via a mirror onto a cooled 16bit CCD camera (resolution: 1024 x 1024 pixels), which registers the signal. A pinhole diameter of 40mm in diameter was set and the distance between pinhole and detector was 10000mm leading to a pixel resolution of 59µm. The exposure time was 30s per image.

8.2.2.2 Dielectric analysis under controlled RH (DEA-RH)

A material which has a dipole activity can be subjected to dielectric technique to study its behaviour upon applied field at selected frequency. Dielectric Analysis measures the complex capacitance *C**.

$$C^* = C' - iC'' \quad (1.3)$$

From the complex capacitance *C**, the complex dielectric constant ε^* is then calculated. This consists of a real part ε' which is the dielectric permittivity under an AC field and an imaginary part ε'' which is the dielectric loss:

$$\varepsilon^* = \varepsilon' - i\varepsilon'' \quad (1.4)$$

Magnitude of dipoles and ease of orientation in an AC electric field is expressed by the dielectric permittivity (*ε'*) and contributions from conductive and dipole relaxations are denoted by dielectric loss factor (*ε''*). As such, dielectric permittivity (*ε'*) can also be expressed as follow:

$$\varepsilon' = {}^{C'}/_{C_0} \qquad (1.5)$$

where:

$$C_0 = {}^{\varepsilon_0 . A}/_{d} \qquad (1.6)$$

and A is the sample area and d its thickness.

The samples were measured at 5 different frequencies (0.3, 1, 3, 10, 30 kHz) here the results are only given for the permittivity measured at 1kHz as the trend of the response measured were independent of the frequency used. Prior to the measurement, canvas samples (10 mm x 10 mm) were pre-dried for at least 24 hours and mounted between parallel plates electrodes in the dielectric analyser (Lacerta Technology DS6000). Measurements were made under controlled RH programme at 25 °C. The untreated and 2-sides coated cotton canvases as well as the untreated and treated primed linen canvases were measured by dielectric analysis using the same RH program as used during the neutron radiography experiment.

8.2.2.3 RH program

The RH program closely followed the testing that had been performed previously using dynamic mechanical on the cotton samples (see 5.2.2.3 Chapter 5).

The samples were all pre-dried before measurement in a desiccator with silica gel. The boundary RH conditions of the experiment were set at a minimum of 20%RH and a maximum 75%RH. The samples were exposed to 1 to 2 RH cycles (neutron radiography) or 3 RH cycles (dielectric experiment) as described below:

- **RH cycles 20-75-20%RH** at 25°C. The humidity level was stabilised at 20%RH for 1 hour. RH was then increased at 4%RH/min to 75%RH and left at 75%RH for 90 min. RH was then decreased back to 20%RH at 4%RH/min and left at that RH level for 60 min. One to 3 consecutive RH cycles were applied depending of the samples or the technique used.

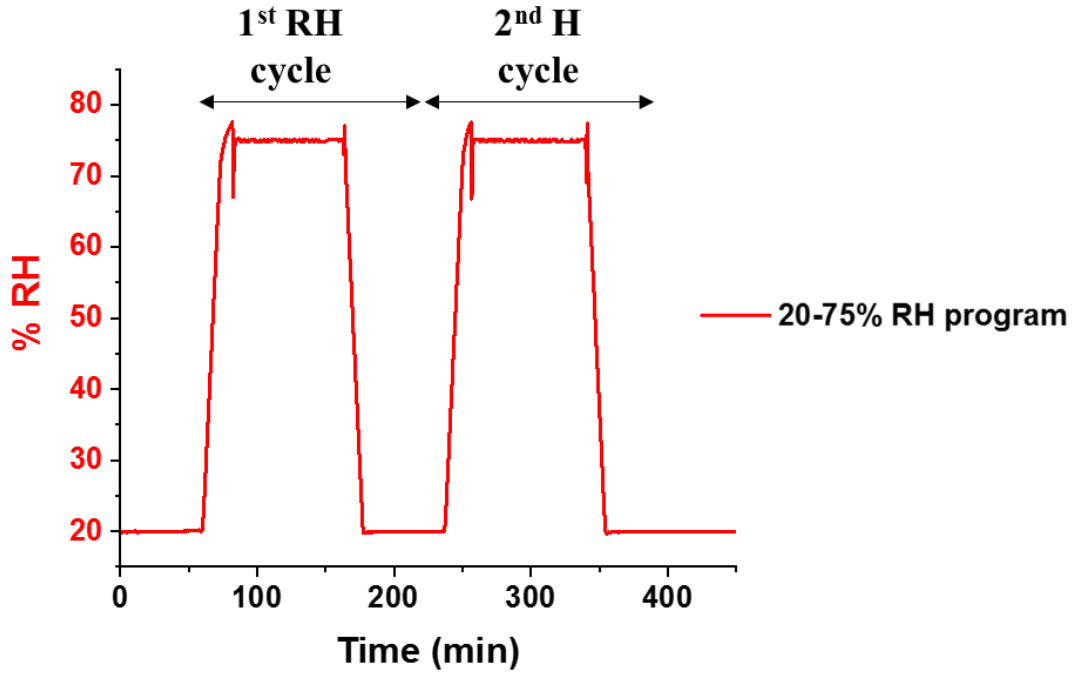

Figure 8.5: RH cycle 20-75-20%RH (4%RH/min, RH plateaus of 60min (20%RH) or 75min (75%RH)) used to study moisture sorption and desorption in canvas and historical primed canvas by neutron radiography.

For some samples, difficulties to stabilised the RH level at 75%RH were faced. At this RH level, rapid and important increases or losses in RH were measured. They were caused by the condensation forming in the tube connecting the RH controller and the sample cell. The important length of the tube, the uncontrolled temperature in the room of the measurement as well as the impossibility to heat up the tube on its all length (i.e. as for the DMA measurements), caused this condensation. Controlled temperature of the environment could eliminate such problems. Outliers in the RH program were not discarded and are shown later in the results. Their impact on the neutron images, however, is minimal. For all the samples presented in this part, these events led to intensity variations in the images which were negligible in comparison with the background

noise. However, for longer episodes during which the RH was not controlled, this led to visible variations in intensity (see Figure F.1 in Appendix 7.1).

8.2.2.4 Image analysis

The theory

Raw data provided by neutron area detectors (i.e. CCD, CMOS camera systems, Imaging plates, ...) were stored as 16bit grayscale TIFF image data. These images have to be converted into corrected radiographic transmission images. The images correction was carried out using ImageJ and a macro written specifically for our images and setup. The code is given in Appendix 7.2. The several corrections include applied are reviewed below:

a/ **Noise removal**

The outliers removal plugin with a threshold removes white and dark spots due to g-radiation or pixel failures from the radiographs. This option was preferred over the application of median filter (ref) as it preserved the features of the woven canvas such as the weaving pattern while efficiently removing the noise. The removal of outliers was performed choosing a radius of 2 and a threshold of 500. An example of a raw neutron image before correction and after the application of a median filter (radius 2) and after removal of outliers (chosen option) (see Appendix 7.1, Figure F.2).

b/ The intensity correction scales the measured radiograph so that the same neutron source flux is assumed for all radiographs of a series.

Neutron exposure normalization for a series of images was performed by deriving a scaling factor in an open beam region of interest i.e. a small image area beside the object under investigation. In this way, temporal variations in the neutron source intensity are taken into account. The area selected consists of an area on the frame used to clamp the sample and which does not include part of the sample as seen in Figure 8.6.

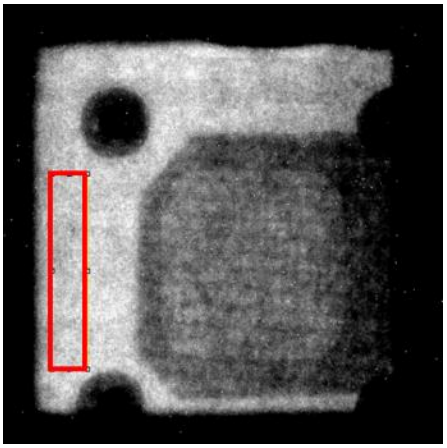

Figure 8.6: Raw image of the sample placed in the chamber with red rectangle indicating the area selected for intensity correction.

c/ **The dark image correction** consists in substracting the CCD camera dark current offset to radiograph. This correction removes the signal coming from the unexposed CCD and the Electronic Amplifiers (i.e.,).

d/ The **flat-field correction** divides the measured flux of a radiograph by the measured open beam flux yielding the transmission through the sample. Spatial variation of the illuminating neutron beam and scintillator in-homogeneity are thereby eliminated.

Additional backgrounds originating from neutron scattering in the sample or some kind of detector/sample environment backscattering were not considered and their removal not included in the corrections. This is because these corrections were only possible by performing additional measurements using of a special B4C grid (Boillat, 2018; Carminati, 2019) which was not available at IMAT at the time of the experiment.

The results of processed radiography data give transmission values (T) i.e. floating point values in the range [0-1]. From transmission values, absorbance values can also be easily calculated (i.e. A= 1-T). As described by Defraeye (2014), to derive quantitative information from transmission (or absorbance) values, the validity of the exponential law of radiation attenuation (aka Beer-Lambert law) is assumed. Thereby material composition e.g. a humidity content can be

calculated. In the framework of this study this was not performed due to the lack of time. The results presented consist in preliminary investigations.

Steps of image correction

Image corrections were applied using the ImageJ software as follow:

1/ Correction Image (background noise & dark image) following equation (8.1)

- Calculation of D(I_n) using an area beside the sample on the frame (see Figure 8.6).
- Subtraction of the dark image (I_{dark}) to the sample radiographic image (I_n)
- Division by correction factor D(I_n)-D(I_{dark}) to account for fluctuations in beam signal

$$I_{corr,n} = \frac{(I_n - I_{dark})}{D(I_n) - D(I_{dark})} \qquad (8.1)$$

Where:

I_n = Radiographic neutron image n of the series of images

I_{dark} = Dark image (neutron beam OFF)

$D(I_n)$ = Mean (grey) value in square (Figure 8.6a) for radiographic neutron image n

$D(I_{dark})$ = Mean (grey) value in square (Figure 8.6a) for mean of 60 radiographic neutron dark images

- Remove outliers (radius 2, threshold 50)

2/ Normalisation with flat image corrected $I_{corr,\,flat}$ following equation (8.2)

$$I_{norm,n} = \frac{I_{corr,n}}{I_{corr,flat}} \qquad (8.2)$$

Using:

$$I_{corr,flat} = \frac{(I_{flat} - I_{dark})}{D(I_{flat}) - D(I_{dark})} \qquad (8.3)$$

Where: I_{flat} = Image of the chamber without sample

8.2.2.5 Contact angle

Contact angle measurements were performed on untreated, the CNF-treated and the MC+CNC(h)-treated cotton canvases to measure the hygroscopic behaviour of the samples. Basic principles and protocol of measurement are given in Chapter 2 (cf. 2.2.3.1).

8.2.2.6 Absorption isotherms

The samples were conditioned at 12%RH using a saturated salt solution in $LiCl.H_2O$. They were then placed in vessels containing a saturated solution in KNO_3 used to fix the RH level at 95%RH. The samples were weighted using an electronic balance after 10, 20, 30, 40, 60, 130 and 180 min exposure to 95%RH to follow the weight increase and moisture uptake in the samples. For each category of sample (cotton or primed canvas, untreated or treated), several pieces were cut. Each time of exposure thus correspond to a new piece of sample placed in an individual container at 95%RH. This was done to avoid errors which could have occurred because of change in RH in the vessel when removing a sample.

8.3 Results

8.3.1 Intensity correction of the neutron images

This part aims to give a clear description of the impact of the corrections applied on a raw neutron radiographic image. Figure 8.7a shows the raw neutron radiographic image obtained for a CNC-treated cotton canvas place in the sample cell during a measurement.

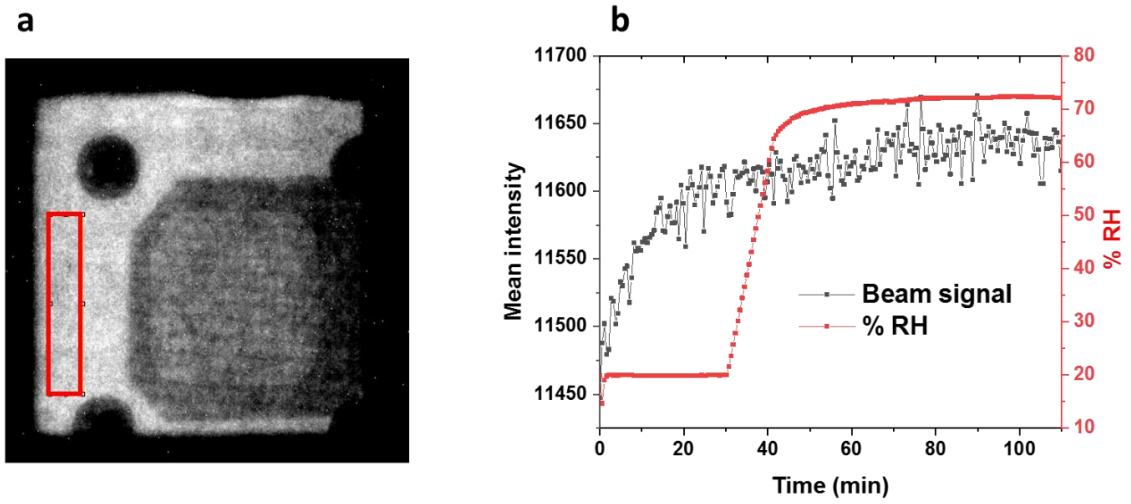

Figure 8.7: Beam signal over time as measured by calculating the mean intensity over time from an area beside the canvas sample (CNC-treated degraded cotton canvas), here chosen as the frame holding the sample. The mean intensity (hence beam signal) measured in the area indicated in (a) by the red rectangle is not stable with time (b). This is problematic as it interferes with the true response of the sample to moisture variations.

For this test, the RH program used consists of 30min at 20%RH followed by an increase in RH at 4%RH/min from 20%RH to 75%RH. The RH level was then maintained at 75%RH for 1h. As shown in Figure 8.7b, the intensity coming from the frame (mean measured in the red area shown in Figure 8.7a) is not constant over time. The mean intensity across the stack of images (n=205) increases logarithmically reaching stabilisation after 60 min of exposure. This same observation was made for all the measurement performed at the beginning of the measurements. Moreover, during the unexpected episodes when the beam was shut down for several minutes during the experiment, the same logarithmic increase in signal was observed on the images after the beam was turned on again. These variabilities in intensity were measured in an area which does not contain the sample or any material sensitive to moisture. The intensity measured in this area can safely be used to give a measure of the instability of the beam. This can also be seen as the increase in mean intensity is independent of the RH variations in the chamber as shown in Figure 8.7b in which the largest increase in intensity occurs at constant the RH level of 20%RH.

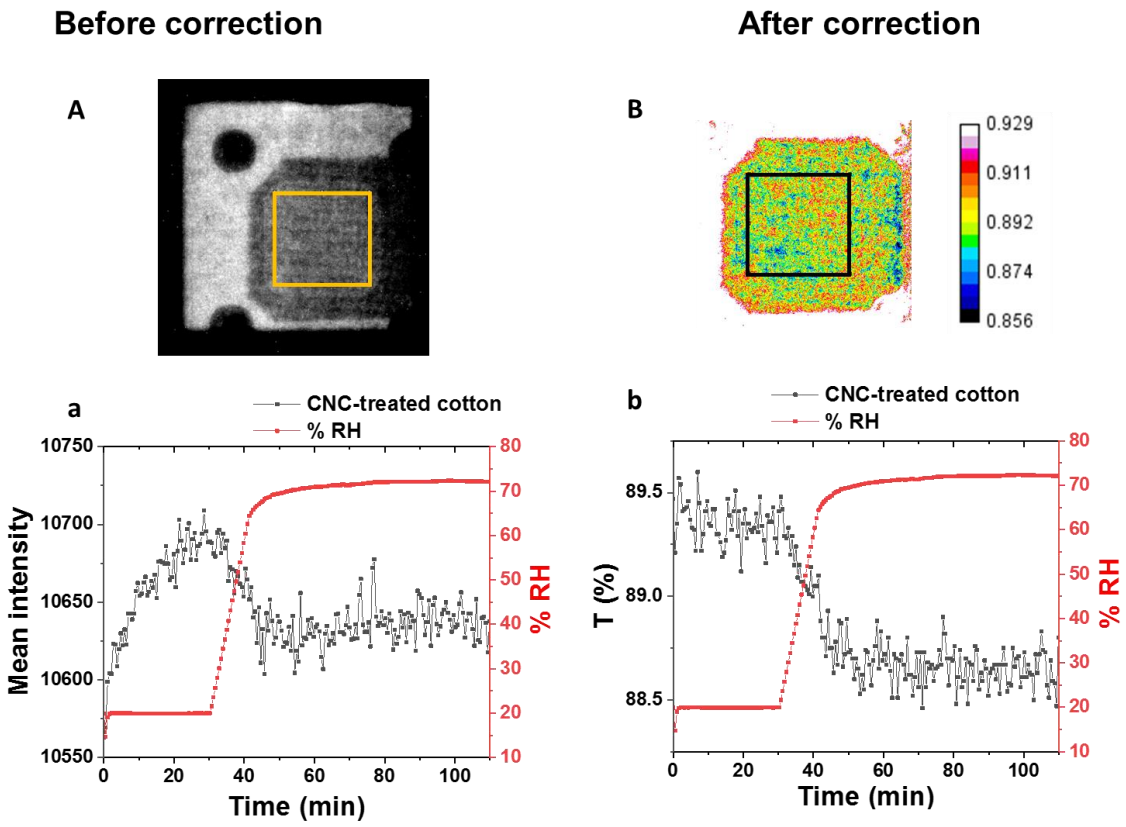

Figure 8.8: Neutron image of the CNC-treated cotton sample before (raw image) (A) and after (transmission image) (B) image corrections which include intensity, dark, flat corrections and removal of the noise. The sample was exposed to an environment at 20%RH (30 min) then increased to 75%RH (60min) at 4%RH/min. A selected area on the sample (yellow rectangle on the images) corresponding to an area directly exposed to the chamber environment was used to integrate the mean intensity (a) and percentage of transmission T(%) (b) measured for the raw images and corrected (or transmission) images (n=205), respectively.

Figure 8.8 shows the raw image of the CNC-treated cotton canvas before (A) and after (B) correction (dark, flat and reduction of the noise) as well as the signal measured in the selected area on the sample (yellow square) (Figure 8.8a and b). For the raw image, the signal measured corresponds to the mean of the intensity of the image (Figure 8.8a) while after correction, a transmission image is obtained and thus the mean percentage of transmission T(%) is given (Figure 8.8b).

As seen in Figure 8.8a, the instability of the beam intensity has a direct impact on the intensity measured on the sample. This is particularly visible for the first 30min of measurement.

The mean intensity measured in the sample area follows a similar logarithmic increase as the one previously measured on the frame (Figure 8.7b). The variations in beam intensity are problematic for the interpretation of the result as they interfere with the true response of the sample to moisture variations. The true response of the sample to moisture sorption/desorption can thus only be extracted if the acquired images are systematically corrected using a correction factor taking into account the beam instability.

After image correction and the use in particular of the correction factor $D(I_n)$-$D(I_{dark})$, the beginning of the curve, from 0 to 30min, is visibly modified. The transmission measured at 20%RH is linear and is characterised by a small decrease in T(%) which could result from moisture sorption by the sample which had been previously dried up at a possibly lower RH level than 20%RH using silica gel.

An area beside the cotton sample was also measured to check the correction as well as to verify that the results were not modified by the variations in moisture level in the chamber. The results gave a linear and flat transmission line which accounts for the efficiency of the correction. Details on the area selected and results are given in Appendix F (Figure F.3).

The last step of the image correction consists in averaging consecutive images of the series of images. This step aims at increasing the signal to noise ratio of the images. The stack of n=205 images was average so that 4 consecutive transmission images were averaged. This led to a new stack of n=202 images whose 1st image corresponds to the average of the 4 first images of the original stack of images.

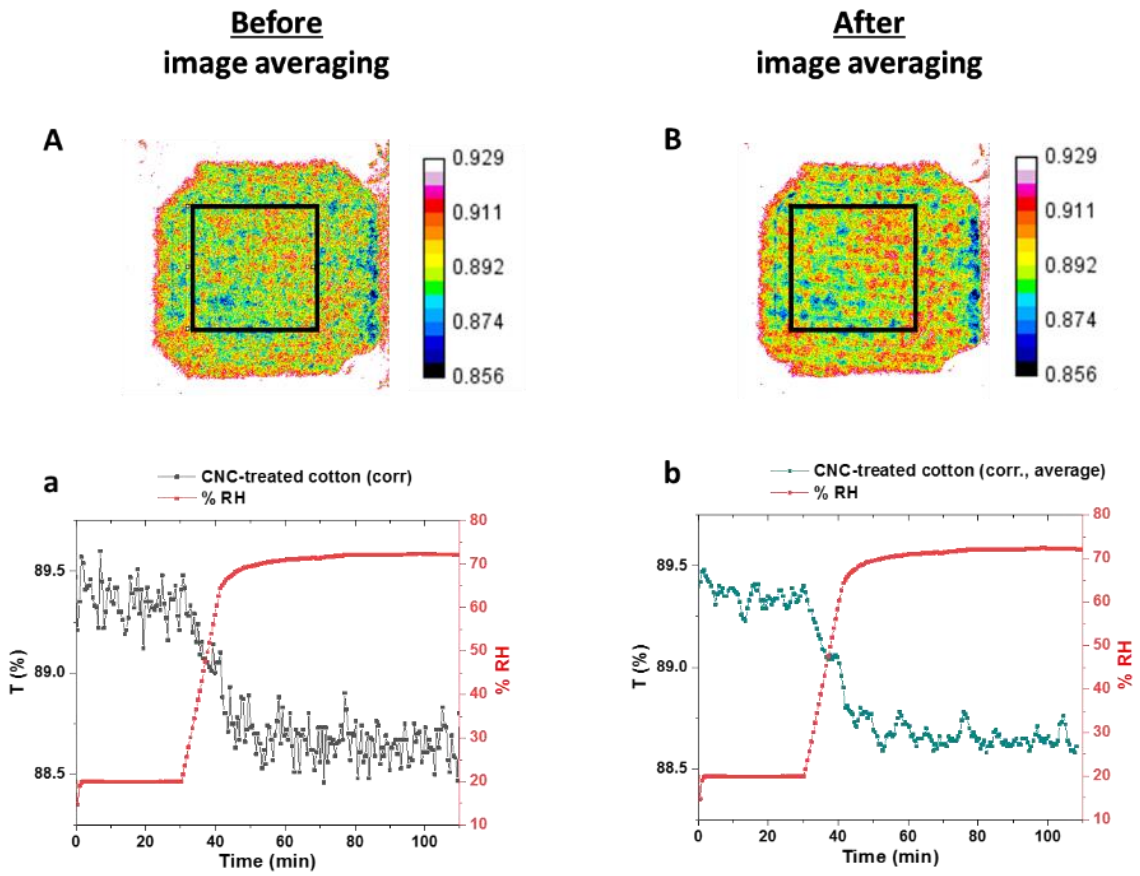

Figure 8.9: Corrected neutron image of the CNC-treated cotton sample, as seen in Figure 8.8B, before (A) and after (B) averaging (4 images averaged). A selected area on the sample (yellow rectangle on the images) corresponding to an area directly exposed to the chamber environment was used to calculate the mean percentage of transmission T(%) (a) and the average in mean of T(%) for 4 successive images (b) measured for the corrected images before and after averaging, respectively. The transmission was integrated over the region shown in A and B (black square).

Figure 8.9A and B show the 1st image of the stack of transmitted neutron images of the CNF-treated cotton taken before (A) and after (B) averaging. As seen in Figure 8.9a and b, the final averaging step leads to a reduction in noise in the curve showing the variation in T(%) for the sample over time. Simultaneously, averaging preserves the global response of the sample to moisture sorption in particular during the rapid 20-75%RH transition (i.e. 30-40min).

After multiple corrections applied on the neutron raw images, transmitted neutron radiographic images are obtained. Time-dependent neutron imaging informs both on the distribution of moisture across the canvas samples as well as the dynamic of moisture diffusion

in the sample (e.g. rate of moisture sorption/desorption). As seen in Figure 8.10, T(%) of the CNC-treated cotton canvas and the RH program applied during the images acquisition are given against time. After 30 mins, there is rapid ingress of moisture in the canvas as RH increases at 4%/min from 20 to 75%RH. This is seen in Figure 8.10a as a decrease in T(%) resulting from the higher absorbance of the neutron beam by the sample due to the presence of absorbed water. This is also observed Figure 8.10b as by the darkening (blue, back area) of the image at 37mins which is associated with lower transmission T(%) (i.e. higher absorbance A(%)=1-T(%)) of the beam. The intensity of this darkening increases in the images after 44mins and 60mins.

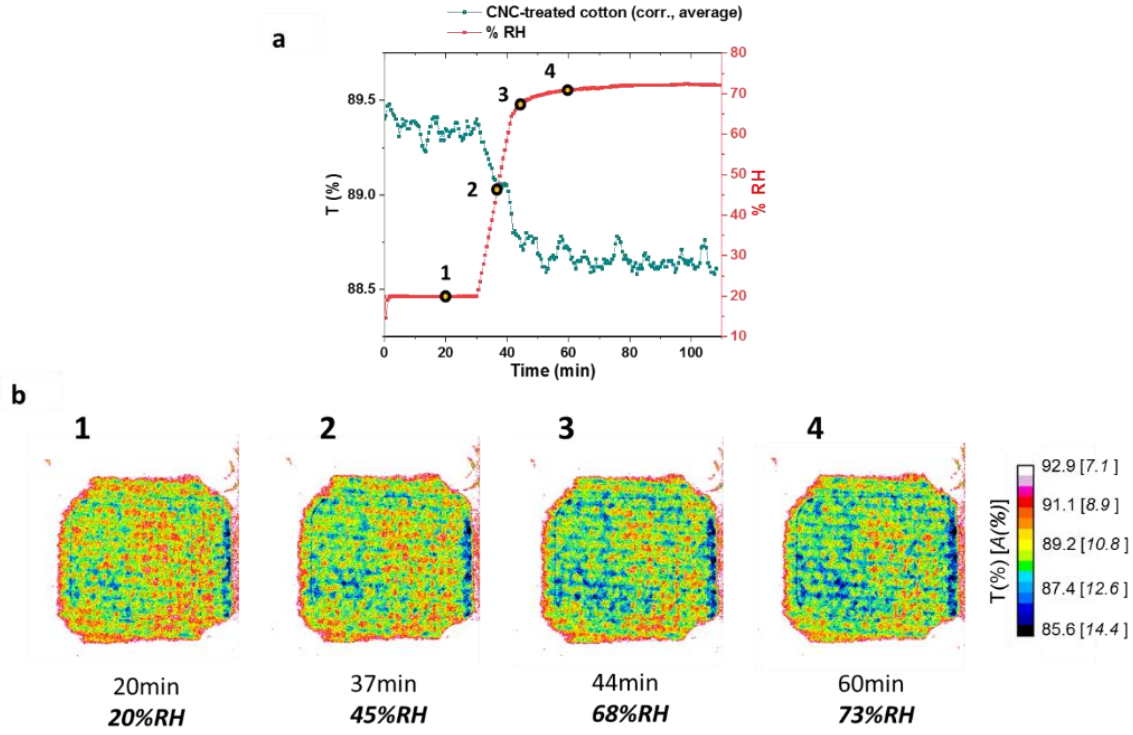

Figure 8.10: (a) Measured percentage transmission integrated over a region previously shown in Figure 8.8a and b for a CNC-treated cotton canvas. (b) Four average transmission radiographic images corresponding to different exposure times and RH levels highlight the dynamic of moisture sorption (20-75%RH) in the canvas sample. Blue to red areas on the images indicate areas with lower transmission T(%) (i.e. higher absorbance A(%) and moisture content) and higher transmission (lower absorbance A(%) and moisture content), respectively.

In terms of moisture distribution, the resolution of the images in Figure 8.10b does not seem high enough to draw substantial conclusions. The area of the canvas which was exposed to

the RH-controlled environment appears to absorb more moisture than the areas clamped between the two plates of the frame. Interestingly, the weft threads which are the horizontal lines on the picture are well defined on the transmission image. At high RH, blue (i.e. high absorbance area) horizontal lines are clearly visible. This is not seen in the warp direction (vertical lines) for which the alignment of the threads is not clear. This difference in the images could indicate a difference in moisture absorption between warp and weft threads. This could also indicate that absorbed water propagation is easier along the weft threads than the warp which would explain why the blue lines spread over the width of the sample and are not only restricted to the exposed area of the canvas.

Subsequently, an attempt to do another normalisation for which neutron images were normalised over the 1st image of the series was also performed. This resulted in different outcomes. Normalised images for the untreated, CNF-treated and MC+CNC(h)-treated cotton canvases is given in Figure 8.11. This normalization enables the removal of the weaving pattern from the images and, as a result, shows the signal coming from the water only. As seen in Figure 8.11, the fact that the weft threads are no more distinguishable on all the normalised images of the series indicate that these threads might not be absorbing/desorbing more moisture than other areas across the canvas. This should, however, be followed up in another study as a higher resolution in the neutron images might have provided more insights into the processes of diffusion of water into canvases and possible the role of each direction in this diffusion.

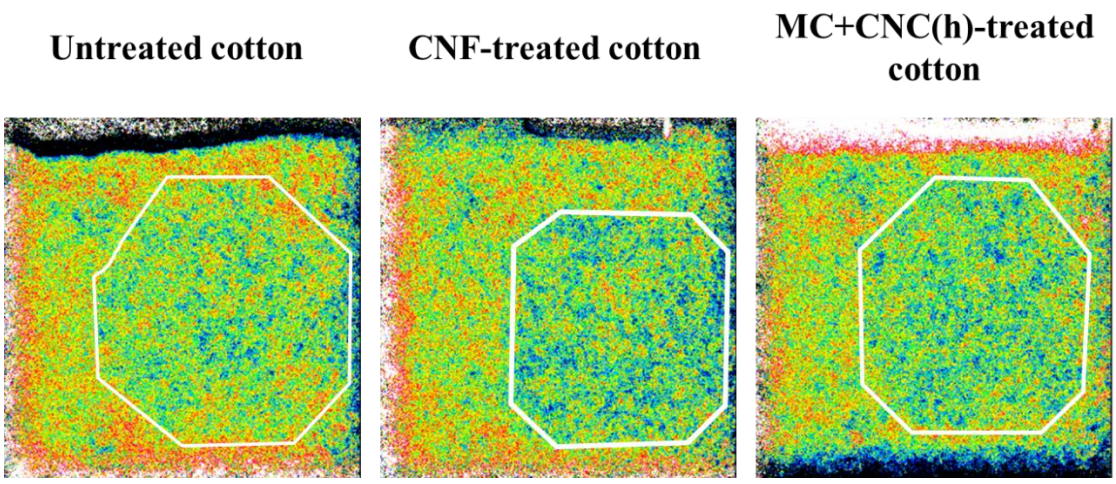

Figure 8.11: Absorbance images after normalization performed over the dry state (i.e. first image of the series measured at 20%RH) (and not the flat image). The contours of the untreated (left), CNF-treated (centre) and MC+CNC(h)-treated (right) cotton samples is indicated by the white line.

The results of the neutron experiment performed on the CNC-treated sample also indicates that the response of the sample to the RH increase is almost immediate and that neutron radiography is sensitive enough to pick up for the change in moisture content in the canvas (also seen for a CNF-treated cotton in Figure F.1 in Appendix 7.1).

Overall, the successive corrections steps applied on the raw neutron images and summarized below in Figure 8.12 have shown to enable the time-dependent study of moisture sorption/desorption in canvas sample (here shown for a CNC-treated degraded cotton canvas).

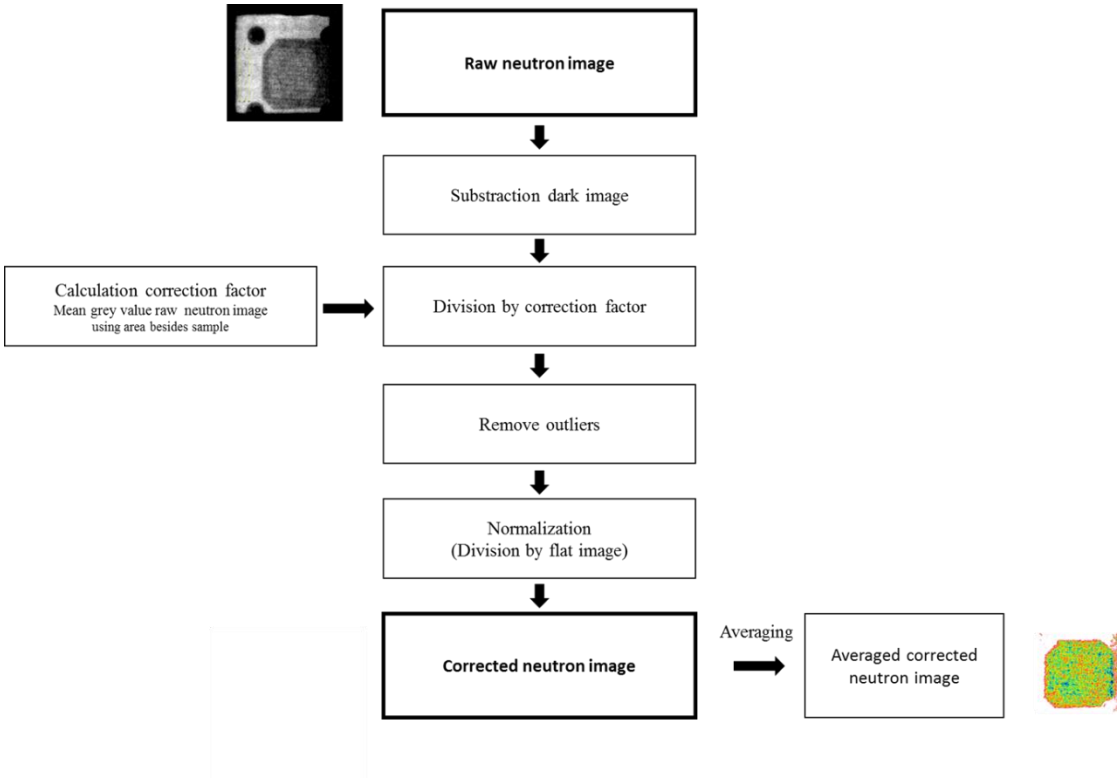

Figure 8.12: Flowchart summarizing the different steps of correction applied on the raw neutron images to obtained the final corrected averaged neutron images which correspond to transmission/absorbance images. These corrections, as described here, were applied on all the neutron images obtained in the frame of this study.

The potential of neutron radiography to explore the time-dependent dynamics of moisture sorption and desorption was thus further used to compare the cotton canvas with a sized and primed linen canvas and how the impact of the treatments on this latter might differ from what had been seen on the cotton canvas. The samples response to moisture variations and the nanocellulose-based treatments impact on their hygroscopic behaviour response were evaluated. All the neutron images obtained in the frame of this study were corrected following the steps in Figure 8.12.

8.3.2 A comparison of the responses to moisture variations measured for the canvas samples before and after treatment.

8.3.2.1 Cotton samples

Hygroscopic behaviour

Neutron radiographic images of an untreated cotton canvas (degraded), a CNF-treated and a MC+CNC(h)-treated cotton canvases were taken while exposing the samples to variations going from 20 to 75%RH (20-75%RH program, 2 RH cycles).

The images were analysed following the steps previously given in part 8.2.2.4. For clarity, the percentage of absorbance (A(%)=100-T(%)) measured on the sample will be given instead of the percentage of transmission T(%).

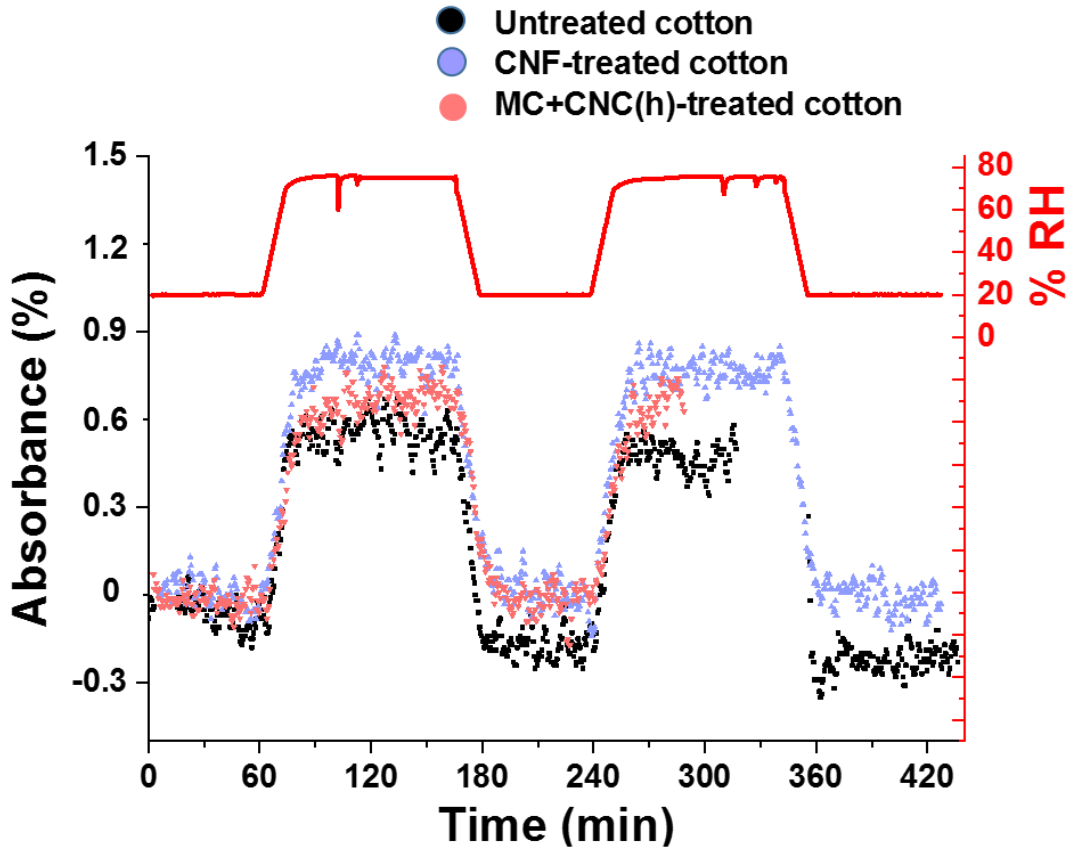

Figure 8.13: Mean percentage in absorbance measured by neutron radiography for an untreated and a CNF-treated and MC+CNC(h)-treated degraded cotton canvas. The mean values were integrated over a region directly exposed to the RH-controlled environment of the sample cell (yellow square previously shown in Figure 8.8a and b).

Figure 8.13 shows the absorbance measured on the untreated and treated canvas samples (area directly exposed to the chamber environment) under the 20-75%RH program. The absorbances measured for all the samples were normalised to 0% at the end of the first 20%RH plateau. As seen in Figure 8.13, the treatments (CNF and MC+CNC(h)) seem to increase the

absorbance of moisture by the canvas sample. An increase in absorbance from 0.59% for the untreated to 0.69% and 0.75% was measure for the MC+CNC(h) and CNF-treated samples, respectively, at 75%RH (end-plateau value) after the first humidification step (Table 8.2). Higher percentage in absorbance $A_{75\%RH}$ at 75%RH were measured again for the treated samples in comparison with the untreated canvas at 75%RH for the second cycle.

RH cycle	**1st RH cycle**			**2nd RH cycle**		
Samples	$A_{75\%RH}$	$A_{20\%RH}$	$\Delta A_{dehumidification}$ (i.e.75-20%RH)	$A_{75\%RH}$	$A_{20\%RH}$	$\Delta A_{dehumidification}$ (i.e.75-20%RH)
Untreated cotton	0.59	-0.16	0.74	0.56	-0.17	0.73
CNF-treated cotton	0.75	-0.14	0.89	0.75	-0.03	0.79
MC+CNC(h)-treated cotton	0.69	0.05	0.64	0.68	-	

Table 8.2: Values in absorbance (A), end-plateau values average of 5, measured at 20 ($A_{20\%RH}$) and 75%RH ($A_{75\%RH}$) for the 2 RH cycles applied (cf. RH cycles as indicated in Figure 8.5) for the untreated and the CNF- and MC+CNC(h)-treated degraded cotton canvas samples. Differences in absorbance ΔA were also calculated between $A_{75\%RH}$ and $A_{20\%RH}$ for each RH cycle.

Table 8.2 also shows that the highest difference $\Delta A_{\text{dehumidification}}$ or ΔA in absorbance measured during dehumidification (75-20%RH), hence in water desorption, was measured for the CNF-treated cotton canvas (ΔA=0.89% for 1st RH cycle) and then for the untreated cotton canvas (ΔA=0.74% for 1st RH cycle), whereas the difference is far lower for the MC+CNC(h) sample (i.e. ΔA=0.64%). These initial results indicate that the high responsiveness induce by the CNF treatment of the CNF-treated sample to variations in RH. It also shows the lower water desorption rate of the MC+CNC(h)-treated cotton canvas. The MC+CNC(h) increases the moisture uptake of the cotton canvas at high RH (i.e. 75%RH) but appears to slow down water desorption.

Dielectric analysis with controlled humidity at 25°C was also used to evaluate susceptibility of sample to moisture uptake. The measurements were performed in the kilohertz region (kHz) as it has shown to be suitable to compare differentiate hygroscopic materials such

as hydroxypropylcellulose from more hydrophobic materials (Sagharlou, 2015). The relative permittivity ε' (measured at 1kHz) of the samples subjected to the same variations in RH (i.e. 20-75%RH) as used during the neutron experiment was measured as it gives a measure of the water absorbed in the sample.

The variations in relative permittivities ε' (1kHz) (i.e. $\Delta\varepsilon'_{75\text{-}20\%RH}$) measured between 75 and 20%RH of the same RH cycle are given in Figure 8.14.

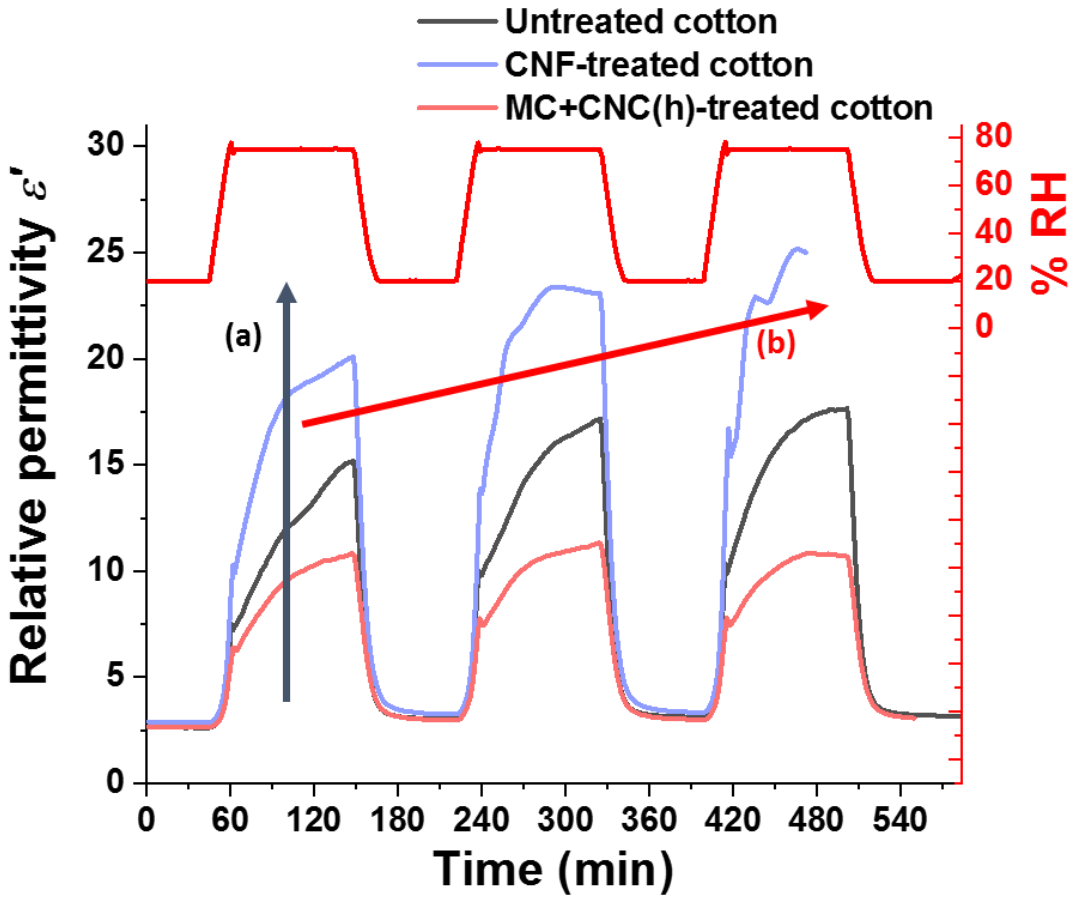

Figure 8.14: Results of the dielectric analysis performed the untreated and treated degraded cotton canvas showing variations in relative permittivity ε‘ measured at 1kHz. The samples were subjected to the same RH program (i.e. 20-75%RH, 4%RH/min) as for the neutron radiography experiment. The graph shows the higher hygroscopic response of the CNF over the untreated canvas whereas MC+CNC(h) shows the lower response to increase in RH (a). A steady increase in relative permittivity ε‘ upon RH cycling was also seen for the untreated degraded cotton canvas and in particularly for the CNF-treated cotton(b).

In Figure 8.14, the relative permittivity ε' (measured at 1kHz) increases at high RH level, i.e. 75%RH, for all the canvas samples. This was expected due to the high relative permittivity of water, i.e. 80.36F.m^{-1} at 20ºC (Sears, 1982). Interestingly, the response measured for all the samples is reversible. At each 20%RH isotherms, the relative permittivity ε' measured for all the samples return to its initial value measured at 20%RH for the first RH plateau. The CNF treatment also shows to increase the response of the canvas to moisture as seen by the higher permittivity measured at 75%RH for the CNF-treated canvas (i.e. 20F.m^{-1}) than for the untreated canvas (15F.m^{-1}). Interestingly, the results of dielectric measurements regarding the MC+CNC(h)-treated sample slightly differ from those obtained by neutron radiography. Among the 3 canvas samples, the lower increase in ε' is measured for the MC+CNC(h)-treated cotton canvas. For this sample, a difference $\Delta\varepsilon'$ in permittivity between dry (20%RH) and wet (75%RH) state of 10F.m^{-1} was measured whereas $\Delta\varepsilon'$ of 15 and 20F.m^{-1} were obtained for the untreated and CNF-treated samples. If the dielectric measurements confirm the higher hygroscopic response of the CNF-treated canvas over the untreated canvas measured by neutron radiography, they also indicate that MC+CNC(h)-treated cotton sample would be less hygroscopic than the untreated and CNF-treated cotton samples. The results seem, first, in contradiction with the results obtained by neutron radiography which had shown that the MC-CNC(h)-treated cotton canvas registered a higher moisture uptake upon humidification (1st, and 2nd RH cycle) (Table 8.2) than the untreated sample. However, it seems to agree with the lower response obtained for the MC+CNC(h) upon dehumidification also by neutron radiography.

It was indeed expected that the MC+CNC(h) treatment would show a more hydrophobic response to moisture sorption/desorption. This is because the MC+CNC(h) composite used in this study correspond to a silylated MC+CNC compound whose silylation enables it to be dissolve in an apolar solvent, here heptane, and makes it at the same time more hydrophobic (more detailed explanation given in paragraph 2.1.2.2 in Chapter 2).

Therefore, the heptane-based treatment MC+CNC(h) was expected to show an increased level of hydrophobic behaviour when compared to the untreated and CNF-treated samples.

Contact angle (CA) measurement and the calculation of weight uptake by DVS or under long-term exposure to humid environment (95%RH) of the 3 different samples were performed to confirm this assumption.

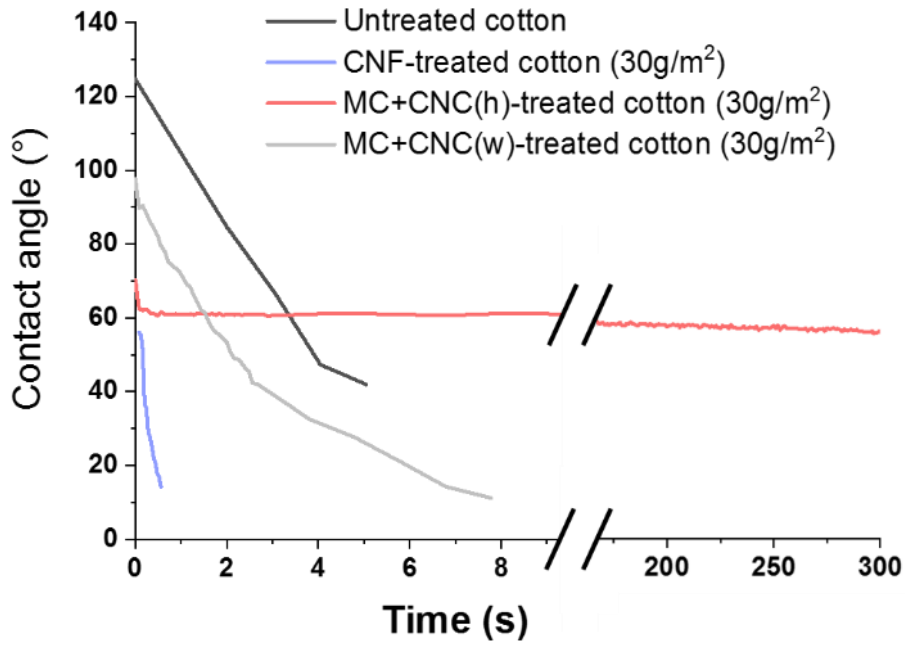

Figure 8.15: Contact angle of the untreated and of 3 treated samples, CNF, MC+CNC(h) as well as MC+CNC(w)-treated degraded cotton canvases.

Figure 8.15 shows the contact angle measured on the untreated, the CNF-treated and the MC+CNC(h)-treated cotton canvases. The water-based MC+CNC(w)-treated canvas is also given for comparison. As can be seen, the contact angle measured for the untreated, the CNF and the MC+CNC(w) sample rapidly decrease and the water droplet is absorbed after only 5, 0.6 and 1s, for each sample respectively. The MC+CNC(h)-treated cotton sample, on the contrary, clearly differs from the other samples. CA remains stable around 60° over a long period, greater than 300s. At the end of the experiment, the water droplet had not yet been absorbed by the treated surface.

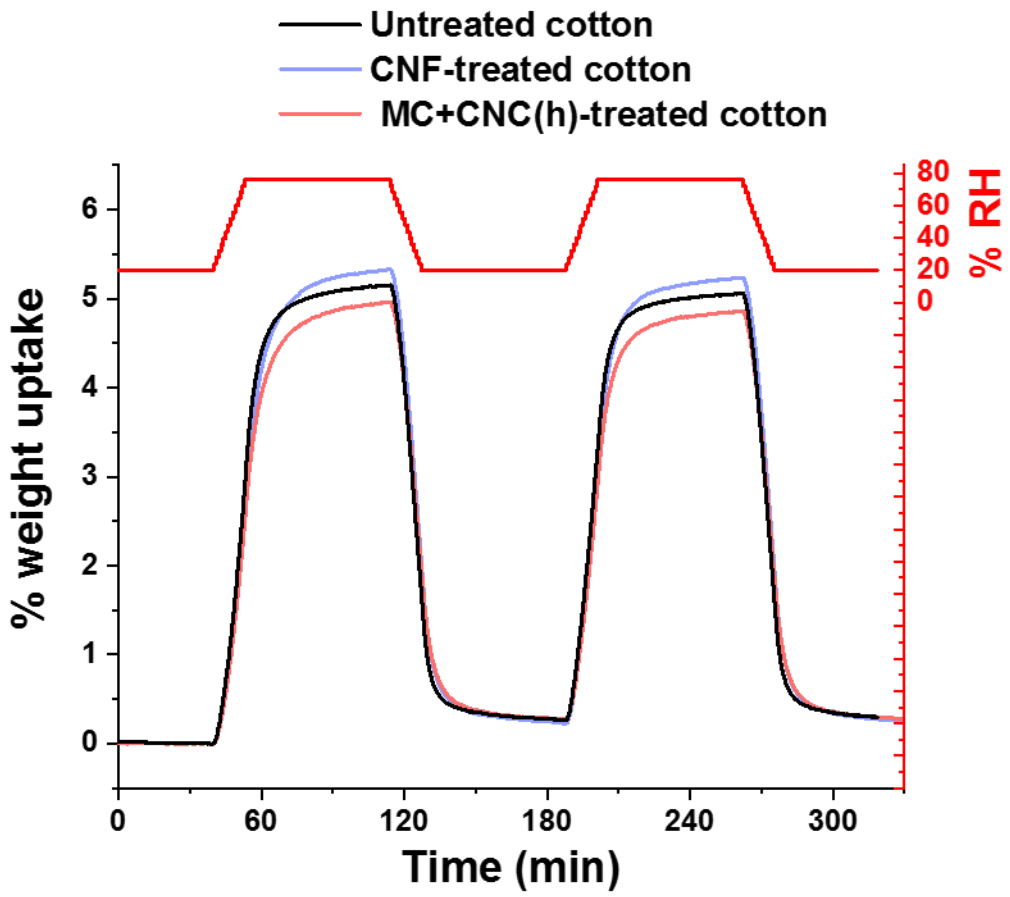

Figure 8.16: Percentage in weight increase measured for an untreated, a CNF-treated and MC+CNC(h) treated degraded cotton canvas subjected to 20-75-20%RH cycling (4%RH/min, 60min RH plateaus). The treated samples were treated from both sides one at 30g/m^2 and the other at 15g/m^2. Samples had been previously dried for 24h with silica gel.

The weight uptake resulting from moisture sorption was also measured by DVS for the 3 untreated/treated cotton samples exposed to a similar RH program than used during the neutron radiography experiment. The results of the DVS measurements shown in Figure 8.16 confirm the hygroscopic responses measured previously by DEA. They indicate the higher hygroscopic response of the CNF-treated cotton canvas over the untreated and MC+CNC(h) samples. The CNF-treated cotton canvas is seen as the most hygroscopic, followed by the untreated and MC+CNC(h) samples. A weight uptake of 5.22±0.08%, 5.10±0.07% and 4.91±0.07% were measured at 75%RH (2nd RH cycle) for the CNF, untreated and MC+CNC(h) samples, respectively.

Two hypotheses could be here formulated to explain the discrepancy in the results and in particular the unexpected response of the MC+CNC(h) sample under neutron radiography:

1/ The moisture has adsorbed on to canvas surface forming micro droplets but has not penetrated and diffused within the canvas. The samples investigated by neutron radiography were measured in-plane (i.e. neutron beam orthogonal to the plane of the sample). The resulting image thus consists of a projection of all the elements that the neutron beam went through in the thickness of the sample. As for X-rays, the resulting image is a 2D projection of a 3D object. Therefore, differentiation between the response to moisture between the sample surface and the bulk cannot be made. Neutron images do not show the true moisture content of the overall canvas to moisture but a mean of the absorbance of the different layers the beam went through (i.e. in this particular case: the canvas and the treatment).

2/ Water vapour has diffused inside the canvas from the edges of the sample, along the threads. This might have occurred despite the canvas edges, which are pressed under the frame plates, being greatly isolated from the sample cell environment.

In both cases, the differences in the results might result from the inhomogeneous diffusion of moisture in the MC+CNC(h) sample. This could originate from both the lower hygroscopic behaviour of the hydrophobic MC+CNC(h) treatment as well as its behaviour in terms of surface deposition. As previously highlighted in Chapter 7 (cf. 7.3.1.1), its surface deposition is characterised by the low penetration of the material into the canvas (Figure 8.17). The treatment is seen as a superficial layer sitting on the canvas surface on the side where it was applied.

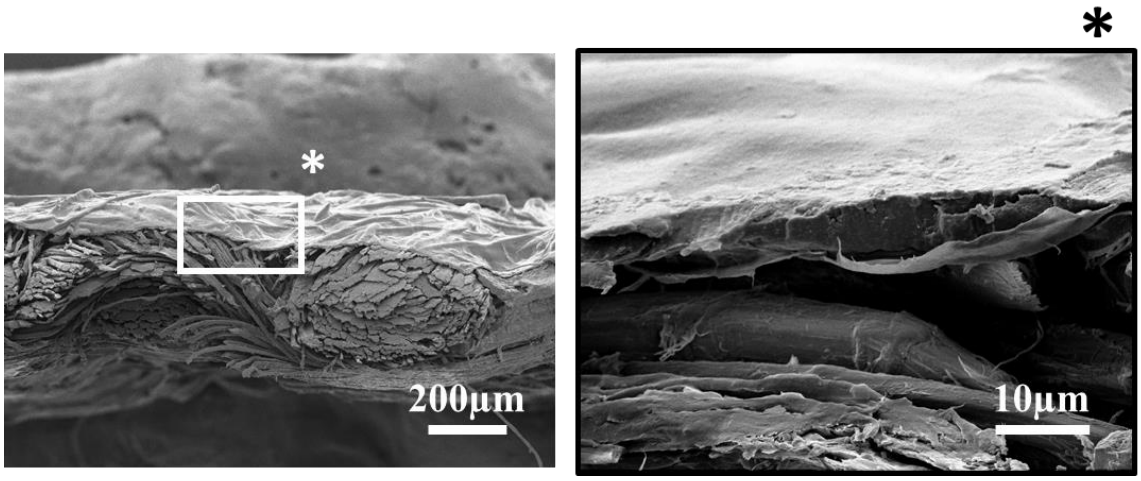

Figure 8.17: SEM images of a MC+CNC(h)-treated linen canvas showing the surface deposition of the treatment. A coating is formed on the canvas surface indicated by (*) and the treatment does not seem to penetrate further into the canvas.

By dielectric analysis (DEA), a lower signal for the hydrophobic MC+CNC(h) was predicted to be measured. This is because the layer of treatment acts as a protective barrier or resistance to the measure of capacitance between the two plates of the DEA (cf. **Error! Reference ource not found.**). In contrast, neutron radiography does not enable to make a distinction between the moisture absorbed by the canvas or adsorbed on its surface and any layer of the sample which contains water (e.g. canvas) will overlap the signal from others, possibly dried, layers (e.g. treatment).

Moisture mapping

Figure 8.18 shows the mapping of the absorbance measured across the untreated and the CNF- and MC+CNC(h) treated cotton canvases at the end of the 1st 20%RH and 75%RH plateaus and of the 2nd 20%RH plateaus (i.e. equilibration at the corresponding RH level for 60, 90 and 60min, respectively). The highest level of absorbance is mainly localised in the area of the sample exposed to the chamber cell environment (i.e. square opening with round edges in the frame). From the images, it can thus be assumed that for the cotton samples, the frame offers a protection against moisture diffusion.

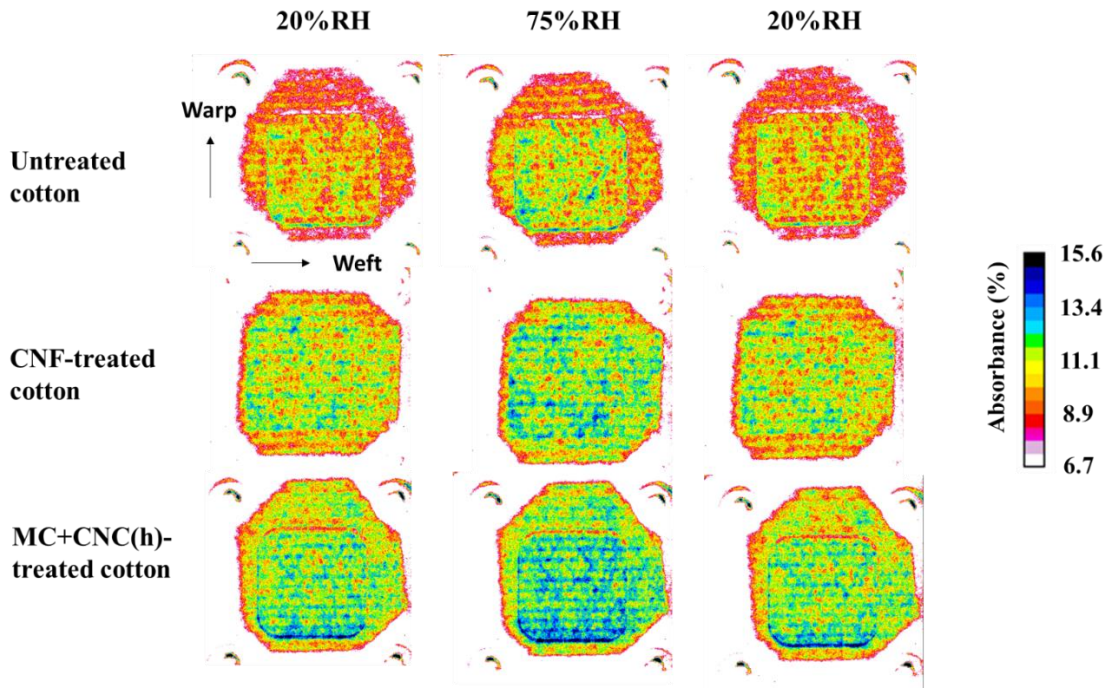

Figure 8.18: Neutron radiographic images of an untreated and a CNF- and MC+CNC(h)-treated degraded cotton canvases after corrections (see corrections steps in 8.2.2.4). These images give the mapping of the neutron beam absorbance by the samples during a 20-75-20%RH cycle (end plateau values, i.e. after 60min at 20%RH and after 90min at 75%RH). The samples were all orientated the same way (weft=horizontal, warp=vertical).

Moreover, at 20%RH, the higher absorbance was measured for the treated than for the untreated samples. This is indicated by the important number of areas at 12% of absorbance (green areas) for the CNF- and MC+CNC(h) samples than for the untreated sample for which bigger areas at 8.5% in absorbance (red areas) are seen. The images agree with the weight uptake data shown previously in Figure 8.13 where MC+CNC(h) shows a high response to moisture uptake. However, these differences might only result from the higher thickness of the treated samples due to the treatment layer(s) (see Table 8.1). The evaluation whether the treated samples could have a higher moisture content than the untreated canvas even at low RH levels would require prior calibration using samples with a known amount of absorbed water (Boon, 2015) or absorption of different water layer thickness (Kang, 2013). In a study by Boon, for example, on time-resolved moisture sorption in paintings, the total attenuating water thickness, hence the layer of water

absorbed by the material, was calculated using as calibration the weight uptake measured in the sample in laboratory experiments.

Kinetics in moisture sorption

Another important aspect of the study of moisture diffusion is time-dependency. As it will be shown the hygroscopic response of the canvas samples to moisture variations can differ in the long and short term. Over the long term, the repetitive exposure to rapid RH cycles does not let enough time for some cotton samples to reach equilibrium in moisture content. This can be seen for example for the treated CNF-treated cotton canvas and, to a lower extent, for the untreated sample previously measured by dielectric analysis (Figure 8.13B and again in Figure 8.19). The relative permittivity ε' (1kHz) measured at 75%RH for each sample over the 3 RH cycles is given below in the table in Figure 8.19. As seen it can be seen, the permittivity ε' measured for these samples at 75%RH keeps increasing with the successive RH cycles from 20.2, to 22.9, to 25.1F.m^{-1} for the CNF-treated sample and from 15.0 to 17.0, to 17.4F.m^{1} for the untreated sample measured at the end 75%RH plateau of the 1st, 2nd and 3rd cycle, respectively. Whereas for the MC+CNC(h)-treated canvas, ε' measured at 75%RH remains constant around 0.7±0.3F. m^{-1} across the cycles. This trend was not observed by neutron radiography but this could be due to differences in the clamping systems. Under dielectric analysis, the sample is pressed between two metallic plates; in neutron radiography, the measured area of the sample was directly exposed to moisture. In the latter configuration, the sample can absorb moisture and, as a consequence, can reach equilibrium faster than in the dielectric analysis configuration in which moisture can only diffuse from the sample edges.

	Relative permittivity ε' (at 75% RH)		
Samples	1st RH cycle	2nd RH cycle	3rd RH cycle
Untreated cotton	15.0	17.0	17.4
CNF-treated cotton	20.2	22.9	25.1
MC+CNC(h)-treated cotton	10.6	11.2	10.6

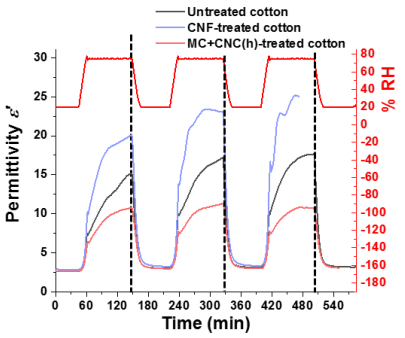

Figure 8.19: Values in dielectric relative permittivity ε' (1kHz) measured for the untreated, CNF-treated and MC+CNC(h)-treated degraded cotton canvas at 75%RH over the 3 RH cycles of 20-75%RH RH program (on the left). Note the increase in ε' measured over the cycles for the untreated and the CNF-treated samples. These values are calculated from the dielectric response of the 3 samples to the 3 RH cycles, shown on the right (black dotted lines) as already presented in Figure 8.13B.

Over the short term, the time-dependent response of the canvas samples to moisture can be seen both by dielectric and neutron radiography. In Figure 8.13A, after reaching RH equilibrium at 75%RH, the absorbance measured for the treated sample (CNF and MC+CNC(h)) still follow an increase before reaching equilibrium after 6 min and more than 15min for the CNF and MC+CNC(h) treated samples, respectively. By dielectric analysis, equilibrium in *ε'*, or moisture content, is not reached for the untreated and treated canvas samples during the first 75%RH even after 90min of exposure. Again, the lower exposure of the sample to the humid environment during dielectric measurements could be responsible for their apparent lower response to moisture. This delayed response observed during the 75%RH plateau could also be observed during the RH transition. In Figure 8.20, the absorbance measured in the exposed area of the sample during the neutron radiography was plotted over the RH in the chamber. The slower response to humidification (solid lines) and dehumidification (dashed lines) of the treated samples, in particular for the MC+CNC(h)-treated sample, in comparison with the untreated sample is highlighted by the hysteresis seen in the graph.

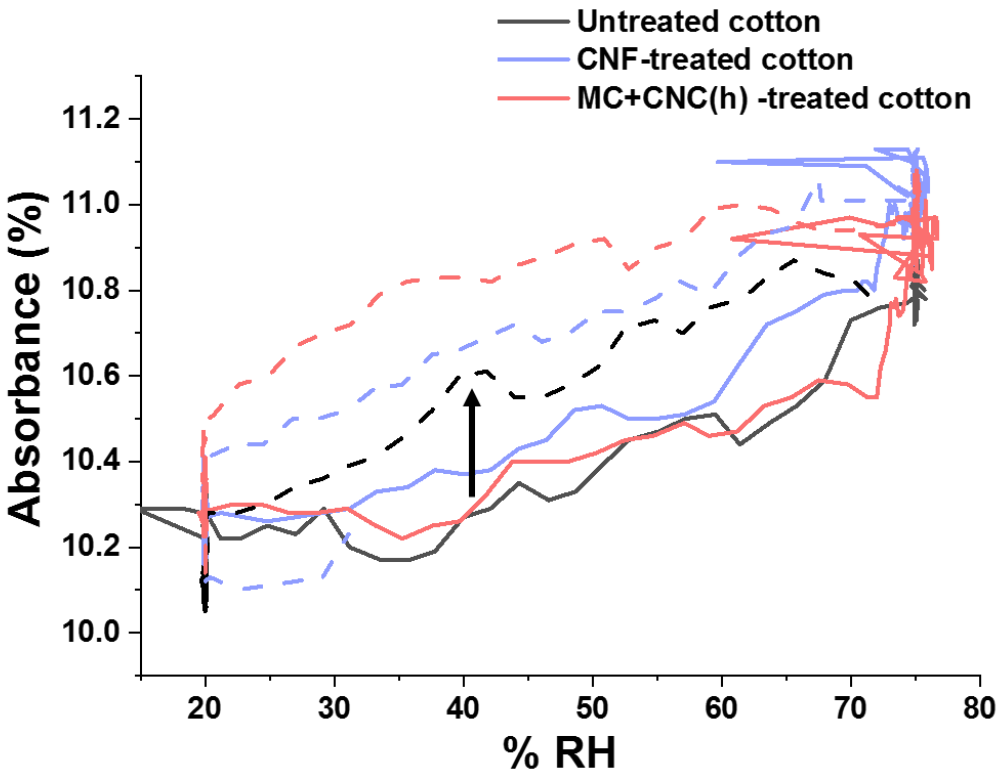

Figure 8.20: Variations in mean absorbance plotted over relative humidity (%RH) of untreated and treated cotton canvas. The absorbance was measured in the selected area of the sample exposed to the RH-controlled environment of the sample cell (yellow square in Figure 8.8a). The humidification (solid lines) and dehumidification (dashed lines) transitions are shown. The graph shows the higher hysteresis in moisture sorption-desorption, indicated by the arrow, measured for the treated samples (i.e. CNF- and MC+CNC(h) treated samples) than for the untreated one.

Finally, the mapping of the change in absorbance occurring across the sample can inform on the distribution of moisture inside the samples. Based on the assumption that moisture would diffuse from the exposed area to the edges, unexposed areas of the sample, the response of 3 different areas on the radiographic images were compared: the exposed one (used previously, see Figure 8.8a) and 2 unexposed areas place on top and on the right side of the sample. The areas are shown in Figure 8.21.

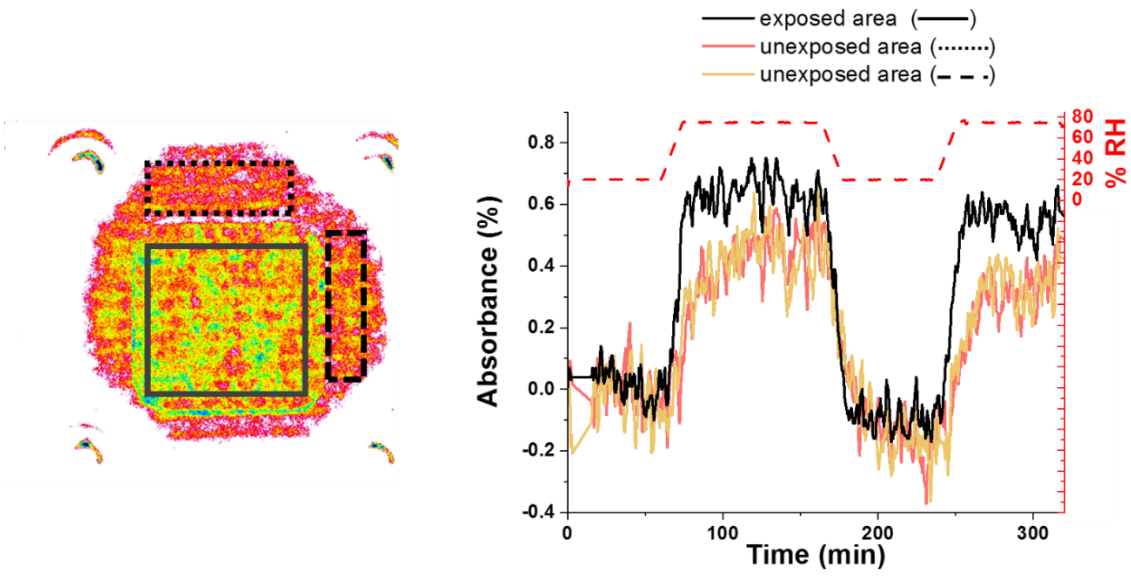

Figure 8.21: On the left, absorbance map of an untreated cotton sample with rectangular areas indicating the area directly exposed to the RH-controlled environment (solid line) and areas protected unexposed under the frame (dotted and dashed lines). The corresponding variations in mean absorbance measured over time in these 3 areas are given in the graph on the right.

As seen in curve in absorbance in Figure 8.21, moisture sorption and desorption in the area exposed the RH-controlled environment is almost immediate and follow the variations in RH (red dashed line). On the contrary, the 2 unexposed areas, which behave in a similar way, show a delay in response characterised by a slow increase in absorbance during the first 45min at 75%RH for both the 1st and 2nd cycle. As seen in Figure 8.21, during the 20 to 75%RH transition, the absorbance of the unexposed area increases by 0.08 and 0.16% for the area on top (dotted line) or on the right side (dashed line) of the sample, respectively. Whereas, the absorbance measured for the exposed area increases already by 0.41%. During the 75%RH plateau (from start to end of the RH plateau), the absorbance of the unexposed area increases by 0.25% only. Whereas, for the exposed areas, increases of 0.48% and 0.41% were measured for the top and right hand side area, respectively. The sample finally reaches equilibrium in moisture content after this first period. After dehumidification (i.e. 75%RH to 20%RH), during the 2nd 20%RH plateau, a similar delay in response is observed. After 60min, however, the sample still seems to lose moisture as seen by the negative slope in absorbance measured for the unexposed areas. A more refined image analysis was performed to measure the variations in absorbance measured along a line going from

on edge, through the centre of the sample to the other edge of the sample. The high noise of the images, low resolution and the inherent inhomogeneous thickness of the canvas (holes in interstitial spaces and thick threads) did not allow for more information to be drawn. Similar observations as those already presented were made. The results are shown in the Appendix (Figure F.4 in Appendix 7.3). In terms of comparison between untreated and treated sample, similar delay in response between exposed and unexposed areas were seen for the untreated and CNF and MC+CNC(h)-treated samples.

8.3.2.2 Historical primed canvas (Landseer)

The primed canvas samples from a Landseer canvas sized and primed were measured before and after treatment by neutron radiography following the same RH program and using the same treatments (i.e. CNF and MC+CNC(h)) than for the degraded cotton samples. Comparison with dielectric measurements was performed. The results are given in light of the previous observations made for the cotton untreated and treated samples. Differences in hygroscopic behaviour between untreated/treated samples, moisture distribution across the samples and kinetics in moisture sorption will be investigated. They will help highlight similarities and/or differences between the response of historical samples (linen canvas) and modern cotton canvas mock-ups.

Hygroscopic behaviour

It has been previously shown that for the cotton canvas, the treatments induced a small increase in response to moisture sorption of the sample characterised by larger variations in absorbance between the dry (20%RH) and humid state (75%RH). The same analysis was performed on the untreated and treated primed canvas samples. Figure 8.22A shows the mean percentage of absorbance measured in the area of the samples directly exposed to the humid environment. On first observation, the variations in percentage of absorbance (%A) measured for the 3 primed canvas samples untreated/treated are similar in magnitude ($\Delta A_{humidification}$ =0.59% for the CNF-treated primed canvas sample) than those previously registered with the cotton samples

($\Delta A_{humidification}$ =0.79% for the CNF-treated cotton sample). A global reduction in variations in absorbance between dry (20%RH) and humid (75%RH) state can, however, be observed for the primed canvas sample in comparison with the cotton samples. This could indicate the role of protective layer against moisture played by the ground layer present on the primed canvas sample.

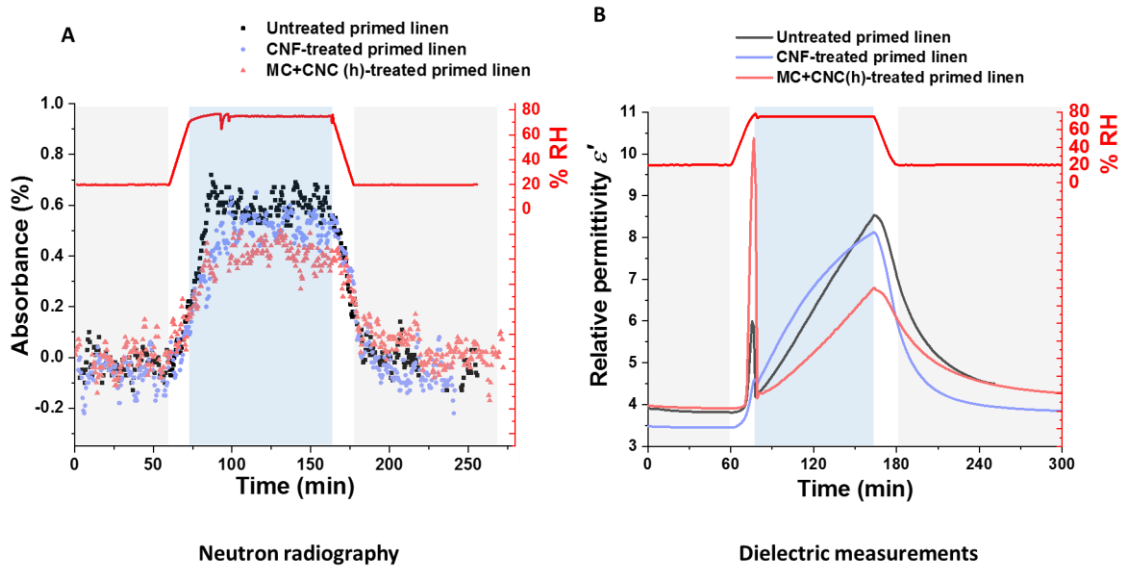

Figure 8.22: In A, mean percentage in absorbance measured by neutron radiography for an untreated and a CNF-treated and MC+CNC(h)-treated primed canvas sample (Landseer). The mean values were integrated over a region directly exposed to the RH-controlled environment of the sample cell (yellow square previously shown in Figure 8.8a and b). The curves in absorbance have been normalized at the end of the 1st 20%RH plateau. In B, variations in dielectric relative permittivity ε' (1kHz) for the 3 same samples, untreated and treated primed canvas sample. For both the neutron imaging and dielectric analysis, the samples were subjected to the same RH program (i.e. 20-75%RH, 4%RH/min).

However, contrary to the cotton samples, the treatments do not induce higher variations in absorbance measured for the treated samples. The higher response to moisture was measured for the untreated sample and the CNF-treated sample. Differences in absorbance ΔA during humidification (20 to 75%RH) and dehumidification (75 to 20%RH) are reported in Table 8.3. The biggest increase in absorbance measured during humidification (i.e. $\Delta A_{humidification}$) and dehumidification (i.e. $\Delta A_{humidification}$) were obtained for the untreated sample ($\Delta A_{humidification}$=0.66%, $\Delta A_{dehumidification}$=0.62%) followed by the CNF-treated ($\Delta A_{humidification}$=0.59%,

$\Delta A_{dehumidification}$=0.62%) and the MC+CNC(h)-treated ($\Delta A_{humidification}$=0.40%, $\Delta A_{dehumidification}$=0.35%) primed canvas samples.

Samples	$\Delta A_{humidification}$ (in %) (i.e.20-75%RH)	$\Delta A_{dehumidification}$ (in %) (i.e.75-20%RH)
Untreated primed linen	0.66	0.62
CNF-treated primed linen	0.59	0.62
MC+CNC(h)-treated primed linen	0.40	0.35

Table 8.3: Differences in absorbance ΔA (in %) measured for the untreated and the CNF- and MC+CNC(h)-treated primed canvas samples on the neutron radiographic images. The images selected for calculation were taken at the end of the 20%RH and 75%RH plateaus. Absolute values of ΔA are given here.

The high hygroscopic behaviour of the CNF and untreated sample in comparison with the MC=CNC(h) sample was also measured by dielectric analysis. As seen in Figure 8.22B, the CNF sample and untreated sample present a similar increase in ε' during the 75%RH plateau (i.e. similar slope coefficient seen by the superposition of the curves). The response of the CNF-treated sample seems slightly higher than the untreated sample as indicated by the difference in permittivity ε' measured at the end of the 20%RH and 75%RH plateaus. Differences in relative permittivity ε' measured between 20 and 75%RH of 3.5 and 4F.m^{-1} were measured for the untreated and the CNF-treated sample respectively. However, as already mentioned (in kinetics of moisture sorption in 8.3.2.1), the delayed response seen in dielectric measurements does not allow the samples to reach equilibrium. These observations thus only inform on the immediate hygroscopic response of the sample but not on the final moisture content or water absorbance capacity.

The results thus highlight the difference in moisture response between the linen historical canvas, sized and primed (i.e. the primed Landseer canvas) and the modern degraded cotton canvas. The CNF treatment still induces a higher hygroscopic response in the primed canvas

sample than the MC+CNC(h), However, contrary to the cotton samples, the treatments seem to maintain (CNF treatment) and reduce (MC+CNC(h) treatment) the hygroscopic response of the primed canvas.

Moisture mapping

In terms of moisture mapping and distribution across the samples, the results obtained for the primed canvas samples also differ in different ways with those obtained with the degraded cotton, unsized and unprimed, samples.

First, as seen in Figure 8.23, the area directly exposed to the chamber cell environment does not show higher absorbance rate than other, unexposed, areas of the sample. The area exposed or unexposed cannot be distinguished from one another on the absorbance radiographic images.

Moreover, the absorbance measured for the untreated primed canvas sample is the highest among the 3 samples. At 20%RH (1st cycle), the untreated sample presents a larger surface with high absorbance (blue to black colour). The MC+CNC(h) sample, on the contrary, shows the lowest absorbance. These difference in absorbance could indicate a difference in moisture content at the beginning of the measurement but could also, most probably, result from a difference in thickness of the samples.

Finally, the absorbance measured for all the samples is greatly lower than those measured for the cotton sample. Again, this is probably the result of the lower thickness of the samples (≈0.5mm for the primed canvas samples against 0.9mm for the cotton samples, see Table 8.1). The ground and size layers do not seem to compensate, in terms of absorbance of the neutron beam, for the difference in canvas thickness.

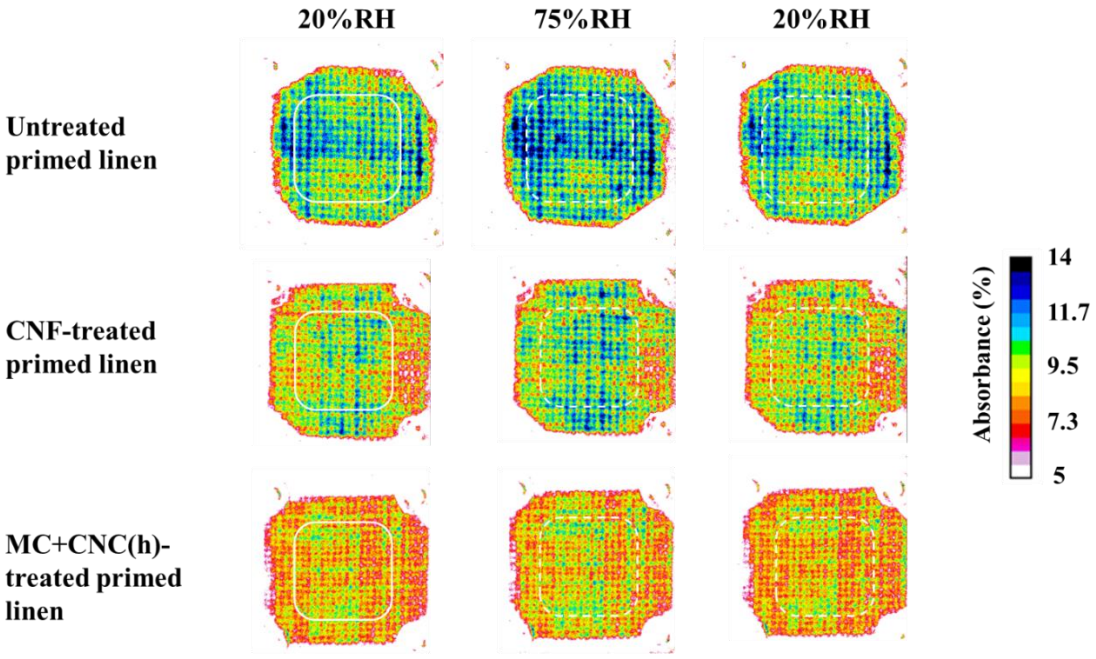

Figure 8.23: Neutron radiographic images of an untreated and a CNF- and MC+CNC(h)-treated primed linen canvas after corrections (see corrections steps in 8.2.2.4). These images give the mapping of the neutron beam absorbance by the samples during a 20-75-20%RH cycle (end plateau values, i.e. after 60min at 20%RH and after 90min at 75%RH).

Kinetics in moisture sorption

In terms of kinetic in moisture sorption, it is interesting to note that the samples behave similarly to the cotton untreated and treated samples. The variations in neutron beam absorbance during RH transition and RH plateau were analysed.

Firstly, Figure 8.24 shows that during RH transitions the unexposed areas of the treated samples have a delayed response to moisture desorption. This is seen in the graph by the hysteresis which characterised the absorbance measured over RH for the CNF- and MC+CNC(h)-treated primed canvas samples. The untreated sample, to the contrary, did not show any hysteresis. Hysteresis in the curve of absorption had been also observed for the cotton samples, for the treated as well as the untreated canvas.

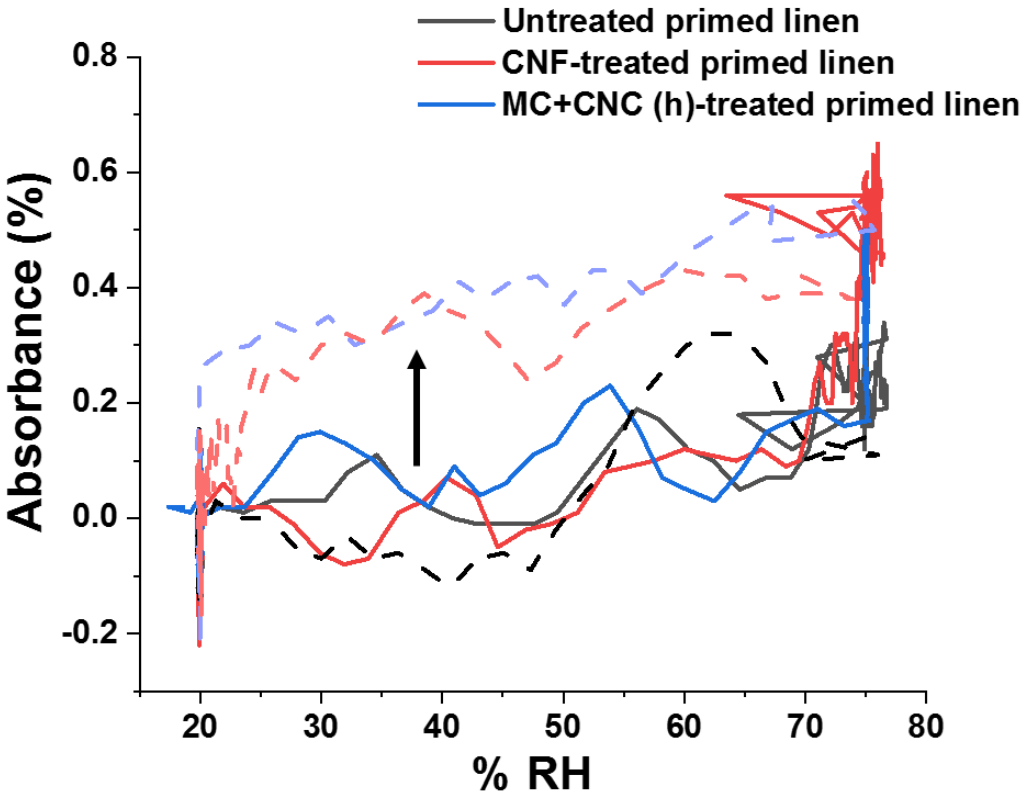

Figure 8.24: Variations in mean absorbance plotted over relative humidity (%RH) of untreated and treated primed canvas canvas. The absorbance was measured in the selected area of the sample exposed to the RH-controlled environment of the sample cell (yellow square in Figure 8.8a). The humidification (solid lines) and dehumidification (dashed lines) transitions are shown. The graph shows the higher hysteresis in moisture sorption-desorption, indicated by the arrow, measured for the treated samples (i.e. CNF- and MC+CNC(h) treated samples) than for the untreated one.

During the RH plateaus, the delayed response of the unexposed areas of the sample over the response of the exposed area can also be seen (Figure 8.25). This is in agreement with the results previously obtained for the cotton canvas. This indicates that contrary to the first assumption made for Figure 8.23, the frame does offer protection against moisture diffusion to the primed canvas samples as well. The protection offered in the case of the untreated linen sample seems however lower than the one seen for the untreated cotton. As seen in Figure 8.25, during the 20 to 75%RH transition, the absorbance of the unexposed area increases by 0.27 and 0.23% for the area on top (dotted line) or on the right side (dashed line) of the sample, respectively.

Whereas, the absorbance measured for the exposed area increases already by 0.45%. During the 75%RH plateau (from start to end of the RH plateau), the absorbance of the unexposed area increases by 0.24% only. Whereas, for the exposed areas, increases of 0.40% and 0.36% were measured for the top and right hand side area, respectively. The results obtained for the untreated cotton sample show the same trend in behaviour characterised by the delay in moisture diffusion in the unexposed area. However, the delay in moisture sorption for the unexposed area is larger for the cotton untreated sample than for the untreated primed canvas canvas. The increase in absorbance measured during the first 20-75%RH RH transition is larger, respectively to the final absorbance measured at the end of the 75RH plateau, for the primed linen canvas than for the cotton sample.

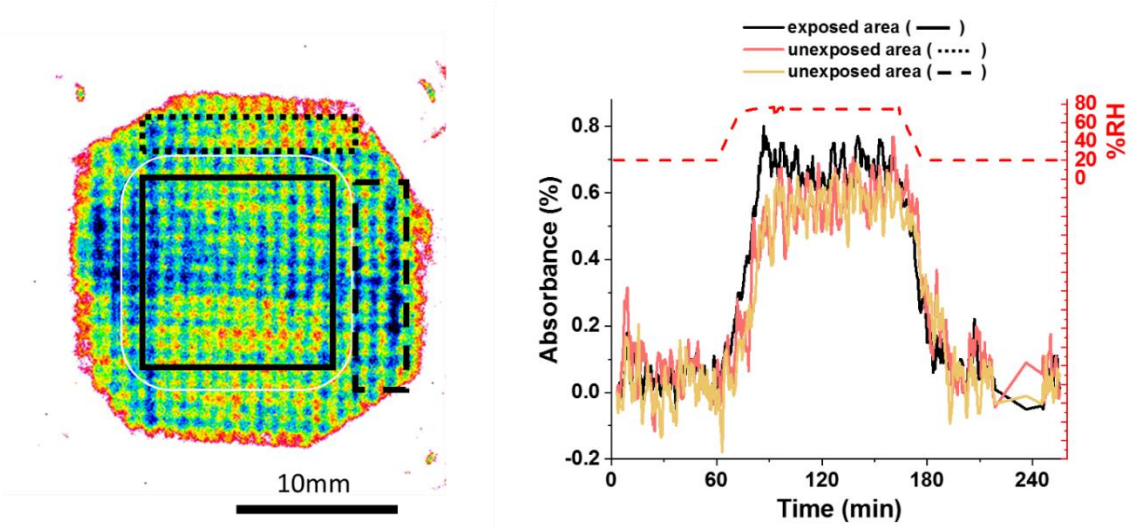

Figure 8.25: On the left, absorbance map of an untreated primed linen canvas with rectangular areas (black lines) indicating the area directly exposed to the RH-controlled environment (solid line) and areas protected unexposed under the frame (dotted and dashed lines). The corresponding variations in mean absorbance measured over time in these 3 areas are given in the graph on the right. On the left, the white line indicated the total exposed area (not used for the calculation).

Despite some differences in the results between cotton canvas and primed linen canvas, the results globally agree between the two types of support used. Treatments tend to slow down moisture diffusion during RH transitions and RH plateaus. As expected and confirm by neutron radiography and dielectric analysis, the CNF treatment also shows a higher hygroscopic behaviour

than the MC+CNC(h) treatment. Depending on the material used as support (cotton degraded canvas or sized and primed historical linen) the impact of the treatments on the hygroscopic response varied. On the cotton canvas, the CNF, as well as the MC+CNC(h) treatments, seem to increase the hygroscopic behaviour of the support. Whereas, with the primed canvas, the CNF does not modify the response of the sample to moisture (similar ΔA) while the MC+CNC(h) treatment reduces its response to moisture.

These preliminary observations, in particular those obtained on the primed canvas, could be complemented with additional measurements. If performed, these measurements should consider the heterogeneous composition of the historical painting with the presence of size and a ground layer. These aspects could be a factor in explaining this difference in the results and interpretation. The size layer, for example, is known to be highly hygroscopic and the ground layer less (Mecklenburg, 1982b). Glutin-based adhesives (i.e. bone glue, hide glue, fish glue) are effectively known to absorb more moisture and to also have higher diffusion coefficients than other adhesives (Mannes, 2014; Volkmer, 2012). Depending on the thickness of these additional layers (size and ground layer), the absorbance measured could greatly change. Errors could be eliminated by using samples with size and ground layers of the exact same thickness. This is in the practice hard to obtain. In the particular case of the Landseer primed canvas, the canvas having been prepared by hand, controlled application of size and ground of the same thickness across the canvas might have been even harder to achieve.

8.4 Conclusion

This innovative and real-time study of moisture sorption in unprimed cotton and primed linen canvases gave valuable insights into the kinetics of moisture diffusion and distribution of moisture across the sample. The results have highlighted general patterns in diffusion, observed for both the primed canvas samples and the cotton canvas samples. Notably, these include a delayed response in moisture absorption of the areas of the sample placed under the frame, as well as of the treated samples in comparison with the untreated references. The results also show some differences between cotton and primed linen samples regarding the variations in absorbance (i.e. variations in moisture content) measured for the untreated in comparison with the untreated samples. These differences were reinforced using complementary analyses performed such as dielectric analysis which reconfirmed these results. A better understanding of the source of these differences in behaviour and of the role of the size and ground layer in the total absorbance measured by neutron radiography on the primed linen canvas untreated and treated with consolidants could be further investigated. Analyses on the samples cross-sections (plane of the sample placed parallel to the beam axis) would be valuable to separate the response of each individual layers but would require a higher resolution as demonstrated by Hendrickxs (2017).

Further work should focus on collecting measurements of the sample cross-sections as well as image calibration for the quantitative assessment of the moisture content in the samples.

9 Conclusions and future developments

Novel nanocellulose based materials have been evaluated as possible new materials for the consolidation of canvas-supported paintings, in particular canvases made of linen as well as cotton, a material which was increasingly used in 20th century paintings. As cotton has proved to be more prone to degradation than linen, it is expected that in the future more and more paintings whose canvas is made of this material might arrive in conservation studios for structural consolidation. The effects of these treatments have been quantified and advantages, disadvantages, and limitations of their application are presented. An analytical approach linking the nano- to the macro-scale was used and led to the improvement of existing techniques and the development of new protocols of evaluation. Additionally, this novel work demonstrated the capabilities of dynamic mechanical analysis (DMA) with programmed and controlled relative humidity (RH), measuring the response of painting canvases to cycles of variations in RH ranging from low (20%) to high values (80%).

Overall, the results have successfully shown the potential of the newly developed nanocellulose-based consolidants for canvas consolidation. This evaluation was initially performed on model degraded cotton canvases and then in collaboration with paintings conservators on genuine lining canvases and historical paintings. A comparative study was also carried out on traditional consolidants. This places the results in the wider context of the study of the mechanical properties of paintings. The study of the response of these materials to RH variations is especially relevant due to the risks associated to environments which are not controlled as found in small galleries, museums, historical houses or castles and possibly during transport.

9.1 Viscoelastic response of painting canvas and other layers to RH variations

Initial investigation sought to identify, the baseline mechanical, in terms of its viscoelastic properties, and dimensional response to RH variations of a degraded cotton canvas. This is the

first time that cotton canvases have been studied in this way. Once these control baselines were established, a modern linen canvas (unsized and sized), as well as historical 19th century samples (with and without priming) were studied. In these investigations, DMA was used to provide a measurement of the viscoelastic parameters (*E'*, Tan δ) with variations in RH for each of the sample, which together with elongation measurements revealed the following:

(a) Warp and weft directions in the degraded cotton canvas presented different mechanical response to RH cycling. A higher plasticization (i.e. loss in stiffness) at high RH levels was found for the canvas in the warp when compared to its weft direction.

(b) Modern cotton and linen canvases (measured in the warp direction) also differed in their response to RH cycling. Linen was found to stiffen at high RH levels.

(c) The washing and subsequent ageing of cotton canvas significantly affected its mechanical response to RH. An inversion in the periodic response of the canvas to RH cycling from stiffening to plasticization at low RH was measured.

(d) For the linen samples, the effects of sizing (modern canvas) and presence of priming (19th century sample) modified the mechanical response of the canvas to RH variations. The sizing induced a decrease in stiffness of the canvas at high RH whereas priming increases the overall stiffness.

It is worth noting however, that the fast rate of increase/decrease in RH used for the study of the canvases samples (i.e. 4%RH/min) does not allow for direct comparison with the response the samples might show in real environments such as galleries or museums. The results also emphasised the unique characteristics of each canvas found in collections with regards to their response to RH. This preliminary study laid the foundation for the following chapters of the thesis, which focusses on the application of traditional adhesives and consolidants (chapter 4) and newly developed nanocellulose treatments (Chapter 5) to the degraded cotton canvas.

9.2 Assessment of traditional consolidants and adhesives used for painting structural consolidation

The previous chapter (Chapter 3) had reaffirmed the importance of RH on the mechanical properties of canvases, as well as size and priming layers. However, in the cases of degraded fragile canvases which need to be consolidated, it is paramount to understand the mechanical response of the materials used in conservation for the consolidation of the canvas, especially considering that these materials are exogeneous to the painting. Therefore, it was essential to investigate the viscoelastic response to RH variations of traditional canvas consolidants and adhesives. The materials chosen for this study are currently used in painting conservation, so their behaviours are immediately relevant to cultural heritage. Additionally, these materials were compared with two novel and developing nanocellulose-only treatments (CNF and CCNF).

The results showed that traditional treatments and novel CNF and CCNF treatments differ in terms of surface deposition, reinforcement provided and response to RH variations. The traditional treatments penetrate more into the canvas but offer a lower consolidation than nanocellulose. In terms of mechanical response to RH, it was possible to evaluate the effect of RH cycling on traditional consolidants applied to canvases and demonstrate effectively differences between the more hydrophilic (Aquazol200, KlucelG and Animal glue) and hydrophobic (Beva371, Paraloid B72 and PlexisolP550) materials, both in film form and applied to cotton canvases. Contact angle measurement and measurement of moisture content by DVS complemented the information gained. Time-dependent responses to RH variations were also seen for the animal glue and ParaloidB72 treated canvases.

The long-term stability of the traditional and nanocellulose consolidants was also evaluated but should be re-evaluated as the ageing program with the high temperature (80°C) and RH level (80%RH) used might not have been appropriate for all the treatments.

One of the main challenges of this study also is the evaluation of the long-term behaviour of the different treatments. The fast RH cycling used gives a first idea of the changes in mechanical properties resulting from fast RH changes. Further studies are, however, needed to

understand the long-term behaviour of these materials. Mechanical modelling of the materials could answer this question, which is of utmost importance in conservation.

9.3 Evaluation of the nanocellulose-based consolidants

The previous chapter (Chapter 4) showed that there are significant differences between some of the novel nanocellulose treatments and the traditional materials current employed by conservators. Building on the conclusions of the last two chapters, this following study is the central component of this thesis. In this study, the chemical, physical and mechanical properties of two main categories of nanocellulose-based consolidants were fully evaluated. These are (1) the nanocellulose consolidants introduced in Chapter 4 and (2) the nanocellulose composites CNC-reinforced cellulose derivatives.

The three treatments could be first distinguished by their surface deposition and by their penetration into the canvas. The nanocellulose treatments (solution 1) form a superficial layer sitting on top of the canvas (i.e. nano-lining) as previously observed in Chapter 4 (cf. Figure 4.13). The nanocomposite (solution 2), instead, offered a higher penetration into the canvas. The level of surface deposition observed for the nanocomposites consolidants was found to be similar to those observed for previously in Chapter 4 for the traditional consolidants (cf. Figure 4.13).

This surface deposition had an impact on the consolidation as well as mechanical response to RH variations. In terms of consolidation, the higher consolidation was conferred by the nanocellulose treatments and nanocomposites treatments. However, mechanical failure of the nanocellulose films was observed at low elongations during the tensile tests. These were attributed to the known brittleness of nanocellulose films and surface deposition characteristic of these treatments. The nanocellulose treatments and nanocomposite also showed a high response to RH variations except for the CNC-treated canvas. This was attributed to the highly-dense coating formed upon application of the treatment. The superficial layer proved to be beneficial as it lowers the mechanical response of the canvas and thus reduces mechanical stresses to which other painting layers (priming, paint) could be exposed.

Moreover, the impact of treatment penetration on the consolidation achieved was investigated separately using the nanocellulose composite solution. The results showed that improved penetration leads to greater consolidation at same weight added in treatment. Additionally, higher penetration would induce lower reversibility which would be a disadvantage for conservators.

Overall, both the nanocomposite and nanocellulose treatments appeared to provide a higher consolidation than the traditional treatments tested in Chapter 4. The low penetration of the nanocellulose-only consolidants could facilitate their reversibility and acceptance in conservation but is also responsible for the mechanical failures measured when applied on canvas. In the frame of the application of nanocellulose-based treatments in conservation, it is expected that compromises between good coupling (i.e. adhesion and mechanical performance) and reversibility should be found.

9.4 Case-study: Improvement of the adhesion and performance of a nanocellulose consolidant using polyamidoamine epichlorohydrin (PAAE)

A separate study was performed to determine if the addition of the cationic polymer PAAE would have an impact on the adhesion of CNF. The results showed an increase in stiffness, an improved surface deposition of the CNF treatment upon the use of PAAE as an intermediate layer between canvas and CNF. The improved adhesion of the fibre/PAAE/CNF layered system was measured at the nanoscale using atomic force microscopy (AFM) and demonstrates the suitability of working with paintings given the very small sample required. It is anticipated that the nanoscale approach presented in this study could be further developed in the future for testing the adhesion properties of other consolidation approaches.

An increase in response to RH was however measured for the samples treated with PAAE. RH has already been shown to be a crucial factor in the stability and mechanical behaviour of canvases (cf. 1.1.2.2 in Chapter 1). Due to this shortcoming, PAAE was not further considered as suitable for canvas consolidation. Chemical functionalisation of nanocellulose might offer an alternative route to the introduction of non-cellulosic additives.

9.5 Nanocellulose-based consolidants tested on real samples from paintings

Chapter 7 focused on the validation of the applicability and performance of the nanocellulose-based consolidants on naturally aged historical canvas and paintings. This was performed in the framework of a workshop with the participation of both conservators and scientists, and reinforced the applicability of the developments made and conclusions drawn thus far in the thesis

The results showed that most of the treatments performed well on the historical materials in terms of handling properties, penetration and surface appearance, with the exception of the treatments containing deacidification particles (i.e. MgO and $CaCO_3$). These treatments induced a whitening of the surface of the canvas. The best results were obtained with the MC+CNC treatments in both water and heptane. The high viscosity of the treatments offered good control during treatment application and lower the penetration of the solvent into the priming and paint layers of the painting. This is essential as water could trigger chemical and physical degradation in the priming and paint layers. The consolidation provided by the treatments on a historical linen lining canvas was also quantified. Higher consolidation was reached with the nanocellulose (CNF and CCNF) as well as with the MC+CNC(w) consolidants. The impact of the solvents alone on the canvas was also highlighted by the results.

Although the outcomes of these extensive investigations were positive, it is also worth noting that the historical canvases and paintings used were not in an advanced stage of degradation. According to the observations made by the painting conservator with whom the tests were performed, the paintings and canvases tested may not have reached the stage at which a conservator might have to intervene on the entire painting. Local consolidation might have been more suited such as tear mending or local patches. Nonetheless, these results here were promising. The novel treatment methods proved beneficial in treating canvases that were noticeably weakened. Future investigations should consider canvases in a highly advanced state of degradation and in this approach it would be interesting to evaluate if the nanocellulose treatments are as effective as when used on less damaged canvases.

One of the challenges in this project has been to establish with certainty the state of degradation at which paintings should be consolidated using the treatments developed. Further tests on an entire painting in real need for consolidation, as defined by painting conservators, should be performed. The application of the coatings at the manufacturer stage is also an alternative route that could be explored.

9.6 Real-time visualisation of moisture distribution in canvases before and after treatment

Once the principal research questions of this thesis had been successfully addressed, a different challenge was investigated to both support and extend the main research question. The impact of moisture on the viscoelastic properties of canvas and traditional and nanocellulose-based consolidants had been a significant challenge to overcome, and the work in the previous chapters had given a potential pathway to dealing with those challenges. However, there was still a concern over the impact the treatments have on the moisture distribution upon RH variations in treated canvases.

A separate study was performed using neutron radiography to study the dynamics of moisture sorption and desorption in untreated and treated cotton canvases and primed linen canvases, with the aim of obtaining the distribution of moisture within the untreated/treated samples. A sample chamber was specially designed and attached to the RH controller used in the DMA-RH experiments. It is to our knowledge, the first time that neutron radiography was used to follow visually moisture sorption/desorption in a material subjected to dynamic and remotely controlled RH cycles at a fixed temperature.

The model degraded cotton canvas, as well as a historical lining linen canvas, were treated with the more hydrophilic CNF and more hydrophobic MC+CNC (in heptane) treatments. Images were obtained which showed an increase in absorbance with moisture sorption and a decrease on dehumidification. Higher and lower hydrophilic response upon exposure to high RH level (i.e.

75%RH) was measured for the CNF and MC+CNC(h)-treated samples, respectively. This was confirmed by complementary RH dielectric analysis and DVS measurements.

At this stage, however, the neutron measurement did not allow for the mapping the canvas surface and the identification of spots of moisture absorption. The evaluation was limited to the observation of an increase/decrease in moisture content of the canvas upon RH increase/decrease, respectively. The main limitation of this study was the low resolution available in the neutron facility at the time of the measurement. A number of image corrections were tested during the post processing of the raw neutron images and included taking into account the variations in beam intensity during sample exposure. These corrections provided a means of verifying that a change in the image did occur on exposure to moisture which was complemented by changes recorded by other techniques. However, the processes of moisture diffusion into the canvas (e.g along the threads) and effect of various treatments on this process could not be clearly identified. The moisture sorption/desorption dynamics could also not be followed from studies of the samples in cross-sections due to the low values of sample thickness.

Finally, for future work it is suggested that the averaging used to improve the resolution of the neutron images should be reviewed. The neutron images could be improved but this processing introduces errors in particular during RH transitions, where the RH was changed quickly. This rendered accurate correlations between RH level and moisture content in the canvas impossible. Further attempt to increase the resolution of the images during the experiment as well as during post-processing should be made.

9.7 Future developments

Though the work performed for this thesis did manage to demonstrate the effects of various nanocellulose-based treatments in terms of the consolidation of the test canvases and to demonstrate the potential of a multi-scale approach introducing DMA-RH to study the impact of moisture on canvas and canvas consolidants, the following developments are suggested:

- Use of a lower RH rate during RH transitions in the DMA-RH studies. It would provide more accurate results on the mechanical responses of painting materials placed in real environments.

- Evaluation of the degree of penetration into the canvas of the traditional and newly developed consolidants and the impact of RH cycling and/or ageing on this penetration. This would bring valuable information to understand the changes in mechanical properties measured upon RH cycling and accelerated ageing.

- Further developments of the ageing program used to compare the long-term stability of nanocellulose treatments with the traditional consolidants. The difficulty faced during the design of the experiment has been to define the temperature and %RH to be used. Accelerated ageing should be done below Tg to avoid degradation of the material which might not be representative of the natural ageing of the material. Yet, the traditional consolidants tested had a low Tg (<80C and some around 40C) and the use of RH cycling and high RH levels might have lowered further their Tg. A compromise between ageing parameter, temperature and RH, and duration of the experiment need to be found.

- Chemical functionalization of nanocellulose to improve adhesion of the treatment onto canvas cellulose fibres and reduce hydrophilic behaviour. This would help to reduce the mechanical response of the canvas to RH and thus to limit risks of fatigue and/or mechanical failure of the painting.

- Use of finite element modelling (amended to include the viscoelastic properties of materials) and which would use the viscoelastic data collected in the framework of this project. This will help to quantify the risks associated with the variations in *E'* measured in a cost- and time-

effective way. This would also help to define acceptable ranges of variations in *E'* within which mechanical failures in paintings can be avoided and predict long-term behaviours.

- Study of the risks associated with local application of the nanocellulose-based treatments as this might trigger additional mechanical damages to the painting due to the concentration of stresses.

- Improvement of the resolution of the neutron radiographic images. This would help to get precise information on the diffusion of water molecules inside the canvas. The study should also be carried out on the cross-section of the samples to study the processes of moisture diffusion through the samples. This would provide the possibility to study barrier properties of some of the treatments, in particular, those identified as more hydrophobic such as MC+CNC in heptane or those who showed to slow down more moisture diffusion processes such as the CNC treatment.

9.8 Summary

Throughout this thesis the viscoelastic behaviour of canvas and the way this behaviour could be altered by application of other materials has been investigated and quantified by testing its response to fluctuations in RH. Such testing of canvases, before and after treatment, has shown to be suited to the evaluation of new materials for canvas consolidation. Novel treatment methods for the conservation of valuable historical paintings have been potentially identified, and treatments with less promising outcomes have been discounted. These new treatment methods have been compared to currently available materials, and the advantages and disadvantages of each was shown. Lastly a novel investigation using neutron imaging showed the complexities of water distribution in a material such as canvas.

In conclusion this thesis has demonstrated which of the treatment types involving novel nanocellulose-based materials, methods and accompanying knowledge could be of use in the preservation of priceless cultural heritage involving canvas-supported paintings.

10 Bibliography

Abdel-Kareem, O. M. A. (2005). The long-term effect of selected conservation materials used in the treatment of museum artefacts on some properties of textiles. *Polymer Degradation and Stability*. https://doi.org/10.1016/j.polymdegradstab.2004.07.014

Ackroyd, P. (2002). The structural conservation of canvas paintings: changes in attitude and practice since the early 1970s. *Studies in Conservation*, *47*(sup1), 3–14. https://doi.org/10.1179/sic.2002.47.Supplement-1.3

Ackroyd, P., Phenix, A., & Villers, C. (2002). Not lining in the twenty-first century: Attitudes to the structural conservation of canvas paintings. *The Conservator*, *26*(1), 14–23. https://doi.org/10.1080/01410096.2002.9995172

Ahmed, H. E., & Kolisis, F. N. (2012). A study on using of protease for removal of animal glue adhesive in textile conservation. *Journal of Applied Polymer Science*, *124*(5), 3565–3576.

AIC Ethics and Standards Committee. (n.d.). AIC Code of Ethics, section II. E.: "Principle of reversibility".

Akushla Wijesekara, D. (2018). *Application of Methylcellulose and Nanocellulose (CNC) based Coatings on Aged Cotton Canvases and Evaluation of the Properties of the Consolidated Cotton Canvas*. Birkbeck University of London.

Alam, M. K., Khan, M. A., & Lehmann, E. H. (2006). Comparative study of water absorption behavior in biopol® and jute-reinforced biopol® composite using neutron radiography technique. *Journal of Reinforced Plastics and Composites*, *25*(11), 1179–1187. https://doi.org/10.1177/0731684406066365

Alfthan, J. (2005). The Effect of Humidity Cycle Amplitude on Accelerated Tensile Creep of Paper, *i*(2004), 289–302.

Ali, O. (2013). *High Performance Regenerated Cellulose Membranes from Trimethylsilyl Cellulose*. King Abdullah University of Science and Technology.

Alihosseini, F. (2016). Plant-based compounds for antimicrobial textiles. In *Antimicrobial Textiles* (pp. 155–195). Woodhead Publishing Series in Textiles.

Allen, N. S., Edge, M., Rodriguez, M., Liauw, C. M., & Fontan, E. (2000). Aspects of the thermal oxidation of ethylene vinyl acetate copolymer. *Polymer Degradation and Stability*. https://doi.org/10.1016/S0141-3910(00)00020-3

Andersen, Cecil K., Mecklenburg, M. F., Scharff, M., & Wadum, J. (2018). With the best intentions. Wax-resin lining of Danish Golden Age paintings (early 19th cent4ry) on canvas and changed response to RH. In J. Bridgland (Ed.), *ICOM-CC 14th triennal conference preprints - Melbourne* (p. art. 1301, 9 pp.). Paris: International Council of Museums.

Andersen, Cecil Krarup, Filtenborg, T., & Scharff, M. (2009). The industrialisation of canvas production in Denmark and its implications for the preservation of Danish nineteenth century paintings. In *Incredible Industri : Preserving the evidence of industrial society: Conference Proceedings* (pp. 39–49). Nordisk Konservator Forbund. https://doi.org/10.13140/2.1.1143.7768

Andreasson, B., Forsström, J., & Wågberg, L. (2005). Determination of fibre pore structure: Influence of salt, pH and conventional wet strength resins. *Cellulose*, *12*(3), 253–265. https://doi.org/10.1007/s10570-004-5837-6

Apolinario, G., Ienny, P., Corn, S., Léger, R., Bergeret, A., & Haudin, J. M. (2016). Effects of water ageing on the mechanical properties of flax and glass fibre composites: Degradation and reversibility. In *Natural Fibres: Advances in Science and Technology Towards Industrial Applications* (RILEM Book, pp. 183–196). Springer, Dordrecht. https://doi.org/10.1007/978-94-017-7515-1_14

Appelbaum, B. (1987). Criteria for Treatment: Reversibility. *Journal of the American Institute for Conservation*, *26*(2), 65–73. https://doi.org/10.1179/019713687806027852

Area, M. C., & Cheradame, H. (2011). Paper aging and degradation: Recent findings and research methods. *BioResources*, (6), 5307–5337. https://doi.org/10.15376/biores.6.4.5307-5337

Armstrong, L. G., & Christensen, G. N. (1961). Influence of moisture changes on deformation of wood under stress. *Nature*, (4791), 869–970.

Arslanoglu, J. (2004). Aquazol as Used in Conservation Practice by. *WAAC Newsletter*, *25*(2), 10–15.

Astley, O. M., & Donald, A. M. (2001). A small-angle X-ray scattering study of the effect of hydration on the microstructure of flax fibers. *Biomacromolecules*, *2*(3), 672–680. https://doi.org/10.1021/bm005643l

Azeredo, H. M. C. d. (2009). Nanocomposites for food packaging applications. *Food Research International*, *42*(9), 1240–1253. https://doi.org/10.1016/j.foodres.2009.03.019

Baglioni, P. (2015). *Nanotechnologies in the conservation of cultural heritage : a compendium of materials and techniques /Piero Baglioni, David Chelazzi, Rodorico Giorgi.*

Baglioni, P., & Chelazzi, D. (2013). *Nanoscience for the conservation of works of art*. RSC Publishing.

Baglioni, P., & Giorgi, R. (2006). Soft and hard nanomaterials for restoration and conservation of cultural heritage. *Soft Matter*, *2*(4), 293–303.

Bahadar, H., Maqbool, F., Niaz, K., & Abdollahi, M. (2016). Toxicity of Nanoparticles and an Overview of Current Experimental Models. *Iranian Biomedical Journal*, *20*(1), 1–11.

Baley, C. (2002). Analysis of the flax fibres tensile behaviour and analysis of the tensile stiffness increase. *Composites - Part A: Applied Science and Manufacturing*, *33*(7), 939–948. https://doi.org/10.1016/S1359-835X(02)00040-4

Banavath, H. N., Bhardwaj, N. K., & Ray, A. K. (2011). A comparative study of the effect of refining on charge of various pulps. *Bioresource Technology*, *102*(6), 4544–4551. https://doi.org/10.1016/j.biortech.2010.12.109

Bardet, R. (2014). *Nanocelluloses as potential materials for specialty papers*. Université de Grenoble.

Barros D'Sa, Angelina (Ed.). (2012). *Adhesives and consolidants in painting conservation*. London: London : Archetype in association with the ICON Paintings Group.

Barros, S. C., da Silva, A. A., Costa, D. B., Costa, C. M., Lanceros-Méndez, S., Maciavello, M. N. T., … Silva, M. M. (2015). Thermal–mechanical behaviour of chitosan–cellulose derivative thermoreversible hydrogel films. *Cellulose*, *22*(3), 1911–1929. Retrieved from http://dx.doi.org/10.1007/s10570-015-0616-0.

Baty, J. W., Maitland, C. L., Minter, W., Hubbe, M. A., & Jordan-Mowery, S. K. (2010). Deacidification for the conservation and preservation of paper-based works: A review. *BioResources*, *5*(3), 1955–2023. https://doi.org/10.15376/biores.5.3.1955-2023

Belbekhouche, S., Bras, J., Siqueira, G., Chappey, C., Lebrun, L., Khelifi, B., … Dufresne, A. (2011). Water sorption behavior and gas barrier properties of cellulose whiskers and microfibrils films. *Carbohydrate Polymers*, *83*(4), 1740–1748. https://doi.org/10.1016/j.carbpol.2010.10.036

Bella, J., Brodsky, B., & Berman, H. M. (1995). Hydration structure of a collagen peptide. *Structure*, *3*(9), 893–906. https://doi.org/10.1016/S0969-2126(01)00224-6

Beltrame, P. L., Paglia, E. D., Seves, A., Pellizzoni, E., & Romanò, M. (1992). Structural features of native cellulose gels and films from their susceptibility to enzymic attack. *Journal of Applied Polymer Science*, *44*(12), 2095–2101.

Bergeaud, C., Hulot, J., & Roche, A. (1997). *La dégradation des peintures sur toile. Méthode d'examen des altérations*. (E. N. Du Patrimoine, Ed.). Paris.

Berger, G. A. (1970). New Adhesive for the Consolidation of Paintings, Drawings and Textiles. *Bulletin*

of the American Group. *International Institute of Conservation of Historic and Artistic Works*, *11*(1), 36–38.

Berger, G., & Zeliger, H. (1974). Wax Impregnation of Cellulose: An Irreversible Process. In *Conference on Comparative Lining Techniques*. Greenwich.

Berger, Gustav A. (1972). Testing Adhesives for the Consolidation of Paintings. *Studies in Conservation*, *17*(4), 173–194. https://doi.org/10.2307/1505565

Berger, Gustav A. (1972). Maney Publishing Testing Adhesives for the Consolidation of Paintings TESTING ADHESIVES FOR THE CONSOLIDATION OF PAINTINGS. *Source: Studies in Conservation Studies in Conservation*, *17*(17), 173–194. Retrieved from http://www.jstor.org/stable/1505565

Bianco, L., Avalle, M., Scattina, A., Croveri, P., Pagliero, C., & Chiantore, O. (2015). A study on reversibility of BEVA®371 in the lining of paintings. *Journal of Cultural Heritage*, *16*(4), 479–485.

Bílková, L. (2012). Application of infrared spectroscopy and thermal analysis to the examination of the degradation of cotton fibers. *Polymer Degradation and Stability*, *97*(1), 35–39. https://doi.org/10.1016/j.polymdegradstab.2011.10.018

Binnig, G., Gerber, C., Stoll, E., Albrecht, T. R., & Quate, C. F. (1987). Atomic resolution with atomic force microscope. *EPL*, *3*(12), 1281–1286. https://doi.org/10.1209/0295-5075/3/12/006

Boillat, P., Carminati, C., Schmid, F., Grünzweig, C., Hovind, J., Kaestner, A., … Lehmann, E. H. (2018). Chasing quantitative biases in neutron imaging with scintillator-camera detectors: a practical method with black body grids. *Optics Express*, *26*(12), 15769. https://doi.org/10.1364/OE.26.015769

Boldizar, A., C. Klason, J. Kubát, P. N. & P. S. (1987). Prehydrolyzed Cellulose as Reinforcing Filler for Thermoplastics. *International Journal of Polymeric Materials and Polymeric Biomaterials*, *11*(4), 229–262. Retrieved from https://doi.org/10.1080/00914038708078665

Bomford, D. (2001). The Conservator as Narrator: Changed Perspectives in the Conservation of Paintings. In M. Leonard (Ed.), *Personal Viewpoints: Thoughts About Paintings Conservation* (p. 5). Los Angeles, USA: The Getty Conservation Institute.

Bomford, D., & Staniforth, S. (1981a). Wax–Resin Lining and Colour Change: An Evaluation. *National Gallery Technical Bulletin*, *5*, 58–65. Retrieved from http://www.nationalgallery.org.uk/technical-bulletin/bomforth_staniforth1981

Bomford, D., & Staniforth, S. (1981b). Wax–Resin Lining and Colour Change: An Evaluation. *National Gallery Technical Bulletin*, *5*, 58–65.

Bonaduce, I., Odlyha, M., Di Girolamo, F., Lopez-Aparicio, S., Grontoft, T., & Colombini, M. P. (2013). The role of organic and inorganic indoor pollutants in museum environments in the degradation of dammar varnish. *Analyst*, *138*(2), 487–500. https://doi.org/10.1039/c2an36259g

Bonnaillie, L. M., & Tomasula, P. M. (2015). Application of humidity-controlled dynamic mechanical analysis (DMA-RH) to moisture-sensitive edible casein films for use in food packaging. *Polymers*, *7*(1), 91–114. https://doi.org/10.3390/polym7010091

Boon, J. J., Hendrickx, R., Eijkel, G., Cerjak, I., Kaestner, A., & Ferreira, E. S. B. (2015). Neutron radiography for the study of water uptake in painting canvases and preparation layers. *Applied Physics A: Materials Science and Processing*, *121*(3), 837–847. https://doi.org/10.1007/s00339-015-9381-z

Borrega, M., & Kärenlampi, P. P. (2010). Hygroscopicity of heat-treated Norway spruce (Picea abies) wood. *European Journal of Wood and Wood Products*, *68*(2), 233–235. https://doi.org/10.1007/s00107-009-0371-8

Boryskina, O. P., Bolbukh, T. V., Semenov, M. A., Gasan, A. I., & Maleev, V. Y. (2007). Energies of peptide-peptide and peptide-water hydrogen bonds in collagen: Evidences from infrared spectroscopy, quartz piezogravimetry and differential scanning calorimetry. *Journal of Molecular*

Structure, *827*, 1–10. https://doi.org/10.1016/j.molstruc.2006.05.002

Bowditch, M. R. (1996). The durability of adhesive joints in the presence of water. *International Journal of Adhesion and Adhesives*, *16*(2), 73–79. https://doi.org/10.1016/0143-7496(96)00001-2

Bridarolli, A., Odlyha, M., Nechyporchuk, O., Holmberg, K., Ruiz-Recasens, C., Bordes, R., & Bozec, L. (2018). Evaluation of the Adhesion and Performance of Natural Consolidants for Cotton Canvas Conservation. *ACS Applied Materials and Interfaces*, *10*(39), 33652–33661. https://doi.org/10.1021/acsami.8b10727

Buchert, J., Pere, J., Johansson, L. S., & Campbell, J. M. (2001). Analysis of the surface chemistry of linen and cotton fabrics. *Textile Research Journal*, *71*(7), 626–629. https://doi.org/10.1177/004051750107100710

Burca, G., Kockelmann, W., James, J. A., & Fitzpatrick, M. E. (2013). Modelling of an imaging beamline at the ISIS pulsed neutron source. *Journal of Instrumentation*, *8*(10). https://doi.org/10.1088/1748-0221/8/10/P10001

Burchard, W. (2003). Solubility and solution structure of cellulose derivatives. *Cellulose*, *10*(3), 213–225. https://doi.org/10.1023/A:1025160620576

Burnham, D. K. (1980). *Warp and weft : a textile terminology /Dorothy K. Burnham*. Toronto: Royal Ontario Museum.

Burnstock, A., & White, R. (2014). the Effects of Selected Solvents and Soaps on a Simulated Canvas Painting. *Studies in Conservation*, *35*(sup1), 111–118. https://doi.org/10.1179/sic.1990.35.s1.024

Butler, S. (1988). *The ageing of Paraloid B-72 based adhesives : I. Solubility and infrared UV-Vis spectroscopy studies*. London.

Butler, S. (1989). *The ageing of Paraloid B-72 based adhesives: II. Viscometry*. London.

Butt, H. J., Cappella, B., & Kappl, M. (2005). *Force measurements with the atomic force microscope: Technique, interpretation and applications*. *Surface Science Reports* (Vol. 1). https://doi.org/10.1016/j.surfrep.2005.08.003

Buzzegoli, E., Landi, L., & Minotti, D. (2006). The phenomenon of diffusion of materials used for painting consolidation in a porous support. In *The Care of Painted Surfaces. Materials and methods for consolidation, and scientific methods to evaluate their effectiveness* (pp. 82–83). Milan: Saonara : Il prato.

Cao, X., Chen, Y., Chang, P. R., Muir, A. D., & Falk, G. (2008). Starch-based nanocomposites reinforced with flax cellulose nanocrystals. *Express Polymer Letters*, *2*(7), 502–510. https://doi.org/10.3144/expresspolymlett.2008.60

Cappitelli, F. (2000). Difficulties In The Scientific Study of Synthetic Materials In Paints. *Conservation Journal*, (34). Retrieved from http://www.vam.ac.uk/content/journals/conservation-journal/issue-34/difficulties-in-the-scientific-study-of-synthetic-materials-in-paints/

Carlisle, B. S., Johns, R. C., & Hassan, Y. A. (1994). Two-Phase Fluid Flow Measurements in Small Diameter Channels Using Real-Time Neutron Radiography. In *4th Int. Topical Meeting on Nuclear Thermalhydraulics, Operations, and Safety, 43-B-1* (pp. 1–6). Taipei, Taiwan (1994).

Carminati, C., Boillat, P., Schmid, F., Vontobel, P., Hovind, J., Morgano, M., … Kaestner, A. (2019). Implementation and assessment of the black body bias correction in quantitative neutron imaging. *PLoS ONE*, *14*(1), 1–24. https://doi.org/10.1371/journal.pone.0210300

Cassie, A. B. D., & Baxter, S. (1944). Wetting of porous surfaces. *Transactions of the Faraday Society*.

Cataldi, A., Deflorian, F., & Pegoretti, A. (2015). Poly 2-ethyl-2-oxazoline/microcrystalline cellulose composites for cultural heritage conservation: Mechanical characterization in dry and wet state and application as lining adhesives of canvas. *International Journal of Adhesion and Adhesives*, *62*, 92–100. https://doi.org/10.1016/j.ijadhadh.2015.07.002

Cataldi, A., Dorigato, A., Deflorian, F., & Pegoretti, A. (2014). Effect of the water sorption on the mechanical response of microcrystalline cellulose-based composites for art protection and

restoration. *Journal of Applied Polymer Science*, *131*(18), 40741. https://doi.org/10.1002/APP.40741

Cataldi, A., Dorigato, A., Deflorian, F., & Pegoretti, A. (2015). Innovative microcrystalline cellulose composites as lining adhesives for canvas. *Polymer Engineering and Science*, *55*(6), 1349–1354. https://doi.org/10.1002/pen.24074

Célino, A., Fréour, S., Jacquemin, F., & Casari, P. (2014). The hygroscopic behavior of plant fibers: a review. *Frontiers in Chemistry*, 1–43. https://doi.org/10.3389/fchem.2013.00043

Cheng, C. L., Kang, M., Perfect, E., Voisin, S., Horita, J., Bilheux, H. Z., … Hussey, D. S. (2012). Average Soil Water Retention Curves Measured by Neutron Radiography. *Soil Science Society of America Journal*, *76*(4), 1184. https://doi.org/10.2136/sssaj2011.0313

Cheng, D., Wen, Y., An, X., Zhu, X., Cheng, X., Zheng, L., & Nasrallah, J. E. (2016). Improving the colloidal stability of Cellulose nano-crystals by surface chemical grafting with polyacrylic acid. *Journal of Bioresources and Bioproducts*, *1*(3), 114–119.

Cheng, L. H., Karim, A. A., & Seow, C. C. (2006). Effects of Water-Glycerol and Water-Sorbitol Interactions on the Physical Properties of Konjac Glucomannan Films. *Journal of Food Science*, *71*(2), E62–E67. https://doi.org/10.1111/j.1365-2621.2006.tb08898.x

Cheng, Q., Wang, S., & Rials, T. G. (2009). Poly(vinyl alcohol) nanocomposites reinforced with cellulose fibrils isolated by high intensity ultrasonication. *Composites Part A*, *40*(2), 218–224.

Chevalier-Menu, A. (2010). *Comment concevoir un protocole d'application des technologies laser et nanogels pour la conservation/restauration des peintures sur toile*. École Nationale Supérieure d'Arts et Métiers.

Chevalier-Menu, Aurélia. (2010). *How to conceive an innovative method based on the application of lasers and nanogels to the conservation of easel paintings*. École Nationale Supérieure d'Arts et Métiers.

Chevalier, A., Chelazzi, D., P., B., Giorgi, R., Caretti, E., Stuke, M., & Menu, M. (2008). Extraction d'adhesifs de rentoilage en peinture de chevalet: nouvelle approche. In *ICOM-CC 15th Triennial Conference, New Delhi*.

Chiriboga Arroyo, P. G. (2013). *Finite Element Modeling of Vibrations in Canvas Paintings*. University TU Delft, Netherlands.

Chung, Y. (2011). Storage and management of paper and textile objects. In L. Kyushik & Y. Eeun (Eds.), *Conservation of papers and textiles* (p. 324). Daejeon, Korea: National Research Institute of Cultural Heritage.

Cipriani, G., Salvini, A., Baglioni, P., & Bucciarelli, E. (2010). Cellulose as a Renewable Resource for the Synthesis of Wood Consolidants. *Journal of Applied Polymer Science*, *118*, 2939–2950.

Coddington, J., & Young, C. (2018). Structure and lining: A review. *AIC News*, *43*(3), 6–9.

Cognard, J. (2004). *Science et technologie du collage*. Lausanne: Presses polytechniques et universitaires romandes.

Collins, G. E. (1939). Fundamental Principles that Govern the Shrinkage of Cotton Goods by Washing. *Journal of the Textile Institute Proceedings*, *30*(3), 37–41. https://doi.org/10.1080/19447013908687452

Conserving canvass symposium. (2019). In *Conserving canvas symposium*. Yale.

Conti, W., Tassinari, E., & Urbani, G. (1972). *Analysis of Creep Curves on Lining Canvas*. *ICOM Report 21/72/6*. London.

Cook, R. D. (1995). *Finite element modeling for stress analysis*. *Choice Reviews Online*. John Wiley & Sons, Ltd. https://doi.org/10.5860/choice.32-6245

CottonIncorporated. (2004). *A guide to improved shrinkage performance of cotton fabrics*. Cary, North carolina, USA.

Crawshaw, J., & Cameron, R. E. (2000). A small angle X-ray scattering study of pore structure in Tencel® cellulose fibres and the effects of physical treatments. *Polymer*, *41*(12), 4691–4698. https://doi.org/10.1016/S0032-3861(99)00502-9

Crisp, M. T., & Riehle, R. J. (2009). Wet-strengthening of paper in neutral pH papermaking conditions. In *Applications of Wet-End Paper Chemistry: Second Edition*. https://doi.org/10.1007/978-1-4020-6038-0_8

Cui, S. Z., & Wang, S. Y. (1999). Nonlinear Creep Characterization of Textile Fabrics. *Textile Research Journal*, *69*(12), 931–934. https://doi.org/10.1177/004051759906901208

D'haenens, M. (2013). La pénétration des adhésifs de doublage. Retrieved July 5, 2019, from http://ceroart.revues.org/3082

Dai, D., Fan, M., & Collins, P. (2013). Fabrication of nanocelluloses from hemp fibers and their application for the reinforcement of hemp fibers. *Industrial Crops and Products*, *44*, 192–199. https://doi.org/10.1016/j.indcrop.2012.11.010

Darque-Ceretti, E., & Felder, E. (2003). *Adhésion et adhérence*. Paris: CNRS Editions.

Das, B., Das, A., Kothari, V. K., & Fangueiro, R. (2011). Development of mathematical model to predict vertical wicking behaviour. Part I: flow through yarn. *Journal of The Textile Institute*, *102*(11), 957–970.

Das, B., Das, A., Kothari, V. K., Fanguiero, R., & de Araújo, M. (2007). Moisture transmission through textiles: Part I: Processes involved in moisture transmission and the factors at play. *Autex Research Journal*, *7*(2), 100–110.

Davies, G. C., & Bruce, D. M. (1998). Effect of Environmental Relative Humidity and Damage on the Tensile Properties of Flax and Nettle Fibers. *Textile Research Journal*, *68*(9), 623–639. https://doi.org/10.1177/004051759806800901

de Britto, D., & Assis, O. B. G. (2009). Thermal degradation of carboxymethylcellulose in different salty forms. *Thermochimica Acta*, *494*(1–2), 115–122. https://doi.org/10.1016/j.tca.2009.04.028

De la Orden, M. U., Matías, M. C., & Urreaga, J. M. (2004). Spectroscopic Study of the Modification of Cellulose with Polyethylenimines. *Journal of Applied Polymer Science*, *92*(4), 2196–2202. https://doi.org/10.1002/app.20236

de Souza Lima, M., & Borsali, R. (2002). Static and dynamic light scattering from polyelectrolyte microcrystal cellulose. *Langmuir*, *18*(4), 992–996.

de Witte, E., Goessens-Landrie, M., Goethals, E. J., & Simonds, R. (1978). The Structure of "Old" and "New" Paraloid B 72. *ICOM Committee for Conservation 5th Triennial Mtg, Zagreb*.

Defraeye, T., Derome, D., Aregawi, W., Cantré, D., Hartmann, S., Lehmann, E., … Nicolai, B. (2014). Quantitative neutron imaging of water distribution, venation network and sap flow in leaves. *Planta*, *240*(2), 423–436. https://doi.org/10.1007/s00425-014-2093-3

Dei, L., & Giorgi, R. (2013). The Degradation of Works of Art Materials. In P. Baglioni & D. Chelazzi (Eds.), *Nanoscience for the conservation of works of art*. RSC Publishing.

Delcroix, G., & Havel, M. (1988). *Phénomènes physiques et peinture artistique* (EREC). Puteaux.

Deloid, G. M., Cao, X., Molina, R. M., Silva, D. I., Bhattacharya, K., Ng, K. W., … Demokritou, P. (2019). Toxicological effects of ingested nanocellulose in in vitro intestinal epithelium and in vivo rat models. *Environmental Science: Nano*, *6*(7), 2105–2115. https://doi.org/10.1039/c9en00184k

Dhar, P., Bhardwaj, U., Kumar, A., & Katiyar, V. (2017). Investigations on rheological and mechanical behavior of poly(3-Hydroxybutyrate)/cellulose nanocrystal based nanobiocomposites. *Polymer Composites*, *38*(1), E392–E401. https://doi.org/10.1002/pc.23859

Doerner, M. (1984). *The Materials of the Artist and their Use in Painting*. Harvest Book.

Down, J. L. (2015). The evaluation of selected poly(vinyl acetate) and acrylic adhesives: A final research update. *Studies in Conservation*, *60*(1), 33–54. https://doi.org/10.1179/2047058414Y.0000000129

Dreyfuss-Deseigne, R. (2017). Nanocellulose Films in Art Conservation: A New and Promising Mending Material for Translucent Paper Objects. *Journal of Paper Conservation*, *18*(1), 18–29. https://doi.org/10.1080/18680860.2017.1334422

Drinberg, A., & Yakovlev, A. D. (1953). Transformation of polybutyl methacrylate into a tridimensional polymer. *Zhurnal Prikladnoi Khimii*, *26:532*(7).

Dufresne, A. (2013). Nanocellulose: a new ageless bionanomaterial. *Materials Today*, *16*(6), 220–227. https://doi.org/10.1016/j.mattod.2013.06.004

Dufresne Alain, & Cavaillé Jean-Yves. (1998). Clustering and percolation effects in microcrystalline starch-reinforced thermoplastic. *Journal of Polymer Science Part B: Polymer Physics*, *36*(12), 2211–2224. Retrieved from http://dx.doi.org/10.1002/(SICI)1099-0488(19980915)36:12%3C2211::AID-POLB18%3E3.0.CO;2-2

Duncan, J. (2008). Principles and Applications of Mechanical Thermal Analysis. In P. Gabbott (Ed.), *Principles and Applications of Thermal Analysis* (pp. 119–153). Blackwell Publishing. https://doi.org/10.1002/9780470697702

Eischen, J. W., Deng, S., & Clapp, T. G. (1996). Finite-element modeling and control of flexible fabric parts. *IEEE Computer Graphics and Applications*, *16*(5), 71–80. https://doi.org/10.1109/38.536277

El Messiry, M., El Ouffy, A., & Issa, M. (2015). Microcellulose particles for surface modification to enhance moisture management properties of polyester, and polyester/cotton blend fabrics. *Alexandria Engineering Journal*, *54*(2), 127–140. https://doi.org/10.1016/j.aej.2015.03.001

Endes, C., Camarero-Espinosa, S., Mueller, S., Foster, E., Petri-Fink, A., Rothen-Rutishauser, B., … Clift, M. (2016). A critical review of the current knowledge regarding the biological impact of nanocellulose. *Journal Of Nanobiotechnology*, *14*(78). https://doi.org/10.1186/s12951-016-0230-9

Environmental Guidelines ICOM-CC and IIC Declaration. (2014). Retrieved July 30, 2019, from http://www.icom-cc.org/332/-icom-cc-documents/declaration-on-environmental-guidelines/#.XUAO0_lKipp

Erhardt, D., & Mecklenburg, M. (1994). Relative humidity re-examined. *Studies in Conservation*, *39*(2), 32–38. https://doi.org/10.1179/sic.1994.39.supplement-2.32

Espy, H. H. (1995). The mechanism of wet-strength development in paper. *TAPPI Journal*.

Farag, R., & Elmogahzy, Y. (2009). Tensile properties of cotton fibers. In A. R. Bunsell (Ed.), *Handbook of Tensile Properties of Textile and Technical Fibres* (pp. 51–72). Sawston, Cambridge: Woodhead Publishing Series in Textiles.

Farmakalidis, H. V., Douvas, A. M., Karatasios, I., Sotiropoulou, S., Boyatzis, S., Argitis, P., … Kilikoglou, V. (2016). Accelerated thermal ageing of acrylic copolymers, cyclohexanone-based and urea-aldehyde resins used in paintings conservation. *Mediterranean Archaeology and Archaeometry*, *16*(3), 213–228. https://doi.org/10.5281/zenodo.163773

Favier, V., Canova, G. R., Cavaillé, J. Y., Chanzy, H., Dufresne, A., & Gauthier, C. (1995). Nanocomposite materials from latex and cellulose whiskers. *Polymers for Advanced Technologies*, *6*(5), 351–355.

Feller, R. L., & Curran, M. (1970). Solubility and Crosslinking Characteristics of Ethylene/Vinylacetate Copolymers. *Bulletin of the American Group. International Institute for Conservation of Historic and Artistic Works*, *11*(1), 42–45. https://doi.org/10.2307/3179081

Feller, R., & Wilt, M. (1990). *Evaluation of Cellulose Ethers for Conservation*. *Research in Conservation* (Vol. 3). Retrieved from http://www.bcin.ca/Interface/openbcin.cgi?submit=submit&Chinkey=109521

Feller, Robert L, Curran, M., & Bailie, C. (1981). Photochemical Studies of Methacrylate Coatings for the Conservation of Museum Objects. In *Photodegradation and Photostabilization of Coatings* (pp. 183–196). https://doi.org/10.1021/bk-1981-0151.ch013

Fernandes Diniz, J. M. B., Gil, M. H., & Castro, J. A. A. M. (2004). Hornification - Its origin and

interpretation in wood pulps. *Wood Science and Technology*, *37*(6), 489–494. https://doi.org/10.1007/s00226-003-0216-2

Flor, G., Campari-Vigano, G., & Feduzi, R. (1989). A thermal study on moisture absorption by epoxy composites. *Journal of Thermal Analysis*, *35*(7), 2255–2264.

Forney, C. F., & Brandl, D. G. (1992). Control of Humidity in Small Controlled- environment Chambers using Glycerol-Water Solutions. *Technology and Products Reports*, 53–54.

Forsgren, L., Sahlin-Sjövold, K., Venkatesh, A., Thunberg, J., Kádár, R., Boldizar, A., … Rigdahl, M. (2019). Composites with surface-grafted cellulose nanocrystals (CNC). *Journal of Materials Science*, *54*(4), 3009–3022. https://doi.org/10.1007/s10853-018-3029-2

Foster, G., Odlyha, M., & Hackney, S. (1997). Evaluation of the effects of environmental conditions and preventive conservation treatment on painting canvases. *Thermochimica Acta*, *294*(1), 81–89. https://doi.org/10.1016/S0040-6031(96)03147-4

Frihart, C. R. (2012). Wood adhesion and adhesives. In *Handbook of Wood Chemistry and Wood Composites, Second Edition*. https://doi.org/10.1201/b12487

Gardner, D. J., Oporto, G. S., Mills, R., & Samir, M. A. S. A. (2008). Adhesion and surface issues in cellulose and nanocellulose. *Journal of Adhesion Science and Technology*, *22*(5–6), 545–567. https://doi.org/10.1163/156856108X295509

Geiger, T., & Michel, F. (2005). Studies on the Polysaccharide JunFunori Used to Consolidate Matt Paint. *Studies in Conservation*, *50*(3), 193–204. https://doi.org/10.1179/sic.2005.50.3.193

Gelse, K., Pöschl, E., & Aigner, T. (2003). Collagens--structure, function, and biosynthesis. *Advanced Drug Delivery Reviews*, *55*(12), 1531-46.

Gettens, R. J., & Stout, G. L. (1966). *Paintings Materials*. NY: Dover Publications.

Gicquel, E., Martin, C., Garrido Yanez, J., & Bras, J. (2017). Cellulose nanocrystals as new bio-based coating layer for improving fiber-based mechanical and barrier properties. *Journal of Materials Science*, *52*(6), 3048–3061.

Golden, M. (2013). Painting support: Cotton Canvas.

Golden, M. (2015). Defining the acrylic patina. *Just Paint by Golden Artist Colors*, (23), 11.

Gong, G. (2014). *Handbook of Green Materials: Processing Technologies, Properties and Applications*. (K. Oksman, P. Mathew Aji, & A. Bismarck, Eds.), *vol. 5* (World Scie).

Gottsegen, M. D. (1993). *The Painter's Handbook*. NY: Watson-Guptill.

Grassie, N. (2008). Photodegradation of methacrylate/acrylate copolymers. *Pure and Applied Chemistry*, *34*(2), 247–258. https://doi.org/10.1351/pac197334020247

Graves, D. J. (2004). A comparative study of consolidants for waterlogged wood: polyethylene glycol, sucrose and silicone oil. *SSCR Journal*, *15*(3), 13–17.

Gray, K. L. (1971). The swelling and shrinkage of untreated fabrics. In H. Mark, N. S. Wooding, & S. M. Atlas (Eds.), *Chemical aftertreatment of textiles* (Wiley-Inte, pp. 115–33). New York.

Grøntoft, T., Odlyha, M., Mottner, P., Dahlin, E., Lopez-Aparicio Susana, S., Jakiela, S., … Wadum, J. (2010). Pollution monitoring by dosimetry and passive diffusion sampling for evaluation of environmental conditions for paintings in microclimate frames. *Journal of Cultural Heritage*, *11*(4), 411–419. https://doi.org/10.1016/j.culher.2010.02.004

Guan, Y., & Li, Y. (2008). Fabrication of cotton nano-powder and its textile application. *Chinese Science Bulletin*, *53*(23), 3735–3740.

Guo, X., Wu, Y., & Xie, X. (2017). Water vapor sorption properties of cellulose nanocrystals and nanofibers using dynamic vapor sorption apparatus. *Scientific Reports*, *7*(14207), 1–12. https://doi.org/10.1038/s41598-017-14664-7

Habibi, Y., Lucia, L., & Rojas, O. (2010). Cellulose Nanocrystals: Chemistry, Self-Assembly, and

Applications. *Chemical Reviews*, *110*(6), 3479–3500.

Hackney, S., Reifsnyder, J., te Marverde, M., & Scharff, M. (2012). Lining easel paintings. In J. H. S. and R. Rushfield (Ed.), *The conservation of easel paintings*. London: Routledge.

Hackney, S, & Hedley, G. (1981). MEASUREMENTS OF THE AGEING OF LINEN CANVAS. *Conservation Studies in Conservation*, *26*(26), 1–14. Retrieved from http://www.jstor.org

Hackney, Stephen. (1984). The distribution of gaseous air pollution within museums. *Studies in Conservation*, *29*(3), 105–116.

Hackney, Stephen. (2004a). Paintings on Canvas: Lining and Alternatives. *Tate Papers*.

Hackney, Stephen. (2004b). Paintings on Canvas: Lining and Alternatives. *Tate Papers*. Retrieved from http://search.proquest.com/docview/911909302/

Hackney, Stephen. (2007). The evolution of a conservation framing policy at Tate. In *Museum microclimates* (pp. 229–235). Copenhagen.

Hackney, Stephen, & Ernst, T. (1994). The applicability of alkaline reserves to painting canvases. *Studies in Conservation*, *39*(2), 223–227. https://doi.org/10.1179/sic.1994.39.supplement-2.223

Hamm, J., Gavett, B., Golden, M., Hayes, J., Kelly, C., Messinger, J., … Suffield, B. (1993). The Discoloration of Acrylic Dispersion Media. In D. Grattan (Ed.), *Saving the Twentieth Century: The Conservation of Modern Materials* (pp. 381–392). Ottawa: Canadian Conservation Institute.

Han, J., Zhou, C., Wu, Y., Liu, F., & Wu, Q. (2013). Self-assembling behavior of cellulose nanoparticles during freeze-drying: Effect of suspension concentration, particle size, crystal structure, and surface charge. *Biomacromolecules*, *14*(5), 1529–1540. https://doi.org/10.1021/bm4001734

Hansen, E. F., Derrick, M. R., Schilling, M. R., & Garcia, R. (1991). The effects of solution application on some mechanical and physical properties of thermoplastic amorphous polymers used in conservation: Poly(vinyl acetate)s. *Journal of the American Institute for Conservation*, *30*(2), 203. https://doi.org/10.1179/019713691806066764

Harmon, R. E., De, K. K., & Gupta, S. K. (1973). New procedure for preparing trimethylsilyl derivatives of polysaccharides. *Carbohydr. Res.*, *31*(2), 407–409.

Harper, B., Clendaniel, A., Sinche, F., Way, D., Hughes, M., Schardt, J., … Harper, S. (2016). Impacts of chemical modification on the toxicity of diverse nanocellulose materials to developing zebrafish. *Cellulose*, *23*(3), 1763–1775.

He, M. Y., Heredia, F. E., Wissuchek, D. J., Shaw, M. C., & Evans, A. G. (1993). The mechanics of crack growth in layered materials. *Acta Metallurgica Et Materialia*, *41*(4), 1223–1228. https://doi.org/10.1016/0956-7151(93)90171-N

Hearle, J. W. S. (1963). The fine structure of fibers and crystalline polymers. III. Interpretation of the mechanical properties of fibers. *Journal of Applied Polymer Science*, *7*, 1207–1223. https://doi.org/10.1002/app.1963.070070403

Hebeish, A., Farag, S., Sharaf, S., & Shaheen, T. I. (2018). High performance fabrics via innovative reinforcement route using cellulose nanoparticles. *The Journal of The Textile Institute*, *109*(2), 186–194.

Hedley, G., Odlyha, M., Burnstock, A., Tillinghast, J., & Husband, C. (1991). A study of the mechanical and surface properties of oil paint films treated with organic solvents and water. *Journal of Thermal Analysis*, *37*(9), 2067–2088. https://doi.org/10.1007/BF01905579

Hedley, G., Villers, C., & Mehra, V. R. (1993). Artists' canvases: their history and future. In C. Villers (Ed.), *Measured opinions : collected papers on the conservation of paintings* (p. 53). London: United Kingdom Institute for Conservation.

Hedley, Gerry. (1975). The effect of beeswax/resin impregnation on the tensile properties of canvas. In ICOM (Ed.), *Icom committee for conservation. 4th triennial meeting*. Paris.

Hedley, Gerry. (1988a). Relative Humidity and the Stress/Strain Response of Canvas Paintings: Uniaxial

Measurements of Naturally Aged Samples. *Studies in Conservation*, *33*(3), 133. https://doi.org/10.2307/1506206

Hedley, Gerry. (1988b). Relative Humidity and the Stress / Strain Response of Canvas Paintings : Uniaxial Measurements of Naturally Aged Samples. *Studies in Conservation*, *33*(3), 133–148.

Hedley, Gerry. (1993a). Artits' Canvases: their History and Future. In Caroline Villers (Ed.), *Measured opinions : collected papers on the conservation of paintings* (pp. 50–56). London: United Kingdom Institute for Conservation.

Hedley, Gerry. (1993b). *Measured opinions : collected papers on the conservation of paintings /Gerry Hedley ; edited by Caroline Villers.* London: United Kingdom Institute for Conservation.

Hendrickx, R., Desmarais, G., Weder, M., Ferreira, E. S. B., & Derome, D. (2016). Moisture uptake and permeability of canvas paintings and their components. *Journal of Cultural Heritage*, *19*, 445–453. https://doi.org/10.1016/j.culher.2015.12.008

Hendrickx, R., Ferreira, E. S. B., Boon, J. J., Desmarais, G., Derome, D., Angelova, L., … Richardson, E. (2017). Distribution of moisture in reconstructed oil paintings on canvas during absorption and drying: A neutron radiography and NMR study. *Studies in Conservation*, *62*(7), 393–409. https://doi.org/10.1080/00393630.2016.1181899

Herrick, F.W., Casebier, R.L., Hamilton, J.K. and Sandberg, K. R. (1983). Microfibrillated cellulose: morphology and accessibility. *J. Appl. Polym. Sci. Polym. Symp.*, *37*, 797–813.

Hill, C. A. S., Norton, A., & Newman, G. (2009). The water vapor sorption behavior of natural fibers. *Journal of Applied Polymer Science*, *112*(3), 1524–1537. https://doi.org/10.1002/app.29725

Hock, C. W. (1942). Microscopic structure of flax and related bast fibers. *Journal of Research of the National Bureau of Standards*, *29*, 41–50. https://doi.org/10.6028/jres.029.024

Hocker, E., Almkvist, G., & Sahlstedt, M. (2012). The Vasa experience with polyethylene glycol: A conservator's perspective. *Journal of Cultural Heritage*, *13*(3 SUPPL.). https://doi.org/10.1016/j.culher.2012.01.017

Horie, C. V. (Charles V. (2010). *Materials for conservation : organic consolidants, adhesives and coatings /Velson Horie.* (2nd ed.). Amsterdam ; London: Butterworth-Heinemann.

Horton-James, D., Walston, S., & Zounis, S. (1991). Evaluation of the Stability, Appearance and Performance of Resins for the Adhesion of Flaking Paint on Ethnographic Objects. *Studies in Conservation*, *36*(4), 203–221. https://doi.org/10.1179/sic.1991.36.4.203

Hubbe M., Rojas O.J., L. L. (2015). Green modification of surface characteristics of cellulosic materials at the molecular or nano scale: A review. *BioResources*, *10*, 6095–6206.

Hummelen, Y., & Scholte, T. (2012). Collecting and Archiving Information from Living Artists for the Conservation of Contemporary Art. *Conservation of Easel Paintings: Principles and Practice*, 39–47.

Hutchinson, J. W. (1996). *Stresses and failure modes in thinfilms and multilayers. Notesfor a Dcamm Course.* Technical University of Denmark, Lyngby.

Hutchinson, J. W., & Suo, Z. (1991). Mixed Mode Cracking in Layered Materials. *Advances in Applied Mechanics*, *29*, 63–191. https://doi.org/10.1016/S0065-2156(08)70164-9

Iaccarino Idelson, A. (2019). About the choice of tension for canvas paintings. *CeROArt*. https://doi.org/10.4000/ceroart.1269

Iler, R. K., & K, I. R. (1979). *The Chemistry of Silica: Solubility, Polymerization, Colloid and Surface Properties and Biochemistry of Silica*. *Endeavour*. https://doi.org/10.1016/0160-9327(80)90074-5

Islam, M. N., Khan, M. A., Alam, M. K., Zaman, M. A., & Matsubayashi, M. (2003). Study of water absorption behavior in wood plastic composites by using neutron radiography techniques. *Polymer - Plastics Technology and Engineering*, *42*(5), 925–934. https://doi.org/10.1081/PPT-120025004

Isogai, A. (2013). Wood nanocelluloses: fundamentals and applications as new bio-based nanomaterials.

Journal of Wood Science, *59*(6), 449–459. https://doi.org/10.1007/s10086-013-1365-z

Jackson, J. K., Letchford, K., Wasserman, B. Z., Ye, L., Hamad, W. Y., & Burt, H. M. (2011). The use of nanocrystalline cellulose for the binding and controlled release of drugs. *International Journal of Nanomedicine*, *6*, 321–330.

Jaïs-Camin, C. (1997). Etude sur la réversibilité d'une nouvelle méthode de doublage avec la Beva 371 vaporisée chaude. *Conservation Restauration Des Biens Culturels*, *10*, 46–53.

Janson, H. W., Zerbe, K., & Mayer, R. (2006). The Artist's Handbook of Materials and Techniques. *Parnassus*. https://doi.org/10.2307/772092

Jiang, Y., Lawrence, M., Hussain, A., Ansell, M., & Walker, P. (2019). Comparative moisture and heat sorption properties of fibre and shiv derived from hemp and flax. *Cellulose*, *26*(2), 823–843. https://doi.org/10.1007/s10570-018-2145-0

Jin, J., Chen, S., & Zhang, J. (2010). UV aging behaviour of ethylene-vinyl acetate copolymers (EVA) with different vinyl acetate contents. *Polymer Degradation and Stability*, *95*(5), 725–732. https://doi.org/10.1016/j.polymdegradstab.2010.02.020

Johansson, L. S., Campbell, J., Koljonen, K., Kleen, M., & Buchert, J. (2004). On surface distributions in natural cellulosic fibres. *Surface and Interface Analysis*, *36*(8), 706–710. https://doi.org/10.1002/sia.1741

Johansson, L. S., Tammelin, T., Campbell, J. M., Setälä, H., & Österberg, M. (2011). Experimental evidence on medium driven cellulose surface adaptation demonstrated using nanofibrillated cellulose. *Soft Matter*, *7*(10917), 10917–10924. https://doi.org/10.1039/c1sm06073b

Kaboorani, A., Auclair, N., Riedl, B., & Landry, V. (2016). Physical and morphological properties of UV-cured cellulose nanocrystal (CNC) based nanocomposite coatings for wood furniture. *Progress in Organic Coatings*, *93*, 17–22. https://doi.org/10.1016/j.porgcoat.2015.12.009

Kadi, N., & Karnoub, A. (2015). The Effect of Warp and Weft Variables on Fabric's Shrinkage Ratio. *Journal of Textile Science & Engineering*, *5*(2). https://doi.org/10.4172/2165-8064.1000191

Kaka, D. O., Rongong, J. A., Hodzic, A., & Lord, C. (2015). Dynamic mechanical properties of woven carbon fibre reinforced thermoplastic composite. In *20th International Conference on Composite Materials*. Copenhagen, Denmark.

Kalia, S., Dufresne, A., Cherian, B. M., Kaith, B. S., Avérous, L., Njuguna, J., & Nassiopoulos, E. (2011). Cellulose-based bio- and nanocomposites: A review. *International Journal of Polymer Science*, (837875). https://doi.org/10.1155/2011/837875

Kalia, S., Thakur, K., Celli, A., Kiechel, M. A., & Schauer, C. L. (2013). Surface modification of plant fibers using environment friendly methods for their application in polymer composites, textile industry and antimicrobial activities: A review. *Journal of Environmental Chemical Engineering*, *1*(3), 97–112.

Kalugina, E. V., Gumargalieva, K. Z., & Zaikov, G. E. (2004). Degradation of polysulfones and polyesterimides. In *Thermal Stability of Engineering Heterochain Thermoresistant Polymers* (pp. 98–151). Utrecht/Boston: VSP.

Kang, M., Bilheux, H. Z., Voisin, S., Cheng, C. L., Perfect, E., Horita, J., & Warren, J. M. (2013). Water calibration measurements for neutron radiography: Application to water content quantification in porous media. *Nuclear Instruments and Methods in Physics Research, Section A: Accelerators, Spectrometers, Detectors and Associated Equipment*. https://doi.org/10.1016/j.nima.2012.12.112

Karbowiak, T., Hervet, H., Léger, L., Champion, D., Debeaufort, F., & Voilley, A. (2006). Effect of plasticizers (water and glycerol) on the diffusion of a small molecule in iota-carrageenan biopolymer films for edible coating application. *Biomacromolecules*, *7*(6), 2011–2019. https://doi.org/10.1021/bm060179r

Karpowicz, A. (1989). In-plane deformations of films of size on paintings in the glass transition region. *Studies in Conservation*, *34*(2), 67–74.

Khan, F., Pilpel, N., & Ingham, S. (1988). The effect of moisture on the density, compaction and tensile strength of microcrystalline cellulose. *Powder Technology*, *54*(3), 161–164. https://doi.org/10.1016/0032-5910(88)80074-3

Khan, R. A., Salmieri, S., Dussault, D., Uribe-Calderon, J., Kamal, M. R., Safrany, A., & Lacroix, M. (2010). Production and properties of nanocellulose-reinforced methylcellulose-based biodegradable films. *Journal of Agricultural and Food Chemistry*, *58*(13), 7878–7885. https://doi.org/10.1021/jf1006853

Kiziltas, A., Gardner, D. J., Han, Y., & Yang, H.-S. (2011). Dynamic mechanical behavior and thermal properties of microcrystalline cellulose (MCC)-filled nylon 6 composites. *Thermochimica Acta*, *519*(1), 38–43.

Klebe, J. F. (1964). Silylsubstituted Polyureas. *Journal of Polymer Science Part B: Polymer Letters*, *2*(11), 1079–1983.

Klemm, D., Schumann, D., Kramer, F., Hebler, N., Koth, D., & Sultanova, B. (2009). Nanocellulose materials - Different cellulose, different functionality. *Macromolecular Symposia*, *280*(1), 60–71. https://doi.org/10.1002/masy.200950608

Kockelmann, W., Burca, G., Kelleher, J. F., Kabra, S., Zhang, S. Y., Rhodes, N. J., … Tremsin, A. S. (2015). Status of the Neutron Imaging and Diffraction Instrument IMAT. *Physics Procedia*, *69*(October 2014), 71–78. https://doi.org/10.1016/j.phpro.2015.07.010

Kohan, M. I. (1996). *Nylon Plastics Handbook*. *IEEE Electrical Insulation Magazine*. https://doi.org/10.1109/MEI.1996.537196

Kolman, K., Poggi, G., Baglioni, M., Chelazzi, D., Baglioni, P., Persson, M., … Bordes, R. (2019). pH-Controlled Assembly of Polyelectrolyte Layers onto Silica Nanoparticles. *In Preparation*.

Kolman, Krzysztof, Nechyporchuk, O., Persson, M., Holmberg, K., & Bordes, R. (2018a). Combined Nanocellulose/Nanosilica Approach for Multiscale Consolidation of Painting Canvases. *ACS Applied Nano Materials*, *1*(5), 2036–2040. https://doi.org/10.1021/acsanm.8b00262

Kolman, Krzysztof, Nechyporchuk, O., Persson, M., Holmberg, K., & Bordes, R. (2018b). Combined Nanocellulose/Nanosilica Approach for Multiscale Consolidation of Painting Canvases. *ACS Applied Nano Materials*, *1*(5), 2036–2040. https://doi.org/10.1021/acsanm.8b00262

Kramer, F., Klemm, D., Schumann, D., Heßler, N., Wesarg, F., Fried, W., & Stadermann, D. (2006). Nanocellulose Polymer Composites as Innovative Pool for (Bio)Material Development. *Macromolecular Symposia*, *244*(1), 136–148.

Krarup Andersen, C. (2013). *Lined canvas paintings, Mechanical properties and structural response to fluctuating relative humidity, exemplified by the collection of Danish Golden Age paintings at Statens Museum for Kunst (SMK)*. *ACM SIGMultimedia Records*. Royal Danish Academy of Fine Arts. https://doi.org/10.1145/3300001.3300014

Krueger, J. (2014). Aqueous Bleaching of Color Field Paintings. *Modern Materials and Contemporary Art Newsletter*, pp. 15–16.

Kubiak, K. J., Wilson, M. C. T., Mathia, T. G., & Carval, P. (2011). Wettability versus roughness of engineering surfaces. *Wear*. https://doi.org/10.1016/j.wear.2010.03.029

Kühn, H. (1986). *Conservation and restoration of works of art and antiquities / Volume 1. / Hermann Kühn ; translated by Alexandra Trone.*

La Nasa, J., Di Marco, F., Bernazzani, L., Duce, C., Spepi, A., Ubaldi, V., … Modugno, F. (2017). Aquazol as a binder for retouching paints. An evaluation through analytical pyrolysis and thermal analysis. *Polymer Degradation and Stability*, *144*, 508–519. https://doi.org/10.1016/j.polymdegradstab.2017.09.007

Lagarón, J. M., Cabedo, L., Cava, D., Feijoo, J. L., Gavara, R., & Gimenez, E. (2005). Improving packaged food quality and safety. Part 2: Nanocomposites. *Food Additives and Contaminants*, *22*(10), 994–998. https://doi.org/10.1080/02652030500239656

Lagerwall, J. P. F., Schütz, C., Salajkova, M., Noh, J., Park, J. H., Scalia, G., & Bergström, L. (2014). Cellulose nanocrystal-based materials: from liquid crystal self-assembly and glass formation to multifunctional thin films. *NPG Asia Materials*, *6*(1).

Landi, S. (2012). *Textile Conservator's Manual* (Rev. ed.). Routledge Ltd.

Lardet, G. (2014). Comparaison du Plexisol® P550 et du Medium de Consolidation® 4176. Retrieved from https://journals.openedition.org/ceroart/3986

Lasyk, Ł., Łukomski, M., Bratasz, Ł., & Kozłowski, R. (2008). Vibration as a hazard during the transportation of canvas paintings. In S. W. D. Saunders, J.H. Townsend (Ed.), *Conservation and Access: Contributions to the London Congress 15–19 September 2008* (pp. 64–68.). London: The International Institute of Conservation of Historic and Artistic Works. https://doi.org/10.1179/sic.2008.53.supplement-1.64

Lavoine, N., Bras, J., & Desloges, I. (2014). Mechanical and barrier properties of cardboard and 3D packaging coated with microfibrillated cellulose. *Journal of Applied Polymer Science*, *131*(8), n/a-n/a. https://doi.org/10.1002/app.40106

Lavoine, N., Desloges, I., Khelifi, B., & Bras, J. (2014). Impact of different coating processes of microfibrillated cellulose on the mechanical and barrier properties of paper. *Journal of Materials Science*, *49*(7), 2879–2893.

Lavoratti, A., Scienza, L. C., & Zattera, A. J. (2015). Dynamic Mechanical Analysis of Cellulose Nanofiber / Polyester Resin Composites, (July), 19–24.

Lazzari, M., & Chiantore, O. (2000). Thermal-ageing of paraloid acrylic protective polymers. *Polymer*, *41*, 6447–6455. https://doi.org/10.1016/S0032-3861(99)00877-0

Learner, T. J. S., Smithen, P., Krueger, J. W., & Schilling, M. R. (Eds.). (2007). Modern paints: uncovering the choices. In *Modern paints uncovered: proceedings from the modern paints uncovered symposium*.

Lee, K. Y., Aitomäki, Y., Berglund, L. A., Oksman, K., & Bismarck, A. (2014). On the use of nanocellulose as reinforcement in polymer matrix composites. *Composites Science and Technology*, *105*, 15–27. https://doi.org/10.1016/j.compscitech.2014.08.032

Li, S., & Lee, P. S. (2017). Development and applications of transparent conductive nanocellulose paper. *Science and Technology of Advanced Materials*, *18*(1), 620–633.

Li, W., Yue, J., & Liu, S. (2011). Preparation of nanocrystalline cellulose via ultrasound and its reinforcement capability for poly(vinyl alcohol) composites. *Ultrasonics - Sonochemistry*, *19*(3).

Li, Y., & Luo, Z. X. (2000). Physical mechanisms of moisture diffusion into hygroscopic fabrics during humidity transients. *Journal of the Textile Institute*, *91*(2), 302–316. https://doi.org/10.1080/00405000008659508

Lin, N., & Dufresne, A. (2014). Nanocellulose in biomedicine: Current status and future prospect. *European Polymer Journal*, *59*, 302–325.

Lin, N., Huang, J., & Dufresne, A. (2012). Preparation, properties and applications of polysaccharide nanocrystals in advanced functional nanomaterials: a review. *Nanoscale*, *4*(11), 3274–3294.

Lindstrom, S. B., Kulachenko, A., Karabulut, E., & Sehaqui, H. (2012). Mechanosorptive creep in nanocellulose materials, (19), 809–819. https://doi.org/10.1007/s10570-012-9665-9

Lindström, T., Wågberg, L., & Larsson, T. (2005). On the nature of joint strength in paper – a review of dry and wet strength resins used in paper manufacturing. *13th Fundamental Research Symposium*, *32*(May 2005), 457–562.

Lodge, R. G. (1988). A history of synthetic painting media with special reference to commercial materials. In *The American Institute for Conservation of Historic and Artistic Works: preprints of papers presented at the sixteenth annual meeting, New Orleans, Louisiana, June 1-5, 1988*.

Lodish H, Berk A, Z. S. et al. (2000). Collagen:The Fibrous Proteins of the Matrix. In *Molecular Cell Biology*.

López-Aparicio, S., Grøntoft, T., Odlyha, M., Dahlin, E., Mottner, P., Thickett, D., … Scharff, M. (2010). Measurement of organic and inorganic pollutants in microclimate frames for. *E-Preserv Sci*, *7*, 59–70.

Ly, B., Thielemans, W., Dufresne, A., Chaussy, D., & Belgacem, M. N. (2008). Surface functionalization of cellulose fibres and their incorporation in renewable polymeric matrices. *Composites Science and Technology*, *68*, 3193–3201. https://doi.org/10.1016/j.compscitech.2008.07.018

Macbeth, R., Odlyha, M., Burnstock, A., Villers, C., & Bruce-Gardner, R. (1993). Evaluation of moisture treatment of fabric-supported paintings. In *ICOM Committee for Conservation 10th triennial meeting: Washington, DC, 22-27 August 1993: preprints*.

Mäkelä, T., Kainlauri, M., Willberg-Keyriläinen, P., Tammelin, T., & Forsström, U. (2016). Fabrication of micropillars on nanocellulose films using a roll-to-roll nanoimprinting method. *Microelectronic Engineering*, *163*, 1–6. https://doi.org/10.1016/j.mee.2016.05.023

Malešič, J., Kolar, J., Strlič, M., Kočar, D., Fromageot, D., Lemaire, J., & Haillant, O. (2005). Photo-induced degradation of cellulose. *Polymer Degradation and Stability*, *89*(1), 64–69. https://doi.org/10.1016/j.polymdegradstab.2005.01.003

Mannes, D., Sanabria, S., Funk, M., Wimmer, R., Kranitz, K., & Niemz, P. (2014). Water vapour diffusion through historically relevant glutin-based wood adhesives with sorption measurements and neutron radiography. *Wood Science and Technology*, *48*(3), 591–609. https://doi.org/10.1007/s00226-014-0626-3

Mannes, David, Schmid, F., Wehmann, T., & Lehmann, E. (2017). Design and Applications of a Climatic Chamber for in-situ Neutron Imaging Experiments. *Physics Procedia*, *88*(September 2016), 200–207. https://doi.org/10.1016/j.phpro.2017.06.028

Mannes, David, Sonderegger, W., Hering, S., Lehmann, E., & Niemz, P. (2009). Non-destructive determination and quantification of diffusion processes in wood by means of neutron imaging. *Holzforschung*, *63*(5), 589–596. https://doi.org/10.1515/HF.2009.100

Maor, Y., & Murray, A. (2007). Delamination of Oil Paints on Acrylic Grounds. *MRS Proceedings*. https://doi.org/10.1557/proc-1047-y04-01

Martin, A., Rouchon, V., Aubry, T., Cauliez, N., Desroches, M., & Margez, M. (2011). Local Strenghtening of Mould-Damaged Manuscripts, A Case Study on Logbooks of Early French Expeditions in Louisiana (1684-1722). *Journal of Paper Conservation*.

Mayer, R., & Smith, E. (1973). *The Artist's Handbook of Materials and Techniques, 3rd Rev. ed.* (E. Smith, Ed.) (Faber). London.

McGlinchey, C., Ploeger, R., Colombo, A., Simonutti, R., Palmer, M., Chiantore, O., … de la Rie, E. R. (2011). and Consolidating Adhesives: Some New Developments and Areas of Future Research. In *Adhesives and Consolidants for Conservation: Research and Applications, Canadian Conservation Institute*. Ottawa.

Mecklenburg, M. F., Fuster-Lopez, L., Ottolini, S. (2012). The glass transition temperature of adhesives : preliminary guidelines for canvas painting treatments. In A. Barros D'Sa (Ed.), *Adhesives and consolidants in painting conservation* (pp. 30–36). Institute of Conservation. Paintings Group., London: Archetype in association with the ICON Paintings.

Mecklenburg, M. F. (1982a). *Some Aspects of the Mechanical Behaviour of Fabric Supported Paintings'. Report to the Smithsonian Institution*. Washington, D.C.

Mecklenburg, M. F. (1982b). *Some Aspects of the Mechanical Behaviour of Fabric Supported Paintings'. Report to the Smithsonian Institution*. Washington, D.C. Retrieved from https://repository.si.edu/handle/10088/55639.

Mecklenburg, Marion F. (2007). *Determining the Acceptable Ranges of Relative Humidity And Temperature in Museums and Galleries, Part 1, Structural Response to Relative Humidity*. Suitland, Maryland.

Mecklenburg, Marion F., & Fuster Lopez, L. (2006). Failure Mechanisms in Canvas Supported Paintings:

Approaches for Developing Consolidation Protocols. In *The Care of Painted Surfaces. Materials and methods for consolidation, and scientific methods to evaluate their effectiveness. Proceedings of the Conference, Milan, November 10-11, 2006 (Third International Conference: Colour and Conservation, Materials a*.

Mecklenburg, Marion F., McCormick-Goodhart, M., & Tumosa, C. S. (1994). Investigation into the Deterioration of Paintings and Photographs Using Computerized Modeling of Stress Development. *Journal of the American Institute for Conservation*, *33*(2). https://doi.org/10.2307/3179424

Mecklenburg, Marion F., McCormick-Goodhart, M., & Tumosa, C. S. (2006). Investigation into the Deterioration of Paintings and Photographs Using Computerized Modeling of Stress Development. *Journal of the American Institute for Conservation*, *33*(2), 153. https://doi.org/10.2307/3179424

Mehra, V. (1981). The cold lining of paintings. *The Conservator*, *5*(1), 12–14. https://doi.org/10.1080/01410096.1981.9994946

Mehra, V. R. (1975). Further develoments in cold lining (nap-bond system). In *ICOM Triennal Meeting, 4th Venise* (p. 90). Paris: ICOM committe for conservation.

Mehra, Vishwa R. (1972). Comparative study of conventional relining methods and materials and research towards their improvement. In *Interim report ICOM comittee for conservation, 3rd Triennial meeting*. Madrid, Spain.

Mehra, Vishwa R. (1975). Comparative Study of Conventional Relining Methods and Materials and Research Towards Their Improvement. In *ICOM Committee for Conservation, 4th Triennial Meeting, Venice*. Venice.

Meinert, M. C., & Delmer, D. P. (1977). Changes in Biochemical Composition of the Cell Wall of the Cotton Fiber During Development. *Plant Physiology*, *59*(6), 1088–1097. https://doi.org/10.1104/pp.59.6.1088

Menard, K. P., & Menard, N. R. (2015). Dynamic Mechanical Analysis in the Analysis of Polymers and Rubbers. In *Encyclopedia of Polymer Science and Technology*. https://doi.org/10.1002/0471440264.pst102.pub2

Mhetre, S., & Parachuru, R. (2010). The effect of fabric structure and yarn-to-yarn liquid migration on liquid transport in fabrics. *Journal of The Textile Institute*, *101*(7), 621–626.

Michalski, S. (1991). Paintings-their response to temperature, relative humidity, shock, and vibration. In *Art in Transit: Studies in the Transport of Paintings* (pp. 223–248). Washington, DC, USA: National Gallery of Art Washington. Retrieved from http://hdl.handle.net/10088/8128

Michalski, S., & Daly Hartin, D. (1996). Preliminary Testing of Lined Model Paintings. In W. Mourey & L. Robbiola (Eds.), *CCI Lining Project, ICOM Committee for Conservation 11th Triennial Meeting Edinburgh* (pp. 288–96). Preprints. London: James & James.

Michalski, S. W. (2016). 2016. Climate Guidelines for Heritage Collections: Where We Are in 2014 and How We Got Here_with addendum. In *Smithsonian Institution Summit on the Museum Preservation Environment* (pp. 9–33). Government of Canada, Canadian Conservation Institute.

Missoum, K., Belgacem, M., & Bras, J. (2013). Nanofibrillated Cellulose Surface Modification: A Review. *Materials*, *6*(5), 1745–1766. Retrieved from http://search.proquest.com/docview/1530318038/

Mitchell, R., Carr, C. M., Parfitt, M., Vickerman, J. C., & Jones, C. (2005). Surface chemical analysis of raw cotton fibres and associated materials. *Cellulose*, *12*(6), 629–639. https://doi.org/10.1007/s10570-005-9000-9

Mormann, W., & Wagner, T. (2000). Silylation of cellulose with hexamethyldisilazane in liquid ammonia. *Carbohydrate Polymers*, *43*(3), 257–262. https://doi.org/10.1016/S0144-8617(00)00173-9

Mormann, Werner, Demeter, J., & Wagner, T. (1999). Partial silylation of cellulose with predictible degree of silylation – stoichiometric silylation with hexamethyldisilazane in ammonia. *Macromolecular Chemistry and Physics*, *200*(4), 693–697. https://doi.org/10.1002/(sici)1521-

3935(19990401)200:4<693::aid-macp693>3.3.co;2-a

Mukherjee, S. M., & Woods, H. J. (1953). X-ray and electron microscope studies of the degradation of cellulose by sulphuric acid. *Biochimica et Biophysica Acta*, *10*(4).

Muros, V. (2012). Investigation into the use of Aquazol as an adhesive on archaeological sites. *Newsletter (Western Association for Art Conservation)*, *34*(1), 9–11.

Murugan, R., Ramesh, R., & Padmanabhan, K. (2014). Investigation on static and dynamic mechanical properties of epoxy based woven fabric glass/carbon hybrid composite laminates. In *Procedia Engineering*. https://doi.org/10.1016/j.proeng.2014.12.270

Mustary, S. (2017). *Synthesis and characterization of biocomposite films, in particular methylcellulose based films with nanocellulose.* Birkbeck University, University of London.

Nair, S. S., & Yan, N. (2015). Bark derived submicron-sized and nano-sized cellulose fibers: From industrial waste to high performance materials. *Carbohydrate Polymers*, *134*, 258–266.

Nakagaito, A. N., Iwamoto, S., & Yano, H. (2005). Bacterial cellulose: the ultimate nano-scalar cellulose morphology for the production of high-strength composites. *Applied Physics A*, *80*(1), 93–97.

Nechyporchuk, O., Belgacem, M. N., & Pignon, F. (2016). Current Progress in Rheology of Cellulose Nanofibril Suspensions. *Biomacromolecules*, *17*(7), 2311–2320. https://doi.org/10.1021/acs.biomac.6b00668

Nechyporchuk, O., Kolman, K., Bridarolli, A., Odlyha, M., Bozec, L., Oriola, M., … Bordes, R. (2018). On the potential of using nanocellulose for consolidation of painting canvases. *Carbohydrate Polymers*, *194*, 161–169. https://doi.org/10.1016/j.carbpol.2018.04.020

Nechyporchuk, O., Kolman, K., Oriola, M., Persson, M., Holmberg, K., & Bordes, R. (2017). Accelerated ageing of cotton canvas as a model for further consolidation practices. *Journal of Cultural Heritage*, *28*, 183–187. https://doi.org/10.1016/j.culher.2017.05.010

Nechyporchuk, O., Yu, J., Nierstrasz, V. A., & Bordes, R. (2017). Cellulose Nanofibril-Based Coatings of Woven Cotton Fabrics for Improved Inkjet Printing with a Potential in E-Textile Manufacturing. *ACS Sustainable Chemistry and Engineering*, *5*(6), 4793–4801. https://doi.org/10.1021/acssuschemeng.7b00200

New ways to remove lignin. (1986). *The Abbey Newsletter*, *10*(1).

Obokata, T., & Isogai, A. (2007). The mechanism of wet-strength development of cellulose sheets prepared with polyamideamine-epichlorohydrin (PAE) resin. *Colloids and Surfaces A: Physicochemical and Engineering Aspects*, *302*(1–3), 525–531. https://doi.org/10.1016/j.colsurfa.2007.03.025

Obokata, T., Yanagisawa, M., & Isogai, A. (2005). Characterization of polyamideamine-epichlorohydrin (PAE) resin: Roles of azetidinium groups and molecular mass of PAE in wet strength development of paper prepared with PAE. *Journal of Applied Polymer Science*. https://doi.org/10.1002/app.21893

Odlyha, M. (1998). *Characterisation of Cultural Materials by Measurement of their Physicochemical Properties*. University of London.

Odlyha, M., Chan, T. Y. A., & Pages, O. (1995). Evaluation of relative humidity effects on fabric-supported paintings by dynamic mechanical and dielectric analysis. *Thermochimica Acta*, *263*(1), 7–21. https://doi.org/10.1016/0040-6031(94)02387-4

Okubayashi, S., Griesser, U. J., & Bechtold, T. (2004). A kinetic study of moisture sorption and desorption on lyocell fibers. *Carbohydrate Polymers*, *58*(3), 293–299. https://doi.org/10.1016/j.carbpol.2004.07.004

Olsson, A. M., Salmén, L., Eder, M., & Burgert, I. (2007). Mechano-sorptive creep in wood fibres. *Wood Science and Technology*, *41*(1), 59–67. https://doi.org/10.1007/s00226-006-0086-5

Oriola, M., Campo-Francés, G., Ruiz-Recasens, C., & Nualart-Torroja, A. (2019). Canvas consolidation survey and treatment requirements for the NANORESTART project. In *Technoheritage 2017, 3rd*

International Congress Science and Technology for the Conservation of Cultural Heritage. Cadiz (Spain): Balkema.

Oriola, Marta, Campo, G., Ruiz-Recasens, C., Pedragosa, N., & Strlič, M. (2015). Collections care scenario appraisal for painting canvases at Museu Nacional d'Art de Catalunya, Barcelona, Spain. *Studies in Conservation*, *60*(1), 193–199. https://doi.org/10.1179/0039363015z.000000000224

Oriola, Marta, Campo, G., Strlič, M., Csefalvayova, L., Odlyha, M., & Možir, A. (2011). Non-Destructive Condition Assessment of Painting Canvases using Near Infrared Spectroscopy. In *Preprints ICOM-CC 16th Triennial Conference*. Lisbon (Portugal): ICOM-CC.

Oriola, Marta, Možir, A., Garside, P., Campo, G., Nualart-Torroja, A., Civil, I., … Strlič, M. (2014). Looking beneath Dalí's paint: Non-destructive canvas analysis. *Analytical Methods*, *6*(1), 86–96. https://doi.org/10.1039/c3ay41094c

Ormsby, B. A., Hagan, E., Smithen, P., & Learner, T. J. S. (2008). Comparing contemporary titanium white-based acrylic emulsion grounds and paints: characterisation, properties and conservation. In J. H. Townsend, T. Doherty, G. Heydenreich, & J. Ridge (Eds.), *Preparation for painting: the artist's choice and its consequences* (pp. 163–171). London: Archetype.

Ormsby, B., Foster, G., Learner, T., Ritchie, S., & Schilling, M. (2007a). Improved controlled relative humidity dynamic mechanical analysis of artists' acrylic emulsion paints: Part II. General properties and accelerated ageing. *Journal of Thermal Analysis and Calorimetry*, *90*(2), 503–508. https://doi.org/10.1007/s10973-006-7725-9

Ormsby, B., Foster, G., Learner, T., Ritchie, S., & Schilling, M. (2007b). Improved controlled temperature and relative humidity DMA of artists' acrylic emulsion paint films : Part I. *Journal of Thermal Analysis and Calorimetry*, *90*(1), 243–253. https://doi.org/10.1007/s10973-006-7724-x

Ormsby, Bronwyn, Learner, T., Schilling, M., Druzik, J., Khanjian, H., Foster, G., & Sloan, M. (2006). The effects of surface cleaning on acrylic emulsion paintings : A preliminary investigation. *Tate Papers [Tate's Online Research Journal]*.

Osong, S., Norgren, S., & Engstrand, P. (2016). Processing of wood-based microfibrillated cellulose and nanofibrillated cellulose, and applications relating to papermaking: a review. *Cellulose*, *23*(1), 93–123.

Pääkkö, M., Ankerfors, M., Kosonen, H., Nykänen, A., Ahola, S., Osterberg, M., … Lindström, T. (2007). Enzymatic hydrolysis combined with mechanical shearing and high-pressure homogenization for nanoscale cellulose fibrils and strong gels. *Biomacromolecules*, *8*(6).

Padanyl, Z. V. (1993). Physical Aging and Glass Transition: Effects on the Mechanical Properties of Paper and Broad. In C. F. Baker (Ed.), *Products of Papermaking* (pp. 521-545.). Leatherhead, UK: PIRA International.

Paralikar, S. A., Simonsen, J., & Lombardi, J. (2008). Poly(vinyl alcohol)/cellulose nanocrystal barrier membranes. *Journal of Membrane Science*, *320*(1–2), 248–258. https://doi.org/10.1016/j.memsci.2008.04.009

Patnode, W. I. (1942). Method of rendering materials water repellent.

Pearson, C. L. (2003). Animal glues and adhesives. In and K. L. M. A. Pizzi (Ed.), *Handbook of Adhesive Technology* (2nd Editio, pp. 479–494). New York: Marcel Dekker.

Penava, Ž., Penava, D. Š., & Tkalec, M. (2016). Experimental analysis of the tensile properties of painting canvas. *Autex Research Journal*, *16*(4), 182–195. https://doi.org/10.1515/aut-2015-0023

Percival-Prescot, W. W. (1974). The Lining Cycle. In *Conference on Comparative Lining Techniques*. Greenwich.

Pereira, F. (2016). Nanocellulose-based composites for conservation and restoration of cultural heritage on paper: Comparative studies between traditional and innovative methods. In *TAPPI international conference on nanotechnology for renewable materials* (pp. 348–65). Grenoble.

Peresin, M. S., Habibi, Y., Vesterinen, A., Rojas, O. J., Pawlak, J. J., & Seppa, J. V. (2010). Effect of

Moisture on Electrospun Nanofiber Composites of Poly (vinyl alcohol) and Cellulose Nanocrystals, 2471–2477.

Pertegato, F. (1993). *I tessili : degrado e restauro*. (Nardini, Ed.). Firenze: Nardini.

Phanthong, P., Reubroycharoen, P., Hao, X., Xu, G., Abudula, A., & Guan, G. (2018). Nanocellulose: Extraction and application. *Carbon Resources Conversion*, *1*(1), 32–43.

Phenix, A. (2010). Lining without heat or moisture. *The Conservator*, *9*(1), 45–46.

Phenix, A., & Sutherland, K. (2014). The cleaning of paintings: effects of organic solvents on oil paint films. *Studies in Conservation*, *46*(sup1), 47–60. https://doi.org/10.1179/sic.2001.46.supplement-1.47

Pireaux, J. J. (1993). High resolution XPS of organic polymers: the scienta ESCA300 database. *Journal of Electron Spectroscopy and Related Phenomena*, *70*(1), 25. https://doi.org/10.1016/0368-2048(93)85006-7

Pizzorusso, G., Fratini, E., Eiblmeier, J., Giorgi, R., Chelazzi, D., Chevalier, A., & Baglioni, P. (2012). Physicochemical characterization of acrylamide/bisacrylamide hydrogels and their application for the conservation of easel paintings. *Langmuir : The ACS Journal of Surfaces and Colloids*, *28*(8).

Placet, V., Cisse, O., & Boubakar, M. L. (2012). Influence of environmental relative humidity on the tensile and rotational behaviour of hemp fibres. *Journal of Materials Science*, *47*(7), 3435–3446. https://doi.org/10.1007/s10853-011-6191-3

Ploeger, R., McGlinchey, C. W., & de la Rie, E. R. (2014). Original and reformulated BEVA ® 371: Composition and assessment as a consolidant for painted surfaces . *Studies in Conservation*, *60*(4), 217–226. https://doi.org/10.1179/2047058414y.0000000132

Ploeger, R., René De La Rie, E., McGlinchey, C. W., Palmer, M., Maines, C. A., & Chiantore, O. (2014). The long-term stability of a popular heat-seal adhesive for the conservation of painted cultural objects. *Polymer Degradation and Stability*, *107*, 307–313. https://doi.org/10.1016/j.polymdegradstab.2014.01.031

Pocobene, G., & Hodkinson, I. (2006). Use of a Pressure-Sensitive Adhesive to Facilitate the Transfer of a Severely Tented Painting. *Journal of the American Institute for Conservation*, *31*(2), 161–173. https://doi.org/10.2307/3179490

Poletto, M., Ornaghi Júnior, H. L., & Zattera, A. J. (2014). Native cellulose: Structure, characterization and thermal properties. *Materials*, *5*(9), 6105–6119. https://doi.org/10.3390/ma7096105

Poletto, M., Pistor, V., Santana, R. M. C., & Zattera, A. J. (2012). Materials produced from plant biomass: part II: evaluation of crystallinity and degradation kinetics of cellulose. *Materials Research*, *15*(3), 421–427. https://doi.org/10.1590/s1516-14392012005000048

Pommet, M., Juntaro, J., Heng, J. Y. Y., Mantalaris, A., Lee, A. F., Wilson, K., … Bismarck, A. (2008). Surface modification of natural fibers using bacteria: Depositing bacterial cellulose onto natural fibers to create hierarchical fiber reinforced nanocomposites. *Biomacromolecules*, *9*(6), 1643–1651. https://doi.org/10.1021/bm800169g

Ranta-Maunus, A. (1975). The Viscoelasticity of Wood at Varying Moisture Content. *Wood Science and Technology*, *9*, 189–205.

Rastogi, V. K., Samyn, P., Bonwick, G., & Birch, C. S. (2016). Synthesis of Polyhydroxybutyrate Particles with Micro-to-Nanosized Structures and Application as Protective Coating for Packaging Papers. *Nanomaterials*, *7*(1).

Rastogi, V., & Samyn, P. (2015). Bio-Based Coatings for Paper Applications. *Coatings*, *5*(4), 887–930.

Ravnikar, A. (2014). Mist-lining of a baroque painting. *CeROArt : Conservation, Exposition, Restauration d'Objets d'Art*, (EGG4). Retrieved from https://journals.openedition.org/ceroart/4049

Reddy, N., & Yang, Y. (2005). Properties and potential applications of natural cellulose fibers from cornhusks. *Green Chemistry*, *7*(4), 190–195. https://doi.org/10.1039/b415102j

Reeve, A., Ackroyd, P., & Stephenson-Wright, A. (1988). The multi-purpose low pressure conservation table. *National Gallery Technical Bulletin*.

Reuber, L. (2008). *Klebstoffe für die Rissverklebung an Leinengeweben*. Fachhochschule Köln.

Richardson, J. (1983, June). Crimes Against the Cubists. *The New York Review of Books*.

Ridge, J. (2006). THE TATE BRAND: ITS CONSEQUENCES FOR THE CARE AND PRESENTATION OF TATE COLLECTIONS. *Studies in Conservation*, *51*(3), 23–29.

Roche, A. (1989). Etude comparative des toiles de lin et de polyester dans les doublages de tableaux. In *2ième colloque de l'ARAAFU* (pp. 149–156).

Roche, Alain. (2003). Approche du principe de réversibilité des doublages des peintures sur toile TT - Toward a principle of reversibility for the linings of paintings on canvas. *Studies in Conservation*, *48*(2), 83–94.

Rodgers, S. M., Cobbledick, S., Evers, J., & Williams, E. (1988). Consolidation/Fixing/Facing. In N. Ash, D. Hamburg, S. Page, S. Bertalan, L. Kruth, D. van der Reyden, … T. Vitale (Eds.), *Paper Conservation Catalog, AIC Book and Pap* (p. 9).

Rojo, E., Peresin, M. S., Sampson, W. W., Hoeger, I. C., Vartiainen, J., Laine, J., & Rojas, O. J. (2015). Comprehensive elucidation of the effect of residual lignin on the physical, barrier, mechanical and surface properties of nanocellulose films. *Green Chemistry*, *17*(3), 1853–1866. https://doi.org/10.1039/c4gc02398f

Roman, M. (2015). Toxicity of Cellulose Nanocrystals: A Review. *Industrial Biotechnology*, *11*(1), 25–33. https://doi.org/10.1089/ind.2014.0024

Ropret, P., Zoubek, R., Škapin, A. S., & Bukovec, P. (2007). Effects of ageing on different binders for retouching and on some binder-pigment combinations used for restoration of wall paintings. *Materials Characterization*, *58*(11-12 SPEC. ISS.), 1148–1159. https://doi.org/10.1016/j.matchar.2007.04.027

Rose, C., & von Endt, D. W. (1984). *Protein Chemistry for Conservators* (American i). Washington, D.C.

Rossi, R. M., Stämpfli, R., Psikuta, A., Rechsteiner, I., & Brühwiler, P. A. (2011). Transplanar and in-plane wicking effects in sock materials under pressure. *Textile Research Journal*, *81*(15), 1549–1558.

Roudet, L. (2007). *L'intervention minimale en conservation-restauration des Biens Culturels : Exploration d'une notion*. Universite Paris I Pantheon-Sorbonne.

Ruhemann, H. (1953). The impregnation and lining of paintings on a hot table. *Studies in Conservation*, *1*(2), 73–76. https://doi.org/10.1179/sic.1953.009

Sagharlou, M. H. (2015). *Development of an Injectable Nanocomposite Hydrogel System for In Vitro Delivery of Rat Olfactory Ensheathing Cells*. University College London.

Sahputra, I. H., Alexiadis, A., & Adams, M. J. (2019). Effects of Moisture on the Mechanical Properties of Microcrystalline Cellulose and the Mobility of the Water Molecules as Studied by the Hybrid Molecular Mechanics–Molecular Dynamics Simulation Method. *Journal of Polymer Science, Part B: Polymer Physics*, *57*(8), 454–464. https://doi.org/10.1002/polb.24801

Saiman, M. P., Wahab, M. S., & Wahit, M. U. (2014). The Effect of Fabric Weave on the Tensile Strength of Woven Kenaf Reinforced Unsaturated Polyester Composite. *Proceedings of the International Colloquium in Textile Engineering, Fashion, Apparel and Design 2014 (ICTEFAD 2014)*, 25–29. https://doi.org/10.1007/978-981-287-011-7_5

Salmén, L. (1984). Viscoelastic properties ofin situ lignin under water-saturated conditions. *Journal of Materials Science*, *19*(9), 3090–3096. https://doi.org/10.1007/BF01026988

Salmén, L., & L. Back, E. (1980). Moisture-dependent thermal softening of paper evaluated by its elastic modulus. *Tappi Journal*, *63*, 117–120.

Salvant, J., Barthel, E., & Menu, M. (2011). Nanoindentation and the micromechanics of Van Gogh oil

paints. *Applied Physics A: Materials Science and Processing*, *104*(2), 509–515. https://doi.org/10.1007/s00339-011-6486-x

Sanchez-Garcia, M. D., Gimenez, E., & Lagaron, J. M. (2008). Morphology and barrier properties of solvent cast composites of thermoplastic biopolymers and purified cellulose fibers. *Carbohydrate Polymers*, *71*(2), 235–244. https://doi.org/10.1016/j.carbpol.2007.05.041

Sandbakken, E. G., & Tveit, E. S. (2012). Edvard Munch's monumental sketches (1909-1916) for the Aula of Oslo University, Norway: Conservation issues and treatments. *Studies in Conservation*, *57*(1), 258–267. https://doi.org/10.1179/2047058412Y.0000000030

Santiso, E. E., Herdes, C., & Müller, E. A. (2013). On the calculation of solid-fluid contact angles from molecular dynamics. *Entropy*, *15*(9), 3734–3745. https://doi.org/10.3390/e15093734

Savadekar, N. R., & Mhaske, S. T. (2012). Synthesis of nano cellulose fibers and effect on thermoplastics starch based films. *Carbohydrate Polymers*, *89*(1), 146–151.

Saville, B. P. (1999). *Physical testing of textiles*. *Physical testing of textiles*. Woodhead Publishing/CRC Press. https://doi.org/10.1533/9781845690151

Sawicki, M. (2017). Non-traditional gilding revisited: evaluation of gilded surfaces exposed to uncontrolled diurnal fluctuations for over 10 years. *AICCM Bulletin*, *38*(1), 15–24. https://doi.org/10.1080/10344233.2017.1342889

Schellmann, N. C. (2014). Animal glues: a review of their key properties relevant to conservation. *Studies in Conservation*, *52*(sup1), 55–66. https://doi.org/10.1179/sic.2007.52.supplement-1.55

Schlüter, K. (2011). Textile Auxiliaries, 3. Sizing Agents. In *Ullmann's Encyclopedia of Industrial Chemistry*. https://doi.org/10.1002/14356007.o26_o07

Sears, F. W., Zemansky, M. W., & Young, H. D. (1982). *University Physics* (6th Ed.). Addison-Wesley.

Sease, C. (1998). Codes of Ethics for Conservation. *International Journal of Cultural Property*. https://doi.org/10.1017/S0940739198770092

Seery, M. (2013). Saving paper. Retrieved June 27, 2019, from https://www.rsc.org/images/EiC0213-paper-conservation-chemistry_tcm18-227485.pdf

Sehaqui, H., de Larraya, U. P., Liu, P., Pfenninger, N., Mathew, A. P., Zimmermann, T., & Tingaut, P. (2014). Enhancing adsorption of heavy metal ions onto biobased nanofibers from waste pulp residues for application in wastewater treatment. *Cellulose*, *21*(4), 2831–2844. https://doi.org/10.1007/s10570-014-0310-7

Sehaqui, H., Zhou, Q., Ikkala, O., & Berglund, L. A. (2011). Strong and tough cellulose nanopaper with high specific surface area and porosity. *Biomacromolecules*, *12*(10), 3638–3644. https://doi.org/10.1021/bm2008907

Sengupta, A. K., De, D., & Sarkar, B. P. (1972). Anisotropy in Some Mechanical Properties of Woven Fabrics. *Textile Research Journal*, *42*(5), 268–271. https://doi.org/10.1177/004051757204200504

Seves, A. M., Sora, S., Scicolone, G., Testa, G., Bonfatti, A. M., Rossi, E., & Seves, A. (2000). Effect of thermal accelerated ageing on the properties of model canvas paintings. *Journal of Cultural Heritage*, *1*, 315–322.

Sheykhnazari, S., Tabarsa, T., Ashori, A., Shakeri, A., & Golalipour, M. (2011). Bacterial synthesized cellulose nanofibers; Effects of growth times and culture mediums on the structural characteristics. *Carbohydrate Polymers*, *86*(3), 1187–1191.

Shore, S. K. (1994). Review of loss compensation techniques used in textile conservation. In *Loss compensation symposium postprints: Western Association for Art Conservation annual meeting 1993*.

Silvério, H. A., Flauzino Neto, W. P., Dantas, N. O., & Pasquini, D. (2013). Extraction and characterization of cellulose nanocrystals from corncob for application as reinforcing agent in nanocomposites. *Industrial Crops & Products*, *44*, 427–436.

Singer, B., Aslaksby, T. E., Topalova-Casadiego, B., & Tveit, E. S. (2014). Investigation of Materials Used by Edvard Munch. *Studies in Conservation*, *55*(4), 274–292. https://doi.org/10.1179/sic.2010.55.4.274

Siqueira, E. J. (2012). *Polyamidoamine Epichlorohydrin-based Papers: Mechanisms of Wet Strength Development and Paper Repulping*. Université Grenoble Alpes, Grenoble, France.

Siroka, B., Noisternig, M., Griesser, U. J., & Bechtold, T. (2008). Characterization of cellulosic fibers and fabrics by sorption/desorption. *Carbohydrate Research*, *343*(12), 2194–2199. https://doi.org/10.1016/j.carres.2008.01.037

Soignet, D. M., Berni, R. J., & Benerito, R. R. (1976). Electron spectroscopy for chemical analyses (ESCA)—A tool for studying treated textiles. *Journal of Applied Polymer Science*. https://doi.org/10.1002/app.1976.070200917

Sonderegger, W., Hering, S., Mannes, D., Vontobel, P., Lehmann, E., & Niemz, P. (2010). Quantitative determination of bound water diffusion in multilayer boards by means of neutron imaging. *European Journal of Wood and Wood Products*, *68*(3), 341–350. https://doi.org/10.1007/s00107-010-0463-5

Sonoda, N., Rioux, J.-P., Duval, A. R., & Duval, A. R. (2006). Identification des materiaux synthetiques dans les peintures modernes. II. Pigments organiques et matiere picturale. *Studies in Conservation*, *38*(2), 99–127. https://doi.org/10.2307/1506462

Spence, K., Habibi, Y., & Dufresne, A. (2011). Nanocellulose-Based Composites. In *Cellulose Fibers: Bio- And Nano-polymer Composites* (pp. 179–213). https://doi.org/10.1007/978-3-642-17370-7_7

Spence, K., Venditti, R., Rojas, O., Habibi, Y., & Pawlak, J. (2011). A comparative study of energy consumption and physical properties of microfibrillated cellulose produced by different processing methods. *Cellulose*, *18*(4), 1097–1111.

St. Lawrence, S., Willett, J. L., & Carriere, C. J. (2001). Effect of moisture on the tensile properties of poly(hydroxy ester ether). *Polymer*, *42*(13), 5643–5650. https://doi.org/10.1016/S0032-3861(00)00836-3

Stamm, A. J. (1956). Thermal Degradation of Wood and Cellulose. *Industrial & Engineering Chemistry*, *48*(3), 413–417. https://doi.org/10.1021/ie51398a022

Stephenson, J. (1989). *The materials and techniques of painting / by Jonathan Stephenson.* New York: New York : Watson-Guptill Publications, 1989.

Stoner, Joyce Hill. (1994). The Impact of Research on the Lining and Cleaning of Easelpaintings. *Journal of the American Institute for Conservation*, *33*(2), 131–140.

Stoner, Joyce Hill, & Rushfield, R. (2013). *Conservation of Easel Paintings*. *Conservation of Easel Paintings*. Abingdon: Routledge. https://doi.org/10.4324/9780080941691

Stoner, Joyce Hill, & Rushfield, R. A. (2012). *The conservation of easel paintings / edited by Joyce Hill Stoner and Rebecca Rushfield.* London: London : Routledge.

Stoudmann, N., Nowack, B., & Som, C. (2019). Prospective environmental risk assessment of nanocellulose for Europe. *Environmental Science: Nano*, (6), 2520–2531. https://doi.org/10.1039/c9en00472f

Strange, A. P. (2019). *Quantitative Nanohistology: Collagen Disorders of Connective and Mineralised Tissues*. University College London.

Strlic, M., & Kolar, J. (2003). Evaluating and enhancing paper stability - needs and recent trends. *Cultural Heritage Research: A Pan-European Challenge*.

Su, J., Mosse, W. K. J., Sharman, S., Batchelor, W., & Garnier, G. (2012). Paper strength development and recyclability with polyamideamine-epichlorohydrin (PAE). *BioResources*, *7*(1), 913–924.

Sukhanova, A., Bozrova, S., Sokolov, P., Berestovoy, M., Karaulov, A., & Nabiev, I. (2018). Dependence of Nanoparticle Toxicity on Their Physical and Chemical Properties. *Nanoscale Research Letters*, *13*(1), 1–21. https://doi.org/10.1186/s11671-018-2457-x

Sun, X., Wu, Q., Zhang, X., Ren, S., Lei, T., Li, W., … Zhang, Q. (2018). Nanocellulose films with combined cellulose nanofibers and nanocrystals: tailored thermal, optical and mechanical properties. *Cellulose*, *25*(2), 1103–1115. https://doi.org/10.1007/s10570-017-1627-9

Svagan, A. J., Hedenqvist, M. S., & Berglund, L. (2009). Reduced water vapour sorption in cellulose nanocomposites with starch matrix. *Composites Science and Technology*. https://doi.org/10.1016/j.compscitech.2008.11.016

Symington, M. C., Banks, W. M., West, O. D., & Pethrick, R. A. (2009). Tensile testing of cellulose based natural fibers for structural composite applications. In *Journal of Composite Materials*. https://doi.org/10.1177/0021998308097740

Taylor, R. A. (1997). Natural waxes on cotton contribute to yarn and fabric quality. *Text. Chem. & Col.*, *29*, 32–35.

Teixeira, A. C. (2016). Canvas support impregnation materials and techniques: a study of Portuguese painting and its conservation issues. *CeROArt : Conservation, Exposition, Restauration d'Objets d'Art*. Retrieved from https://journals.openedition.org/ceroart/4918

Testa, G., Surdella, A., Rossi Bozii, E. C., & Seves, A. (1994). The kinetics of cellulose fiber degradation and correlation with some tensile properties. *Acta Polymerica*, *45*(1), 47–49. https://doi.org/10.1002/actp.1994.010450109

Thomson, G. (1956). Test for cross-linking of linear polymers. *Nature*, (4537), 807.

Thummanukitcharoen, P., Limpanart, S., Srikulkit, K. (2011). Preparation of organosilane treated microcrystalline cellulose (SIMCC) and the polypropylene/SIMCC composite. In *18th International conference on composite materials*. Jeju Island.

Timár-Balázsy, Á. (1998). *Chemical principles of textile conservation / Ágnes Tímar-Balázsy and Dinah Eastop*. Oxford ; Boston: Butterworth-Heinemann.

Timár-Balázsy, Á., & Eastop, D. (1998). Binding media on printed and painted textiles. In *Chemical principles of textile conservation* (p. 120). Oxford ; Boston: Butterworth-Heinemann.

Tobler-Rohr, M. I. (2011). The supply chain of textiles. In *Handbook of Sustainable Textile Production*. https://doi.org/10.1533/9780857092861.45

Tsetsekou, E., Platanianaki, A., & Pournou, A. (2018). Assessing wood adhesives used in conservation by testing their bond strength and ageing behavior. *Procedia Structural Integrity*, *10*, 227–234. https://doi.org/10.1016/j.prostr.2018.09.032

Unger A., Schniewind A.P., U. W. (2001). Consolidants. In *Conservation of Wood Artifacts. Natural Science in Archaeology.* (Springer). Berlin/Heidelberg.

Van de vorst, A. (1997). *Introduction à la physique, premier cycle* (2nd editio). Bruxelles: De Boeck.

Van Der Reyden, D. (1992). Recent Scientific Research in Paper Conservation. *Journal of the American Institute for Conservation*, *31*(1), 117–138.

Van Look, G., Simchen, G., & Heberle, J. (1995). *Silylating Agents: Derivatization Reagents, Protecting-group Reagents, Organosilicon Compounds, Analytical Applications, Synthetic Applications.* (Fluka Chem).

Van Loon, A., Noble, P., & Burnstock, A. (2012). Ageing and deterioration of traditional oil and tempera paintings. In J.H. Stoner & J. H. Rushfield (Eds.), *Conservation of Easel Paintings* (pp. 214–241). Routledge, London.

Van Tilborgh, Louis, Meedendorp, T., Hendriks, E., Johnson, D. H., & Johnson, C. Richard, Erdmann, R. G. (2012). Weave matching and dating of Van Gogh' s paintings: an interdisciplinary approach. *The Burlington Magazine*, 112–122.

Vanlandingham, M., Villarrubia, J., Guthrie, W., & Meyers, G. (2001). Nanoindentation of polymers: An overview. *Macromolecular Symposia*, *167*, 15–43.

Vieira, M. G. A., Da Silva, M. A., Dos Santos, L. O., & Beppu, M. M. (2011). Natural-based plasticizers

and biopolymer films: A review. *European Polymer Journal*, *47*(3), 254–263. https://doi.org/10.1016/j.eurpolymj.2010.12.011

Vilde, V. (2016). Vilde, V Thickett, D Hollis, D Grau-Bove, J Richardson, E. In *BSSM's 11th International Conference on Advances in Experimental Mechanics*.

Villers, Caroline. (2003). *Lining paintings : papers from the Greenwich Conference on Comparative Lining Techniques*. (Caroline Villers, Ed.).

Viñas, S. M. (2011). Contemporary theory of conservation. *Studies in Conservation*, *47*(1), 1–239. https://doi.org/10.4324/9780080476834

Vinçotte, A., Beauvoit, E., Boyard, N., & Guilminot, E. (2019). Effect of solvent on PARALOID® B72 and B44 acrylic resins used as adhesives in conservation. *Heritage Science*, *7*(42). https://doi.org/10.1186/s40494-019-0283-9

Voisin, H., Bergström, L., Liu, P., & Mathew, A. (2017). Nanocellulose-Based Materials for Water Purification. *Nanomaterials*, *7*(3), 57. https://doi.org/10.3390/nano7030057

Völkel, L., Ahn, K., Hähner, U., Gindl-Altmutter, W., & Potthast, A. (2017). Nano meets the sheet: adhesive-free application of nanocellulosic suspensions in paper conservation. *Heritage Science*, *5*(1), 1–17.

Volkmer, T., Schmidt, J. A., Kranitz, K., & Niemz, P. (2012). Untersuchungen zum Einfluss der Klebstoffart auf den Diffusionswiderstand von Holzverklebungen. *Bauphysik*, *34*(2), 55–60. https://doi.org/10.1002/bapi.201200006

von Endt, D. W., & Baker, M. T. (1991). The chemistry of filled animal glue systems. In D. Bigelow (Ed.), *Gilded Wood Conservation and History* (pp. 155–162). Sound View Press.

Wågberg, L., & Bjőrklund, M. (1993). On the mechanism behind wet strength development in papers containing wet strength resins. *Nordic Pulp & Paper Research Journal*, *8*(1), 53–58. https://doi.org/10.3183/npprj-1993-08-01-p053-058

Wang, F. (2018). *Engineering of high-performance textiles*. (M. Menghe & X. John H., Eds.) (First edit). Duxford, United Kingdom: Woodhead Publishing.

Wang, J., Yiu, B., Obermeyer, J., Filipe, C. D. M., Brennan, J. D., & Pelton, R. (2012). Effects of temperature and relative humidity on the stability of paper-immobilized antibodies. *Biomacromolecules*. https://doi.org/10.1021/bm2017405

Watson, W. (1921). *Textile Design and Colour; Elementary Weaves and Figured Fabrics* (2nd editio). London: Longmans, Green and Co.

Weaving process. (n.d.). Retrieved July 30, 2019, from http://www.tikp.co.uk/knowledge/technology/warping-and-weaving/weaving-process/

Wenzel, R. N. (1936). Resistance of solid surfaces to wetting by water. *Industrial and Engineering Chemistry*. https://doi.org/10.1021/ie50320a024

Whitmore, Paul M., & Bogaard, J. (1994). Determination of the Cellulose Scission Route in the Hydrolytic and Oxidative Degradation of Paper. *Restaurator*, (15), 26–45.

Williams, J. C. (1981). A review of paper quality and paper chemistry. *Library Trends*, *30*(2), 203–224.

Wojciech, M., & Maciej, T. (2011). Color difference Delta E - A survey. *Machine Graphics and Vision*, *20*(4), 383–411. Retrieved from http://mgv.wzim.sggw.pl/MGV20.html%0Ahttp://www.researchgate.net/publication/236023905_Color_difference_Delta_E_-_A_survey

Wolansky, G., & Marmur, A. (1999). Apparent contact angles on rough surfaces: The Wenzel equation revisited. *Colloids and Surfaces A: Physicochemical and Engineering Aspects*, *156*(1–3), 381–388. https://doi.org/10.1016/S0927-7757(99)00098-9

Wolbers, R. C., McGinn, M., & Duerbeck, D. (1994). *Poly(2-Ethyl-2-Oxazoline): A New Conservation Consolidant*. (V. Dorge & F. C. Hault, Eds.), *Painted Wood: History and Conservationed*. Los

Angeles: Getty Conservation Institute.

Wood, J. D., Gauvin, C., Young, C. R. T., Taylor, A. C., Balint, D. S., & Charalambides, M. N. (2018). Cracking in paintings due to relative humidity cycles. *Procedia Structural Integrity*, *13*, 379–384.

Works, A. (2018). Measurements of Solvent Cleaning Effects on Oil Paintings Author (s): Ken Sutherland Source : Journal of the American Institute for Conservation , Vol . 45 , No . 3 (Fall - Winter , Published by : Taylor & Francis , Ltd . on behalf of The American Inst, *45*(3), 211–226.

Xu, X., Liu, F., Jiang, L., Zhu, J. Y., Haagenson, D., & Wiesenborn, D. P. (2013). Cellulose nanocrystals vs. cellulose nanofibrils: a comparative study on their microstructures and effects as polymer reinforcing agents. *ACS Applied Materials & Interfaces*, *5*(8), 2999–3009.

Yang, X., Bakaic, E., Hoare, T., & Cranston, E. D. (2013). Injectable polysaccharide hydrogels reinforced with cellulose nanocrystals: Morphology, rheology, degradation, and cytotoxicity. *Biomacromolecules*, *14*(12), 4447–4455. https://doi.org/10.1021/bm401364z

Young, C., & Ackroyd, P. (2001). The mechanical behaviour and environmental response of paintings to three types of lining treatment. *National Gallery Technical Bulletin*, *22*, 85–104.

Young, C., & Jardine, S. (2012a). Fabrics for the twenty-first century: As artist canvas and for the structural reinforcement of easel paintings on canvas. *Studies in Conservation*, *57*(4), 237–253. https://doi.org/10.1179/2047058412Y.0000000007

Young, C., & Jardine, S. (2012b). Fabrics for the twenty-first century: As artist canvas and for the structural reinforcement of easel paintings on canvas. *Studies in Conservation*, *57*(4), 237–253. https://doi.org/10.1179/2047058412y.0000000007

Young, C. R. T., & Hibberd, R. D. (1999). Biaxial tensile testing of paintings on canvas. *Studies in Conservation*, *44*(2), 129–141. https://doi.org/10.1179/sic.1999.44.2.129doi.org/10.1179/sic.1999.44.2.129

Youssef, B., Soumia, A., Mounir, E. A., Omar, C., Abdelaziz, L., Mehdi, E. B., & Mohamed, Z. (2015). Preparation And Properties Of Bionanocomposite Films Reinforced With Nanocellulose Isolated From Moroccan Alfa Fibres. *Autex Research Journal*, *15*, 1–9. https://doi.org/10.1515/aut-2015-0011

Zhang, P., Wittmann, F. H., Zhao, T. J., Lehmann, E. H., & Vontobel, P. (2011). Neutron radiography, a powerful method to determine time-dependent moisture distributions in concrete. *Nuclear Engineering and Design*, *241*(12), 4758–4766. https://doi.org/10.1016/j.nucengdes.2011.02.031

Appendices

A Appendix Chapter 3

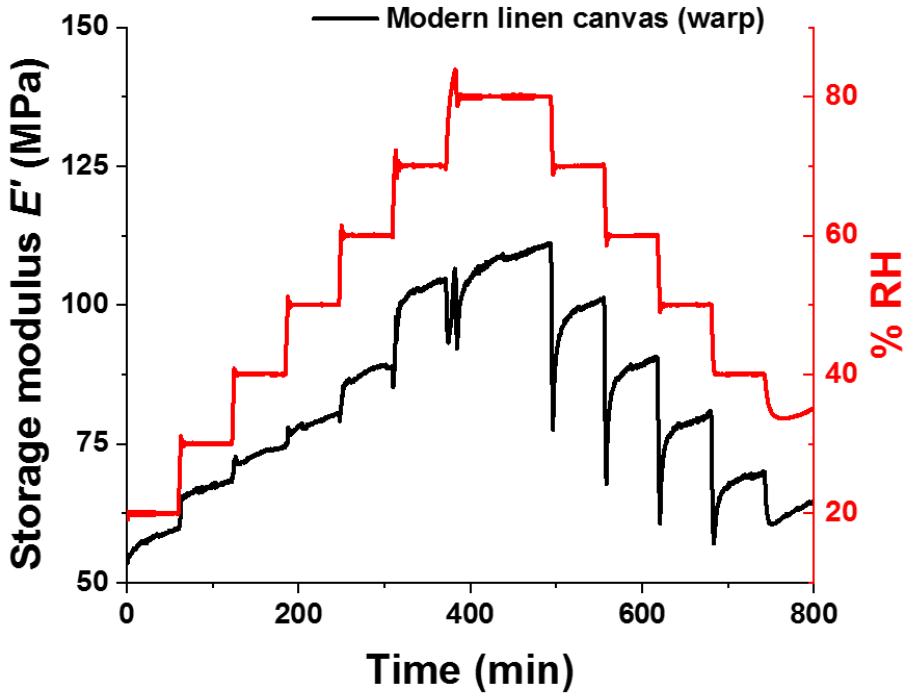

Figure A.1: Mechanical response to RH steps of modern linen canvas measured in the warp direction

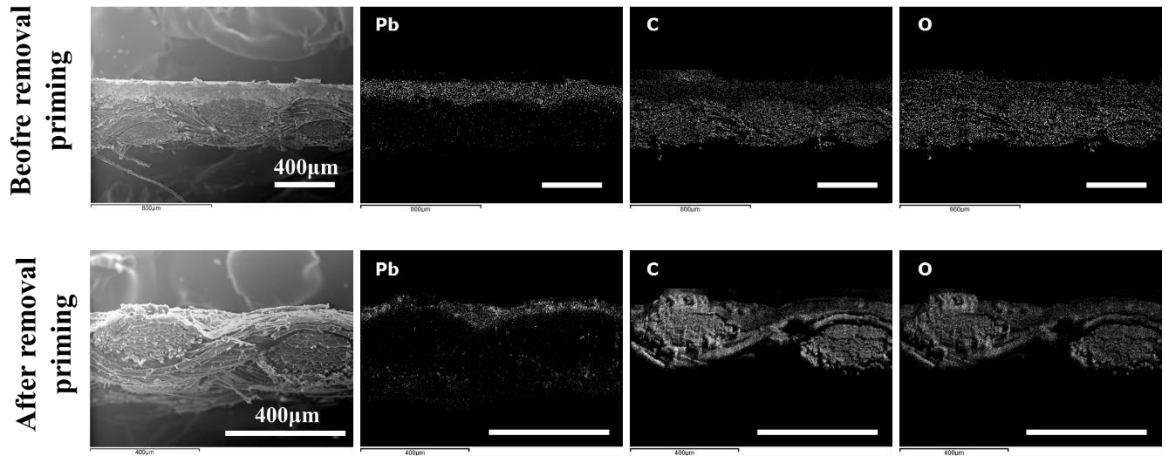

Figure A.2: SEM-EDX mapping images of the 19th century linen primed and sized canvas before and after removal of the priming layer. The thick layer of priming is no more visible on the unprimed sample. Traces of lead (Pb) from the priming layer (i.e. lead white $2PbCO_3 \cdot Pb(OH)_2$) can, however, still be seen on the canvas surface of the canvas after removal.

B Appendix Chapter 4

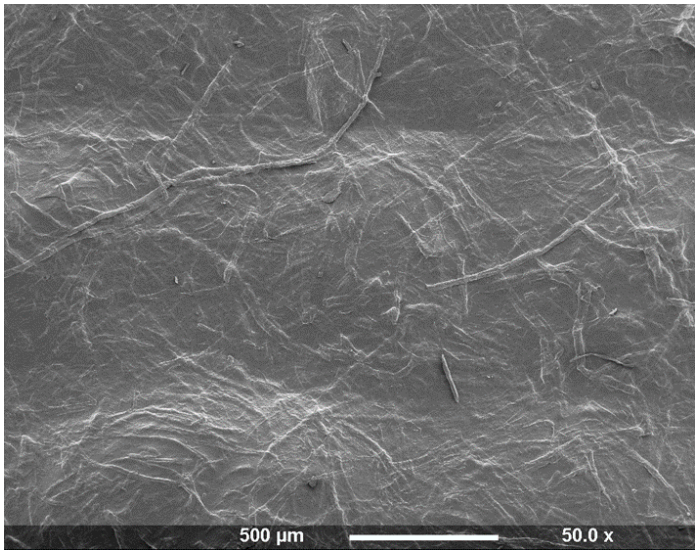

Figure B.1: SEM image of a CCNF-treated canvas (unaged). The treatment covers the canvas threads. Cotton fibres embedded in the film can be seen.

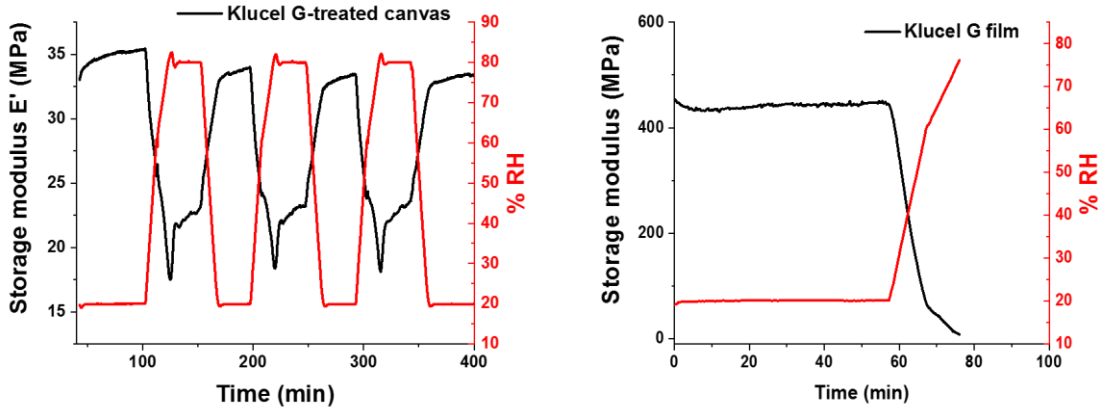

Figure B.2: Variations in E' measured for a Klucel film upon application of the 20-80-20 RH program. Note that upon humidification (20-80%RH transition), the tension of the film dropped to 0 (resulting in a drop in E') leading the DMA to stop the measurement.

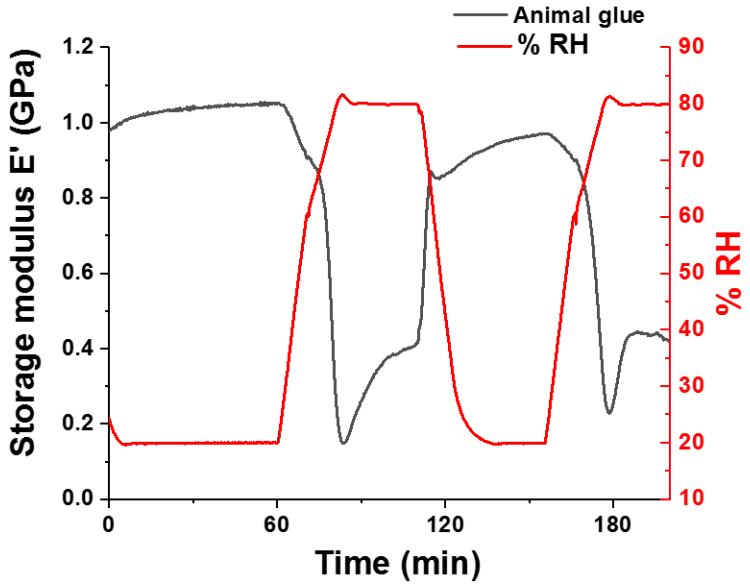

Figure B.3: Variations in E' measured for animal glue film upon application of the 20-80-20 RH program. Note that upon humidification (20-80%RH transition), the tension of the film dropped to 0 (resulting in a drop in E') leading the DMA to stop the measurement.

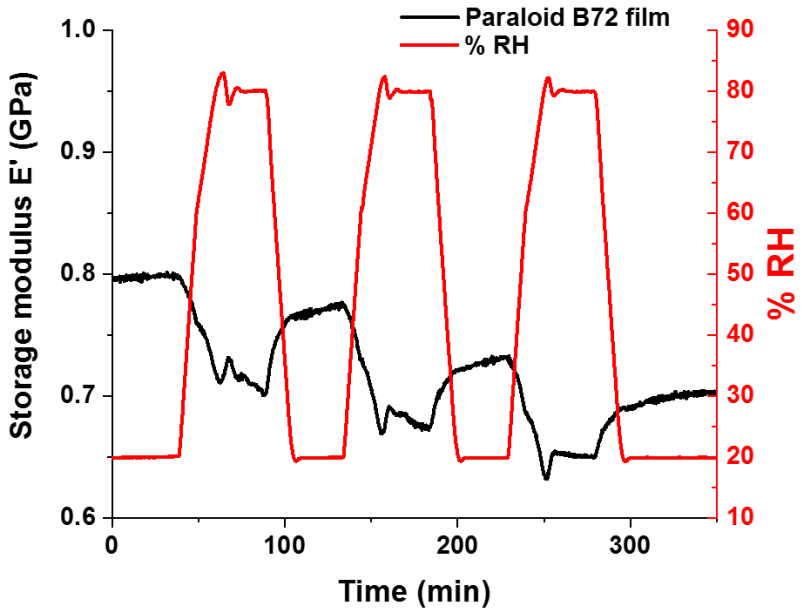

Figure B.4: Variations in E' measured for a Paraloid B72 film upon application of the 20-80-20%RH program.

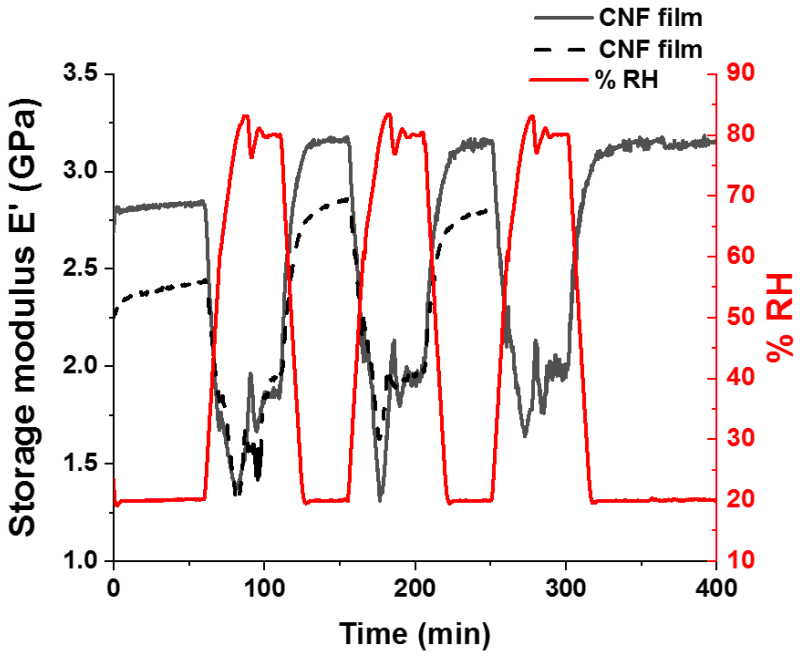

Figure B.5: Variations in E' measured for a CNF film (2 samples) upon application of the 20-80-20 RH program. Note that the mechanical response of the 2 pieces of CNF films are slightly different in terms of intensity but that the response is stable over time. After the first RH cycle during which E'(20%RH) increases by ≈700MPa, storage moduli E' measured at 20 and 80%RH does not seem to vary over time.

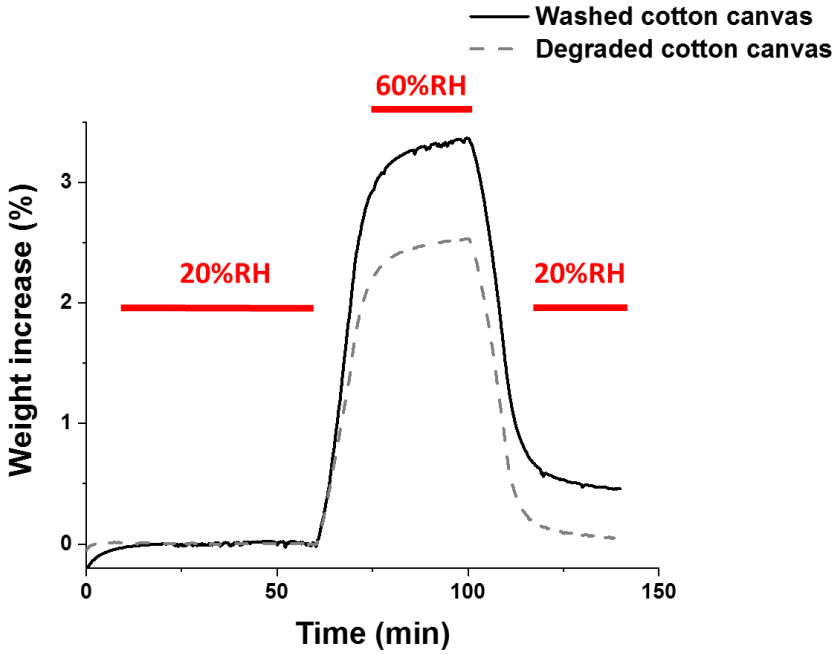

Figure B.6: DVS of a washed and degraded cotton canvas subjected to a 20(1h)-60(30min)-20 (30min)%RH cycle. Note the higher hygroscopic behaviour (higher uptake mass) of the washed cotton canvas over the degraded cotton canvas.

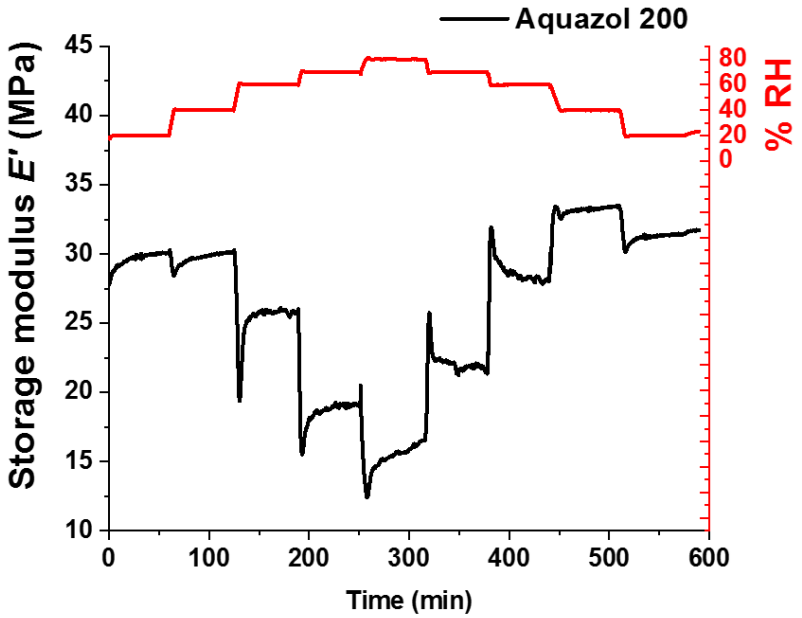

Figure B.7: Variations in storage modulus E' measured for an Aquazol 200-treated canvas upon application of 1 cycle of RH-steps (20-40-60-70-80%RH, 4%RH/min)

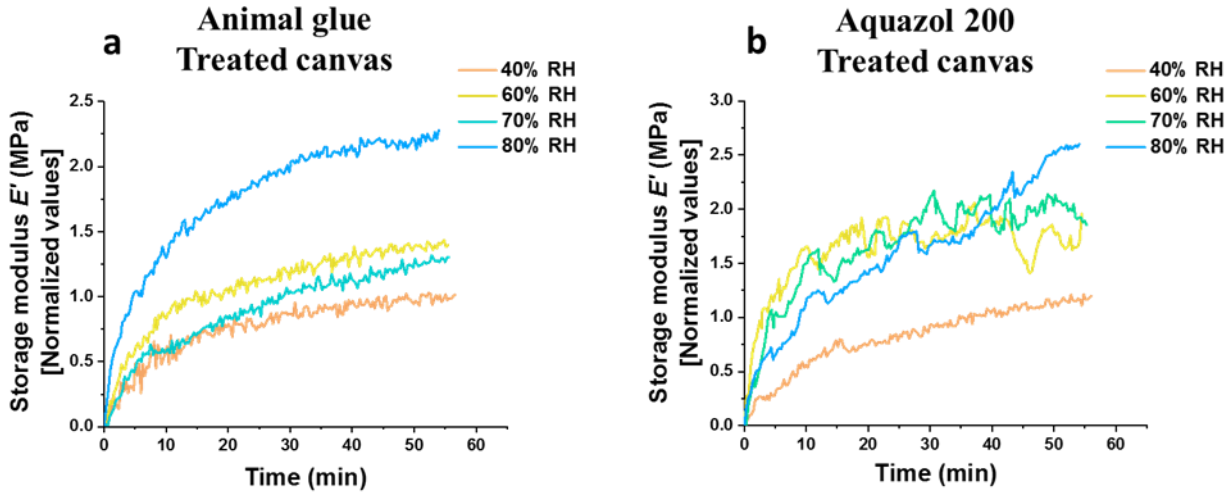

Figure B.8: Logarithmic increase in storage modulus E' measured for the Animal glue and Aquazol200-treated degraded cotton canvases at the 40, 60, 70 and 80%RH isotherms (25°C). The results show the higher response of the animal glue sample at 80%RH than at 40, 60 and 70%RH seen by the noticeable increase in E' under exposure to 80%RH. Increase in the mechanical response of Aquazol 200 to moisture can already been seen between the 40 and 60%RH isotherms. Note that all the curves from Animal glue and Aquazol 200 at the different isotherms present a logarithmic increase except Aquazol200 at 80%RH. At that level, the response of the Aquazol20 sample is particularly high and unstable.

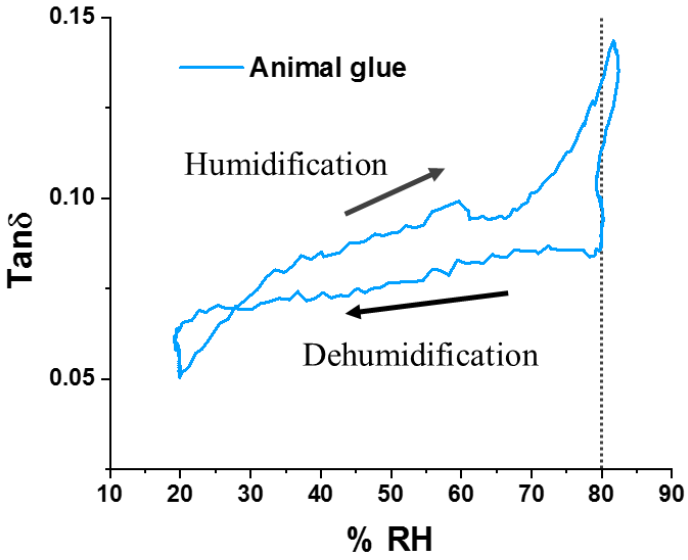

Figure B.9: Tanδ variations upon RH shown for 1 20-60-80-20%RH RH cycle (2nd RH cycle, RH cycling program) for the animal glue-treated degraded cotton canvas. Trend on humidification (20-80%RH) and dehumidification (80-20%RH) are shown. Note the important exponential increase in Tanδ measured above 70%RH (including overshoot in RH above 80%RH) during the humidification ramp. Between 30 and 70%RH, the viscoelastic response of the sample remains quite steady.

Figure B.10: Animal glue film after ageing. Note that the film has strongly degraded as seen by the strong darkening of the film, cracks have appeared and because the film had started to melt, it was put on the sailcloth seen on the picture.

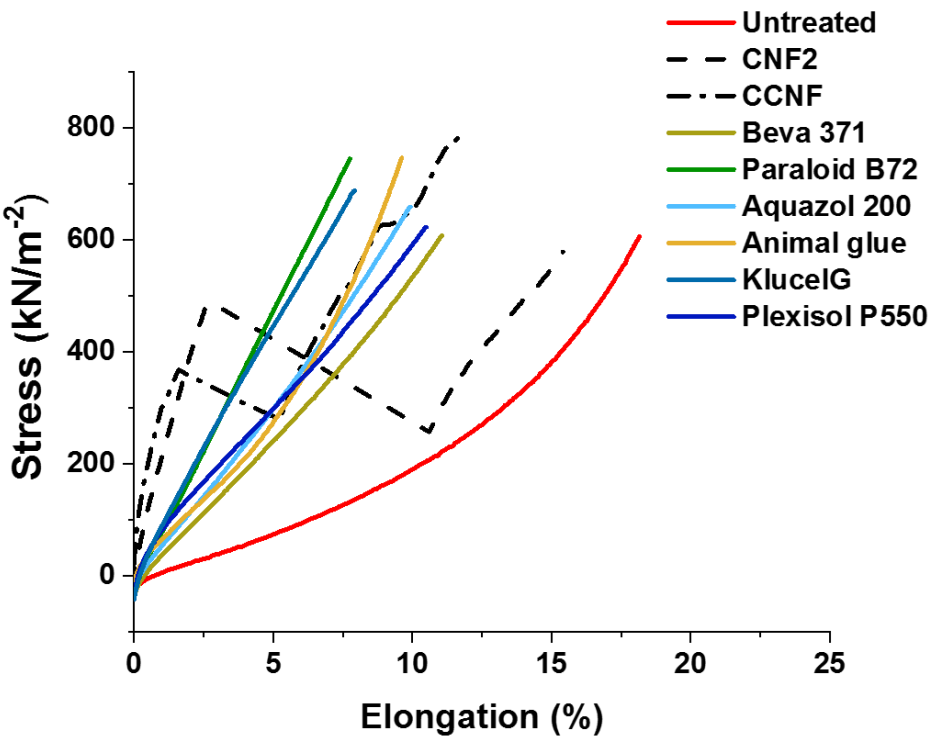

Figure B.11: Tensile curves (20%RH, 25°C) measured after ageing for the modern cotton canvas untreated and treated with traditional consoldiatn and the CNF and CCNF nanocellulose treatments.

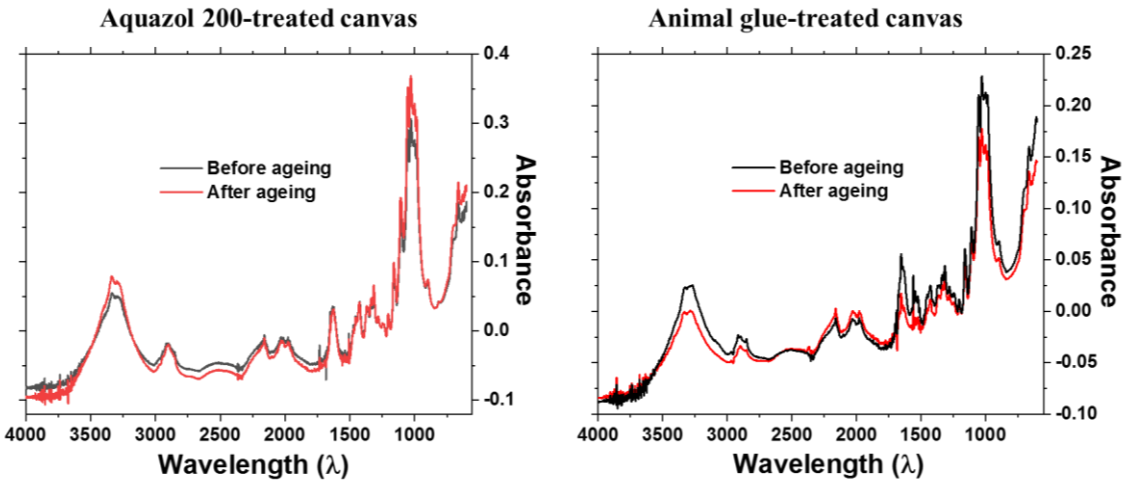

Figure B.12: FTIR spectra of degraded cotton canvases treated with Aquazol 200 and animal glue before and after ageing.

C Appendix Chapter 5

C.1. Solution 1, nanocellulose consolidants

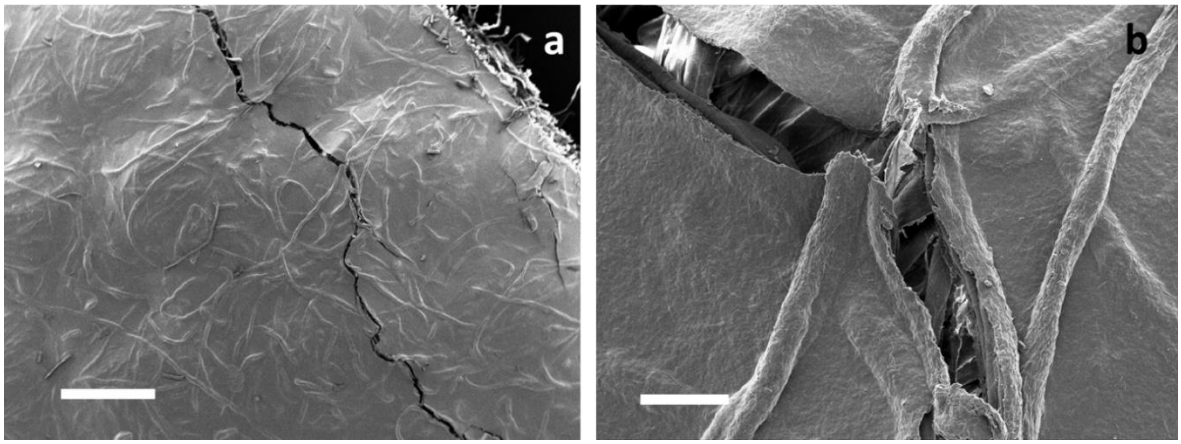

Figure C.1: Rupture of the coating layer observed after tensile testing for a CNF-treated canvas (a). The cracks are spread perpendicular to the direction along which the force was applied. They often seem to propagate along cotton fibres and to cause the rupture of fibre embedded in the coating and perpendicular to the direction of the cracks propagation (b).

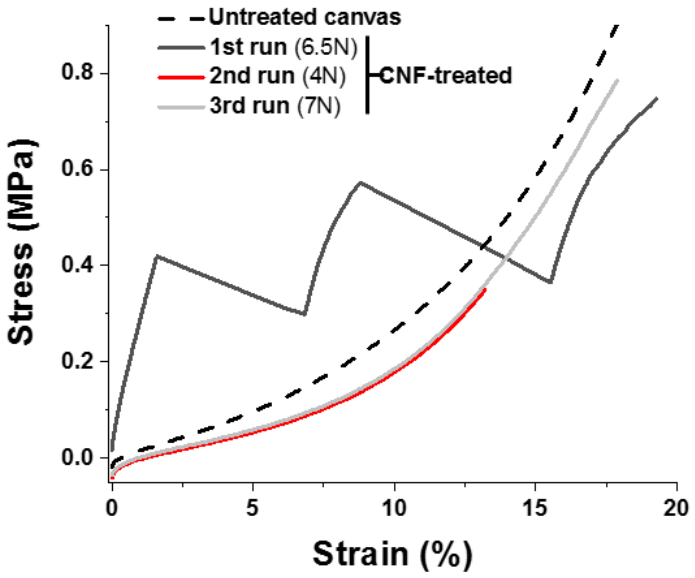

Figure C.2: Three consecutive tensile measurements on a CNF-treated sample showing complete loss of the reinforcement after the first test. This loss result from the tension applied (6.5N, i.e. 1300N/m) and consecutive rupture of the coating layer. After the 1st run (black solid line), the slopes of the CNF-treated curves for the 2nd (red) and 3rd (grey) are lower than the one measured for the untreated sample. Note that the tension applied is above the recommended

values given in the literature (cf. Table 1.1 in Chapter 1) established around 200N.m^{-1}. Only **Mecklenburg (2006)** *suggested higher tensions around 2000N.m^{-1}.*

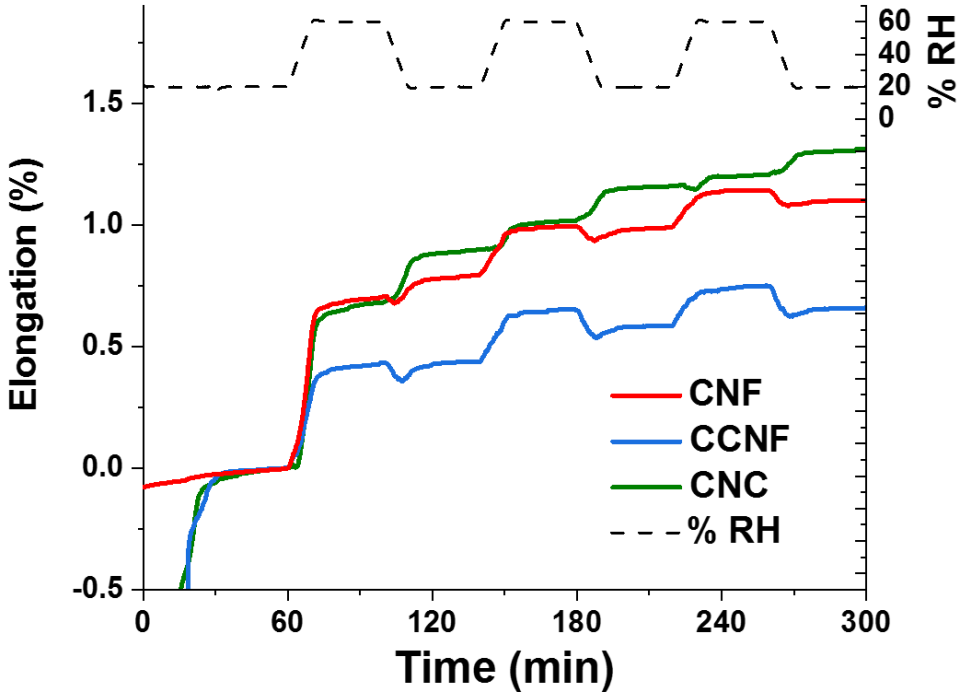

Figure C.3: Elongation measured for the CN-F, CCNF- and CNC-treated degraded cotton canvas upon application of the 20-60-20%RH RH cycles (2 cycles, 25°C). The continuous elongation measured for the 3 samples which was attributed to mechanosorptive creep of the material and had been already observed previously in Chapter 3 and 4 for the canvas and treated canvas with traditional consolidants. However, note the distinct response of the CNC-treated sample for which elongation is increased at each RH transition, humidification (20-60%RH) as well as dehumidification (60-20%RH). For the CNF- and CCNF-treated samples, instead, shrinkage (i.e. reduction in elongation) of the samples is seen during dehumidification. This could be due to the more compact structure of the CNC layer and result from reorganisation of the CNCs nanocristals within the layer leading in end effect to irreversible deformation of the coating.

C.2. Solution 2: nanocomposites CNC/cellulose derivative consolidants

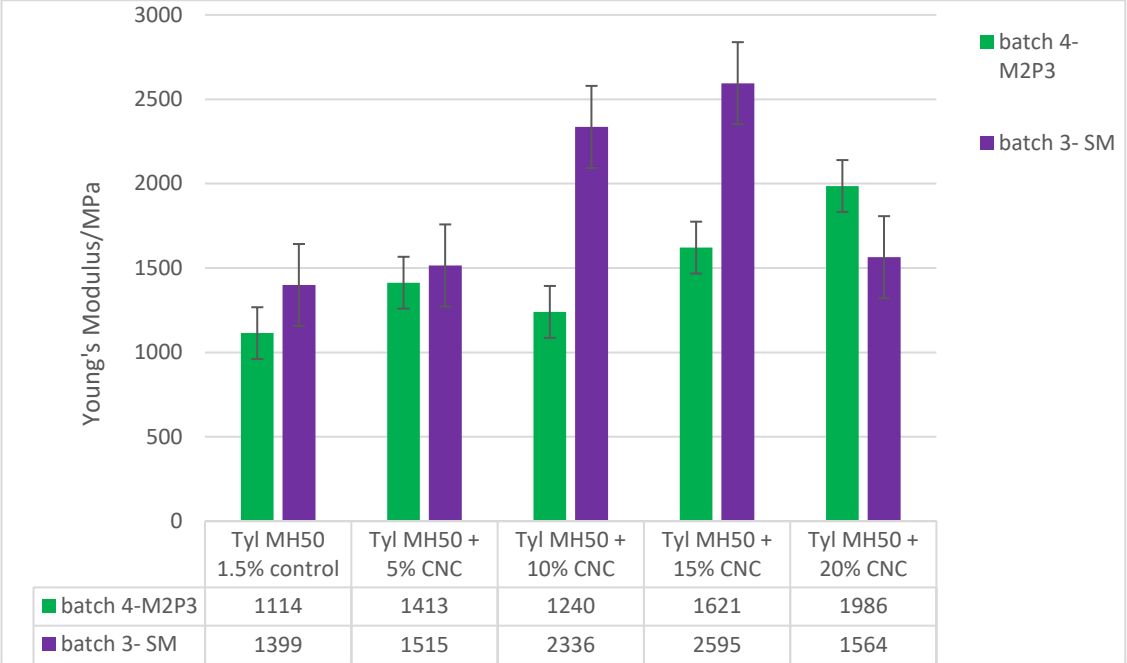

	Tyl MH50 1.5% control	Tyl MH50 + 5% CNC	Tyl MH50 + 10% CNC	Tyl MH50 + 15% CNC	Tyl MH50 + 20% CNC
batch 4-M2P3	1114	1413	1240	1621	1986
batch 3- SM	1399	1515	2336	2595	1564

Figure C.4: Young's modulus measured at 20% RH and 25°C for pre-dried Tylose film and Tylose films loaded with 5%, 10%, 15% and 20%CNC (percentage in total dry weight of the film). The graph was taken from the Master's thesis of Akushla Wijesekara (2018). The results of 2 batches prepared following similar protocols are compared, i.e. batch 4 and 3. Discrepancies in the results, especially at high concentrations in CNC (10 to 20%CNC) were attributed to differences in samples' thickness. This was probably due to the removal of bubbles by vacuum during the dry casting of the samples of batch 4 and absent of the preparation of batch 3.

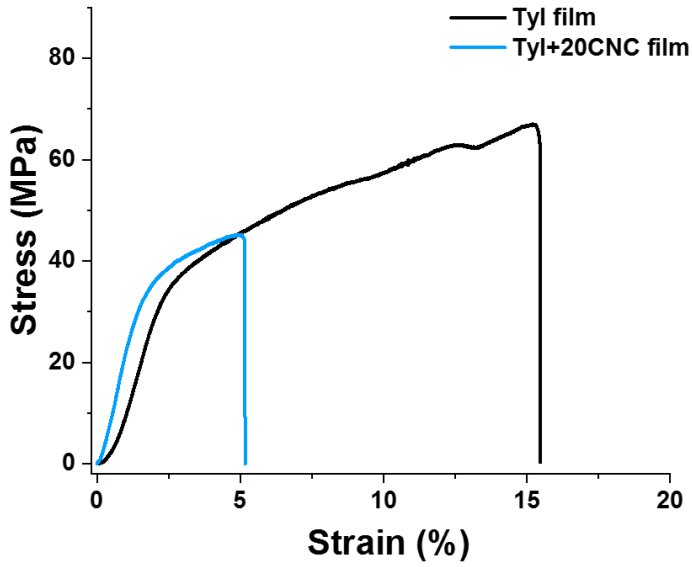

Figure C.5: Stress-strain curve of a Tyl film and reinforced Tyl+20CNC film measured by an Instron tensile tester. The films were brought to rupture. The elongation at break of the films is compared and highlights the higher brittleness of the CNC-loaded film. *Tensile tests were performed using Instron tensile tester with a gauge length of 30mm and cross-head speed of 10mm/min (room conditions). The films (70mm(l)x10mm(w)) had been preconditioned at 30%RH for at least 24h prior to the measurement.*

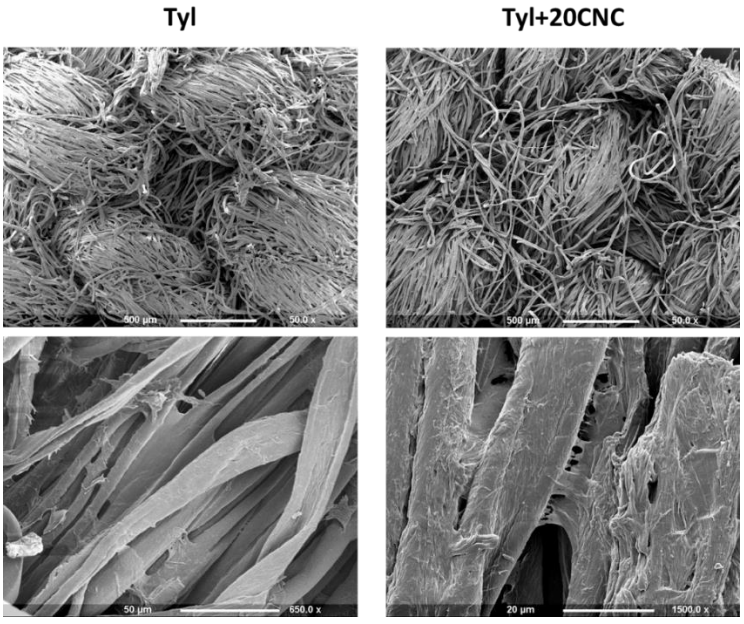

Figure C.6: Comparison of the surface deposition of Tylose MH50 and Tylose MH50+CNC. Similar deposition and penetration seem to be achieved with or without the addition on CNC nanoparticles.

a

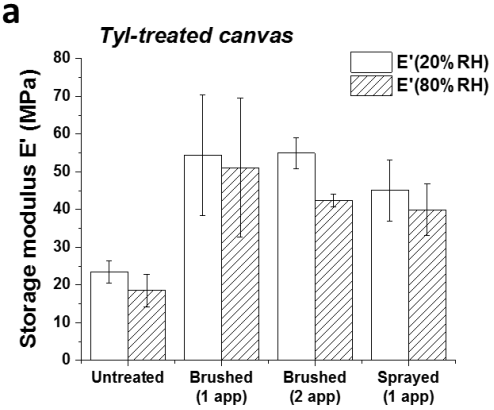

b

Tyl treated canvas	**ΔE' (20-60%RH) (MPa)**
Untreated	4.9±1.4
Brushed (1 app)	3.3±2.6
Brushed (2 app)	12.5±3.1
Sprayed (1 app)	5.3±4.6

Figure C.7: Storage moduli E' measured at 20% and 80%RH (end-plateau value) for untreated and Tylose MH50-treated degraded cotton canvases (a) and difference in E' measured between the 20%RH and 80%RH plateaus as shown in Figure 5.26 (i.e. $\Delta E'_{20\text{-}60\%RH}$) (b). The results enable to compare the impact of the mode of application used (sprayed (1app, 15g.m^{-2}), brushed (1app, 15g.m^{-2}) and brushed (2app, 30g.m^{-2})) on the mechanical properties and mechanical response to moisture variations of the treated samples.

C.3. Solution 3: Multilayered nanoparticles combined with CNF (CNF:Sil/PEI/CMC) for canvas consolidation

C.3.1. Materials and methods

C.3.1.1. Materials

Aqueous dispersions of PEI(polyethylenimine)-coated silica NPs (Sil/PEI), CMC-coated Sil/PEI NPs (Sil/PEI/CMC) and CNF were tested separately as well as combined, i.e. CNF:Sil/PEI/CMC.

This treatment consists in multilayered nanoparticles made from the centre to the surface of a silica core covered with a layer of polyethylenimine (PEI) and a layer of carboxymethylcellulose (CMC) (cf. 2.1.2.3 in Chapter 2). These particles are also found in dispersion mixed with CNF nanofibrils (CNF:Sil/PEI/CMC).

C.3.1.2 Methods

Sample preparation

Treated canvases used in this study were received from Chalmers University (Gothenburg, Sweden). The treatments tested included aqueous dispersions of Sil/PEI, Sil/PEI/CMC, CNF and a combination of CNF and Sil/PEI/CMC (i.e. CNF:Sil/PEI/CMC). The treatments had been applied by spraying on pieces (7x8cm) of a degraded cotton canvases. The protocol of application, described elsewhere (Kolman, 2018), is given below.

The formulations were applied on the surface of a degraded cotton canvas by spraying using an airbrush (i.e. Cotech Airbrush Compressor AS18B (Clas Ohlson AB, Sweden) at a pressure of 2 bar. When more than one layer of treatment was applied, the subsequent applications were sprayed in 30 min time intervals to allow some water to evaporate. The treatments were applied at a distance of around 20 cm of the canvas. The treatments were applied in 2 applications depending of the treatment. This correspond to weight uptake of 8.6wt% for the CNF-treated sample and around 2.5wt% for the Sil/PEI/CMC, Sil/PEI-treated samples. The mass uptake for the CNF:Sil/PEI/CMC was found around 5.0%wt.

RH program for DMA-RH measurements

The RH program used consist in three successive RH cycles 20-60-20 % RH at 25°C. The rate of change from 20-60%RH was 4%RH/min. The samples were set to equilibrate at 20 or 60 % RH for 30 min between each transition. The samples were preconditioned before the DMA-RH measurement for at least 24h at 20%RH at room temperature and were tested in the warp direction as described in Chapter 2 (cf. 2.2.4.2).

C.3.2. Results

The multi-layered treatments developed in the framework of the Nanorestart project by Chalmers university consist of a dispersion in Sil/PEI/CMC mixed with a CNF dispersion. As seen previously (cf. 5.3.2), the CNF treatment has shown to greatly reinforce degraded cotton canvases at low elongation. The combination of Sil/PEI/CMC and CNF aim at providing additional reinforcement which will be discussed in more details below.

C.3.2.1. Appearance

The surface appearance of the sample was investigated by SEM. As seen in Figure C.8, the surface appearance of the treated canvases is strongly affected by the use of CNF. For the CNF: Sil/PEI/CMC and the CNF treated canvases, a coating of treatment is formed on the treated side (Figure C**.8**d.1 and e.1). This coating covers the entire surface of the canvas, inter-fibres and inter-threads spaces are not visually accessible anymore. This had been already observed in 5.3.1 when analysing the deposition behaviour of CNF. With the addition of Sil/PEI/CMC nanoparticles (NPs) to the CNF dispersion, the distinctive surface deposition of CNF is maintained. The SEM images at higher magnification of the CNF:Sil/PEI/CMC and CNF-treated samples (Figure C**.8**d.3 and e.3, respectively) also show that the surface coating of the CNF:Sil/PEI/CMC-treated sample seems to be made of both CNF nanofibrils intertwined with Sil/PEI/CMC NPs. The surface coating of the CNF:Sil/PEI/CMC presents a more granular appearance than for the CNF sample for which the coating consists of a mesh of nanofibrils. On the contrary, the surface appearance of the Sil/PEI/CMC-treated canvas, seen at low magnification (Figure C**.8**c.1), is similar to the one of the untreated canvas (Figure C**.8**a.1). The individual cotton fibres and threads

are clearly visible. The Sil/PEI/CMC NPs does not form a film but covered individual cotton fibres. The coverage is often homogeneous but also tend to agglomerate between cotton fibres as seen in the area indicated by arrows in Figure C.8c.2 and c.3 (similar observations can be made for the Sil/PEI-treated sample in Figure C.8b.2 and b.3). As seen on these images, those interfibrillar bridges are often seen broken which tend to highlight their high brittleness. Contrary to the interfibrillar bridges, in the form of films, seen for the cellulose derivative treatments or the traditional consolidants (cf. Figure 4.13 in Chapter 4), this suggests that for Sil/PEI/CMC-treated canvases, those bridges might not participate to the expected canvas consolidation.

From these observations, the question thus arises whether for the mixed CNF:Sil/PEI/CMC consolidant, the CNF treatment and the superficial layer formed upon drying does not prevent the penetration of Sil/PEI/CMC NPs into the canvas. It was, however, shown by Kolman (2018) that the Sil/PEI/CMC nanoparticles present in the mixed consolidant CNF:Sil/PEI/CMC can penetrate further down in the canvas. This occurs when several successive applications (>2) are made. The solvent plays the role of carrier for the Sil/PEI/CMC NPs.

Further mechanical testing was carried out to evaluate the consolidation provided by the multilayered nanocellulose-based treatment CNF:Sil/PEI/CMC and Sil/PEI/CMC.

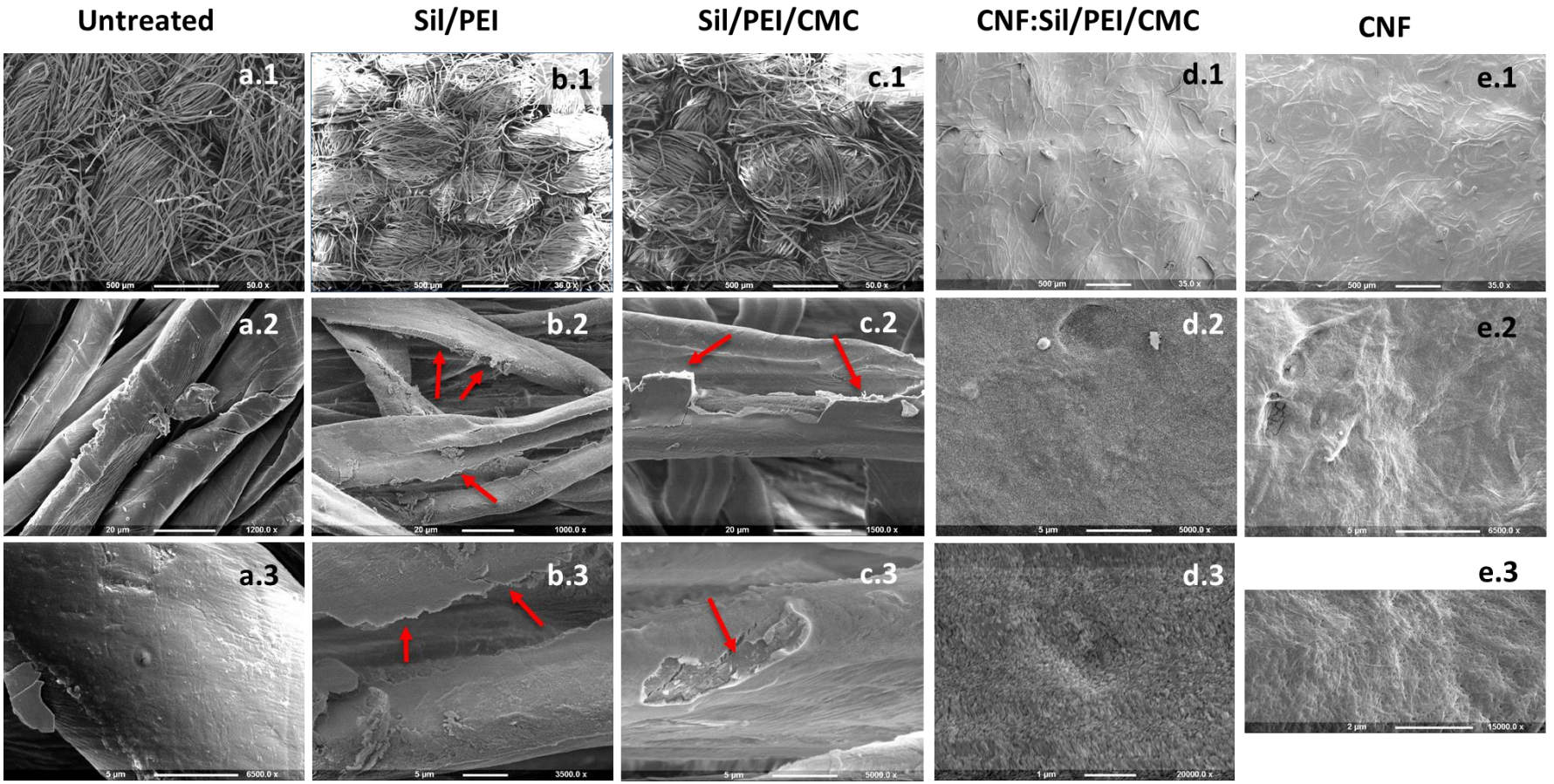

Figure C.8: SEM images of the surface of a degraded cotton canvas untreated (a) and treated with Sil/PEI (b), Sil/PEI/CMC (c), CNF:Sil/PEI/CMC (d) and CNF (e). The number indicates different magnifications of SEM images of the same sample (indicated by a letter) from low (1, x35) to high (3, x3500-20000) magnification.

C.3.2.2. Consolidation

The samples could not be tested by tensile testing using the DMA apparatus available in this project due to the limited amount of samples available. The results of previous tensile testing performed on the same samples using an Instron tensile tester and bringing the samples up to rupture were, however, reported by Kolman (2018). It was shown that the CNF treatment increased the breaking force value and elongation at break (Figure C.9A), while the stiffness of the sample was not affected much (inset in Figure C.9A). The Sil/PEI/CMC treatment, instead, increased the breaking force and decreased the extension at break (Figure C.9B) of the canvas. The stiffness (inset in Figure C.9B) of the Sil/PEI/CMC-treated canvas was increased compared to that of CNF. It is important to note, however, that the same number of applications correspond to a higher weight uptake for the Sil/PEI/CMC treatment than for the CNF treatment. As reported in this study, 2 applications in Sil/PEI/CMC led to a weight uptake of 8.6%w/w whereas for CNF it corresponded to a weight uptake of 2.5%w/w (cf. . This difference could explain the surprisingly low stiffness of the CNF-treated canvas measured by Kolman (2018) which also contradict what was measured by Nechyporchuk (2018). This latter had tested the same samples (CNF-treated degraded cotton canvas, application by spray) but a higher weight uptake (i.e. up to 7.2%w/w) had been applied. From those results, both the Sil/PEI/CMC and the CNF treatments are expected to bring high stiffness to the degraded canvas. The Sil/PEI/CMC treatment seems to increase the brittleness of the canvas but since the forces required to reach rupture of the canvas are beyond those that would be applied on a painting (i.e. 2kN/m, 1-2% elongation) (Iaccarino Idelson, 2019; Mecklenburg, 1982; Young, 1999), this region of the tensile curves will not be investigated here.

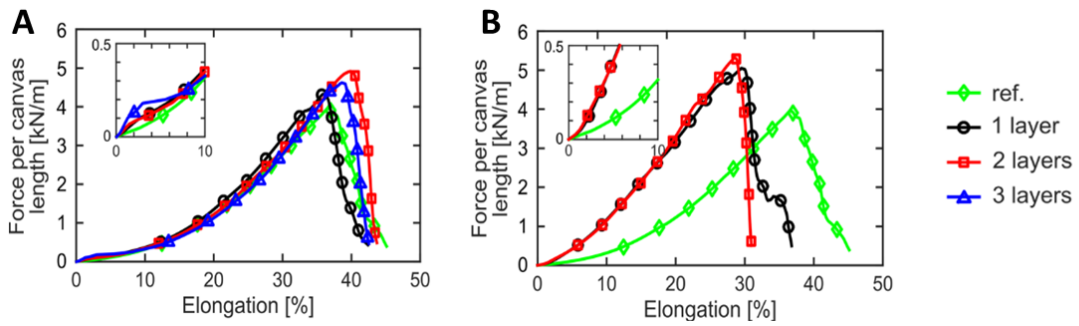

Figure C.9: Tensile test curves of degraded cotton canvas treated with (A) CNF and (B) Sil/PEI/CMC. The treatments were applied with up to three repetitions (layers). The insets present the curves in the low elongation region. (taken from* (Krzysztof Kolman et al., 2018a)*). The tensile curves were obtained using an Instron tensile tester.

Since no tensile testing could be performed on the samples, the viscoelastic mechanical data from the DMA-RH analysis (using controlled RH cycles) was used. As it was previously shown (cf. 4.3.3.2.1 in Chapter 4), storage moduli *E'* measured for the samples during RH cycling can inform on the stiffness of the samples. The results are here given for the storage moduli measured at 20%RH (Figure C.10). Similar results were obtained at 60%RH and can be seen in the following part (Figure C.11) in which the mechanical response of the samples to moisture variations will be discussed.

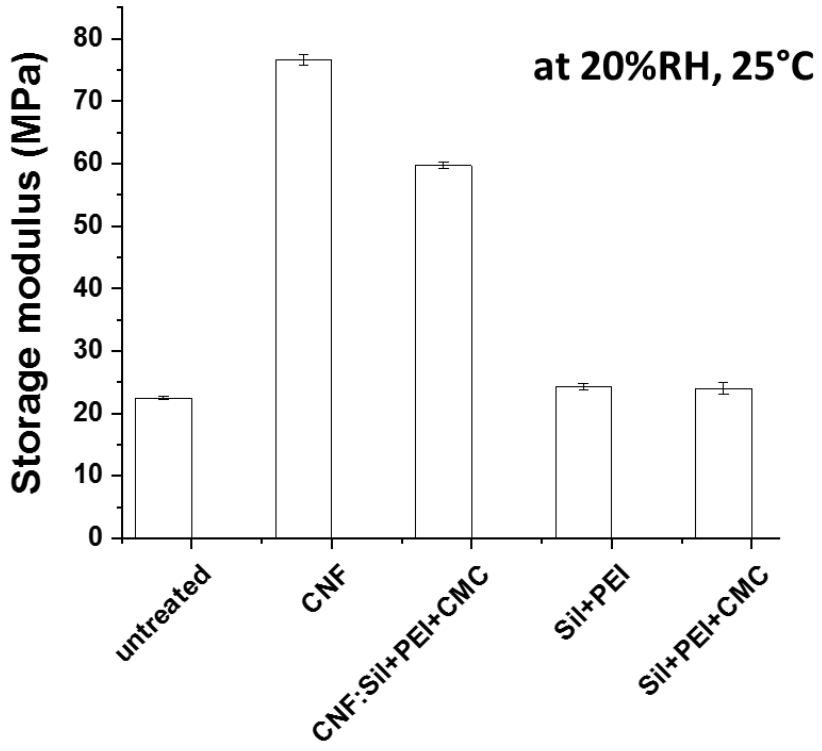

Figure C.10: Storage moduli E' measured at 20%RH (25°C) for the untreated canvas and the Sil/PEI, Sil/PEI/CMC and Sil/PEI/CMC:CNF as well as the CNF- treated degraded cotton canvases. The impact of each individual constituent of the consolidation on the final mechanical performance of the treated canvas is analysed.

In Figure C.10, the storage moduli measured for the untreated cotton canvas and the Sil/PEI-, Sil/PEI/CMC, Sil/PEI/CMC:CNF and CNF-treated canvases are shown. The higher reinforcement provided by CNF is highlighted in the results. The CNF and the CNF:Sil/PEI/CMC treatments present the highest storage moduli E' at 20%RH measured at 76.6±0.8 and 59.7±0.5 MPa, respectively. The Sil/PEI and Sil/PEI/CMC treatments, on the contrary, do not seem to provide any reinforcement to the canvas. Storage moduli *E'* of 24.2±0.5 and 24.0±0.9 MPa were obtained for these samples. This is similar to the 22.5±0.3MPa measured for the untreated canvas. The low stiffness of the canvas reached for the Sil/PEI and Sil/PEI/CMC treatments is surprising and was not expected from the results previously obtained by Kolman (2018). Two assumptions could be made. First, mechanical damages of the samples during transport might have occurred due to the high brittleness of these samples (Kolman 2018). This is also supported by SEM of the Sil/PEI/CMC and Sil/PEI/CMC samples (Figure C.8) which shows the numerous cracks and

ruptures of the secondary arms formed between cotton fibres. Second, the amount of treatment applied might not have been sufficient to observe any consolidation.

It is also interesting to notice that the use of CNF with the dispersion in Sil/PEI/CMC lead to a reduction in stiffness of the treated material. This is to be put in relation with the changes in surface coating shown previously in Figure C.8d.3 and Figure C.8e.3 for the surface layer of the CNF: Sil/PEI/CMC and CNF treatments, respectively. The presence of Sil/PEI/CMC particles mixed with CNF as seen from the granular appearance of the surface coating (Figure C.8d.3) may have caused the change in mechanical properties of the coating layer. This change could result in a loss in stiffness or, as suggested by the tensile tests performed by Kolman (2018), a higher brittleness (Figure C.9).

C.3.2.3. Response to RH

The impact of the treatments on the samples mechanical response to moisture was also investigated. Storage moduli measured at the end of the 20 and 60%RH plateau for the 2nd RH cycle are given in Figure C.11a. The differences in E' measured between 20% and 60%RH were also calculated (i.e. $\Delta E'_{20\text{-}60\%RH}$) (Figure C.11b). In terms of response to moisture, the Sil/PEI/CMC and Sil/PEI-treated samples showed again a very similar mechanical response to RH variations than the untreated sample. Variation in E' of 4.4±0.3MPa, 5.8±0.9MPa and 3.4±0.1MPa were calculated for the untreated and the Sil/PEI and Sil/PEI/CMC samples, respectively. These low values could be an indication of the treatment similar response to moisture than the canvas but this could also be the result of the defect in consolidation previously noticed for these two samples. Slightly higher response than the untreated canvas was measured for the Sil/PEI/CMC-treated sample. This could result from the high hygroscopic behaviour of CMC (REF). The Sil/Pei sample instead shows to slightly reduce the mechanical response of the untreated canvas to moisture. This could be due to the high concentration in hydrophobic silica particles in the treatment. Overall, however, the results highlight that despite the presence of NPs of treatments on the cotton fibres (Figure C.8b.2, c.2), the mechanical behaviour to moisture, hence hygroscopic behaviour of the samples, seemed unchanged by the use of Sil/PEI/CMC or

Sil/PEI. The treatments do not strongly hinder or increase the diffusion of water molecules into the cotton fibres.

a

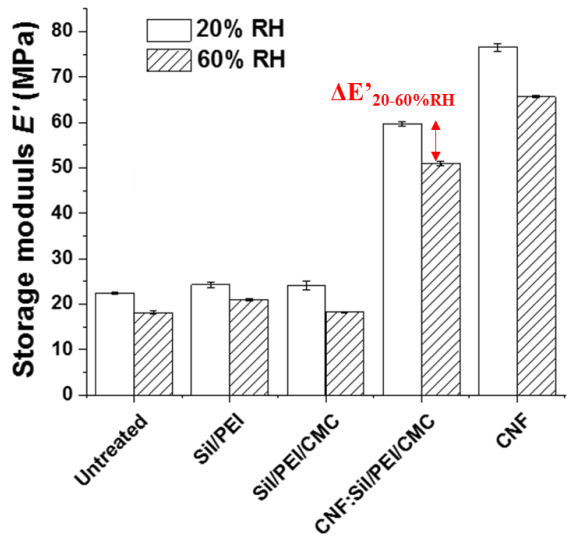

b

Sample	ΔE'(20-60%RH) (MPa)
Untreated	4.4±0.3
Sil/PEI	3.4±0.1
Sil/PEI/CMC	5.8±0.9
CNF: Sil/PEI/CMC	8.7±1.3
CNF	10.9±0.8

Figure C.11: Storage moduli E' measured at 20% and 60%RH (end-plateau value) for untreated and Sil/PEI-, Sil/PEI/CMC-, CNF:Sil/PEI/CMC and CNF-treated degraded cotton canvases (a). Difference in E' measured between the 20%RH and 60%RH plateaus were calculated (i.e. $\Delta E'_{20\text{-}60\%RH}$) (b). The results enable to compare the individual components of the CNF:Sil/PEI/CMC treatments on the sample mechanical properties and mechanical response to moisture variations.

The higher mechanical response is seen for the mixed consolidant CNF:Sil/PEI/CMC ($\Delta E'_{20\text{-}60\%RH}$=8.7±1.3MPa) and, as expected from previous results (cf. 5.3.3) for the CNF-treated canvas ($\Delta E'_{20\text{-}60\%RH}$=10.9±0.8MPa). Those strong mechanical responses are most probably caused by CNF which might governs most of the CNF:Sil/PEI/CMC mechanical behaviour. As already shown in 5.3.3, CNF is highly hygroscopic (cf. Figure 5.8) and strongly increases the mechanical response of treated cotton canvases subjected to variations in RH (20-80%RH). However, as seen in Figure C.**11**b by the lower $\Delta E'_{20\text{-}60\%RH}$ measured for the CNF:Sil/PEI/CMC sample, the presence of Sil/PEI/CMC NPs in the surface coating seems to reduce its hygroscopic behaviour, hence the one of the sample.

C.3.2.4. Stability upon ageing

Colour change upon ageing

Upon accelerated ageing (cf. 5.2.2.4), colour changes were measured for all the samples, untreated and treated. As seen in Figure C**.12**, the strong colour change measured for the samples is characterised by losses in luminance($\Delta L^*<0$) and the yellowing of the samples ($\Delta b^*>0$). The colour change after accelerated ageing is particularly pronounced for the treated samples with the exception of Sil/PEI/CMC for which similar values in ΔE^*, ΔL^* and Δb^* to those of the untreated canvas were measured, i.e. 13.8, -10.0 and 9.0 respectively. The stronger colour changes were measured for the Sil/PEI and the CNF:Sil/PEI/CMC-treated canvas with ΔE^* of 24.4 and 22.4, respectively. The Sil/PEI colour change is characterised by the strong yellowing ($\Delta b^*=18.5$) of the canvas, stronger than any other samples. This probably results from the degradation of the PEI cationic polymer which tends to yellow upon thermo-oxidative ageing (Kalugina, 2004). It is also known that the PEI amine groups reacted with cellulose carbonyl groups at moderate temperatures to form Schiff bases, which are responsible for the yellowing of the material (De la Orden, 2004). This was not directly observed here for the treated unaged samples but the ageing might have promoted the interactions between cellulose and PEI leading to an increase yellowing observed for this material. The lower colour change observed for the Sil/PEI/CMC particles could indicate that the CMC offers a protection against the degradation of the PEI layer.

As for the Sil/PEI sample, the colour change of the CNF:Sil/PEI/CMC-treated is seen as a combination of the strong darkening ($\Delta L^*=-15.8$) and yellowing of the canvas ($\Delta b^*=14.9$). However, the canvas yellowing is much less pronounced than for the Sil/PEI sample for which an increase yellowing of $\Delta b^*=18.5$ was measured. The darkening of the canvas, instead, was similar to what was observed for the Sil/PEI sample as well as the CNF-treated sample. It is assumed that CNF could be causing the darkening observed for the CNF:Sil/PEI/CMC-treated canvas as the same sample without CNF (i.e. Sil/PEI/CMC) does not show any colour change.

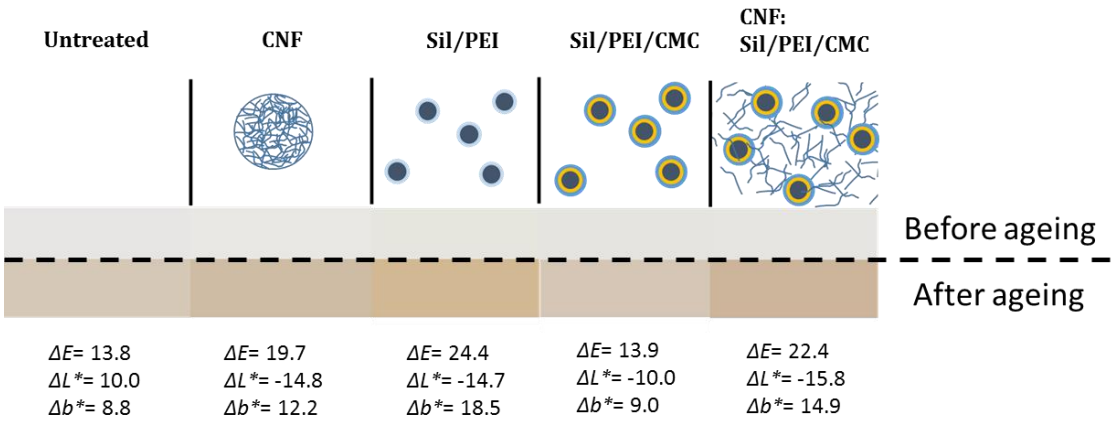

Figure C.12: Colour change measured after ageing for the untreated, CNF-, Sil/PEI-Sil/PEI/CMC and CNF:Sil/PEI/CMC-treated degraded cotton canvas. The overall colour change, the change in luminosity and the yellowing of the sample are shown for all the sample as well as the colour of the canvas surface before and after ageing. Note that the colours shown on the image were produced by computing the Cielab* colour information collected by colourimetry.

Consolidation and mechanical response to moisture after ageing

The mechanical response of the samples before and after ageing are compared in Figure C.13. The way the thermal and RH ageing might have affected both the consolidation provided by the consolidants, as well as the mechanical response of the samples to RH, are investigated. Following accelerated ageing, a strong loss in storage modulus E' was measured at 20%RH for the CNF:Sil/PEI/CMC and CNF samples from 59.7±0.5MPa to 51.0±0.5MPa and from 76.6±0.8 to 65.7±0.8MPa, respectively (Figure C.13a). The loss in E', hence stiffness, probably result from the degradation of the CNF which has shown to be the only constituent of the treatment providing consolidation at low elongation to the degraded canvas (see 0 Consolidation). The Sil/PEI- and Sil/PEI/CMC-treated canvases, instead, do not seem to be affected mechanically by the ageing. They do not contribute either to any modifications in the viscoelastic behaviour of the degraded canvas. As seen in Figure C.13a, storage moduli E' measured for both samples remain unchanged and similar to E' measured for the untreated canvas before and after ageing.

In terms of response to moisture, Figure C.13b shows that differences in E 'between 20 and 60%RH (i.e. $\Delta E'_{20\text{-}60\%RH}$) are greatly reduced after ageing for the CNF:Sil/PEI/CMC, CNF as well as the Sil/PEI/CMC. $\Delta E'_{20\text{-}60\%RH}$ values go from 8.7 to 3.6MPa and 10.9 to 3.8MPa after ageing for the CNF:Sil/PEI/CMC and CNF samples, respectively. $\Delta E'_{20\text{-}60\%RH}$ after ageing are lower than half of the values measured before ageing. Interestingly, the hygroscopic response of the Sil/PEI/CMC-treatde sample seems also affected. This is seen as a reduction by a factor 2 of the $\Delta E'_{20\text{-}60\%RH}$ measured for this sample after ageing. The hygroscopic response of the untreated and Sil/PEI samples remain, on the contrary, almost unchanged. A small increase in response from 4.4. to 5.5MPa seem to be observed for the untreated sample but remain significantly low.

Previous results (see 0) on unaged samples suggested that the high mechanical response to RH of CNF:Sil/PEI/CMC and CNF samples was mainly triggered by the CNF component. Yet, the results could suggest that the lower hygroscopic response measured for the CNF:Sil/PEI/CMC sample after ageing is here the result of changes in mechanical behaviour observed for both CNF and Sil/PEI/CMC NPs. Reduction in hygroscopic behaviour might be caused by the degradation of both CNF and Sil/PEI/CMC NPs.

a

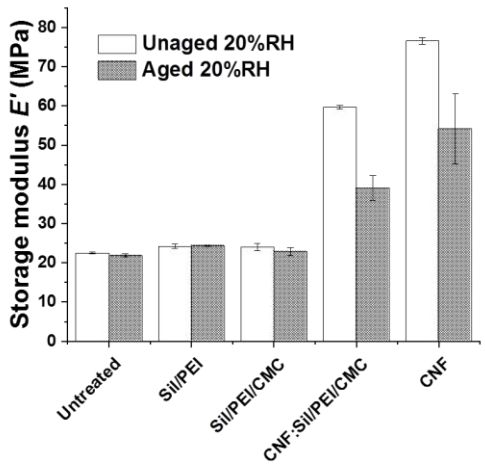

b

Sample (treatment)	$\Delta E'_{20\text{-}60\%RH}$	
	Unaged	Aged
Untreated	4.4±0.3	5.5±0.6
Sil/PEI	3.4±0.1	3.7±0.6
Sil/PEI/CMC	5.8±0.9	2.5±0.1
CNF:Sil/PEI/CMC	8.7±1.3	3.6±0.8
CNF	10.9±0.8	3.8±1.0

Figure C.13: Variations in mechanical properties and response to moisture measured for the treatments part of solution 3. In (a), the storage moduli measured at 20%RH (25°C) for untreated and Sil/PEI, Sil/PEI/CMC, CNF:Sil/PEI/CMC- and CNF-treated degraded cotton canvases. In (b), the difference $\Delta E'_{20\text{-}60\%RH}$ measured between 20 and 60%RH RH plateau (end-plateau values) for unaged and aged samples.

Conclusions

The main outcomes of the evaluation of the solution 3 of nanocellulose-based consolidants are given below in Table C.1). Consolidation (i.e. increase in stiffness) of the degraded cotton canvas was measured for the CNF treatment only. The Sil/PEI/CMC multi-layered particles, instead, did not increase the stiffness of the canvas. The mechanical results obtained here for the unaged samples treated with Sil/PEI/CMC appear to contradict those presented in another study (Kolman,2018). The results of this early work on the Sil/PEI/CMC treatment had showed that the treatment provided as much consolidation to a degraded cotton canvas as CNF.

The results are also surprising as the SEM images clearly indicate that treatments have been applied to all the samples that were tested. Possibly, the transport of the sample and the low amount in consolidant might have affected the samples, hence the results on consolidation. The absence of a noticeable increase in stiffness resulting from the application of Sil/PEI/CMC contributed to the difficulty to measure either any modification of the response of the samples to moisture. Further assessment of newly prepared samples is required.

Mechanical behaviour of the Sil/PEI and Sil/PEI/CMC samples remain similar to the one of the untreated canvas. When Sil/PEI/CMC and CNF were combined, a loss in consolidation compared to the CNF-only treated canvas was observed but was also accompanied by a reduction in mechanical response to moisture, beneficial for the canvas. Upon ageing, consolidation provided by the CNF: Sil/PEI/CMC as well as CNF (also observed in Figure 5.21 in 5.4.2.4) treatment was maintained and also lead to a lower mechanical response of the treated samples to moisture. The presence of Sil/PEI/CMC also retarded change in colour and as such showed a protective action on ageing.

	Solution 3 Multilayered nanoparticles
Visual appearance	- High penetration of the treatment into the canvas - Homogeneous distribution on individual cotton canvass fibres
Consolidation	Low *[possibly due to issue with the samples]*
Hygroscopic behaviour / mechanical response to RH variations	Similar to untreated sample *[possibly due to issue with the samples]*
Stability upon accelerated ageing	- Colour change but lower than CNF
Main advantages	- High consolidation and high penetration (according to Kolman (2018)) [not seen here]
Main disadvantages	- Absence of consolidation measured in this study [cause unknown]

Table C.1: Summary of the results obtained for the solution 3 nanocellulose-based consolidants.

D Appendix Chapter 6

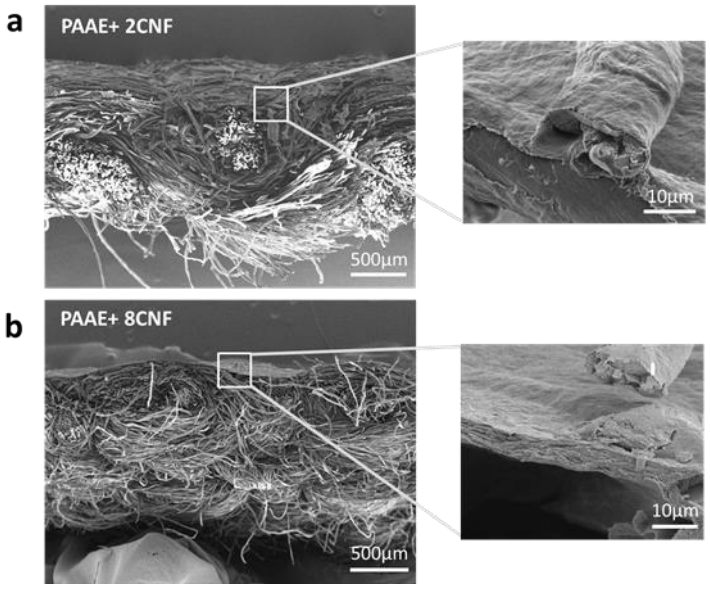

Figure D.1: SEM images of cross-sections of the 'PAAE + 2CNF' (a) and 'PAAE + 8CNF' (b) samples showing thicknesses of the CNF layer around 1-2 and 5µm, respectively.

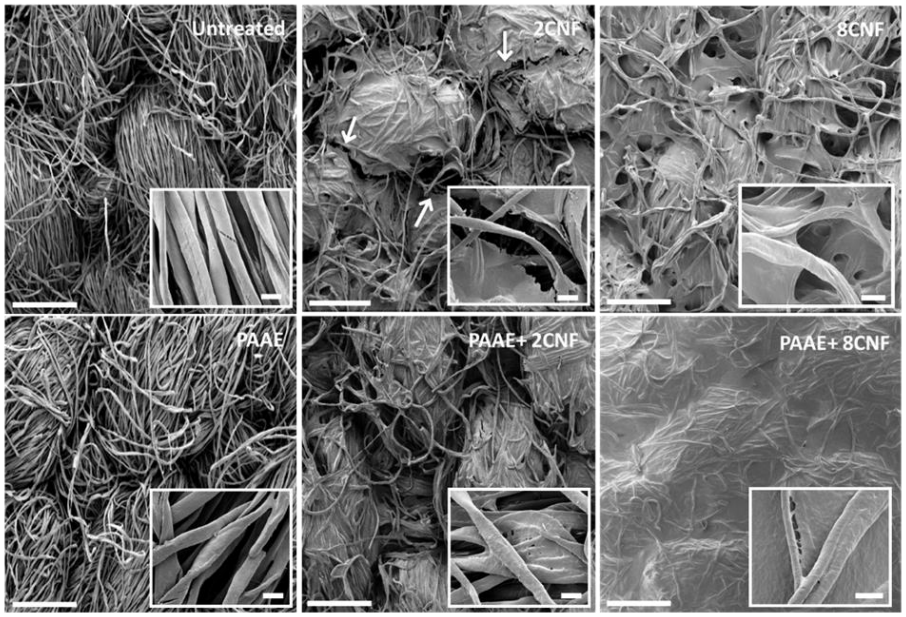

Figure D.2: SEM images showing the deposition of the treatment (2 applications (i.e. 2CNF) and 8 applications (i.e. 8CNF) with or without PAAE) onto the surface (scale of 500µm) and the fibres (scale of 20µm) of the canvas.

E Appendix Chapter 7

	MC+CNC (w)	MC+CNC +CaCO3	MC+CNC (h)	MC+CNC +MgO (h)	CNF	CCNF	$CaCO_3$@CMC	$CaCO_3$@	$CaCO_3$
Tight weave n°1 (1st)	4	4			4	5	1	1	
Tight weave n°1 (2nd)	3	3	2	3			3		
Tight weave n°2	3	3	3	3	3	3	3		
Loose weave n°1 (1st)	3	3					4	4	4
Loose weave n°1 (2nd)	3	3	3	3	3		3	3	

Table E.1: Number of applications carried out for each treatment on the densely and loosely woven lining canvases

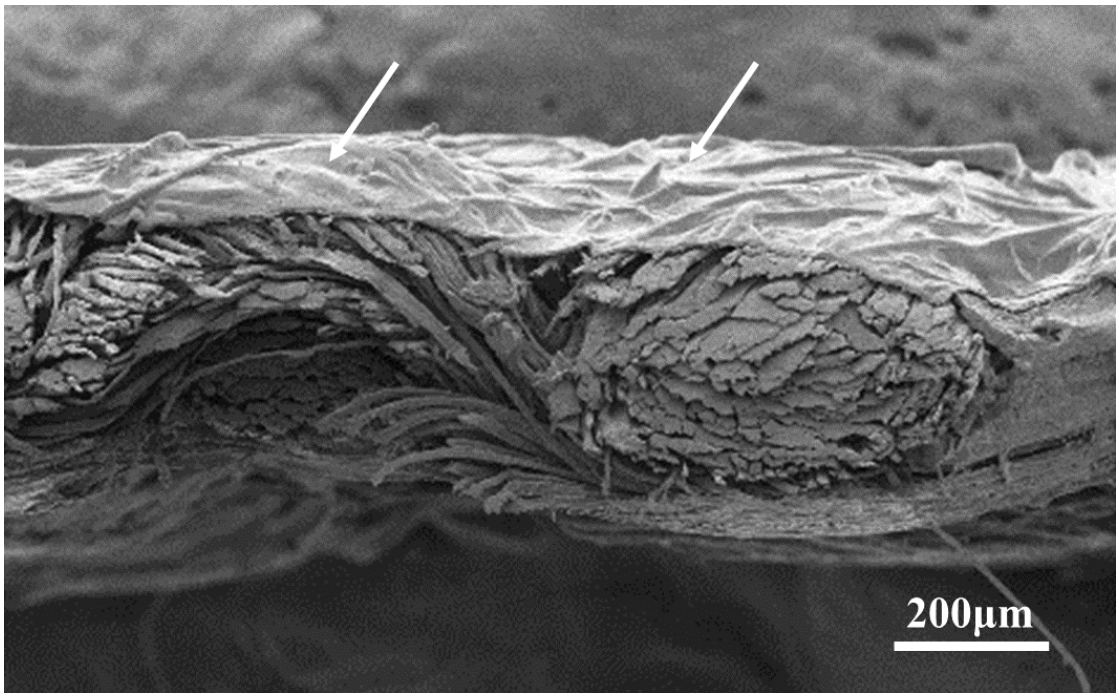

Figure E.1: SEM images of the cross-section of the 19th century lining canvas (linen canvas, dense weaving n°1) treated with MC+CNC+MgO in heptane. Note the layer of treatment deposited on the surface of the canvas corresponding to the treated side (top).

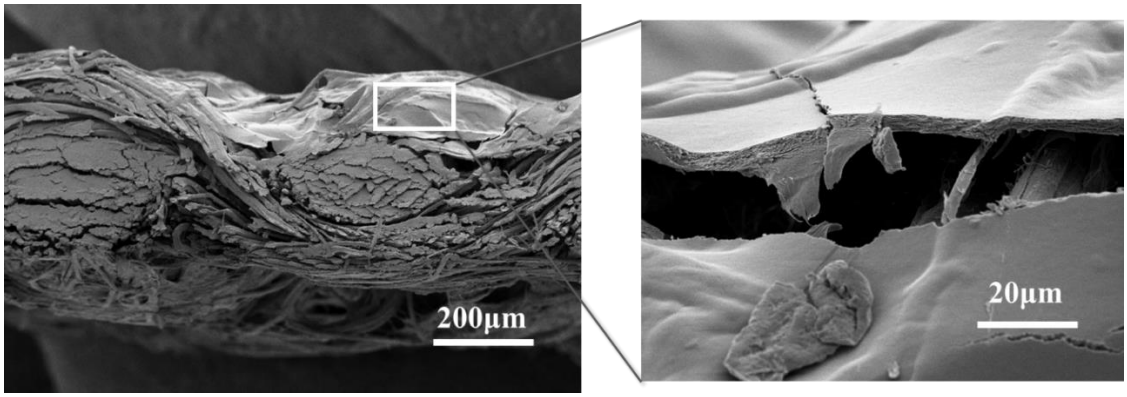

Figure E.2: SEM images of the cross-section of the 19th century lining canvas (linen canvas, dense weaving n°1) treated with CNC in water:ethanol (1:1). Note the layer of treatment deposited on the surface of the canvas corresponding to the treated side (top).

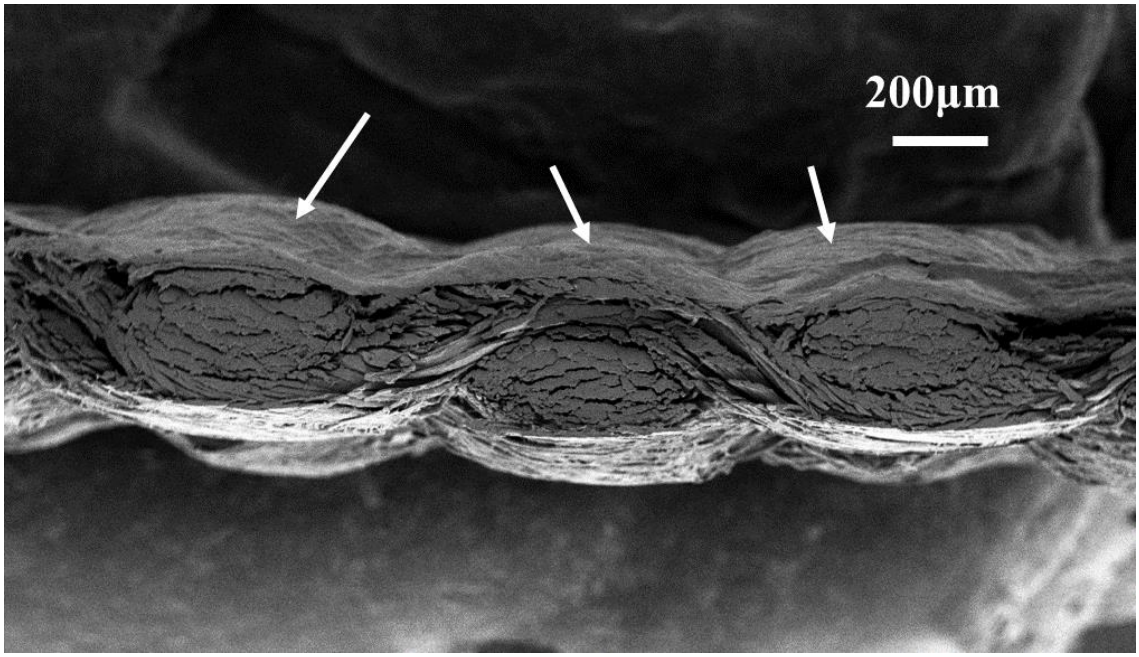

Figure E.3: SEM images of the cross-section of the 19th century lining canvas (linen canvas, dense weaving n°1) treated with CNF in water. Note the layer of treatment deposited on the surface of the canvas corresponding to the treated side (top).

F Appendix Chapter 8

F.1. Supplement to image correction

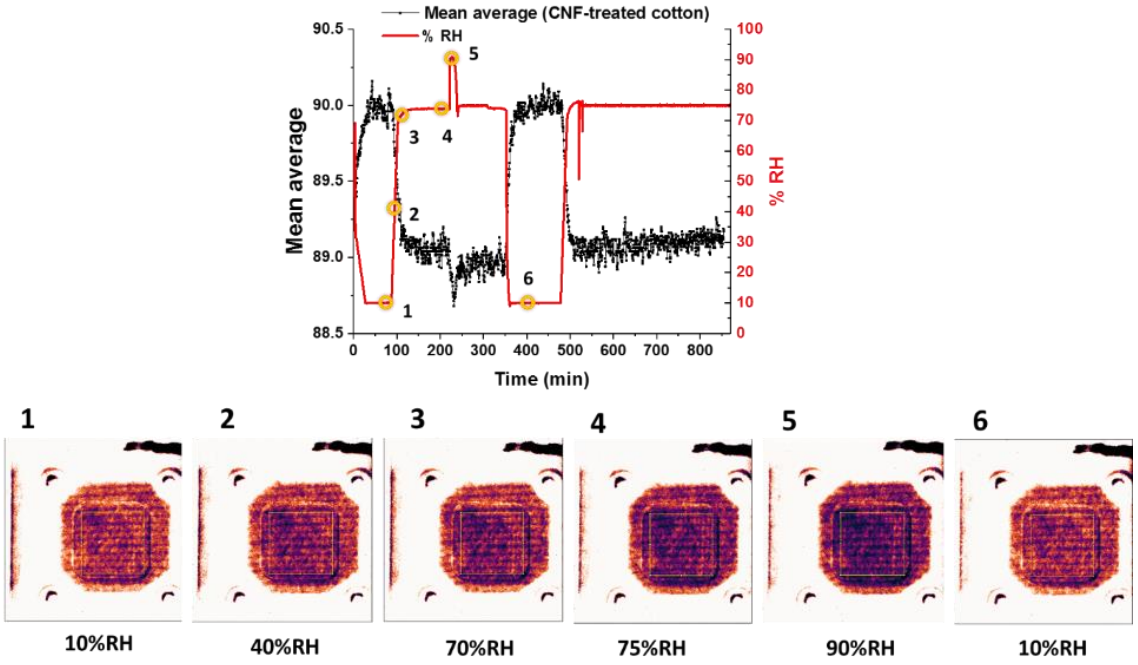

Figure F.1: Absorbance in neutron intensity measured for a CNF-treated cotton canvas. The RH program used for this sample differs from the one used on the other samples (cf. 8.2.2.3). The sample was equilibrated at 10%RH for 1hour and 30minutes. The RH was then increased to 75% at 4%RH/min and stabilize at 75%RH for 6hours. The RH was decreased back to 10%RH at 4%RH/min and left for 10hours at 10%RH.

Figure F.1 shows the mean average intensity measured in the centre of a CNF-treated cotton canvas (i.e. exposed area, yellow square in Figure 8.8a). The intensity is given before corrections of the image using the correction factor D(I_n)-D(I_{dark}) (see paragraph 8.2.2.4). The impact of the variations, programmed or accidental (e.g. event nb. 5 in Figure F.**1**) are clearly seen. The jump in RH from 75 to 90%RH observed around 230min leads to an immediate response of the canvas as seen by the peak in intensity (mean Intensity) measured for the sample (black curve). This can also be seen in image 5 taken which corresponds to the average of 4 images during this episode at 95%RH.

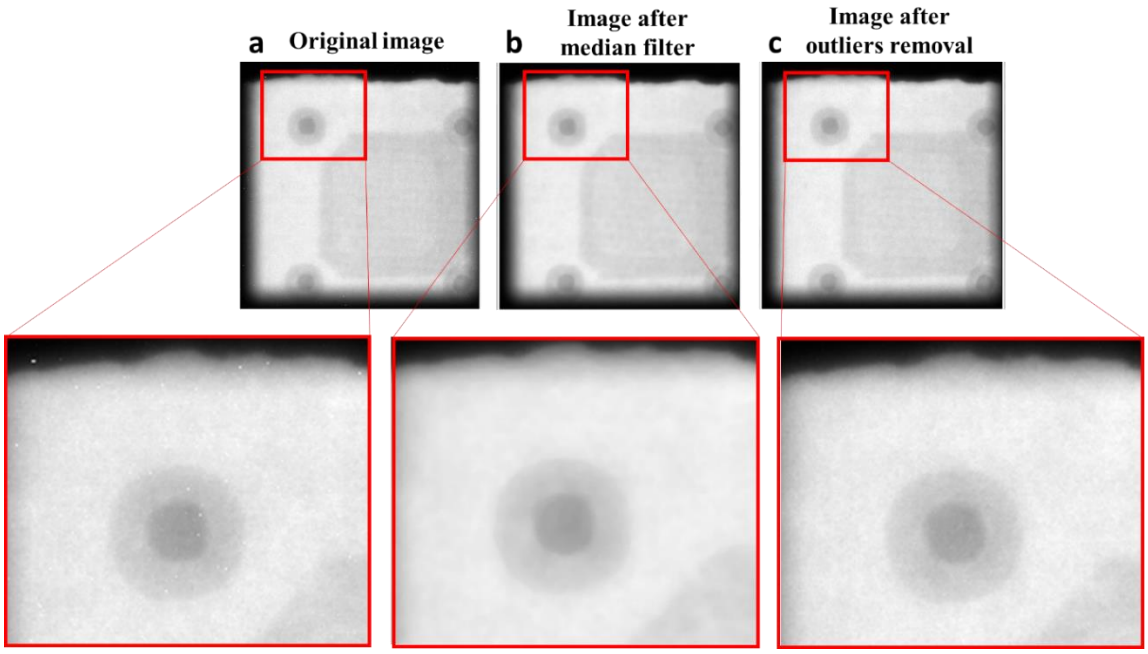

Figure F.2: Neutron images before (a) and after noise removal using a median filter (radius=2) (b) or the outliers removal (radius=2, threshold=500) (c).

The filters were used to remove the noise, white and black speckles, seen on the raw images Figure F.2a. As seen in Figure F.2b the use of the median filter eliminates the speckles seen in Figure F.2a but also induces the loss in the definition and resolution of the image. The image appears more blur. The removal of outliers (Figure F.2c) enables the removal of part of the speckles (reduction in white spots) while preserving the overall features (threads, weaving). This second option was thus privileged over the median filter for the correction of the images.

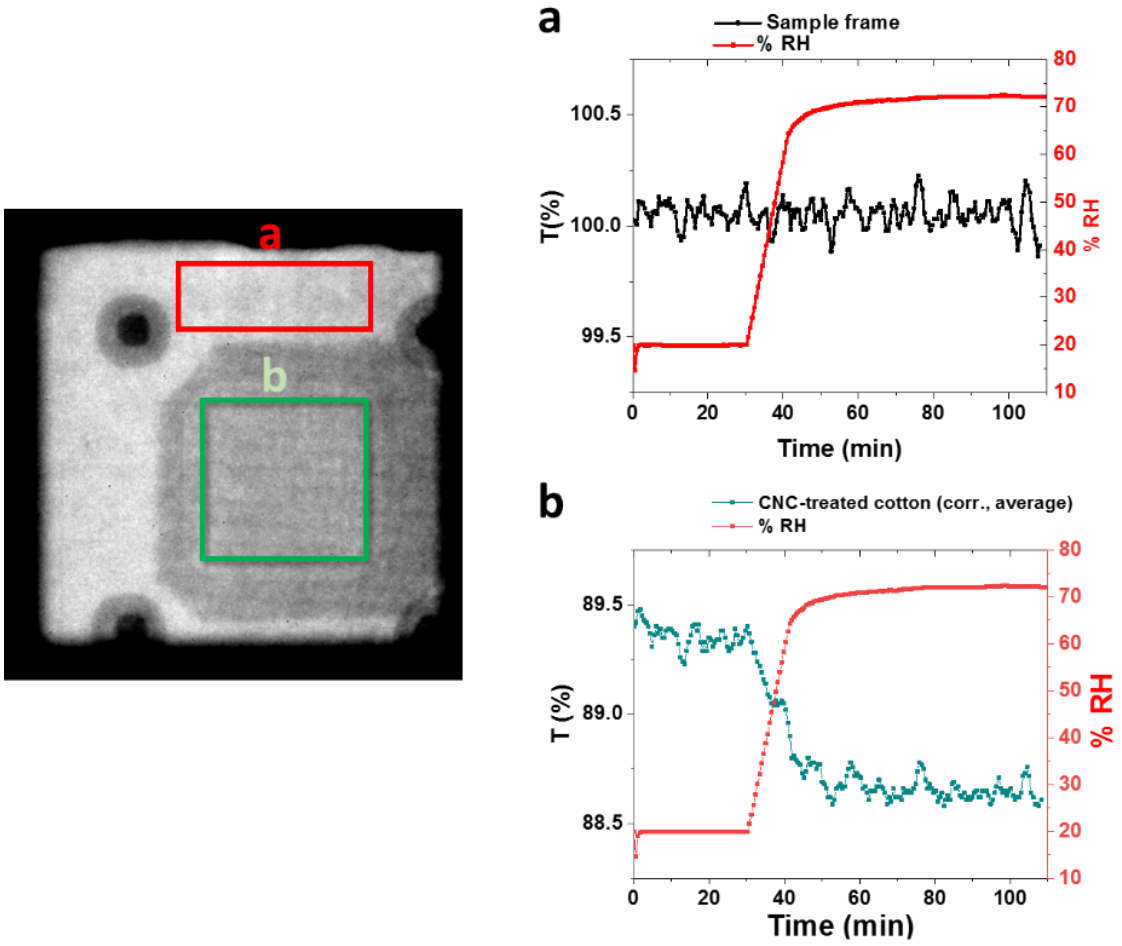

Figure F.3: On the left, neutron radiographic image of the CNC-treated cotton canvas. The transmission measured in (a) an area on the frame and in (b) an area on the sample are given on the right over time.

The transmission T(%) shown in Figure F.3a and b were calculated after corrections of the series of neutron images obtained for a CNC-treated cotton canvas. To evaluate the validity and efficiency of the corrections and in particular of the correcting factor D(I_n)-D(I_{dark}) (see paragraph 8.2.2.4). This factor had been calculated using an area on the frame located on the left hand side (Figure 8.6a). The evaluation of the correction was thus performed by measuring the transmission given on another location on the frame (i.e. red rectangle on the neutron image in Figure F.**3**). As seen in Figure F.**3**a, the transmission measured on the frame is not influenced by the variations in RH. The noise of the signal, however, remains relatively important. This could originate from the back scattering which could not be corrected but could also be a result of the correction using the correcting factor. Additional filters could have been applied on the images to

smoothen the signal. However, such corrections are also associated with the risk of losing some features of the images as well as overcorrections leading to misleading results. Since the signal-to-noise ratio of the transmission measured on the sample remains low, as seen in Figure F**.3**b, the corrections implemented can be considered acceptable. The use of a correcting factor and a filter (outliers removal) were used to correct all the images of the series of measurements.

F.2. ImageJ macro for image analysis

```
/*specify 2 rectangles
 * first is the frame, duplicate it.
 * second is sample, duplicate.
 * make each a 32 bit image
 */

dir1 = getDirectory("F:/data/Projects/isis/RB1820595/Cotton/CMCCNCw2/longrun20");

dir2 = getDirectory("F:/data/Projects/isis/RB1820595/Cotton/CMCCNCw2/Results/R1");

list = getFileList(dir1);


setBatchMode(true);
for (i=0; i<list.length; i++) {
showProgress(i+1, list.length);
filename = dir1 + list[i];
if (endsWith(filename, ".tif")) {


open(filename);

Imagename = File.nameWithoutExtension;        // this lets you use the string "Imagename" in the macro to save files with the name of the input file


selectWindow(Imagename+".tif");
makeRectangle(1096, 986, 72, 156);
run("Duplicate...", "title=frame duplicate");

selectWindow(Imagename+".tif");
makeRectangle(1048, 824, 417, 429);
run("Duplicate...", "title=sample duplicate");

selectWindow("IMAT00010979_cellulose1_dark_025.tif");
makeRectangle(1048, 824, 417, 429);
run("Duplicate...", "title=dark duplicate");

selectWindow("frame");
run("32-bit");
selectWindow("sample");
run("32-bit");

selectWindow("dark");  //Calculation of D(I_dark)
run("Measure");
d=getResult("Mean", nResults-1);

imageCalculator("Subtract create 32-bit stack", "sample","dark");          //Dark correction

for (i=0; i<nSlices; i++) {                    //Calculation of D(I_n)
          selectWindow("frame");
          setSlice(i+1);
          run("Measure");

          x=getResult("Mean", nResults-1);
          y=x-d;  //Calculation of D(I_n) - D(I_dark)
```

```
        selectWindow("Result of sample");
        setSlice(i+1);
        run("Divide...", "value="+y+" slice");     //Correction intensity with factor D(In) - D(Idark)

        run("Remove Outliers...", "radius=2 threshold=500 which=Bright");        //Noise removal

        print(x);

        }


imageCalculator("Divide create 32-bit stack","Result of sample", "Flatcorrdale.tif");
        //Correction with flat image

run("Running ZProjector", "running=4 projection=[Average Intensity]");

//Averaging images (4 images) using plugin Running ZProjector


saveAs("tif", dir2+ Imagename + "processedWAv");       //Save stack of averaged and corrected images

close();

  }

}
```

F.3.Study on moisture inhomogeneities

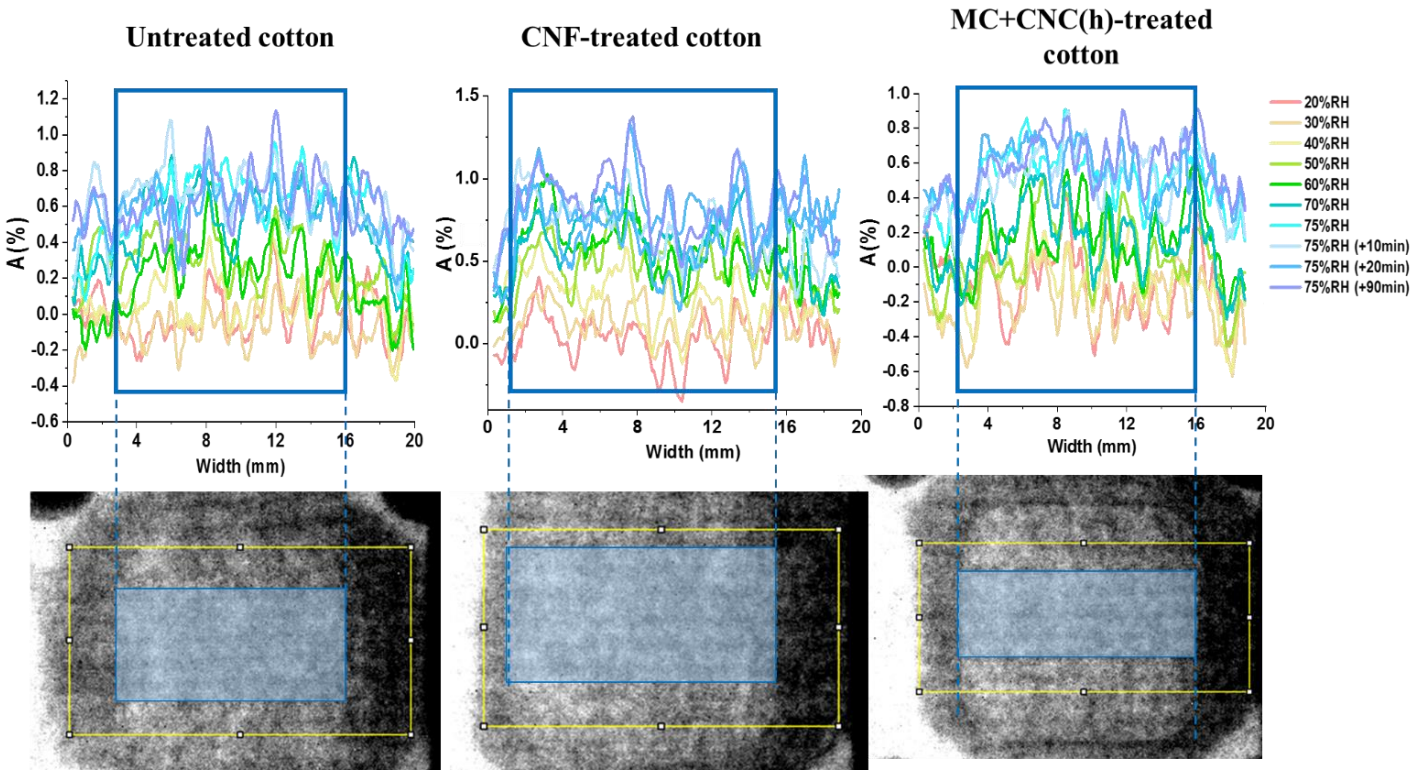

Figure F.4: Variations in absorbance upon increases in RH measured at different point on the sample (unexposed/exposed area), from one to the other edge. Each point on the curves in absorbance (A(%)) indicates the average absorbance measured along a line in the yellow rectangle which is associated to a fixed width. The blue area corresponds to the area on the canvas sample directly exposed to moisture. Note the high noise of the data calculated from the images. This is due to the high noise of the images, their low resolution and the inherent inhomogeneous thickness of the canvas (holes in interstitial spaces and thick threads).

The results presented in Figure F**.4** show the high noise obtained when analysing the images. An overall increase in absorbance was measured across the sample upon increase in RH from 20 to 75%RH. The results also indicate that the unexposed areas, placed under the frame, do not absorb moisture as fast as the exposed area. This is seen by the lower increase in *A*(%) measured upon RH increase. At 75%RH, the curves of the average absorbance measured along the sample have a curve shaped characterised by lower absorbance measured at the edges (i.e. unexposed areas). This is seen in particular for the untreated and MC+CNC(h)-treated samples. Further improvement of the signal-to-noise ratio should be done to confirm these findings.